

AD-A007 566

MINUTES OF THE EXPLOSIVES SAFETY
SEMINAR (16TH), HELD AT THE DIPLOMAT
HOTEL, HOLLYWOOD, FLORIDA, ON 24-26
SEPTEMBER 1974. VOLUME II

Department of Defense Explosives Safety
Board
Washington, D. C.

26 September 1974

DISTRIBUTED BY:

NTIS

National Technical Information Service
U. S. DEPARTMENT OF COMMERCE

AD-A007 566

MINUTES

OF THE SIXTEENTH

EXPLOSIVES SAFETY SEMINAR

VOLUME II

DIPLOMAT HOTEL

HOLLYWOOD, FLORIDA

24-25-26 September 1974

Sponsored by

Department of Defense Explosives Safety Board

Washington, D. C. 20314

Approved for public release; distribution unlimited

Reproduced by
NATIONAL TECHNICAL
INFORMATION SERVICE
US Department of Commerce
Springfield, VA. 22151

i a

764

TABLE OF CONTENTS

VOLUME II

DESIGN OF A SUPPRESSIVE STRUCTURE FOR A MELT LOADING OPERATION Messrs P.A. Cox & E.D. Esparza, SW Res Inst, San Anton, TX	793
STRUCTURAL ANALYSIS OF CONTAINMENT STRUCTURES Messrs N.J. Huffington & S.R. Robertson, BRL, Aberdeen PG, MD	817
METHODS OF PREDICTING LOADING AND BLAST FIELD OUTSIDE SUPPRESSIVE STRUCTURES Messrs W.E. Baker & P.S. Westine, SW Res Inst, San Anton, TX	831
ENERGY SOLUTIONS FOR PREDICTING DEFORMATIONS IN BLAST LOADED STRUCTURES Messrs P.S. Westine & W.E. Baker, SW Res Inst, San Anton, TX	849
ESTIMATES OF FRAGMENTATION HAZARDS FOR SELECTED SUPPRESSIVE SHIELDING APPLICATIONS Mr. J.H. Kineke, Jr., BRL, Aberdeen PG, MD	879
FRAGMENT PENETRATION ESTIMATES FOR THE 81MM SUPPRESSIVE SHIELD Messrs C.J. Brown & A.J. Ricchiazzi, BRL, Aberdeen PG, MD	889
AIRBLAST ATTENUATION BY PERFORATED PLATES Mr. Charles Kingery, BRL, Aberdeen PG, MD	901
200 PSI PROOF TEST OF THE 81mm SUPPRESSIVE SHIELD Mr. A.H. Lasseigne, General Electric Co, Bay St Louis, MS	911
SUPPRESSIVE SHIELDING CONCEPT AS AN ANTIPROPAGATION BARRIER FOR THE 81mm, M374 HE MORTAR ROUND Mr. A. K. Keetch, Dugway Proving Ground, UT	913
DEMILITARIZATION CONSIDERATIONS OF TOXICS ASSOCIATED WITH EXPLOSIVES Mr. A.L. Waschler, Ofc ProgMgr. emilChemMat, Aberdeen PG, MD	935
AMC DEPOT DISPOSAL SYSTEM Mr. J. L. Byrd, AMC Ammunition Center, Savanna, IL	961
TREATMENT AND DISPOSAL OF SENSITIVE PRIMING MIXTURE WASTES Dr. P.M. Broudy, Frankford Arsenal, Philadelphia, PA	1007
REPLACEMENT OF BENZENE FOR IMPROVED TOXICITY IN THE NITROCELLULOSE RECOVERY PHASE OF BALL PROPELLANT MANUFACTURE Messrs J.M. Goldman & J.A. Sipia, Frankford Arsenal, Phila, PA	1039

HAZARDOUS WASTE DISPOSAL THROUGH FLUIDIZED BED INCINERATION Messrs J.S. Santos & J.J. Canavan, Picatinny Arsenal, Dover, NJ	1051
A PREDESIGN ANALYSIS TECHNIQUE FOR REINFORCED CONCRETE STRUCTURES Mr. J. O. Davis, Sandia Corp, Albuquerque, NM	1075
PRIMARY FRAGMENT CHARACTERISTICS AND IMPACT EFFECTS IN PROTECTIVE DESIGN Messrs J.J. Healey & Samuel Weissman, Ammann & Whitney, NY, NY	1107
STEEL STRUCTURES TO RESIST THE EFFECTS OF H.E. EXPLOSIONS Mr P. Price, Picatinny Arsenal & Mr N. Dobbs, Ammann & Whitney	1143
EXPLOSIVE-RESISTANT DESIGN FOR THE DEMILITARIZATION FACILITY, NAVAL AMMUNITION DEPOT, HAWTHORNE, NEVADA Mr Dirk VanErp, Keller & Gannon & Frits Fenger, Tudor Eng Co,SF	1179
TREATMENT OF EXPLOSIVE-CONTAMINATED WASTEWATER BY PHYSICAL- CHEMICAL MEANS IN A 10 GPM PILOT PLANT Mr. J.S. Teter, Tudor-Keller & Gannon, San Fran, CA	1195
SECRETARY OF LABOR v. GEARHART-OWEN INDUSTRIES, INC D. E. Ray, Esq., USA Armament Command, Rock Island, IL	1203
A NEW METHODOLOGY FOR WOUNDING AND SAFETY CRITERIA Mr. Wm Kokinakis, BRL, Aberdeen PG, MD	1209
ELECTRONIC INITIATION OF ENERGETIC SOLIDS Messrs T.Gora, D.S.Downs, & H.D.Fair, Picatinny Arsenal, Dover,NJ	1227
GENERATION AND DISSIPATION OF ELECTROSTATIC CHARGES ON EXPLOSIVE POWDERS Mr. B.D. Pollock, Picatinny Arsenal, Dover, NJ	1251
CLOTHING MATERIALS AND STATIC GENERATION Mr. F.J. Rizzo, USA Natick Laboratories	1269
RENOVATION OF OLD CONDUCTIVE FLOORS Mr. I.T. Cruz, NWS Yorktown, VA	1291
NAVSEA SYSTEMS SAFETY GUIDELINES Mr. T.M. Leach, NAVSEA Safety School, NAD Crane, IN	1297
SAFETY AND HAZARDS ANALYSIS OF THE AUTOMATED PRODUCTION SYSTEM FOR 155MM AND 8" PROPELLING CHARGES Mr K.K. Arora, GARD & J.S. Chiappa, Picatinny Arsenal	1313
AN ANALYTICAL MODEL TO PREDICT EXPLOSION PROPAGATION Mr J.M. Dobbie & Mr D.S. Allan, A.D. Little, Cambridge, MA	1343

SAFE SEPARATION AND SECONDARY FRAGMENT IMPACT STUDIES Messrs R.M. Rindner & R.S. Kuvka, Picatinny Arsenal, Dover, NJ	1363
EXPLOSIVE LOAD RESPONSE TO NAVAL GUN SYSTEMS ENVIRONMENT AND ITS RELATIONSHIP TO IN-BORE SAFETY AND PERFORMANCE Mr M.C. Shamblen & J.S. O'Brasky, NWL Dahlgren, VA	1397
MULTI-BURST SIMULATION Messrs J.H. Keefer & R.E. Reisler, BRL, Aberdeen PG, MD	1455
MEASUREMENT OF PRESSURES AND IMPULSES OF GASEOUS EXPLOSIONS AT HIGH INITIAL PRESSURES Mr. A. B. Wenzel, SW Research Institute, San Antonio, TX	
PRESSURE RELIEF AND DECAY IN INTERNAL EXPLOSIONS Messrs R.G.S. Sewell & G.F. Kinney, NWC China Lake, CA	1517
BLAST ENVIRONMENT FROM FULLY AND PARTIALLY VENTED EXPLOSIONS IN CUBICLES Messrs W.A. Keenan & J.E. Tancreto, CEL, NCBC Port Hueneme, CA	1527
PERSONAL ASPECTS OF PUBLIC AFFAIRS Mr. J.J. Foley, Army Materiel Command, Alexandria, VA	1553
LIST OF ATTENDEES	1561

DESIGN OF A SUPPRESSIVE STRUCTURE FOR A MELT LOADING OPERATION*

by

P. A. Cox
E. D. Esparza

Southwest Research Institute
San Antonio, Texas

ABSTRACT

This paper discusses the present design and analysis of a suppressive structure for a melt loading operation having a capacity of 2500 lb of high explosive. The primary purpose of a suppressive structure is to reduce the required spacing of facilities which contain and process high-explosives by reducing the overpressure outside of the structure and controlling the fragments from an internal explosion.

A development program is being supported by the Edgewood Arsenal to establish the technology for designing suppressive structures so that they can be routinely applied to explosive processing operations. This program is divided into several phases which will culminate in a full scale design and test.

Design loads for the structure include those due to the internal blast wave plus those due to the long term pressure buildup in the structure generated by the heat of explosion. Appropriate methods of analyses were used to assess the effect of both the dynamic and quasi-static loads in the structural design. The design was also influenced by the fragmentation requirements which often controlled structural sizing rather than blast loading.

The suppressive structure consists of a structural steel frame to which vented steel panels are attached. Several panel concepts were developed and designed for the full scale structure. These panels will be tested in full scale against simulated primary fragments. Blast attenuation tests will also be conducted using subscale panels to determine venting characteristics. In addition, a one-quarter scale replica model structure

*Work performed under Contract DAAD05-74-C-0751 with Army Materiel Systems Analysis Agency, Aberdeen Proving Ground, Maryland.

will be tested to obtain additional information on venting and on the structural integrity of the frame and panels. The present quarter-scale frame design is presented in this paper. All venting and structural data obtained in these tests will be used to design the full scale prototype. Its venting characteristics, fragment suppression capabilities, and structural integrity will then be verified by full scale testing.

INTRODUCTION

Hazards produced by accidental explosions within facilities that contain and process high explosives have concerned safety engineers for many years. One obvious way to reduce the hazards is to separate such facilities as far apart as possible to avoid the potential for propagation of such an explosion and also to place the facilities as far away from populated areas or other nonrelated operations as possible. Another approach, which is the subject of this paper, is to use a suppressive structure to contain the fragments and suppress the air blast wave from the detonation in order to reduce the required spacing to a minimum. This paper represents a progress report on the design and analysis of a structure to contain the fragments and suppress the air blast from the detonation of 2500 lb of Composition-B explosive being processed in a melt kettle.

The technology for vented suppressive structures has not yet reached the stage where the design is a straightforward process. Most of the development to date has taken place at the NASA National Space Technology Laboratories (NSTL) and has been for the containment of relatively small explosive charges. (1, 2, 3)*

To establish the technology for the design of suppressive structures, development programs are being conducted to determine acceptable panel configurations and frame designs to defeat the fragment hazard and to reduce the air blast to acceptable levels. The present program, supported by the Edgewood Arsenal, will develop the technology for suppressive structures so that they can be routinely applied to explosive processing operations.

This particular development program is for the Category 1 shield and represents the probable upper limit in charge weight for which suppressive structures will be designed. The program is divided into several phases which will culminate in a full-scale design and test. The phases are:

* Superscript numbers denote references included at the end of the paper.

Fragment Hazard Evaluation

This evaluation will consist of two subphases: (1) a melt kettle fragment analysis whereby the worst case fragment from a melt kettle is determined by actual tests, and (2) panel penetration tests whereby simulated full-scale primary fragments are fired at full scale panel components.

Blast Hazards Analysis

In the blast hazards analysis the venting characteristics of the panels will be investigated in order to determine qualitative comparisons between candidate panels. In addition, a one-quarter scale replica of a full-scale prototype structure will be designed and tested. This test will provide information not only on the venting characteristics of the panels but also on the structural integrity of the frame and panels.

Full-Scale Prototype Design and Test

Information from the fragment hazard evaluation and blast hazards analysis, including the structural information from the quarter-scale tests, will be used to design the full-scale prototype. Its venting characteristics, fragment suppression capabilities and structural integrity will then be verified by testing.

As related to the development program, this paper describes the panel concepts which will be evaluated in the fragment hazard evaluation and blast hazard analysis, as well as the frame which will be evaluated in the quarter scale testing.

DESIGN REQUIREMENTS

Primary requirements for a suppressive structure designed for a melt loading operation having a capacity of 2500 lb of high explosives are:

- (1) Maintain structural integrity for a charge weight of 3125 lb, thus ensuring a margin of safety of 25% based on charged weight.
- (2) Contain all primary fragments within the structure. Reference 4 translates this requirement into a 16-oz fragment with a velocity of 7200 fps.

- (3) Reduce the side-on overpressure outside the structure to 5 psi at a distance of 75 ft from the center of a 2500-lb high explosive charge.
- (4) Floor area of approximately 40 ft by 40 ft with an internal volume of about 64,000 ft³.
- (5) Incorporate to the extent possible existing technology and test results of past suppressive structure designs.

DESIGN APPROACH

Many concepts were considered in the design of this suppressive structure. The most obvious design configuration for a structure which is to contain internal pressure is either spherical or cylindrical. Although such configurations result in much more efficient structures for resisting the internal blast loading, it so happens that the steel thickness in the walls of the structure required to defeat the primary fragment are much greater than the thickness required to resist the blast loading. In addition, venting the walls of curved cylinders and spheres significantly complicates construction over that for a straight sided rectangular box. After considering the alternatives, the following guidelines were established to define the design approach for this suppressive structure.

- Structure would be square or rectangular in shape
- All steel construction would be used for both panels and frame. Also, frame members which form the sides and the roof of the structure would continue through the floor to complete the rectangular box.
- Maximum venting would be designed into the walls and roof of the structure consistent with the external overpressure requirements.
- The structure would be designed to have a central charge location which would result in an intermediate vented steel grid floor.
- In order to reduce structural weight to a minimum, extensive plastic deformation of both panels and frame is allowed.

Following these guidelines, several panel concepts were developed and a one-quarter scale replica of the prototype frame developed for the quarter-scale testing.

PANEL CONCEPTS

Four different panel designs were formulated using standard structural angles, perforated plates and tubes. All four panels were designed for the full-scale prototype structure. Since quarter-scale tests will first be conducted, the panels tested will be replica models of those presented here. For this type of model, pressure, stress and strain levels are the same as in the prototype; length and time become 1/4 the value; and the charge weight required to produce these analogous conditions is $(1/4)^3$ times the prototype charge weight. Furthermore, any nondimensional parameters, such as the vented area ratio, remain the same in the model as in the prototype.

In designing the panels, an effective venting area ratio was first computed to provide the required side-on overpressure reduction. Using the equation⁽⁵⁾

$$\alpha_{\text{eff}} = \frac{P_s^2 R^3 X}{(976.3)^2 W^{4/3}} \quad (1)$$

where

$$\begin{aligned} P_s &= 5 \text{ psig} & X &= 40 \text{ ft} \\ R &= 75 \text{ ft} & W &= 2500 \text{ lb} \end{aligned}$$

the effective venting ratio, α_{eff} , needed is 0.013. From this, the venting ratio, α_i , of each element in a panel is computed by assuming that⁽⁵⁾

$$\frac{1}{\alpha_{\text{eff}}} = \sum_{i=1}^N \frac{1}{\alpha_i}, \quad N = \text{number of elements} \quad (2)$$

In each element, α is defined as the ratio of open area divided by the total area of the wall.

To defeat the primary fragment threat using four spaced plates requires a total thickness of 2.35 in. of steel.^(4, 6) All the panels were therefore designed such that each configuration would provide at least four spaced plates with the necessary total steel thickness. Each geometry was then checked to ensure that the dynamic and quasi-static blast loads were also contained. Since the structure is to be designed to contain the detonation of 3125 lb of explosive, the dynamic design loads, the reflected impulse and pressure, were determined from data by Goodman⁽⁷⁾ to be 2.43 psi-sec and 4057 psi, respectively. The quasi-static design load was determined by computing the charge weight to structure volume ratio and using the methods presented by Baker and Westine⁽⁵⁾. Since the effective venting of the structure is very small, the quasi-static pressure rise of 165 psig for an unvented enclosure is used.

The first panel design (Figure 1) uses a set of angles spaced so that the specific impulse can be assumed to be absorbed and dispersed by the angles and the perforated plates need only be sufficient to withstand the quasi-static pressure. Since the angles are spaced to provide about a 30% vent area, the quasi-static pressure does not load them.

In this case, the angles provide the majority of the material thickness required to stop the primary fragments. Using this criterion, several angles were selected and checked against the dynamic loading using the following equation:⁽⁹⁾

$$\frac{i_r^2 b^2 L}{\rho A M_p} = 16 \frac{w_0}{L} \quad (3)$$

where

$$\begin{aligned} i_r &= 2.43 \text{ psi-sec} & w_0 &= 0.15 L \text{ (in)} \\ b &= \text{angle spacing (in)} & A &= \text{cross-section area (in}^2\text{)} \\ L &= 116 \text{ in} & \rho &= 0.283/386 \text{ lb-sec}^2/\text{in}^4 \end{aligned}$$

From these results, 3-1/2 x 3-1/2 x 1/2 angles were selected.

Two perforated plates were sized to back the angles and contain the quasi-static pressure by allowing the plates to develop uniaxial membrane action as well as bending. From⁽⁸⁾

$$\frac{P_{\max} x^2}{\sigma_y h^2} = \frac{3}{4} + \frac{4}{5} \frac{w_0}{h} \quad (4)$$

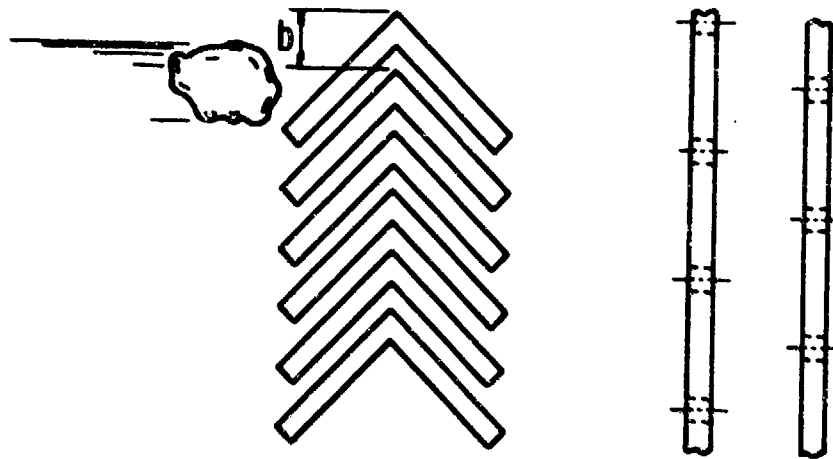
where

$$\begin{aligned} P_{\max} &= 165 \text{ psi} & L &= 116 \text{ in} \\ X &= 58 \text{ in} & w_0 &= 0.15 L \\ \sigma_y &= 36,000 \text{ psi} \end{aligned}$$

the thickness of each plate was computed to be 9/16 in. allowing for the perforations.

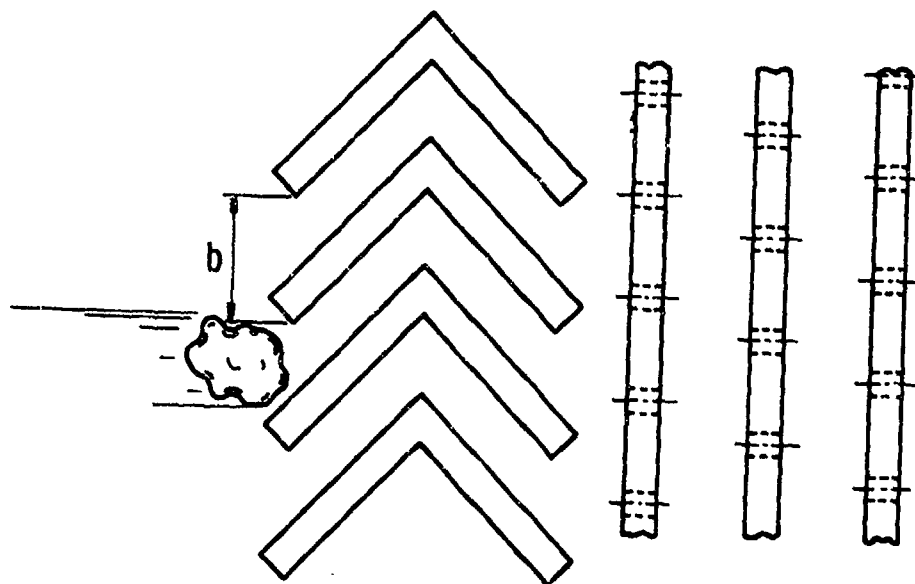
The second panel design (Figure 2) is similar to the first. However, in this case, the size and spacing of the angles were chosen such that the required material is distributed between the angles and plates. Furthermore, the vent area of the angles is larger than on the first configuration so that it can be assumed that the plates will also be loaded dynamically. After some selective computations using Eq. (2), 5 x 5 x 3/4 angles were chosen for this panel.

In sizing the plates, both the dynamic and quasi-static loadings were considered. For the dynamic loading, the following equation was used to determine the total plate thickness allowing uniaxial membrane and bending action⁽⁸⁾



	<u>Full Scale</u>	<u>1/4 - Scale</u>
Angles	L 3-1/2 x 3-1/2 x 1/2	L 7/8 x 7/8 x 1/3
Angle Spacing	b = 1.24 in	b = 0.31
Plates	9/16 in	9/64 ≈ 10 Ga
Holes	1/2 in Diameter	1/8 in Diameter
Hole Spacing	2.7 in	0.675 in

Figure 1. Panel Concept 1



	<u>Full Scale</u>	<u>1/4 - Scale</u>
Angles	L 5 x 5 x 3/4	L 1-1/4 x 1-1/4 x 3/16
Angle Spacing	b = 2.71 in	b = 0.678
Plates	5/8 in	5/32 in = 3/16 in
Holes	1/2 in Diameter	1/8 in Diameter
Hole Spacing	2.19 in	0.548 in

Figure 2. Panel Concept 2

$$\frac{i_r^2 X^2}{\rho \sigma_y h^4} = \frac{2}{3} \left(\frac{w_o}{h} \right) + \frac{32}{35} \left(\frac{w_o}{h} \right)^2 \quad (5)$$

Arbitrarily selecting three plates to back the angles, a plate thickness of 5/8 in. was computed. Since the total plate thickness required using Eq. (4) is greater than that for Eq. (3) (quasi-static), the impulsive load governs in this case.

Having sized the plates, a check was made to determine if sufficient material was available to defeat the primary fragment threat. Since the angles provide 1 in. of steel and the plates 1-7/8 in., the fragment criteria have been met.

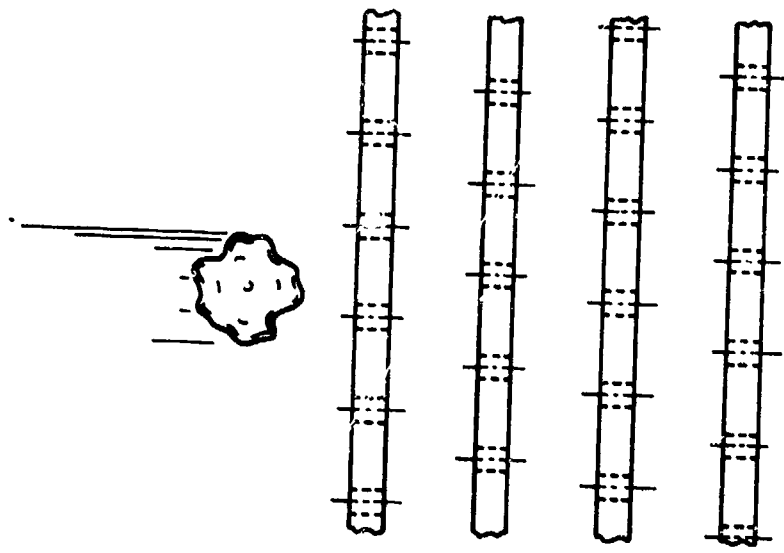
For the third panel design (Figure 3), a set of four perforated plates are used to contain the primary fragments, as well as to carry the total air blast loading. Since a total thickness of 2.35 in. of steel is required to meet the primary fragment threat, each plate should be one-fourth the total thickness plus the thickness required to account for the vented area. Each plate was computed to be 11/16 in. thick. From Eqs. (3) and (4), the plate thicknesses required to carry the quasi-static and dynamic loads are less than those needed against the primary fragments. Therefore, the four perforated plates will be more than adequate against the blast loading.

The last panel design (Figure 4) we considered consists of tubes in a staggered arrangement. The tubes were sized and spaced such that a primary fragment would encounter at least 2.5 in. of steel with four effective layers as it traverses the panel. The spacing must also provide the effective venting area ratio required.

In sizing the tubes, it became evident that this panel concept would be the heaviest of the four as well as require considerably more fabrication time. Consequently, this design has been dropped from the testing program.

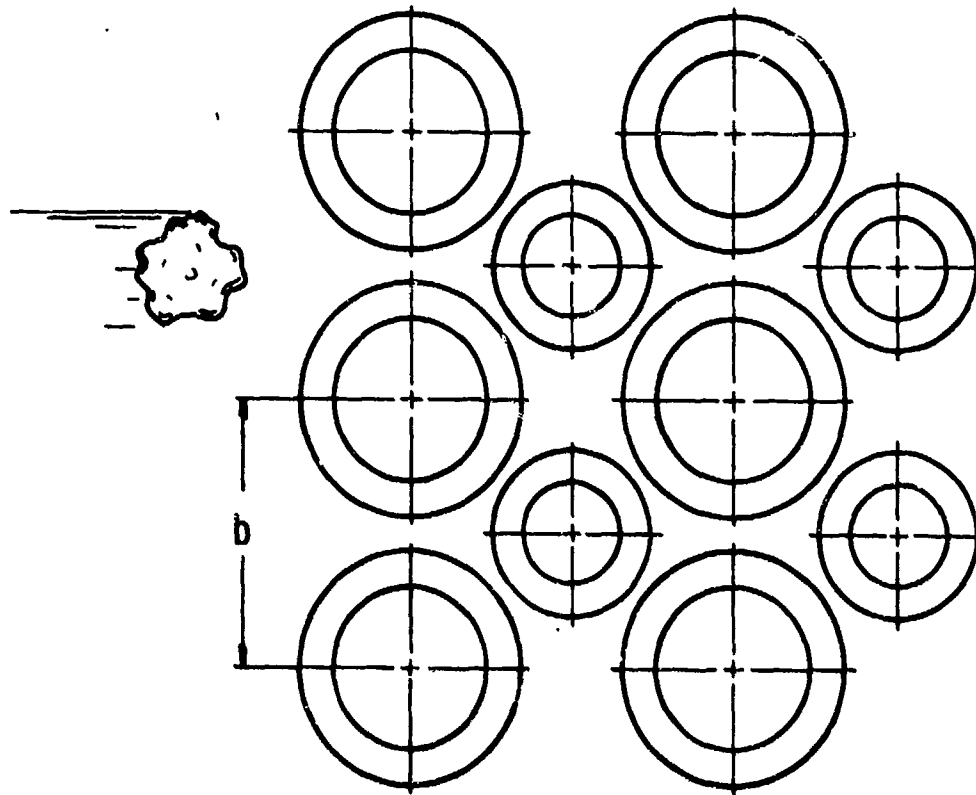
PRELIMINARY DESIGN OF QUARTER-SCALE FRAME

This section discusses the design of the frame for the quarter-scale model which is to be tested in the Blast Hazards Evaluation Phase of the development program. The frame was designed in quarter scale for the loads which the quarter-scale model will experience. It could just as easily have been designed in full scale and geometrically reduced to model size except that, in quarter scale, stock structural members can be more readily selected to aid in fabrication. Most, if not all, full-scale members must be full-up members.



	<u>Full Scale</u>	<u>1/4 - Scale</u>
Plates	11/16 in	11/64 \approx 3/16 in
Holes	3/4 in Diameter	3/16 in Diameter
Hole Spacing	2.90 in	0.725 in

Figure 3. Panel Concept 3



	<u>Full Scale</u>	<u>1/4 - Scale</u>
Large Tubes	5 in OD, 3.5 in ID	1.25 in OD, 0.875 in ID
Small Tubes	3.5 in OD, 2.25 ID	0.875 in OD, 0.56 in ID
Spacing	$b = 5.6$ in	$b = 1.4$ in

Figure 4. Panel Concept 4

According to Hopkinson's scaling, for scaled charge weights (3125 lb full scale and 50 lb quarter scale) quasi-static and dynamic pressures on the inside of the model will be identical to those of the full-scale structure. However, as pointed out earlier, time scales by the ratio of geometric lengths and is thus reduced by a factor of four in quarter scale. Hence, pressure loads on the design of the quarter-scale frame will be the same as those used for the design of the panels (designed in full scale), and the impulse will be reduced to one-fourth of the full-scale value. Summarizing, the loads are:

- Maximum quasi-static pressure: $P_{qs} = 165$ psi
- Maximum reflected pressure from the blast wave:
 $P_r = 4057$ psi
- Maximum reflected specific impulse: $i_r = 0.6$ psi-sec

In the design of the frame, the following assumptions and guidelines were adhered to:

- Although attenuation of the load on the frame due to the panel response is possible for the dynamic loading, such effects were neglected. For the quasi-static loading, which has a very long duration relative to the response time of the panels or frame, such attenuation is not probable.
- The maximum allowable deflection of the side members was set as $0.15 L$ (15% of the member's length).
- A maximum strain in the material of 10% was allowed for dynamic loading.
- A maximum allowable tensile or compressive stress of 45,000 psi was set for the quasi-static loading. This is approximately midway between the minimum yield and minimum ultimate tensile properties of the material and will probably result in some deformation of the structure and strain hardening in order to develop this strength.
- Strain rate effects on the material strength were ignored since quasi-static loads governed the design.

The configuration developed for the frames is shown in Figure 5. Intersecting box beams form the roof and floor of the structure, and vertical members with no cross supports form the four sides. Box beams were chosen for the main structural elements in the frame for several reasons:

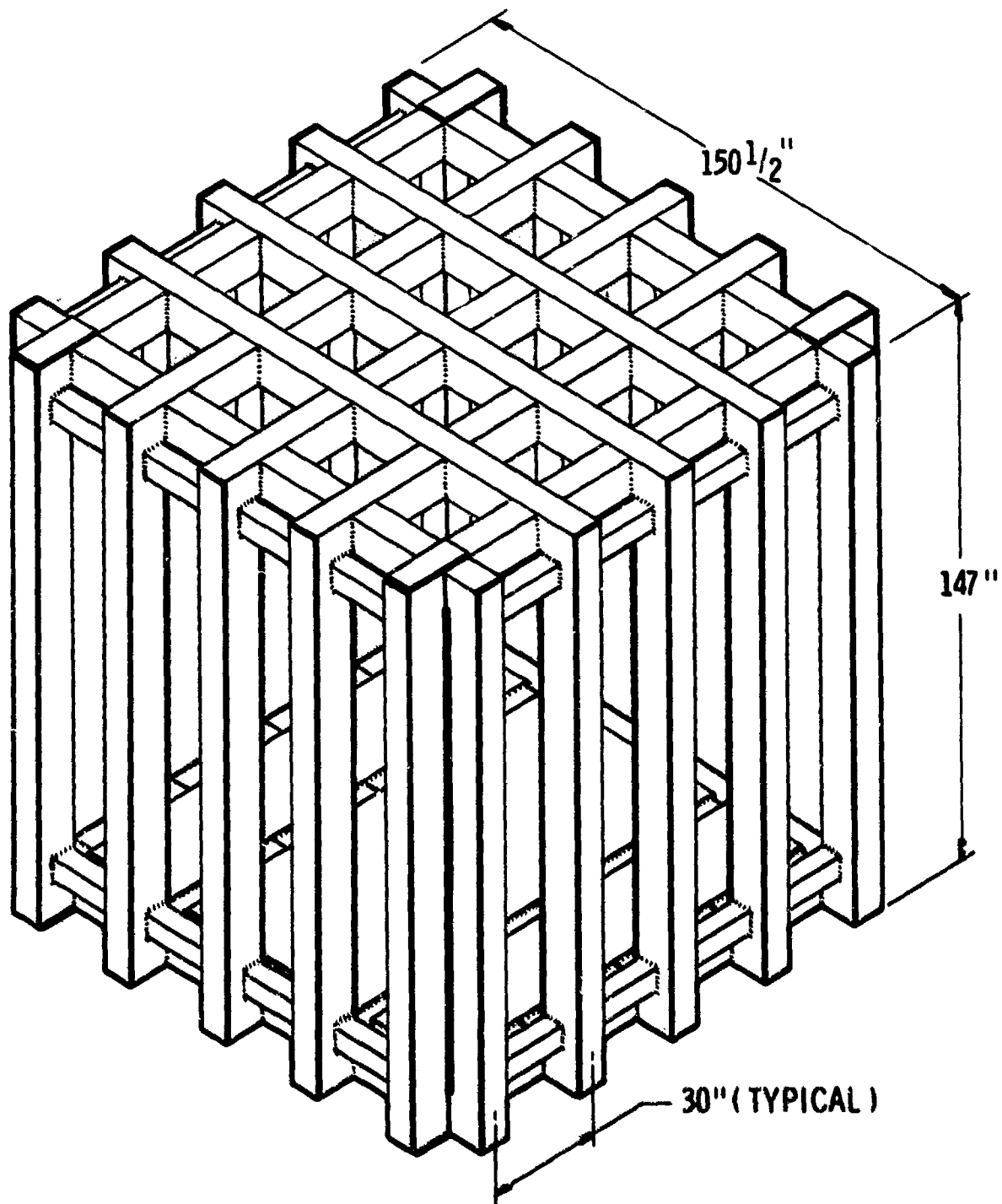


Figure 5. Jarter - Scale Frame

- (1) The members are compact, which is essential for both dynamic and plastic deformations.
- (2) The experience with members of similar proportions in Reference 2 showed good resistance to local buckling under high plastic deformations.
- (3) The section has a high shear strength to bending strength ratio.
- (4) Good support is provided for the panels by box beams because the panel loads are transferred directly through the webs of the box rather than through flanges as would be the case for wide-flange beams.

Preliminary sizing of frame members was made using equations developed by Westine and Baker⁽⁹⁾ or derived following the same procedures but using different deformed mode shape assumptions. A more detailed analysis of the elastic-plastic deformations in the frame will also be made using a finite element computer program. The equations used for preliminary sizing of the frame are summarized below:

Clamped Beam

Deformed shape and strain equation:

$$w = \frac{16 w_0}{L^4} \left[x^2 - \left(\frac{L}{2} \right)^2 \right]^2 \quad (6)$$

$$\epsilon_{\max} = \frac{32 c}{L} \left(\frac{w_0}{L} \right) \quad \text{at ends} \quad (7)$$

Elastic behavior - impulsive load:

$$M_{\max} = 2.236 \frac{i b}{r} \sqrt{\frac{EI}{\rho A}} \quad \text{at ends} \quad (8)$$

$$V_{\max} = \frac{13.417 i b}{L} \sqrt{\frac{EI}{\rho A}} \quad \text{at ends} \quad (9)$$

Plastic behavior - impulsive load:

$$\frac{i_r^2 b^2 L}{M_p \rho A_{\text{eff}}} = 24.64 \left(\frac{w_o}{L} \right) \quad (10)$$

Plastic behavior - quasi-static load:

$$\frac{P_{qs} b L^2}{M_p} = 23.09 \quad (11)$$

Simply-Supported Beam

Deformed shape and strain equation:

$$w = w_o \cos \left(\frac{\pi x}{L} \right) \quad (12)$$

$$\epsilon_{\text{max}} = \frac{\pi^2 c}{L} \left(\frac{w_o}{L} \right) \quad \text{at center} \quad (13)$$

Elastic behavior - impulse load:

$$M_{\text{max}} = i_r b \sqrt{\frac{2EI}{\rho A}} \quad (14)$$

$$V_{\text{max}} = \frac{\pi i_r b}{L} \sqrt{\frac{8EI}{\rho A}} \quad (15)$$

Plastic behavior - impulsive load:

$$\frac{i_r^2 b^2 L}{M_p \rho A_{\text{eff}}} = 12.566 \left(\frac{w_o}{L} \right) \quad (16)$$

Plastic behavior - quasi-static load:

$$\frac{P_{qs} b L^2}{M_p} = 9.87 \quad (17)$$

where:

- c = distance to external fibers
- w = lateral deflection in the beam at any point x
- w_0 = maximum center deflection
- L = beam length
- ϵ_{\max} = maximum strain
- M_{\max} = maximum moment under impulsive loading for elastic behavior
- V_{\max} = maximum shear under impulsive loading for elastic behavior
- M_p = fully plastic moment in the beam
- A = beam cross-sectional area
- EI = beam bending rigidity
- b = loaded width (approximately equal to the panel width)
- ρ = material density
- A_{eff} = area of beam plus an effective area of the panel to account for both panel and beam masses for dynamic response calculations.

Loading terms of pressure and impulse have been defined previously. To apply the equations for impulsive loading, w/L is computed from Eqs. (7) or (13) for a maximum strain of 10% (w_0/L is limited to 0.15, maximum). The required plastic moment, M_p , and effective area, A_{eff} , are then determined from Eqs. (10) or (16). For quasi-static loading M_p is determined from the force balance in Eqs. (11) or (17).

Because the members in the frame are neither fully clamped nor simply supported, calculations were performed for both conditions, and judgment was applied to select a member which fit somewhere in between the two extremes. Requirements for the frame members can be determined from Eqs. (10) and (11) for clamped beams and from Eqs. (16) and (17) for simply supported beams. These requirements are expressed in terms of the plastic moment for the quasi-static loading, and in terms of the product

of the plastic moment and the cross-sectional area for the dynamic loading. In addition, the quasi-static shearing load at the ends of the members is simply the product of the quasi-static pressure and the total panel area which the member must support. Using the geometry of Figure 5, these requirements for the vertical members in the sides of the structure are:

Clamped Beam

Quasi-static load: $M_p = 3.91 \times 10^6 \text{ lb-in}$

$V = 297,000 \text{ lb}$

Impulsive loading: $M_p A = 11.4 \times 10^6 \text{ lb-in}^3$

Simply-Supported Beam

Quasi-static loading: $M_p = 9.14 \times 10^6 \text{ lb-in}$

$V = 297,000 \text{ lb}$

Impulsive loading: $M_p A = 22.4 \times 10^6 \text{ lb-in}^3$

An 8 x 10-in. box beam with a 1/2-in. wall and a 1/2-in. reinforcing plate across each 8-in. dimension (see Figure 6) was chosen as the best structural component to satisfy the above requirements. For a maximum allowable tensile stress of 45,000 psi and a maximum shearing stress of 30,000 psi, * the beam develops the following properties:

$$M_p = 4.51 \times 10^6 \text{ lb-in}$$

$$V = 330,000 \text{ lb}$$

$$M_p A = 107.8 \times 10^6 \text{ lb-in}^3$$

The requirement for the impulsive load, expressed as $M_p A$, is adequately satisfied for both clamped and simply supported conditions. Also, the quasi-static shearing load of the beam ends is satisfied where V has been computed on the basis of uniform shear in the 10-in. webs (sides) of the beam with a small portion of the 8-in. section assumed to be effective in shear as well. Note that the plastic moment required for the quasi-static loading falls somewhere in between that required for clamped and simply supported beams. Even though the members in the roof have less bending rigidity than the side beams (as will be explained shortly, the 8 x 10-in. box beams without the reinforcing plates were used in the roof and floor), the end condition is more nearly clamped than simply supported, and, for

* This stress is slightly less than the minimum ultimate shearing stress (34,400 psi) computed as 60% of the minimum tensile strength of the material.

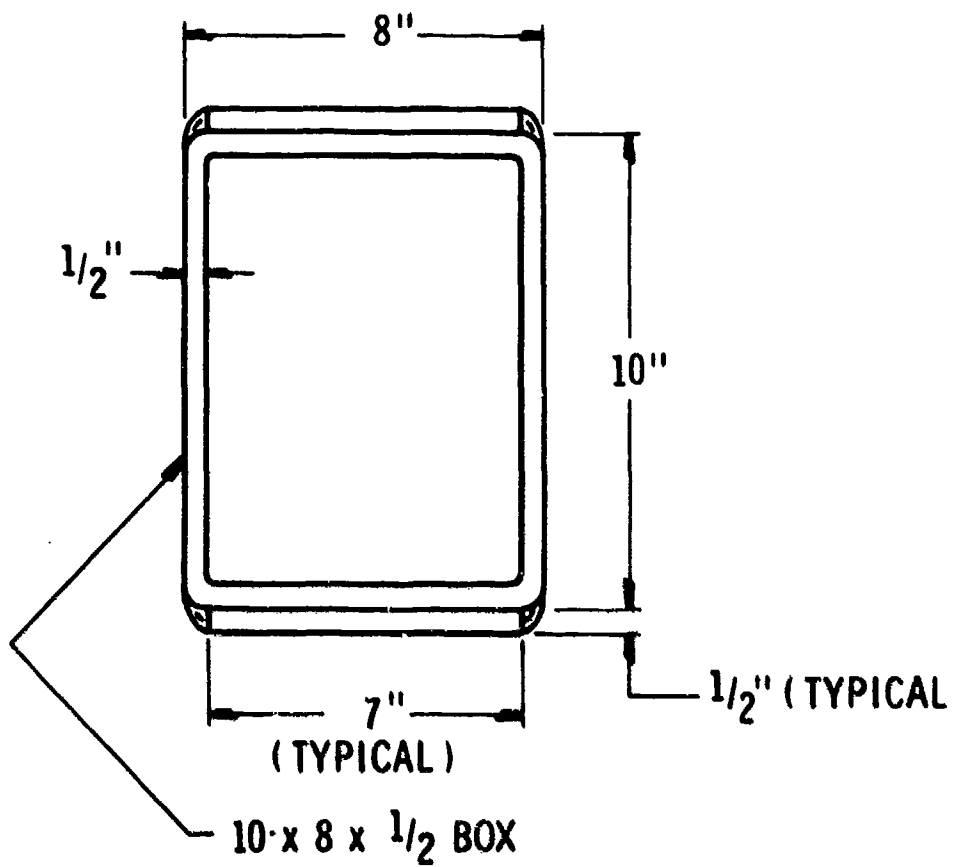


Figure 6. Cross-Section of Frame Vertical Members

the preliminary selection, the plastic moment developed by the reinforced box beam was judged to be adequate. Tensile stresses in the side members were also checked and found to be small (approximately 8,000 psi). Because of the uncertainty in the end conditions for the beam, which can have a significant effect on the stresses, the effect of the axial load was not considered in the preliminary selection of the beam properties. It will, of course, be included in the more exact analysis.

The shearing stress in the beam under the impulsive loading has not yet been addressed. It was computed on the basis of the maximum curvature corresponding to the deflection which first produces an equivalent fully plastic bending moment in the beam. This curvature is set by the assumed deflection shape. Deep beams with high bending stiffness were eliminated by this criterion, but it was not a factor for the compact box section chosen. Equations (8), (9), (14) and (15) were used for these calculations.

The roof members were sized based on an elastic distribution of stresses in the grid of intersecting beams. From this we estimated that the bending strength of the members in the grid should be approximately 60% of that for the side members. This happens to be very close to the strength of the 8 x 10-in. box member without reinforcing plates, and these members were chosen for the roof and floor. The non-vented floor is closed by a solid plate of 0.375-in. thickness designed to resist the loads in membrane action in the same manner as for the vented panels.

The frame attachments for the membrane plate panels are such that the inplane loads are transferred continuously through the panels to the corner members of the frame. Details of the panel-to-panel and panel-to-corner attachments are shown in Figure 7.

CLOSURE

In this paper, we have presented in the status of the design of a suppressive structure which will first be tested in quarter-scale as part of a program to build and test a prototype Category I suppressive shield. This current quarter-scale frame design will be scrutinized further before it is finalized and tested. The work that is in progress towards this end is

- (1) Possible panel redesign to fit the panels between the frame members. The panels were initially designed for other earlier frame concepts, and it is possible that modifications can be made to reduce panel size and simplify field installation.
- (2) Along this same line, the frame may be slightly modified to simplify fabrication of the roof and floor. Figure 8 shows a variation of the frame in which the beams in the roof and floor would overlap instead of intersect.

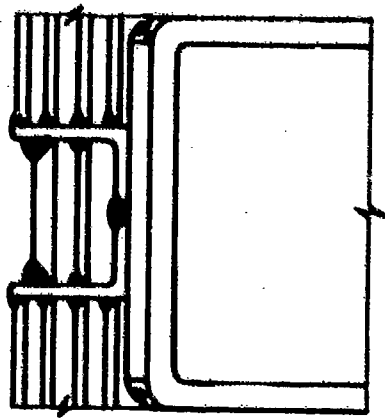
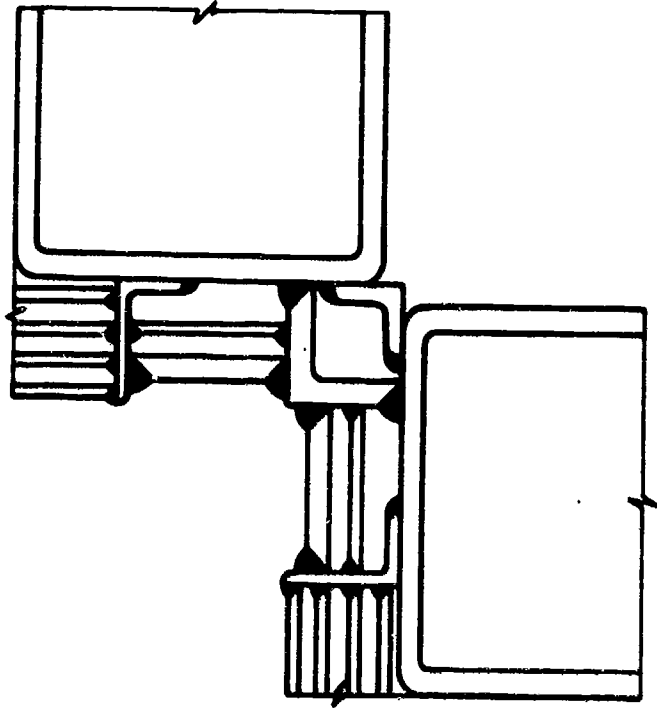


Figure 7. Typical Panel Installation

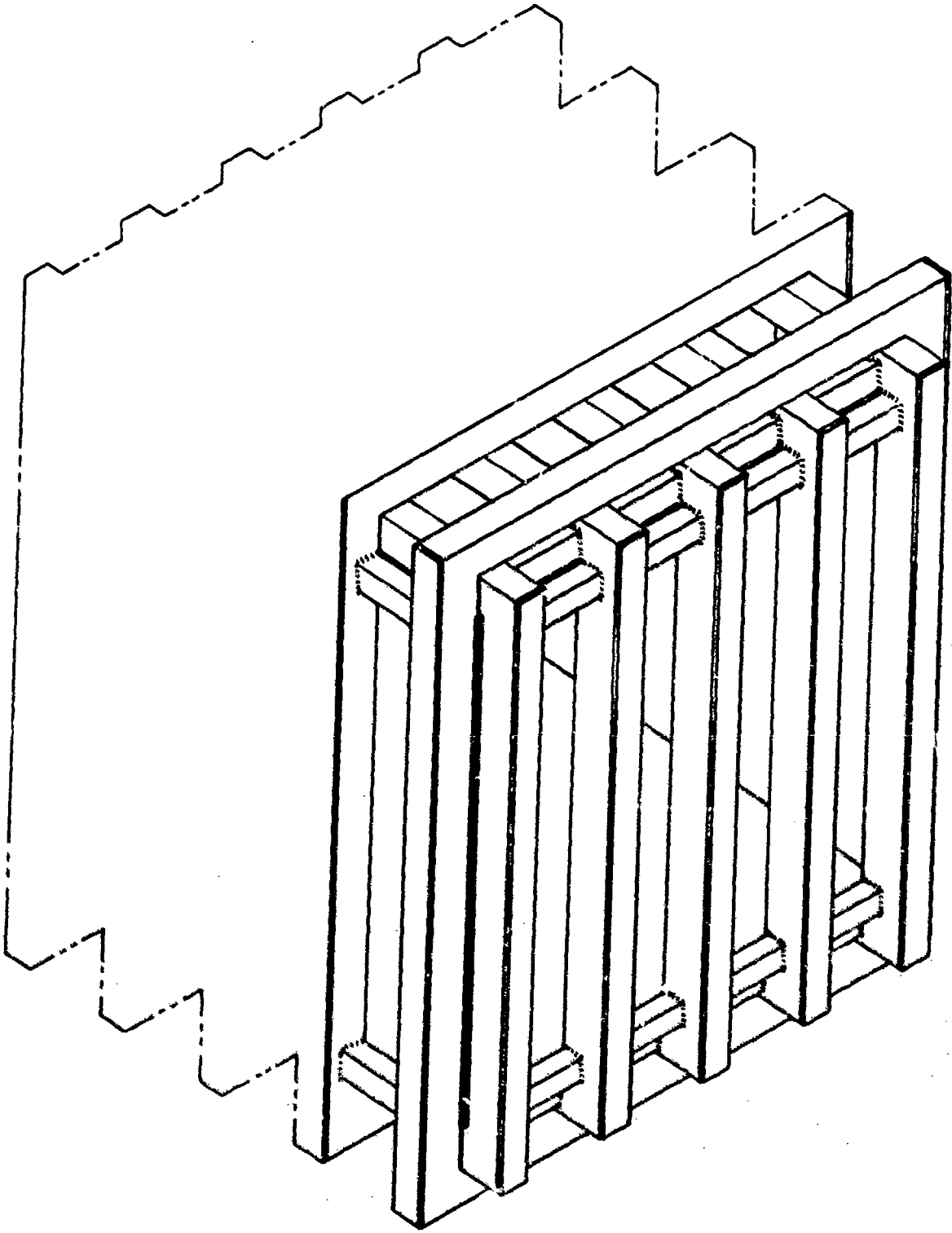


Figure 8. Modified Quarter Scale Frame

- (3) Additional analyses will be performed on the frame as soon as design modifications are finalized. Deformations and stresses will be computed for the governing quasi-static loading at maximum charge weight. This will be a static analysis including large deflections and plastic strains. Elastic-plastic dynamic response for the impulsive loading will perhaps be determined also.

The panel and frame designs presented are just one phase in the development of the prototype structure. By conducting properly instrumented tests with the quarter-scale model we hope to improve the design of the prototype. Also, a long range Applied Technology Program being conducted by the Edgewood Arsenal should help fill in gaps in our knowledge concerning the fragment and blast threats, venting characteristics, inter-panel pressures, etc., so that future suppressive structures can in fact be routinely designed and applied to explosive processing operations

REFERENCES

1. Report EA1002, "Study of Suppressive Structures Applications to an 81 mm Automated Assembly Facility," prepared for Manufacturing Technology Directorate, Chemical and Plants Division, Edgewood Arsenal, 16 April 1973.
2. Report EA-4E33, "81 mm Suppressive Shielding Technical Data Package," January 1974.
3. Report EA-FR-2B02, "Final Report Application of Suppressive Structure Concepts to Chemical Agent Munition Demilitarization System (CAMDS)," July 27, 1973.
4. J. Coutinho, N. Hags and J. Liu, "Current State of Design Procedures for Suppressive Structures," AMSAA Interim Note No. R-29, Aberdeen Proving Ground, Maryland, May 1974.
5. W. E. Baker and P. S. Westine, "Methods of Predicting Load and Blast Field Outside Suppressive Structures", DoD 16th Annual Explosives Safety Seminar, September 1974.
6. B. Bertrand, C. Brown, D. J. Dunn, et al., "Suppressive Structures--A Quick Look," BRL Interim Memorandum Report No. 190, Aberdeen Proving Ground, Maryland, February 1974.
7. H. J. Goodman, "Compiled Free-Air Blast Data on Bare Spherical Pentolite," BRL Report No. 1092, Aberdeen Proving Ground, Maryland, February 1960.
8. W. E. Baker, P. S. Westine, P. A. Cox and E. D. Esparza, "Analysis and Preliminary Design of a Suppressive Structure for a Melt Loading Operation," Technical Report No. 1, Contract No. DAAD05-74-C-0751, Southwest Research Institute, San Antonio, Texas, March 1974.
9. P. S. Westine and W. E. Baker, "Energy Solutions for Predicting Deformations in Blast Loaded Structures", DoD 16th Annual Explosives Safety Seminar, September 1974.

STRUCTURAL ANALYSIS OF CONTAINMENT STRUCTURES

Norris J. Huffington, Jr.
Struan R. Robertson

U.S. Army Ballistic Research Laboratories
Aberdeen Proving Ground, Maryland

ABSTRACT

As part of a study of the suppressive structure concept, analyses of the large deflection, elastoplastic response of two configurations (a hemispherical shell and a cylindrical shell with closed ends) subjected to internal blast were performed. These blast and fragment containment structures may be regarded as limiting cases of suppressive structures and the results obtained are believed to constitute useful baseline data for evaluating efficiency of suppressive structure designs. Suggestions regarding more practical containment/suppressive structural configurations are included.

INTRODUCTION

The concept of a suppressive structure entails the use of multi-component panels which are supported by a relatively rigid bent-type framework. The complete structure, consisting of framework plus panels, is fabricated from commercial low carbon steel and forms an enclosure surrounding the region where an accidental explosion may occur. The panels consist of arrays of bar elements (angles, zees, etc.), perforated plates, and louvred plates at various spacings. These panels are intended to provide total containment of fragments and to permit a restricted venting of the contained blast, resulting in a significant decrease in external overpressures over what would be realized if no suppressive structure were present. For an optimum design the entire structure would experience limited elastoplastic deformation, thus providing a sink for the released explosive energy.

Complete analytical modeling of the response of such a complex structure would be extremely tedious and costly. However, such structures have been produced through a combination of approximate analytical procedures and proof testing. In response to a request for more rigorous dynamics analysis it was decided to begin with an idealized configuration which would be amenable to analysis by an existing large deflection elastoplastic structural shell response computer program, PETROS 3 (Ref. 1). This analytical tool would be employed to design an efficient closed (total containment) shell structure which would have the same protective capacity as an existing suppressive structure which was developed for application to an 81 mm mortar round automated

assembly facility (Ref. 2). This suppressive structure is a welded steel framework 20 feet long by 15 feet wide by 13 feet high having 4 feet by 12 feet wall panels and 4 feet square ceiling panels, the total weight being 51000 pounds. The comparison between the total containment and suppressive structural designs should be meaningful because the suppressive structure, while not necessarily optimized, was certainly not grossly overdesigned (a fragment nearly perforated an outer louvred panel and the whole structure experienced appreciable permanent deformation).

ANALYSIS OF TOTAL CONTAINMENT STRUCTURE

Hemispherical Configuration

To achieve nearly homogeneous elastoplastic straining a hemispherical configuration was selected, this to be bolted down to a horizontal rigid foundation as shown in Figure 1. As was the case for the suppressive structure of Ref. 2, this configuration must survive the simultaneous detonation of two 81 mm mortar rounds. For simplicity in the analysis, these rounds were located at a central point on the foundation so that the blast loading is spherically symmetric. The mathematical problem may now be posed as follows: For a shell thickness h determined by the requirement for fragment containment*, how small can the midsurface radius R of the hemisphere be made without causing structural failure due to blast loading?

In order to solve this problem it was necessary to formulate the pressure pulse as a function of the radius R . Data for this formulation are presented in Ref. 3. For a selected value of R the pressure experienced by the target is represented in the following manner. At the arrival of the blast wave there is a jump to the peak reflected pressure, followed by an exponential decay which is terminated when the thermodynamic equilibrium pressure is reached corresponding to the release of detonation energy and explosion products in a constant volume process. Subsequent to this the pressure is taken to remain constant at the equilibrium pressure. This loading pulse is illustrated in Figure 2 for the case $R=5$ feet.

The material was taken to be 1020 steel, which was represented in the analysis as a strain hardening material with stress-strain properties modeled by the succession of linear segments shown in Figure 3. Strain-rate effects were neglected, which should be conservative.

*For this case, $h=1$ inch of steel is sufficient, as discussed in Ref. 3.

The foregoing numerical quantities which have been discussed are the only physical data input required for the PETROS 3 code (Ref. 1), which treats the transient response of shells by obtaining a finite difference solution of the nonlinear partial differential equations of motion. Since the loading and response are axisymmetric it is only necessary to use two meridional rows of mesh points. Owing to the highly nonlinear character of this transient response problem it is necessary to determine the minimum value for R by trial. When calculations were performed for R=10 feet the response was found to be entirely negligible. Results for R=5 feet are shown in the figures which follow. Figure 4 shows the transient rectangular components of displacement in a meridional plane at point A which is at 45° from the vertical axis of the hemisphere. From this it may be determined that the maximum displacement is only 0.036 inches, essentially radially outward. Displacements at other locations are correspondingly small. A typical transient strain response is shown in Figure 5, this prediction being for the circumferential and meridional components of strain on the inner surface of the shell at point A. These strains are seen to be small, as was the case for all mesh locations (maximum calculated value was 0.0018). The suspicion that the stresses for this case barely exceeded the yield stress is confirmed by the energy balance diagram of Figure 6. This diagram, part of the graphical output provided by the BRL version of the PETROS 3 code, shows the temporal variation of total energy and work quantities for the hemispherical shell. There is a gradual increase in the amount of (irreversible) plastic work but this will be bounded as the shell "shakes down" to purely elastic oscillations.

From the above it may be inferred that the radius R of the hemisphere could be made considerably less than 5 feet before danger of rupture would arise. However, to be conservative and because the size of the containment structure is already inconveniently small for necessary machinery and service personnel further reductions in R were not pursued. Rather, the total weight of the containment structure for R=5 feet was determined to be approximately 7000 pounds, or about 14% of the weight of the corresponding suppressive structure of Ref. 2. Since the cost of monocoque construction employed for the total containment structure should be considerably less than the cost of fabricating the panel arrays used in the suppressive structure, a comparison on a cost basis should be even more favorable to the containment structure.

Hemicylindrical Configuration

Although the previously considered hemispherical configuration has advantages with respect to optimal stressing of the material it clearly has drawbacks regarding access and the shape of the interior volume afforded. Consequently, consideration was given to analysis of the response of a compromise configuration: specifically, a hemicylinder with closed ends, one-quarter of which is illustrated in Figure 7.

While certainly not as efficient from a structural viewpoint*, it is regarded as a closer approximation to a configuration which could be employed for an assembly line operation.

This response problem was also treated using the PETROS 3 code for the case $h=1$ inch, $R=5$ feet and a cylinder length L of 10 feet. The weight of this structure would be approximately 10500 pounds. The same charge, two 81 mm mortar rounds, was assumed to be detonated on the axis of the cylinder midway between the ends. The peak reflected pressure on the cylinder at $z=L/2$ and on the end plates on the cylinder axis is 1000 psi as for the hemisphere. At other locations the peak pressure is less due to spherical divergence of the blast wave and oblique reflection. Empirical data on this pressure were fitted by a quadratic approximation in the response calculations. The pressure at each location was then assumed to decay exponentially until the equilibrium pressure (100 psi) is reached, which is less than for the hemisphere due to the greater internal volume.

The deflections at B and C (Figure 7) are the greatest for the end plate and the hemicylinder, respectively. At both locations the maximum deflections exceed those for the hemisphere, which is in agreement with expectations since the deformation of the hemicylinder is highly inhomogeneous. While strains at certain points are greater than for the hemisphere, the structure should still be able to contain the explosion.

COMMENTS AND RECOMMENDATIONS

While the containment structural configurations discussed in the foregoing may appear too idealized for practical application, it was possible to perform more complete and rigorous response analyses for these configurations than is possible at present for the more complex suppressive structure. Also, the containment structures may be viewed as limiting cases of suppressive structures having zero venting and with the multilayered panels fused into a single monocoque shell. On this basis it may be useful to define a structural efficiency for protective structures using an optimal containment structure as the baseline. For fabrication procedures and materials having about the same cost per unit weight one may define:

$$\text{Structural Efficiency} = \frac{\text{weight of optimal containment structure}}{\text{weight of equivalent capacity structure being evaluated}} \times 100$$

* It would certainly be possible to design a more structurally efficient end closure than a flat plate but other considerations relating to the intended application may indicate a preference for a vertical wall.

For example, for the structures which were considered for protection against accidental detonation of two 81 mm mortar rounds (using the hemispherical configuration as a baseline), the efficiency of the hemicylinder with end plates would be 67% while that of the suppressive structure of Ref. 2 would be 14%. While the latter factor may seem very low, it is typical of many engineering calculations that practical considerations prevent the achievement of high efficiencies. Rather, it was felt that the establishment of a criterion for efficiency might permit a useful comparison of two or more suppressive structural designs.

An examination of the characteristics of the near-optimal hemispherical structure permits the identification of factors which contribute to efficiency of suppressive structures:

1. Shapes which promote the development of membrane restoring forces before large deformations occur are desirable. Flat plates supported at the edges which resist deformation principally by nonuniformly distributed bending stresses are inefficient.
2. Since structural weight of fragment sensitive structures varies approximately as the midsurface area, the structure should be made as small as the requirement of blast survivability permits. However, it is recognized that considerations of internal volume required for necessary machinery and for service personnel may dictate the use of a somewhat larger, less efficient structure.
3. While the use of vented spaced plates may be desirable from the viewpoint of blast and fragment suppression, in configurations where significant bending cannot be avoided (as in box-type structures) the use of multiple plates with no shear ties is less efficient than a single plate of the same total thickness.

In comparing suppressive structures with those designed for total containment it was believed that the ventilated structure might be somewhat lighter because it does not have to resist the full blast loading. Conversely, it was recognized that stress concentrations associated with openings in the ventilated structure would require added weight so that the net effect could not be determined a priori. However, the apparent greater weight of "equivalent" suppressive structures (aside from that part due to greater size) would indicate that either the stress concentration effect is dominant or designers have not been able to take advantage of the reduced blast loading due to uncertainty as to its extent. Further, it appears from examinations of calculations that structures which have been designed to survive the initial portion of a blast load such as depicted in Figure 2 can withstand the much lower equilibrium pressure indefinitely, thus obviating the need for rapid venting of the confined pressure.

The writers prefer to leave for future judgment any determination as to whether suppressive structures can be designed to be competitive with total containment structures from an engineering viewpoint. However, considerable research and methodology development in the areas of blast dissipation, structural component loading, and structural response of complex configurations will be required before rational design of suppressive structures can be performed with the same degree of confidence as presently exists for containment structures. Perhaps some combination of these concepts will eventually prove most satisfactory for practical applications. Figure 8 illustrates such a compromise which may be useful for an assembly line operation. Munitions on pallets are brought by conveyor belt to and away from a station where a hazardous operation is performed. This station is enclosed in a containment structure which has openings for the conveyor belt and pallets at each end. Suppressive panels to cover the openings required for pallets as well as deflectors to divert residual blast upwards would be raised and lowered hydraulically to permit passage of pallets. In the closed position the ends of the suppressive panel would be nested in wedge supports capable of resisting any loads produced by an accidental detonation. While probably not necessary, additional suppressive panels could be located in the upper portion of the cylindrical structure to provide additional upward directed venting.

REFERENCES

1. S. Atiuri, E. A. Witmer, J. W. Leech, and L. Marino, "PETROS 3: A Finite Difference Method and Program for the Calculation of Large Elastic-Plastic Dynamically-Induced Deformations of Multilayer Variable-Thickness Shells", BRL Contract Report No. 60, November 1971.
2. "Design, Fabrication and Test of a Suppressive Structure for Application to an 81 mm Mortar Round Automated Assembly Facility", Draft Report, Edgewood Arsenal Resident Office, National Aeronautics and Space Administration, Bay St. Louis, MS, 9 January 1974.
3. B. Bertrand, C. Brown, D. Dunn, N. Huffington, J. Kineke, C. Kingery, R. Meissner, A. Ricchiazzi, S. Robertson, and R. Vitali, "Suppressive Structures - A Quick Look", BRL Interim Memorandum Report No. 190, February 1974.

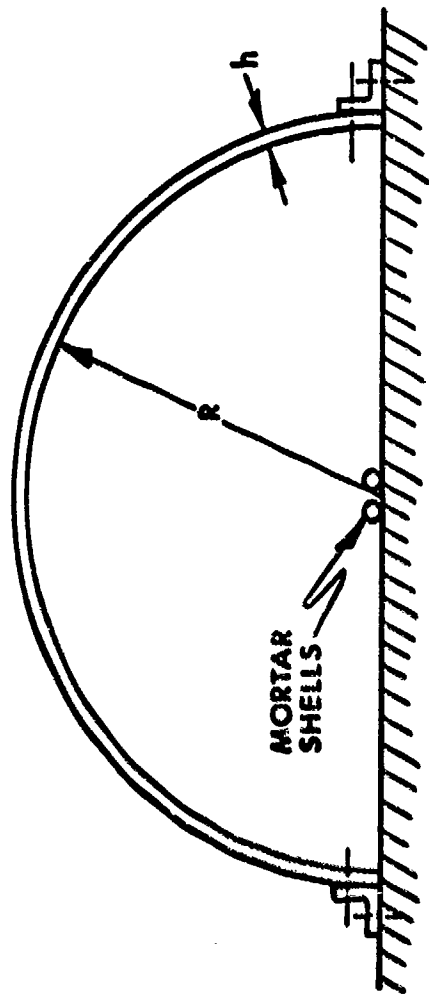


Figure 1. Section through Hemispherical Containment Structure

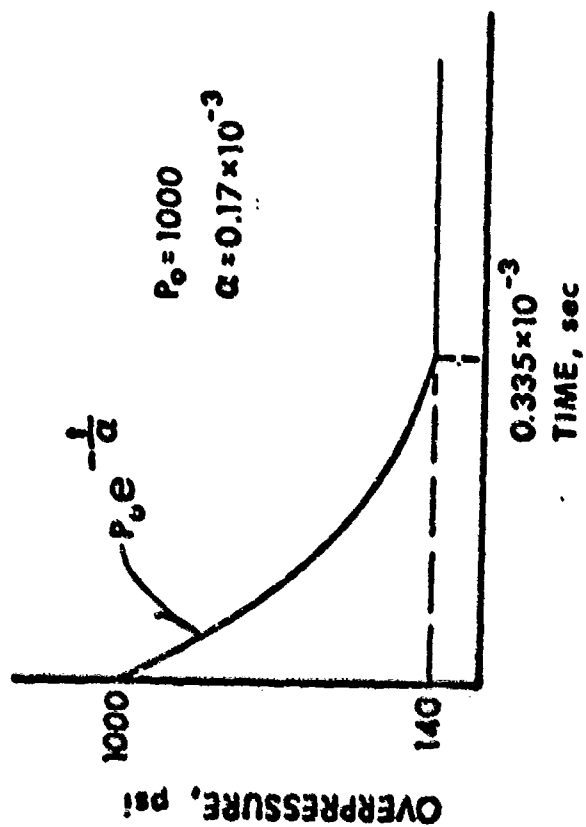


Figure 2. Blast Loading for R=5 Feet

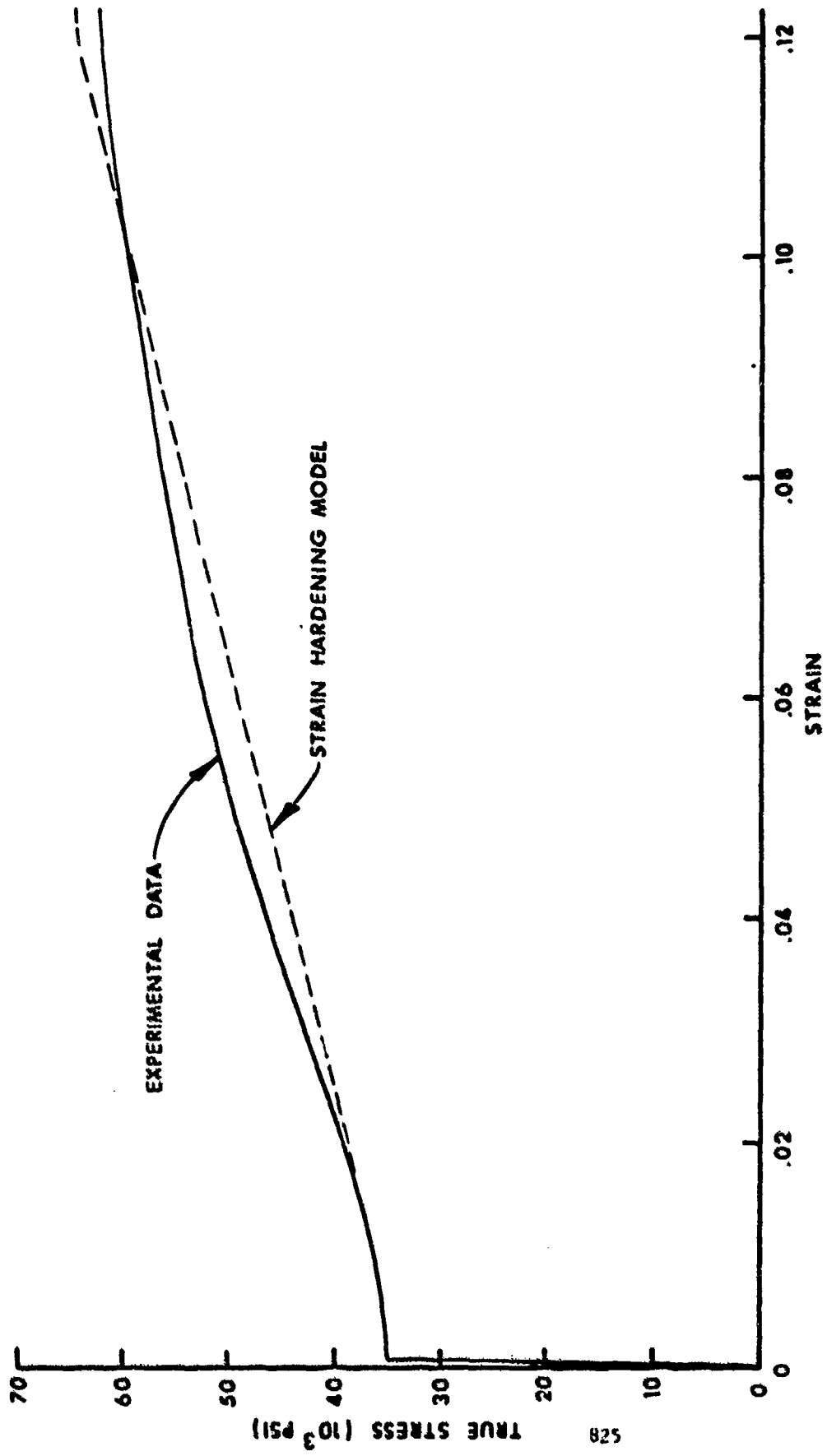


Figure 3. Stress-Strain Property Modeling

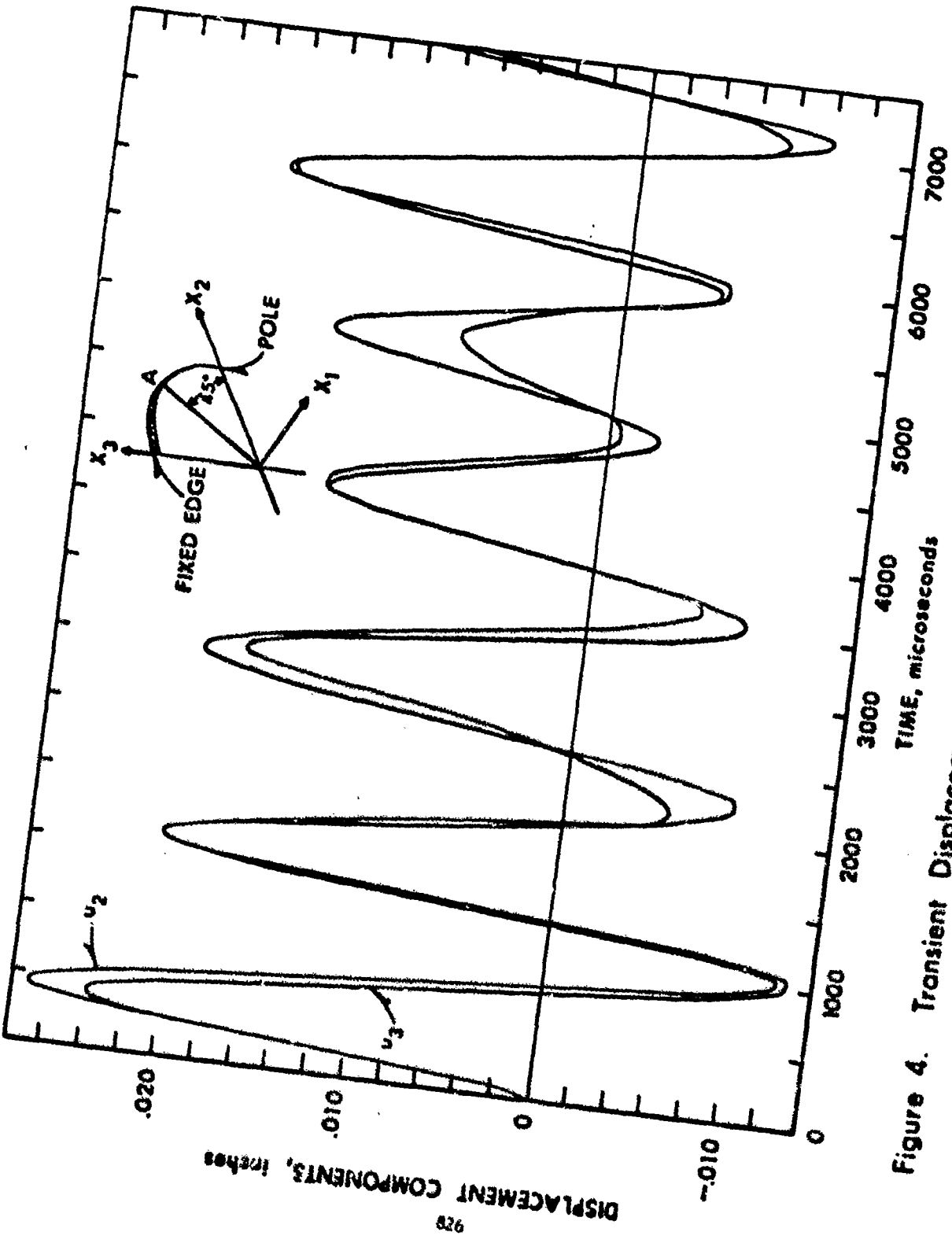


Figure 4. Transient Displacement Components at Point A, $R = 5$ Feet.

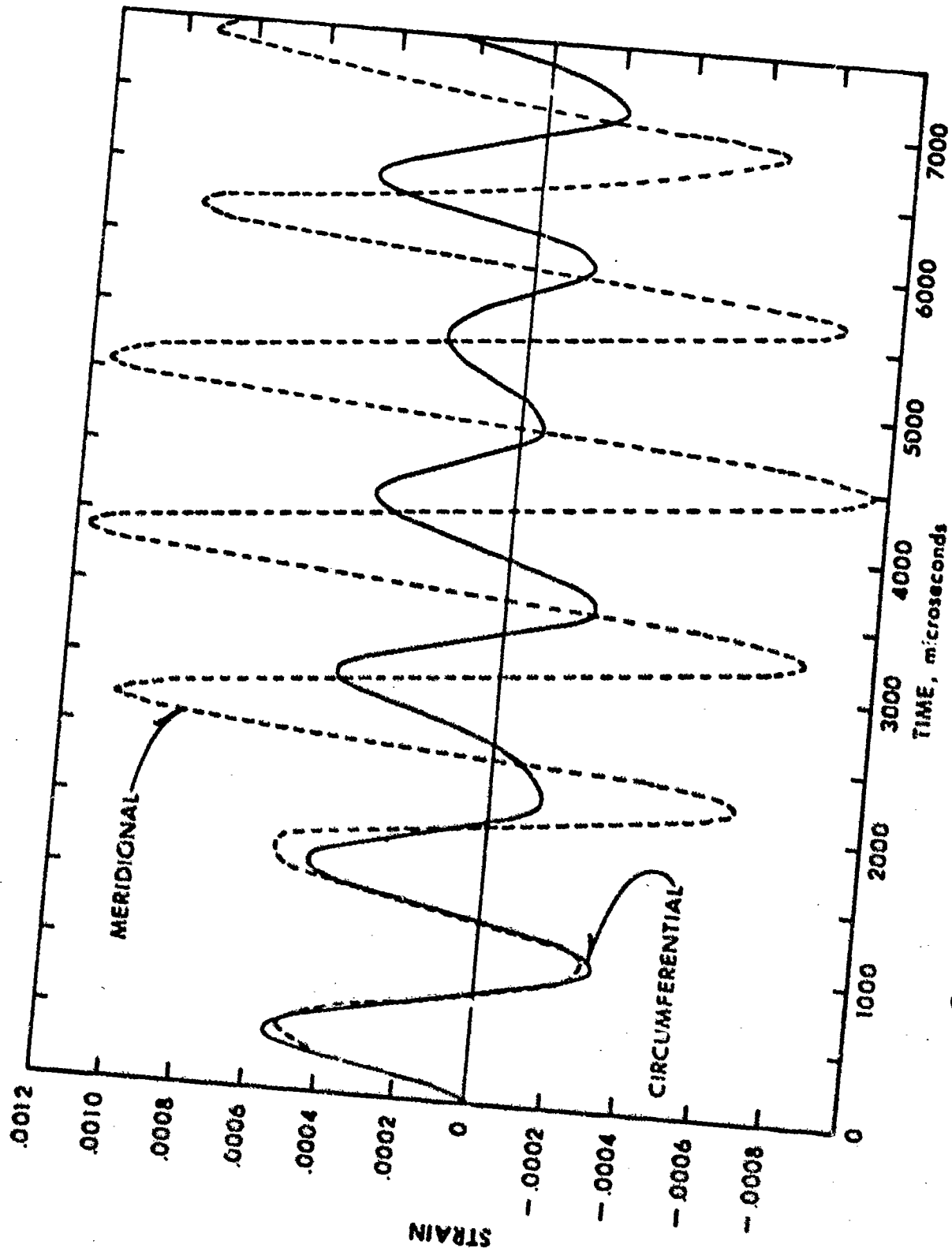


Figure 5. Inner Surface Strains at Point A, R=5 Feet

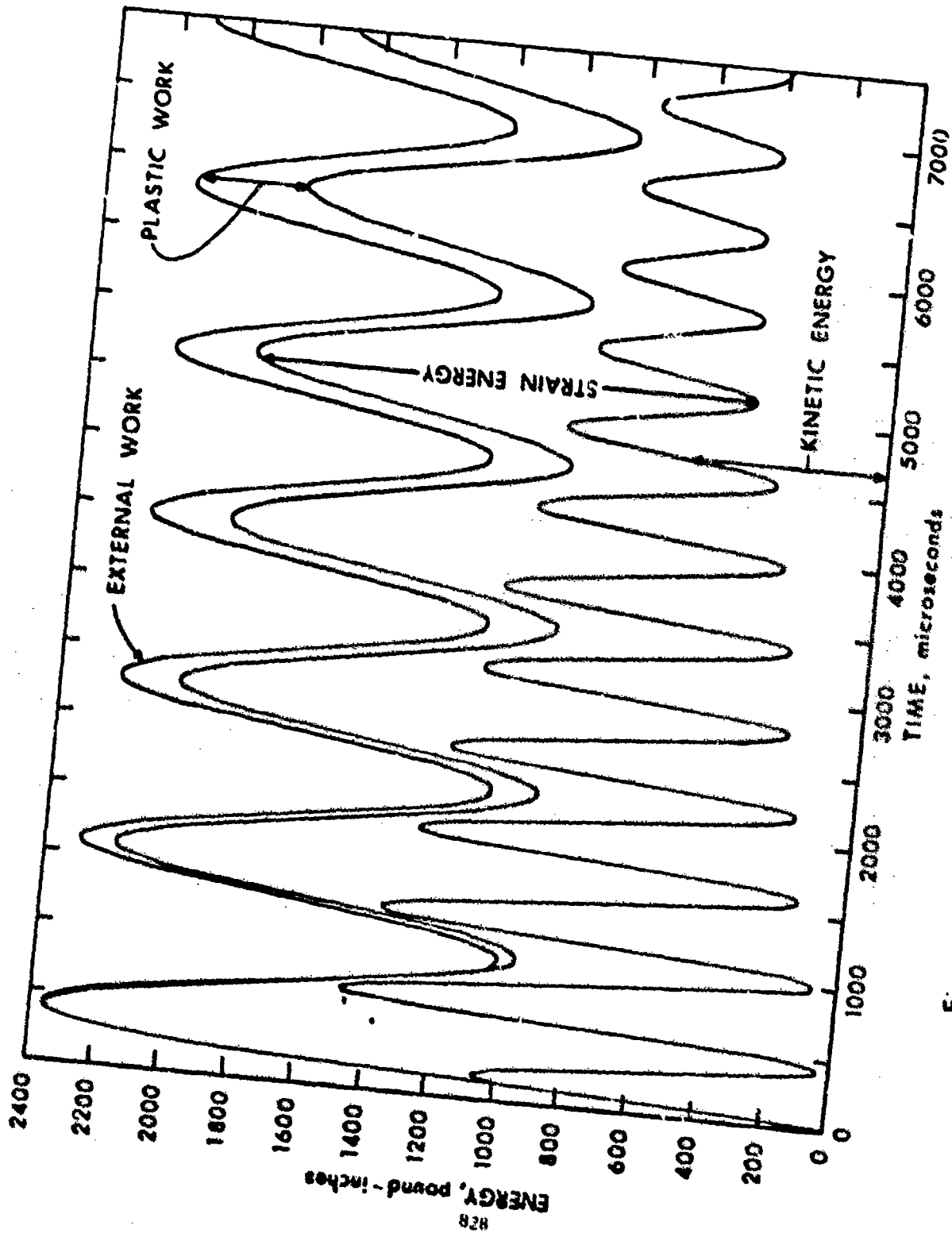


Figure 6. Energy Balance Diagram, R=5 Feet

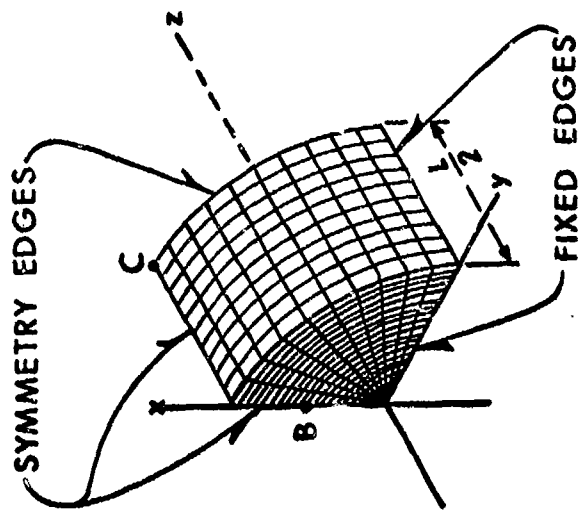


Figure 7. Hemicylinder Geometry, Including Finite Difference Grid

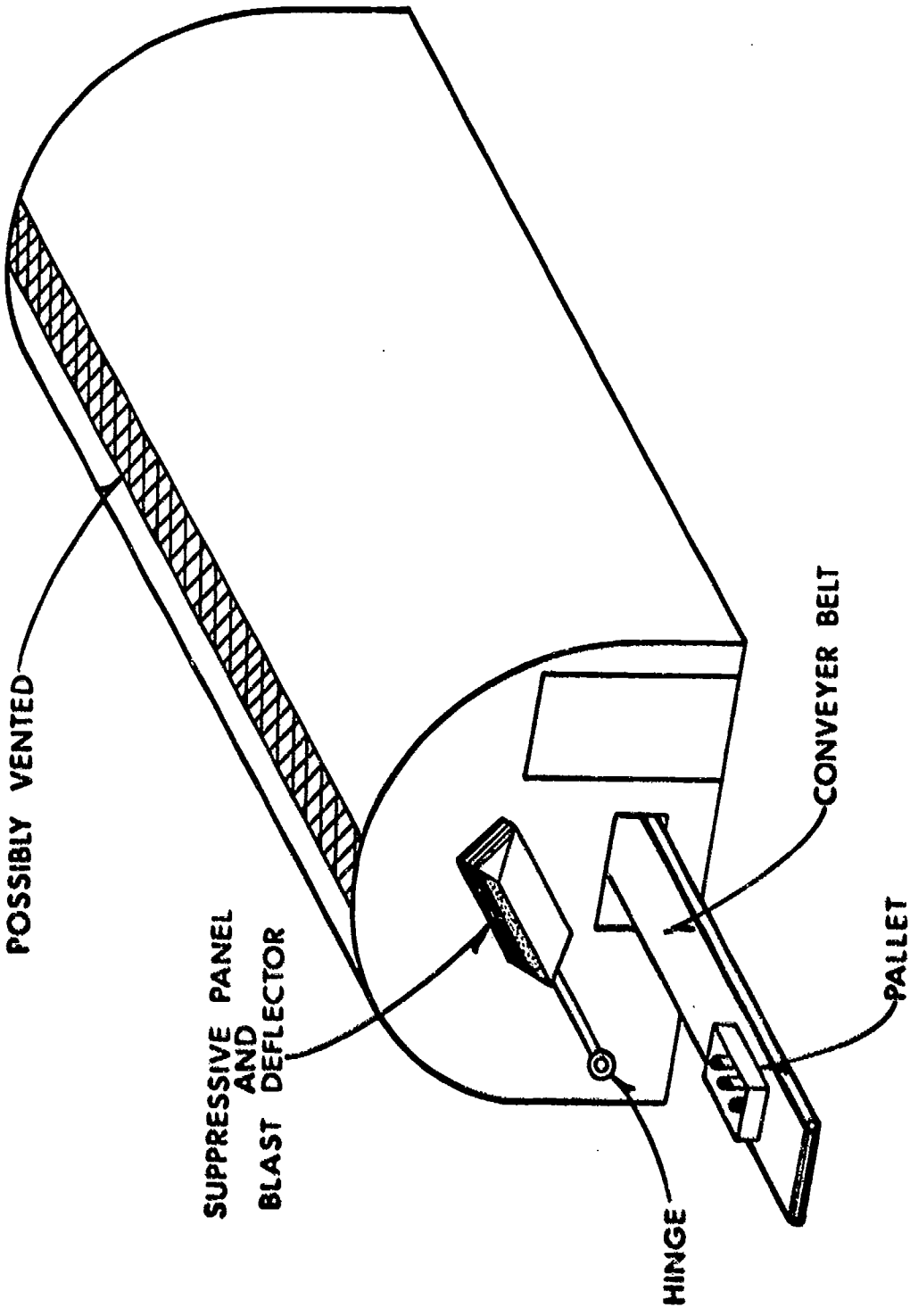


Figure 8. Protective Structure Concept for Assembly Line

METHODS OF PREDICTING LOADING AND BLAST FIELD OUTSIDE SUPPRESSIVE STRUCTURES*

by

W. E. Baker
P. S. Westine

Southwest Research Institute
San Antonio, Texas

ABSTRACT

Methods have been developed for predicting the blast loads, quasi-static pressure rise, and duration of the quasi-static pressure rise within a suppressive structure. In addition, the side-on overpressures outside a vented suppressive structure are estimated.

Before any prediction procedure could be developed, the effective vented area ratio ($\alpha_{eff} = A_{vent}/A$) for a multi-walled structure with various size vents in each wall had to be developed. This relationship was assumed, and then employed in a model analysis to develop pi terms for predicting loads and durations inside the structure as well as overpressures outside the structure. Finally, experimental test data taken from the literature were used to develop functional relationships. Whereas in the past, investigators have assumed that the influence of a vented suppressive structure was a reduction in effective charge weight, this solution shows that a more accurate concept is the creation of an effective standoff distance less than the free-field standoff distance at which blast pressures are the same for a given size energy release. This effective standoff distance is a function of the effective vented area ratio α_{eff} , the free-field standoff distance for a given overpressure, and the width of a suppressive cubical structure. Data from a variety of test structures show that the procedure predicts outside pressures to within one standard deviation of 18.6%.

For the vast majority of suppressive structures, the quasi-static pressure rise within the structure is independent of the vented areas. Test data indicate that provided $\frac{(\alpha_{eff} A)^{3/2}}{V}$ is less than 0.0775, the maximum internal quasi-static pressure is a function only of the charge weight divided

*Work performed under Contract DAAD05-74-C-0751 with Army Materiel Systems Analysis Agency, Aberdeen Proving Ground, Maryland.

by the volume because the maximum pressure is reached before significant venting occurs.

INTRODUCTION

The loading from an explosive charge detonated within a vented or unvented structure consists of two almost distinct phases. The first phase is that of reflected blast loading. It consists of the initial high pressure, short duration reflected wave, plus perhaps several later reflected pulses arriving at times closely approximated by twice the average time of arrival at the chamber walls. These later pulses are attenuated in amplitude because of irreversible thermodynamic process, and they may be very complex in waveform because of the complexity of the reflection process within the structure, whether vented or unvented. If the structure has solid walls, the blast loading can be estimated by using sources of compiled blast data for normally reflected blast pressures and impulses such as Refs. 1 and 2, and the well-known Hopkinson's blast scaling law (see Chapter 3 of Ref. 3). The effect of vented panels in the suppressive structures on reduction of the reflected blast loading can be very complex, and will not be addressed in detail in this paper.

As the blast waves reflect and re-reflect within the structure and as unburned detonation products combine with the available oxygen,* a quasi-static pressure rise occurs and the second phase of loading takes place. Proctor and Filler⁴ present some data on these pressures, Proctor⁵ has developed a computer program to calculate both blast and quasi-static pressure rises, and Sewell and Kinney⁶ also present methods for estimating this later phase. In addition, Keenan and Tancreto^{7,8} have made measurements of blast pressures emitted from rectangular box cubicles with various vent areas and pressure rises within the cubicles. Finally, Lasseigne⁹ has measured static pressure rises in closed chambers to obtain design information for a specific suppressive structure. From these references, one obtains the answer that for the particular ratios of vent area to chamber volume tested, the venting has no effect on the peak quasi-static pressure. Thus, peak static pressures for unvented or poorly vented structures are the same. Unfortunately, essentially no data exist for quasi-static pressures within well-vented structures and the crucial question of the actual maximum pressure rise within such chambers remains unanswered. We must at present use the unvented pressure rise for design purposes. We have, however, conducted a model analysis and fitted curves to all data available to date to obtain the best possible estimate of this pressure. The model analysis and curve fits are presented later in this paper.

*The amount of oxygen available within any complete structure is apparently little affected by venting, until the venting area becomes very large.

A third important question regarding blast loading and suppressive structures is, "Can blast pressures outside these structures be predicted for specific designs?" Many of the past measurements of effectiveness of these structures have been based on blast attenuation which they provide (see Refs. 9-12). Using these references and more recent data from MTF, we have generated a method of correlating emitted blast waves with suppressive structure design based on comparing free-field blast data to blast data for waves emanating from suppressive structures. This method introduces an effective vent area ratio, α_{eff} , which can be computed for any combination of vented elements in a suppressive structure panel. Using this parameter and least-squares curve fits to free-field and suppressive structures blast data, we have shown that the influence of the suppressive structure is to create an effective standoff distance R_{st} , less than the free-field standoff distance R_f at which side-on overpressure P_s is the same for a given blast source energy W . Alternatively, this method will predict the reduction in overpressure over a considerable range of distances outside the structure. Details of the method are also given later.

BLAST PRESSURES OUTSIDE SUPPRESSIVE STRUCTURES

The side-on overpressures P_s in the free-field around an explosive charge are given by a functional relationship as expressed in Eq. (1).

$$P_s = f\left(\frac{R}{W^{1/3}}\right) \quad (\text{free field}) \quad (1)$$

where

R = standoff distance

W = charge weight

This functional relationship is the famous Hopkinson blast scaling law for the blast field around geometrically similar sources at sea-level ambient atmospheric conditions.³ Assume that a cubical blast suppressive structure whose length on any side is X and whose walls are fabricated of a single metal sheet with holes drilled in it is now centered over the explosive charge. The ratio of the vent area of a wall to the total cross-sectional area of the wall will be defined as equaling α . Equation (1) for free-field blast will now be modified by the additional geometric parameters defining the size of the suppressive cube X and the vent area ratio α . If we elect to write a modified form for Eq. (1) in nondimensional terms, a functional equation for predicting blast pressures outside the suppressive structure becomes:

$$P_s = f_1\left(\frac{R}{W^{1/3}}, \frac{X}{R}, \alpha\right) \quad (\text{suppressive structure equation}) \quad (2)$$

Equation (2) represents a four-parameter space of nondimensional numbers or pi terms. Although no functional format is expressed by Eq. (2), sufficient quantities of experimental data can be used to obtain an empirical relationship. This is precisely what is done to develop a relationship for predicting blast pressures outside of the suppressive structure; however, we must first realize that most suppressive structures do not have walls which are a single sheet with holes. The vast majority of structures have three to six wall layers with various staggered venting patterns so fragments will not escape the confinement. This means that, for a multi-walled confinement, we must compute an effective α , α_{eff} , so Eq. (2) can be used to predict blast pressures. To compute α_{eff} for a multi-walled structure, we have assumed that:

$$\frac{1}{\alpha_{\text{eff}}} = \frac{1}{\alpha_1} + \frac{1}{\alpha_2} + \dots + \frac{1}{\alpha_N} \quad (3a)$$

where N = number of elements in a suppressive structure panel. Or,

$$\frac{1}{\alpha_{\text{eff}}} = \sum_{i=1}^{i=N} \frac{1}{\alpha_i} \quad (3b)$$

Although no theoretical proof of this relationship is presently possible, it does reach the appropriate limits for small and large numbers of plates. For example, if only one plate is present, $\alpha_{\text{eff}} = \alpha_1$, as it should. If an infinite number of plates are present, $\alpha_{\text{eff}} = 0$, with the flow completely choked. If one of the plates is solid and thus has a zero α , $\alpha_{\text{eff}} = 0$, as it should. If all plates have the same value for α , $\alpha_{\text{eff}} = \alpha/N$, which is a number smaller than α for a single plate, as would be expected. In each member, α is defined according to Eq. (4).

$$\alpha = \frac{A_{\text{vent}}}{A_{\text{wall}}} \quad (4)$$

For plates, the meaning of this definition is obvious; however, in angles and louvres, the definition is less obvious. Figure 1 defines α in a series of angles.

In a louvre, we use a similar definition of α , except that the α , determined on the basis of Eq. (4), is multiplied by a factor equal to 1/2. This factor was applied because the data of Ref. 12 indicate that louvres are more efficient in constricting flow than are plates with holes. Perhaps this is explained by the fact that the entrance of a louvre is perpendicular to the entrance of a hole in a wall. As will be shown later, the factor of

1/2 appears to be justified by a curve fit to the experimental data. Figure 2 illustrates our definition of α for a louvre.

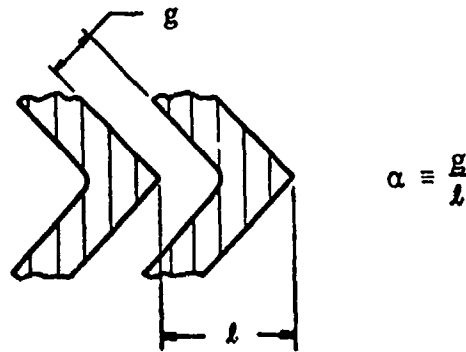


FIGURE 1. DEFINITION OF α IN A SERIES OF ANGLE MEMBERS



FIGURE 2. DEFINITION OF α IN A LOUVRE

Now that α_{eff} has been defined, we are prepared to develop a functional format for Eq. (2). This format was developed by assuming that Eq. (2) can be expressed as

$$P_s = A \left(\frac{R}{W^{1/3}} \right)^{N_1} \left(\frac{X}{R} \right)^{N_2} \left(\alpha_{\text{eff}} \right)^{N_3} \quad (5)$$

If logarithms are taken of both sides of this equation,

$$(\log P_s) = (\log A) + N_1 \left(\log \frac{R}{W^{1/3}} \right) + N_2 \left(\log \frac{X}{R} \right) + N_3 (\log \alpha_{\text{eff}}) \quad (6)$$

The equation is made linear, and a least-squares curve fit can be developed by stating that:

$$\left[1.0, \log \frac{R}{W^{1/3}}, \log \frac{X}{R}, \log \alpha_{\text{eff}} \right] \begin{bmatrix} \log A \\ N_1 \\ N_2 \\ N_3 \end{bmatrix} = [\log P_s] \quad (7)$$

Substituting matrix notation yields:

$$[L][N] = [P] \quad (8)$$

and a least squares curve fit results for $\log A$, N_1 , N_2 , and N_3 or the N matrix when:

$$[N] = [L^T L]^{-1} [L^T][P] \quad (9)$$

Experimental test data from Refs. 9-12 were used to develop this curve fit. The resulting equation is

$$P_s = 976.3 \frac{W^{2/3} \alpha_{\text{eff}}^{1/2}}{R^{3/2} X^{1/2}} \quad (10)$$

where

P_s = side-on pressure (psi)

W = charge weight (lb)

R = standoff distance from charge (ft)

X = width of suppressive cube (ft)

α = effective vented area ratio (-)

Figure 3 is a plot of Eq. (10) versus the experimental data points used to compose this plot. Equation (10) appears to experimentally curve fit the test results excellently. One standard deviation for the experimental data about the line in Figure 3 equals 18.6%, which is only slightly worse than would be obtained for free-field data. Because this is a curve fit to test data, Eq. (10) should only be used when input conditions fall within variations in individual pi terms. The variations included in test results were:

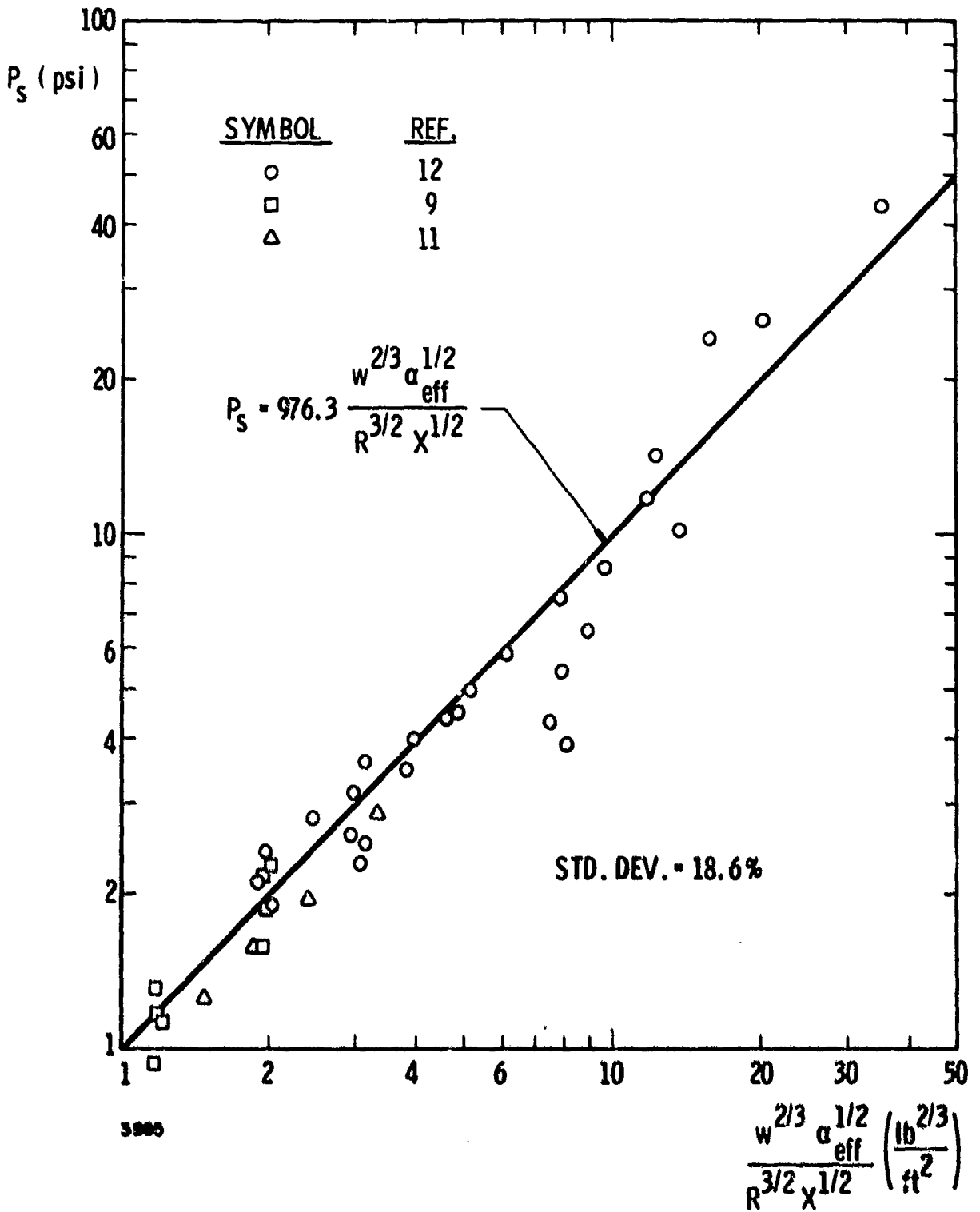


Figure 3. Curve Fit To Blast Pressures Outside Suppressive Structures

$$0.0263 \leq \alpha_{\text{eff}} \leq 0.60$$

$$0.323 \leq \frac{X}{R} \leq 1.77 \quad (11)$$

$$4.27 \text{ ft/lb}^{1/3} \leq \frac{R}{W^{1/3}} \leq 17.5 \text{ ft/lb}^{1/3}$$

The test data include results for a wide variety of panel geometries and numbers of vented layers in each panel. These range from as few as two layers to as many as five, and combinations of spaced angles, zeas, perforated plates, and louvres.

It is interesting to curve fit free-field side-on blast pressure data from Refs. 9-12 using the same procedure over the same range as for the suppressive structure blast field data. The resulting equation for free-field data is

$$P_s = 976.3 \left(\frac{W^{2/3}}{R^2} \right) \quad (12)$$

A comparison between Eq. (12) and the test data points can be seen in Figure 4. The standard deviation for blast pressures in the free-field is 13.1% which is only slightly better than the standard deviation for the suppressive structure blast field equation. Naturally, Eq. (12) should only be applied whenever $R/W^{1/3}$ is between the limits established by Eq. (11).

If one compares Eq. (10) for suppressive structures to Eq. (12) for free-field blast, it is immediately apparent that the influence of the suppressive structure is to create an effective standoff distance less than the free-field standoff distance at which blast pressures are the same for a given energy release. This standoff distance with a structure suppressing the blast R_{st} is related to the free-field standoff distance R_f by:

$$R_f^2 = R_{st}^{3/2} \frac{X^{1/2}}{\alpha_{\text{eff}}^{1/2}} \quad (13)$$

or

$$R_{st} = \alpha_{\text{eff}}^{1/3} \left(\frac{R_f^{4/3}}{X^{1/3}} \right) \quad (14)$$

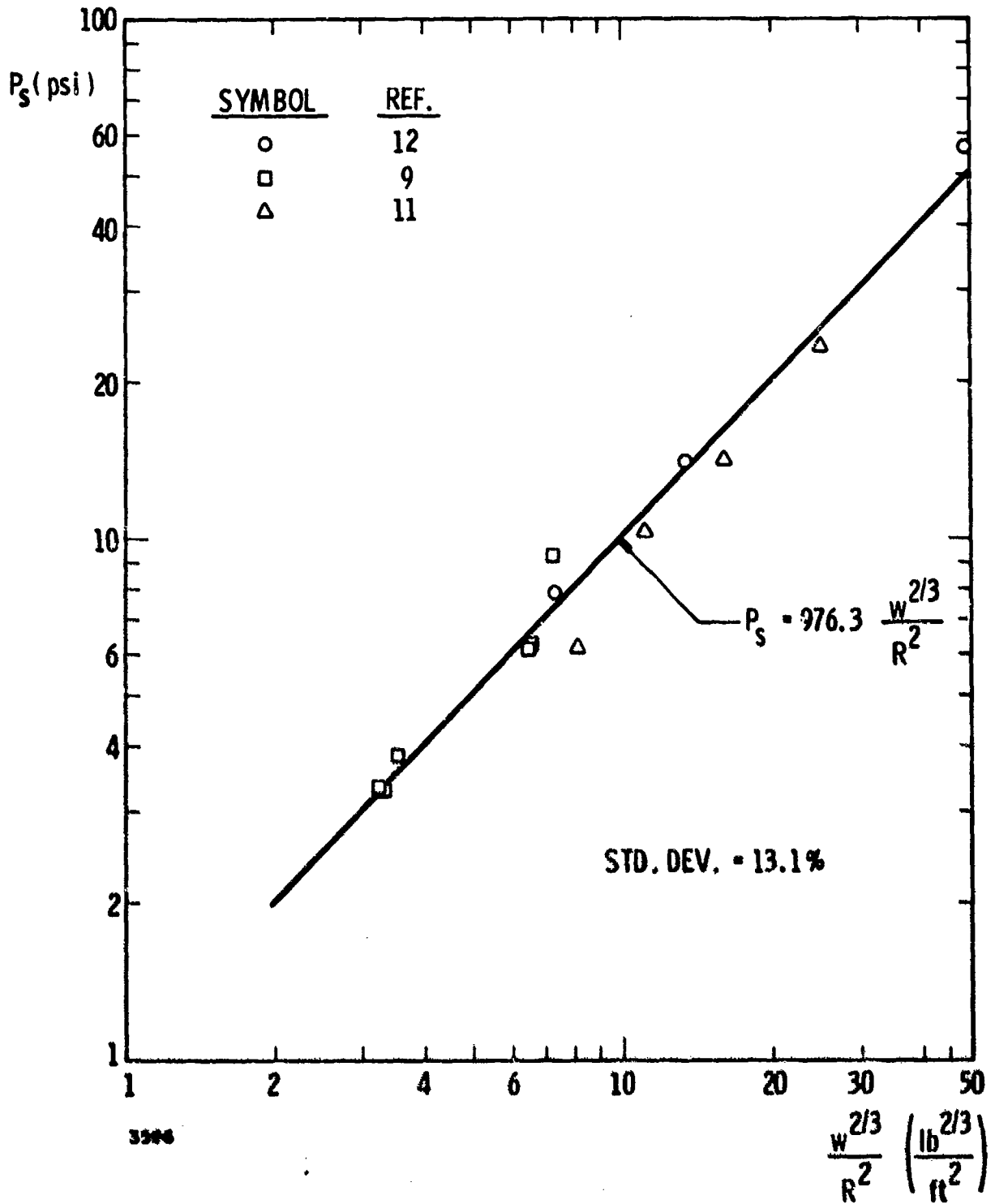


Figure 4. Curve Fit To Free Field Blast Pressures

PRESSURE RISE INSIDE STRUCTURE

In this section, we will discuss the quasi-static pressure rise within a suppressive structure. To create a solution, we will first perform a model analysis. The problem is envisioned as an instantaneous energy release of magnitude W inside a confined volume V . A vent area ($\alpha_{eff}A$) exists through which internal gases can escape. We are interested in predicting the internal pressure rise p and its decay as functions of time t . Ambient atmospheric pressure p_0 exists initially inside and outside the confined volume. To define an equation of state for the gases in this problem, we need two additional parameters, the ratio of specific heats γ and speed of sound c . Table 1 summarizes the parameters in this problem and lists their fundamental dimensions in an engineering system of force, length and time (F, L, T).

TABLE 1. PARAMETERS DETERMINING QUASI-STATIC PRESSURE INSIDE A VENTED CONTAINMENT VESSEL

Parameter	Symbol	Fundamental Dimensions	Description
Volume	V	L^3	Geometry
Vented Area	$(\alpha_{eff}A)$	L^2	
Energy Release	W	FL	Input energy
Atmospheric Pressure	p_0	F/L^2	Initial state of air
Sound Speed in Air	c	L/T	
Specific Heat Ratio Air	γ	---	
Pressure Increase	p	F/L^2	Response
Time	t	T	

Texts such as Ref. 13 tell how nondimensional numbers or pi terms can be developed from this list of variables. Because no new assumptions are inserted in developing pi terms, we will present only the results and not perform all of the algebra. The assumptions in this analysis are all included in the definition of the problem, so that phenomena are not considered which have no parameter listed in Table 1. Probably the major assumption is that no thermal effects are considered; in other words, the pressures dissipate through the venting and not through the conduction of heat into the walls of the suppressive structure. An acceptable set of pi terms which can result is:

$$\begin{aligned}\pi_1 &= p/p_o \\ \pi_2 &= \frac{(\alpha_{\text{eff}} A)^{3/2}}{V} \\ \pi_3 &= \gamma \\ \pi_4 &= \frac{W}{p_o V} \\ \pi_5 &= \frac{ct}{V^{1/3}}\end{aligned}\tag{15}$$

If we assume γ is a constant and are only interested in predicting peak pressure, the result would not be dependent upon time or the pi term $ct/V^{1/3}$ and the pi term γ would be invariant. Hence,

$$\frac{p_{\text{max}}}{p_o} = f \left(\frac{W}{p_o V}, \frac{(\alpha_{\text{eff}} A)^{3/2}}{V} \right)\tag{16}$$

Because p_o is invariant, we can also write a dimensional functional format for Eq. (16).

$$p_{\text{max}} = f \left(\frac{W}{V}, \frac{(\alpha_{\text{eff}} A)^{3/2}}{V} \right)\tag{17}$$

Figure 5 is a plot of p_{max} versus W/V for various values of $\frac{(\alpha_{\text{eff}} A)^{3/2}}{V}$. Provided $\frac{(\alpha_{\text{eff}} A)^{3/2}}{V}$ is less than 0.0775, the experimental data indicate that

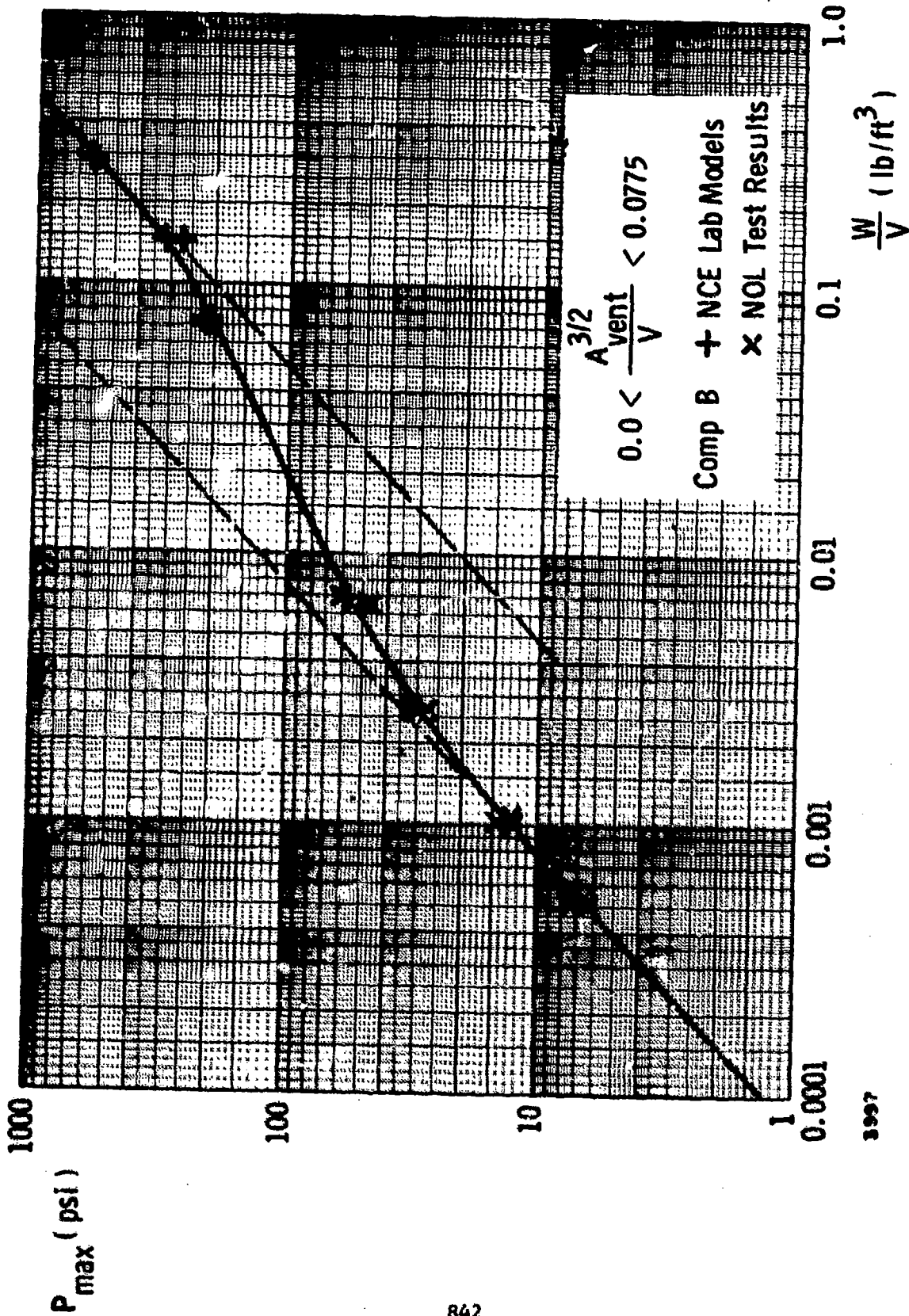


Figure 5. Quasi-Static Pressure Rise Inside An Unvented Enclosure

the maximum pressure p_{\max} is independent of $\frac{(\alpha_{\text{eff}} A)^{3/2}}{V}$. This can be written as

$$p_{\max} = f\left(\frac{W}{V}\right), \frac{(\alpha_{\text{eff}} A)^{3/2}}{V} \leq 0.0775 \quad (18)$$

The data used in developing Figure 5 come from Refs. 7 and 8. In addition to presenting their own data which were obtained at the Naval Civil Engineering Laboratory, Keenan and Tancreto also report test data obtained by Proctor at the Naval Ordnance Laboratory. Both groups of experiments used Comp B explosive, but, as can be seen in Figure 5, their experiments were in different domains of W/V .

The dashed straight lines in Figure 5 are the asymptotes for complete energy conversion or for p_{\max} proportional to (W/V) . If (W/V) is too large, insufficient oxygen is available to convert all the energy in the explosive charge; hence, the energy release is reduced by the ratio of the heat of detonation divided by the heat of combustion. Figure 5 implies that for $W/V \leq 0.003$ complete oxidation occurs; $W/V \geq 0.1$, the only oxidizer available is that in the explosive itself, and W/V between 0.003 and 0.1 results in partial afterburning.

If the maximum pressure is reached before significant venting occurs, the blow-down time will be independent of $W/p_0 V$, and we can write a functional equation for time of blow-down.

$$\frac{ct}{V^{1/3}} = f\left(\frac{p}{p_0}, \frac{(\alpha_{\text{eff}} A)^{3/2}}{V}\right) \quad (19)$$

Neglecting the invariant ambient gas parameters in Eq. (19) permits us to write a dimensional form of Eq. (19).

$$\frac{t}{V^{1/3}} = f\left(p, \frac{(\alpha_{\text{eff}} A)^{3/2}}{V}\right) \quad (20)$$

The data used to develop Figure 5 can also be used to empirically solve Eq. (20). Figure 6 is a plot of $\frac{t}{p^{1/6} V^{1/3}}$ versus $\frac{(\alpha_{\text{eff}} A)^{3/2}}{V}$. The ordinate of this graph is based on the empirical observation that the two pi terms $\frac{t}{V^{1/3}}$ and p can be combined to form $\frac{t}{p^{1/6} V^{1/3}}$. We can now write Eq. (20) as Eq. (21):

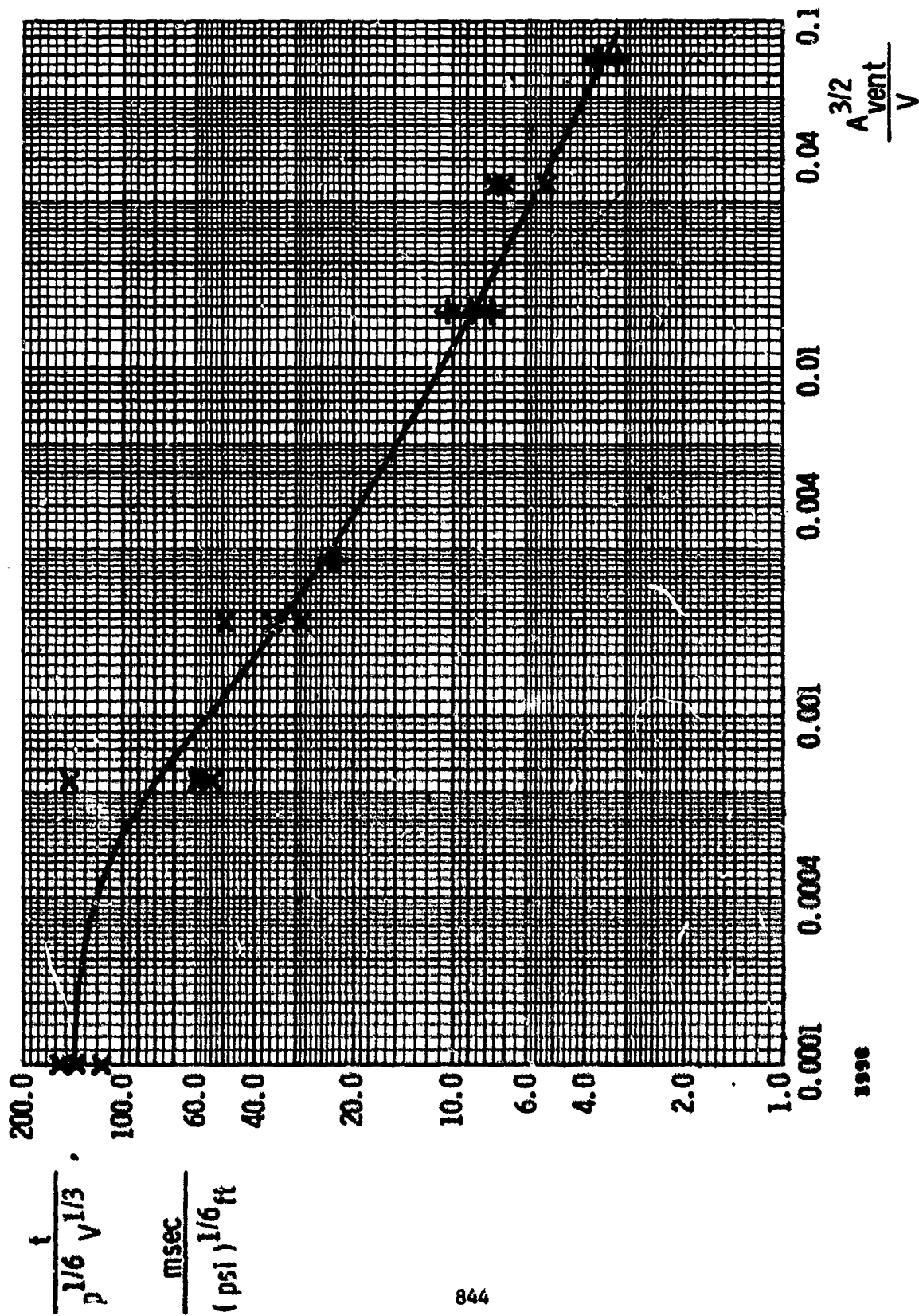


Figure 6. Scaled Blow-Down Time For Vented Structure

$$\frac{t}{p^{1/6} V^{1/3}} = f \left(\frac{(\alpha_{\text{eff}} A)^{3/2}}{V} \right)$$

The function format for Eq. (21) is obtained from Figure 6.

CONCLUSIONS

In this paper, we have presented methods for estimating long term (quasi-static) pressures generated by internal explosions within vented suppressive structures, and attenuated blast pressures escaping from suppressive structures with various vent panel designs. Scaled curves for appropriate parameters are presented, based on fits to available experimental data.

We have several suggestions for improving methods for estimating blast loading and attenuation of suppressive structures:

- (1) Initial reflected blast loads have conservatively been estimated to be the reflected pressures and impulses on rigid, non-vented walls. We suggest that shock-tube or field tests be conducted to measure these loads more accurately, for several typical vent panel designs.
- (2) Experimental data for quasi-static pressure rises caused by internal explosions in vented structures have been limited to such small values of scaled vent areas that the maximum pressure rises are unaffected by the vent areas. Tests should be run on well-vented structures to determine scaled vent areas which cause significant reduction in quasi-static pressures.
- (3) As additional data on attenuated blast pressures outside suppressive structures are obtained in the course of subsequent testing, these data should be factored into the design curves and equations in this paper to obtain better fits. In addition, curve fits should be made to scaled data for blast impulse outside the structures, when sufficient data are available.

REFERENCES

1. H. J. Goodman, "Compiled Free-Air Data on Bare Spherical Pentolite," BRL Report No. 1092, Ballistic Research Laboratories, Aberdeen Proving Ground, Md., Feb. 1960 (AD 235-278).
2. W. H. Jack, Jr., "Measurements of Normally Reflected Shock Waves from Explosive Charges," BRL Memorandum Report No. 1499, Ballistic Research Laboratories, Aberdeen Proving Ground, Md., 1963.
3. W. E. Baker, Explosions in Air, Univ. of Texas Press, Austin, Texas, 1973.
4. J. F. Proctor and W. S. Filler, "A Computerized Technique for Blast Loads from Confined Explosions," 14th Annual Explosives Safety Seminar, New Orleans, La., 8-10 Nov. 1972, pp. 99-124.
5. J. F. Proctor, "Internal Blast Damage Mechanisms Computer Program," 61 JTCG/ME-73-3, Joint Technical Coordinating Group for Munitions Effectiveness, 10 April 1973.
6. R. G. S. Sewell and G. F. Kinney, "Internal Explosions in Vented and Unvented Chambers," 14th Annual Explosives Safety Seminar, New Orleans, La., 8-10 Nov. 1972, pp. 87-98.
7. W. A. Keenan and J. E. Tancreto, "Effects of Venting and Frangibility on Blast Environment from Explosions in Cubicles," Minutes of the Fourteenth Explosives Safety Seminar, New Orleans, Nov. 1973, pp. 125-161.
8. W. A. Keenan and J. E. Tancreto, "Blast Environment from Fully and Partially Vented Explosions in Cubicles," Tech. Rept. 51-027, Civil Engineering Laboratory, Naval Construction Battalion Center, Port Hueneme, Ca., Feb. 1974.
9. A. H. Lasseigne, "Static and Blast Pressure Investigation for the Chemical Agent Munition Demilitarization System: Sub-Scale," Rept. EA-FR-4C04, Nov. 30, 1973.
10. Report EA1002, "Study of Suppressive Structures Applications to an 81 mm Automated Assembly Facility," prepared for Manufacturing Technology Directorate, Chemical and Plants Division, Edgewood Arsenal, 16 April 1973.

REFERENCES (Cont'd)

11. Report EA-4E33, "81 mm Suppressive Shielding Technical Data Package," Jan. 1974.
12. Report EA-FR-2B02, "Final Report Application of Suppressive Structure Concepts to Chemical Agent Munition Demilitarization System (CAMDS)," July 27, 1973.
13. W. E. Baker, F. S. Westine and F. T. Dodge, Similarity Methods in Engineering Dynamics, Hayden Book Co., Inc., Rochelle Park, N. J., 1973.

ENERGY SOLUTIONS FOR PREDICTING DEFORMATIONS IN BLAST LOADED STRUCTURES

by

P. S. Westine*
W. E. Baker**

ABSTRACT

Energy solutions are excellent analysis procedures for predicting residual strains or deformations in structural elements when transient behavior is of little interest. In this paper, we demonstrate how energy procedures can be used in rigid-plastic structural solutions when members are loaded either impulsively or quasi-statically by blast waves.

In the impulsive loading realm, the kinetic energy imparted to a structural member is equated to the plastic strain energy, whereas in the quasi-static loading realm, the work performed in deforming a structural member is equated to the plastic strain energy. An assumed first mode structural deformation pattern works well when calculating plastic strain energy in either of the loading realms. Experimental test data on deformed simply-supported and cantilever beams, clamped circular plates, and clamped rectangular plates demonstrate the validity of these solutions.

The test data on different types of structural elements are important, as the beam data involve only bending behavior, the circular plates have both bending and extensional action, and the rectangular plates introduce shearing behavior into the strain energy calculations. Because all solutions are closed-form ones, design formulae result which can be used by others to evaluate plastic deformation in blast loaded structural members.

INTRODUCTION

Energy solutions are excellent analysis procedures for predicting residual strains or deformations in structural components whenever transient (time-dependent) behavior is of little interest. Although schools

* Senior Research Engineer, Southwest Research Institute, San Antonio, Texas.

** Institute Scientist, Southwest Research Institute, San Antonio, Texas.

readily teach energy procedures for obtaining elastic solutions, few investigators apply the approach to dynamic plasticity problems.

Dynamic rigid-plastic energy solutions began in the early 1950's when Lee and Symonds [1] used the static plastic-hinge concept, considered beam inertia, and propagated a traveling hinge to analytically obtain the upper bound for permanent deformation in a beam under a transverse load. Their Brown University associates and graduates such as S. R. Bodner, W. Prager, N. Jones, J. B. Martin, R. M. Haythornthwaite and others then added refinements, illustrations of which are given in Refs. 2-6. It was J. E. Greenspon in the 1960's who pointed out that one could obtain solutions without going through the details of propagating a plastic hinge along structural members [Refs. 7-11]. Greenspon noted that the residual strain energy stored in a plastically deformed member could be calculated by assuming a final deformed shape. This strain energy was then equated to the energy flux in an explosive blast wave.[11] We disagree with this last step, which made deformations independent of structural orientation relative to the enveloping blast wave, thus ignoring an important effect observed in many experiments. In addition, Greenspon's procedure forces pressures and impulses in the blast wave to obey the relationship $PI = \text{constant}$, whose asymptotes for both pressure and impulse are $P = 0$ and $I = 0$. The response of real targets is related to non-zero P and I limits, so this conclusion is also unacceptable.

We would emphasize that Greenspon was correct in his strain energy estimation procedures. Estimates of structural deformation would have been correct had he equated strain energy to the kinetic energy imparted to the structure for short duration impulsive loads. When durations are long relative to the structural response time, the strain energy is equated to the work performed when the peak load moves through the distance that the structure deforms. Hence, two separate procedures are required, one to obtain the solution for the impulsive loading realm, and the other to obtain the solution for the quasi-static loading realm. We will proceed to illustrate these procedures by computing results and comparing to test data. Our first illustration is a rheological model whose exact solution can be obtained and compared to the answers given by energy procedures.

RIGID-PLASTIC SINGLE DEGREE-OF-FREEDOM SYSTEM

Consider first a single-degree-of-freedom, rigid-plastic system as in Figure 1a. The motion of the mass m is resisted by a Coulomb friction element f when the blast load $p(t)$ is applied to the structure. We will approximate the blast loading with an exponential decay as in Figure 1b (where P is the maximum applied force and T is the time constant associated with the duration of loading). If $P/f \leq 1.0$, we have the trivial case where the residual deformation X equals 0 because the mass never moves.

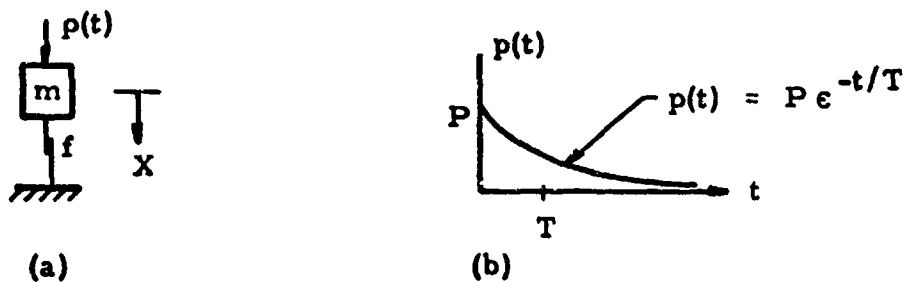


FIGURE 1. RIGID-PLASTIC, SINGLE-DEGREE-OF-FREEDOM DAMAGE MODEL

If $P/f \geq 1.0$, we must write the differential equation of motion:

$$P e^{-t/T} - f = m \frac{d^2 x}{dt^2} \quad (1)$$

By direct integration, we obtain for the case of zero initial velocity, the velocity relationship:

$$\frac{dx}{dt} = \frac{PT}{m} \left[1 - e^{-t/T} - \left(\frac{f}{P}\right) \left(\frac{t}{T}\right) \right] \quad (2)$$

Integrating again, we obtain for the case of zero initial displacement, the displacement equation:

$$x = \frac{PT^2}{m} \left[\frac{t}{T} + e^{-t/T} - \frac{1}{2} \left(\frac{f}{P}\right) \left(\frac{t}{T}\right)^2 - 1 \right] \quad (3)$$

Motion continues until the velocity, Eq. (2), equals zero or until:

$$e^{-t/T} + \left(\frac{f}{P}\right) \left(\frac{t}{T}\right) = 1.0 \quad (4)$$

We cannot explicitly solve for t/T in Eq. (4), as it is a transcendental equation; therefore, we assume values of P/f , solve for t/T , and substitute into the displacement equation (Eq. (3)) to obtain the maximum deformation X . Table 1 gives the results of such a calculation.

The maximum deformation X in the third column of Table 1 has been made nondimensional by dividing the left and right sides of Eq. (3) by $\frac{PT^2}{m}$. A solution can be presented for the maximum displacement by plotting

TABLE 1

t/T	P/f	X_m/PT^2	$(PT)^2/X_{mf}$
---	1.00	0	∞
0.09	1.033	0.001	1033
0.35	1.18	0.003	394
0.50	1.27	0.009	141
0.75	1.42	0.024	59.2
1.00	1.58	0.052	30.3
1.50	1.94	0.143	13.6
2.00	2.31	0.270	8.56
3.00	3.16	0.630	5.02
4.00	4.08	1.06	3.84
6.00	6.01	2.00	3.01
9.00	9.00	3.50	2.57
13.0	13.0	5.50	2.36
20.0	20.0	9.00	2.22
35.0	35.0	16.50	2.12
50.0	50.0	24.0	2.08
75.0	75.0	36.5	2.05
100.0	100.0	49.0	2.04
---	∞	---	2.00

$\frac{X_m}{PT^2}$ versus P/f . We have elected to divide P/f by $\frac{X_m}{PT^2}$ to form a new fourth column in Table 1 and to plot this new column $\frac{(PT)^2}{X_{mf}}$ versus P/f .

The reason for this manipulation is that the product PT equals the applied total impulse I , and in this manner we create a scaled load-impulse or P-I diagram. The solid line in Figure 2 is this scaled P-I diagram for a simple rigid-plastic structure.

Observe in Table 1 and Figure 2 that whenever $\frac{I^2}{X_{mf}}$ is greater than about 60, the duration of loading T is larger than the response time t and P/f equals 1.0. Similarly, whenever P/f is greater than about 20, durations of loading T are smaller than the response times t of the responding structure, and $\frac{I^2}{X_{mf}}$ equals 2.0. The energy solutions which we will apply estimate both of these asymptotes.

The strain energy U stored in plastic deformation is given by:

$$U = fX \quad (5)$$

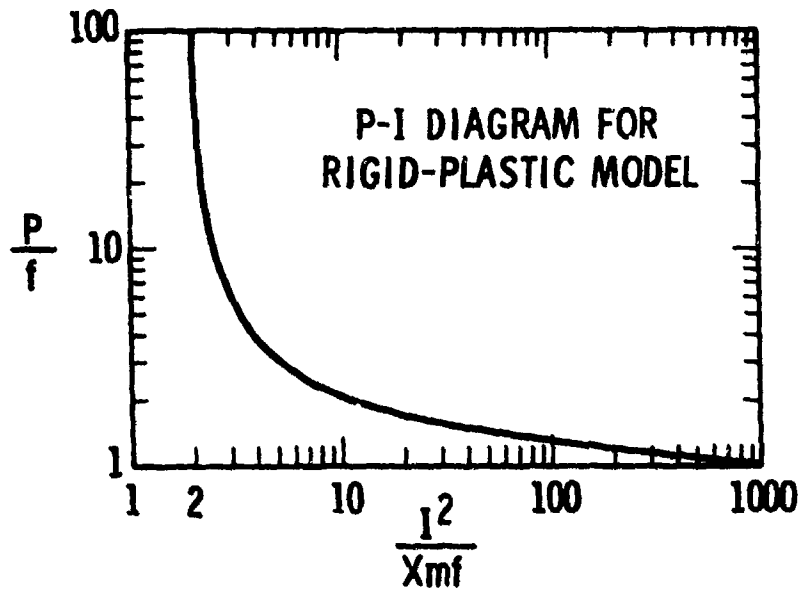


FIGURE 2. P-I DIAGRAM FOR RIGID-PLASTIC SYSTEM

The kinetic energy KE imparted to the mass equals:

$$KE = \frac{1}{2} m V_0^2 = \frac{1}{2} m \left(\frac{I}{m} \right)^2 = \frac{I^2}{2m} \quad (6)$$

The work WK done by the maximum force P acting through the distance X is:

$$WK = PX \quad (7)$$

Equating the strain energy U, Eq. (5), to the kinetic energy KE, Eq. (6), yields the asymptote for the impulsive loading realm or:

$$\frac{I^2}{Xmf} = 2.0 \quad (\text{impulsive loading realm}) \quad (8)$$

The other asymptote is obtained by equating U, Eq. (5), to the work WK, Eq. (7).

$$\frac{P}{f} = 1.0 \quad (\text{quasi-static loading realm}) \quad (9)$$

Had we wished to calculate maximum elastic deformations rather than plastic ones, the same procedures would apply. Replacing the Coulomb friction element with a linear elastic spring in Figure 1a would have yielded the analytical solid curved line shown in Figure 3. This solution also has asymptotes for the impulsive and quasi-static loading realms that can be

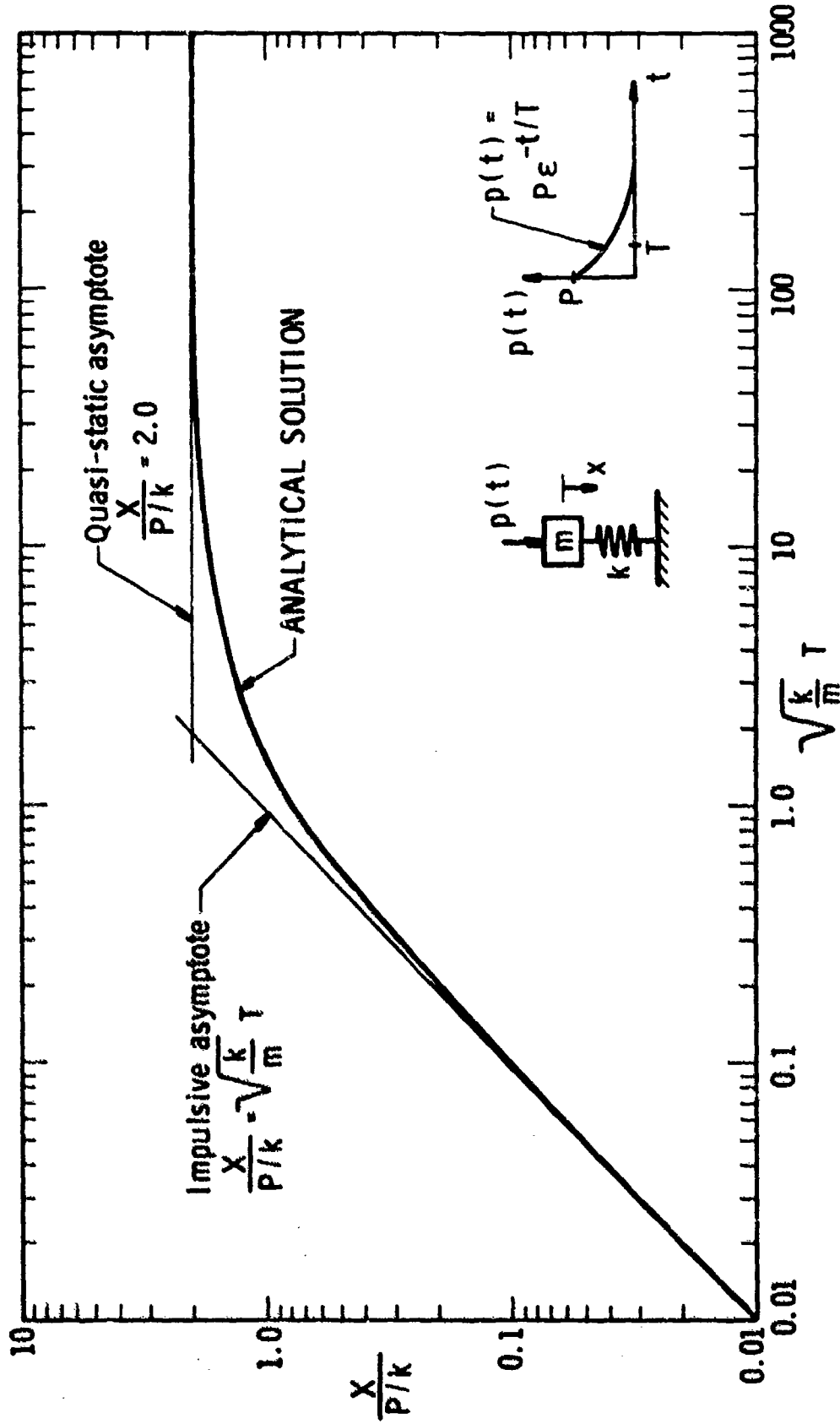


Figure 3. Maximum Response to Force Pulse

obtained using energy procedures. The strain energy in an elastic system would be given by Eq. (10) rather than Eq. (5).

$$U = \frac{1}{2} k X^2 \quad (10)$$

In an elastic system the kinetic energy KE and work WK are still given by Eqs. (6) and (7), respectively. For an elastic system, equating Eq. (10) to Eq. (6) yields the asymptote for the impulsive loading realm.

$$X = \frac{I}{\sqrt{km}} \quad (11)$$

or

$$\frac{X}{P/k} = \sqrt{\frac{k}{m}} T \quad (\text{impulsive loading realm}) \quad (12)$$

Similarly, equating Eq. (10) to Eq. (7) yields the quasi-static loading realm asymptote:

$$\frac{X}{P/k} = 2.0 \quad (\text{quasi-static loading realm}) \quad (13)$$

Both the impulsive loading realm asymptote and quasi-static loading realm asymptote are shown in Figure 3. Figure 3 illustrates that, if these asymptotes are known for an elastic as well as plastic system, the deformations can be predicted using energy procedures.

As has been illustrated in these simple models, the principles are as follows:

- (1) To estimate the impulsive loading realm structural deformation asymptote, estimate the strain energy in a deformed structure and equate this strain energy to the kinetic energy imparted to the structure.
- (2) To obtain the quasi-static structural deformation asymptote, equate the strain energy to the work performed by the peak force deflecting with the structure.

We are now prepared to illustrate these principles as they are applied to beam, plates, and similar more complex structural components which are loaded by blast waves or other transient pulses. The first structural components that we will study are cantilever beams.

BLAST LOADED CANTILEVER BEAMS

Consider a clamped cantilever beam of rectangular cross section as depicted in Figure 4.

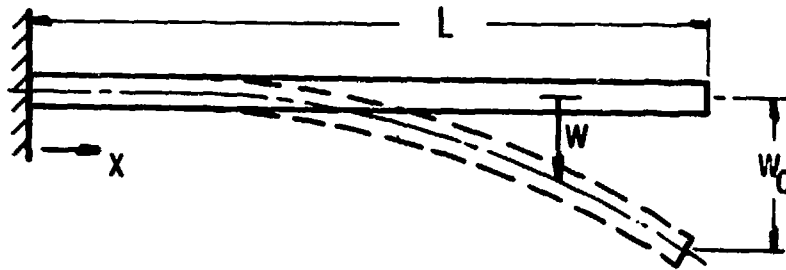


FIGURE 4. SCHEMATIC DRAWING OF CLAMPED CANTILEVER BEAM

We will assume that the deformed shape for this structural component is given by

$$w = w_0 \left[1 - \cos \frac{\pi x}{2L} \right] \quad (14)$$

Notice that the assumed deformed shape has no deflection and no slope at $x = 0$ and no moment at $x = L$. The maximum deformation and maximum slope occur at $x = L$, and the maximum moment occurs at $x = 0$. These are the correct boundary conditions. A good solution does depend upon selecting an appropriate deformed shape.

Because membrane action is not developed, the strain energy is dissipated in bending. In an elastic member, the bending strain energy is given by:

$$U = \int_0^L \frac{M^2 dx}{2EI} \quad (15)$$

where the moment M is equal to $-EI \frac{d^2 w}{dx^2}$. Differentiating Eq. (14) and substituting into Eq. (15) then yields:

$$U = \frac{\pi^4 EI w_0^2}{32 L^4} \int_0^L \cos^2 \left(\frac{\pi x}{2L} \right) dx \quad (16)$$

Or, upon integrating:

$$U = \frac{\pi^4 EI w_o^2}{64 L^3} \quad \left(\begin{array}{l} \text{bending in elastic} \\ \text{cantilever beam} \end{array} \right) \quad (17)$$

The kinetic energy imparted to the cantilever beam of mass density ρ , width b , and thickness h by a uniform specific impulse of intensity i is given by:

$$KE = \sum_{\text{beam}} \frac{1}{2} m V_o^2 \quad (18)$$

or

$$KE = \int_0^L \frac{1}{2} (\rho b h dx) \left(\frac{i b dx}{\rho b h dx} \right)^2 \quad (19)$$

Integration of the preceding quantity then yields:

$$KE = \frac{i^2 b L}{2 \rho h} \quad (20)$$

The equation defining the impulsive loading realm asymptote for the elastic maximum tip deformation is then obtained by equating Eq. (20) to Eq. (17).

The width b drops out of the solution when $\frac{1}{12} b h^3$ is substituted for the second moment of area I in Eq. (17).

$$\frac{w_o}{L} = \frac{\sqrt{384}}{\pi^2} \left(\frac{L}{h} \right) \left(\frac{i}{h \sqrt{E \rho}} \right) \quad (21)$$

The quasi-static loading realm asymptote is predicted by estimating the work WK associated with the peak drag load Q . The work is:

$$WK = \sum_{\text{beam}} C_D Q b dx w \quad (22)$$

or

$$WK = C_D Q b w_o \int_0^L \left(1 - \cos \frac{\pi x}{2L} \right) dx \quad (23)$$

Integration of the preceding quantity then yields:

$$WK = \left(1 - \frac{2}{\pi}\right) C_D Q b L w_o \quad (24)$$

Equating Eq. (24) to Eq. (17) and substituting for the second moment of area then yields the quasi-static asymptote for the elastic maximum tip deformation.

$$\frac{w_o}{L} = \frac{875.5}{\pi^5} \left(\frac{C_D Q}{E}\right) \left(\frac{L}{h}\right)^3 \quad (25)$$

Maximum elastic strains at the root of the cantilever beam can also be calculated from the maximum tip deformations, either Eq. (21) or Eq. (25), dependent upon the loading realm. Substituting the second derivative of Eq. (14) into the moment-curvature relationship, the moment into $\sigma = \frac{Mc}{I}$, the stress σ into $\epsilon = \frac{\sigma}{E}$, and $\frac{1}{12} b h^3$ for the second moment of area I , yields the strain equation in terms of the maximum tip deformation. This equation is given by:

$$\epsilon = \frac{\pi^2 h w_o}{8 L^2} \cos \frac{\pi x}{2L} \quad (26)$$

The strain ϵ will be a maximum at the root of the cantilever beam where $\cos \frac{\pi x}{2L}$ equals 1.0. Substituting Eq. (21) for w_o into Eq. (26) then yields the maximum strain equation for the impulsive loading realm.

$$\epsilon = 2.45 \frac{i}{h\sqrt{E\rho}} \quad (\text{impulsive loading realm}) \quad (27)$$

Equation (26) for the impulsive loading realm can be compared to experimental test data to demonstrate the validity of this analysis procedure. In 1958, W. E. Baker, et.al.,^[12] detonated H. E. explosive charges in the vicinity of 6061-T6 aluminum cantilever beams. Plotted in Figure 5 is the maximum bending strain as a function of $\frac{i}{L\sqrt{\rho E}}$ for beams with a length of 12 in. and thickness of 0.051 inch. Some uncertainty exists in computing the impulse imparted to the beams because of an air blast wave diffracting around the beams; hence, the test data are plotted as bars. As can be seen in Figure 5, Eq. (27) for the maximum elastic strain at the root of the cantilever beams accurately predicts experimentally observed results.

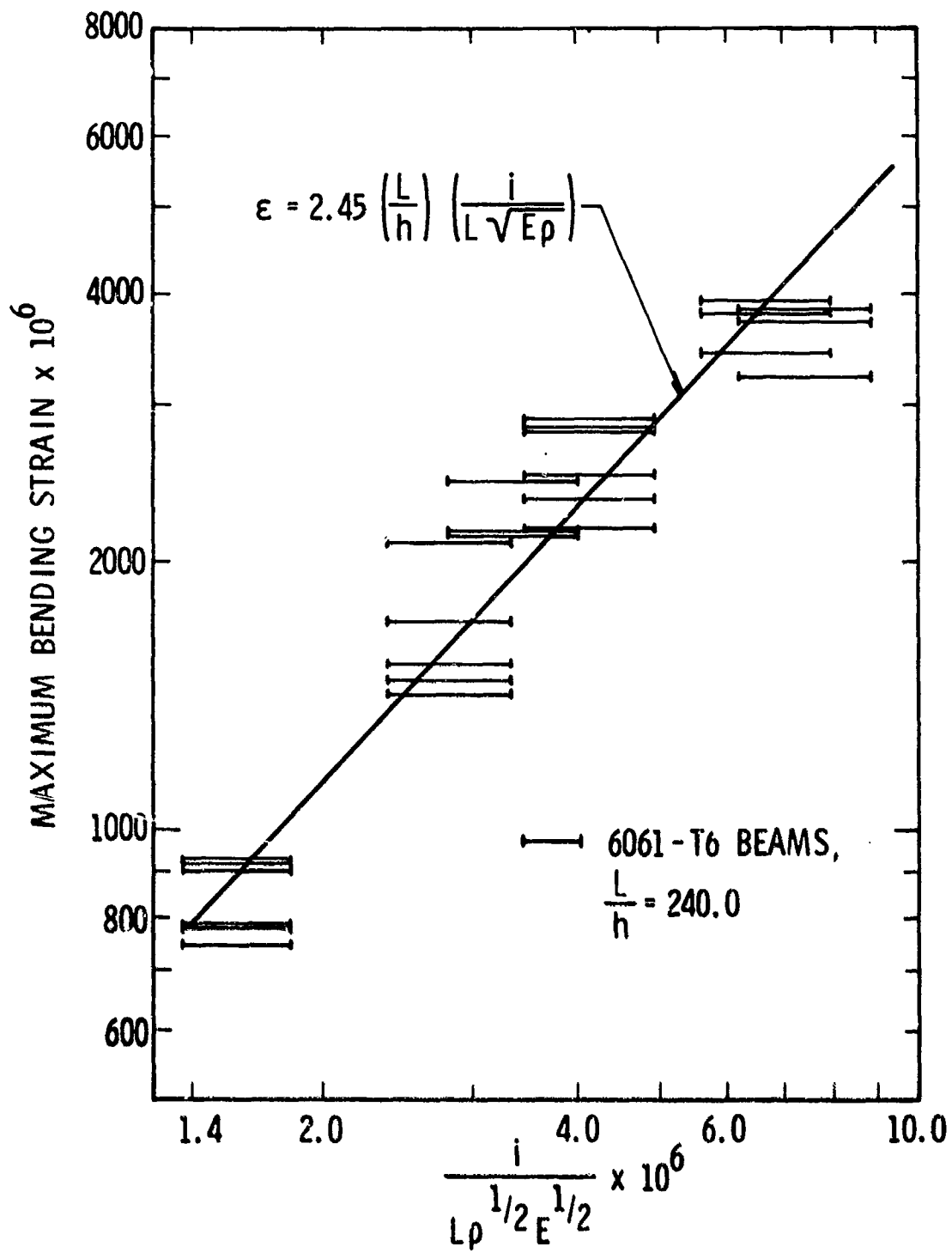


Figure 5. Elastic Response of Cantilevers, Impulsive Loading Realm

The strain at the root of cantilever beams in the quasi-static loading realm can be obtained by substituting Eq. (25) into Eq. (26) and setting the $\cos \frac{\pi x}{2L}$ equal to 1.0. This result yields:

$$\epsilon = 3.534 \left(\frac{L}{h} \right)^2 \left(\frac{C_D Q}{E} \right) \quad (\text{quasi-static realm}) \quad (28)$$

J. D. Day in unreported tests ran five blast loading experiments on clamped cantilever steel beams with strain gauges at the root of the beam. The steel beams were $6 \times 3/4 \times 3/4$ in. and were exposed to side-on overpressures P_s as summarized in Table 2. The drag pressure Q can be calculated from P_s , and assuming that C_D equaled 1.75, we obtain calculated strains as shown in the last column of Table 2. These calculated strains compare very favorably with experimental observed results.

TABLE 2. ELASTIC STRAINS IN CANTILEVERS,
QUASI-STATIC LOADING REALM

Test No.	P_s (psi)	Q (psi)	Experimental $\epsilon \times 10^{+6}$	Calculated $\epsilon \times 10^{+6}$
1	8.80	1.76	23.2	23.6
2	8.68	1.74	22.9	23.4
3	10.48	2.42	32.5	32.5
4	16.10	5.47	80.4	73.5
5	20.78	8.73	141.0	117.5

Plastic response of cantilever beams can be estimated as easily as elastic response. If we assume a rigid-plastic model, the bending strain energy now becomes the integration of the moment-curvature relationships over the length of the beams. In other words:

$$U = \int_0^L M_y \frac{d^2 w}{dx^2} dx \quad (29)$$

Differentiating Eq. (14), the assumed deformed shape and substituting it into Eq. (29) gives:

$$U = \frac{\pi^2 M_y w_0}{8 L^2} \int_0^L \cos \frac{\pi x}{2L} dx \quad (30)$$

But in a rectangular member the yield moment $M_y = \frac{\sigma_y b h^2}{4}$; hence, upon substituting for M_y and completing the integration, we obtain:

$$U = \frac{\pi \sigma_y b h^2 w_o}{16 L} \quad (31)$$

Equating Eq. (31) to the kinetic energy, Eq. (20), then yields the asymptote for permanent residual tip deflection in the impulsive loading realm.

$$\frac{w_o}{L} = \frac{8}{\pi} \left(\frac{L}{h} \right) \left(\frac{i}{h \sqrt{\rho \sigma_y}} \right)^2 \quad (32)$$

Reference 12 also presents test data on permanent tip deflections for the same 6061-T6 aluminum cantilever beams as were used in the elastic strain, Figure 5, comparison. Plotted in Figure 6 are these scaled tip deflections as a function of $\frac{i}{L \sqrt{\rho E}}$. Equation (32) was placed in the same format as the data in Figure 6 by multiplying and dividing Eq. (32) by the elastic modulus E . As can be seen in Figure 6, the agreement is relatively good. The disagreement that does arise at small values of scaled impulse $\frac{i}{L \sqrt{\rho E}}$ is caused by our use of a rigid-plastic rather than elastic-plastic analysis.

The writers have no data for a cantilever beam permanent tip deflection comparison in the quasi-static loading realm. In the quasi-static loading realm, the displacement X becomes indeterminate when U , Eq. (31), is equated to WK , Eq. (24). The solution in the quasi-static loading realm is given by:

$$\frac{P}{\sigma_y} = 0.540 \left(\frac{h}{L} \right)^2 \quad (33)$$

The displacement w_o in Eq. (33) is indeterminate just as X was indeterminate in the rigid-plastic rheological model, Eq. (9), for the quasi-static loading realm. This conclusion is correct for perfectly plastic nonhardening systems in the quasi-static loading realm. A hardening stress-strain law does result in finite displacements.

BENDING IN SIMPLY-SUPPORTED AND CLAMPED BEAMS

Our next illustration will be plastic bending in a simply-supported beam being loaded with a uniform load. Figure 7 shows the deformed shape of a bent simply supported beam. To calculate strain energy in this member,

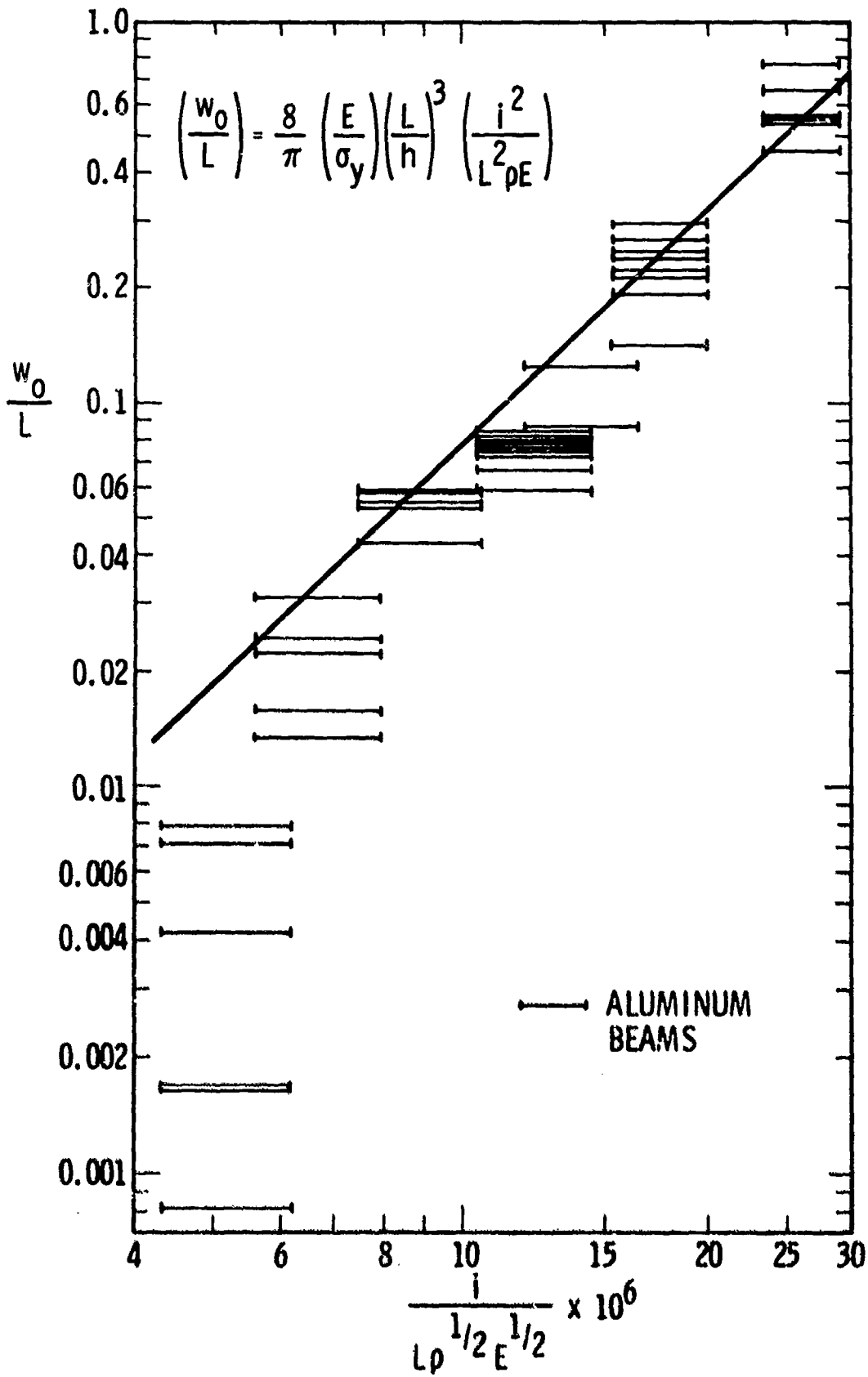


Figure 6. Damage to Cantilever Beams, Impulsive Loading Realm

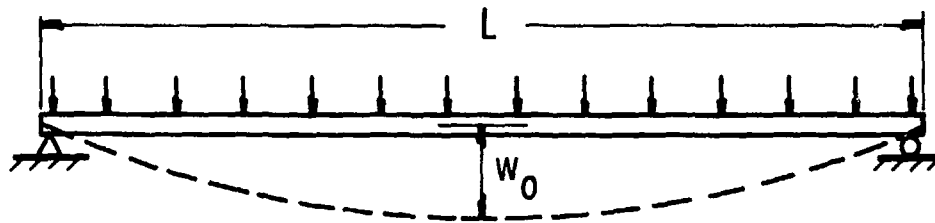


FIGURE 7. DEFORMED SHAPE OF SIMPLY-SUPPORTED BEAM

we must assume a deformed shape. Selecting:

$$w = w_0 \left(1 - \frac{4x^2}{L^2} \right) \quad (34)$$

as an appropriate deformed shape gives the appropriate boundary conditions.

At $x = 0$, center of the beam, $w = w_0$ and the slope $\frac{dw}{dx} = 0$, while at the ends of the beam, $x = \pm \frac{L}{2}$, the deflections $w = 0$ and the slopes $\frac{dw}{dx} = -\frac{8xw_0}{L^2}$,

a maximum value. The strain energy equals the plastic yield moment M_y for the beam cross-section times the change in angle of rotation integrated over the entire beam. Because the beam is symmetric and the change in angle of rotation with respect to x approximately equals $-\frac{d^2w}{dx^2}$, the strain energy U equals:

$$U = -2 \int_0^{L/2} M_y \frac{d^2w}{dx^2} dx \quad (35)$$

Differentiating Eq. (34), substituting it into Eq. (35) and integrating then yields:

$$U = \frac{8 M_y w_0}{L} \quad (36)$$

The kinetic energy KE is obtained by summing the impulse squared divided by two times the incremental mass (see Eq. (6)) over the entire beam. If b is the width of the loaded member, ρ the density, A the cross-sectional area, and i the specific impulse, this summation yields the following integration.

$$KE = 2 \int_0^{L/2} \frac{i^2 b^2 (dx)^2}{2 \rho A (dx)} \quad (37)$$

or

$$KE = \frac{i^2 b^2 L}{2 \rho A} \quad (38)$$

Equating U, Eq. (36), to KE, Eq. (38), yields the asymptote for the impulsive loading realm.

$$\frac{i^2 b^2 L}{\rho M_y A} = 16 \left(\frac{w_o}{L} \right) \quad \left(\begin{array}{l} \text{impulsive realm} \\ \text{s. s. beam} \end{array} \right) \quad (39)$$

The work WK is obtained by integrating over the length of the beam, the forces times the distances through which they move. This operation is performed by integrating $p b dx$ times the assumed deformed shapes, Eq. (34).

$$WK = 2 \int_0^{L/2} p b w_o \left(1 - \frac{4x^2}{L^2} \right) dx \quad (40)$$

or

$$WK = \frac{2}{3} p b L w_o \quad (41)$$

Equating WK, Eq. (41), to U, Eq. (36), yields the quasi-static asymptote,

$$\frac{p b L^2}{M_y} = 12 \quad \left(\begin{array}{l} \text{quasi-static realm} \\ \text{s. s. beam} \end{array} \right) \quad (42)$$

So far these calculations have assumed that the beam is simply-supported and free to rotate at the ends. If the beam is clamped at the ends, no rotation occurs, but can move inwards so that no membrane action is developed; we can use many of the results which have already been developed. To do this, assume that a clamped beam is really two simply-supported beams that have been split and joined end to end as in Figure 8.

This new configuration implies that:

$$U = 2 U_{s. s.} = \frac{16 M_y w_o}{l} \quad (43)$$

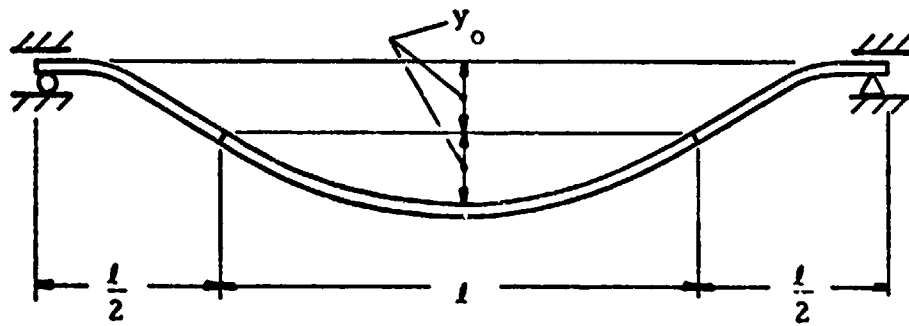


FIGURE 8. DEFORMED SHAPE OF CLAMPED BEAMS

and that

$$KE = 2KE_{s.s.} = \frac{i^2 b^2 l}{\rho A} \quad (44)$$

but $l = \frac{L}{2}$ and $y_0 = \frac{w_0}{2}$, so substituting for l and y_0 and equating U to KE yields:

$$\frac{i^2 b^2 L}{\rho A M_y} = 32 \frac{w_0}{L} \quad \left(\begin{array}{l} \text{impulsive realm} \\ \text{clamped beam} \end{array} \right) \quad (45)$$

Because Eq. (45) for clamped beams is twice Eq. (39) for simply-supported beams, we can write

$$\frac{i^2 b^2 L}{N \rho A M_y} = 16 \frac{w_0}{L} \quad \left(\begin{array}{l} \text{impulsive realm} \\ \text{beam bending} \end{array} \right) \quad (46)$$

where

$N = 1.0$ for simply-supported beams

$N = 2.0$ for clamped beams

To experimentally demonstrate the validity of this solution, we have plotted experimental data taken by Florence and Firth^[13] and compared these data to Eq. (46). Because Florence and Firth used beams with rectangular cross-sections, $M_y = \frac{\sigma b h^2}{4}$. Substituting for M_y , bh for A , and $2l$ for L (they used half spans), yields:

$$\frac{i^2}{N \rho \sigma_y h^2} = \left(\frac{h}{l} \right) \left(\frac{w_0}{l} \right) \quad \left(\begin{array}{l} \text{impulsive realm} \\ \text{rectangular beam bending} \end{array} \right) \quad (47)$$

All of the beams tested by Florence and Firth had an l/h ratio of 36, so this comparison is made by plotting $\frac{i}{h\sqrt{N\rho\sigma_y}}$ versus $\frac{w_0}{l}$. All beams are impulsively loaded using sheet explosive. Both clamped and pinned beams made of 2024-T4 aluminum, 6061-T6 aluminum, 1018 cold rolled steel, and 1018 annealed steel are included in this comparison. Figure 9 demonstrates the validity of Eq. (47) and this analysis procedure.

Because we have no data for clamped beams or simply-supported beams in the quasi-static realm, we will not develop the equations, but will give the results. Because the clamped beam in bending is 8/3 times Eq. (42) for simply-supported bending, we can write:

$$\frac{pbL^2}{M_y} = 12N^{1.415} \quad \left(\begin{array}{l} \text{quasi-static realm} \\ \text{beam bending} \end{array} \right) \quad (48)$$

where

$N = 1$ simply-supported beam

$N = 2$ clamped beam

CIRCULAR PLATE (BENDING AND EXTENSIONAL BEHAVIOR)

The next solution that we will evaluate is for the residual mid-point deformation in uniformly impulsed clamped circular plates. This problem adds an additional term to the strain energy expression, as both bending and extensional action will be present. An appropriate assumed deformed shape for a clamped plastically deformed circular plate is:

$$w = \frac{w_0}{2} \left(1 + \cos \frac{\pi r}{R} \right) \quad (49)$$

The deformed shape is being described by a radial (radius r and angle θ) coordinate system with its origin at the center of the plate. Because of symmetry, the deformed shape is independent of the angle θ . Equation (49) meets the appropriate boundary conditions for a clamped circular plate in that at the center with $r = 0$, w is a maximum deformation of w_0 , and $\frac{dw}{dr} = 0$ while at the edge of the plate with $r = R$, $w = 0$ and $\frac{dw}{dr} = 0$. An inflection point occurs at $r = \frac{R}{2}$ when the curvature changes from negative to positive for increasing values of r .

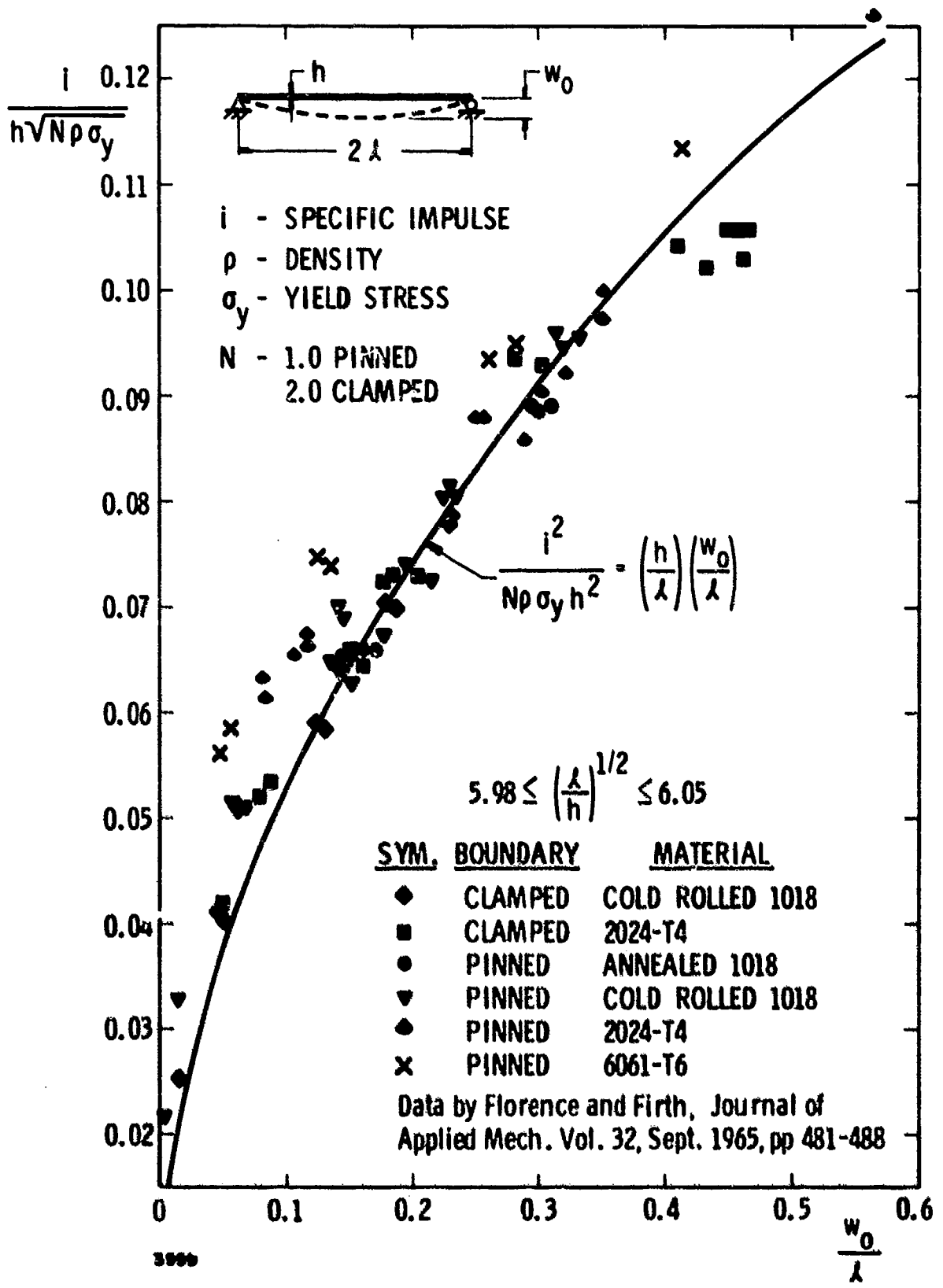


Figure 9. Beam Bending In The Impulsive Loading Realm

Because no change in length occurs circumferentially, there is no circumferential strain and no circumferential strain energy in a clamped circular plate. The radial strain energy per unit volume equals the stress σ times the strain ϵ in any structural element. If we assume that the plate is yielding, the stress σ must equal the yield stress σ_y in a rigid plastic constitutive relationship, and if plane sections remain plane, the bending strain for small deformations is given by $-z \frac{d^2 w}{dr^2}$ where z is the plate coordinate perpendicular to the r and θ coordinates. To compute the bending strain energy contribution U_b , create a circular differential torus of circumference $2\pi r$, thickness dz , and width dr . The differential bending strain energy dU_b equals this volume times σ_y times $-z \frac{d^2 w}{dr^2}$. The total bending strain energy U_b is obtained by integrating the differential strain energy over the plate thickness and plate radius. Equation (50) describes this mathematical procedure.

$$U_b = \int_{-h/2}^{+h/2} \int_0^{R/2} (2\pi r dr dz) (\sigma_y) \left(-z \frac{d^2 w}{dr^2} \right) + \int_{-h/2}^{+h/2} \int_{R/2}^R (2\pi r dr dz) (-\sigma_y) \left(-z \frac{d^2 w}{dr^2} \right) \quad (50)$$

Equation (50) must be integrated in parts because the sign of the bending stress changes at the inflection point which is located at $R/2$. Differentiating Eq. (49), substituting it into Eq. (50), and integrating over dz plus dr then yields:

$$U_b = \frac{\pi^2 \sigma_y h^2 w_0}{4} \quad (51)$$

Next we estimate the extensional strain energy U_e through a similar procedure. Extensional strains in a circular plate are generally given by $\epsilon = \sqrt{1.0 + \left(\frac{dw}{dr}\right)^2} - 1.0$. Using the binomial expansion and retaining only the first two terms leads to the approximate expression for extensional strains, $\epsilon \approx \frac{1}{2} \left(\frac{dw}{dr}\right)^2$. We will use the same differential torus to compute extensional strain energy as was used to compute bending strain energy. The total extensional strain energy U_e is obtained by integrating the differential volume times σ_y times $\frac{1}{2} \left(\frac{dw}{dr}\right)^2$ over plate thickness and plate radius. Equation (52) mathematically describes this procedure for obtaining extensional strain energy.

$$U_e = \int_{-h/2}^{+h/2} \int_0^R (2\pi r dr dz) (\sigma_y) \left(\frac{1}{2} \left[\frac{dw}{dr} \right]^2 \right) \quad (52)$$

Differentiating Eq. (49), substituting it into Eq. (52), and integrating yields:

$$U_e = \frac{\pi^3 \sigma_y h w_o^2}{16} \quad (53)$$

The total strain energy U is the sum of U_e (Eq. (53)) and U_b (Eq. (51)), or:

$$U = \frac{\pi^2}{4} \sigma_y h^2 w_o^2 + \frac{\pi^3}{16} \sigma_y h w_o^2 \quad (54)$$

The kinetic energy KE for a uniformly applied impulsive load imparted to the plate is obtained just as it was for a beam, by summing up the impulse squared divided by two times the incremental mass over the surface of the entire plate. This summation leads to the following integration.

$$KE = \int_0^R \frac{i^2 (2\pi r)^2 (dr)^2}{2 \rho h (2\pi r) (dr)} \quad (55)$$

or:

$$KE = \frac{\pi i^2 R^2}{2 \rho h} \quad (56)$$

Equating U (Eq. (54)) to KE (Eq. (56)) yields the asymptote for the impulsive loading realm.

$$\left[\frac{iR}{\sqrt{\rho \sigma_y} h^2} \right]^2 = \frac{\pi}{2} \left(\frac{w_o}{h} \right) + \frac{\pi^2}{8} \left(\frac{w_o}{h} \right)^2 \left(\begin{array}{l} \text{impulsive realm} \\ \text{clamped circular} \\ \text{plate} \end{array} \right) \quad (57)$$

A comparison between Eq. (57) for a uniform impulse on a clamped circular plate and experimental test data can be made using test results by Florence.^[14] Residual permanent mid-span deformations were measured on both clamped circular 6061-T6 aluminum plates and 1018-cold rolled steel plates that had been loaded uniformly with various layers of sheet explosive. The 22 aluminum data points, 20 steel data points, and Eq. (57) are all shown in Figure 10. Once again the validity of this solution and analysis procedure are substantiated. If there exists a systematic error, it is a tendency for the analytical

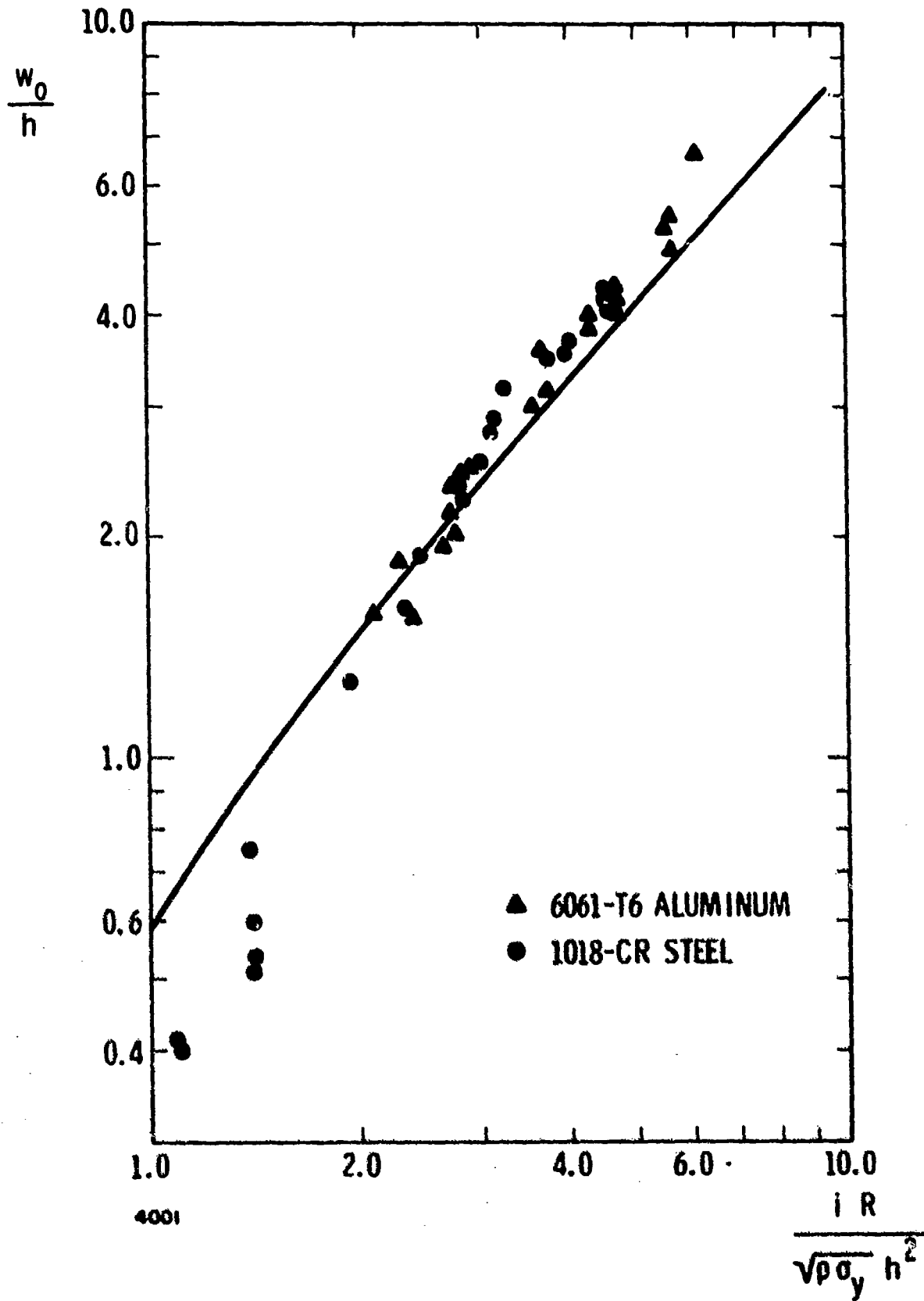


Figure 10. Comparison Of Equation 84 With Experimental Plate Data

curve to slightly underestimate deformations whenever $\frac{w_0}{h}$ is large. This error is probably caused by the assumed deformed shape not yielding the minimum strain energy. For small values of $\frac{w_0}{h}$, the analytical curve overestimates deformations. This error is created because we assume that deformations extend over the entire span of the plate. When loads are small and deformations small, the deformed shape covers only a portion of the entire plate.

RECTANGULAR PLATE (ADDITION OF SHEARING STRAINS)

The final solution that we will develop is for the plastic response of rectangular plates from uniformly applied transverse impulses. This solution introduces a new complication associated with a lack of radial symmetry and the bending plus extensional shearing forces that are created thereby. For a clamped-clamped uniformly loaded rectangular plate, we will assume a deformed shape given by:

$$w = \frac{w_0}{4} \left(1 + \cos \frac{\pi x}{X} \right) \left(1 + \cos \frac{\pi y}{Y} \right) \quad (58)$$

where

X and Y are half spans

x and y are the rectangular coordinate system with its origin in the center of the plate.

This assumed deformed shape meets the appropriate deflection and slope criteria in the middle of the plate and along all boundaries. Lines of inflection occur at $y = \frac{Y}{2}$ and $x = \frac{X}{2}$. The strain energy per unit volume in a structural element under a biaxial state of stress is:

$$\frac{U}{\text{Vol.}} = \int_{\text{strains}} \left[\sigma_{xx} d\epsilon_{xx} + 2\sigma_{xy} d\epsilon_{xy} + \sigma_{yy} d\epsilon_{yy} \right] \quad (59)$$

Because we have yielding, we will assume that $\sigma_{xx} = \sigma_y$ and $\sigma_{yy} = \sigma_y$, but for the shearing stress we will use a Huber-Mises-Hencky distortion energy yield criteria of $\sigma_{xy} = \frac{\sigma_y}{\sqrt{3}}$. The normal bending strains are as in the circular plate problem with $\epsilon_{xx} = -z \frac{\partial^2 w}{\partial x^2}$ and $\epsilon_{yy} = -z \frac{\partial^2 w}{\partial y^2}$. The bending shearing strain $\epsilon_{xy} = 2z \frac{\partial^2 w}{\partial x \partial y}$. The bending strain energy U_b is then given by:

$$U_b = 8 \int_0^{h/2} dz \int_0^X dx \int_0^Y dy \sigma_y \left(-z \frac{\partial^2 w}{\partial x^2} - z \frac{\partial^2 w}{\partial y^2} \right) + 8 \int_0^{h/2} dz \int_0^X dx \int_0^Y dy \left(2 \frac{\sigma_y}{\sqrt{3}} \right) \left(2z \frac{\partial^2 w}{\partial x \partial y} \right) \quad (60)$$

The bending strain energy contributions from the normal stress and strains must be obtained by four part integration (from 0 to $\frac{X}{2}$ and 0 to $\frac{Y}{2}$, from $\frac{X}{2}$ to X and 0 to $\frac{Y}{2}$, from 0 to $\frac{X}{2}$ and $\frac{Y}{2}$ to Y, plus from $\frac{X}{2}$ to X and from $\frac{Y}{2}$ to Y) because the lines of inflection change the sign of the stress. Differentiating Eq. (58), substituting it into Eq. (60), and performing the triple integration then yields:

$$U_b = \frac{\pi}{2} \sigma_y h^2 w_o \left[\frac{Y}{X} + \frac{X}{Y} \right] + \frac{4}{\sqrt{3}} \sigma_y h^2 w_o \quad (61)$$

The first term on the right hand side of Eq. (61) is the contribution from the normal bending strains, and the second term is the contribution from the bending shear strains.

Equation (59) applies to the extensional response as well as bending response. The normal extensional strains are as in the circular plate problem with $\epsilon_{xx} = \frac{1}{2} \left(\frac{\partial w}{\partial x} \right)^2$ and $\epsilon_{yy} = \frac{1}{2} \left(\frac{\partial w}{\partial y} \right)^2$. The extensional shearing strain $\epsilon_{xy} = \left(\frac{\partial w}{\partial x} \right) \left(\frac{\partial w}{\partial y} \right)$ as a first approximation. These additional observations mean that the extensional strain energy U_e is given by:

$$U_e = 4 \int_0^X dx \int_0^Y dy \int_0^h dz \sigma_y \left[\frac{1}{2} \left(\frac{\partial w}{\partial x} \right)^2 + \frac{1}{2} \left(\frac{\partial w}{\partial y} \right)^2 \right] + 4 \int_0^X dx \int_0^Y dy \int_0^h dz \left(\frac{2\sigma_y}{\sqrt{3}} \right) \left(\frac{\partial w}{\partial x} \right) \left(\frac{\partial w}{\partial y} \right) \quad (62)$$

Differentiating Eq. (58), substituting it into Eq. (62), and performing the triple integration yields:

$$U_e = \frac{3\pi^2}{32} \sigma_y h w_o^2 \left[\frac{Y}{X} + \frac{X}{Y} \right] + \frac{8}{\sqrt{3}} \sigma_y h w_o^2 \quad (63)$$

The total strain energy U is then the sum of U_e (Eq. (63)) and U_b (Eq. (61)), or:

$$U = \frac{\pi}{2} \sigma_y h^2 w_o \left[\frac{Y}{X} + \frac{X}{Y} \right] + \frac{4}{\sqrt{3}} \sigma_y h^2 w_o + \frac{3\pi^2}{32} \sigma_y h w_o^2 \left[\frac{Y}{X} + \frac{X}{Y} \right] + \frac{8}{\sqrt{3}} \sigma_y h w_o^2 \quad (\text{clamped plate}) \quad (64)$$

The strain energy in a simply-supported plate can also be estimated using the same procedure, with an assumed deformed shape described by:

$$w = w_o \cos \frac{\pi X}{2X} \cos \frac{\pi Y}{2Y} \quad (65)$$

The previous procedure gives as a value for the strain energy U ,

$$U = \sigma_y h^2 w_o \left[\frac{Y}{X} + \frac{X}{Y} \right] + \frac{4}{\sqrt{3}} \sigma_y h^2 w_o + \frac{\pi^2}{8} \sigma_y h w_o^2 \left[\frac{Y}{X} + \frac{X}{Y} \right] + \frac{4}{\sqrt{3}} \sigma_y h w_o^2 \quad (\text{s. s. plate}) \quad (66)$$

Notice that Eq. (66) for strain energy in a simply-supported plate is similar to Eq. (64) for strain energy in a clamped plate. The only difference in these equations is in the numerical values of the coefficients which accompany each term on the right hand side of these expressions. This observation means that if we insert a coefficient N that is equal to 1.0 for simply-supported plate and equal to 2.0 for clamped plates, a general strain energy equation can be written as in Eq. (67).

$$U = \frac{\pi^{N-1}}{N} \sigma_y h^2 w_o \left[\frac{Y}{X} + \frac{X}{Y} \right] + \frac{4}{\sqrt{3}} \sigma_y h^2 w_o + \frac{3^{N-1} \pi^2}{8 N^2} \sigma_y h w_o^2 \left[\frac{Y}{X} + \frac{X}{Y} \right] + \frac{4N}{\sqrt{3}} \sigma_y h w_o^2 \quad (67)$$

The kinetic energy KE imparted to a plate is not dependent upon the deformed shape. For a uniformly applied impulsive load imparted to a plate, the kinetic energy is obtained (as it was for a circular plate) by summing up the impulse squared divided by two times the incremental mass over the surface of the plate. The appropriate integration is given by:

$$KE = 4 \int_0^X \int_0^Y \frac{i^2 (dx)^2 (dy)^2}{2 \rho h (dx) (dy)} \quad (68)$$

or

$$KE = \frac{2i^2 XY}{\rho h} \quad (69)$$

Equating Eq. (67) and Eq. (69) finally yields a general rectangular plate equation for deformations caused by uniform impulsive loads. The following equation is this relationship.

$$\left[\frac{iX}{\sqrt{\rho \sigma_y} h^2} \right]^2 = \frac{\pi^{N-1}}{2N} \left[1 + \left(\frac{X}{Y} \right)^2 \right] \left(\frac{w_o}{h} \right) + \frac{2}{\sqrt{3}} \left[\frac{X}{Y} \right] \left(\frac{w_o}{h} \right) + \frac{3^{N-1} \pi^2}{16N^2} \left[1 + \left(\frac{X}{Y} \right)^2 \right] \left(\frac{w_o}{h} \right)^2 + \frac{2N}{\sqrt{3}} \left[\frac{X}{Y} \right] \left(\frac{w_o}{h} \right)^2 \quad (70)$$

We will demonstrate the validity of this solution by using clamped ($N = 2$) rectangular plate data reported by N. Jones, T. O. Uran, and S. A. Tekin.^[15] Rectangular plates with an aspect ratio $\left(\frac{Y}{X} \right)$ equal to 1.695 were loaded with sheet explosive in these experiments. Both hot-rolled mild steel plates and 6061-T6 aluminum plates were tested and can be seen plotted in Figure 11. Equation (69) is also shown in Figure 11; however, left and right sides of Eq. (69) were multiplied by $\left(\frac{Y}{X} \right)^2$ to cast it into the format of their data. Excellent correlation appears in Figure 11 when Eq. (70) is compared to experimental test results.

Unfortunately, no experimental quasi-static loading realm data exist on dynamically loaded, plastically deformed plates, simply-supported beams, or clamped beams. The analytical solution is easily developed for a plate. The work WK performed on either simply-supported or clamped plates is obtained by integrating $p w dx dy$ and equals:

$$WK = \frac{\pi^{2(N-2)}}{16^{N-2}} p w_o X Y \quad (71)$$

When this work is equated to the general strain energy expression, Eq. (67), we obtain the solution for the quasi-static loading realm of rectangular plates.

$$\frac{p}{\sigma_y} \left(\frac{X}{h} \right)^2 = \frac{\pi^{2/N}}{2^4/N^2} \left[1 + \left(\frac{X}{Y} \right)^2 \right] + \frac{4^{(2N-3)}}{\sqrt{3} \pi^{2(N-2)}} \left[\frac{X}{Y} \right] + \frac{3^{(N-1)} 4^{(N-2)} \pi^{2(3-N)}}{32} \left[1 + \left(\frac{X}{Y} \right)^2 \right] \left(\frac{w_o}{h} \right) + \frac{2^{(N-1)} 4^{(2N-3)}}{\sqrt{3} \pi^{2(N-2)}} \left[\frac{X}{Y} \right] \left(\frac{w_o}{h} \right) \quad (72)$$

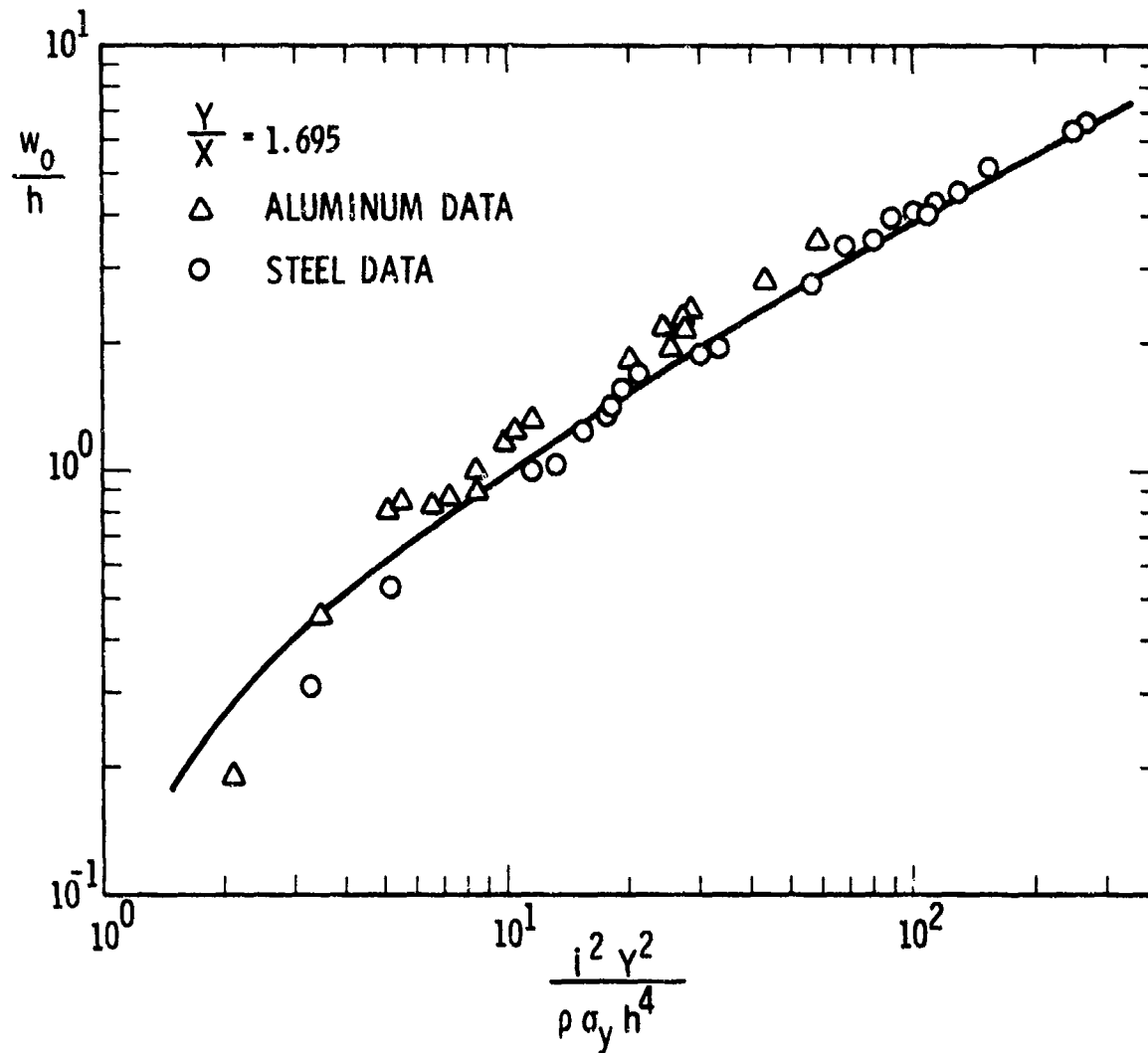


Figure 11. Predicted and Experimental Deformations in Uniformly Loaded Rectangular Plates

RESUME

These procedures and the resulting formulae comprise the structural analysis approach that was used by SwRI to control deformations in the design of a plastically-yielding, blast-suppressing structure. This analysis procedure yields explicit expressions for nondimensional deformations in terms of nondimensional loading parameters. If other deformed shapes were to be assumed, the same nondimensional parameters would occur and would be to the same powers; however, the numerical coefficients preceding each term would have other values. These analyses can also be applied to shell type structures with no more difficulty than was demonstrated in the development of the plate solutions. The approach is attractive because no involved solutions to complex differential equations are required--only integrations of work, kinetic energy, and strain energies are needed for a given structural element.

The illustrations shown in this paper have included a single-degree-of-freedom plastic rheological model, an elastic rheological model, elastic cantilever beams, plastic cantilever beams, plastic simply-supported beams, plastic clamped beams, plastic clamped circular plates, plastic simply-supported rectangular plates, and plastic clamped rectangular plates. Experimental test data obtained by other investigators have been used to demonstrate the validity of these solutions, especially in the impulsive loading realm. It is interesting to note that all plastic beam solutions have the functional formats

$$\frac{i^2 L^2}{\rho \sigma_y h^3} = f\left(\frac{w_o}{L}\right) \quad \left(\begin{array}{l} \text{impulsive realm} \\ \text{any beam} \end{array} \right) \quad (73)$$

and

$$\frac{p L^2}{\sigma_y h^2} = \text{constant} \quad \left(\begin{array}{l} \text{quasi-static realm} \\ \text{any beam} \end{array} \right) \quad (74)$$

As extensional behavior is developed by elements such as plates, these general functional formats are:

$$\frac{i^2 X^2}{\rho \sigma_y h^4} = f\left(\frac{Y}{X}, \frac{w_o}{h}\right) \quad \left(\begin{array}{l} \text{impulsive realm} \\ \text{plates} \end{array} \right) \quad (75)$$

and

$$\frac{p X^2}{\sigma_y h^2} = f\left(\frac{Y}{X}, \frac{w_o}{h}\right) \quad \left(\begin{array}{l} \text{quasi-static realm} \\ \text{plates} \end{array} \right) \quad (76)$$

One could use experimental test data that had been nondimensionalized to graphically present solutions following these formats.

ACKNOWLEDGEMENTS

This paper is a result of work performed under two different contracts with two different agencies. We have been studying suppressive structure behavior for Mr. Paul King at Edgewood Arsenal and Dr. John Coutinho at the Army Materiel Systems Analysis Agency under Contract DAAD05-74-C-0751 with AMSAA. Other illustrations were developed for Mr. John Hennessey under Contract DAAE07-74-C-0192 with the U. S. Army Tank Automotive Command. The cooperation of these individuals and others at their agencies and SwRI is appreciated.

REFERENCES

1. E. H. Lee and P. S. Symonds, "Large Plastic Deformation of Beams Under Transverse Impact," J. Appl. Mech., Vol. 19, No. 3, 1952, p. 308.
2. S. R. Bodner and P. S. Symonds, "Plastic Deformations In Impact and Impulsive Loading of Beams," Plasticity, Pergamon Press, 1960, pp. 488-500.
3. S. R. Bodner and P. S. Symonds, "Experimental and Theoretical Investigations of the Plastic Deformation of Cantilever Beams Subjected to Impulsive Loading," J. Appl. Mech., Vol. 29, No. 4, 1962, pp. 719-728.
4. J. B. Martin, "On the Application of the Bounding Theorems of Plasticity to Impulsively Loaded Structures," Dept. of Navy Contract N00014-67-A-0191-0003, Tech. Rept. 13, with Brown Univ., July 1971.
5. J. B. Martin, "Extremum Principles for a Class of Dynamic Rigid-Plastic Problems," Dept. of Navy Contract N00014-67-A-0191-0003, Tech. Rept. 14, with Brown Univ., August 1971.
6. N. Jones, "Influence of Strain-Hardening and Strain-Rate Sensitivity on the Permanent Deformation of Impulsively Loaded Rigid-Plastic Beams," Advanced Research Projects Agency Contract SD-86, with Brown Univ., July 1967.
7. J. E. Greenspon, "Plastic Behavior of Control Surfaces and Plates Subjected to Air Blast Loading, Part 2, Detailed Analysis and Numerical Results for Beam Type Structures," Contract No. DA36-034-ORD-3081RD with BRL, March 1962.

REFERENCES (Cont'd)

8. J. E. Greenspon, "Plastic Behavior of Control Surfaces and Plates Subjected to Air Blast Loading, Part 1, Simplified Theoretical Relations," Contract No. DA36-034-ORD-3081RD with BRL, Nov. 1960.
9. J. E. Greenspon, "Prediction of Iso-Damage Curves," Contract No. DAAD05-67-C-0331 with BRL, July 1967.
10. J. E. Greenspon, "Elastic-Plastic Response of Structures to Blast and Impulse Loads," Contract No. DA-18-001-AMC-1019(X) with BRL, March 1967.
11. J. E. Greenspon, "Theoretical Calculations of Iso-Damage Characterizations," Contract No. DAAD05-69-C-0116 with BRL, Feb. 1960.
12. W. E. Baker, W. O. Ewing, Jr., and J. W. Hanna, "Laws for Large Elastic and Permanent Deformation of Model Structures Subjected to Blast Loading," BRL Report No. 1060, Dec. 1958.
13. A. L. Florence and R. D. Firth, "Rigid-Plastic Beams Under Uniformly Distributed Impulses," J. Appl. Mech., 32, Series E, 1, March 1965, pp. 7-10.
14. A. L. Florence, "Circular Plate Under a Uniformly Distributed Impulse," J. Solids and Structures, 2, 1966, pp. 37-47.
15. N. Jones, T. O. Uran, and S. A. Tekin, "The Dynamic Plastic Behavior of Fully Clamped Rectangular Plates," Int. Jour. Solids Structures, 6, 1970, pp. 1499-1512.

ESTIMATES OF FRAGMENTATION HAZARDS FOR SELECTED SUPPRESSIVE SHIELDING APPLICATIONS

JOHN H. KINEKE JR.
BALLISTIC RESEARCH LABORATORIES
ABERDEEN PROVING GROUND, MD 21005

INTRODUCTION

Suppressive shielding is currently being examined by the Army as a design option for the containment of hazards which can result from an accidental high explosive detonation. Hazards generally can be bi-classified as products in the gaseous state and products in the solid state. Each hazard class leads to its peculiar threats and thus each must be assessed during a shielding design exercise. Gaseous products, the fireball and detonation products, can induce blast loading and failure of the containing structure, fire, undesired overpressure outside the containing structure, and earth excavation. Solid products, metal fragments, represent a penetration and perforation threat.

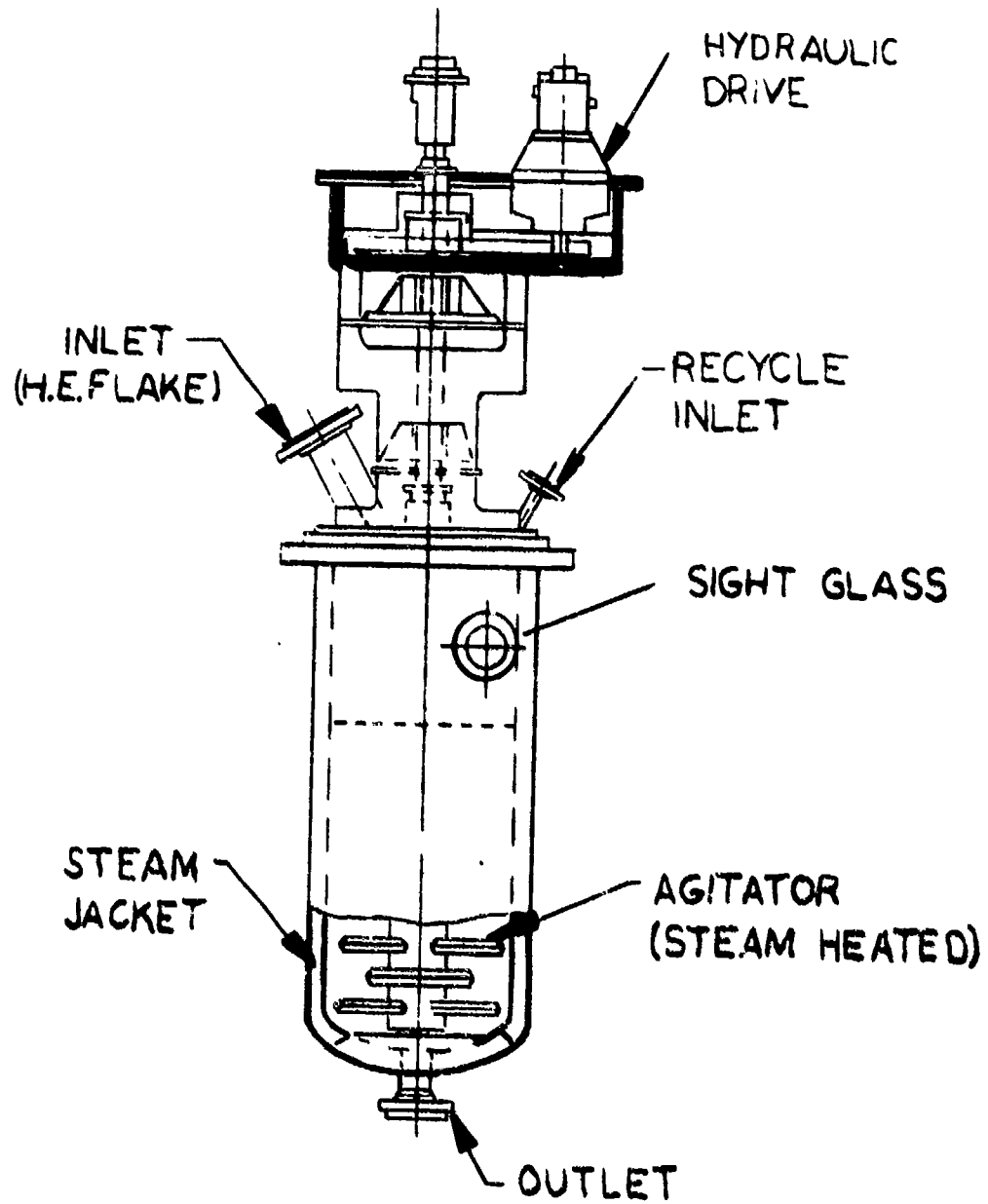
This paper is concerned with the assessment of fragment hazards from accidental detonations. These hazards are typed as either primary fragments or secondary fragments. Primary fragments are defined as those which originate from material essentially in intimate contact with the explosive, such as the casing of an explosive-filled artillery shell, or the walls of an explosive melt kettle. Secondary fragments are defined as material, usually metal, proximate to the explosive but not in contact with it, which could undergo substantial acceleration. In either case a penetration threat obtains.

In the following sections primary and secondary fragment hazards are illustrated by example. In each case the procedures will be indicated by which the characteristics of the fragments: speed, mass and shape, are estimated. In addition, for each an estimate of threat in terms of penetration into monolithic steel will be described. In assessing both hazards and threats a worst case philosophy has been adopted.

PRIMARY FRAGMENTS

High explosive warheads are of course the principal source of primary fragments. Their characteristics are available to anyone who would consult the Joint Munitions Effectiveness Manual. On the other hand explosive melt kettles are usually not evaluated for their fragmentation potential. One such is the melt-pour operation on the proposed 105mm load, assembly and packout line at the Lone Star Army Ammunition plant.

The kettle, illustrated in Figure 1, is supposed to contain about 900 kilograms of Composition B. About 6.1 meters tall, filled, usually nearly to the top, with liquid explosive and surrounded with a steam



PORCUPINE PROCESSOR
 (CONTINUOUS TYPE MELTER)
 FIGURE 1

jacket, it contains a concentric agitator hub, also steam-bearing, and agitator blades. All available details of construction are shown in Figure 2. Wherever an initiation may commence, fragments will result.

Since the quantity of explosive present is variable and no information was available on the state variables of the steam contained in the jacket and in the agitator, only a simplistic statement can be made for those fragments originating from the lower explosive-filled portion of the kettle.

The ratio of explosive mass to metal mass for the kettle is given by:

$$\frac{C \rho_{HE} (r_1^2 - r_a^2)}{M \rho_{steel} (r_2^2 - r_1^2 + r_4^2 - r_3^2)} = 1.024 \quad (1)$$

where $\rho_{HE} = 1.75 \text{ gm/cm}^3$

$\rho_{steel} = 7.8 \text{ gm/cm}^3$

Implicit in this calculation is the assumption that the melter wall, given a high order detonation, will expand without fracture, at least until it contacts the steam jacket, requiring an expansion ratio $r_3/r_2 = 1.2$. This compares with an expansion ratio at fracture for

most metal in an internally loaded cylindrical warhead configuration of 1.5 to 2; thus it is a relatively safe assumption.

Two limit calculations of fragment speed have been performed. The simpler calculation ignores the presence of the agitator, other than the fact that it reduced the volume of the explosive by 17%, which is reflected in the C/M above. In this case:

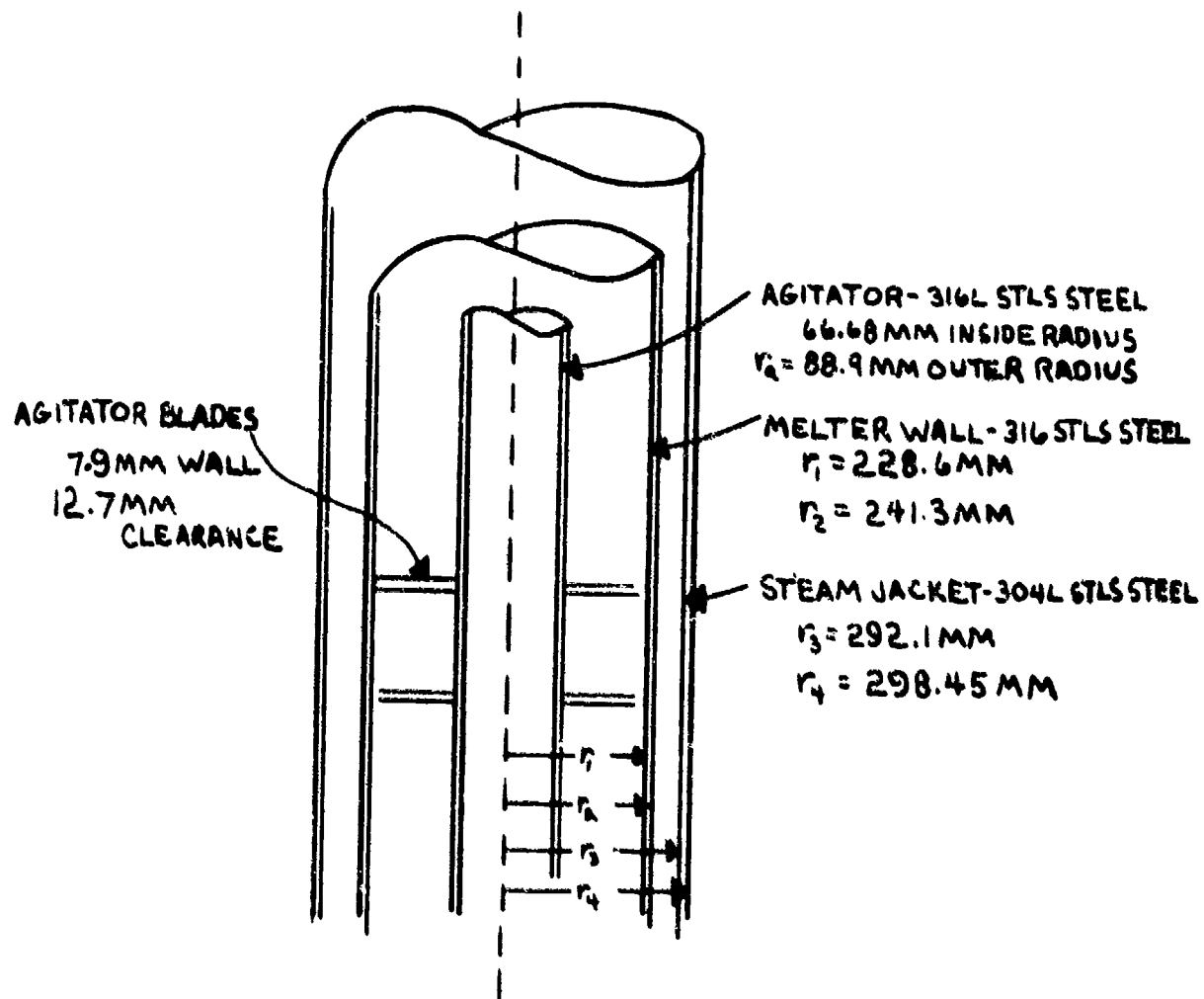
$$V = \sqrt{2E} \sqrt{\frac{C/M}{1 + C/2M}} = 2.14 \text{ km/sec} \quad (2)$$

where $\sqrt{2E} = 2.0 \text{ km/sec}$ for Composition B. A second calculation, treating the agitator as rigid yields

$$V = \sqrt{2E} \sqrt{\frac{C/M}{1 + (C/2M) \frac{3 + A_r}{2(1 + A_r)}}} = 2.18 \text{ km/sec} \quad (3)$$

where $A_r = 1.6$ = the expansion ratio at which fracture occurs. In either case, since no energy consumption in compressing the agitator and the steam contained therein, nor in compressing the steam in the outer jacket has been accounted for, the maximum fragment speeds might be expected to be 5 to 10% less.

Representing the melt kettle as a relatively thin-walled cylinder, both tensile and shear fracture mechanisms, due to circumferential (hoop) stress and the resultant of circumferential stress and radial compressive stress, can be operative. Invoking a dominant shear fracture mechanism, with no debilitation of fragment cross-section by tensile fracture



PORCUPINE PROCESSOR DETAIL
 FIGURE 2

leads to a worst case fragment cross-section of 362.9mm^2 . For reasonably equiaxed (i.e. chunky) fragments then the mean dimensions will be

$$\sqrt{\frac{4A}{\pi}}, \text{ producing a mass of:} \\ m (\text{chunky}) = \rho_{\text{steel}} A \sqrt{\frac{4A}{\pi}} = 60.8\text{gm.} \quad (4)$$

Since fracture propagation in an axial direction for internally-loaded warheads frequently leads to sliver-shaped fragments with a fineness ratio (f) up to approximately ten, a worst case rod-like fragment mass can be estimated.

$$m (\text{rod-like}) = \rho_{\text{steel}} f A \sqrt{\frac{4A}{\pi}} = 608 \text{ grams.} \quad (5)$$

Based on the estimated worst case fragment masses and speeds, maximum fragment energies of 134 kilojoules for chunky fragments and 1340 kilojoules for rod-like fragments are calculated.

Numerous empirical correlations of the penetration capability of steel fragments striking mild steel targets are extant. Chosen for estimating the penetration which could be achieved by the postulated chunky fragment is a regression due to Tolch and Bushkovitch (reference 1):

$$P = 4.55m^{1/3}v^{4/3}\cos\theta \quad (6)$$

where P = penetration in mm

m = fragment mass in gm

v = fragment speed in km/sec

θ = impact obliquity from target normal

Penetration estimated with equation (6) involves an extrapolation of its range of validity from 1.2km/sec, the upper limit of the data from which it was derived, to 2.1km/sec; thus into a regime where penetration would be expected to become less strongly dependent upon the impact speed than the $4/3$ power, but not less than the $2/3$ power. Using a $4/3$ power computation at 1.2km/sec to anchor a $2/3$ power relation yields, then, a lower limit estimate for the penetration threat of a chunky fragment.

Use of a worst case philosophy with the rod-like fragments requires that the assumption be made that at, least in some cases, they strike with negligible yaw (i.e. end-on). Grabarek (ref. 2) provides a means of calculating the perforation capability of non-yawed rods against rolled homogeneous armor targets in terms of limit speed:

$$V_L = \left[\frac{B D^3 ((P \sec \theta) / D)^{1.6}}{m} \right]^{1/2} \quad (7)$$

where V_L = protection ballistic limit in m/sec

D = rod diameter in mm

P = thickness of armor perforated in mm

m = rod mass in gm

θ = impact obliquity from target normal

B = empirical constant dependent on rod hardness.

With manipulation and use of

$$m = \frac{\pi}{4} \rho D^3 f \quad (8)$$

where f = length-to-diameter ratio of the rod

P can be expressed in terms of f: $P = D \cos \theta \left[\frac{\pi \rho f V_L^2}{4B} \right]^{5/8}$ (9)

Then, the dependence of perforable thickness on f can be written

$$P(f) = (f)^{5/8} P(f=1) \quad (10)$$

Fragment Characteristics are summarized below:

SHAPE	CHUNKY	ROD-LIKE (f = 10)
SPEED (MAX)	2.1 KM/SEC	2.1 KM/SEC
MASS	61 GM	608 GM
ENERGY	234 KJ	1340 KJ
Steel Protection Thickness Required	32-48 mm	135-205mm (end-on impact)

Consideration of steel protection thickness required must be coupled with the scenario, thus necessitating estimation of the direction in which fragments will be launched. For a spectrum of potential initiation sites for detonation an upper limit to fragment polar projection angle, measured from the normal to the kettle surface should be no more than ten degrees, since the melt kettle is a right circular cylinder. Thus if the kettle were located below grade, no fragment protection would be required for those fragments originating from the explosive-filled portion of the kettle. On the other hand, an above-grade placement would require steel protection upwards of 200mm in thickness. It should be pointed that the fragment hazard described is only one aspect of the total potential hazard. Located at the top of the kettle are the explosive flake inlet and recycle inlets, together with the drive for the agitator. This initial assessment was conducted with a dearth of information on the geometry, mass distribution and materials at the top of the kettle. Similarly, the ullage region of the kettle has not been treated. Certainly in the ullage portion fragment speeds will be substantially less than those of the explosive-filled portion. However, the less severe impetus, which leads to these lower speeds, perforce leads to diminished comminution and thus a potentially more severe frag-

ment penetration threat. It is unlikely that this hazard can be evaluated without a series of experiments designed to elicit the size distribution of ullage fragments.

SECONDARY FRAGMENTS

An example of a secondary fragment hazard is illustrated in Figure 3. An M-374 81mm mortar shell is shown on a pallet during a fuze cavity facing operation. The warhead itself is a source of primary fragments whose characteristics are documented in JMEM. The worst of these would acquire a translational energy of about 13 kilojoules. External to the shell, however, are potential secondary fragments in the form of the roller support and the roller rod.

Because of their threatening shape the rollers could present a serious penetration threat. Used to support the shell on the pallet the rollers intersect the shell periphery slightly below a horizontal cross section. The rollers are fabricated of Delrin ($\rho_o = 1.14\text{gm/cm}^3$), concentrically located on a steel rod. Since the roller-rod complex is contiguous with the shell case, an energy-based (Gurney) calculation of the rod speed should satisfy a worst case philosophy.

An effective ratio of explosive mass to metal mass for the roller is given by:

$$\frac{c}{M} = \frac{\text{operative mass of explosive per unit length}}{\text{operative mass of case per unit length} + \frac{m_{r1} + m_{rd}}{L_{rd}}} \quad (11)$$

$$= \frac{\frac{\alpha}{2\pi} \rho_{HE} R_1^2}{\frac{\alpha}{2\pi} \rho_c (R_2^2 - R_1^2) + \frac{\rho_{r1}(r_{r1}^2 - r_{rd}^2) L_{r1} + \rho_{rd} r_{rd}^2 L_{rd}}{L_{rd}}} \quad (12)$$

$$= 0.194$$

where: $\frac{\alpha}{2\pi}$ = effective fractional azimuthal sector occupied by the rod-roller complex = 0.1

$$\rho_{HE} = \text{density of Composition B} = 1.75\text{gm/cm}^3$$

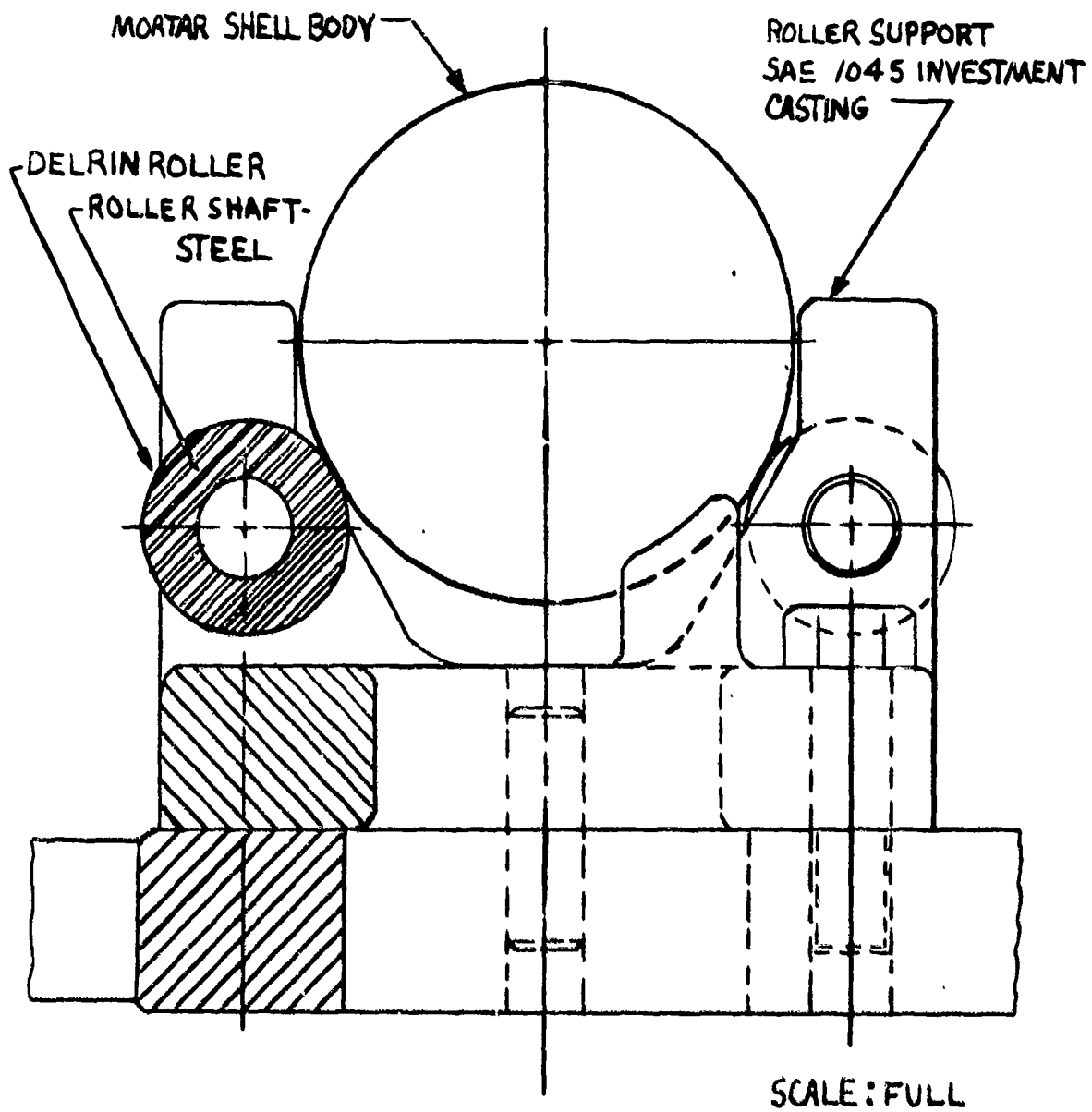
$$\rho_{r1} = \text{density of roller} = 1.14\text{gm/cm}^3$$

$$\rho_{rd} = \text{density of rod} = 7.8\text{gm/cm}^3$$

$$\rho_c = \text{density of case} = 7.8\text{gm/cm}^3$$

$$R_2 = \text{outer case radius} = 3.947\text{cm}$$

$$R_1 = \text{inner case radius} = 3.348\text{cm}$$



81mm MORTAR SHELL HOLDER - PALLET END VIEW
FIGURE 3

r_{rd} = radius of rod = 1.588cm

r_{rl} = outside radius of roller = 3.492cm

L_{rd} = length of rod = 8.255 cm

The secondary fragment hazard, then, calculated with this simplistic model, can be defined as a steel rod of mass 127.5gm with a potential upper limit on speed of 1.1km/sec. Realistically, the 77 kilojoules assigned to the rod by this approach is probably an overestimation. More reasonably, a kinetic energy less than one-fifth is probably justifiable, if a momentum approach had been pursued. However, continuing to follow the worst case philosophy, the penetration threat represented by the higher energy can be determined. With the assumptions that the Delrin roller does not participate in the penetration process, and that the rod could strike a shield in a non-yawed condition, with no obliquity, application of equations (6) and (10) lead to a predicted penetration threat of 47mm.

CONCLUSIONS

Care should be taken, in the design of suppressive shielding, to give due consideration to both blast and fragment hazards, in order to avoid, a serious underestimation of the protection afforded by a candidate structure. The cursory examinations of primary and secondary fragment hazards described in this paper indicate that serious penetration threats can be present in scenarios which associate metal in close proximity with high explosive charges in the context of an accidental detonation. In the current fiscal year the Ballistic Research Laboratories will be pursuing these fragment hazards as part of the Suppressive Shielding Applied Technology Program. It is anticipated that some of the gross uncertainties represented here, particularly with respect to ullage fragments and secondary fragments, will be resolved. Moreover, a set of procedures will be developed to define fragment hazards for a variety of scenarios which may become of interest.

REFERENCES

1. T-1ch N.A and Bushkovitch, A.V., "Penetration of Mild Steel by Bomb Fragments", BRLR-568, August 1945
2. Grabarek, C.L., "Penetration of Armor by Steel and High Density Penetrators", BRL MR-2134, October 1971

FRAGMENT PENETRATION ESTIMATES FOR THE 81MM SUPPRESSIVE SHIELD

Mr. C. J. Brown

Ballistic Research Laboratories, Aberdeen Proving Ground, MD

Mr. A. J. Ricchiazzi

Ballistic Research Laboratories, Aberdeen Proving Ground, MD

ABSTRACT

Penetration predictions were made for the most severe case fragment threats for an 81mm M374 mortar shell to determine the effectiveness of a lightweight suppressive structure. The equations predicted that a steel rod weighing 128 grams with a velocity of 1.09 km/sec would penetrate into the sixth plate of a six plate array for two different target arrays. Future programs are designed to check the validity of the penetration equations used in this report and if necessary to modify them or initiate the development of predictive techniques which delineate the effect of spacing.

I. INTRODUCTION

Ballistic Research Laboratories were requested by the Hazardous Material Engineering Office of the Edgewood Arsenal to provide penetration predictions into a lightweight suppressive structure by fragments from an 81mm M374 mortar shell. A hasty survey of the literature on available penetration equations was performed to determine those that would provide the best estimate of ballistic limit velocity, residual mass and residual velocity for the particular problem at hand. The fragments of concern are those emanating from artillery shell, mortar shell and fragmenting warheads which are termed primary fragments and those fragments launched which are portions of holding devices or other surrounding equipment which are called secondary fragments. The panels which provide the target configuration consist of several sheets of mild steel of varying thicknesses placed in a spaced array.

A comparison of experimental data and calculated data from existing fragment penetration equations were used as a basis of selecting the "best" equation for predicting penetration into the suppressive shield. Because of the spaced target configuration it was decided to use the residual velocity and residual mass as a basis of comparison. In the following sections the equations, panel configuration and prediction results are presented. Future goals in fragment penetration into suppressive structures is also included.

II. METHODOLOGY

A. Thor Equations

In order to calculate a first approximation of the terminal ballistic performance of a fragment against a spaced target array the residual velocity and residual mass of the fragment perforating successive spaced layers must be known. Equations were examined in the following reports: Project Thor Report TH-47¹, BRL Report Number 568² and BRL Memorandum Report Number 1777³. Estimates of residual velocity were made using the methods of reference 1, employing an equation of the following form.

$$V_R = V_S - [10^C e^D m_S^B (\sec \theta)^Y V_S^A] \quad (1)$$

where V_R = fragment residual velocity (ft/sec)

V_S = fragment striking velocity (ft/sec)

e = plate thickness (inches)

m_S = fragment striking mass (grains)

θ = angle of obliquity (angle between fragment trajectory and normal to target)

V_S = fragment striking velocity (ft/sec)

c , α , β , γ and λ are constants which are dependent on target material. In this case for mild homogeneous steel $c = 4.520$, $\alpha = 0.889$, $\beta = -0.352$, $\gamma = 1.262$ and $\lambda = 0.019$. Estimates of residual mass were performed using the methods of reference 2, employing an equation of the following form.

$$M_R = M_S - [10^c e^\alpha M_S^\beta (\sec \theta)^\gamma V_S^\lambda] \quad (2)$$

where M_R = fragment residual mass (grains)

M_S = fragment striking mass (grains)

e = plate thickness (inches)

θ = angle of obliquity (angle between fragment trajectory and normal to target)

V_S = fragment striking velocity (ft/sec)

c , α , β , γ and λ are constants which are dependent on target material. In this case for mild homogeneous steel $c = -2.798$, $\alpha = 0.138$, $\beta = 0.926$, $\gamma = 0.143$ and $\lambda = 0.761$.

B. Johnson Equations

In reference 3, a very detailed, systematic, statistical study was performed on the data to obtain regression equations. An estimate of the logarithm of the loss of velocity of a fragment perforating a target is given by:

$$\log_{10} (V_S - V_R) = b_0 + \sum_{i=1}^4 b_i \log_{10} x_i \quad (3)$$

V_S = fragments striking velocity (ft/sec)

V_R = residual velocity of the largest piece of the original fragment after perforation of the target (ft/sec)

x_1 = target thickness (inches)

x_2 = fragment striking mass (grains)

x_3 = secant of the angle of impact obliquity of the fragment (angle between fragment trajectory and normal to target)

x_4 = fragment striking velocity (ft/sec)

where b_i are parameter estimates for homogeneous mild steel

- $b_0 = 3.9064$ (coefficient estimate)
- $b_1 = 0.9496$ (target thickness coefficient estimate)
- $b_2 = -0.3603$ (striking mass coefficient estimate)
- $b_3 = 1.2842$ (impact obliquity coefficient estimate)
- $b_4 = 0.1929$ (striking velocity coefficient estimate)

An equation of this same form to estimate logarithm of the loss of mass of a fragment perforating a target is given by:

$$\log_{10} (M_S - M_R) = b_0 + \sum_{i=1}^4 b_i \log_{10} x_i \quad (4)$$

M_S = fragment original mass (grains)

M_R = fragment residual mass (grains)

x_1 = target thickness (inches)

x_2 = fragment striking mass (grains)

x_3 = secant of the angle of impact obliquity of the fragment (angle between fragment trajectory and normal to target)

x_4 = fragment striking velocity (ft/sec)

b_i are coefficient estimates for homogeneous mild steel

$b_0 = -2.2776$ (coefficient estimate)

$b_1 = 0.1885$ (target thickness coefficient estimate)

$b_2 = 0.9145$ (striking mass coefficient estimate)

$b_3 = 0.1958$ (impact obliquity coefficient estimate)

$b_4 = 0.6394$ (striking velocity coefficient estimate)

C. Comparison of Thor and Johnson Equation Prediction with Experimental Data

In the remainder of this paper equations (1) and (2) will be referred to as the Thor equations while equations (3) and (4) will be called the Johnson equations. To determine which set of equations gave the "best" estimate of residual mass and velocity some calculations were performed and compared with experimental data. Although the number of computations made are not large in number, they serve to point out the differences in

residual mass and velocity utilizing the two sets of equations. These data are presented in Table I.

TABLE I

COMPARISON OF RESIDUAL VELOCITY (V_R)

MHN	t	θ	M_0	Exp. V_S	Exp. V_R	Johnson V_R	Thor V_R
	(in)	(deg)	(grains)	(ft/sec)	(ft/sec)	(ft/sec)	(ft/sec)
135	.125	0	60	2899	1780	1708	1463
135	.125	60	120	4894	2815	2395	2170
135	.060	0	60	1291	840	783	555
100	.132	60	240	6108	4075	3967	3858

COMPARISON OF RESIDUAL MASS (M_R)

MHN	t	θ	M	Exp. V_S	Exp. M_R	Johnson M_R	Thor M_R
	(in)	(deg)	(grains)	(ft/sec)	(grains)	(grains)	(grains)
110	1	0	240	9189	25.2	-23.8	-24.9
120	0.25	0	30	5085	6.8	9.2	9.7
120	.5	0	240	5760	57.4	68.0	71.6
120	.5	0	60	8534	11.1	-2.2	-2.9

If a comparison is made with the residual velocity computations using the Johnson and Thor equations with the experimental data, it may be observed that the Johnson equation gave the "best" estimate for all of the cases tested. If a comparison is made with the residual mass computations utilizing the Johnson and Thor equations with the experimental data and observing Table I, the Johnson equation is only slightly better than the Thor equation. This may possibly be explained by the difficulties normally encountered in the measurement of residual mass. Considering the treatment of the data in reference 3, it would appear reasonable that the Johnson equations would provide the better estimate. A regression analysis was performed on over two thousand firings in which steel fragments were fired against various target materials. A very detailed, systematic, statistical study was performed on the data to obtain the regression equations where confidence intervals for mean values and tolerance intervals for estimating individual values are given by each regression equation.

D. Tolch Equation

The Johnson equations are applied to an array of targets as long as there are residual fragment velocity and residual fragment mass. When a target has succeeded in stopping a fragment or a perforation is not obtained, a negative residual velocity or negative mass is acquired; then it is necessary to compute the depth of penetration into that particular target. This is accomplished in the case of a steel fragment penetrating a mild steel target using the equation given in reference 2 which has the following form.

$$P = [.112 M^{1/3} (V/1000)^{4/3}] \cos \theta \quad (5)$$

where

P = penetration (inches)

M = fragment mass (oz)

V = fragment striking velocity (ft/sec)

θ = cosine of the angle of impact obliquity of the fragment (angle between fragment trajectory and normal to target)

The above equation (5) is good for angles up to 30° according to the report because this is based on irregular bomb fragments penetrating mild steel and it is referred to as the Tolch equation.

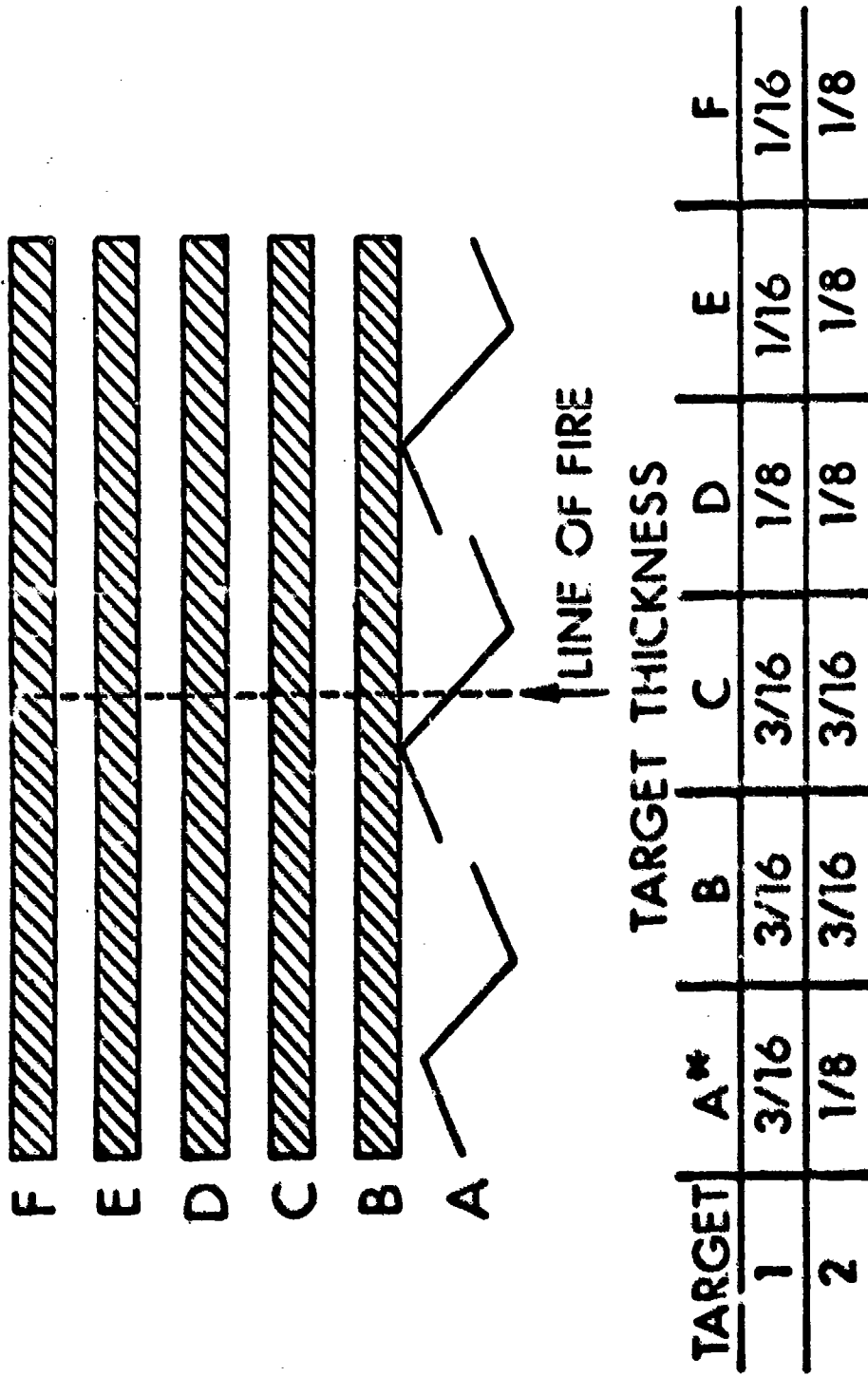
III. COMPUTATIONAL PROCEDURE

A. Panel Configurations

Computations were performed using fragment data for an 81mm M374 mortar shell for two different suppressive structure panels consisting of 2 bars and spaced mild steel plates. Figure 1 shows the panel configuration and thicknesses of mild steel plates. The last two plates in each panel array are louvered plates. The plates are spaced a small distance apart usually about $3/16"$ (.1875").

B. Penetration Predictions for Panels

Penetration predictions were made using the main threat fragments from an 81mm M374 mortar shell as selected by Kinoko in BNL IMR 190⁴ for the two panel configurations shown in Figure 1. The fragment threats for panel 1 are presented in Table II along with the plate number the fragment stopped in and the penetration depth in centimeters. The calculations were performed using the methods of reference 3 (Johnson equations and reference 2 (Tolch equation)). The computations were made using the fragment mass and velocity presented in Table II as striking mass and velocity into the first plate (2 bar) of the panel and a residual mass and velocity were calculated using the Johnson equations. The residual mass and velocity



* A - Z BAR AT 60° OBLIQUITY

FIGURE 1. PANEL CONFIGURATION

obtained from the first plate (Z bar) became the striking mass and velocity impacting the second plate of the panel. This procedure was continued until a negative mass or velocity was obtained which indicated that complete penetration had not occurred in that particular plate of the panel. Using the residual mass and velocity of the fragment from the previous plate, a depth of penetration was calculated for the plate penetrated, but not perforated. The number of the plate the fragment stopped in is presented in Table II and the equivalent thickness of penetration using secant of the angle of obliquity is also shown. Penetration predictions were made using the same methods and fragment threats just described, but for the plate configuration of panel 2. These results are listed in Table III.

TABLE II

PENETRATION ESTIMATES FOR PANEL 1

Frag. No.	Mass (grams)	Type Frag**	Velocity (km/sec)	1/2 MV ² (K Joules)	Plate No. Frag Stopped In	Penetration (cm)***
2	1.64	(S)	1.94	3.22	1	0.66
5	272.48	(A)	0.63	53.19	4****	2.08
7	43.46	(S)	0.78	13.13	2	1.09
8	4.89	(S)	2.04	10.19	2	1.17
9	4.64	(S)	1.92	9.55	2	1.09
12	261.14	(A)	0.53	37.15	3****	1.65
roller	70.45	(S)	0.77	21.00	3	1.50
rod	127.53	(S)	1.09	75.76	6	2.29

** (S) Shell case

(A) Aluminum fragment

*** Estimates using equations in NRLM 1777 and NRLR 568

**** Fragment is aluminum while estimate is for steel (an aluminum fragment will not penetrate as much as steel).

TABLE III

PENETRATION ESTIMATES FOR PANEL 2

Frag. No.	Mass (grams)	Type Frag**	Velocity (km/sec)	$1/2 MV^2$ (K Joules)	Plate No. Frag Stopped In	Penetration (cm)***
2	1.64	(S)	1.98	3.22	2	0.76
5	272.48	(A)	0.63	53.19	5****	2.06
7	43.46	(S)	0.78	13.13	3	1.19
8	4.89	(S)	2.04	10.19	3	1.14
9	4.64	(S)	1.92	8.55	3	1.12
12	261.14	(A)	0.53	37.15	4****	1.75
roller	70.45	(S)	0.77	21.00	4	1.60
rod	127.53	(S)	1.09	75.76	6	2.29

** (S) Shell case

(A) Aluminum fragment

**** Estimated using equations in NRLM 1777 and NRLR 568

*** Fragment is aluminum while estimate is for steel (an aluminum fragment will not penetrate as much as steel).

A study of the penetration results of panel 1 as shown in Table II would appear to indicate that all fragments were stopped by the panel successfully using the assumptions and methods indicated. Essentially the same results may be observed for panel 2 in Table III where all fragments are stopped in the panel. The fragments are suppressed in different plates because of the target panel thicknesses. Any component plate of either panel array should be made of thicker material for safety considerations for this shell threat.

IV. FUTURE WORK

The suppressive structures study involving BML in relation to penetration of a structure by a fragment threat has two major objectives:

1. to provide test support for suppressive structures.
2. to provide technical support.

Experimental tests will be conducted to measure behind the target effects, residual mass, residual velocity and spatial distribution of the pre-impact fragment. These data are required to check the validity of existing fragment penetration equations and if necessary modify them or initiate the development of new equations which delineate the effect of spacing. Field tests of full scale panels will be conducted to provide end proof testing.

V. CONCLUSIONS

At the time this study was performed, the confidence using the Johnson equations to predict fragment penetration into spaced structures had not been fully tested. It was noted that the residual masses predicted by this method differ appreciably from those estimated by Thor equations. The uncertainty of the results as a consequence of the uncertainty in residual mass was not studied. The degradation due to holes in the center layers of the spaced panel structure was not taken into account in the predictions.

In conclusion, it is estimated that either of the two panel configurations will stop any of the given fragment threats. The most severe threat in the 75.76KJ rod for which the margin of safety is very slim. For comparison purposes then, a minimal shell thickness of 1.0 inch should be considered in the analysis.

REFERENCES

1. Ballistic Analysis Laboratory, Johns Hopkins University, "The Resistance of Various Metallic Materials to Perforation by Steel Fragments; Empirical Relationships for Fragment Residual Velocity and Residual Weight", Project Thor Technical Report No 47, April 1961.
2. Tolch, N. A. and Bushkovitch, A. V., "Penetration of Mild Steel by Bomb Fragments", BRLR 568, August 1945.
3. Johnson, J. R. and Mioduski, R. E., "Estimation of the Loss of Velocity and Mass of Fragments During Target Perforation (U)", BRLM 1777, September 1966, CONFIDENTIAL.
4. Bertrand, B., Brown, C., Dunn, D. J., Huffington, N. J. Jr., Kineke, J. H. Jr., Kingery, C., Meissner, R., Ricchiazzi, A., Robertson, S. R. and Vitali, R., "Suppressive Structures - A Quick Look", BRL IMR 190, February 1974.

AIRBLAST ATTENUATION BY PERFORATED PLATES

BY

CHARLES KINGERY

U.S. ARMY BALLISTIC RESEARCH LABORATORIES
ABERDEEN PROVING GROUND, MARYLAND

INTRODUCTION

BACKGROUND

The U. S. Army is continuing with the modernization of munition processing facilities under the Production Base Modernization Program. One phase of the overall program is to develop a technology base for suppressive shields which will allow the preparation of an engineering design handbook.

The basic requirements in the design of suppressive shields for application to munition production lines is to contain the fragments and attenuate the blast developed from accidental explosions.

The Ballistic Research Laboratories (BRL) have the prime responsibility for conducting the applied technology phase of the suppressive shield development program. This includes the definition of the fragment and blast environment created from an explosive detonation within a suppressive structure, the structural loading and response, the containment of primary and secondary fragments and the attenuation of blast. This paper will report on current work associated with blast attenuation.

OBJECTIVES

The objectives of the overall program in blast suppression are as follows:

1. Evaluate the parameters effecting the performance of suppressive structures in attenuating blast.
2. Develop an understanding of the phenomenology of blast suppression to permit a logical, efficient design of blast suppressors.

The experimental phase of this program has just begun and the presentations are made to show the general approach to the problem and the initial results to date.

Preceding page blank

THEORY

Attempts have been made to establish a theoretical treatment to describe the attenuation of shock waves passing through orifices and other restrictions^{1,2,3,4,5,6}. In general the theories developed are restricted to limited ranges of incident peak overpressure, vent area or geometry. Therefore the researcher usually resorts to empirical solutions for specific problems. This paper will present some preliminary experimental results associated with a specific problem.

DESIGN OF EXPERIMENT

APPROACH

The experiments were conducted in the 4 inch diameter shock tube located at the shock tube facility at BRL. Emphasis was put on the study of the effects of single parameter variations. The two variables being reported on are the effect of vent area and peak overpressure.

SHOCK TUBE

The shock tube used was 4 inches in diameter with a compression chamber length of 12 inches. From the diaphragm to the test item is 100 inches. From the test item to the end of the tube is also 100 inches. A sketch of the tube, showing the location of the test item and the pressure transducers is presented in Figure 1. The short compression chamber develops a peaked shock wave representative of a shock wave generated from a high explosive detonation. The range of peak overpressures used for this study was from 200 psi down to 50 psi.

INSTRUMENTATION

Instrumentation required for documenting the overpressure versus time at specific locations in a shock tube usually consists of a transducer, an amplifier and a recorder.

The transducers used for this series of shots were a piezoelectric type with a Tourmaline crystal, Model ST-4, manufactured by the Susquehanna Instruments Company.

The amplifiers were Kistler charge amplifiers Model 566.

The recorders were Techtronic Dual Beam scopes Model 502-A.

ORIFICE PLATE DESIGN

The orifice plates were designed to investigate the effect of vent area on blast attenuation versus input pressure. The plate designs are presented in Table 1. The thickness of the plates are .25 inches and the diameter of the holes are .5 inches.

TEST RESULTS

VENT AREA VERSUS PEAK OVERPRESSURE

The hole size in the orifice plates was held constant (0.5 inches) and the three different venting areas were exposed to three pressure levels. There is an inherent blast attenuation as the shock front propagates down the tube. Therefore the magnitude of the shock pressure was documented at the six stations for the three input pressure in order to determine the target input pressure (P_{T1}) and the transmitted pressure at station 6 with a 100 percent vent area opening. The values of transmitted pressure at four stations down the tube for the three input pressures are presented in Figure 2. The target input pressures established from figure 2, by interpolating between station 3 and 4, are used as a basis for establishing the blast attenuation effects of the different vent areas.

The target input pressures (P_{T1}) versus the transmitted pressure (P_T) for the different vent areas are listed in Table 2 and plotted in Figure 3.

To determine the blast attenuation, and take into account the attenuation associated with the tube, a comparison must be made between the transmitted pressure at station 6 with a 100 percent opening and the pressures at station 6 with the other percent openings. The percent attenuation is determined from the following expression:

$$\frac{P_T(100 \text{ percent}) - P_T(\text{VA percent})}{P_T(100 \text{ percent})} \times 100 = \text{Percent Pressure Attenuation}$$

This percent pressure attenuation is listed in column five of Table 2.

DISCUSSION

It should be noted again that the results obtained from this series of tests are based on a constant hole size (.5 inch diameter). The effect of hole size will be the next parameter to be investigated. Although the data presented in Table 2, and the family of curves developed in Figure 3 are quite consistent more tests are being planned for other vent areas and input pressures.

The results presented in column five of Table 2 show no effect of target input pressure on blast attenuation over the range tested. Therefore an average of the three values for each percent vent area was plotted in figure 4. With the end points fixed one can extrapolate and determine the percent attenuation to be expected for the full range of percent openings with 0.5 inch hole size.

REFERENCES

1. J. M. Ross, C. M. Nixon and W. M. McMurtry, "A Shock Tube Study of Attenuation of Air Flow Through Chokes," Suffield Experimental Station Technical Note No. 152, 11 May 1966.
2. Otto Laporte, "On the Interaction of a Shock Wave with a Constriction," LASL, UCAL, Report LA-1740, August 1954.
3. George Rudinger, "Wave Diagrams for Non-Steady Flow in Ducts," Van Nostrand Company, Inc., New York, 1955.
4. L. Dresner and C. V. Chester, "Attenuation of Shocks in Tubes by Orifice Plates," ORNL-TM-1750, 9 February 1967.
5. Louis L. Monroe, "Investigation of the Transmission of a Shock Wave Through an Orifice," GALCIT Hypersonic Research Project Memo No. 46, 25 September, 1958.
6. Brian F. Bertrand, "Shock Wave Transmission Through a Large Restriction in a Constant Area Duct," BRL Memorandum Report No. 1848, June 1967.

TABLE I
ORIFICE PLATE DESIGNS

VENT AREA PERCENT	NUMBER OF HOLES	SPACING OF HOLES (INCHES)
10	6	1.10
25	16	0.80
50	32	0.56

$$\text{AREA PERCENT} = \frac{\text{VENT AREA}}{\text{TOTAL AREA}} \times 100$$

$$\text{TOTAL AREA} = 12.566 \text{ IN}^2$$

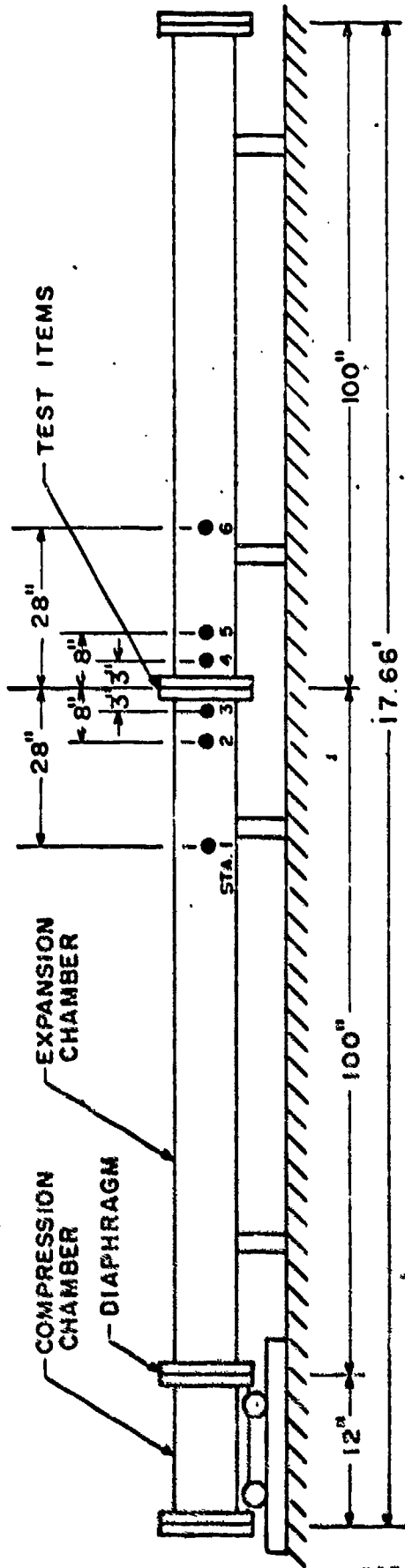
HOLE SIZE = 0.50 INCH DIAMETER

HOLE SPACING MEASURED CENTER TO CENTER

TABLE 2

TRANSMITTED OVERPRESSURE VERSUS TARGET
INPUT OVERPRESSURE FOR DIFFERENT VENT AREAS

VENT AREA	TARGET INPUT PRESSURE	TRANSMITTED PRESSURE (STA. 6)	PRESSURE ATTENUATION	
			RATIO	PERCENT
100	49	37	NA	NA
	113	93	"	"
	189	156	"	"
50	49	30	.81	19
	113	72	.77	23
	189	127	.81	19
25	49	22	.59	41
	113	54	.58	42
	189	94	.60	40
10	49	14	.38	62
	113	33	.35	65
	189	60	.38	62



● -- GAGE PORTS
1/2" - 20 NF

FIGURE 1 SHOCK TUBE TEST SET-UP

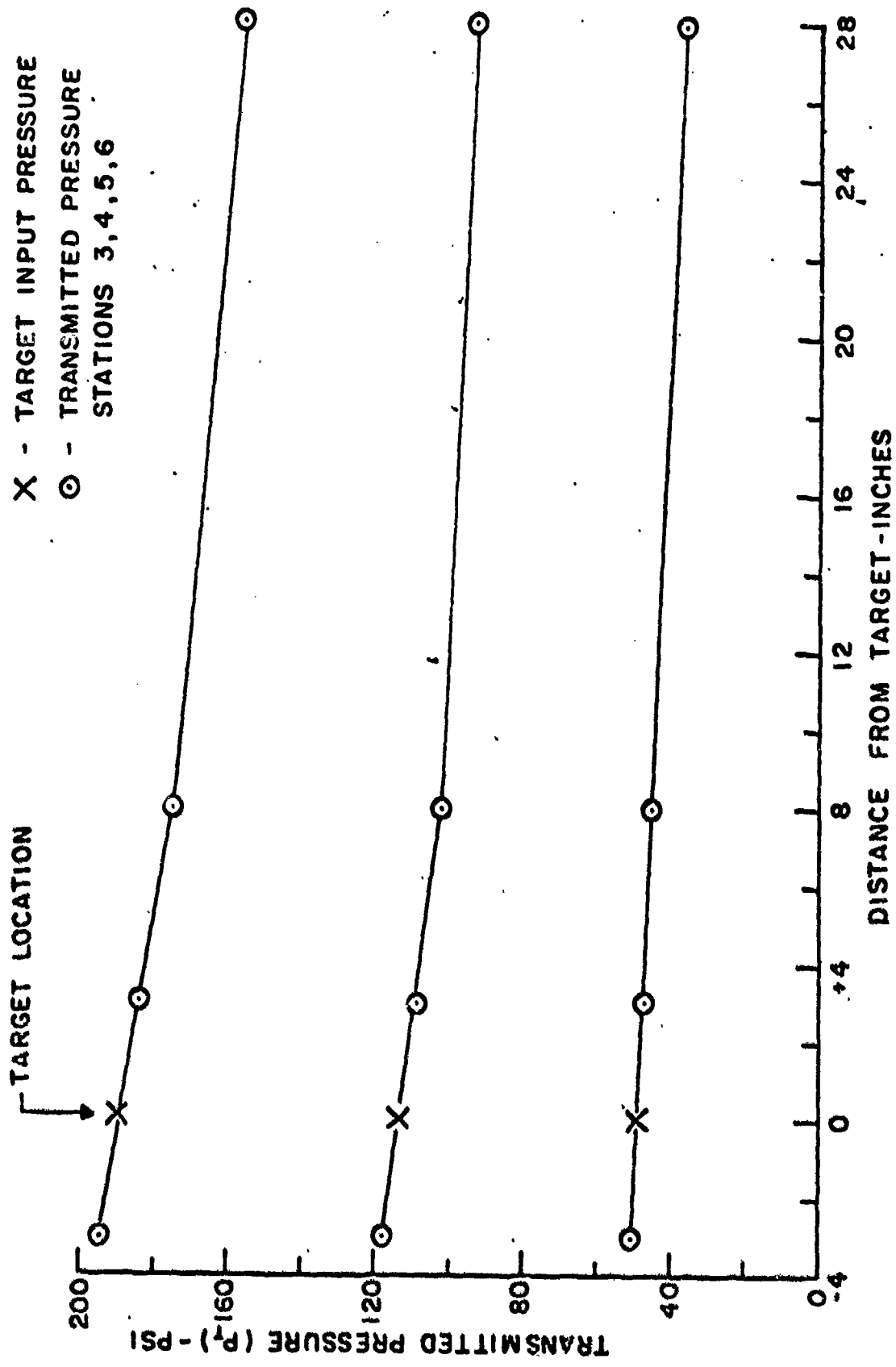


FIGURE 2 PRESSURE ATTENUATION DOWN TUBE FOR DIFFERENT INPUT PRESSURES

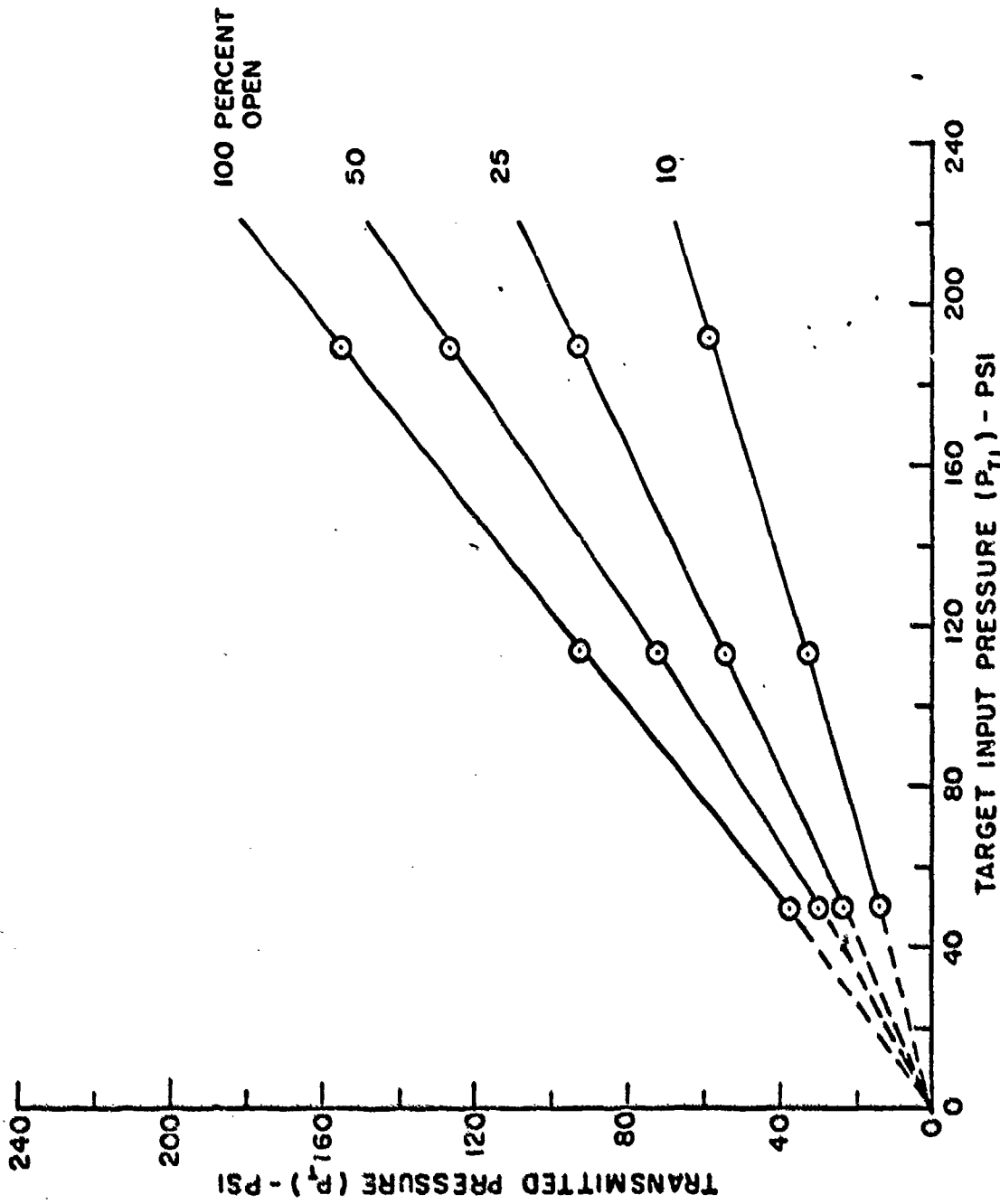


FIGURE 3 TARGET INPUT PRESSURE VS TRANSMITTED PRESSURE FOR DIFFERENT VENT AREAS

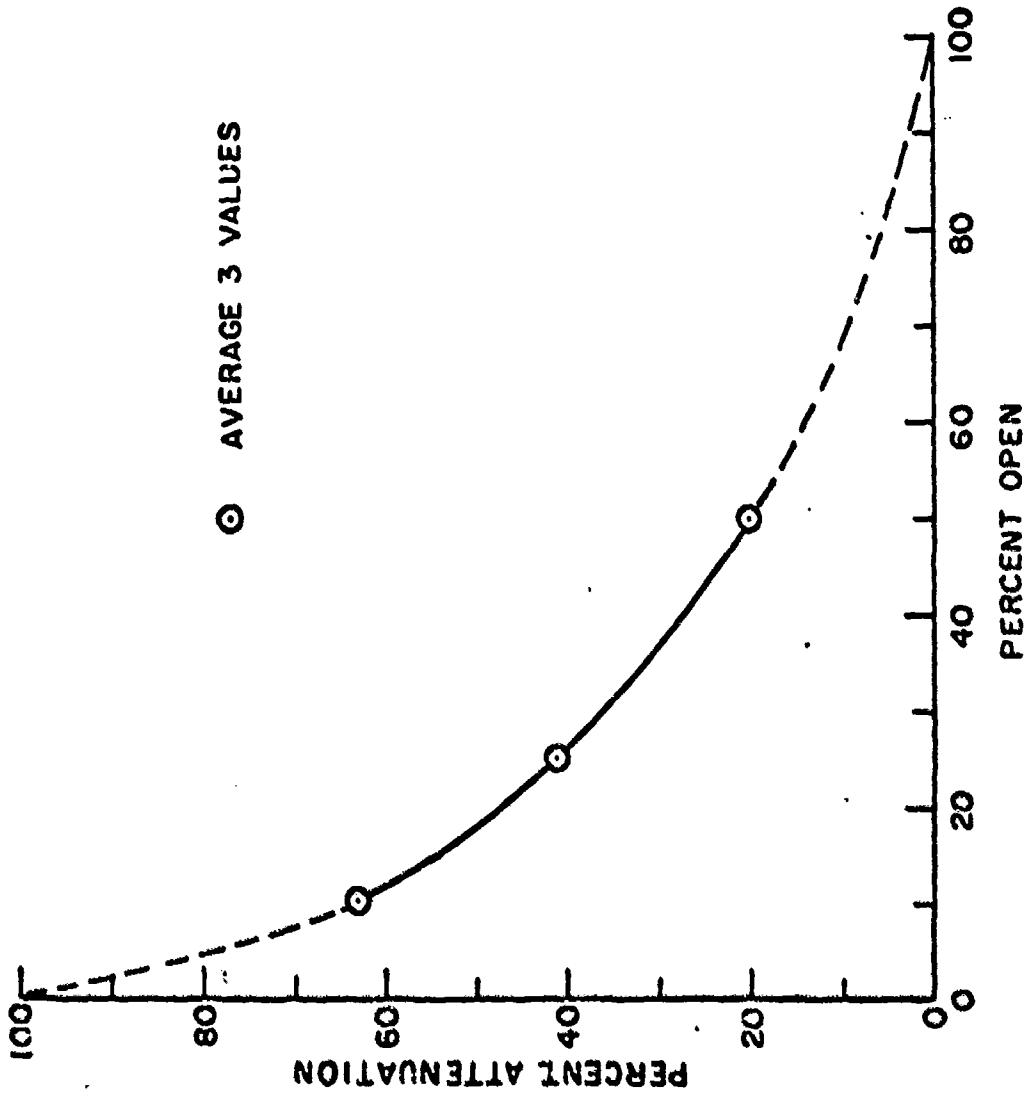


FIGURE 4 - PERCENT VENT AREA Vs PERCENT ATTENUATION

200 PSI PROOF TEST OF THE 81mm SUPPRESSIVE SHIELD

Mr. A. H. Lasseigne
General Electric Co.
Ray St. Louis, MS

DIGEST

Tests were conducted to obtain preliminary data on the structural loading and response characteristics in excess of its design range of a typical full scale suppressive shield, when subjected to overpressures of 200 psi resulting from detonation of a centrally located 35 lb. bare spherical charge. The 81mm prototype suppressive shield, located at the NSTL Kellar Road Test Range, was used for these trials. All major column structural members failed as a result of maximum tension load being developed where the sides of the column were welded to the side beams. This was a result of the roof beams being forced upward while the side columns were being forced outward.

(Mr. Lasseigne presented a summary of Edgewood Arsenal Technical Memorandum EA 4E33K "200 psi Proof Test of the 81mm Suppressive Shield." This document will be placed with the Defense Document Center, Cameron Station, Alexandria, VA 22314 and may be ordered in the regular manner from DDC by authorized users.)

**SUPPRESSIVE SHIELDING CONCEPT AS AN ANTIPROPAGATION BARRIER
FOR THE 81mm, M374 HE MORTAR ROUND**

by

**Alfred K. Keetch
Test Operations Directorate
US Army Dugway Proving Ground
Dugway, Utah 84022**

SUMMARY

An engineering design test program was initiated to determine the effectiveness of suppressive shielding as an antipropagation barrier for the 81mm high explosive mortar round.

This test program was conducted in two phases. Phase I consisted of eight tests designed to establish an optimum safe separation distance between mortar rounds with and without sleeve-type shielding. Phase II was a single trial effort incorporating the sleeve shielding into a container configuration to demonstrate that detonation propagation can be greatly reduced or completely avoided using this concept.

The test results indicate that suppressive shielding is effective in preventing propagation of detonation between 81mm mortar rounds. However, the number of tests conducted was insufficient to statistically confirm the results with any degree of reliability.

Similar tests are planned to further investigate suppressive shielding concepts for various applications in support of the ammunition plant modernization program.

BACKGROUND

The safety of personnel and the protection of equipment and facilities at production plants demands a solution for reducing the propagation of detonation hazards inherent in manufacture, loading, handling, transporting, and storage of ammunition. Suppressive shielding is a promising candidate for solving this problem, and is also less costly than other proposed methods.

Vented wall and perforated shield concepts are being considered for use in the plant modernization program. The limited testing conducted to date indicates that distances between loading operations can be effectively reduced with the use of vented separator.

The testing outlined in this paper was conducted to further demonstrate the capability of suppressive shielding in preventing propagation of detonation between 81mm HE mortar rounds.

DETAILS OF TEST

Phase I - Safe Separation Test for 81mm Mortar Rounds

This test phase consisted of two parts:

Part I dealt with establishment of an optimum safe separation distance between mortar rounds using perforated shielding.

Part II dealt with performing comparison tests to demonstrate that detonation propagation would occur when shields were not used between rounds.

The shield sleeves for Part I were fabricated from 1/8-inch thick perforated steel plate with a pattern of 1/4-inch diameter perforation, located on .413 inch by .413 inch by .510 inch centers as shown in Figure 1.

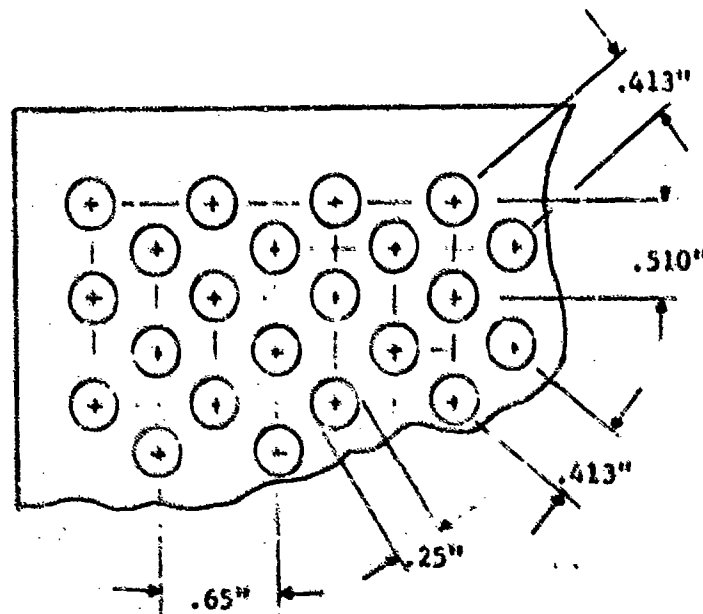


Figure 1. Perforated Pattern of Perforated Plate

The sleeves were both rectangular and cylindrical in shape. The dimensions of the rectangular sleeves varied from 22" x 5.2" x 5.2" to 22" x 11.2" x 11.2". The cylindrical sleeves were 22 inches in length and 5.2 inches in diameter.

A typical test setup for five of the six trials of Part I is shown in Figure 2. It consisted of four acceptor rounds arranged radially with the shielded donor round at the center. The distances from the donor round to the shield wall varied from 1 to 4 inches. The distances from the donor round to the acceptor rounds varied from 2 to 8 inches.

The test setup for the sixth trial of Part I is shown in Figure 3. It consisted of the four radial acceptor rounds and the center donor all arranged within a five compartment sleeve shield. This trial was designed to evaluate the effects of double layer shielding. Distance from the donor to the first layer of shielding was 1 inch. Distance between the two layers of shielding was 0.5 inch. Distance from the donor round to the four acceptor rounds was 2.75 inches edge to edge.

The test of Part I exposed 24 acceptor rounds to the detonation effects of a shielded donor round. The separation distances varied from 2 to 8 inches. No detonation propagation of acceptor rounds occurred during these tests. A partial explosion of one acceptor round was recorded at a separation distance of 2 inches. These tests demonstrated that detonation propagation can be effectively reduced or avoided when shielding is used between rounds.

In Part II tests shields were not used between rounds. A typical test setup is shown in Figure 4. The radial arrangement of the four acceptor rounds with the donor in the center was also used in these tests. Separation distances between acceptor and donor rounds again varied from 2 to 8 inches.

Eight acceptor rounds were exposed to donor detonation in the Part II tests resulting in detonation of seven of the acceptor rounds and explosive propagation of the eighth. These tests demonstrated that there is a high probability of propagation between rounds with a separation distance of less than 8 inches.

Primary fragment analysis was used to determine degree of propagation in these tests. Figure 5 shows a comparison of these fragments from the Part I (trial 7) shielded tests and the Part II (trial 8) unshielded tests.

PHASE II - Propagation Test of a Suppressive Shield Container for 81mm
Mortar Round

This test phase consisted of a single trial incorporating the perforated shield sleeves into a container configuration. The purpose of this test was to demonstrate the Production Pallet/Transportation Module concept as mentioned by Mr. Paul King during the morning presentation.

The suppressive shield container was fabricated from identical 1/8-inch perforated plate as the sleeves of the Phase I tests. The perforated plate was formed into cylinders 22 inches in length and 5.2 inches in diameter. The cylinders were assembled within a perforated box in a 3 x 4 pattern as illustrated in Figure 6. Spacing between the cylinders was 0.5 inch outside edge to outside edge. A detachable lid of perforated material served as a top to the container.

The suppressive shield container was placed on wooden stakes 2 feet above the ground as shown in Figure 7. This was to reduce the effect of blast reflection from the ground and also to aid in photographic coverage.

The donor round, seven acceptor rounds, and four dummy loads were placed in the container as shown in Figures 8 and 9. All mortar rounds were positioned base (fins) down in the container. Distance between the donor and acceptor rounds varied from 2.75 to 9.1 inches. The dummy loads were used due to a limited number of mortar rounds on hand. The dummies were the same length and mass as the mortar rounds to simulate effects.

The donor round was statically detonated as shown in Figure 10. Large fragments can easily be seen projecting from the test package. The detonation was also recorded by motion picture photographs at 24, 1,000, and 10,000 pictures per second.

Primary and secondary fragments were recovered at distances up to 470 feet from the point of detonation as shown in Figure 11. Primary fragments and explosive residue for the acceptor rounds (Figure 12) were analyzed. The results of the analysis indicated that no detonation propagation occurred. Damage sustained by the acceptor rounds was categorized using the guidelines of Table 1.

TABLE I. DAMAGE CATEGORIES FOR ACCEPTOR ROUNDS

-
1. Detonation propagation. Fragments in the same size range as donor.
 2. Explosion propagation. Significantly larger fragments with little or no residual explosive.
 3. Physical rupture or conflagration. Very large fragments with residual explosive.
 4. Physical damage. Fragment penetrations with explosive intact.
 5. No damage. Minor fragment scars with no penetration.
-

The first layer of acceptor rounds, immediately adjacent to the donor, were assessed as damage category 3. The second layer of two acceptor rounds (Figure 13) were assigned category 4 damage. The two remaining, third layer acceptor rounds (Figure 14), with added shielding by other acceptors and furthest from the donor, were virtually undamaged and were classed as damage category 5.

One round from the second layer, category 4 group experienced an unusual deformation of the booster cup as shown in Figure 15. It appears that a negative pressure developed during the donor detonation causing the abnormality.

The cylinders of the suppressive shield container were analyzed for damage and also categorized using the guidelines of Table II.

TABLE II. DAMAGE CATEGORIES FOR SUPPRESSIVE SHIELD CYLINDERS

-
1. Complete destruction of the cylinder.
 2. Major tearing and deformation of the perforated plate. Separation from neighboring cylinders.
 3. Minor tearing and deformation of the perforated plate. No separation from neighboring cylinders.
 4. Minor fragment penetration with no tearing or deformation.
 5. No damage.
-

Damage to the container cylinders (Figure 16) varied according to distance from the donor. The donor cylinder was completely destroyed. (Damage category 1). The eight cylinders adjacent to the donor were assigned damage category 2. The three remaining cylinders, furthest from the donor, were classed category 2+. The plus (+) was assigned because the cylinders had minor tearing, major deformation and separation from neighboring cylinders. Explosive residue from the acceptor rounds impinged on the surface of most cylinders. Damage sustained by the top, sides, and bottom of the container is shown in Figure 17.

CONCLUSION

Testing performed to date is insufficient to statistically confirm results or make judgement with any degree of reliability. However, it is evident that the suppressive shielding concept has potential as an antipropagation barrier. The concept as tested in this program should be investigated for application to in-plant handling of 81mm, and other medium caliber rounds. This concept offers maximum benefit for minimum payload loss. It is also recommended that the suppressive shielding concept be offered to Department of Transportation for investigation or incorporation into the containerized munitions program.

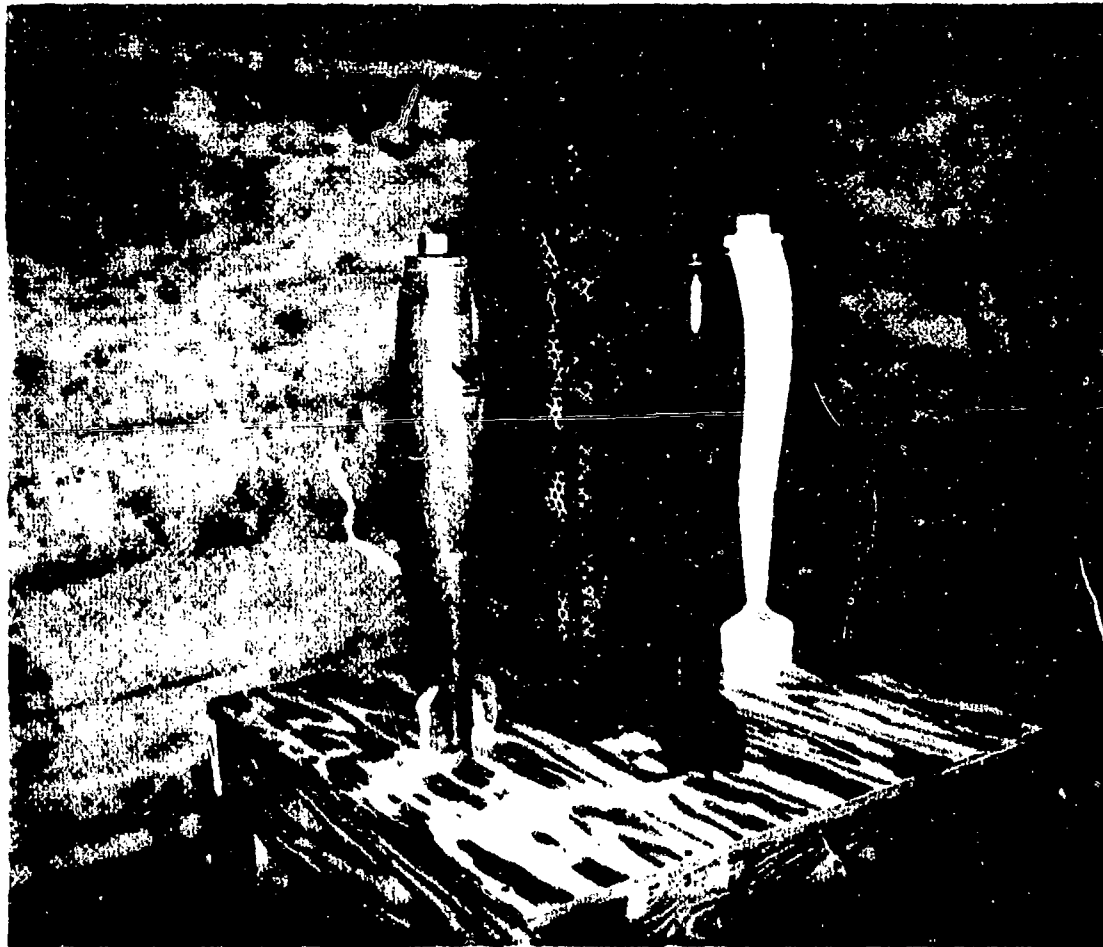


Figure 2. Typical Test Setup of a Part I Trial with Shielding.

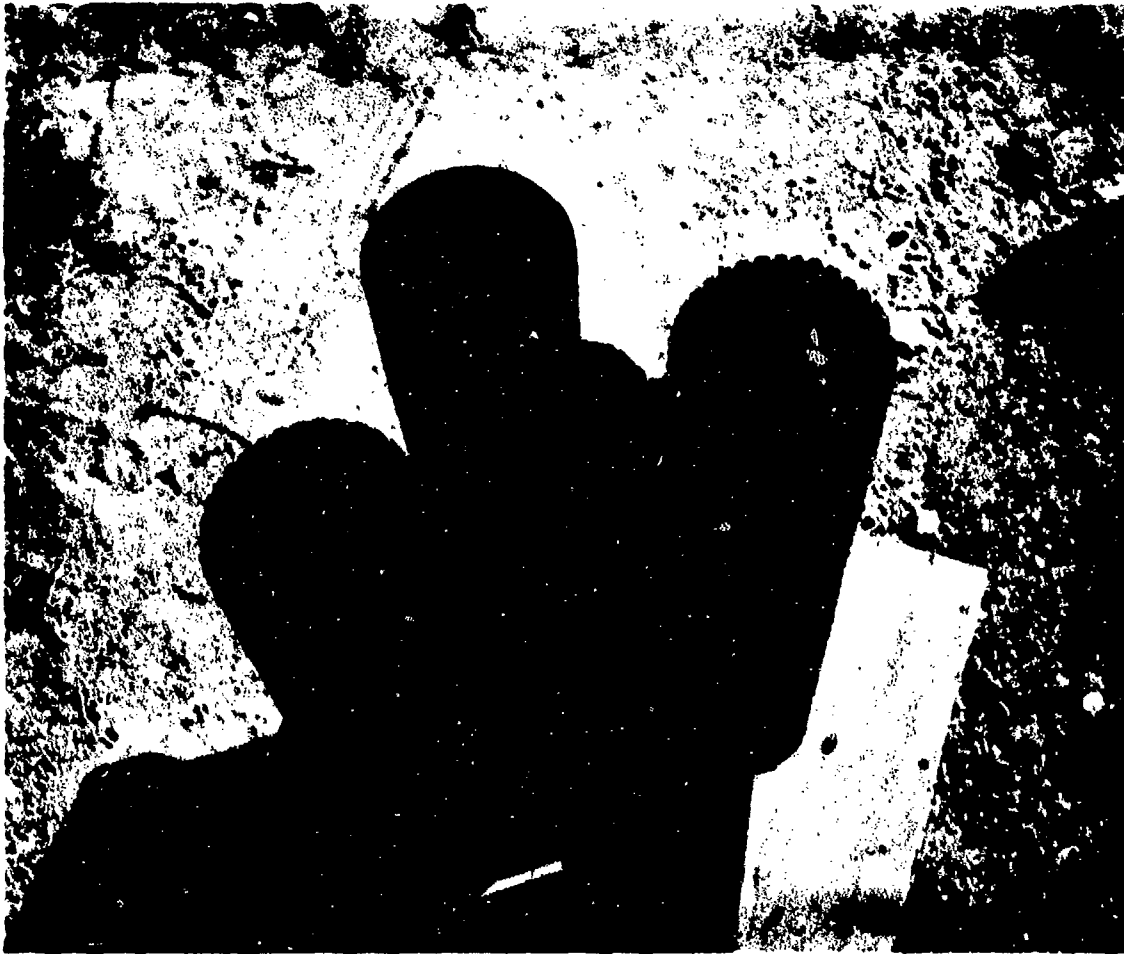


Figure 3. Test Setup for the Sixth Trial of Part I with Five
Compartment Shield.



Figure 4. Typical Test Setup of a Part II Trial without Shielding.



Figure 5. Primary Fragments Analyzed to Determine Degree of Propagation.
Note: Comparison of Fragments from Shielded Test (trial 7)
and unshielded test (trial 8).

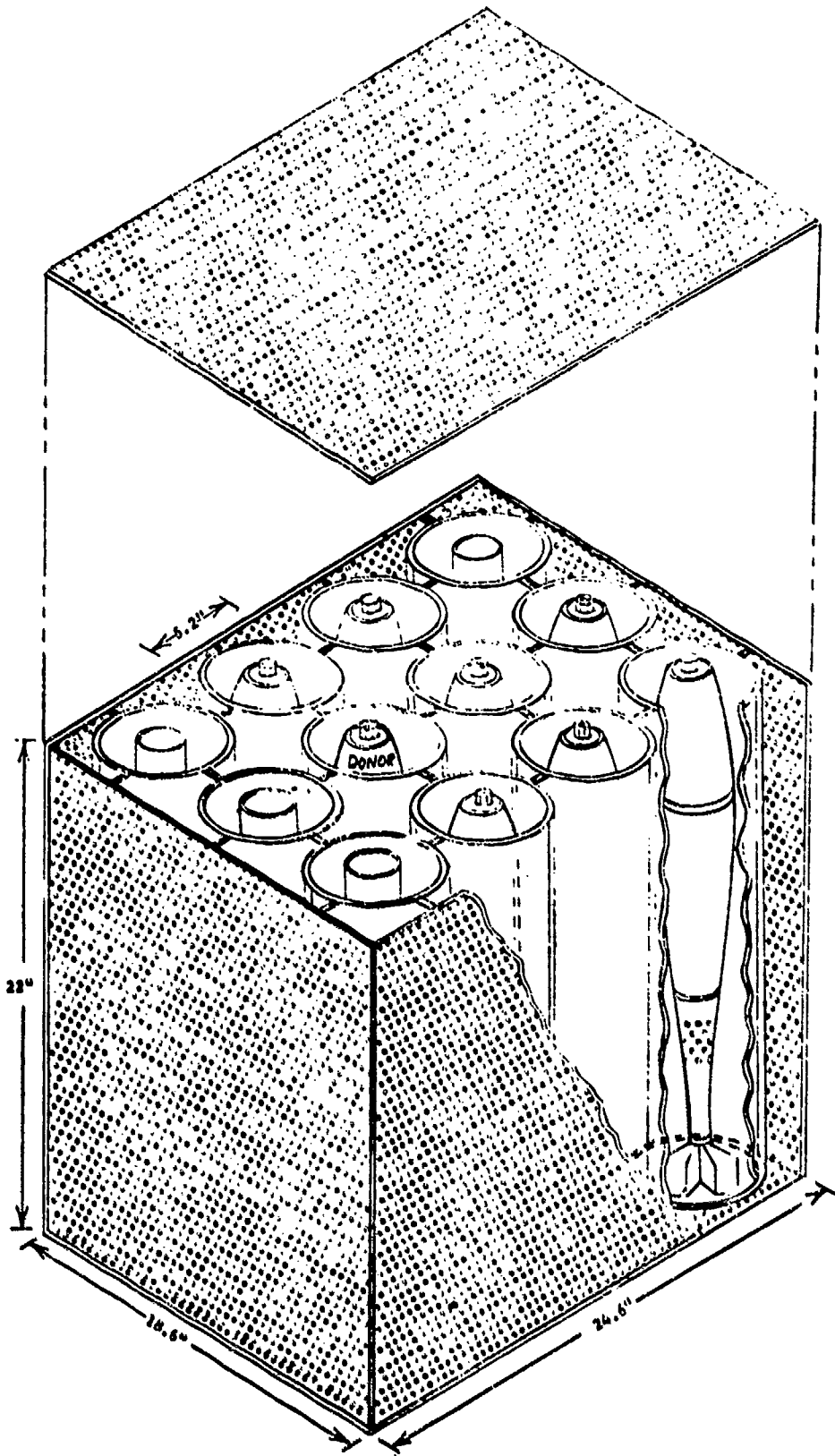


Figure 6. Suppressive Shield Container

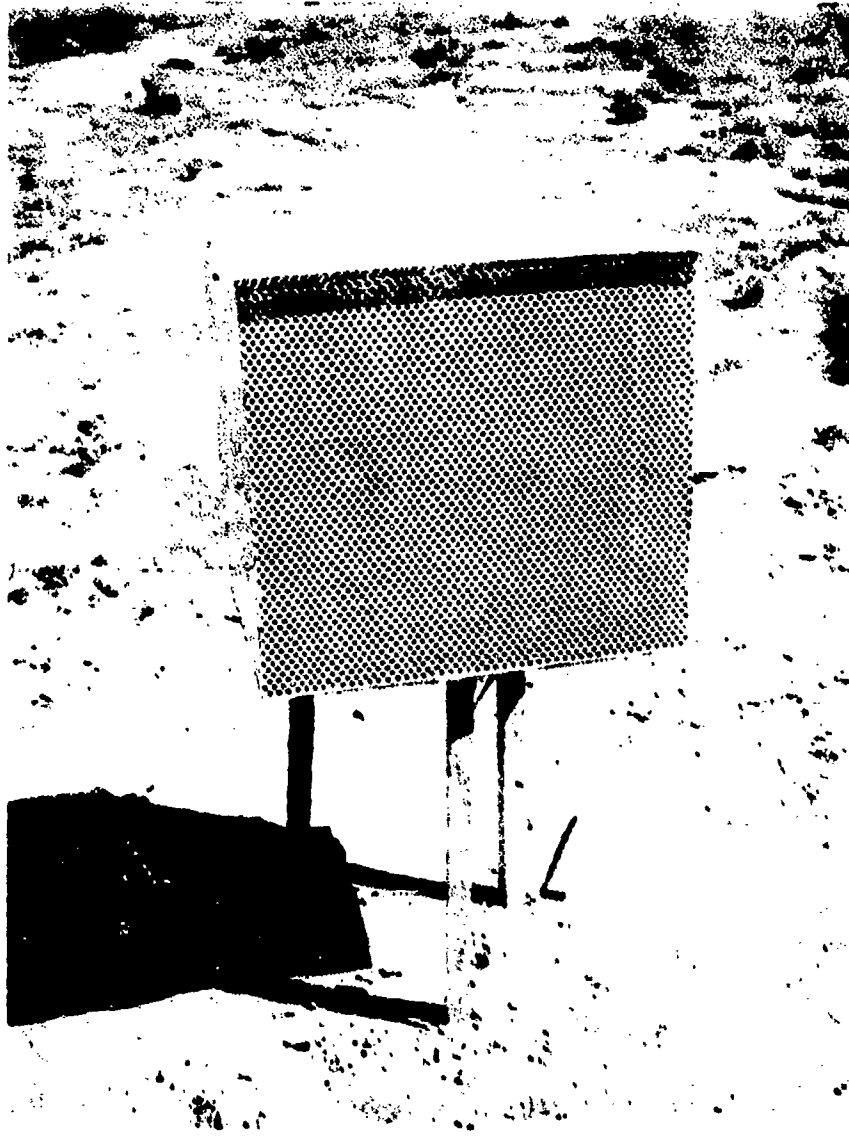


Figure 7. Suppressive Shield Container on Test Platform.

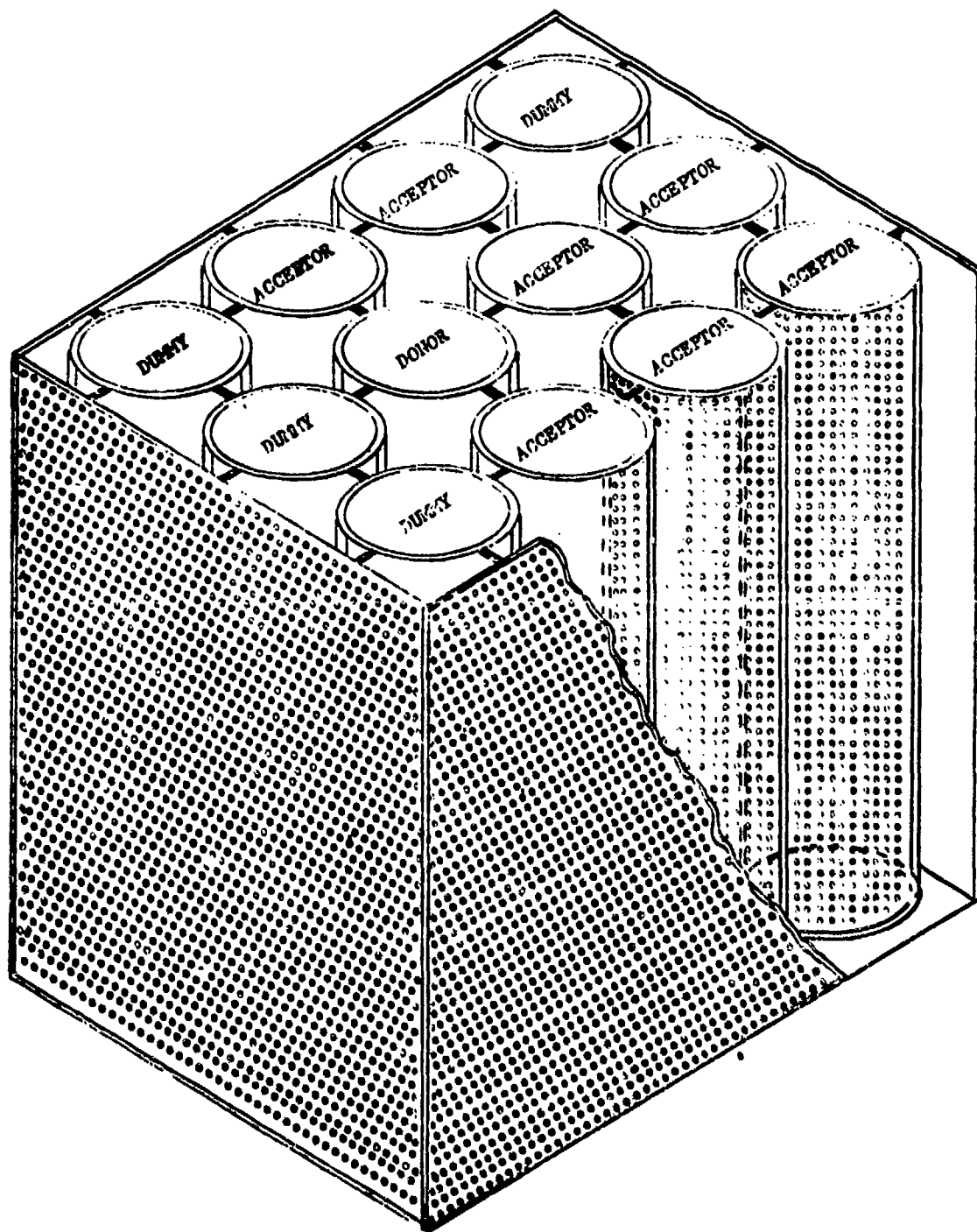


Figure 8. Location of Donor Round, Seven Acceptor Rounds, and Dummy Loads within the Suppressive Shield Container.

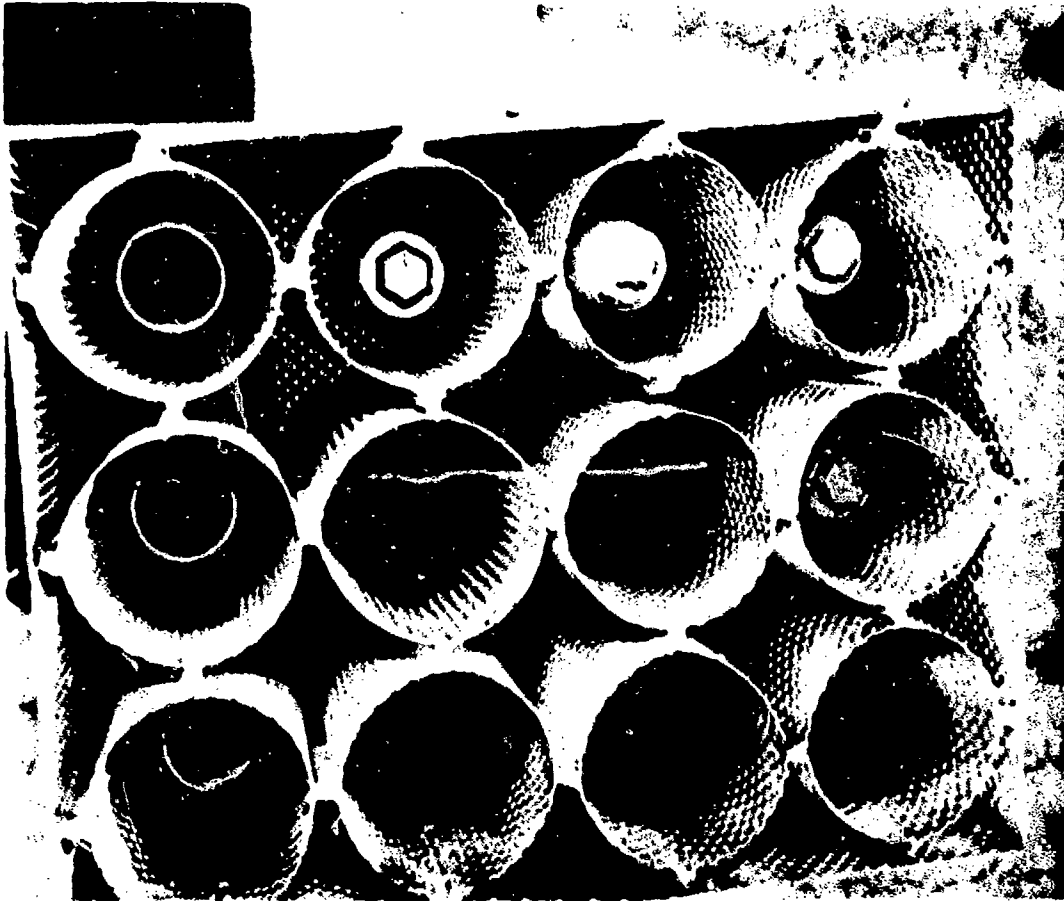


Figure 9. Mortar Rounds and Dummy Loads in Container.

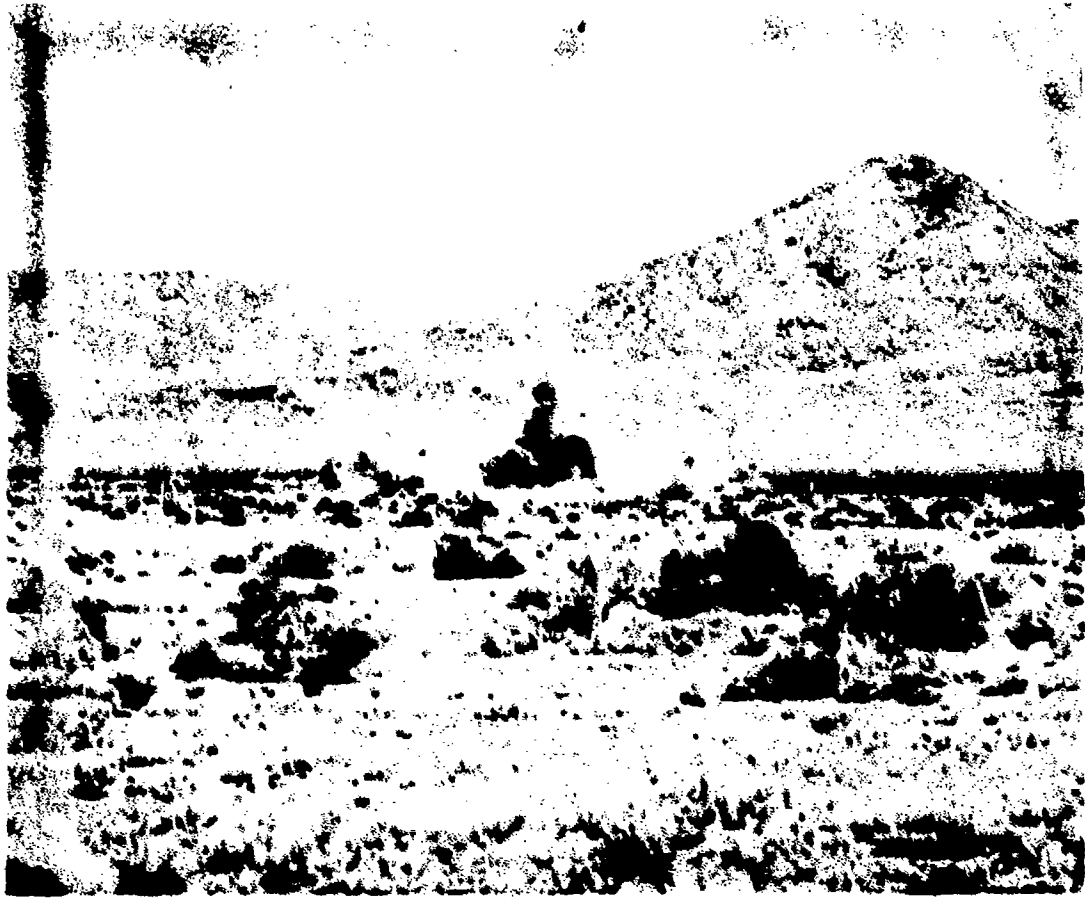
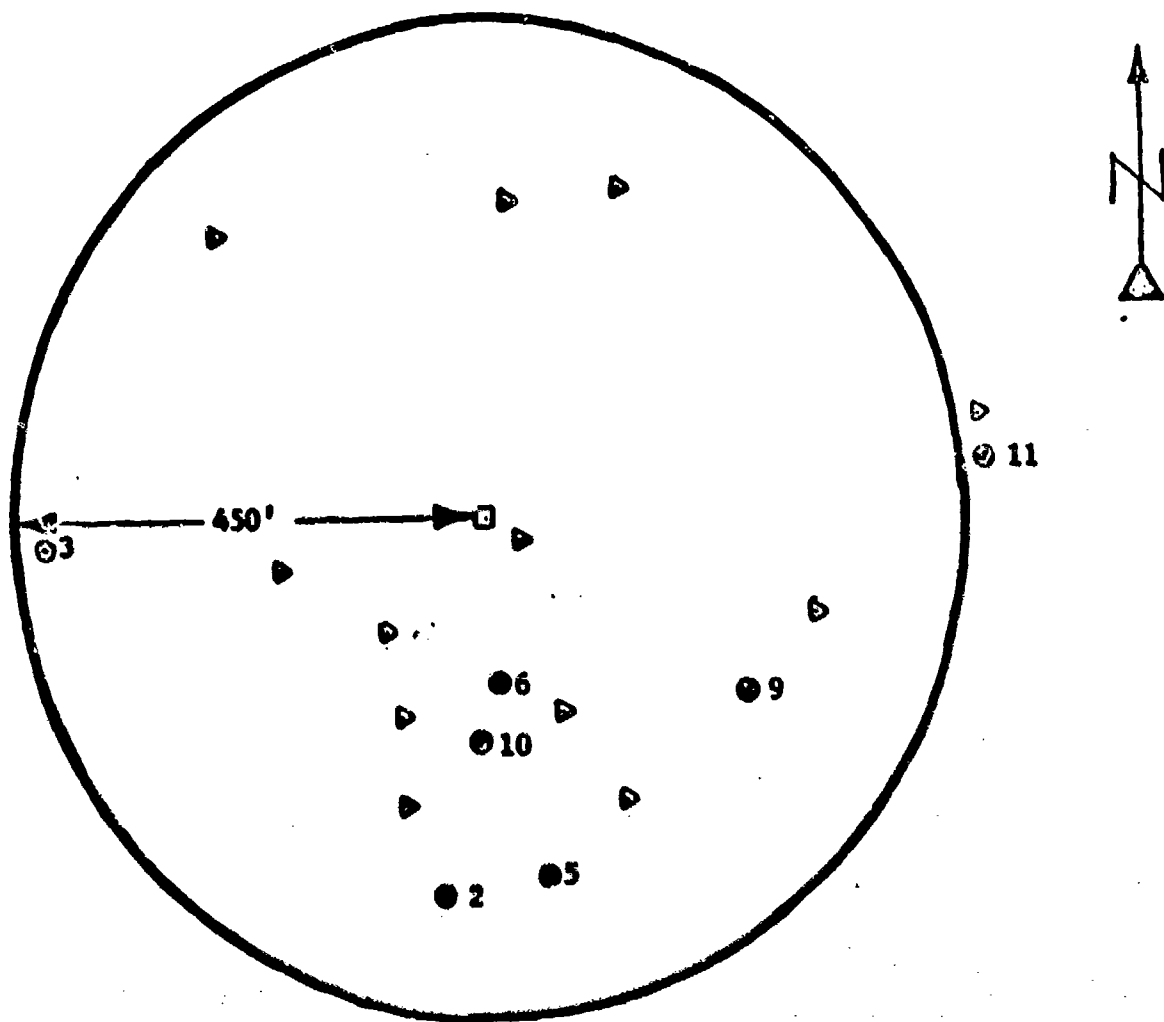


Figure 10. Detonation of Donor Round. Note: Fragments Projecting from Test Package.



- - POINT OF DETONATION
- - PRIMARY FRAGMENTS (Acceptor Rounds)
- ▲ - SECONDARY FRAGMENTS (Container)

Figure 11. Locations of Primary and Secondary Fragments Recovered after Donor Detonation.

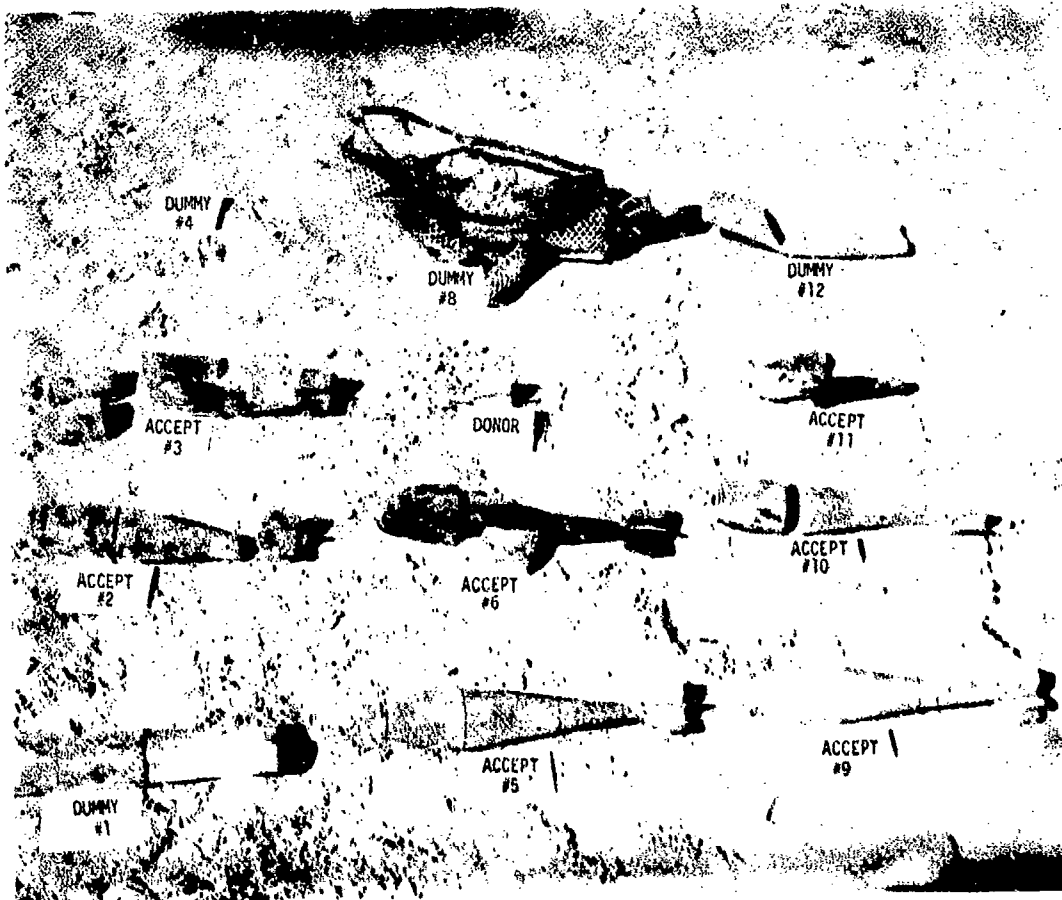


Figure 12. Recovered Primary Fragments used for Propagation Analysis.



Figure 13. Second Layer Acceptor Rounds. Damage Category 4.

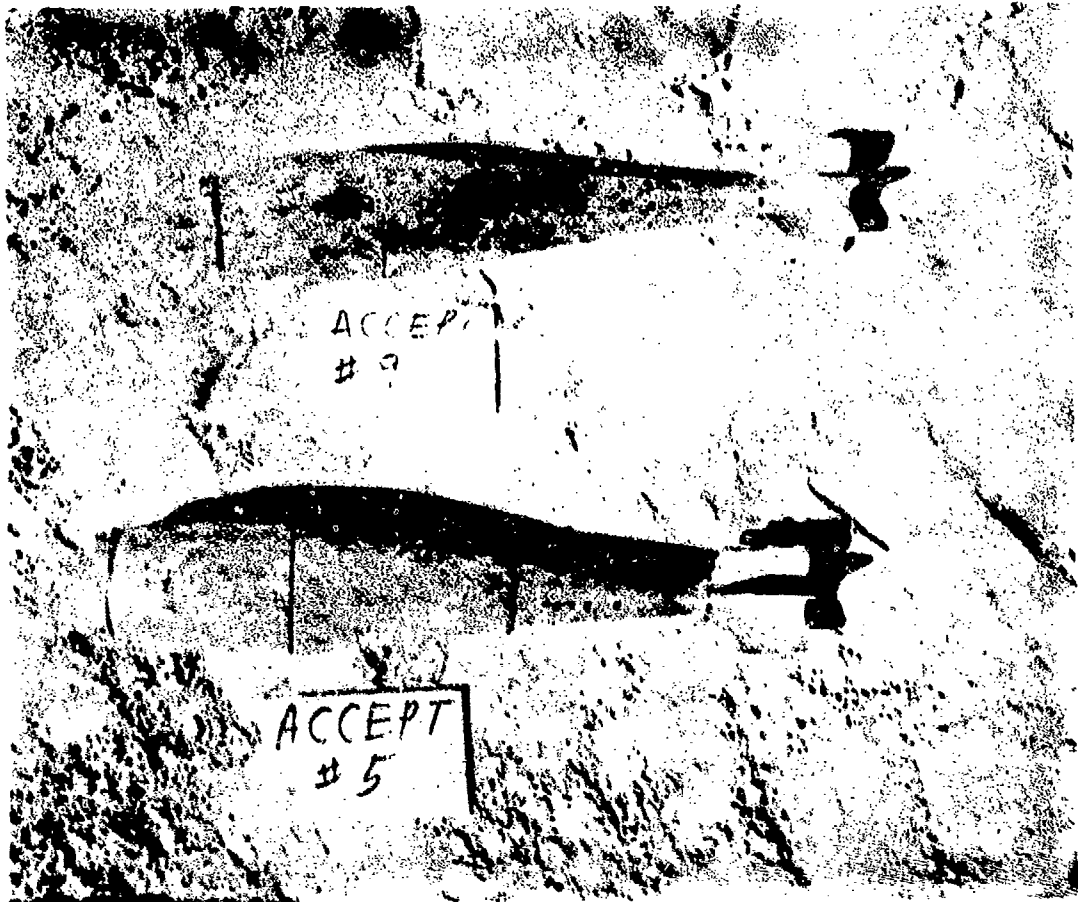


Figure 14. Third Layer Acceptor Rounds. Damage Category 5.
Very Little Damage.



Figure 15. Abnormal Booster Cup Deformation from Second Layer
Acceptor Group. Damage Category 4.



Figure 16. Damage to Container Cylinders from Donor Detonation.



Figure 17. Damage to Top, Sides, and Bottom of Container.

DEMILITARIZATION CONSIDERATIONS OF TOXICS
ASSOCIATED WITH EXPLOSIVES

Presented By
ALBERT L. WASCHLER

OFFICE OF THE AMC PROGRAM MANAGER FOR
DEMILITARIZATION OF CHEMICAL MATERIEL
Aberdeen Proving Ground, MD

Today, I am going to present a summary of events leading to the current approach being applied in disposal of lethal chemicals in bulk and munitions; also, with the ongoing program at Rocky Mountain Arsenal as my illustration, provide some insight into the process selection and operational practices now being utilized at Rocky Mountain Arsenal.

A number of public laws have come into being which restrict transport of chemical material and drive us in most cases to on-site disposal. Since the cancellation of CHASE 69, which was a planned sea dump of chemicals and chemical munitions, the demil program has grown dramatically. Now we have 39 geographically dispersed projects, each complex in its own right. A large number of agencies within DOD as well as external to DOD are involved. The program experiences high visibility from political and public point of view. We are now undertaking tasks never accomplished on such a large scale before. In many areas, we are pushing the state-of-the-art, particularly in the field of pollution abatement. As a result of growth of the program, in October 1972, AMC established the Office of the Program Manager for Demilitarization of Chemical Materiel. This centralized the mission of managing the preparation for and disposal of lethal chemical agents and munitions.

Workload. Chemical munitions and agents were produced and are stored at Rocky Mountain Arsenal. Today I would like to describe a portion of the demilitarization program - the ongoing demilitarization operations at Rocky Mountain Arsenal in Denver, Colorado. At this time, the mustard disposal operation has been successfully completed and work is continuing on the M34 and demilitarization of other lethal chemical material at Rocky Mountain Arsenal. Not only have we begun the demilitarization of the M34 clusters (on the 29th of October), but our schedules for disposal of this cluster form the base point around which we built our plans for disposing of the portion of the remaining stockpile at Rocky Mountain Arsenal.

You can see the cluster on this vugraph (VG 3) as it is being downloaded in a declustering cubicle. It is a one-thousand pound class bomb, produced for the Air Force at Rocky Mountain Arsenal and stored at that location. In this program we are disposing of 21,115 of these clusters.

The clusters were originally planned to be disposed of in Operation CHASE 69. When that operation was suspended, the National Academy of Sciences recommended that we dispose of these clusters onsite at Rocky

Mountain Arsenal. There are personnel at Rocky Mountain Arsenal who are experienced in the handling of the nerve agent GB, its manufacture and the filling of it into various munitions. It was felt that this expertise could certainly be applied to the demilitarization program. Also, there are facilities at Rocky Mountain Arsenal which, with some modification, could be adapted to the demilitarization process.

The next vugraph (VG 4) shows you the cluster as it is currently stored in the toxic yard at Rocky Mountain Arsenal. It is 78 inches long and 19 inches in diameter. This cluster contains a series of smaller bombs called the M125 bomb. There are 76 of these bombs arrayed in four bundles of 19 bombs each. Each bomb contains 2.6 pounds of the non-persistent lethal nerve agent GB and a little over 1/2 pound of explosive in the form of the central burster. In excess of 883,000 pounds of explosives and almost 4.2 million pounds of the agent are being disposed of in this demilitarization program.

The process that we are employing to demilitarize the M34 cluster is shown on this next vugraph (VG 5). As I discuss each major step in the process, I will show pictures of the major pieces of equipment on the screen.

From the toxic yard, the cluster is brought into the disposal facility shown. (VG 6). This is the same building in which M34 clusters were filled many years ago at Rocky Mountain Arsenal. We have modified and adapted it to the demilitarization of that cluster. At the outset, given our stringent safety criteria, we made an assumption. We assumed that one entire cluster could somehow explode during the demilitarization process, although such a possibility is extremely remote. The building as it was originally designed is not strong enough to withstand that explosive force. For example, the plenum chamber was designed to withstand an overpressure of 5 pounds per square inch. If one cluster went off, 7 pounds per square inch would be generated. Thus the plenum chamber had to be modified. Also, the interior walls of the building have been strengthened through the addition of structural steel. Today, when you walk into the facility, it almost looks as if you are entering a battleship.

Before we leave this vugraph, I would like to describe the extent to which we have had to go in pollution abatement. In the lower part of the picture is the exhaust scrubbing system. It consists of five separate scrubbing banks and a 200-foot dilution stack. Its function is to accept the contaminated air from the work area which flows through the 5-foot ductwork and scrub it before the exhaust is emitted into the atmosphere. In order to meet the very stringent limits placed on release of agent GB into the atmosphere, established by the US Surgeon General, this system has to be 99.995% efficient. We exceed that efficiency requirement. After renovation of the system, modifying it and testing it, we are achieving up to 99.9989% efficiency. I cite these numbers merely to indicate to you the extent that we've gone in pollution abatement in the demilitarization field.

Upon arrival in this facility, each individual cluster is placed in a gas leak-proof, explosion-proof cubicle where, using sophisticated remotely controlled equipment, it undergoes a declustering operation. The picture on the screen (VG 7) shows you one such piece of equipment. This is a computer programmed mechanical arm designed to remotely pick up each one of 76 bombs, remove it from the cluster and then place it into a staking device. In the staking device the impact functioning fuze is deformed to prevent it from activating during the remainder of the demilitarization process. Also, the parachute cup is staked to the wall of the bomb to prevent the parachute from deploying during the remainder of the process. Following this, the bomb is remotely conveyed to a station where holes are punched into the wall of the bomb, and the agent is drained off. Then the bomb body with the agent removed, but the explosive component still in it, is remotely conveyed to a shearing station. At this station, a guillotine-like device pierces through the wall of the bomb and shears the central burster away from the impact functioning fuze. In the next step of the operation, the bomb is remotely conveyed into a deactivation furnace shown on the screen (VG 8).

This is nothing more than a rotary kiln which heats the bomb parts to a high temperature. Since the central burster has been sheared away from the impact functioning fuze, the explosive component will merely burn off rather than detonate in high order fashion. Following deactivation, the metal parts are conveyed to a high temperature decontaminating furnace (VG 9). By incinerating the metal components, we assure that all traces of nerve agent have been completely thermally degraded before the metal parts are taken to the salvage yard for disposal. Returning to the punch and drain operation, let us look at what happens to the agent. It is pumped to a nearby facility for destruction; as shown on the screen (VG 10). This is the same building in which we originally manufactured nerve agent GB. It has been modified for destruction of that same agent. GB is destroyed by chemically neutralizing it with caustic (sodium hydroxide). This reduces the agent to a brine solution which is then spray-dried in equipment shown on the screen (VG 11). Thus the liquid solution is reduced to the solid salt form. The dried salts are loaded in 55-gallon drums and placed into temporary storage. The status of this program is shown on the vugraph (VG 12). As you can see, we began its design in the Fall of 1969. It has taken a long time to bring onstream, principally because this is the first time an effort of this nature has been undertaken and the equipment and facility are complex. We began sustained disposal operations 29 October 1973 and expect to complete the demilitarization of the M34 cluster in the Fall of 1976.

Using the M34 cluster program as a base, let us now look at the plans for disposal of the remaining chemical stocks at Rocky Mountain Arsenal. As announced by Mr. Callaway, Secretary of the Army, on 4 October 1973, the JCS determined that the portions of the deterrent stockpile of chemical agents and munitions stored at RMA need no longer be retained. Based on this, detailed plans have been developed for disposal. Our workload requirements are as shown on this next vugraph (VG 13). As you can see, the RMA stockpile of GB is contained in large underground storage tanks, ton

containers, the weteye bomb and the Honest John warhead, with its component M139 bomblet. In this program, we would dispose of over 2,200 tons of the nerve agent GB. At the same time there are over 1,000 tons of the obsolete agent phosgene which must be disposed of, contained in ton containers. Phosgene is the commercial chemical, carbonyl chloride.

In addressing our tasks, we will be demilitarizing and disposing of all GB stocks at Rocky Mountain Arsenal. Also, we are planning for the sale of phosgene to the USAF or the conversion of the materiel by government, onsite, to a useable product, HCl.

The criteria applied to our planning for disposal recognized the need to dispose of stocks at Rocky Mountain Arsenal at an early date and a major criterion was maximum acceleration of our disposal schedules. A hallmark of the study was optimum use of concurrent disposal operations. While accelerating our schedules, we knew that we still had to maintain a high standard of safety and environmental control.

First, the Honest John warhead shown on this vugraph (VG 14). Its demilitarization will be accomplished using procedures and equipment quite similar to that which will be employed in the M34 demilitarization facility. Plans are for the Honest John warhead to be demilitarized concurrently with the M34 demilitarization program in another facility. The warhead contains 368 GB filled M139 bomblets. The bomblet, shown on this vugraph (VG 15), contains 1.3 pounds of the nerve agent GB and about .16 pounds of explosive. Thus, the total warhead contains 478 pounds of agent and almost 60 pounds of explosives.

The process which will be employed to demilitarize the Honest John warhead is shown on this next vugraph (VG 16). The process differs from the M34 in that once the warhead is opened, the bombs are removed from the warhead and placed on the conveyor manually. The balance of the operations are remote.

Our second task involves the disposal of GB in ton containers, in large underground storage tanks, and in the weteye bomb. Since the procedures for the destruction of the agent are similar, I'll discuss this as one task.

First, let's look at the ton container itself. It is shown on this next vugraph (VG 17). It is a commercial container, used to store and transport hazardous liquid. It is very sturdy with steel walls about 9/16 of an inch thick. Each ton container contains approximately 1500 pounds of the agent.

The weteye bomb is shown on this next vugraph (VG 18). It has a thin aluminum case, is 86 inches long and contains 350 pounds of the agent. It does not have an explosive component.

The process by which we would destroy the bulk agent is shown on this next vugraph (VG 19).

In the case of the weteye, the bomb is brought into the disposal facility and placed into an unloading area which is under negative pressure. Holes are punched into the walls of the bomb and the agent is drained off and destroyed in the M34 neutralization facility.

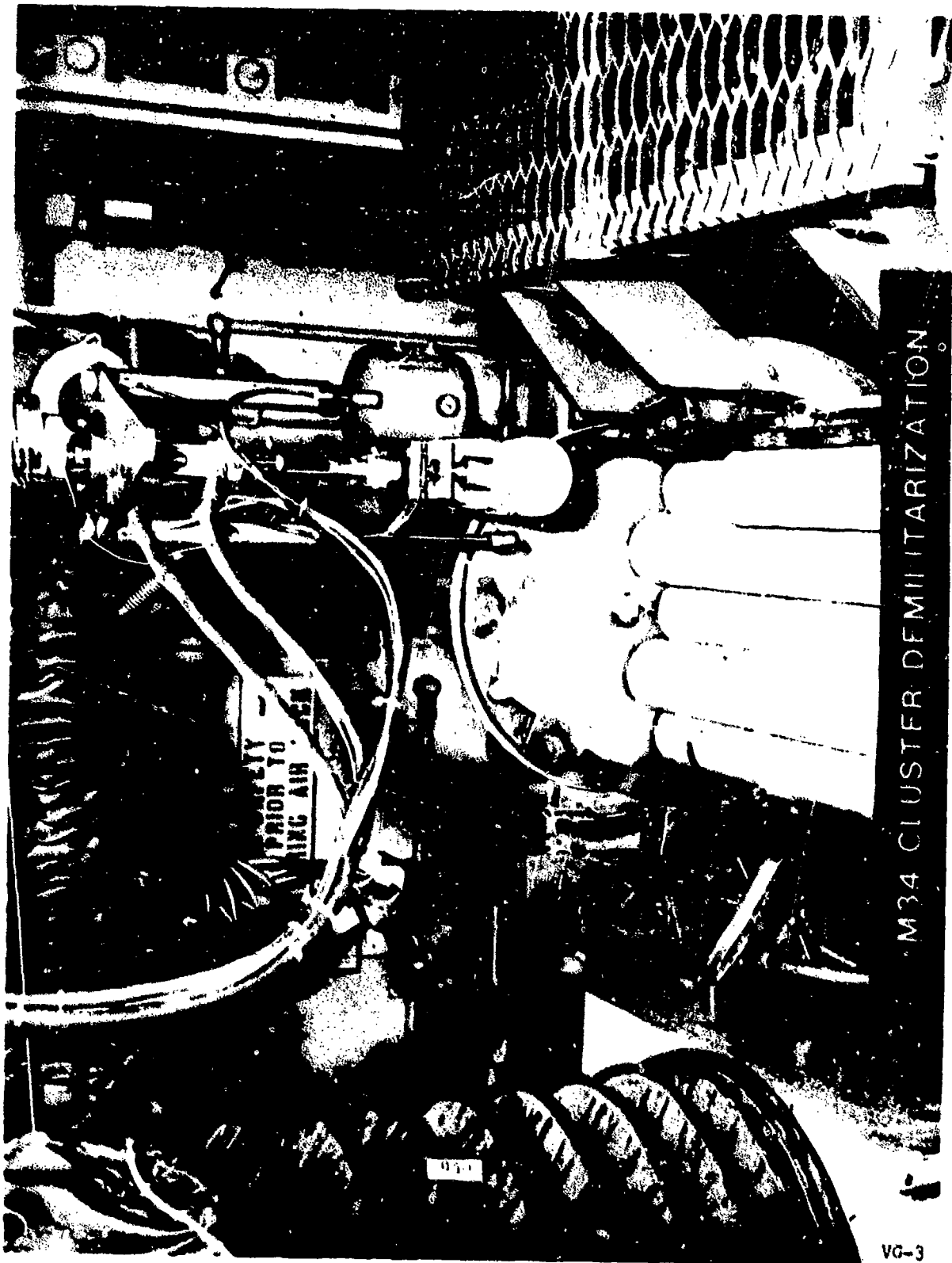
The procedure with the ton container is similar. It is brought into an unloading booth which is under negative pressure and evacuation hoses hooked up to the ton container valves. The agent is evacuated and destroyed in the M34 neutralization facility. In both cases, the metal components are decontaminated and treated at high temperature to assure that all traces of agent have been removed, prior to disposal as scrap.

The bulk GB in underground storage tanks is pumped directly into the M34 neutralization facility for destruction. The storage tanks will then be decontaminated and retained as a part of the mobilization base at Rocky Mountain Arsenal. This latter operation is in the operational phase and is scheduled for completion on 28 December 1974.

Our last task is the disposal of obsolete phosgene. It is stored in ton containers in the toxic yard at Rocky Mountain Arsenal as you can see on this next vugraph (VG 20) and each ton container contains approximately 1500 pounds of the agent.

In summary, using our ongoing M34 cluster demilitarization program as a base, we will concurrently detoxify the bulk agent GB, the Honest John warheads, and transfer the phosgene. To do this, we plan to construct a new facility for the Honest John demilitarization by adding to an existing building in the GB plants area. We awarded the contract for design and construction of this new facility in January 1974.

Rocky Mountain Arsenal experience is serving as a base for accomplishing the many other chemical disposal tasks facing us at other sites. We expect to benefit by this experience and continue this program while maintaining the highest standards of safety and environmental control.



M34 CLUSTER DEMILITARIZATION.

VG-3



941

VG-4

Reproduced from
best available copy. ©

M34 CLUSTER DEMILITARIZATION PROCESS

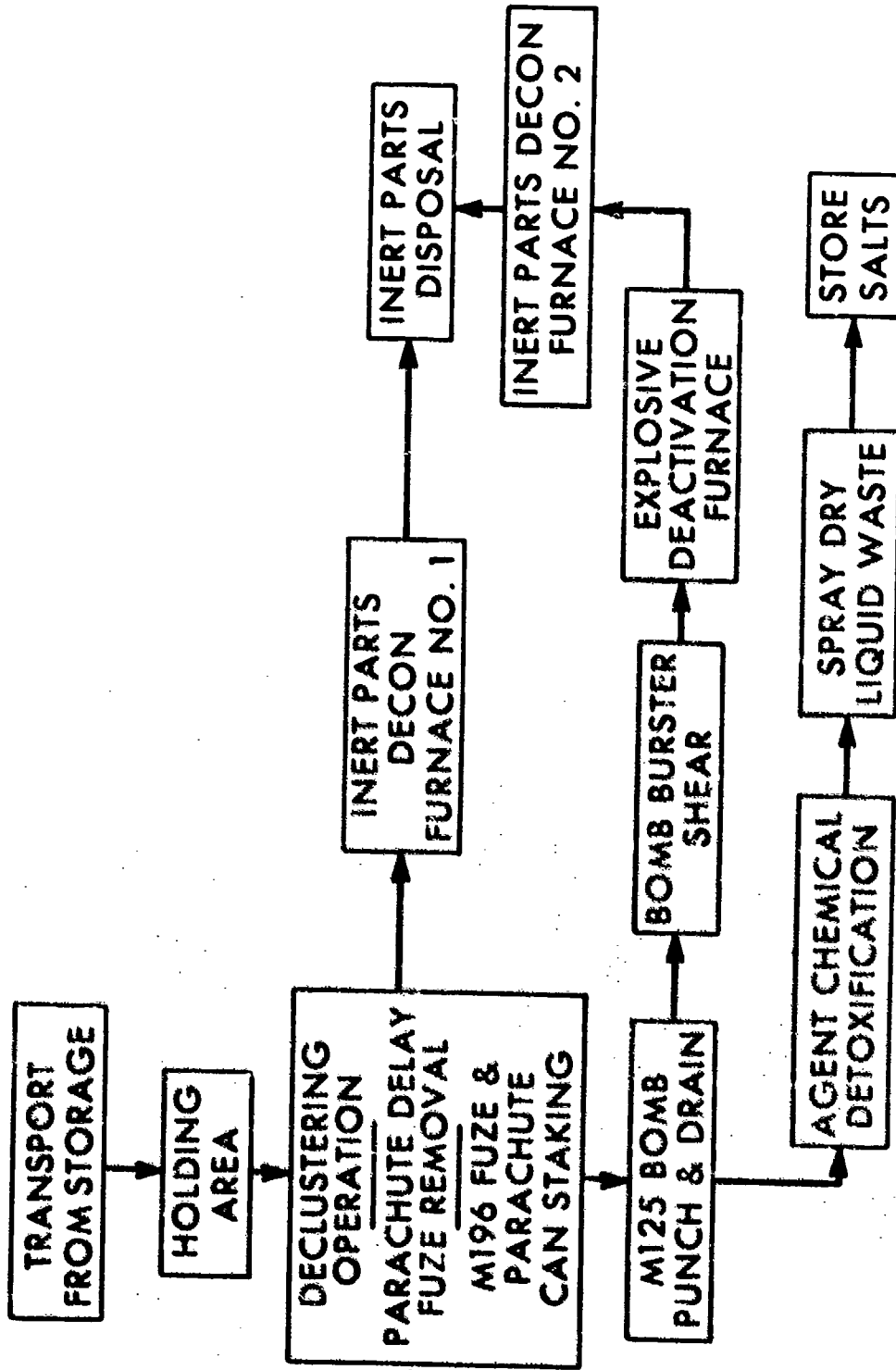
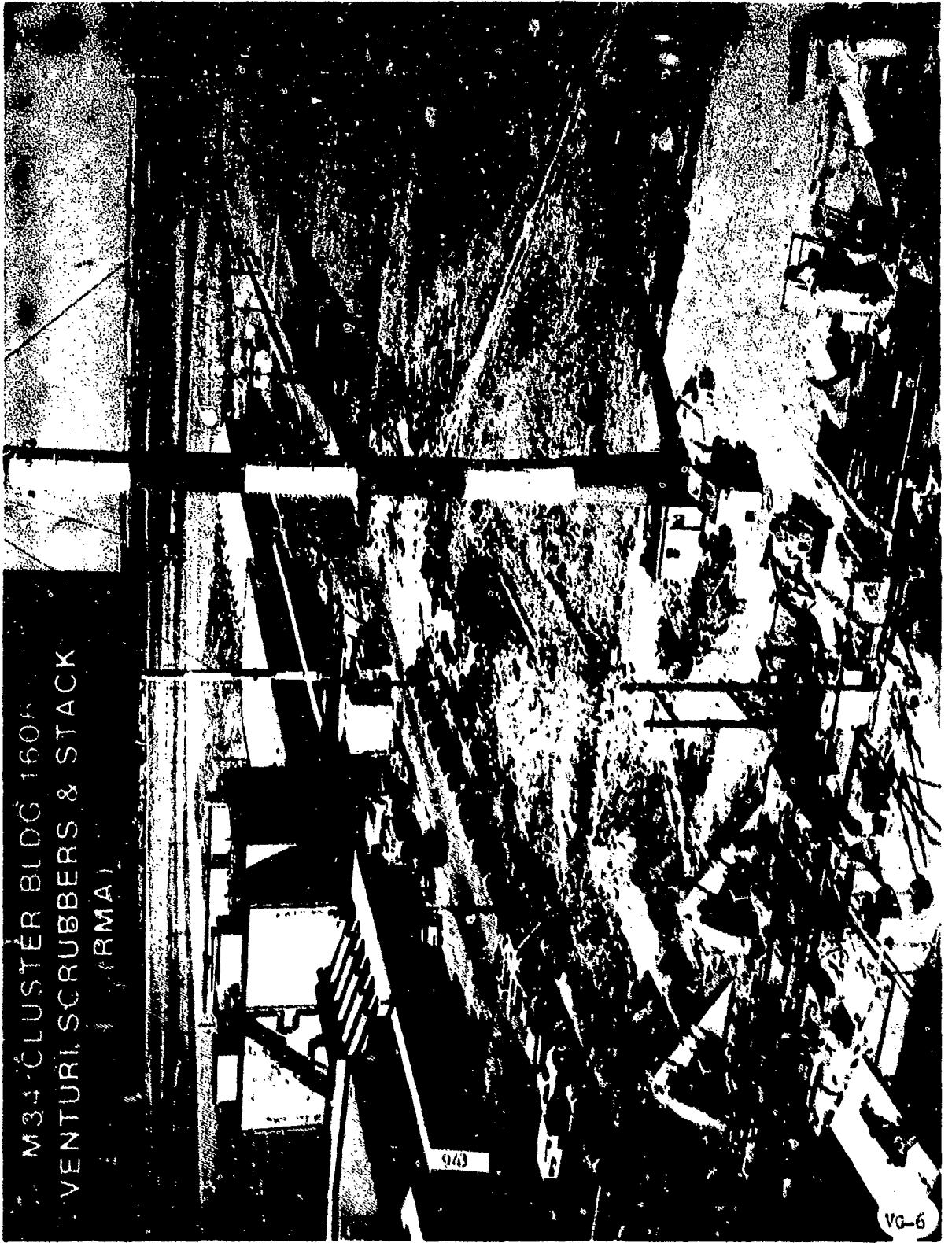


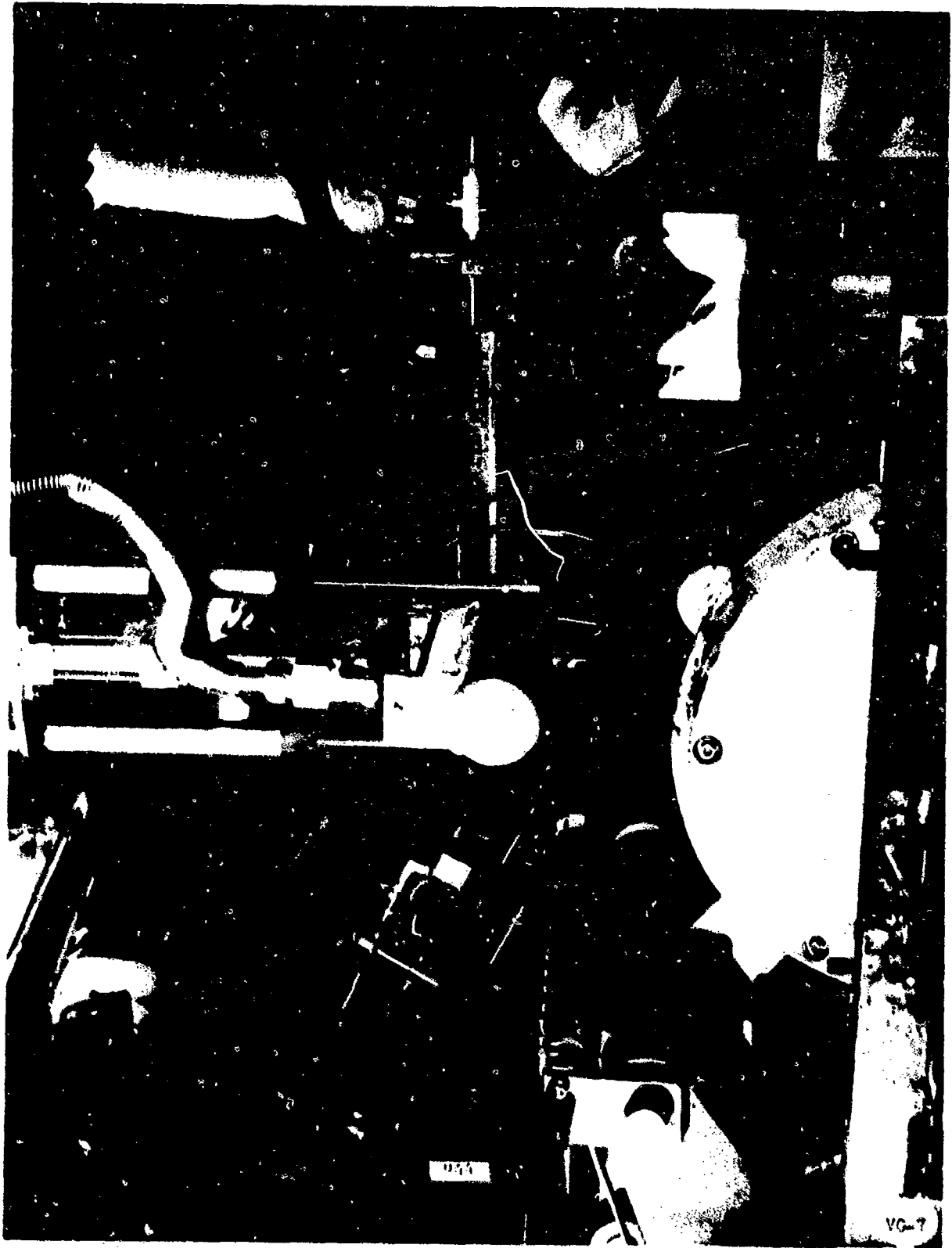
FIGURE C1A

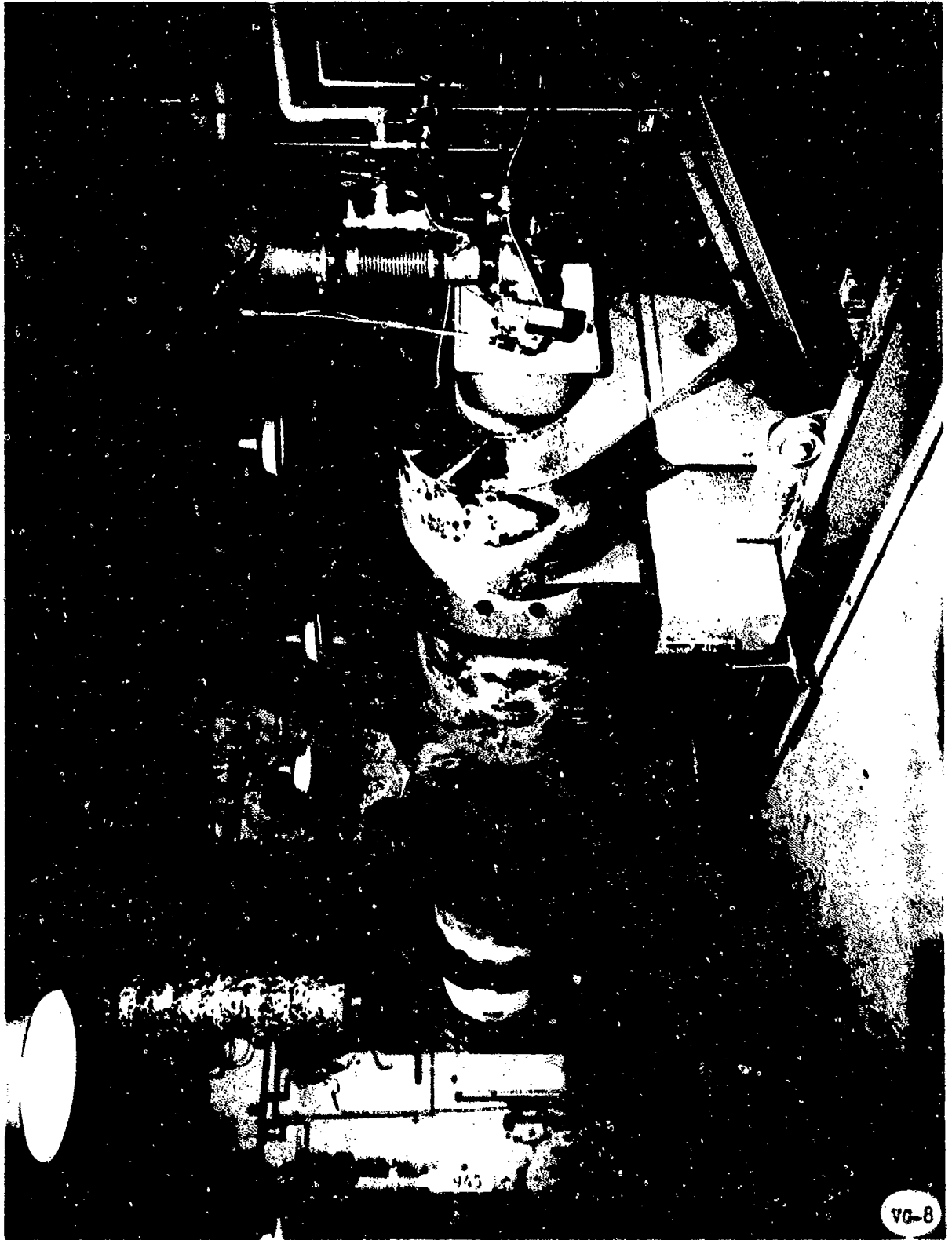
M34 CLUSTER BLDG 160F
VENTURI, SCRUBBERS & STACK
(RMA)



943

VG-6



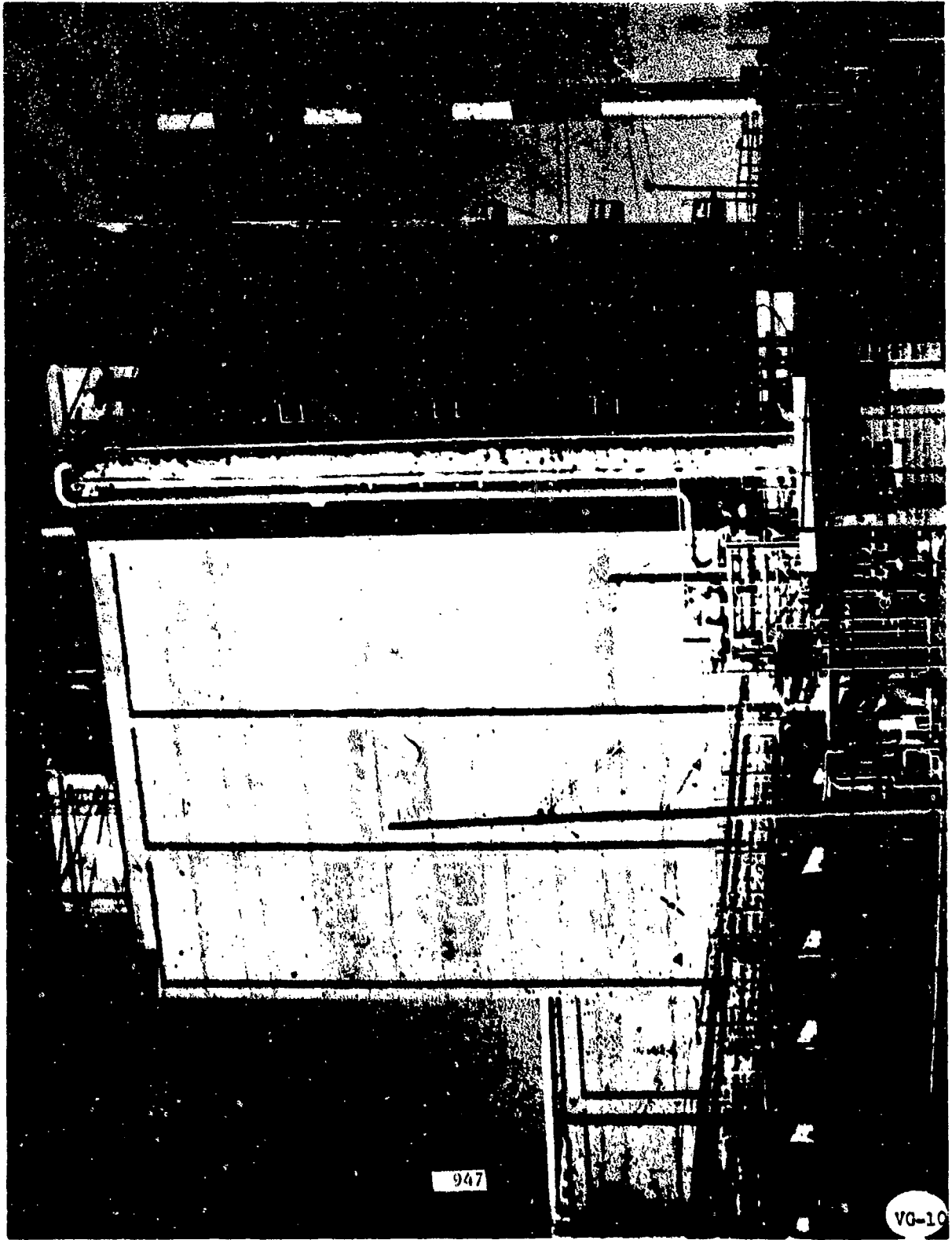


VG-8



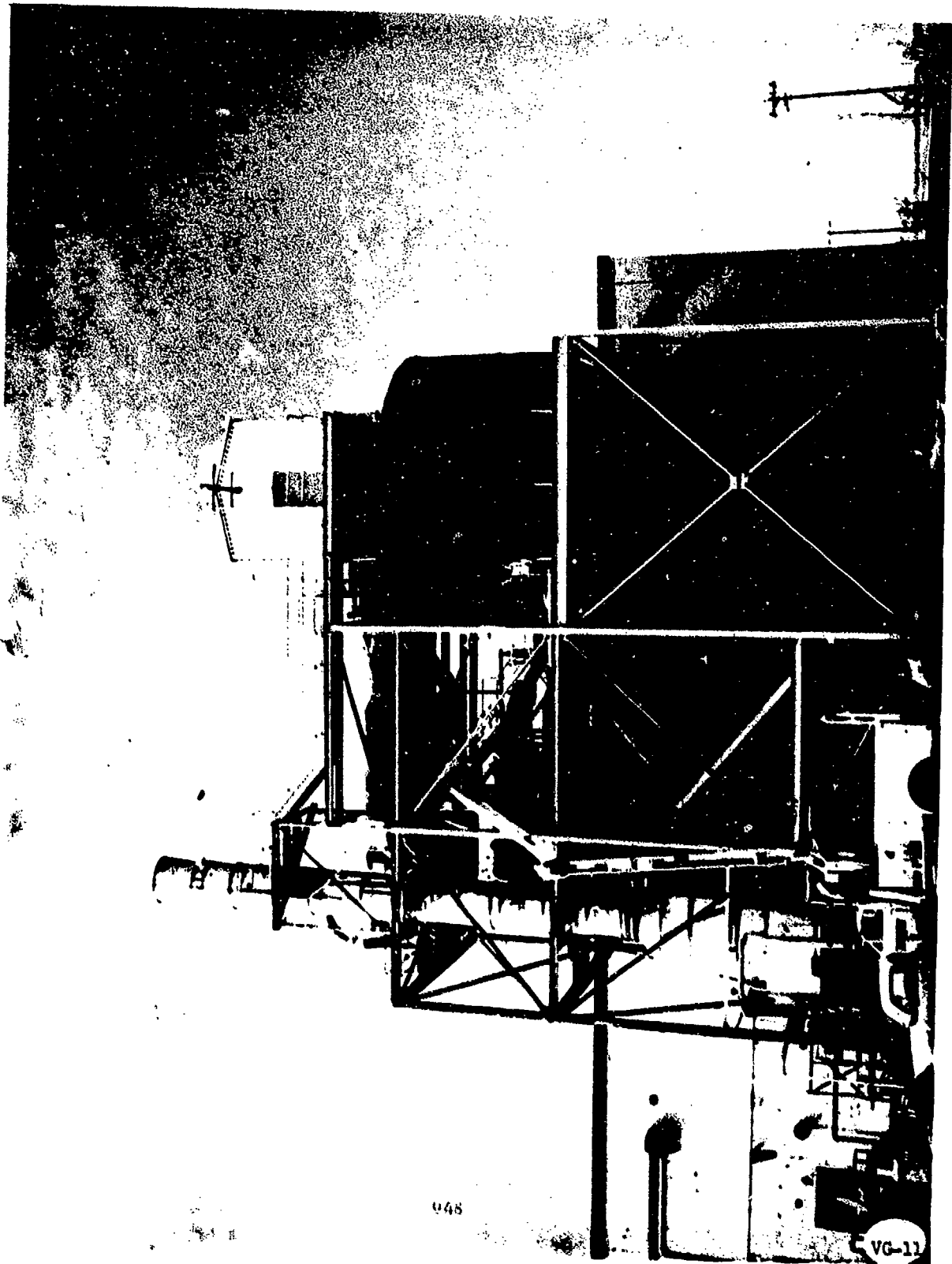
940

VG-9



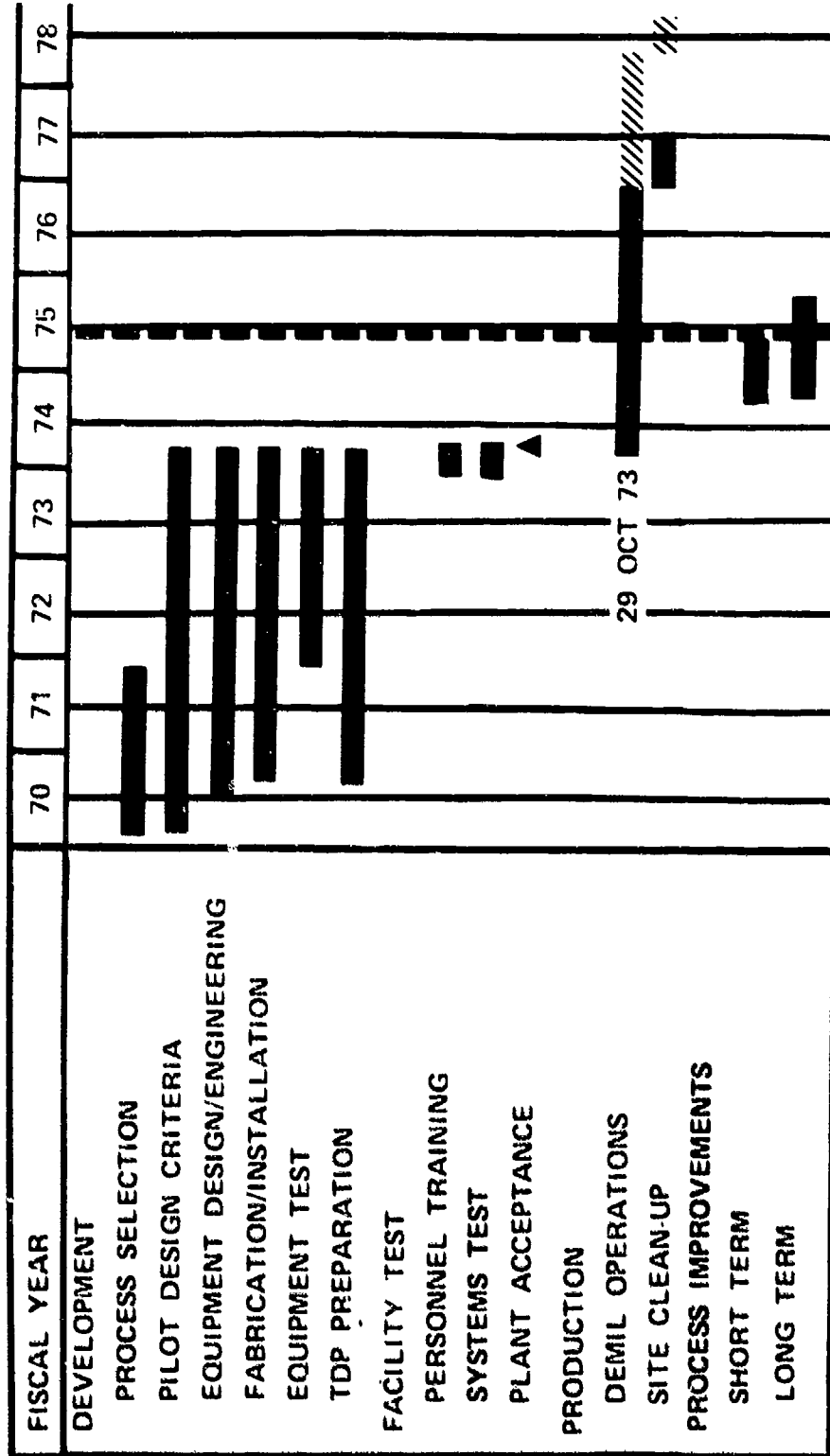
947

VG-10



M34 CLUSTER DEMILITARIZATION

PROJECT SCHEDULE



////// REVISED OPNS SCHEDULE

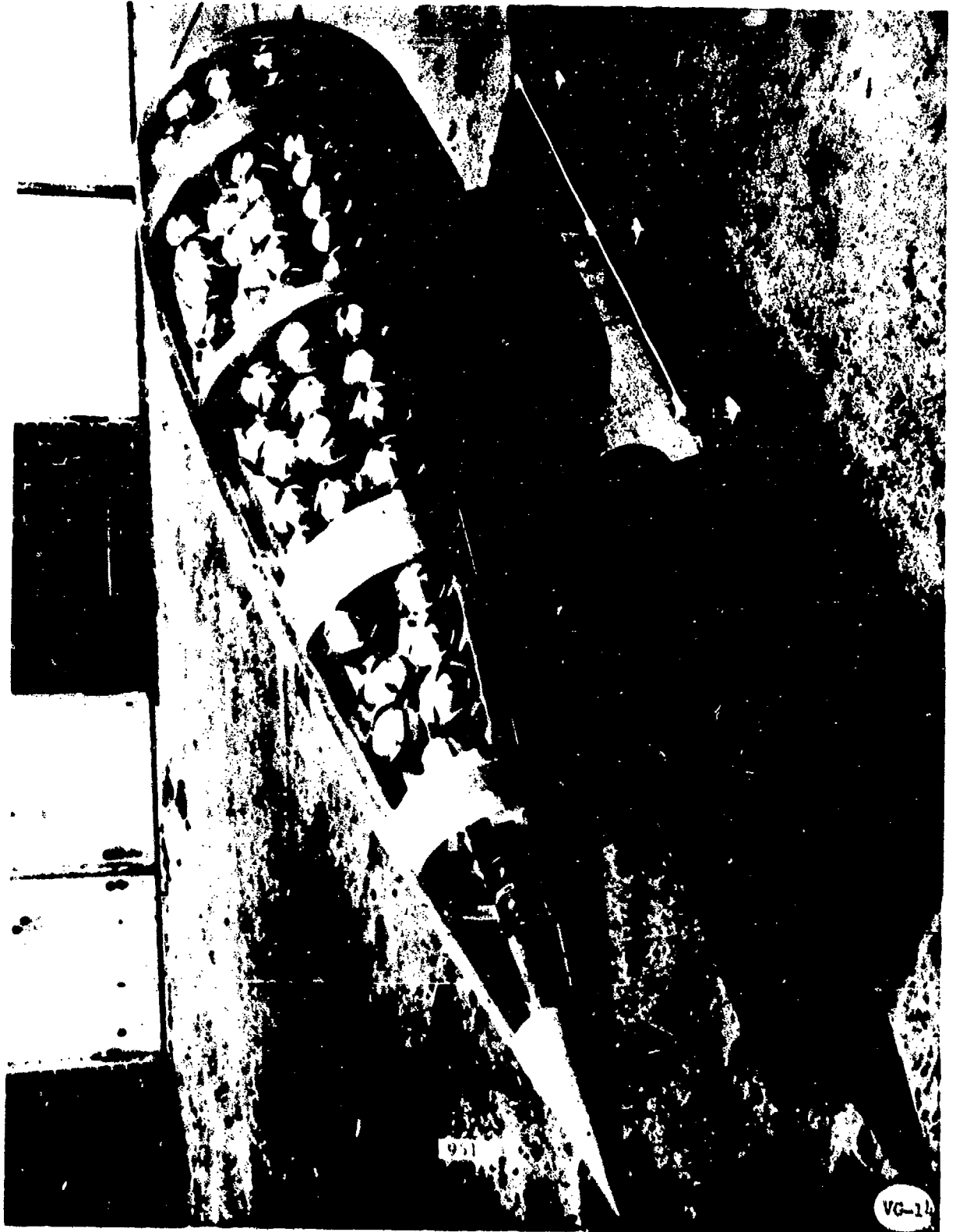
TODAY

FIGURE

WORKLOAD REQUIREMENT

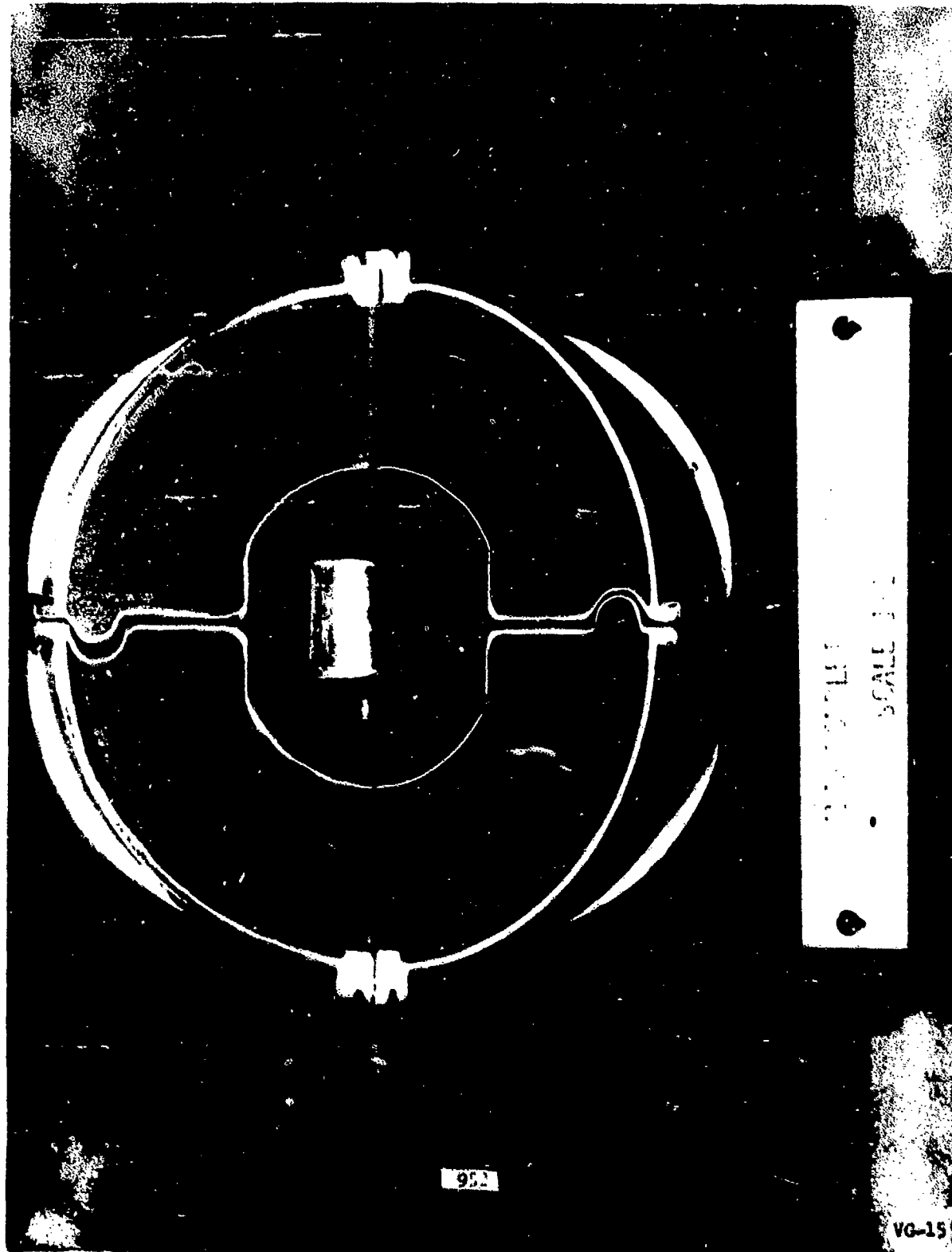
	TONS OF AGENT
GB (WAR RESERVE)	
BULK STOCKS	
(TON CONTAINERS, UNDERGROUND TANKS)	2055
WETEYE BOMBS	157
HONEST JOHN WARHEADS	25
BOMBLETS FOR HONEST JOHN	14
	TOTAL 2251
PHOSGENE (OBSOLETE)	
TON CONTAINERS	1039

950



931

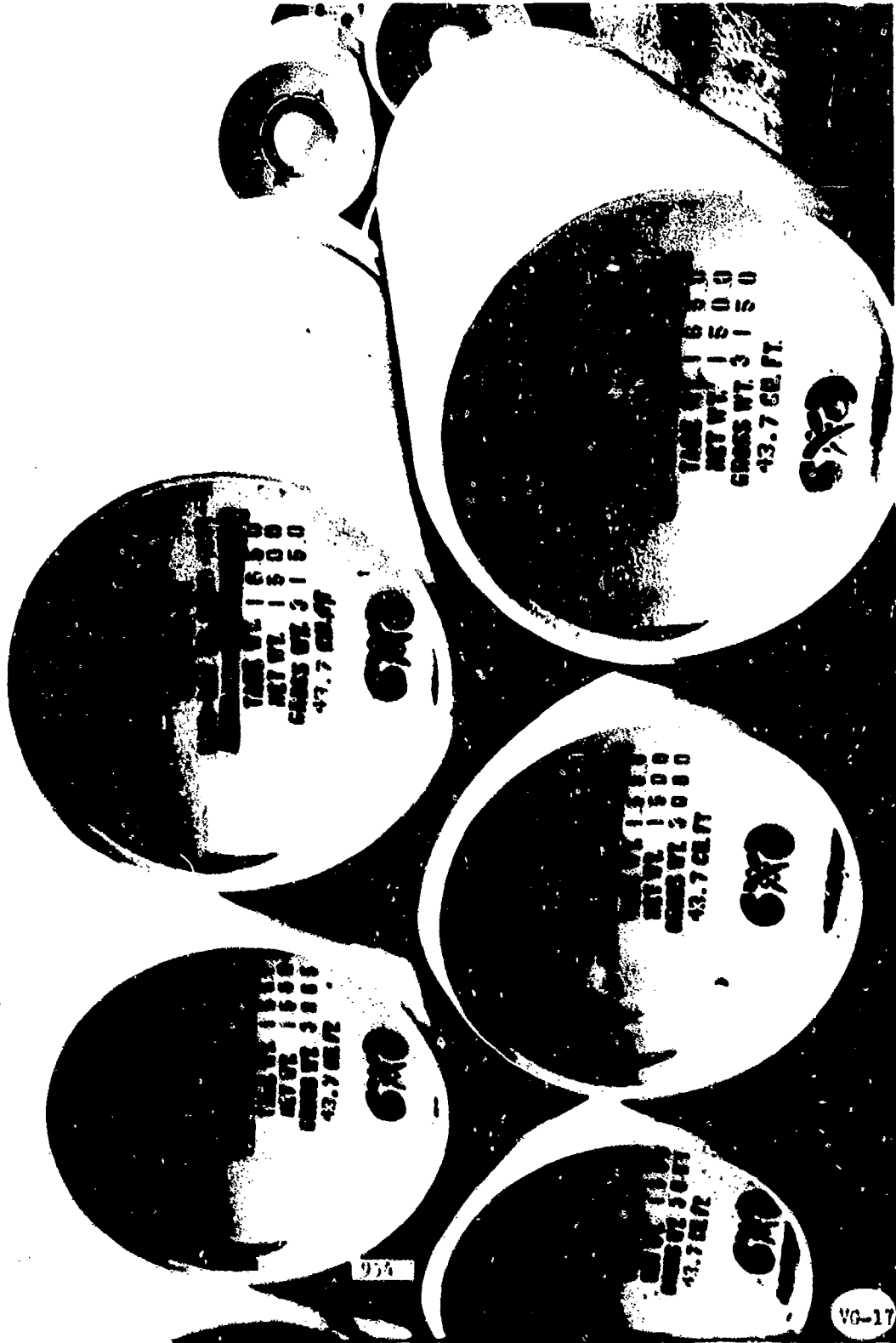
VG-14



SCALE

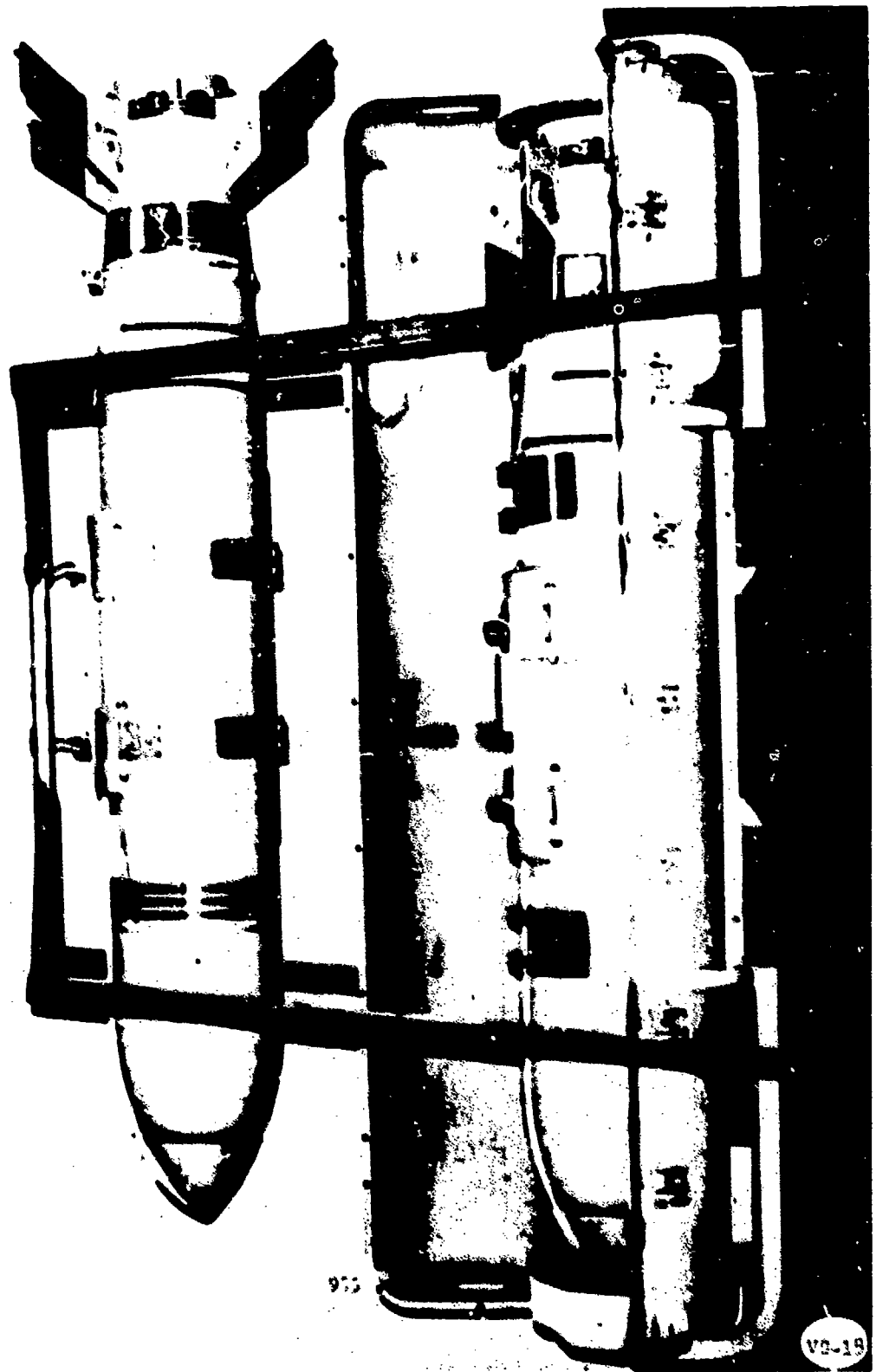
952

VG-15



954

VG-17



955

VC-18

WETEYE BOMB DEMILITARIZATION PROCESS

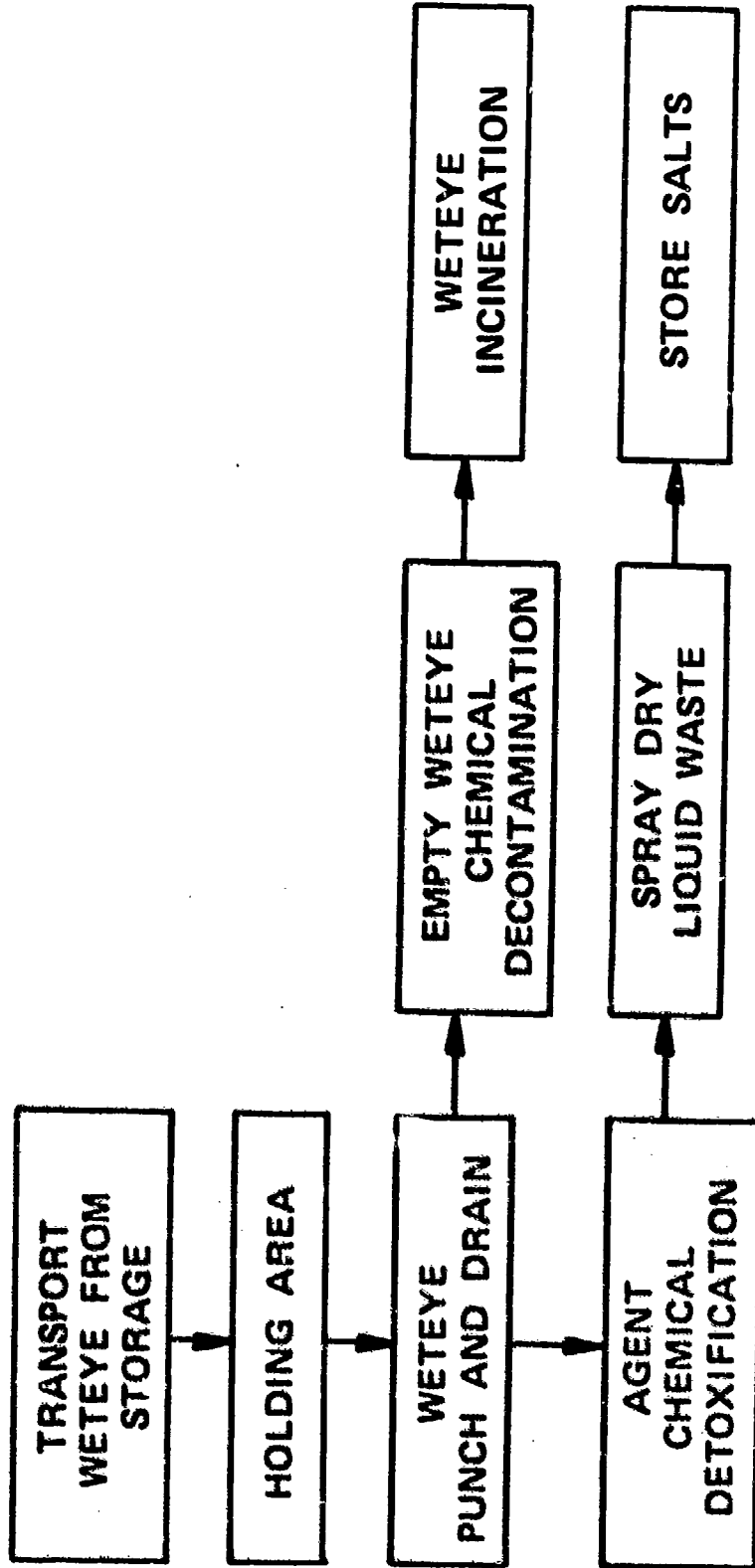
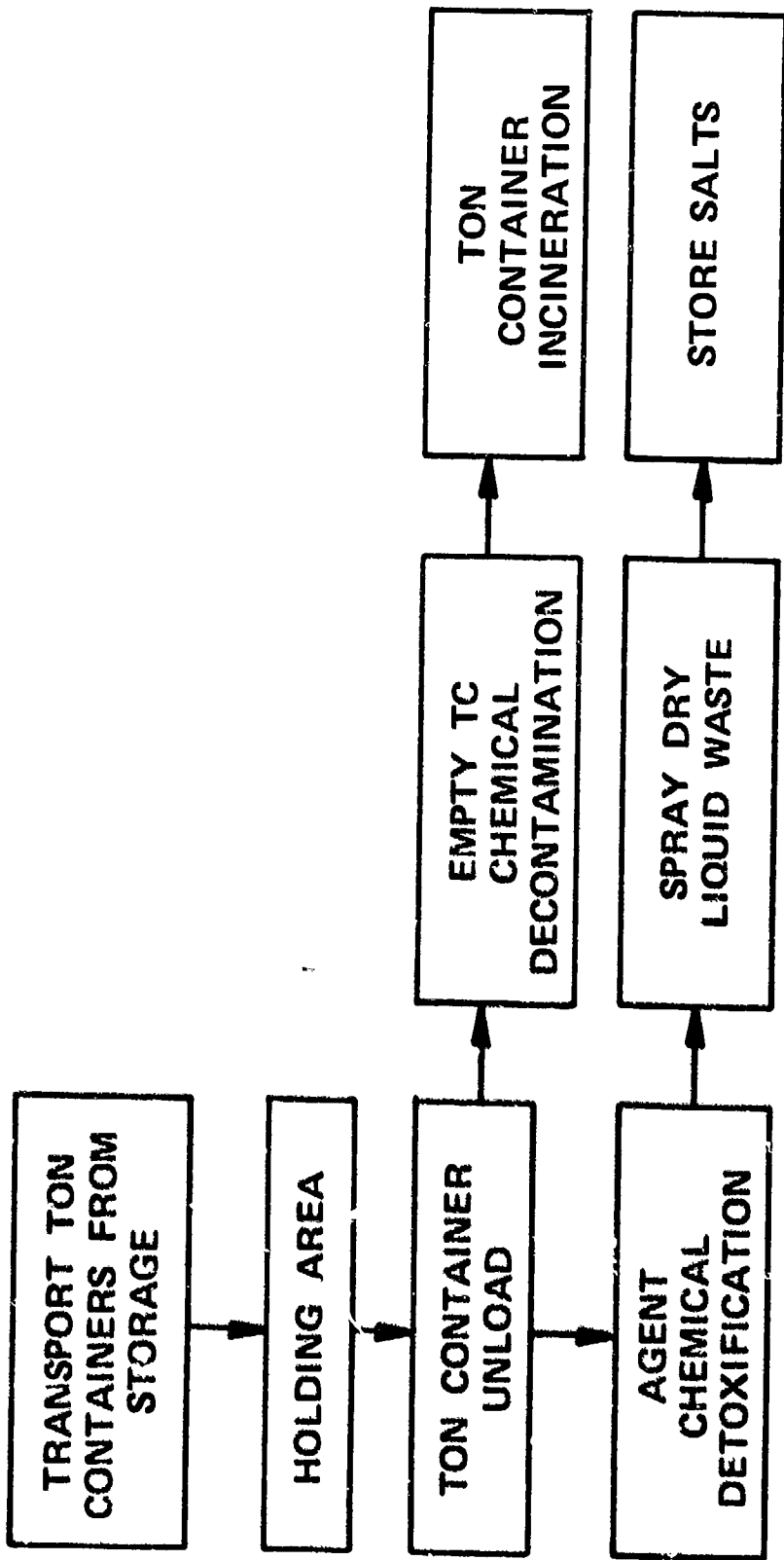


FIGURE W1A

BULK GB IN TON CONTAINERS DEMILITARIZATION PROCESS



957

FIGURE TC1A

BULK GB IN UNDERGROUND TANK DEMILITARIZATION PROCESS

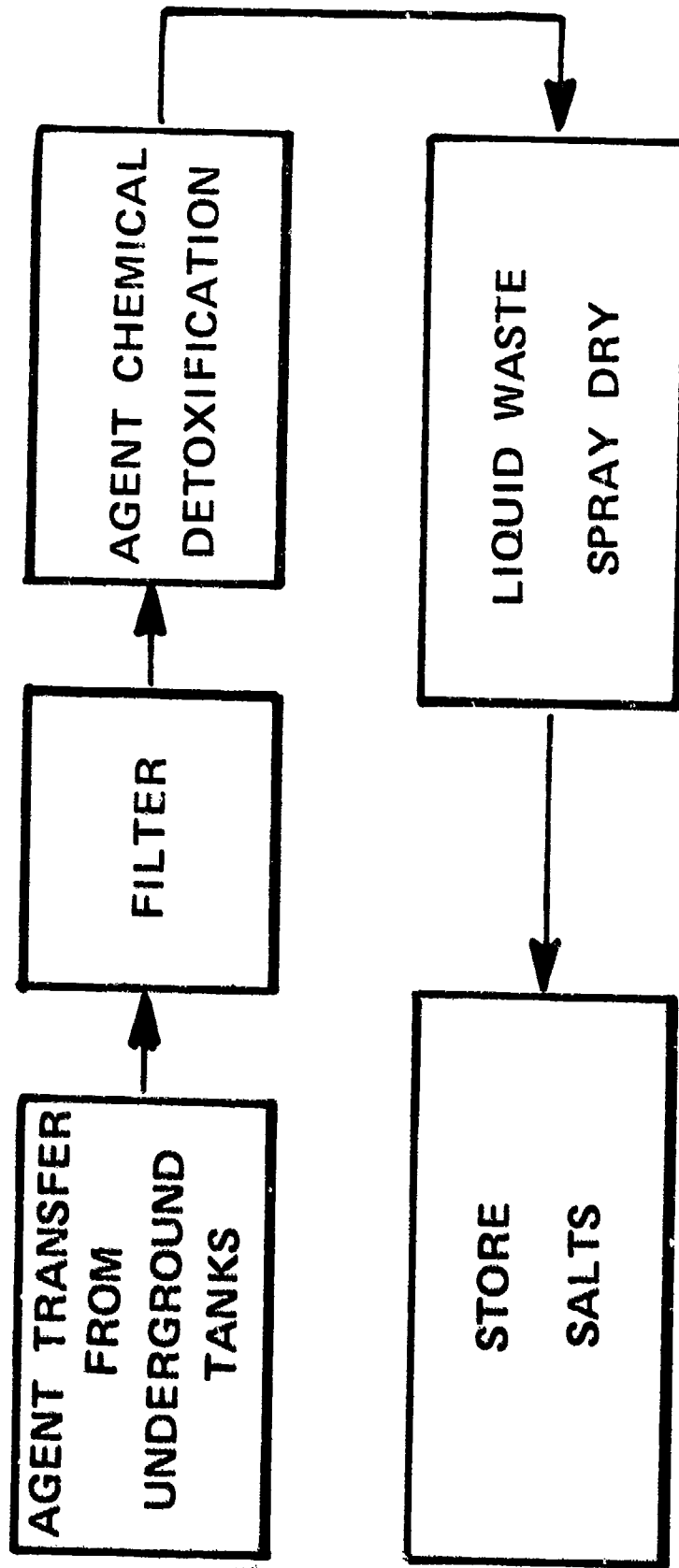
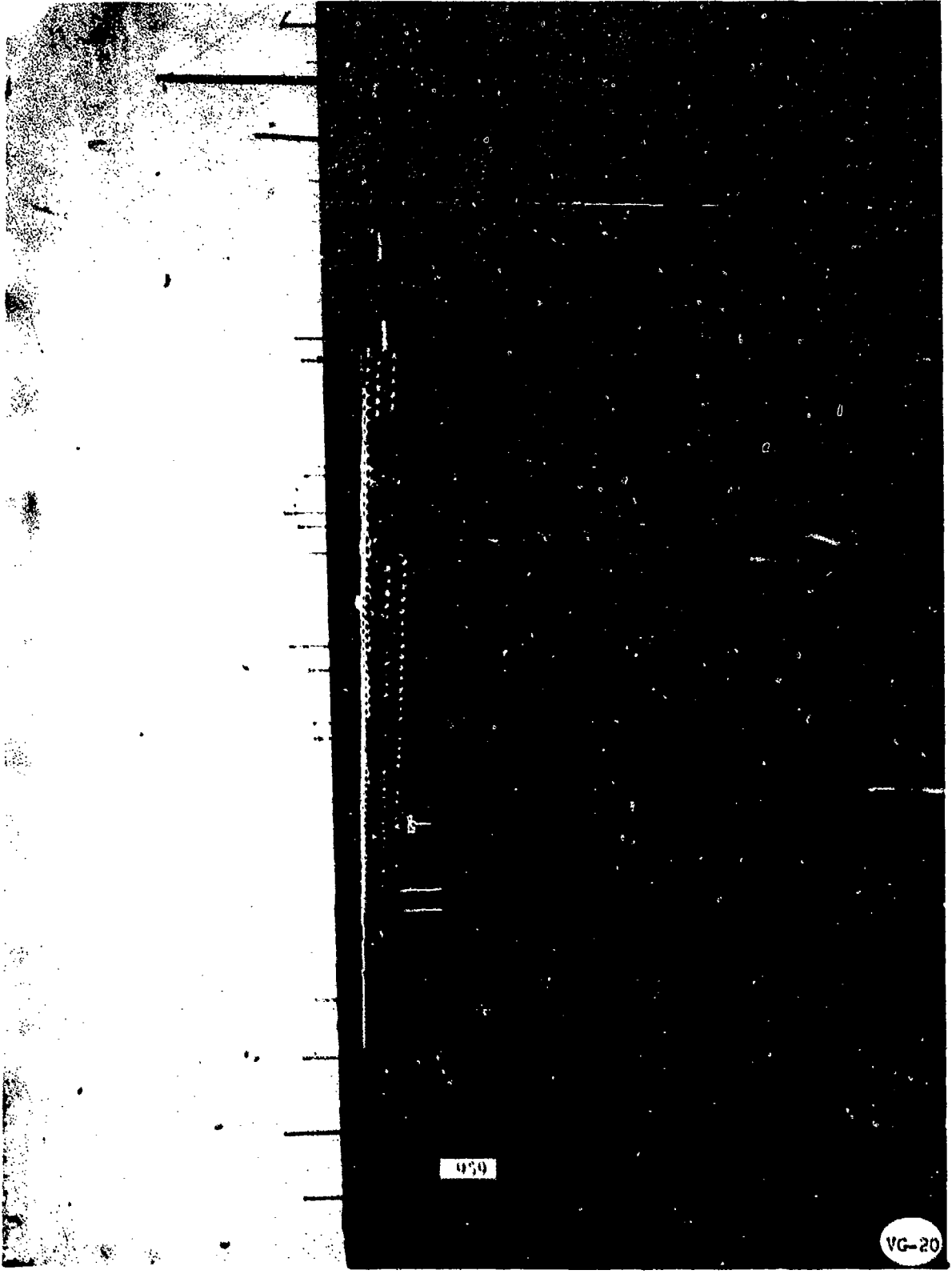


FIGURE UT1A



050

VG-20

MODULAR DISPOSAL PROCESSING FACILITY

I. INTRODUCTION

a. There are a variety of materials generated at an Army Depot that have historically been disposed of by open burning and detonation for munitions and combustibles, and land fill for inert and domestic wastes. Current disposal methods do not meet present and proposed pollution abatement criteria, hence the AMC Ammunition Center was assigned a project by Headquarters Army Materiel Command to recommend new methods for disposal. It appeared possible to use the system conceived for ammunition related waste for all solid wastes generated at an Army Depot.

b. In order to evaluate the feasibility of this enlarged concept a data acquisition phase was initiated to determine the current state-of-the-art that could be applied to a flexible disposal system. Economics dictate that some methods of burning and detonation are the most advantageous techniques for disposal of energetic materials. The area of greatest concern is performance of these techniques without causing pollution to the environment. It was found that commercial equipment and operational techniques for performing specific ecologically acceptable burning and detonation existed at scattered industries, research and development laboratories and government activities. These equipment and operations were fluidized bed reactors for incineration of combustibles, confined detonation chambers for explosives, slurring techniques for incineration of energetic materials, water removal of case-bonded missile propellants and granulation of rocket propellants. The Center's concept brings together the existing equipment development and operational techniques to provide for a modular disposal processing facility for Army Depots' explosives and

solid waste. Other processes such as over-fired open pit incinerators were investigated and found to be severely limited or not acceptable for disposal of energetic materials.

c. Section 211 of the Solid Waste Disposal Act, as amended, requires that all Federal agencies establish guidelines on proven procedures for operation of solid waste management systems. The development of processes and/or procedures which can serve as the basis of adequate hazardous waste management practice require (1) the identification of materials for which adequate methodology does not exist or is economically untenable, and (2) the creation of adequate processes or procedures.

II. PURPOSE

a. To develop an environmentally acceptable disposal processing facility for AMC depots to process "explosive waste" and include the flexibility and variety of capabilities in the disposal system to accommodate all waste materials generated by depots in the accomplishment of their missions. A major objective is the demilitarization of those munitions that current disposal technology limits to open burning and/or open detonation.

b. These objectives can be accomplished as follows:

(1) A modular thermal disposal processing facility utilizing fluidized bed technology for incineration of explosives and solid industrial type and liquid waste, decontamination of metal ammunition components, and waste generated from ammunition operations is a process system that will adequately give the necessary waste management - disposal capabilities for AMC depots. The facility brings together the technologies of shredding, slurring, granulation and re-cycling to provide for complete

thermal processing of the several dissimilar but combustible materials in a single disposal system. With quick and complete combustion possible, the requirement for gas cleaning equipment to meet air pollution regulations is significantly reduced.

(2) For items of explosives that cannot be accommodated by incineration, technology is available for detonation of up to 100 pounds of explosives and for functioning of pyrotechnics within a confinement chamber; exhausting the gases through the fluidized bed reactor for total oxidation with nearly zero environmental (noise, air and water) pollution. Greater explosive weight capabilities can be designed into the chamber.

(3) The hot gases from the fluidized bed reactor can be directed through a chamber and utilized for decontamination (replacing flashing techniques) for washed-out projectiles, bombs, etc. and materials and equipment where size permits. Burn-out of explosive fillers can also be accomplished in this facility.

III. EXISTING DISPOSAL FACILITIES

The following existing disposal facilities are undergoing modifications to provide for pollution control systems that will make these facilities environmentally acceptable.

(1) Deactivation Furnace: APE 1236 Deactivation Furnace is a specially designed rotary kiln furnace used to safely destruct small arms, boosters, fuzes, blasting caps and other munitions that can be sized to 600 grains explosive content. Efforts are under way to develop pollution controls which will satisfy environmental standards and to perform size reduction of munitions such that explosive content is within the destruct limits. Problems of characterizing and measuring emissions are being identified to allow generation of data required for prototype pollution control system development.

(2) Washout Facilities: Washout of explosive fillers from larger items such as bombs, separate loading projectiles, fixed and semi-fixed projectiles and separated ammunition can be adequately accomplished with the APE 1300 Washout Facility. Efforts are in progress to expand this capability through development of additional washout racks to accommodate smaller and/or peculiar shaped items. In addition, development of treatment methods for controlling contaminated waters to meet environmental standards have been identified. A problem still remains in the disposal of explosive laden sludge from the washout plant operations and flashing of metal munition casings.

(3) Open Burning and Detonation: Open burning and detonation facilities existing at all AMC Ammunition Depots are no longer environmentally acceptable.

IV. CONSTRAINED MATERIALS

There are numerous ammunition items that are not suitable for demilitarization by deactivation furnace and washout systems. In addition, current disposal methods for other waste generated at Army Depots present an environmental problem. Most of these materials fall into the following general categories:

- (1) Large missile motors and rocket launchers.
- (2) Rocket motors.
- (3) Permanently enclosed (sealed) H.E. loaded items - bombs, mines, CBU's etc.
- (4) Bulk H.E., demolition charges, bulk artillery and small arms propellant, etc.
- (5) Pyrotechnics.
- (6) Contaminated combustible materials from ammunition maintenance operations - packing materials, dunnage, etc.

(7) Unserviceable combustible fluids, such as solvents, cutting oils, industrial fluids generally.

(8) General domestic and industrial wastes.

V. UNCONSTRAINED PROCESSING. The modular thermal and confined detonation processing facility is intended to replace those disposal operations currently and historically limited to accomplishment by burning or demolition for explosive related materials and open burning or land-fill for inert materials. The system is to accommodate all current inventory as well as projected future disposal inventories. With the exclusion of radioactive materials, the processing facility will be oriented to Army materials but will also be compatible with many materials in the stocks of other services. This system is unique in its versatility such that it will accommodate disposal of combustible general supply waste, industrial shops waste and domestic and office wastes. Salvage and recovery features can be integrated with this system wherever feasible.

VI. SYSTEM CONCEPT. The disposal processing facility will consist of three (3) basic reactor units; fluidized bed reactor, confined detonation unit, and a decontamination oven, each of which is multi-purpose and complements the other in accomplishing an environmentally acceptable disposal process. All of the reactor units are serviced by a single highly flexible exhaust gas treatment section.

(1) Fluidized bed reactor. The fluidized bed reactor will accomplish disposal of all combustible material. It represents a process system that offers several advantages over conventional incineration. The operating temperature conditions in a fluidized bed reactor can be readily controlled within very narrow ranges, a factor

which makes possible the incineration of carbonaceous waste while minimizing the generation of noxious fumes and particulate matter. When a combustible particle is added to the bed, transfer of energy to this particle is rapid, and the particle quickly reaches its ignition temperature. Combustion begins and the heat of combustion is rapidly transferred to the bed of solid particles (sand). Because of the motion of both the gas and the solid, contact between the burning particle and the oxygen in the gas is excellent. No hot zone will develop in the bed.

Energetic materials (explosives and propellants) are amenable to combustion in the fluidized bed reactor since this material can be introduced as water slurries thus controlling the heat energy release to a constant B.T.U. value. Packaging materials, dunnage, domestic and office waste can be shredded to facilitate uniform feed and constant B.T.U. value. Excess air required to sustain combustion can be as low as 5%. This reduces the formation of oxidized gases, resulting in small volume gas cleaning equipment to meet air pollution standards.

(2) Confined detonation chamber. The confined detonation chamber is a reinforced concrete blast containment structure for detonation of explosives in quantities up to 100 lbs. and for functioning of pyrotechnics and munitions that cannot be opened or for which disassembly is uneconomical and whose explosives charge exceed the limits of the deactivation furnace. The chamber attenuates noise, contains explosive particulate, and allows gaseous emissions to be directed through gas cleaning equipment prior to release to the atmosphere. The chamber can be exhausted in 3 to 10 minutes, thus allowing a relatively short cycle time between detonations.

All necessary safety features can be interlocked to prevent any accidental detonation or functioning of munitions when exposure exists. Included are windows in the control room to provide visual surveillance before and after function to determine that all safety features are operative. An emergency entrance hatch is provided should main chamber openings become blocked in the closed position by debris during an explosive event.

(3) Decontamination chamber. Considerable metal parts, projectiles, and bomb casings are generated from explosive washout and possibly microwave melt-out operations. Open flashing of these materials will be in violation of air quality standards. These contaminated metal components will be placed in a chamber positioned in the exhaust gas line of the fluidized bed reactor to accomplish decontamination by "inductive" heating. An advantage of utilizing the exhaust gases (1000°F to 1400°F) from the fluidized bed reactor is the low oxygen content which minimizes the production of oxides emissions yet is of sufficient temperature to completely pyrolyze any contamination to an inert condition.

The decontamination chamber will include provision for expansion of its operational capability to serve as a burn-out station for some fillers.

The emissions from the decontamination of metal components or burn-out will pass directly to the gas cleaning equipment and if necessary may be returned to the fluidized bed reactor for additional oxidation of effluents that otherwise would become secondary emission to assure an efficient cleaning before release to the atmosphere.

VII. POLLUTION CONTROL TECHNOLOGY

a. Air pollution control equipment will be selected to scrub gaseous effluents

which may be grouped into four categories of emission groupings in the following order of difficulty: (1) burning of propellants and explosives, (2) thermal decontamination of metal parts, (3) burning of dunnage, packing materials, and ammunition maintenance operation's scrap and, (4) signals, flares, smoke and incendiary items. The philosophy of air pollution is to "prevent it" or "correct it". Air pollution can be prevented by designing the process or machinery with control equipment that eliminates or reduces the pollution at its source. The fluidized bed reactor system represents this "control of the source" by reducing or eliminating the production of difficult to clean emissions. Because of the relatively low temperatures generated, and small excess air, no appreciable nitrogen oxides are produced. The distillation products are consumed in the bed thus eliminating unburned hydrocarbons leaving the unit. The results are cleaner stack emissions with less scrubbing operations, since the primary pollutant is particulate matter.

b. Control equipment will be venturi collectors and packed tower scrubbers. The venturi collects particles to the 0.1 micron level such as metallurgical fumes and zinc and magnesium oxides, and recovers soluble gases. The venturi design relies on high gas velocities on the order of 100 to 500 ft/sec through a constriction where water is added. The impact breaks the water into droplets with the fineness of spray determined by gas velocity. The packed tower scrubber removes dust but primarily is designed for gas absorption. Gas-liquid flow is counter current and with extended surface packings provides absorption by spreading the liquid surface while collecting particulates by cyclone action.

Particulates, dust, fly ash, etc. are collected in the wet discharge and disposed by land fill.

c. Source testing will be performed to obtain emission data. Continuous sampling devices that provide accurate record of emissions will be utilized. Monitors using spectroscopic, chromatographic or chemiluminescent reactions are available for accurate testing and control of pollutants.

VIII. ENERGY CONSERVATION

a. Since this system utilizes the fluidized bed reactor to process all combustible waste and will be in operation during all disposal operations, recovery of the heat generated will be considered. This heat energy could be recovered in the form of steam which in turn can be used directly as process steam or for facility heating, or for electrical power generation. Considering the disposal facility's necessarily remote location and low requirement for process steam or facility heating, the most practical approach to energy recovery would be to generate electrical power. There is a continuous demand and the power can readily be distributed to points of utilization.

b. In designing the prototype disposal system, provisions to allow energy recovery through power generation will be studied. The equipment associated with this could be installed near the end of the prototype testing phase.

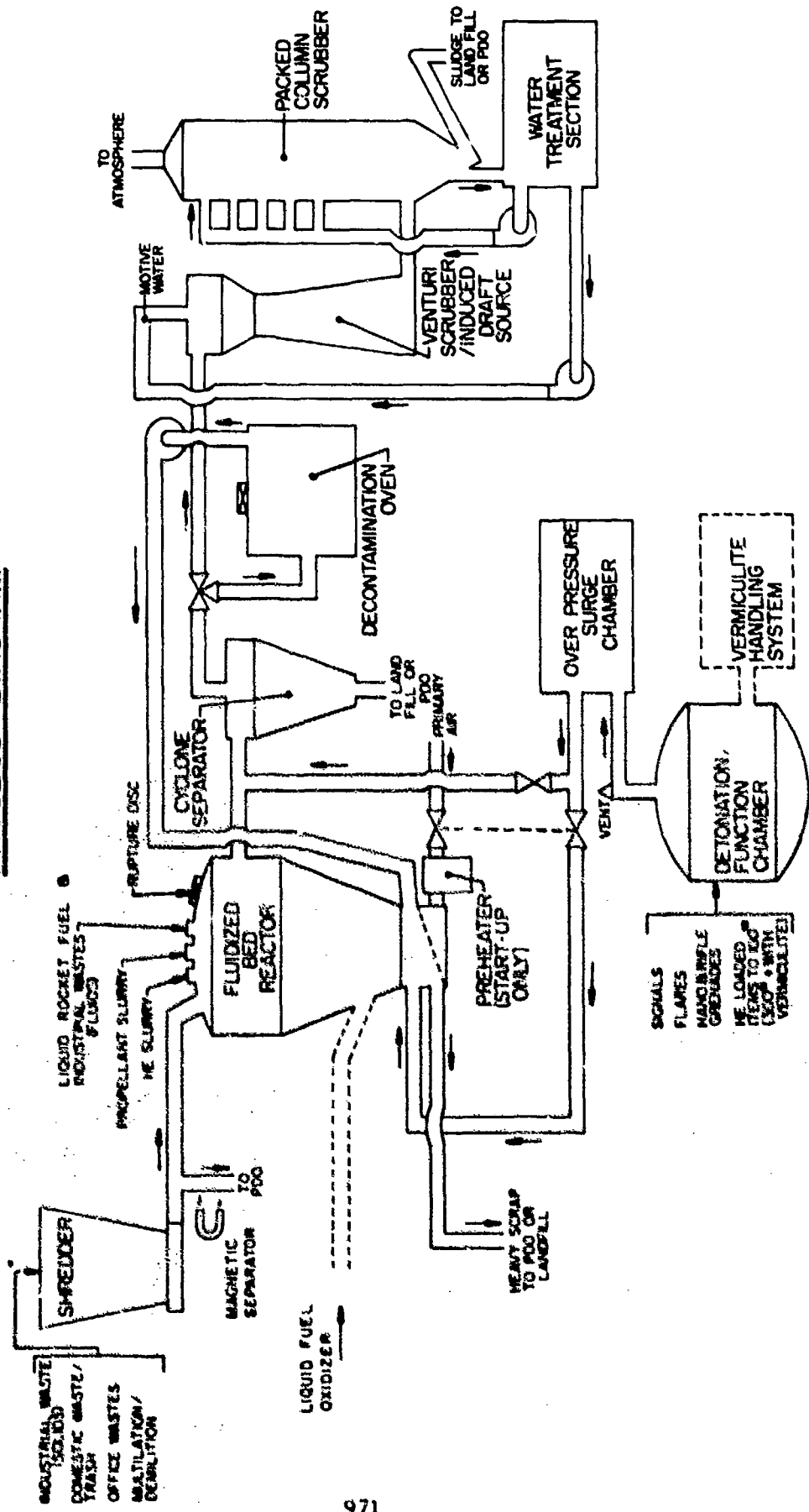
IX. SAFETY

The disposal system concept has been reviewed by both the AMC Safety Office and the Department of Defense Explosives Safety Board. No significant safety problems were discovered during these initial reviews.

PHYSICAL STATE OF DISPOSAL MATERIALS

Types Preparation for Disposal	Artillery/ SAA		Rocket Grains		Slurys		HE Pellets Sludge	← Combustible Granular Filters →	Solids		Combustible Office, Domestic, and Ind. Wastes	
	Case Banded	Case Banded	Case Banded	Case Banded	Packaging	Mutilation/ Demil			Solids	Liquid	Gases	
Receive & Temp. Store	x		x				x				x	
Unpack & Transfer	x		x				x				x	
Surge, for process	x		x				x				x	
Segregate for screen products												
Shoe/puncture												
Chip												
Granulate												
Hydraulic erosion												
Shred												
Magnetic separation												
Air classification (size & Wt.)												
Types of Disposal												
Defonate (confined)												
Function/activate (confined)												
Incinerate-fluidized bed												
Floath/burn off												
Compact/bale												
Safe - PDO												
Land fill												
Pollution Controls												
Cyclone Separator (dry Partic.)												
Venturi scrubber, multi-stage												
Closed water system												
Packed tower, multi-stage, counter flow current												
Catalytic Pkg., as/if reqd.												
Reagent, if reqd.												
Closed water treatment system												

PROCESS DIAGRAM



1. Fluidized Bed Reactor.
2. Function - Purpose in System: Burn combustibles (any combustible material) in various forms.
 - a. Slurries.
 - b. Solids.
 - c. Gases.
 - d. Fluids from industrial operations.
3. Reason for Selection - Advantages/Merits:
 - a. Simple, reliable principle of operation.
 - b. Durable - very little maintenance or attention.
 - c. Highly adaptable to wide operating temperature range, easily controlled.
 - d. Very close temperature control. ($\pm 5^{\circ}\text{F}$. at 1300°F can be maintained.)
 - e. Close control of primary air and operating temperature minimizes off-gas treatment required. (5% excess air can be maintained.)
 - f. Possibly use catalytic bed to further minimize noxious off gases.
 - g. Variable rate of heat generation by numerous types of materials to be processed is no problem.
 - h. Operating temperature highly flexible, readily adaptable to the optimum temperature for the material being processed.
 - i. Combustibles heated very rapidly and uniformly with no hot spots.
 - j. All surfaces exposed to gas stream (oxygen.)
 - k. Hot sand imparts heat to combustible.
 - l. Sand absorbs part of heat generated.
 - m. Sand erodes combustible material.
 - n. 70% water content in slurries (precludes detonation of energetic materials.)
 - o. Concurrent disposal of wide range of materials.

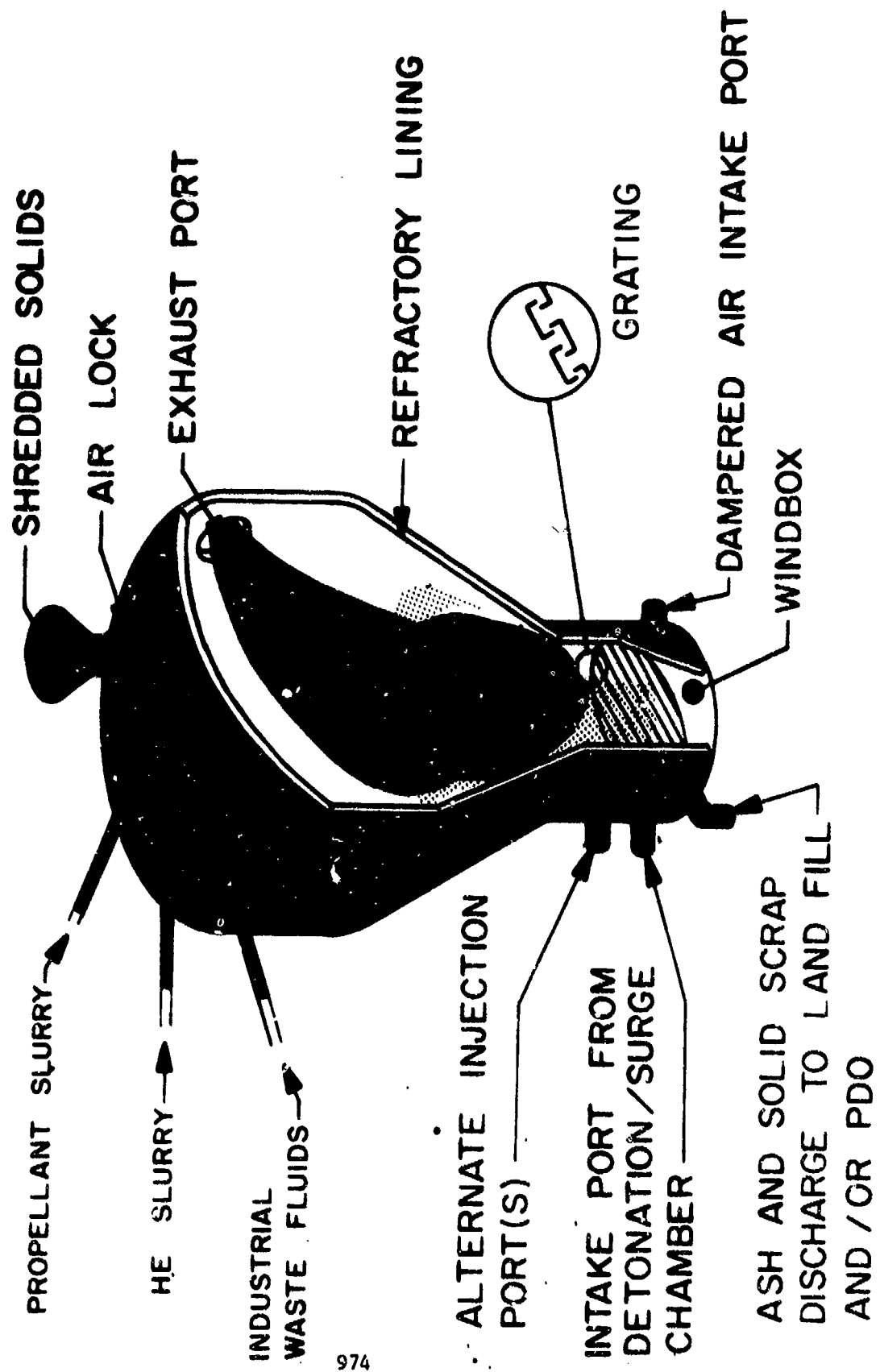
- p. Reduce emission from detonation/function chamber by drawing these through bed.
- q. Intermittent operation with minimum start-up time after brief shut downs, as over-night or week ends. (Fluid bed retains heat.)
- r. Equipment design will provide for removal of non-combustibles (non magnetic scrap, perhaps residue from limited item burn-out).
- s. Minimal external fuel source required after start-up, probably none. (Shredded domestic refuse would be the prime fuel source.)
- t. Unit is run at negative pressure (partial vacuum) which would minimize the effects of any potential detonation.

4. Disadvantages/problem areas.

- a. Higher energy requirements for proper air flow to displace sand bed.
- b. Size control of "fuel" necessary, small, light, loose, or shredded charge - no heavy masses in the fire box to smoulder.

5. Commercial brochures are on hand on various processing methods developed by Coppsland using the fluidized bed concept, the fluidized bed incinerator at Thunderbay, Ontario being one of these. Slides are on file from the Thunderbay installation. There are other manufacturers of fluidized bed reactors.

FLUIDIZED BED REACTOR.



1. Decontamination Oven. Stationary refractory lined chamber equipped with material handling equipment.

2. Purpose:

- a. Burn out of ammunition items and components.
- b. Flash munitions casings from the Washout Operation, etc.
- c. Flash contaminated processing equipment being removed from service, (prior to repair or salvage):

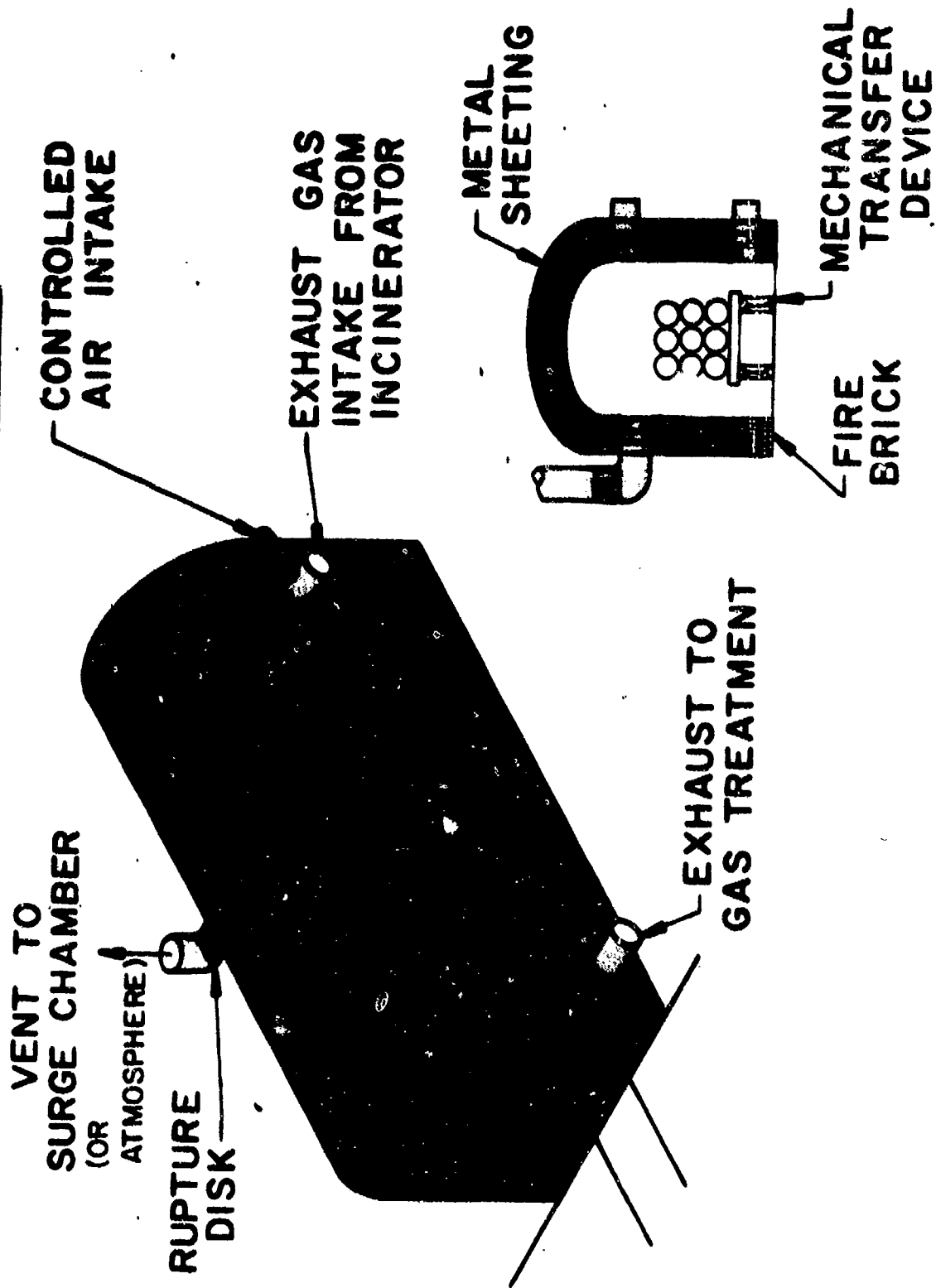
Controlled temperatures will minimize damage to repairable equipment.

3. Merits:

- a. Utilize waste heat in the exhaust gases from the reactor.
- b. Interlocked proportioning dampers in the exhaust line will divert hot exhaust gases from the fluidized bed reactor (less the heavy particulate removed by the Cyclone Separator).
- c. Controlled fresh air intake interlocked with the exhaust duct dampers will provide oxygen as required for controlled combustion.
- d. Above arrangement should ensure very close temperature control, making it possible to effectively decontaminate materials without mutilation beyond re-use, such as when salvaging equipment. Operating temperature will be infinitely variable from about 400°F to 1200°F.
- e. The rupture disc vented to atmosphere would protect the oven and exhaust gas treatment system from excessive over pressures, should a detonation or deflagration occur.
- f. The end opening, "Pass Through" arrangement would facilitate flashing large parts, and would allow mechanical transfer for flashing on a production basis.

4. Drawings are on hand for two decontamination ovens as used by Army Ammunition Plants (AAP's).

DECONTAMINATION OVEN



1. Detonation/function chamber.

2. Purpose in the System: Would be used to function various munitions and components which are not readily amenable or compatible with other disposal methods. Operational economics and minimized operational hazards could be influencing factors in using this method over others potentially applicable.

3. Merits:

a. An effective, highly flexible, universal method of confining products of detonation or functioning items up to the equivalent of 100# of HE when no secondary precautions are taken, and approximately 400# HE when energy retardant procedures are used (such as imbedding the charge in vermiculite or pearlite.)

b. Little, if any, noise or shock external to the facility.

c. Total control of off-gases and fragments.

d. Potential salvage value of fragments recovered.

e. Greatly reduces land area requirements, compared to current demolition ground and burning ground practices.

4. Disadvantages:

a. Relatively slow production compared to current demolition ground procedures, in that smaller shots and fewer sites would be used.

b. Particularly slow if vermiculite is required, although proper design of the materials handling and storage equipment could expedite this phase of the operation.

5. Data:

a. Slides, a brochure, and sources of information relative to the 40' ID reinforced concrete structure at Battelle Memorial Labs are on hand.

b. Photos and drawing of 10' ID X 31' steel test chamber at Los Alamos.

c. Tech data on AEC tests using vermiculite and pearlite to defeat/minimize explosive shock waves, is being submitted to the AMC Ammunition Center.

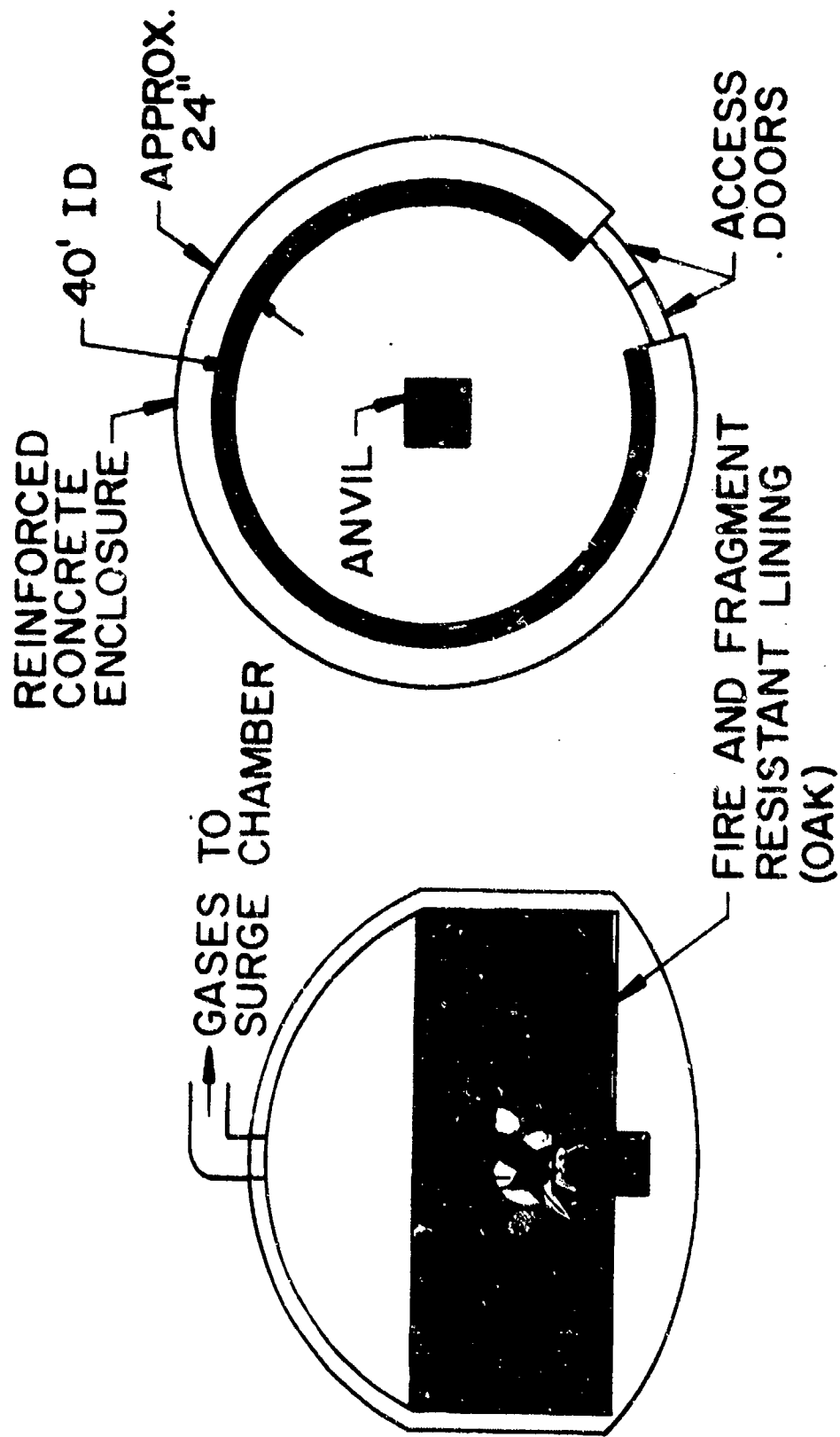
d. Tech data on small metal total containment spheres used experimentally by AEC can be obtained.

Notes:

1. Production rate could be increased by adding a "surge chamber" between the detonation chamber and the reactor. This would allow purging the detonation chamber first, then reloading it while the surge chamber is being evacuated into the reactor.

2. Drawing a partial vacuum prior to the shot would also increase the allowable explosive weight per shot.

DETONATION / FUNCTION CHAMBER



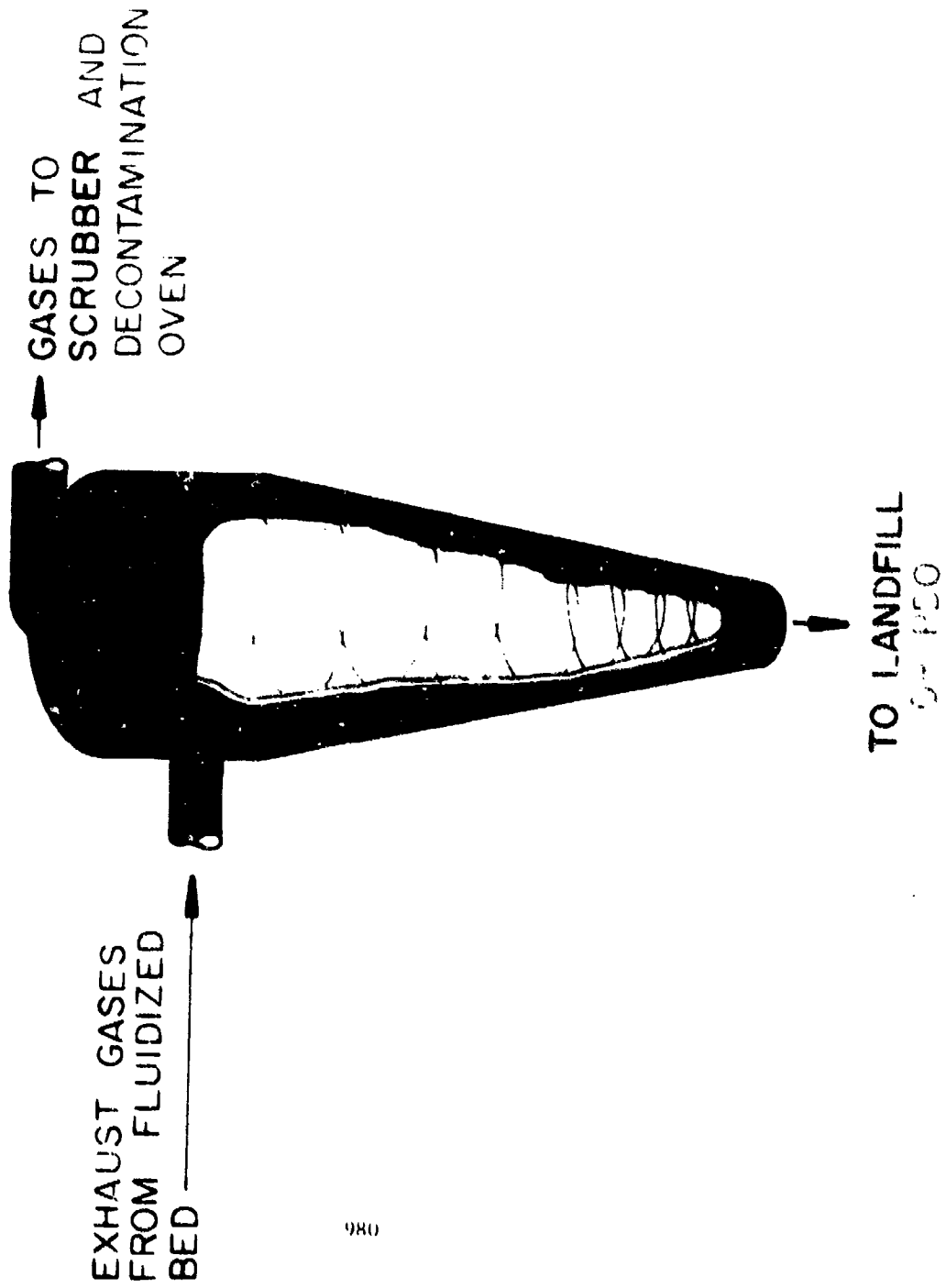
ELEVATION VIEW

PLAN VIEW

1. Cyclone Separator.
2. Purpose: Remove heavier particulate from exhaust gases, prior to using the hot gases to heat the decontamination oven.
3. Advantages:
 - a. Avoid excessive cooling of the exhaust gases.
 - b. Would allow use of relatively clean, hot exhaust gases to heat the decontamination oven.
 - c. Would reduce sediment loading in scrubbing system, and subsequent sludge removal in the clarifier station.
4. Disadvantages: Particulate materials recovered are dry and hot (high temp.) This could pose problems relative to housekeeping and personnel hazards during handling, transporting, etc, if not adequately addressed during design.
5. Particulate separators are widely used industrially.

CYCLONE

(REMOVE HEAVY PARTICULATE)



1. Venturi Type Scrubber .

2. Purpose:

- a. Cools/quenches gas temp (raises scrubber water temp.)
- b. Removes water-soluble materials (both gaseous and fine particulates passing cyclone separator.)
- c. Produces induced draft, pulling gases through system at a negative pressure.

3. Advantages:

- a. Particulate removal to one Micron size.
- b. No moving parts exposed to gas stream, avoiding wear or abrasion, and the associated maintenance.
- c. Entire gas handling system from the intake port of the reactor to the venturi will be under a negative pressure (partial vacuum) precluding escape of gases.

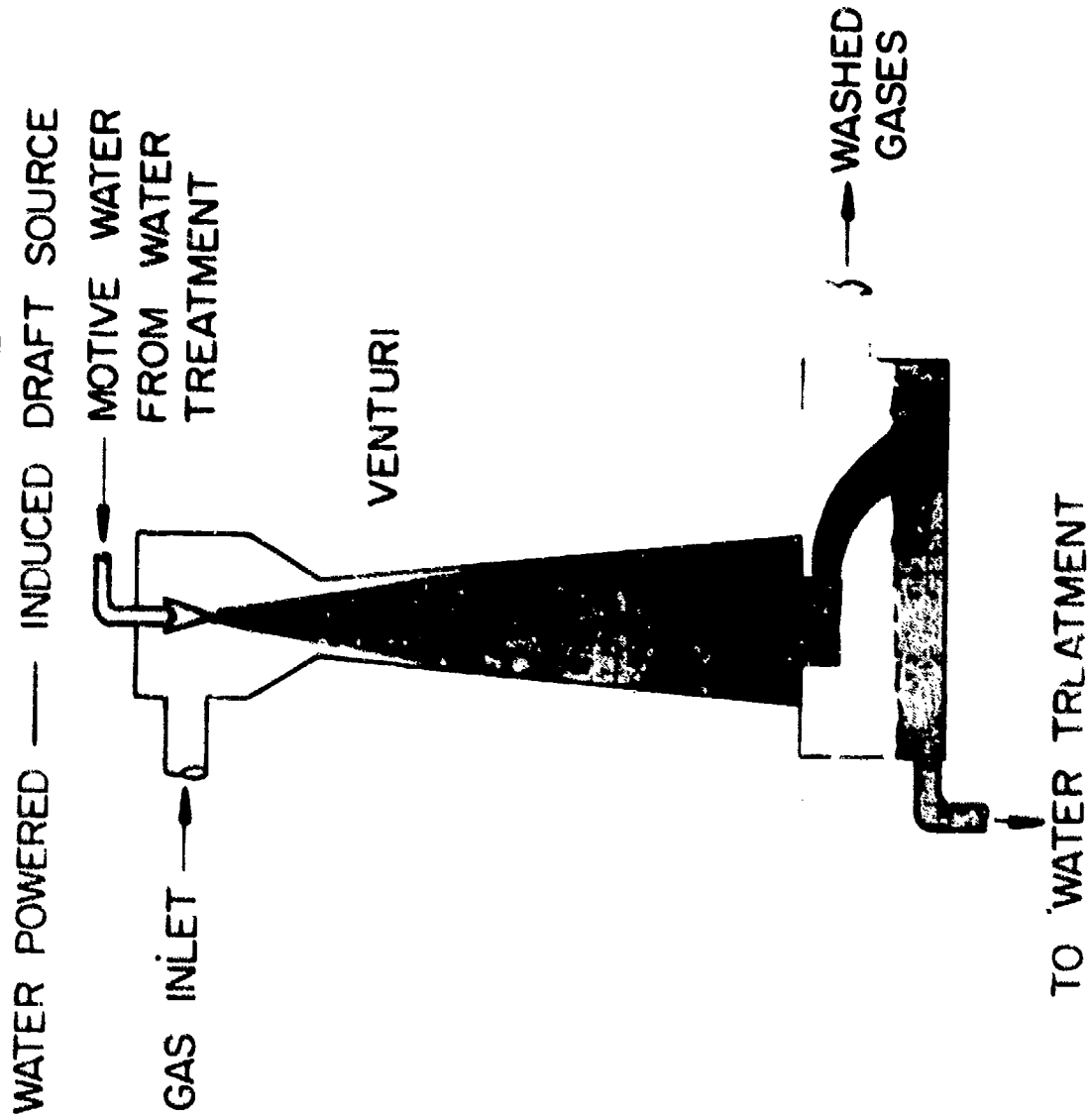
This also simplifies feeding waste materials into the reactor.
- d. Very minimal maintenance - pump for motive water only moving element.
- e. Use waste heat in the form of hot water for heating facility. Hot water may be useful in neutralizing effluent for recirculation.

4. Disadvantages/Associated Problems .

- a. Water treatment required, to allow recirculation (cooling, sediment removal, and possibly chemical treatments.)
- b. May require a secondary exhauster blower after venturi to generate sufficient draft, but if so, a fan down stream from the venturi scrubber will be handling relatively clean, cool, non-abrasive gases - minimizing maintenance requirements.

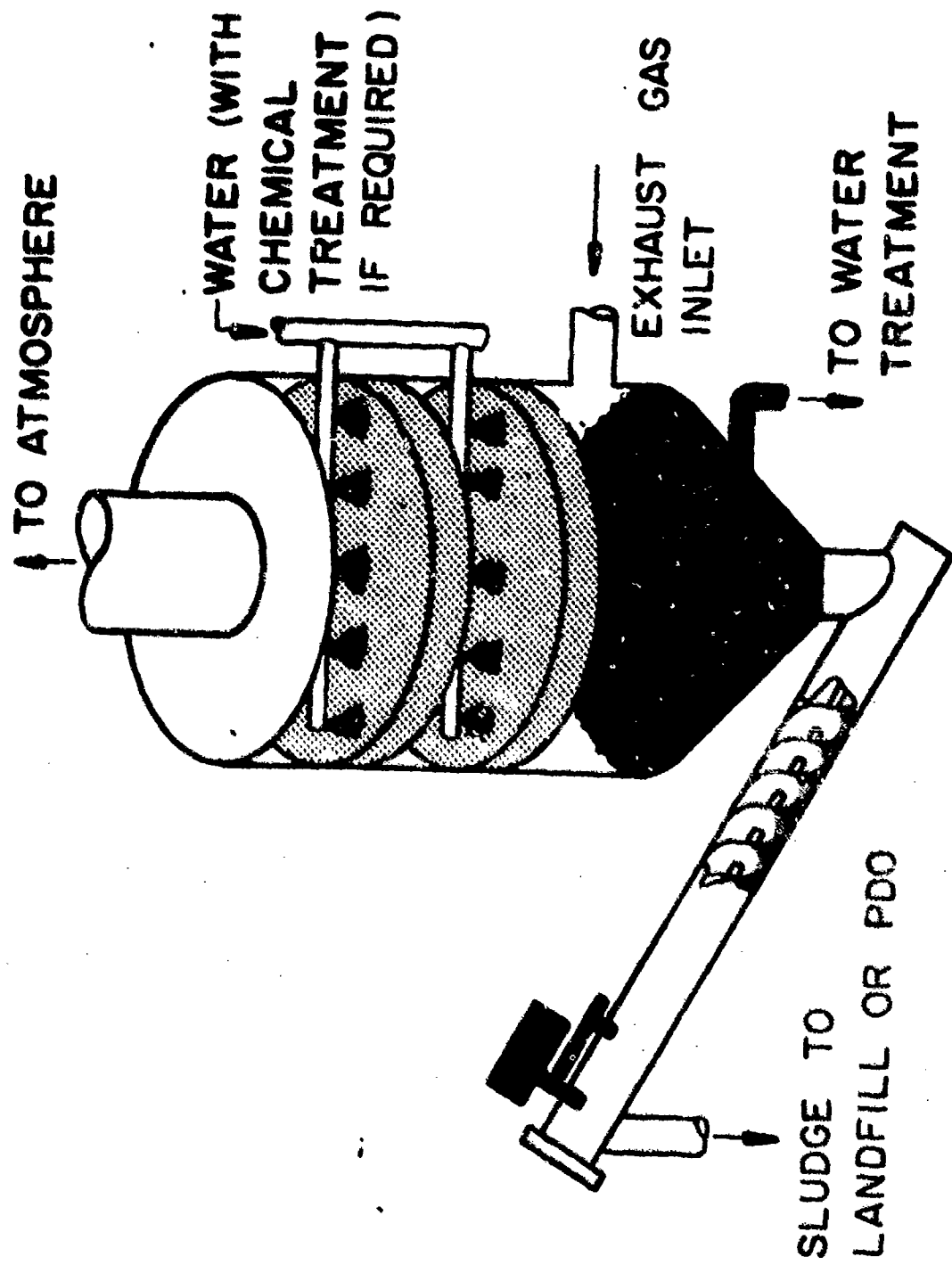
5. Water powered venturi scrubbers and exhausters are commonly used industrially.

GAS SCRUBBER



1. Packed Column Scrubber:
2. Purpose: Secondary treatment of exhaust products. Note: Pilot tests may indicate secondary exhaust treatment to be unnecessary, depending on products liberated and efficiency of the venturi scrubber.
3. Advantages:
 - a. Counter current flow (gases versus media.)
 - b. Multi-stage, progressively finer media, as required.
 - c. Catalytic fluid media, as required could be used.
4. Disadvantages: Effluent treatment for recirculation, and eventual disposal when it becomes saturated.
5. Slides of this type scrubber are included in the Thunderbay incinerator slides. These scrubbers are commonly used in chemical industries.

PACKED TOWER SCRUBBER



1. Clarifier.
2. Purpose: Remove solids from the scrubber effluent to allow recirculation of the water.
3. Merits:
 - a. In the system shown.
 - (1) The 1st stage removes the light materials which float to the surface.
 - (2) The 2d stage removes the heavier materials which tend to settle.
 - b. Solids removed are wet and relatively cool, which should simplify materials handling requirements.
 - c. The type equipment shown minimizes the plant area which could be required to perform this function.
4. Other considerations: The wet sludge removed must be disposed of - probably by land fill, but possibly to PDO for sale if of commercial value.
5. Data: Commercial brochures are on file for equipment elements similar to those shown. There are numerous other models of equipment commercially available for the application.

SEPARATION OF SOLIDS

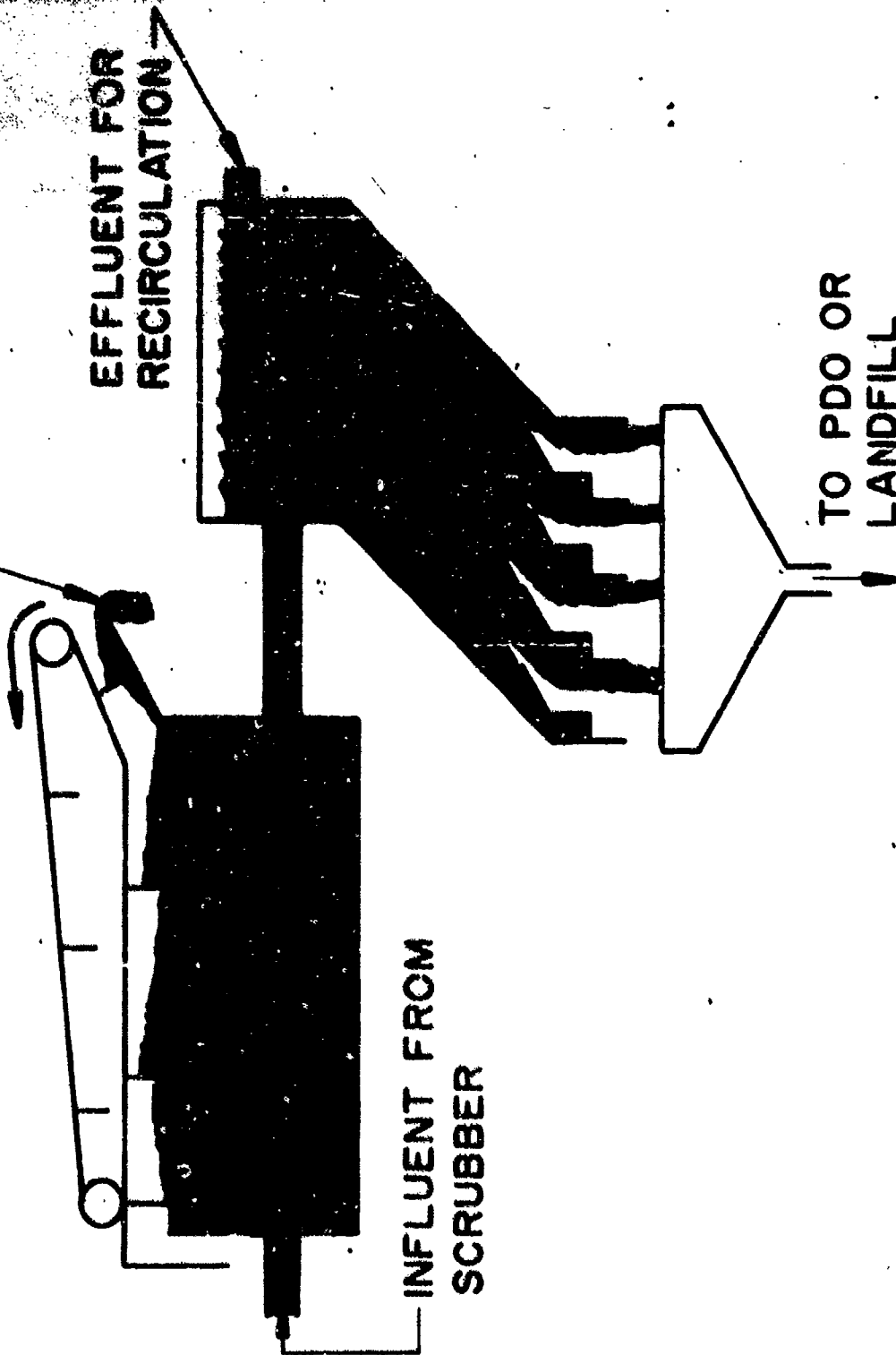
FLOATATION MATERIALS
TO LANDFILL OR PDO

EFFLUENT FOR
RECIRCULATION →

TO PDO OR
LANDFILL

INFLUENT FROM
SCRUBBER

986



1. Feeder system for larger solids.

2. Purpose:

a. Storage area in the pole building will serve as collection point for incoming materials.

b. Materials too large or heavy for fluidization in the reactor bed, or too large for the materials handling system, will be shredded.

Note: The shredder will also have application in mutilation of certain lighter weight inert ammunition items.

c. The magnetic separator will segregate ferrous materials emerging from the shredder for transfer to PDO or as appropriate.

d. During some types of operations, (as shredding clean packaging or mutilation of inert ammunition elements) other materials may be diverted for transfer to PDO or to land fill as appropriate.

e. Solid materials to be disposed of in the fluidized bed reactor will be held temporarily in a storage hopper, then fed to the fluidized bed at a controlled rate. The feed rate will be dependent on heat being generated by other combustion processes under way within the reactor.

Note: Domestic and industrial refuse will be the primary source of fuel. The volume is the largest and most constant of all materials to be processed.

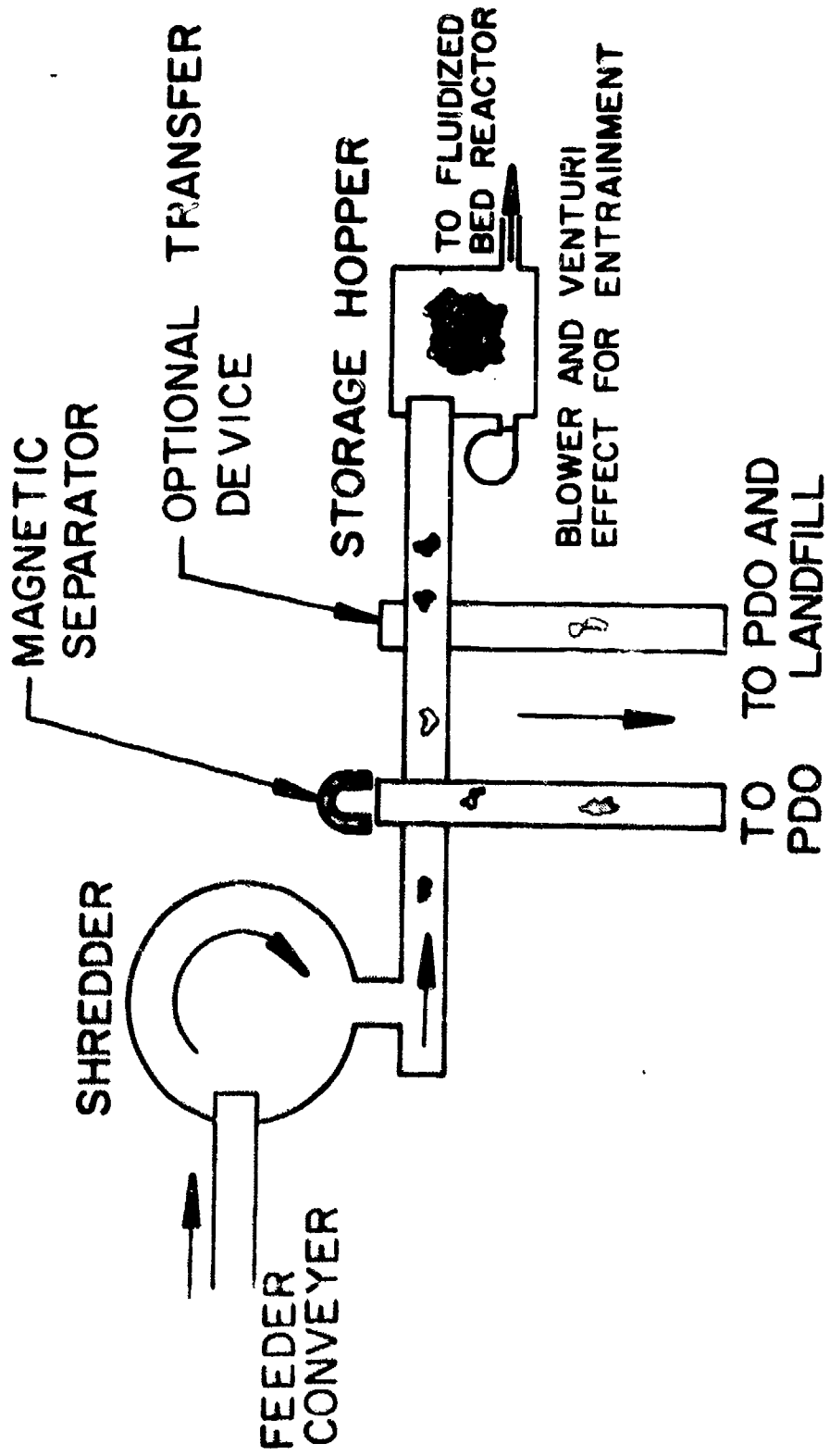
f. A pneumatic conveying system, with a venturi throat section at the load station is shown for transfer of the refuse to the reactor. Other handling systems should also be investigated.

3. Reason for selection: self explanatory.

4. Not applicable.

5. Data available: Commercial literature and slides for the Eidal shredder on hand. Slides are on hand of the storage hopper, feeder equipment, and pneumatic transfer equipment used for shredded refuse at union electric, St. Louis. Pneumatic conveyors and Cyclone separators are used on Army Depot Ammunition Maintenance Lines. Other equipment elements are common industrially.

FEEDER SYSTEM FOR SOLIDS



1. Shredder.
2. Propose to use vertical rotor progressive grinding type, such as Eidal's.
(Eidal 400 HP model suggested.)
3. a. Will accommodate packaging materials including plastics and pallets.

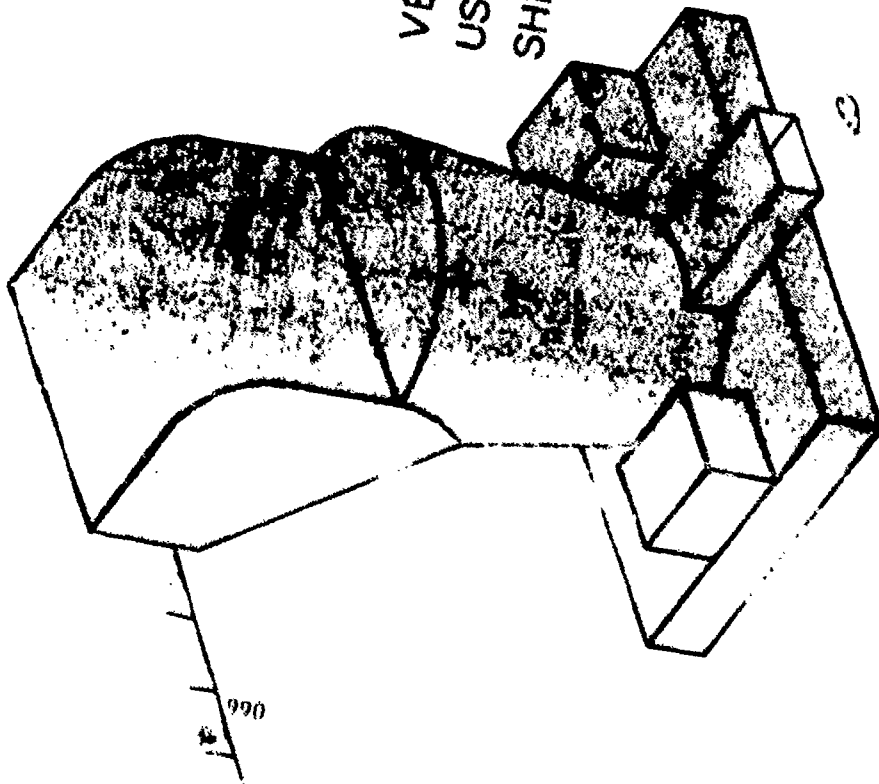
b. Will take metal objects to size of 5 gal pail and density of fractional horse power electric motors.

c. Minimal maintenance when used on low density wood packaging.
4. a. Shredding equipment requires frequent re-conditioning (hard-surfacing) of surfaces which contact the refuse, although this requirement is minimal when processing softer materials such as wood and fiberboard.

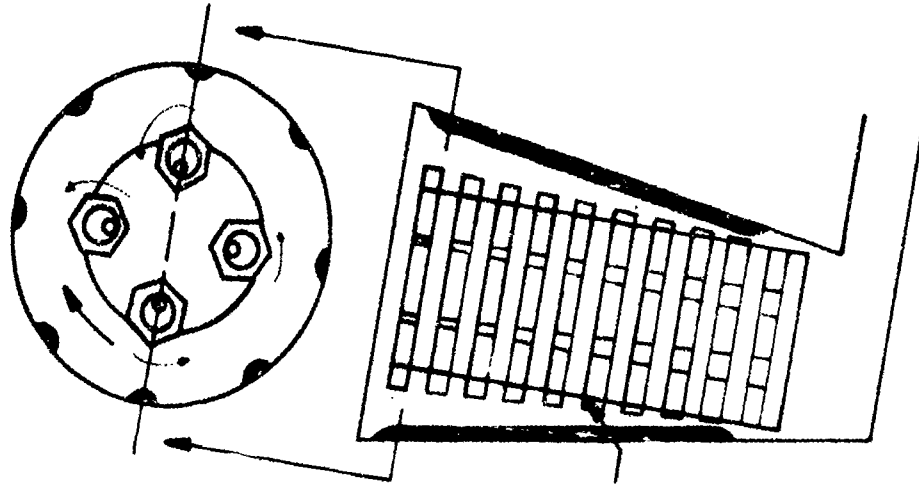
b. Significant electrical power required (approx. 400 HP to drive the rotor.)
5. a. Commercial literature is on hand for various shredders.

b. Also 35MM slides are on hand of three models of Eidal Shredders at the Albuquerque plant, a shredding and materials segregation operation at Denver on junk autos, the Municipal Refuse System at St. Louis, and the Wood By-Products Shredding and Disposal System at Thunderbay, Ontario.

(PACKAGING MTLs., DOMESTIC WASTES, INERT
SHREDDER
AMMUNITION MUTILATION)



VERTICAL ROTOR
USING PROGRESSIVE
SHREDDING PRINCIPLE



1. Magnetic Separator.

2. Purpose: Remove ferrous materials from the shredded refuse which is to be processed in the fluidized bed reactor.

3. Merits:

Compact, durable, minimal maintenance.

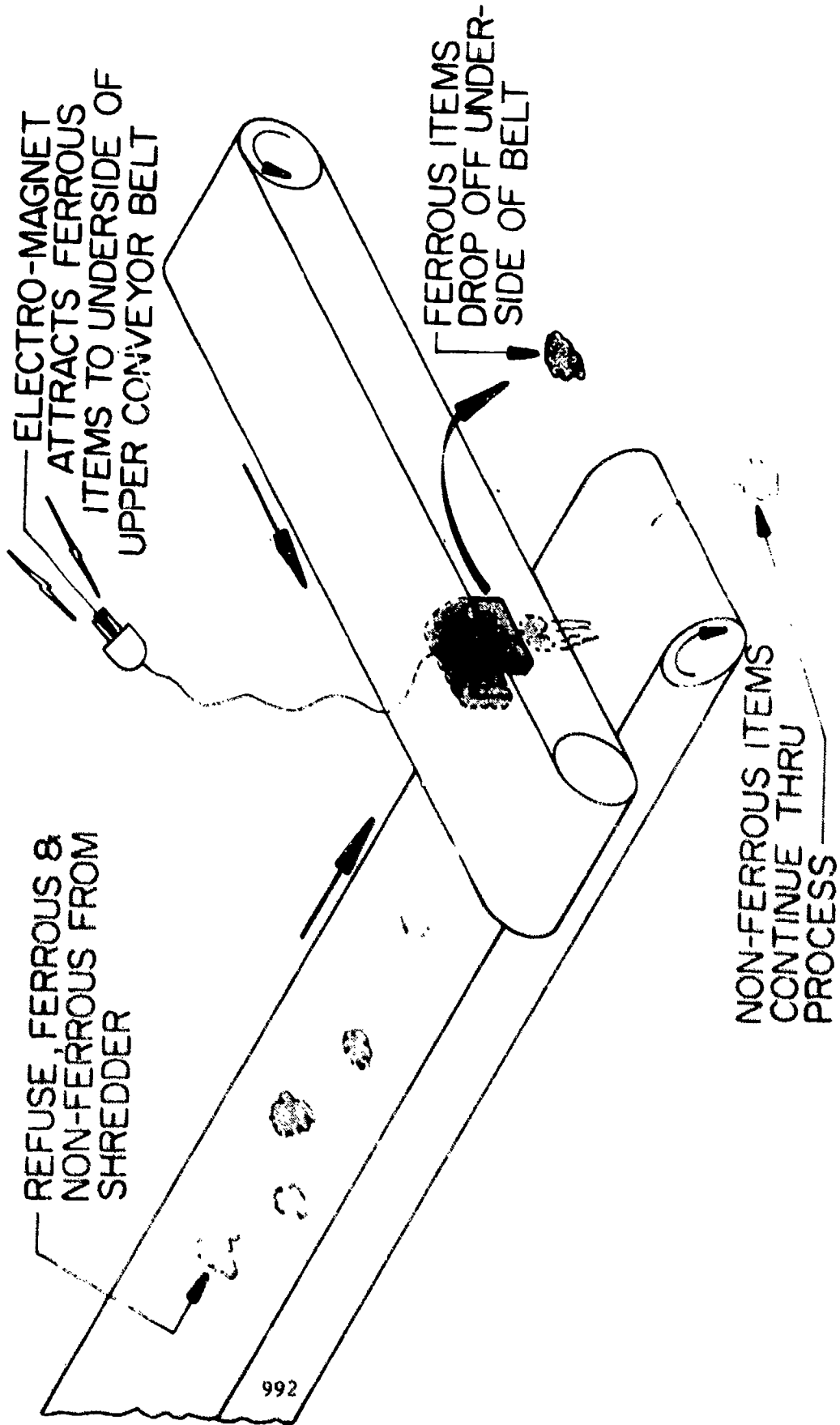
4. Problem areas:

Requires electrical power source.

5. Data available:

Readily available commercially from a number of manufacturers.

ELECTRO-MAGNETIC SEPARATOR



1. Liquid industrial wastes.

2. Purpose in System: a. Small reservoir and pump for transferring to fluidized bed reactor, at a controlled rate of feed.

b. As an alternate, it may be desirable to use a compressed air or steam powered eductor to selectively transfer the industrial wastes from a bank of "dedicated" open top tanks with self-closing lids equipped with fusible links.

3. Reason for selection: Self explanatory.

4. Problem Areas:

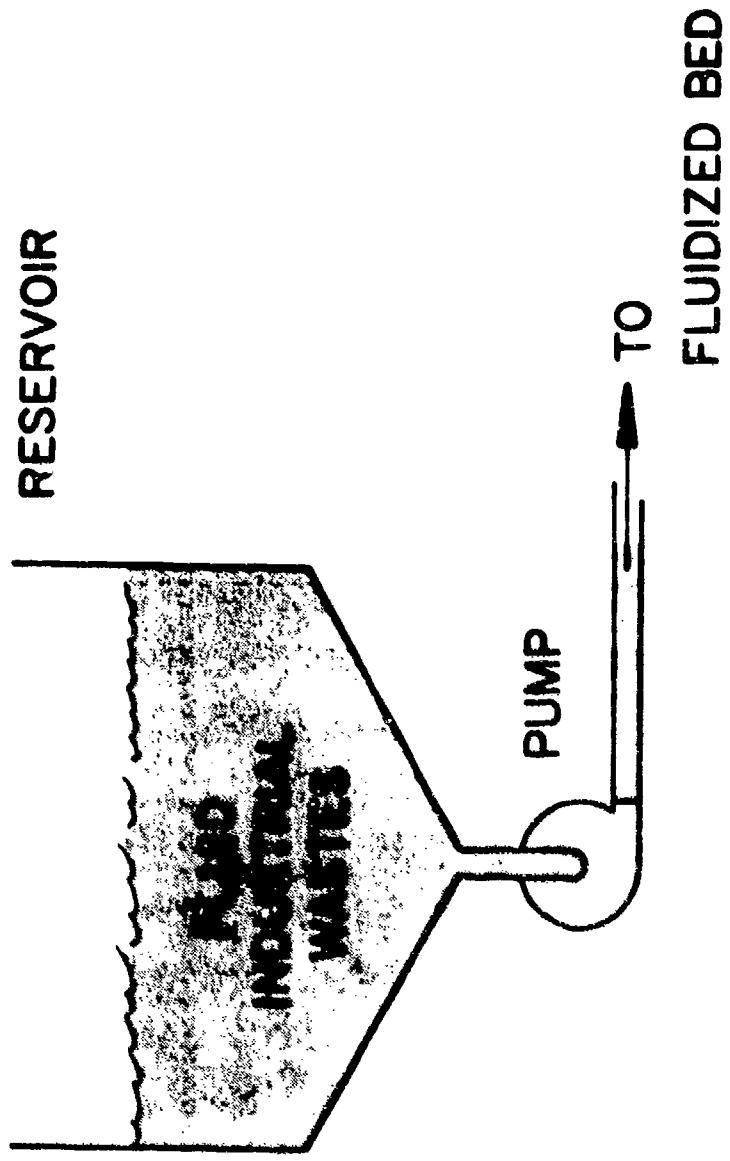
a. The inherent industrial fire hazard will be isolated from the balance of the operation with fire walls.

b. Bay will be equipped with deluge.

c. Quantity of materials in process will be minimal.

5. No unusual equipment design problems.

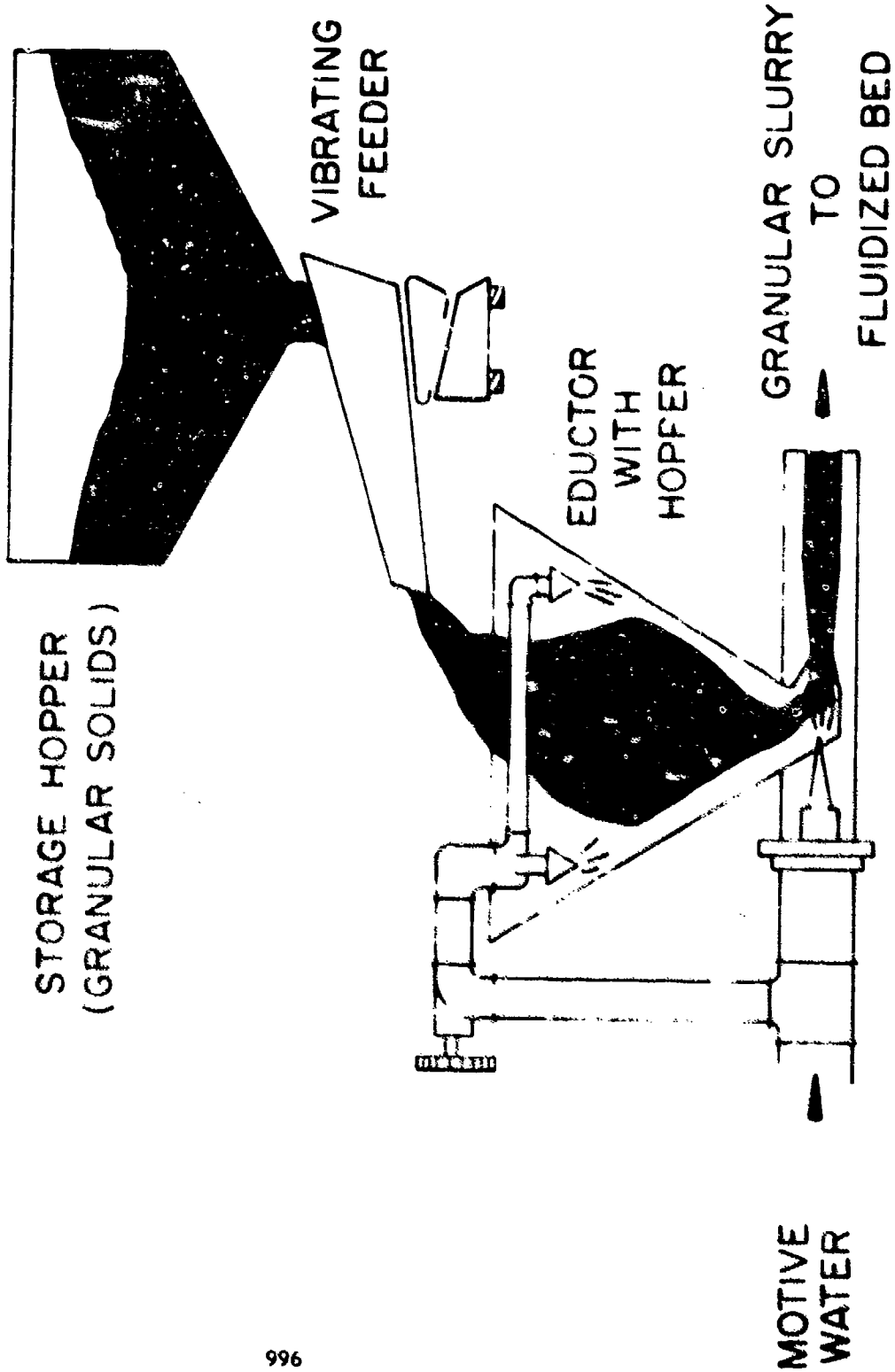
LIQUID INDUSTRIAL WASTE



1. Hydraulic Venturi with hopper intake.
2. Purpose:
 - a. Regulate feed of material, by controlling vibrator frequency and water supply.
 - b. Thoroughly wet and immerse materials in water.
 - c. Transfer /propel/convey material to fluidized bed and inject.
3. Reason for selection:
 - a. Accommodates wide range of physical characteristics of materials being transferred.
 - b. Economical to acquire and operate.
 - c. Flexible operation, readily controlled.
 - d. Combines elements outlined in 2 above into a single piece of equipment.
 - e. Low maintenance - no moving parts, other than water pump on motive water supply.
 - f. Ensures safest conditions for handling hazardous materials.
 - (1) Materials must be thoroughly wet/immersed to be conveyed.
 - (2) No moving parts exposed to the materials.
 - (3) Without proper water flow, material cannot be transferred.
4. Disadvantages:
 - a. Requires water to operate - probably no problem for the process(es) envisioned.
 - b. A hydro-clone may be needed at the reactor to reduce the water content as the material is introduced into the reactor.
5. Data available: Much data published on water powered eductors and hydraulic conveying. Water powered eductors are used to transport propellant considerable distances at Army Ammunition Plants.

WATER POWERED EDUCTOR

TRANSFER



Reproduced from
best available copy. ©

1. Bulk High Explosive Feed.

2. Purpose:

a. To entrain and immerse dry HE pellets (or other HE particles) in a water stream and transfer to fluidized bed.

b. Alternate: Receive wet granular HE materials, hold in small reservoir, and transfer to fluidized bed.

3. Reason for selection:

a. The water powered eductor ensures rapid and thorough wetting of the dry materials.

b. The pump and reservoir may be a more efficient method of handling the materials which are already wetted; although the eductor should be able to handle this sludge as well as the dry pellets. (A rubber lined centrifugal pump is used to convey HE Pellets in water from the pelleting tank to the de-watering screen in the APE 1300 Washout System. A conventional centrifugal pump is used at Badger AAP to transport propellant in water solution.)

c. Use Red water to power eductor, then incinerate automatically.

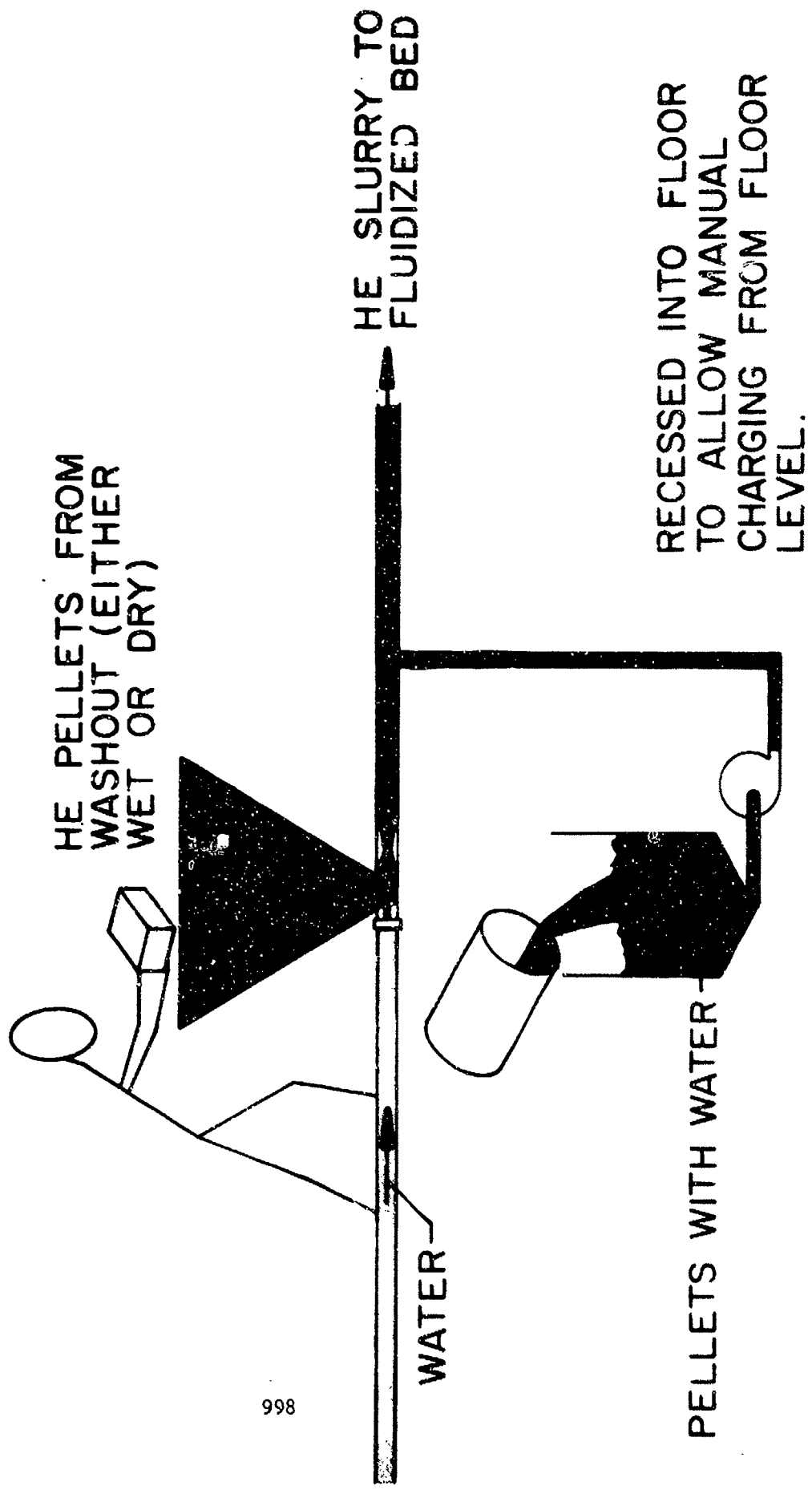
4. Disadvantage:

Additional water is introduced using the eductor. This should be no problem, as the fluidized bed will take 70% excess water with the charge. The excess water would consume heat in vaporizing, allowing more fuel (refuse) to be introduced.

5. Data:

Centrifugal pumps and eductors are now used within Army activities to pump both HE and propellant slurries.

BULK HIGH EXPLOSIVE FEED



1. Propellant preparation and feed systems.

2. Purpose:

- a. Remove propellant from case bonded motors.
- b. Granulate larger grains (probably anything larger than about M19 propellant) reducing the size to allow efficient transfer and incineration.
- c. Wet and transfer propellant particles and inject into fluidized bed.

3. Reason for selection:

- a. SAA and artillery propellant.
 - (1) Most of this could be dumped directly into the hopper of the water powered hydraulic venturi.
 - (2) The storage hopper would be under continuous deluge.
- b. Small rocket motor grains:
 - (1) Granulate with water to form slurry.
 - (2) Transfer to fluidized bed, either via centrifugal pump or the eductor transfer system for SAA and artillery propellant.
- c. Hydraulic erosion process, for large, case bonded rocket motors.

Note: This would be an optional modular element, used only at those stations having the item(s).

(1) Water is injected into motor under high pressure (5800-6000 PSI) and low volume with the propellant eroded and removed continually, and maintained in a wet condition - major safety feature.

(2) Removal semi-auto (similar to current HE washout process), and at acceptable rate (is being done at rates to 2000 Lb per Hr.)

d. Materials could go to PDO, instead of to the reactor, when there is a commercial market or potential for recycling into munitions manufacture.

4. Disadvantages:

- a. A clarifier may be required on water to be re-circulated in Hydraulic erosion process.

b. Some of the largest artillery grains may require granulation prior to transferring with the eductor.

5. Data:

a. An SOP on a washout process at Huntsville is on hand.

b. Pictorial drawing illustrating the washout application at Thoikol, Brigham City, UT is on hand, SOP is available through command channels.

c. Water powered eductors are used to transfer artillery propellant grains considerable distances at Badger AAP.

d. 35MM slides of the Hammermill granulation operation at Badger, including materials handling methods, are on hand.

e. 35MM slides of mechanical Chipper and Shearing Operations at Badger AAP are on hand (applied to small rocket motor grains.) Drawings also on file.

1. Liquid Propellant Oxidizer Feed Station.

2. Function:

Withdraw oxidizer from container, and transfer to fluidized bed reactor at a controlled rate.

3. Advantages of the airlift evacuation system:

- a. No moving parts exposed to oxidizer, as opposed to pumps.
- b. Low air lift pressure clears line to reactor after transfer of the oxidizer.
- c. Continuous oxidizer feed to the reactor provided through use of two air lift stations operated alternately.
- d. System is under low positive pressure (perhaps 10 PSI) and readily controlled via the pressure regulator.

4. Disadvantages:

Compressed air source required, however, the volume required and pressure are very low.

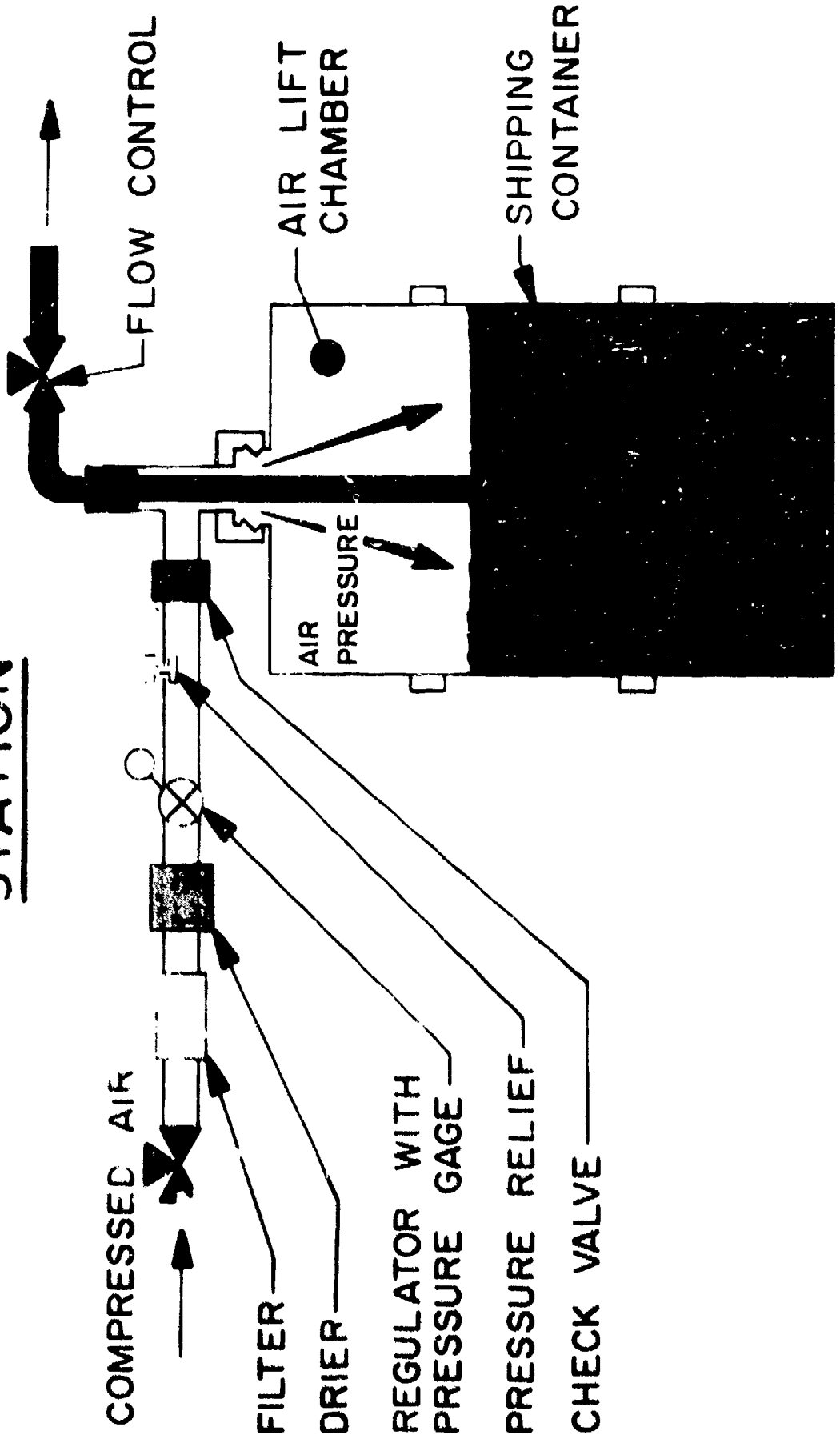
5. Supporting Data:

Air lift means of transfer is in common use industrially. Also, it is used in the oxidizer disposal system outlined in TB 9-1375-200-50/1.

LIQUID PROPELLANT OXIDIZER FEED

STATION

TO FLUIDIZED BED REACTOR



1. Opening Station (to gain access to fillers.)

2. Purpose:

To gain access to the munitions filler, allowing removal by subsequent washout or burn-out.

3. Reason for Selection:

a. Some items cannot now be opened. These have historically been demilled on the demolition ground.

b. A drill or mill station is shown, which would be highly adaptable to a wide range of munitions items.

It would be fairly fast, requiring few operators, and could be fit into existing facilities.

c. Sawing methods which have been under development may be applicable, dependent upon productivity, operational requirements, etc.

d. Could be located in "Preparation Building" for de-contamination oven, or in the current maintenance facilities, or at the "Bomb Disassembly" station which most depots already have

4. Disadvantages:

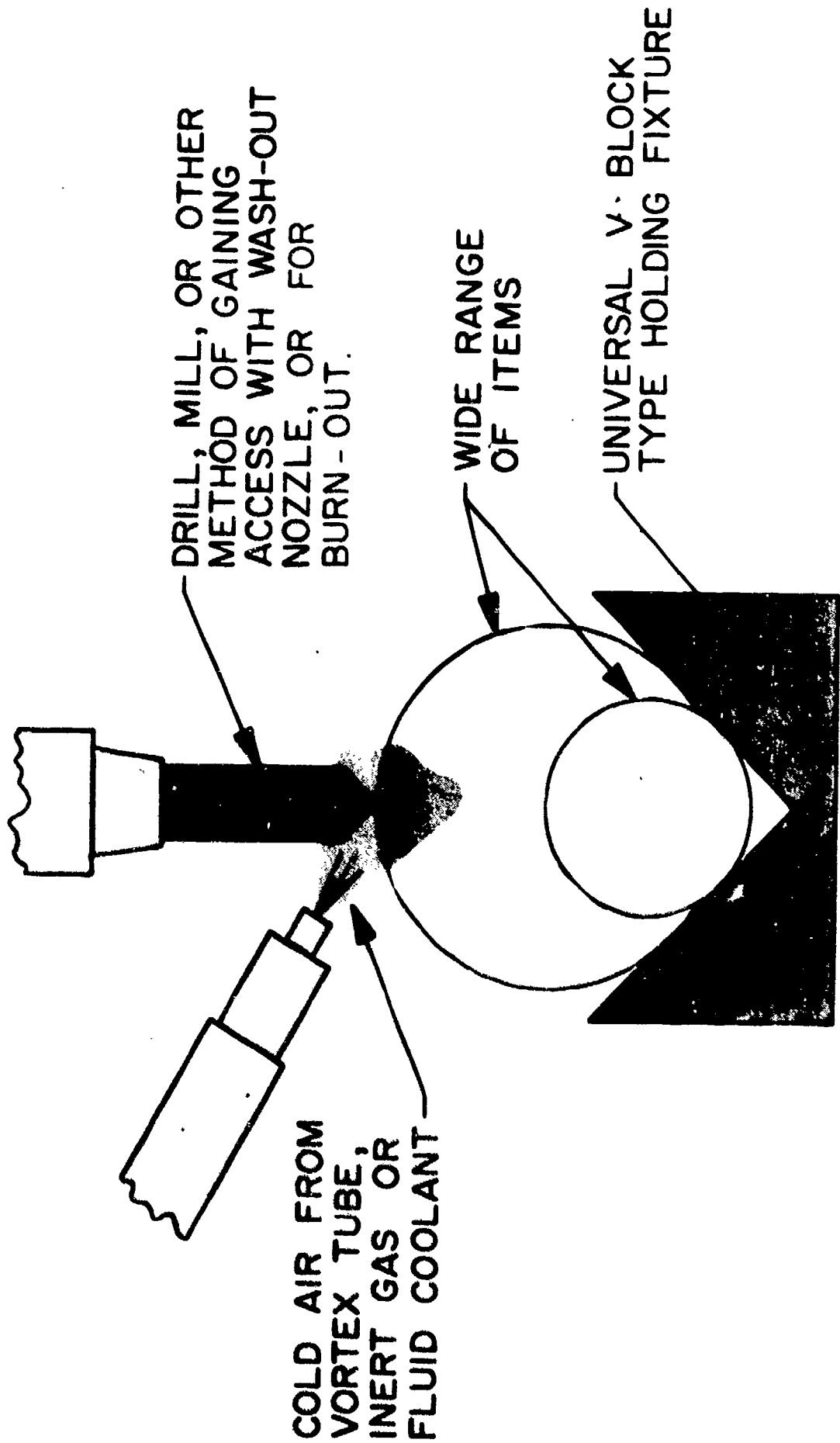
Not applicable.

5. Data:

a. Considerable experience has been gained over the years in sawing and drilling techniques applied to various munitions during manufacture, inspection, modification, and demil programs.

b. From the wide variety of commercial equipment available, some should be adaptable with minimal modification.

"OPENING" OPERATION



TREATMENT AND DISPOSAL OF SENSITIVE PRIMING MIXTURE WASTES*

Philip M. Broudy, Ph. D.

Munitions Development and Engineering Directorate
Frankford Arsenal
Philadelphia, Pennsylvania 19137

The issuance of Executive Order 11507, dated 4 February 1970, provided new impetus to the Federal Government's role in pollution abatement by directing "that the Federal Government in the design, operation and maintenance of its facilities shall provide leadership in the nationwide effort to protect and enhance the quality of our air and water resources". In July 1971 Frankford Arsenal, under the direction of the U.S. Army Materiel Command, initiated pollution abatement activities in those areas for which it has technical responsibility. One such area is the production of primers for small caliber cartridges at Lake City AAP (Army Ammunition Plant), Independence, MO and Twin Cities AAP, New Brighton, MN. Both of these installations are government-owned contractor-operated (GOCO) plants; the latter is currently on standby status. The production of these primers requires the manufacture of very sensitive explosive compounds; the subsequent mixing of these explosives with fuels, oxidizers, binders and other ingredients; and the loading of the resultant priming mixture into the primers.

*This paper is based on work carried out by Battelle Columbus Laboratories, Columbus, OH, under Contract No. DAAA25-74-C-0153.

The composition of the most widely used priming mixture in U.S. Army small caliber cartridges, FA 956, is shown in Table I. Since lead styphnate is a primary initiating explosive, it is manufactured at each plant from trinitroresorcinol (TNR), a high explosive which, in turn, is either manufactured at the plant (Lake City AAP) or purchased commercially (Twin Cities AAP). Tetracene, also a primary initiating explosive, is manufactured at each plant from aminoguanidine bicarbonate. The other ingredients are all purchased or processed from the purchased materials.

Explosive wastes are generated in the manufacture of TNR, lead styphnate, and tetracene; in PETN washing; in the final mixing of the priming mixture; in primer loading; and in various clean-up operations. Considerable quantities of spent acids and toxic heavy metals, which include lead, barium and antimony, are also present in the wastes. In the manufacture of priming mixture, the wastes generated at the two plants can be as high as 80,000 pounds per month. Because of their hazardous nature, these wastes are associated with large quantities of water.

Whereas the standards for drinking water have been relatively constant over the years, the standards for effluent water have been in a continual state of development. In many cases the state standards for effluent water are based on pollutant materials normally found in sanitary wastes and, therefore, should not be expected to include consideration of materials found in primer wastes. For

example, Table II shows that the standards for the Little Blue River, the receiving stream for wastes from Lake City AAP, include only ammonia, lead and dissolved oxygen as parameters for primer wastes. Minnesota standards, however, include ammonia, barium, dissolved oxygen, dissolved solids, lead, nitrate, phenols, sodium, sulfate, BOD (biological oxygen demand) and suspended solids as parameters for primer wastes. Table III presents the industrial wastewater guidelines set by the Ammunition Procurement and Supply Agency (APSA)* and the maximum and minimum standards set by the various states. There are relatively few cases where the APSA values drastically exceed the most stringent state standards.

Table IV, whose data is based on material balances, shows that pollutant concentrations in raw primer waste streams exceed the APSA guidelines by two or three orders of magnitude for pollutants such as sulfate, total nitrogen, lead, antimony, barium and total solids. Other pollutants which exceed the APSA guidelines to a lesser degree are nitrate, nitrite and ammonia. Table V compares a Twin Cities AAP composite stream and the three Lake City AAP waste streams with existing effluent standards and indicates the percentage reduction in pollutant concentration needed to meet the standards.

The current practice at the plants is chemical desensitization of the wastes followed by discharge to leaching pits, evaporation ponds or an industrial waste treatment plant (ITP). Since these

*APSA, the agency responsible for operating the GOCO plants, was incorporated into the U.S. Army Armament Command in July 1973.

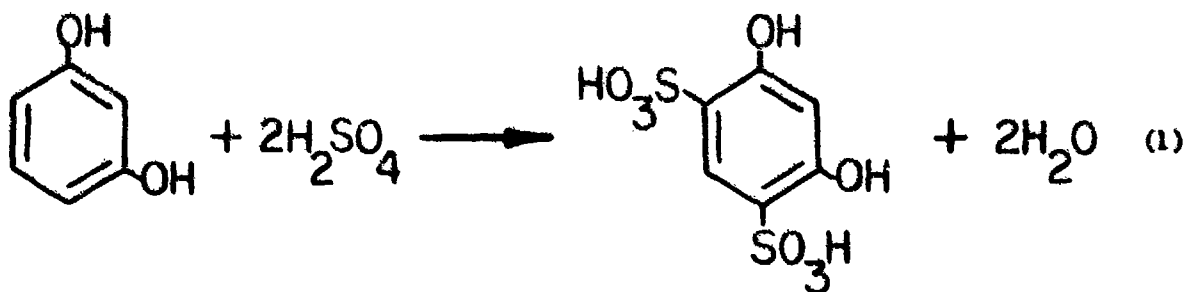
wastes exceed allowable effluent standards, it was decided to carry out a program to evaluate the treatment and disposal methods and to modify or replace them, as required, to preclude pollution of underground waters and/or surface streams. Also, it was not known if desensitization of any of the organic materials in the priming mixture resulted in the formation of unknown compounds which would be highly toxic to life in the environment.

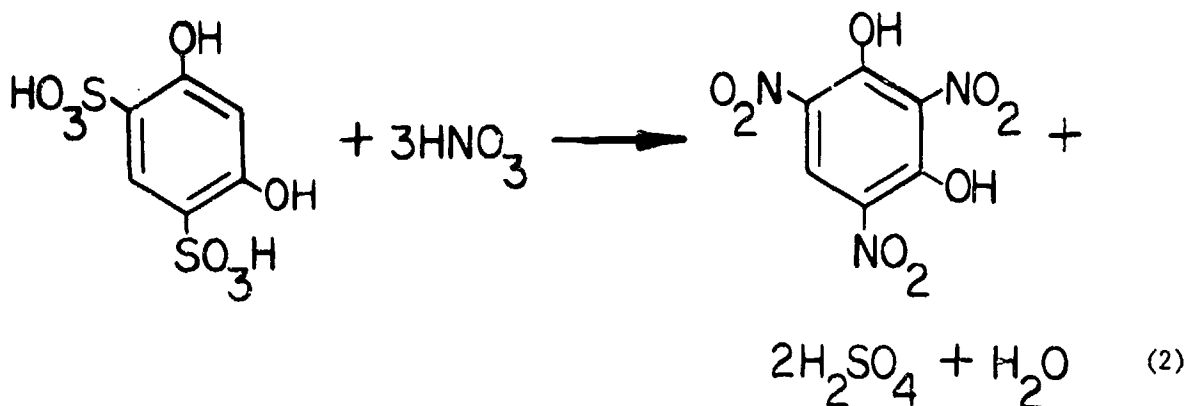
The resulting program was divided into three phases; viz., concept, feasibility and pilot line phases. This paper will be concerned with the concept phase which included identification and quantification of wastes, evaluation of current waste treatment and disposal methods, and concept studies for improved waste treatment and disposal methods.

CURRENT METHODS

Waste Treatment

TNR is manufactured essentially from resorcinol, sulfuric acid and nitric acid according to the equations



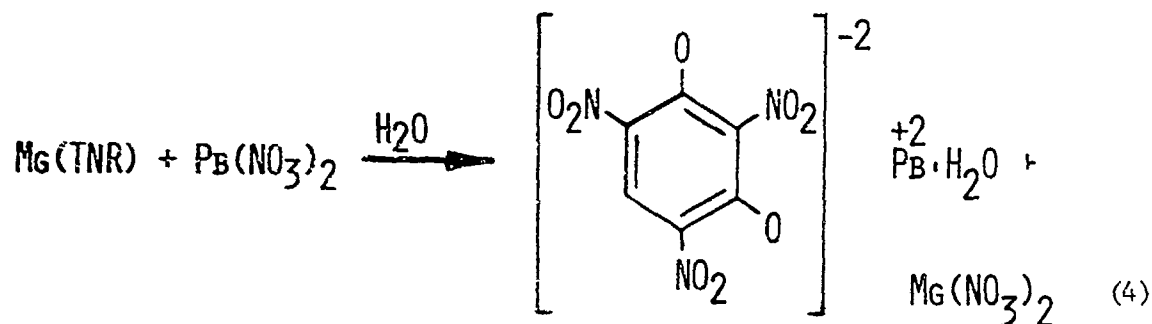


In addition to the approximately 75 to 90% yield of TNR, the final reaction mixture contains considerable quantities of wastes including all of the sulfuric acid employed, excess nitric acid and various by-products. After separation of the TNR by filtration, the wastes are neutralized with soda ash (Na_2CO_3) and then desensitized - that is, made non-explosive - by treatment with sodium hydroxide, aluminum powder and live steam (Remington Arms Company method). Mass spectral analysis of laboratory-desensitized TNR identified materials of molecular weights 151, 167, 256 and 332. Possible molecular formulas are $\text{C}_6\text{H}_5\text{N}_3\text{O}_2$, $\text{C}_6\text{H}_5\text{N}_3\text{O}_3$, $\text{C}_{12}\text{H}_{20}\text{N}_2\text{O}_4$ and $\text{C}_{12}\text{H}_8\text{N}_6\text{O}_6$ (or $\text{C}_{12}\text{H}_{24}\text{N}_6\text{O}_5$). Although the precise structures have not been determined, possible structures which correspond to the molecular weights obtained are shown in Figure 1. These structures show that reduction of the nitro groups and bimolecular coupling are occurring.

Lead styphnate is manufactured from TNR by different methods at Lake City AAP and Twin Cities AAP. At the Lake City Plant the TNR is first converted to a magnesium styphnate solution with magnesium oxide.



To this solution is added a solution of lead nitrate which results in the precipitation of lead styphnate.

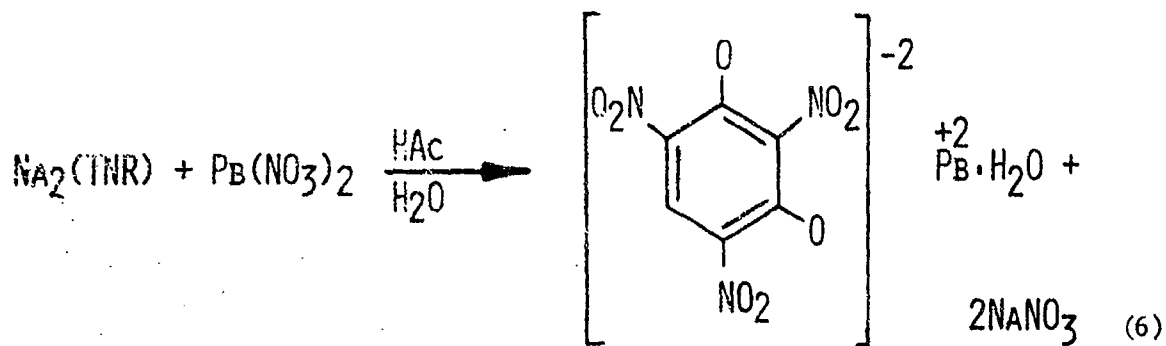


The product is then washed and filtered.

At the Twin Cities plant the process calls for conversion of TNR to a sodium styphnate solution with sodium hydroxide.



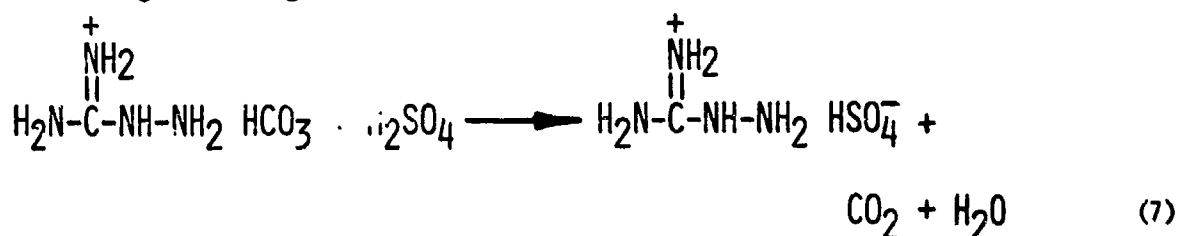
Addition of a lead nitrate-acetic acid solution results in the precipitation of lead styphnate.



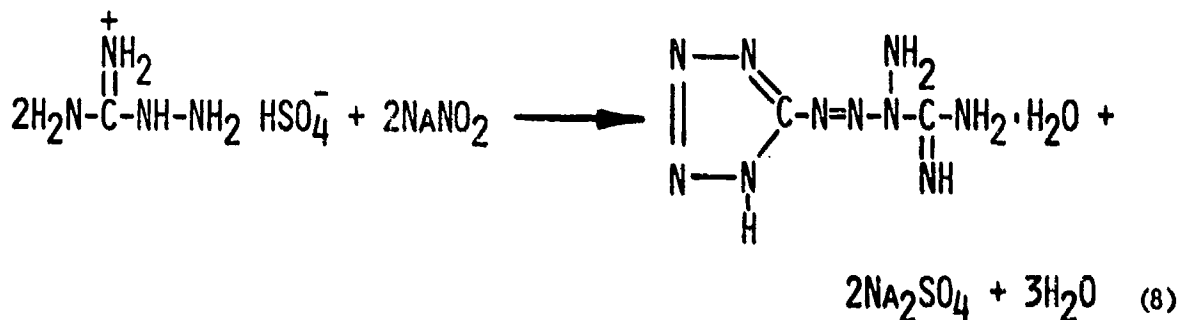
In this process the product is merely washed by repeated decantations.

The lead styphnate wastes do not require neutralization and are desensitized directly by the sodium hydroxide-aluminum powder-steam treatment. The desensitization products should be the same as in the TNR desensitization except for the additional formation of elemental lead.

Tetracene is also manufactured differently at the two plants. At the Lake City plant aminoguanidine bicarbonate is treated with sulfuric acid to give aminoguanidine sulfate.

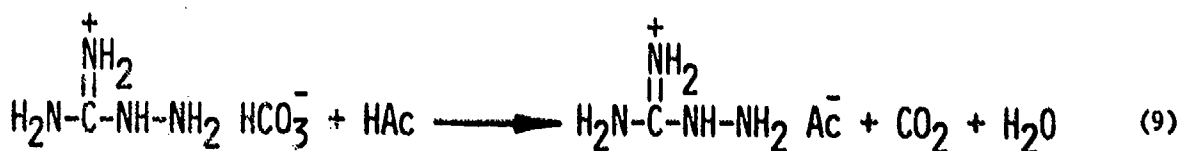


After addition of a sodium nitrite solution, the tetracene precipitates slowly.

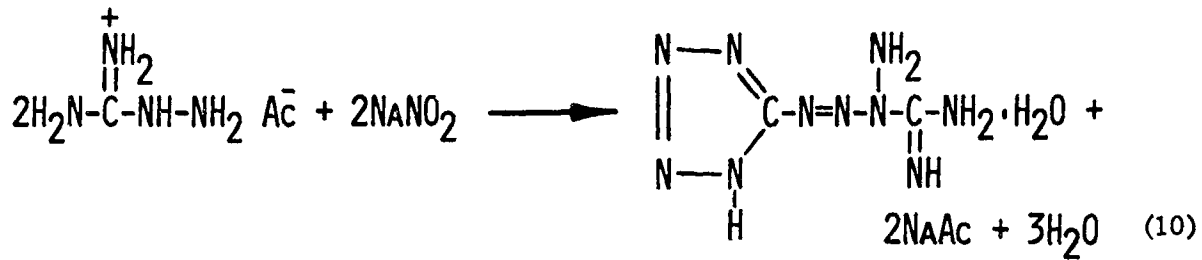


The product is then washed and filtered.

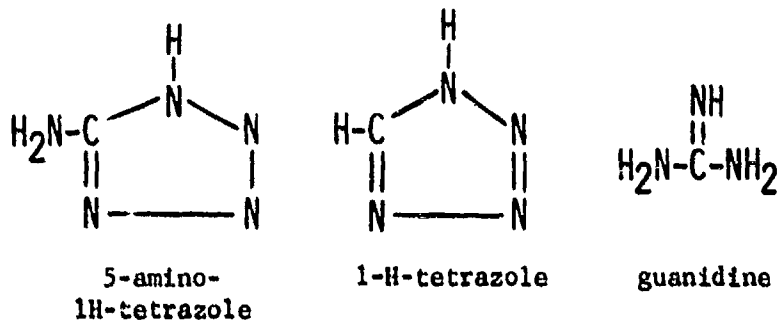
At the Twin Cities plant aminoguanidine bicarbonate is treated with acetic acid to give aminoguanidine acetate.



Again, addition of a sodium nitrite solution results in the slow precipitation of tetracene.



The tetracene wastes are desensitized without the addition of chemicals merely by boiling the aqueous mixture; the tetracene in the wastes decomposes to give ammonia, nitrogen and several other products including those shown below:



The other wastes of concern are generated during the mixing of priming mixture and the subsequent loading of the mixture into primers. These wastes, which contain all the materials in the FA 956 formulation, are desensitized by the sodium hydroxide-aluminum powder-steam treatment. The TMR and lead styphnate probably decompose as described previously. Tetracene, however, decomposes differently than in boiling water to give ammonia, cyanamide and 5-amino-1H-

tetrazole. The above desensitization procedure is only of limited effectiveness in the destruction of PETN because of its only slight solubility in water. At least one hour of heating is required to destroy dissolved PETN and at least six hours for PE-trinitrate and PE-dinitrate.

Waste Disposal

At Lake City AAP the desensitized wastes are segregated into three streams: a TNR waste stream, a lead styphnate-tetracene stream and a priming mixture mixing-loading waste stream. The TNR and lead styphnate-tetracene streams are discharged to evaporation ponds with impervious clay bottoms in order to evaporate the water and collect the solids. Overflow of the ponds has occurred during periods of heavy rain, resulting in discharge to a tributary of the Little Blue River an effluent which exceeds U.S. Army and Missouri standards for dissolved solids, sulfate, lead and possibly dissolved oxygen. The priming mixture waste stream is pumped to the ITP where it is treated with other wastewaters. The effluent from the ITP is discharged into the tributary of the Little Blue River. The heavy metals, lead, barium and antimony, should precipitate in settling ponds as a result of normal alum additions used in the ITP, the aluminum content of the desensitized waste and the sulfate from brass pickling acid waste. Thus, although the desensitized wastes from priming mixture mixing and loading do add to the load on the ITP, they should not adversely affect the quality of the ITP effluent.

At Twin Cities AAP all the wastes are desensitized in a central treatment sump and then trucked to open pits where seepage through approximately 400 feet of sand into ground water is a possibility. Also, the trucking of undesensitized wastes to the central treatment sump, in addition to being costly, could constitute a serious safety hazard.

PROPOSED METHODS

The various concepts considered for treatment and disposal of priming mixture wastes are presented in Table VI.

Waste Treatment

The TNR wastes consist of sulfuric and nitric acids and some organic materials which may be explosive. Although it is effective in neutralizing the acids, soda ash, the current neutralizing agent, also causes a very high dissolved solids content (20-30%) due to sodium sulfate and sodium nitrate. Neutralization by hydrated lime, Ca(OH)_2 , would result in the precipitation of calcium sulfate, thereby substantially reducing the dissolved solids and sulfate contents of the waste solution. After desensitization and discharge to an evaporation pond, the effluent from any overflow would still contain a much smaller concentration of pollutants.

Alternate methods of desensitization were evaluated in order to obtain products less undesirable than those obtained from the sodium hydroxide-aluminum powder-steam treatment. The agents studied experimentally included sodium sulfide, sodium sulfite, sodium

hydrosulfite (dithionite), sodium peroxide, hydrogen peroxide, sodium hypochlorite, chlorine gas, potassium persulfate, potassium bromate, sodium perborate and air (catalyzed and uncatalyzed). Although the experimental work was performed only on TNR, application to lead styphnate and priming mixture was also intended. It is apparent from Table VII that the agents which were chemically effective were sodium hydrosulfite, hydrogen peroxide, sodium hypochlorite, chlorine gas, potassium persulfate and air in the presence of a platinum/aluminum oxide catalyst. However, when cost effectiveness is taken into consideration, only chlorine gas and air appear to be competitive with the current sodium hydroxide-aluminum powder-steam treatment. In the case of chlorine gas, the possible toxicity of the products of chlorination must be investigated. It should be noted that oxidative desensitization would be preferable since it would have the additional desirable feature of reducing the chemical oxygen demand of the waste stream. Reducing agents, of course, would have the opposite effect.

Simple boiling of the wastes from tetracene manufacture, the current desensitization method at Lake City AAP, appears to be the best treatment for this waste. However, the agents tested above for TNR should also be applicable to the tetracene in priming mixture. PETN, on the other hand, was found to be stable to a fifty-fold excess of sodium hypochlorite even after several hours at 80°C. Again, the stability of PETN may be due to its only slight solubility in water. Two other possibilities for PETN are desensitization with ferrous ion

and the use of a wetting agent to promote hydrolysis.

Another approach to the treatment and disposal of TNR wastes is thermal, oxidative desensitization followed by separation and reuse of the acids. In work carried out at Dugway Proving Ground, Dugway, UT it was found that TNR was unstable in hot concentrated sulfuric acid. Since the waste from the manufacture of a 60 pound batch of TNR contains approximately 240 pounds of sulfuric acid and 38 pounds of nitric acid, it appeared that the explosive materials in the waste could be destroyed or desensitized merely by heating the waste mixture. Separation of the acids by distillation would then permit their reuse in the process. This would eliminate both the addition of chemicals for neutralization and desensitization and a substantial disposal problem. Although this approach has been investigated in the laboratory only in a preliminary manner, a recommended acid recovery procedure worthy of further study is the following. Heat the TNR wastes to 100°C and reflux for partial water removal. Raise the temperature to 250°C while distilling off a dilute nitric acid fraction suitable for reuse in drowning and rinsing operations. Increase the temperature to 325°C to give a distillate which is a mixture of nitric acid, sulfuric acid and water. This fraction would be recycled to the next batch of wastes for work-up. The pot residue after heating to 325°C consists of 98% sulfuric acid plus a solid residue of organic material and ferric sulfate. The sulfuric acid could be used as is in TNR manufacture, although build-up of the solid residue would

deserve monitoring, or most of the acid (say 80%) could be redistilled for use in TNR manufacture and the balance (20%) could be recycled to the next batch of wastes. Another possibility is to use the recovered sulfuric acid in another application, such as pickling of brass cartridge cases, where the residue build-up would not be a factor. Irregardless of how the acid is reused, the main points are that no chemicals are added and there is no material requiring disposal.

Incineration, which is used extensively in the destruction of scrap propellant and explosives, would have application to all of the waste streams resulting from the manufacture of priming mixture. In an incinerator the water would be evaporated and the combustible materials in the waste would be burned leaving a non-explosive ash for disposal. However, because of the large quantities of water associated with the waste, there would be a large energy input to evaporate the water. Also, for safety reasons the incinerator should be located several hundred yards from the manufacturing area which would require the transfer of the sensitive primer wastes from the manufacturing area to the incinerator. This would constitute a safety hazard. The wastes could be incinerated after chemical desensitization, but the cost would be approximately one dollar per pound of priming mixture produced. This is much too costly.

Disposal

As noted previously, disposal of desensitized wastes in evaporation ponds has not been entirely satisfactory during periods of heavy

rain. One possibility would be to direct any overflow to the ITP for treatment and disposal. However, since the water in the TNR evaporation pond contains 8,000 to 12,000 ppm of dissolved solids (mainly sodium sulfate) at a pH of about 10 and since the effluent from the ITP is already high in dissolved solids and sulfate³, this additional discharge would aggravate the situation. Precipitation of the excess solids in the ponds and the accompanying reduction in the dissolved solids content would permit discharge of the supernatant liquid to the ITP without degrading the effluent from the ITP. Therefore, studies were performed on the TNR and lead styphnate-tetracene waste streams to reduce the waste solids and organics by pH adjustment and coagulation with lime. HCl was added to the test solutions for pH adjustment as shown in Tables VIII and IX. A decrease in pH of the TNR waste from 11.6 to 6.8 resulted in a 58% decrease in total organic carbon (TOC), but the total solids decreased by only 6%. Addition of lime to the neutralized wastes resulted in a peak decrease in TOC of 75%, but again the total solids were reduced only slightly. In the case of the lead styphnate-tetracene composite waste, lowering the pH from 12.1 to 8.1 reduced the TOC by 53% but had only a small effect on the total solids. Addition of lime to the neutralized wastes resulted in a peak decrease in TOC of 62% and an actual increase in total solids. It is apparent from this data that neither pH adjustment nor the use of a coagulant was satisfactory in significantly reducing the solids content of the wastes.

Of course, lime neutralization of INK wastes, as mentioned previously, would result in the formation of calcium sulfate which after desensitization and discharge to the evaporation pond would settle in the pond. The dissolved solids content of the supernatant should, thereby, be reduced to a level that would not degrade the effluent from the ITP.

The concept of disposal of priming mixture wastes in a biological treatment system is based on the ability of such a plant to both remove the chemical oxygen demand (COD) of the waste and destroy the nitrogen compounds associated with the waste. The wastes must be treatable by biological action and must not poison the plant biomass. A brief study was made to determine the effect of desensitized primer wastes on the biological treatment in a municipal sewage plant. The toxic influence of these wastes was studied experimentally by waste dilution studies on batch activated sludge units and biological oxygen demand (BOD) analyses. The results of this work are presented in Tables X, XI and XII. The BOD data in Table X demonstrate that both TNR and tetracene wastes have definite toxic effects on biota found in municipal biological treatment plants. In the case of TNR the decrease in BOD from 825 to 60 with decrease in dilution from 1:1500 to 1:60 shows that the more concentrated solution reduces the activity of the biota. Similarly, the BOD of tetracene wastes decreases from 143 to 2.7 with decrease in dilution from 1:150 to 1:15. The BOD of lead styphnate, on the other hand, does not drop off as drastically

with increase in dilution, indicating that this waste may not be toxic to the biota. However, at extremely low dilutions it is not unexpected that a toxic effect is observed.

The oxygen uptake and related BOD data in Table XI show that desensitized TNR wastes are toxic to sewage plant biota at dilutions less than 1:100. A similar situation is observed with the BOD of a composite of desensitized lead styphnate and tetracene wastes in Table XII. However, the relative constancy of the BOD's for all dilutions of the wastes after exposure to the activated sludge units for 30 hours shows that the sewage biota acclimatized to the wastes during that time period. The oxygen uptake did not show the same sharp decrease for dilutions greater than 1:100 because the composite waste included the relatively non-toxic lead styphnate waste.

It should be noted that all of the BOD data show that the desensitized TNR, lead styphnate and tetracene wastes are treatable by biological action. Therefore, these wastes can be discharged to a municipal type sewage treatment plant, but the sewage volume should be at least 100 times the primer waste volume to preclude a detrimental effect on the sewage plant. There should be no problem in achieving this dilution with the Metropolitan Disposal System of the Twin Cities area and with the system planned by the Little Blue River Valley Sewer District.

REFERENCES

1. Bravo, J. and Collora, P.J., "Environmental Pollution Standards - A Summary of State and Federal Regulations", U.S. Army Munitions Command, Frankford Arsenal, Philadelphia, PA (November 1972).
2. Anonymous, "Water Quality Standards", APSA Regulation No. 11-11, U.S. Army Ammunition Procurement and Supply Agency, Joliet, IL (July 1970).
3. Graven, J. T., "Water Quality Engineering Special Study 24-030-71/72, Industrial Wastewater, Lake City Army Ammunition Plant, Independence, Missouri", U.S. Army Environmental Hygiene Agency, Edgewood Arsenal, MD (May 1972).

TABLE I. COMPOSITION OF FA 956 PRIMING MIXTURE

<u>Ingredient</u>	<u>Percent</u>
Normal Lead Styphnate	37
Tetracene (1-amino-1-[(1H-tetrazol-5-yl)azo]guanidine hydrate)	4
PETN (Pentaerythritol Tetranitrate)	5
Barium Nitrate	32
Antimony Sulfide	15
Aluminum Powder	7
Gum Solution	<0.1 (Solids)

TABLE II. STATE WATER QUALITY STANDARDS¹

State	pH	Temperature	Dissolved Oxygen, mg/l		Parameter		Miscellaneous		
			Monthly ave 5-7 min	Instantaneous 3-5 min	mg/l	Parameter	mg/l	Parameter	
Minnesota (Standards vary, depend on river)	5.5-10.0 (waste)	95° F (max)			2.0	Ammonia (as N)	200-700	Sulfate	250
	6.0-9.5 (Industry)	10° F over natural			0.01	Arsenic	1.5	Zinc	1.0-5.0
					1.0	Barium	0.3	BOD	25-50
					305.0	Bicarbonate	0.05	Suspended Solids	10-50
					0.5	Boron	0.05	Turbidity	5-50
					500	CaCO ₃	0.5	Oils	Essentially free of oil
					0.01	Cadmium	45		
					0.2	Chloroform extractable	0.01		
					50-250	Chloride	1.0-2.0		
					1.0	Chromium (total)	0.01		
					0.5	Chromium (hex.)	0.05		
					1.0	Copper	60		
					0.2	Cyanide			
Missouri (Little Blue River)	6.5-9.0	95° F (max)	3-5 min		0.3	Ammonia (as N)			
		5° F over natural			1.2	Fluoride			
					0.1	Lead			
					1.0	Zinc			

TABLE III. COMPARISON OF STANDARDS (ppm*)^{1,2}

Constituent	APSA Guidelines		State Standards	
	Effluent	Boundary	Most Stringent	Least Stringent
Ammonia	0.1	.01	0.30	2.00
Arsenic	0.05	.01	0.01	0.05
Barium	1.00	.10	0.01	0.50
Bicarbonate	35.00	35.00	205.00	205.00
Boron	1.00	.10	0.30	1.00
Cadmium	0.01	.01	0.005	0.03
Chloride	150.00	25.00	25.00	400.00
Chromate (HEX)	0.05	.05	0.05	0.05
Chromate (TOT)	1.00	.10	0.0	1.00
Copper	0.02	.02	0.0	1.00
Cyanide	0.025	.01	0.0	0.20
Fluoride	1.00	.70	0.20	2.50
Iron	0.30	.05	0.20	1.50
Lead	0.05	.01	0.04	0.20
Manganese	0.05	.01	0.05	1.00
Mercury	0.01	.01	0.0	0.005
Molybdenum	1.00	.10	0.01	0.01
Nickel	1.00	.10	0.10	1.00
Nitrate	5.00	.50	1.00	45.00
Phosphate	0.50	.05	0.03	2.00
Selenium	0.01	.01	0.005	0.01
Silver	0.05	.01	0.02	0.05
Sodium	100.00	10-60	1.00	82.00
Sulfate	200.00	50.00	100.00	500.00
Uranium	1.00	0.10	5.00	5.00
Zinc	0.50	0.05	0.025	5.00
Max. Temp.	90° ^w	—	80°F	95°F
Dissolved Oxygen	5.0	5.0	100% Sat	1.0
Phenols	0.010	0.010	0.001	1.0
pH	6.0-8.5	6.0-8.5	6.5-8.5	4.3-9.5
Dissolved Solids	200	500	500	2500

* Unless otherwise specified

TABLE IV. WASTE CHARACTERISTICS OF EFFLUENTS FROM PRIMER PLANTS

Plant	COD		Total Solids		TOC	pH	Inorganic Nitrogen (a)		Organic Nitrogen (b)		Al	CO ₂	Ca	Pb	Sb	Ba	Sulf	Maximum Waste Stream			
	PPM	PPM	PPM	PPM			PPM	PPM	PPM	PPM									PPM	PPM	PPM
<u>TPR Waste Streams</u>																					
Lake City AAP	6,200	3,000	3,200	270,000	950	12.9	85,000	4,700	--	3,300	17,000	--	--	--	--	--	--	--	1,250	10,400	
Twin Cities AAP (c)	15,000	3,000	12,000	400,000	3,400	12.9	4,000	7,500	--	3,400	5,700	100,000	--	--	--	--	--	--	1,000	8,300	
<u>Lead Sulfate Streams</u>																					
Lake City AAP	1,250	150	1,100	7,400	370	11.4	940	740	160	160	940	--	740	--	--	--	--	--	4,250	35,400	
Twin Cities AAP	13,000	--	13,000	35,000	4,400	4.8	4,700	2,400	--	--	--	--	3,800	--	--	--	--	--	1,500	12,800	
<u>Tetracane Streams</u>																					
Lake City AAP	7,100	6,000	1,100	36,000	53	8.0	18,000	2,300	250	--	--	--	--	--	--	--	--	--	220	1,800	
Twin Cities AAP	18,900	4,300	14,600	46,000	3,500	11.4	16,000	3,700	840	--	--	--	--	--	--	--	--	--	730	6,050	
<u>Miscellaneous Streams</u>																					
Lake City AAP	1,700	400	800	1,800	360	10.0	570	30	90	370	--	--	70	50	70	18	4,000	32,800	4,160	4,160	
Twin Cities AAP	11,300	1,600	9,700	30,000	2,100	7.0	--	1,200	2,300	1,900	--	--	5,000	3000	5300	1100	1,000	1,000	1,000	1,000	1,000
<u>Loading Streams</u>																					
Lake City AAP	42	30	12	170	4	10.0	60	2	3	35	--	--	7	4	4	4	--	24,000	200,000	200,000	
Twin Cities AAP	30	6	24	65	7	7.0	--	3	5	7	--	--	14	7	7	7	--	19,000	180,000	180,000	

(a) Inorganic nitrogen is all nitrogen not associated with the organics expressed in ppm nitrogen.
 (b) The organic nitrogen is all nitrogen associated with organic compounds and expressed as ppm nitrogen.
 (c) The inorganic carbon is expressed in ppm as calcium carbonate.
 (d) Proposed plant.

TABLE V. DEGREE OF TREATMENT NEEDED FOR MAJOR CONSTITUENTS OF PRIMER WASTES TO MEET WATER QUALITY STANDARDS
(All concentrations in ppm)

Stream	COP		SO ₄		COP & Amm. N		Pb		Sb		Ba	
	Stream Concentration	Percent Removal										
Minimum Standard	20 (a)		200 (a)		2.0 (b)		0.05 (a)		0.05 (a)		1.0 (a)	
Two Cities	3,100	99.4	8,600	97.7	1,660	99.9	240	99.98	10	99.5	16	93.8
Lake City												
TRE Stream	6,400	99.7	112,000	99.9	4,700	99.96	-	-	-	-	-	-
Pb Sulfamate and Tetracene Stream	1,500	98.7	550	63.7	960	99.8	700	99.993	-	-	-	-
Primer Mixing and Loading System	200	90.0	-	-	22	90.9	15	99.7	10	99.5	12	91.7

(a) APWA Guidelines
(b) Minnesota standard

TABLE VI. PROPOSED CONCEPTS AND APPLICATIONS

	THE	Tetracene	Lead Sulfate	FEIN	Priming Mixture	Priming Mixture
					MIXING	LOADING
<u>Neutralization</u>						
CaCO ₃	X					X
CaO	X					X
Ca(OH) ₂	X					X
<u>Desensitization</u>						
Na ₂ S	X		X		X	X
Na ₂ SO ₃	X		X		X	X
Na ₂ SO ₄	X		X		X	X
Na ₂ S ₂ O ₄	X		X		X	X
H ₂ O ₂	X		X		X	X
NaOCl	X		X	X	X	X
Ca(OCl) ₂	X		X		X	X
NaBO ₃ ·4H ₂ O	X		X		X	X
K ₂ S ₂ O ₈	X		X		X	X
KBrO ₃	X		X		X	X
Air Oxidation	X		X		X	X
Cl ₂				X	X	X
Fe ⁺⁺				X	X	X
Wetting Agent						
Boiling						
Acid Recovery	X	X				X
Incineration	X					X
<u>Disposal</u>						
Industrial Waste Treatment	X					X
Sanitary Sewer				X		
Direct	X	X	X		X	X
With Neutralization	X	X	X		X	X
With Desensitization	X	X	X		X	X
With Equalization	X	X	X		X	X
With Elutriation	X	X	X		X	X
With Precipitation	X	X	X		X	X
With Filtration	X	X	X		X	X
Land Fill	X	X	X		X	X
Metals Recovery						
Incineration	X	X	X		X	X

TABLE VII. EVALUATION OF ALTERNATE
TNR DESENSITIZATION METHODS

<u>Agent</u>	<u>Chemical Effectiveness</u>
Na ₂ S	No
Na ₂ SO ₃	No
Na ₂ S ₂ O ₄ · 2H ₂ O	Yes
Na ₂ O ₂	No
H ₂ O ₂	Yes
NaOCl	Yes
Cl ₂	Yes
K ₂ S ₂ O ₈	Yes
KBrO ₃	No
NaBO ₃ · 4H ₂ O	No
Air	No
Air with Pt/Al ₂ O ₃ Catalyst	Yes

TABLE VIII. ATTEMPTED PRECIPITATION OF TNR EVAPORATION POND WASTES

Sample	pH	Lime Dosage (mg/l)	TOC (mg/l)	TOC Removed (%)	Total Solids (mg/l)	Solids Removed (%)
<u>pH Adjustment</u>						
Waste	11.6	-	914	-	140,000	-
1	10.1	-	700	23	139,000	1
2	9.2	-	640	30	134,000	4
3	8.6	-	576	37	135,000	3
4	8.4	-	465	49	138,000	1
5	7.8	-	416	54	140,000	0
6	6.8	-	380	58	131,000	6
<u>Lime Addition</u>						
1	7.1	2,000	238	74	119,000	15
2	8.1	3,000	236	74	134,000	4
3	8.7	4,000	230	75	132,000	6
4	9.9	6,000	238	74	123,000	12
5	10.7	8,000	259	72	129,000	8
6	11.8	10,000	350	62	127,000	9

TABLE IX. ATTEMPTED PRECIPITATION OF LEAD STYFINATE - TETRACENE
COMPOSITE EVAPORATION POND WASTES

Sample	pH	Lime Dosage (mg/l)	TOC (mg/l)	TOC Removed (%)	Total Solids (mg/l)	Solids Removed (%)
<u>pH Adjustment</u>						
Stirred Waste	12.1	-	366	-	14,700	-
1	11.2	-	277	24	11,300	23
2	10.4	-	261	29	11,100	34
3	9.8	-	220	40	11,300	23
4	8.9	-	196	46	11,700	20
5	8.3	-	173	53	12,000	18
6	8.1	-	163	53	12,200	17
<u>Lime Addition</u>						
1	7.8	1000	162	56	18,000	24*
2	8.0	1500	172	53	17,000	16*
3	8.2	2000	160	56	17,000	16*
4	8.9	3000	138	62	16,000	9*
5	10.6	4000	158	57	17,000	14*
6	11.4	5000	154	58	16,000	9*

* Increase in total solids.

TABLE X. BOD₅ OF PRIMER WASTES

<u>Waste Stream</u>	<u>Dilution</u>	<u>BOD₅ (mg/l)</u>	<u>BOD₅ Reduction Due to Toxicity (%)</u>
<u>TNR</u>	1:1500	825	--
	1: 600	540	35
	1: 300	435	47
	1: 150	338	59
	1: 60	80	90
<u>Lead Styphnate</u>	1: 300	195	--
	1: 150	128	34
	1: 60	213	9*
	1: 30	146	25
	1: 15	109	44
<u>Tetracene</u>	1: 150	143	--
	1: 60	21	85
	1: 30	4.5	97
	1: 15	2.7	98

* Increase in BOD₅

TABLE XI. BIOTOXICITY OF TNR WASTES

Sample	Dilution	Oxygen Uptake at 48 hours (mgO ₂ /l MLVSS)	Reduction in		Initial BOD ₅ (mg/l)	Reduction in BOD ₅ (%)		pH	
			Oxygen Uptake (%)	Reduction in BOD ₅ (%)		Initial	Final		
Blank	--	0.688	--	--	777	--	--	7.8	7.2
1	1:10,000	0.768	12*	2**	795	2**	2**	8.0	7.2
2	1:1,000	0.704	2*	2	765	2	2	8.2	7.6
3	1:100	0.688	--	10**	855	10**	10**	9.3	9.0
4	1:20	0.216	69	69	240	69	69	9.8	9.0
5	1:10	0.213	69	69	240	69	69	10.1	9.2

* Percent increase in oxygen uptake.

** Percent increase in BOD₅.

TABLE XII. BIOTOXICITY OF LEAD STYPHNATE-TETRACENE COMPOSITE WASTE

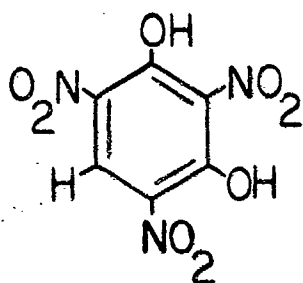
Sample	Dilution	Oxygen Uptake at 30 hours (mgO ₂ /l MLVSS)	Reduction		Reduction		Reduction		pH	
			in Oxygen Uptake (%)	Initial BOD5 (mg/l)	in Initial BOD5 (%)	BOD5 at 30 hrs. (mg/l)	BOD5 (%)	Initial	Final	
Blank		0.632	--	885	--	372	--	8.0	6.7	
1	1:10,000	0.776	23*	795	10	366	2	8.2	6.7	
2	1:1,000	0.652	2*	765	14	384	3**	8.4	7.4	
3	1:100	0.576	9	855	3	378	2**	8.6	8.0	
4	1:20	0.488	23	354	60	354	5	9.4	8.4	
5	1:10	0.552	13	240	73	300	19	9.6	8.6	

* Percent increase in oxygen uptake.

** Percent increase in BOD5.

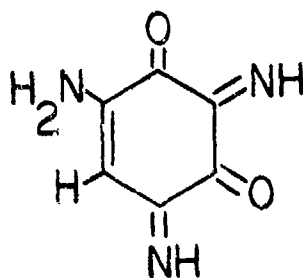
FIGURE 1. POSSIBLE STRUCTURES FOR LABORATORY-DESENSITIZED TNR

TNR: $C_6H_3N_3O_8$ (MW=245)



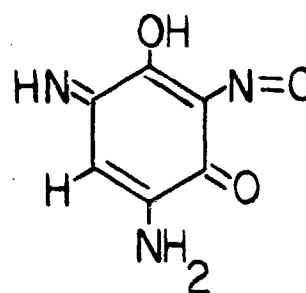
I

$C_6H_5N_3O_2$ (MW=151)



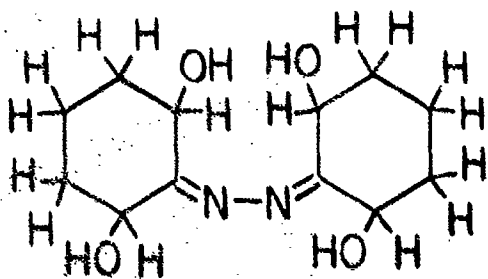
II

$C_6H_5N_3O_3$ (MW=167)

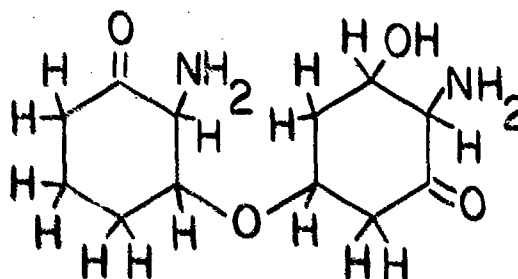


III

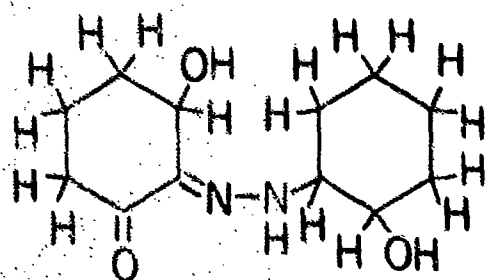
$C_{12}H_{20}N_2O_4$ (MW=256)



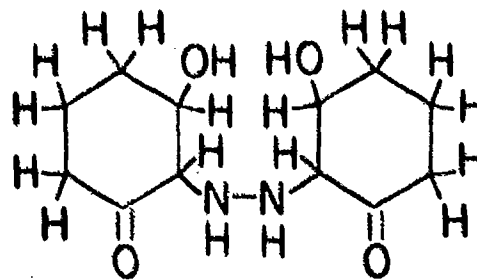
IV



V



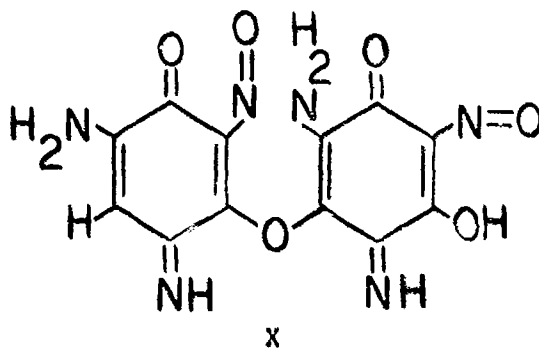
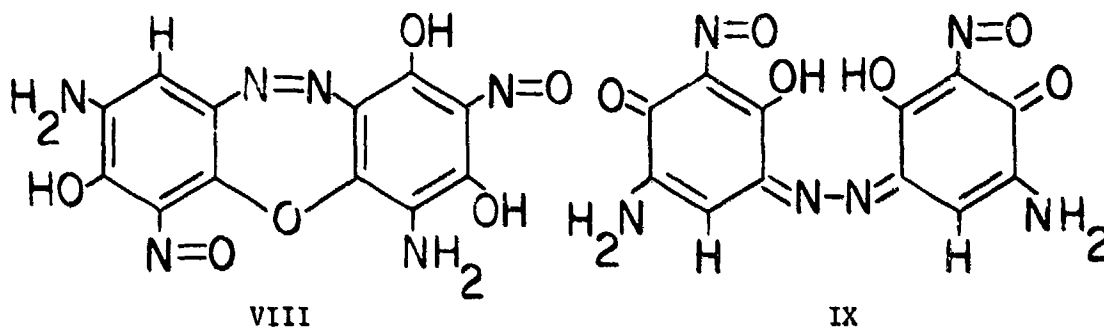
VI



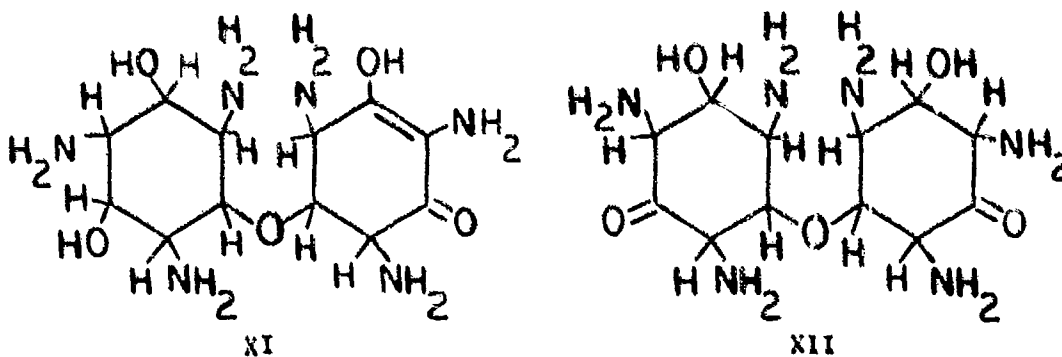
VII

FIGURE 1. POSSIBLE STRUCTURES FOR LABORATORY-DESENSITIZED TNR (CONT)

C₁₂H₈N₆O₆ (MW=332)



C₁₂H₂₄N₆O₅ (MW=332)



REPLACEMENT OF BENZENE FOR IMPROVED
TOXICITY IN THE NITROCELLULOSE RECOVERY
PHASE OF BALL PROPELLANT MANUFACTURE

Messrs J. M. Goldman and J. A. Sipia, Jr.
Frankford Arsenal
Philadelphia, Pennsylvania

ABSTRACT

This study represents one portion of a program directed toward the minimization or elimination of toxicity and flammability hazards associated with the use of benzene in the recovery of nitrocellulose from surplus cannon propellants in the manufacture of ball propellants.

The current extraction operation using the benzene-ethyl acetate cosolvent is described in detail. The toxicity and flammability problems associated with the use of benzene are identified.

The methodology of identifying prospective replacements for benzene is presented along with the results of Soxhlett extractions where dichloromethane is identified as the most promising candidate. The operating temperature for extraction with dichloromethane has been selected based upon a series of batch extractions.

By varying the dichloromethane to propellant ratio the solid-liquid equilibrium relationship was established in a further series of batch extractions. With these data, a new process design for the recovery of nitrocellulose from cannon propellants using dichloromethane is proposed.

This study shows that extraction efficiency and economy of operation need not be sacrificed when correcting environmental problems.

INTRODUCTION

Overview of Extraction Step

In the manufacture of ball propellant, surplus single base cannon propellants are used as the source of nitrocellulose (NC), the major component of the finished product. These surplus propellants contain along with the NC, dinitrotoluene (DNT), dibutylphthalate (DBP), and diphenylamine (DPA), components undesirable in the feedstock for ball propellant processing. In order to utilize the NC in the cannon propellants, the undesirable components must be removed. It is in the extraction or NC recovery step, the first major process step in ball propellant manufacture, that this is achieved.

Description of the Extraction Process

The removal of unwanted modifiers from the cannon propellant is achieved in a 3-step, batch, countercurrent leaching operation. Prior to the extraction operation, the cylindrical multiperforated cannon propellant grains are ground in a hammermill to provide solids with a high surface area to accelerate the leaching rate. This granular feed is pumped in a water slurry to one of the two extraction stills. The feed rests on a perforated false bottom through which water is drained. Following drainage, the cosolvent, containing 90% benzene (B) and 10% ethyl acetate (EA), by weight, is added to the extraction still. The contents are heated to 65°C, the extraction temperature, and agitated for the 90 minute first extraction step. The solvent is then drained and pumped either to recovery for cleanup or to the other extraction still for processing of another batch of propellant. The two stills are operated together in order to achieve countercurrent processing. The schematic in Figure 1 shows how this is achieved. P represents the powder and S the solvent. Superscripts represent one particular batch of either powder or solvent. The subscripts of P refer to the number of prior contacts with solvent. Subscripts of S refer to the number of times the solvent has had prior contact with propellant. After three contacts with the B-EA cosolvent, the powder is pumped as a water slurry, to a stripping still. After solvent has been used three times, it is sent to solvent recovery for removal of the modifiers. After two batches of propellant have been extracted and pumped to the stripping still, the agitated propellant-water slurry is heated and placed under vacuum in order to remove some of the solvent retained either on the surface or in the interstices of the propellant granules. Upon completion of solvent stripping, the propellant chips are pumped forward for the manufacture of ball propellant. Seventeen hours are required to complete two extraction batches and 12 hours more for the stripping of the retained solvent. The product of the NC recovery operation is solid NC with less than 1% residual extractible material.

Toxicity and Flammability

The presence of benzene in the NC recovery step has always generated concern among operators and safety engineers. An accidental spill or leakage of vapors is not considered casually because of the extreme toxicity and flammability of benzene.

The toxicity of benzene is considered very severe. The O.S.H.A. assigned Threshold Limit Value of 10ppm maximum exposure for an 8-hour shift attests to this. If overexposure should occur, underexposure must follow in order to meet the O.S.H.A. guidelines. At low concentrations, prolonged exposure can damage the blood-forming organs. Slightly higher concentrations can result in headache, nausea, and tightness of chest, possibly preventing an operator from removing himself from the contaminated area. At high concentrations, failure of either the central nervous system or respiratory system is a probability. Harmful amounts of benzene may be absorbed by ingestion, inhalation, or direct contact.

During the NC recovery step, extraction stills are opened in order to check if all solvent has drained after a stage. Since high local concentrations of benzene can accumulate when the manhole cover is opened, operators are required to wear air masks or packs to prevent inhalation and possible contamination.

In addition to the severe toxicity exhibited by benzene, it presents a potential for fire and explosion. Because of its low flash point of -11°C (12°F) and lower explosive limit of 1.3% in air, benzene is considered dangerously flammable.

The concern for operator health and safety in the NC recovery operation led to the creation of a program to replace benzene with a less toxic and, if possible, a non-flammable solvent. Below is presented a portion of the program which has resulted in the identification of dichloromethane as an alternate solvent which not only meets the constraints set for toxicity and flammability, but also offers processing and economic advantages for the NC recovery phase of ball propellant manufacture.

METHODOLOGY OF SOLVENT SELECTION

Selection Criteria

The literature was searched in order to find potential replacements for benzene. The criteria were based upon the desire to minimize or eliminate all objectionable characteristics associated with benzene. Therefore, any proposed solvent must have either a higher flash point than benzene or no flash point at all so that the chance of fire or explosion

would be less likely. In order to reduce the possibility of a toxic environment and to ease the management of same, a minimum Threshold Limit Value of 100ppm in air was set following consultation with plant safety personnel. The types of effects a solvent could produce when contacted by humans were considered as a guideline as well, with those solvents having milder effects being more favorably considered.

In order for successful removal of unwanted modifiers to be accomplished in a leaching operation, the proposed solvent had to exhibit good solvent power for the modifiers. At the same time, solubility of NC in the solvent was considered detrimental since this would represent a loss of raw material, an unacceptable processing inefficiency. With all these constraints, one additional one was necessary: the proposed alternate solvent would need to be approximately as efficient or more so than the B-EA cosolvent in use.

Soxhlett Extractions

The literature indicated that the most promising alternates fell in the following two classes: (1) halogenated hydrocarbons and (2) short to medium chain length alcohols. In order to assess the leaching power of each solvent, duplicate 5-hour Soxhlett extractions were run for each candidate. The results indicated that three of the solvents being investigated showed better extraction power than benzene. They were, in order of relative extraction efficiency, as follows: (1) dichloromethane, (2) n-butanol, and (3) isobutanol. These three solvents showed improvement in the flammability and the minimum toxicity level considerations, as well. A summary of results to this point appears in Table I.

TABLE I

Summary of Soxhlett Extractions and Environmental Data

<u>Solvent</u>	<u>Percent Extractibles Removed</u>	<u>Flash Point, °F</u>	<u>TLV, Ppm</u>
Dichloromethane	97.7	None	500
n-butanol	86.6	115	100
Iso-butanol	84.5	100	100
Benzene	73.8	12	10

Only the above three candidate solvents were studied further. Here, only subsequent investigation of dichloromethane is considered, since only with it has experimentation progressed to the point of process design.

Batch Extractions

In the Soxhlett extraction phase of this investigation, dichloromethane could be compared only to benzene, not directly with the 90% benzene-10% ethyl acetate cosolvent in use. Therefore, a series of concurrent batch extractions was planned and subsequently conducted in an agitated, temperature-controlled, 1-liter, 3-necked flask. Standard experimental procedure provided for addition and heating up of the solvent followed by addition of the required amount of ground surplus cannon propellant. In every case, the solvent-to-propellant ratio was 3:1 by weight, the ratio used in production. The duration of the extractions was a standard of 4 hours, sufficiently long for complete equilibrium to have been reached. Prior to extraction, the propellant was towel-dried; following extraction, the propellant was allowed to air dry overnight prior to analysis for residual extractible material.

In this phase of experimentation, two effects were studied: (1) extraction efficiency as a function of temperature, and (2) the impact of 10% by weight ethyl acetate addition to the solvent upon extraction efficiency. Figure 2 compares the extraction efficiencies of dichloromethane and the B-EA cosolvent. In both cases, more extractible matter is removed as the temperature is elevated. The extraction efficiency of dichloromethane is much less sensitive to temperature. Equivalent removal of extractibles can be achieved using dichloromethane at 35°C as compared to 65°C for the B-EA cosolvent.

The effects of addition of ethyl acetate on removal of extractibles from cannon propellant are shown in Table II.

TABLE II

Influence of EA on Extraction Efficiency

<u>Solvent</u>	<u>Temperature, °C</u>	<u>Residual Extractibles</u>
Benzene	65	6.35
Benzene-EA	65	3.33
Dichloromethane	35	3.33
Dichloromethane-EA	35	3.39

The advantage of using ethyl acetate with benzene is clearly shown; however, no significant change in extraction efficiency is shown when EA is combined with dichloromethane. Since no advantage was gained by combining EA with dichloromethane, further experimentation was carried out with dichloromethane alone.

As a result of the batch extractions discussed above, the optimal operating temperature of 35°C was identified for dichloromethane and the ability to use dichloromethane without EA indicated significant processing simplification.

Below is discussed the experimentation which has led to a design for the NC recovery operation, using dichloromethane as the extraction solvent.

DESIGN OF EXTRACTION SCHEME

Equilibrium and Rate Data

In order to properly design the extraction process, an equilibrium relationship between the modifiers in the liquid and solid phases was required. These data were obtained in a series of batch extractions in which the initial solvent-to-propellant ratios were varied over a wide range (1:1 to 20:1). The extractions were conducted in an agitated, temperature-controlled, 2-liter resin flask. Solvent heat up and propellant addition were accomplished in similar fashion to the prior batch extractions. The duration of propellant-dichloromethane contact was 3 hours in all cases. Liquid samples were withdrawn from the resin flask at regular intervals and analyzed by ultraviolet spectrophotometric methods to determine the approach to equilibrium. Upon completion of each experiment, the liquid phase was poured off and the solid phase air dried overnight prior to analysis for residual extractible material. In this way, each experiment yielded a solid-liquid equilibrium point and the time interval to achieve equilibrium conditions. Results from the analyses of solid and liquid phases were curve-fitted by the method of least squares. The curve representing the equilibrium relationship is shown in Figure 3. With the equation representing this curve and overall and component (unwanted modifiers) material balances derived around a theoretical countercurrent leaching stage, a computer program was written to assist in the design of the countercurrent extraction process. The results of this design and how they are incorporated in the existing process equipment are discussed below.

RESULTS

Selection of the Number of Stages and the Solvent/Powder Ratio

With the assistance of a computer simulation, the minimum number of stages and the corresponding solvent-to-propellant ratio could be determined. The simulation was designed to calculate stages proceeding in reverse order. Specifically, the simulation iterated starting with the outlet powder weight fraction of 0.01 extractibles and corresponding

pure solvent input. The simulation iterated until the powder feed modifier weight fraction of 0.13860 was exceeded. The solvent to powder ratio was specified in the data input along with powder feed and product extractibles composition and solvent feed. The data output provided both propellant and solvent inlet and outlet compositions for each stage. The solvent-to-propellant ratio was varied until the minimum number of stages was determined. The results of the calculation for dichloromethane are presented and compared with the current process in Table III.

TABLE III

Comparison of Current Benzene-EA and Proposed Dichloromethane Propellant Extraction Schemes

<u>Solvent</u>	<u>Number of Stages</u>	<u>Solvent to Powder Ratio</u>
Benzene-EA	3	3:1
Dichloromethane	2	3.125:1

A proposed scheme of using the current extraction equipment with dichloromethane as the leaching solvent is shown in Figure 4.

Implications of Using Dichloromethane in Nitrocellulose Recovery

The proposed scheme for extracting unwanted modifiers from single-base cannon propellants with dichloromethane indicates significant potential advantages over the current processing technique. The higher specific gravity of dichloromethane allows more solvent in a batch and, therefore, a 44% increase in propellant processed per batch. Combined with the reduction in stages from 3 to 2, resulting in a 25.5% shorter processing time for 2 batches, a 93% increase in production rate can be effected. This, alone, can mean a 30% reduction in per pound costs for the NC recovery operation.

Further economies, although less significant, are reduced steam requirements because of the lower extraction temperature, 35°C, and the lower specific and latent heats associated with dichloromethane. Btu requirements are compared in Table IV.

TABLE IV

Comparison of Energy Requirements in Extraction and Solvent Stripping

<u>Solvent</u>	<u>Extraction</u> <u>Btu/lb Solvent</u>	<u>Stripping</u> <u>Btu/lb Solvent</u>
Benzene-EA	30.2	212.1
Dichloromethane	5.04	142.57

A further advantage of using dichloromethane is processing simplification. The reduction in stages from 3 to 2 means less handling of each batch of solvent. The ability to use dichloromethane as the sole extraction solvent makes the recovery operation more easily accomplished.

Finally, all the processing efficiencies discussed above have been accomplished as a by-product of the effort to make the NC recovery operation a safer one. The total elimination of a fire hazard attributed to the extraction solvent is achieved when using dichloromethane. The high TLV of 500ppm combined with the reduced toxicity of dichloromethane makes the extraction environment significantly easier to manage.

CONCLUSIONS

Following successful pilot plant process and product testing the change to dichloromethane can be made in the NC recovery operation at Badger AAP. Finally, a toxic working environment can be significantly improved without paying a premium for such a change.

Extraction
Still No. 1

Extraction
Still No. 2

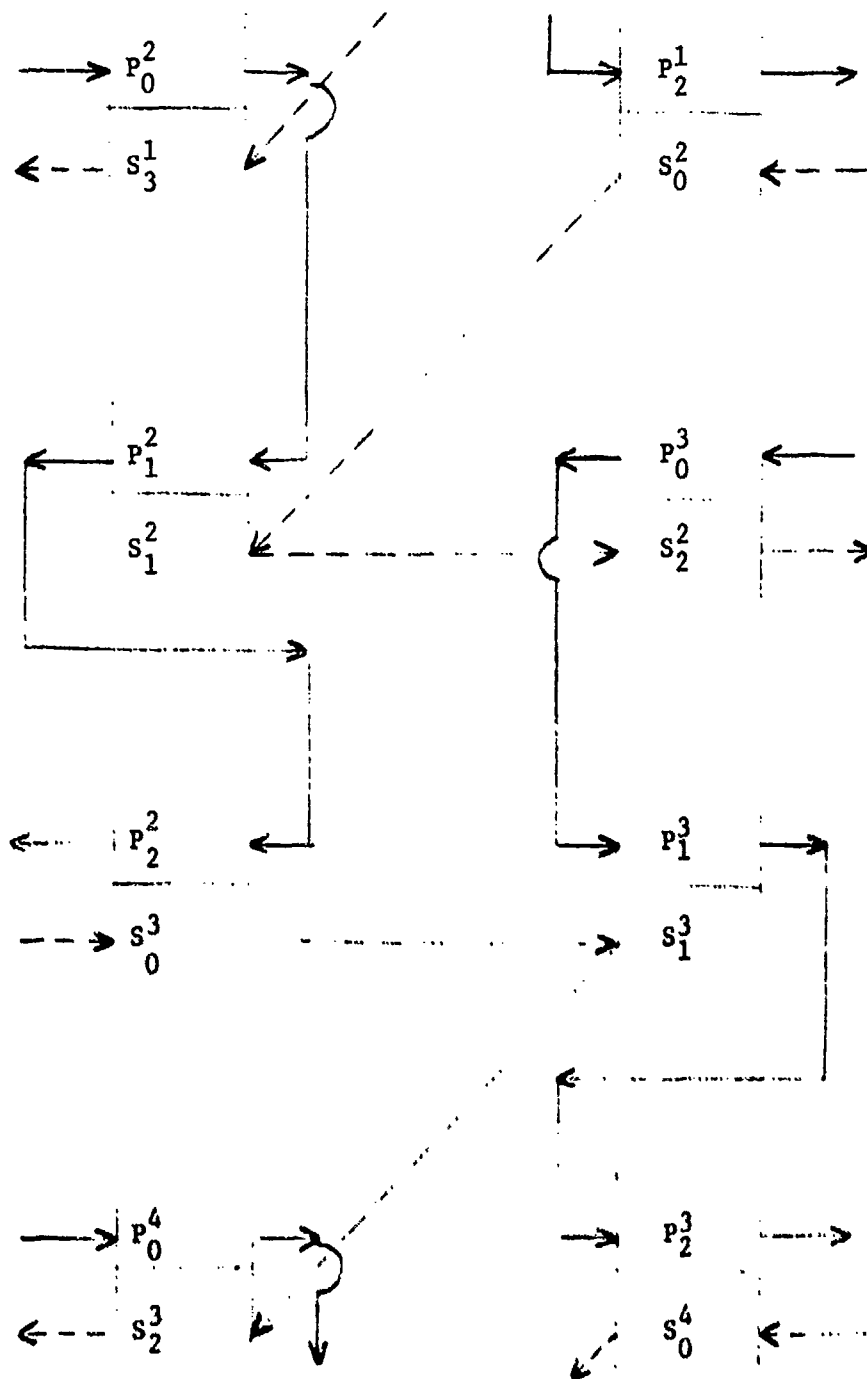


Figure 1. Current Extraction Scheme Using Benzene - Ethyl Acetate Cosolvent

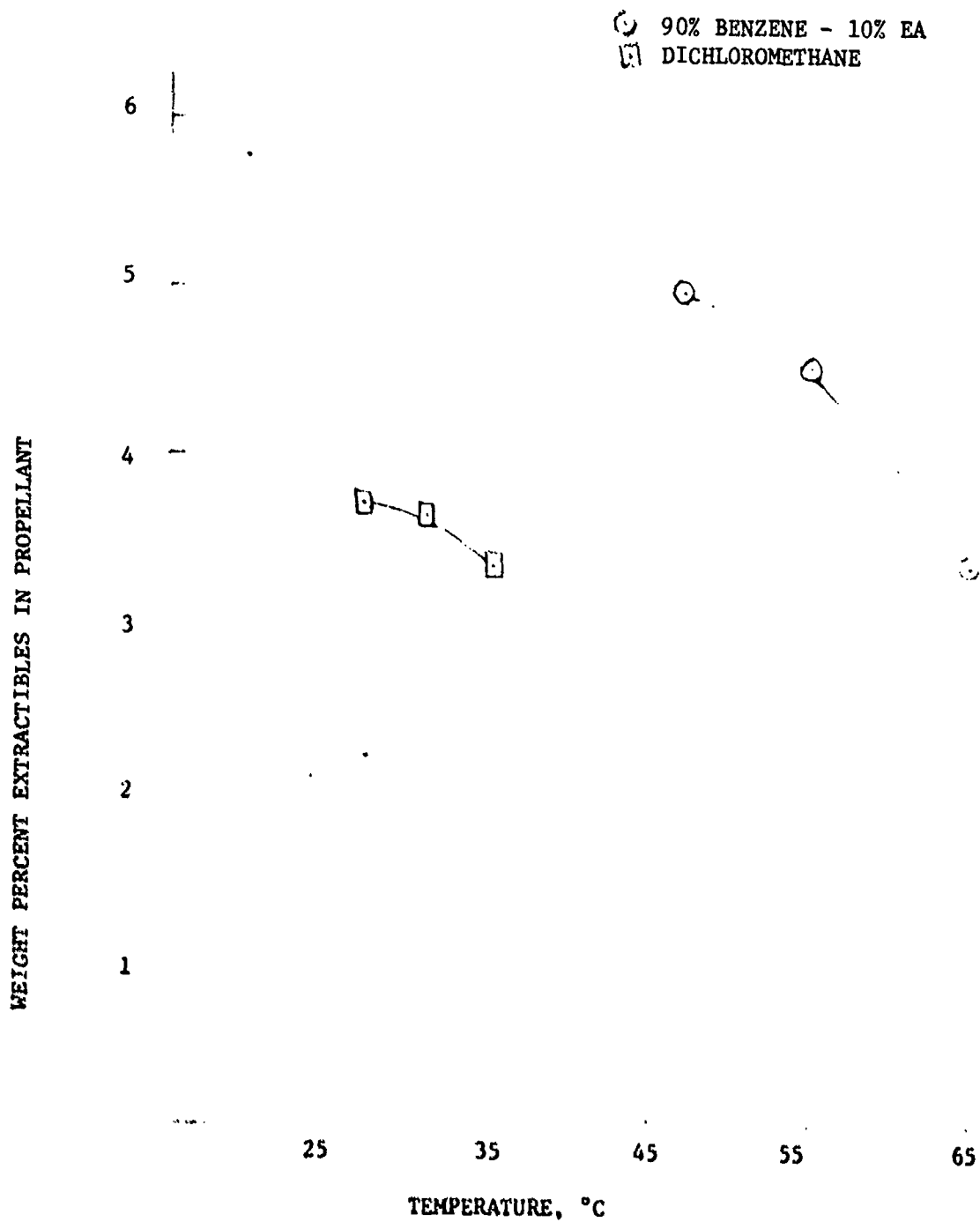
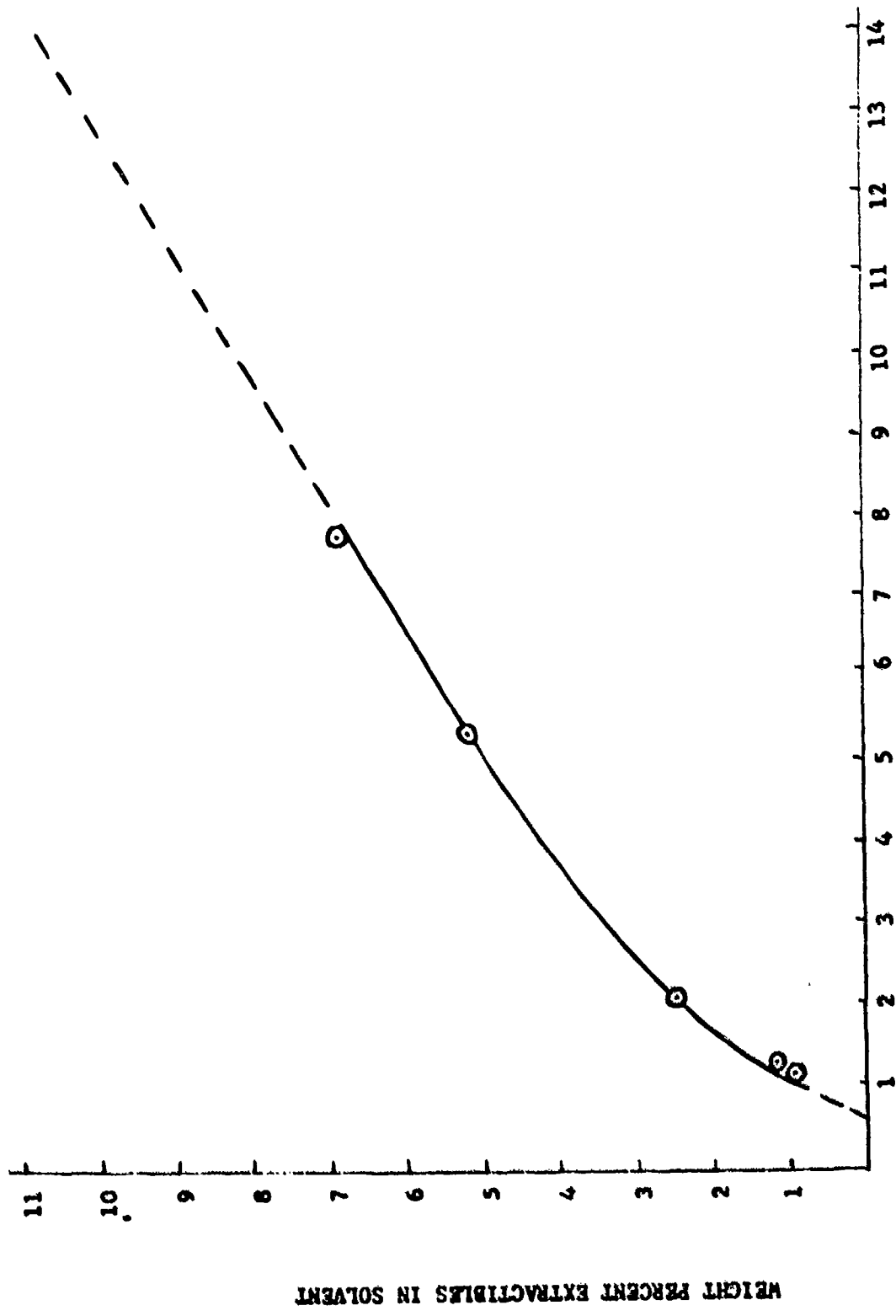


Figure 2. Effect of Temperature on Extraction Efficiency



WEIGHT PERCENT EXTRACTIBLES IN PROPELLANT

Figure 3. Equilibrium Relationship for Extraction with Dichloromethane

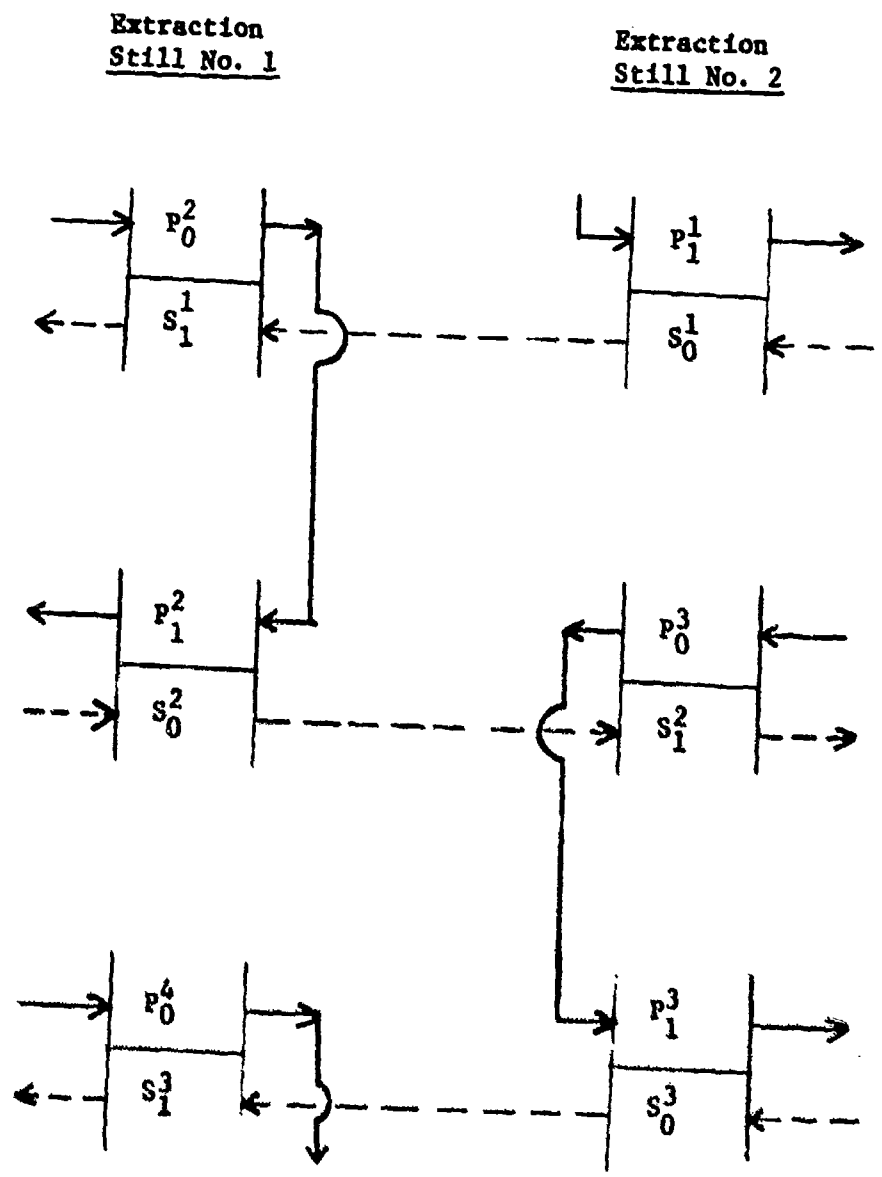


Figure 4. Proposed Extraction Scheme Using Dichloromethane

Hazardous Waste Disposal Through
Fluidized Bed Incineration

By

Joseph S. Santos
John J. Canavan

Facilities and Protective Technology Division
Manufacturing Technology Division
Picatinny Arsenal

ABSTRACT

Picatinny Arsenal has the responsibility for developing the technology and equipment necessary for the elimination of the pollutants generated by the Army's government owned, contractor operated (GOCO) plants manufacturing munitions. One of the major problems at all of these plants is the disposal of explosive and propellant waste material. The current method of "open burning" is unacceptable from safety and environmental aspects. Therefore, it was decided that incineration appeared to be the best approach to eliminate open burning. The feasibility of incinerating explosives in a water slurry was accomplished at Picatinny Arsenal. Concurrently, Redford Army Ammunition Plant evaluated an off-the-shelf rotary kiln incinerator. The nominal feed rate for these systems was 250 lb/hr of waste explosives and propellants. Typical wastes were TNT, Comp B, RDX and HMX explosives; single, double and triple base propellants. In addition to the incineration effort, the ancillary processes of grinding, slurry preparation and pumping, and injection techniques were fully demonstrated. To meet future requirements, an advanced incineration technique, the fluidized bed combustor, was selected for investigation. This system successfully demonstrated the disposal of explosives and propellants in a small scale pilot plant. During the course of this effort, a catalyst was found that reduced the NO_x concentration in the stack gas to virtually zero. In support of the incineration efforts, a pilot plant hazards analysis on the rotary kiln, an engineering development hazards analysis on the fluidized bed and detonation propagation tests on aqueous slurries of explosives and propellants have been accomplished.

INTRODUCTION

The US Army is a major producer of munitions for the United States. In the course of the manufacturing and load assembly pack operations conducted at the GOCO plants throughout the United States nonrecoverable and nonrecyclable waste propellants and explosives are accumulated. The current method of disposing of this waste is by open burning. Here the material is spread on concrete pads and remotely initiated. Stock piling of hazardous waste materials, air and water pollution, personnel exposure, and inefficiency characterize the problems associated with open burning and emphasize the need for a safe, reliable, pollution free alternative.

Controlled combustion is the most logical, technical solution, but little information of an engineering nature is available on this subject. Therefore, the objective of this study was to develop the necessary engineering technology for a total system (Figure 1) and to test and evaluate the systems, developed as pollution abatement vehicles, to eliminate the open burning disposal practice. Three incinerator designs, vertical induced draft, rotary kiln and fluidized bed were operated on a pilot and laboratory scale. The feasibility of this concept was shown by successfully destroying TNT, Composition B, RDX and HMX in the vertical induced draft unit. The rotary kiln incinerator was successfully piloted, at 250 lb/hr, and the results of the pilot plant effort were incorporated into a Design Criteria Package for implementation of a full scale (1350 lb/hr) complex. Studies on a laboratory scale fluidized bed incinerator were extremely interesting. The combustion of the explosives and propellants was rapid and a catalyst was uncovered that drastically reduced the NO_x on the exhaust gas. In addition to the incineration techniques, the ancillary processes of grinding, slurry preparation, pumping and injection were fully demonstrated. In the hazards analysis area, each system was analyzed for normal operations and for abnormal conditions or malfunctions. It was found that for normal operations there are no serious hazards. However, the addition of tramp metal, loss of water, poor housekeeping or operation could lower the safety margin to zero. Hazards analyses identified the potential hazards and operational procedures were then developed that minimized the hazards.

TECHNOLOGY DEVELOPMENT

Three incinerator designs, a vertical induced draft, rotary kiln, and fluidized bed were selected for investigative studies to determine their applicability to explosive and propellant waste disposal.

Vertical Incinerator: Initial work was accomplished in an existing vertical induced draft incinerator designed and built in 1957 for liquid explosive waste disposal (Figure 2). It is a cylindrical steel furnace lined with firebrick. Inside dimensions are 8 feet diameter and 30 feet high. The upper zone contains the oil burners and auxiliary equipment to produce the heat necessary to evaporate the water and bring the temperature of the solid explosive waste up to the

ignition point. Introduction of the explosive waste occurs just under the oil burners. An induced draft fan, with a capacity of 10,000 cubic feet per minute, and a cyclone dust collector are the other main elements of the plant, with the combustion gases exiting via the flue to a 125 foot stack. The furnace is provided with 3 oil burners operating on #2 fuel oil supplied from a 7,500 gallon underground storage tank.

After the furnace is brought up to operating temperature, about 1500°F in the combustion zone, temperature may be controlled by the use of one or two burners as desired. The furnace generally operates under a negative pressure due to operation of the induced draft fan and the natural draft in the stack. About 30% of combustion air is taken in by induction with additional atomizing and combustion air provided by the controllable turbo-blower capable of furnishing 1150 cubic feet per minute maximum. Instrumentation and control equipment are provided for temperature control and automatic shut-down if incinerator equipment malfunction occurs. In addition, 10 explosion blow-out doors are provided as an additional safety measure.

This incinerator was modified to accept solid waste explosives in water slurries. Feasibility and safety requirements, particle size reduction, suspension, injection, combustion and baseline gaseous emission data were established and evaluated. The explosive was ground to a uniform particle size using a rubber-lined steel jar mill and bronze balls. Water was added to the explosive in the grinder in the ratio of 3:2 by weight, respectively. The resulting slurry was sieved through a 20 mesh screen and water added to achieve a water/explosive ratio of 6.7/1 prior to incineration for a disposal rate of 250 pounds per hour equivalent dry explosive. The feed system employed is depicted in Figure 3. Suspension was maintained by a pneumatic agitator and the slurry transferred into the incinerator through a water cooled injection tube. Two means of slurry transfer were evaluated: a steam ejector and a diaphragm pump, both of which performed satisfactorily. The end of the injection tube was equipped with a spray nozzle to disperse the slurry upward into the combustion chamber.

A summary of materials incinerated with the combustion conditions for the initial testing in the vertical induced draft incinerator is shown in Figure 4. A total of 49 tests were completed with explosive slurries. Duration of tests ranged from thirty seconds to twenty minutes. Temperature and photographic data showed controlled, rapid combustion occurring in the injection and combustion zones with only an occasional flaming particle visible. An analysis of the exhaust gases emitted is shown in Figure 5. It is apparent that while the feasibility of the concept was proven, the environmental aspects still required some work. Visual observation indicated that the unsightly dense smoke associated with open burning was eliminated; however, small amounts of NO_x fumes were visible.

The instrumentation and control systems installed on the incinerator performed as required and resulted in the program being completed with no serious incidents. Preliminary hazards analyses identified the potential hazards and operational procedures were then developed that minimized the hazards. This includes the processes of grinding, pumping, injection and incineration of the explosive and propellant/water slurries.

Rotary Kiln Incinerator System: An important task in the overall program to develop an acceptable incineration system was to select an off-the-shelf unit and adapt it to meet immediate needs. The unit selected for this purpose was the rotary kiln incinerator. This system was designed for nominal feed rate of 250 lb/hr of propellant or explosive. It was installed and operated at Radford AAP concurrently with the vertical incinerator effort at Picatinny Arsenal.

The rotary kiln used (Figure 6) was approximately five feet in diameter and eight feet long. The cylinder is lined with alumina fire brick, which can withstand temperatures to 2400°F, and has a variable speed of 0-6 rpm. No. 2 fuel oil or butane can be used for the burner which fires countercurrent to the material and exhaust gas flow. The afterburner is a refractory lined cylinder located above and downstream of the incinerator. A pre-cooler quenches the hot exhaust gases to 600°F prior to entrance into the wet scrubber. The marble bed scrubber washes out particles and water soluble chemicals in the exhaust stream. The exhaust gases then pass through an induced draft fan and up the stack where they are characterized for CO, CO₂, NO, NO₂, SO₂, HC, H₂S and particulates.

The waste explosive or propellant was ground by a rotating knife grinder with water added. The resulting slurry is immediately discharged through an 8 mesh screen in the bottom of the grinder to a slurry tank. Here the proper slurry ratio is maintained, transferred by centrifugal pump from the tank to the incinerator where a metering pump (peristaltic type) delivers the slurry to the combustion chamber. The unmetered slurry is returned to the storage tank at velocities high enough to maintain suspension integrity. Incineration tests have been successfully accomplished on single, double and composite base propellants, HMX, TNT, and RDX-based explosive compositions. Water to explosive ratios and feed rates were varied from 19:1 to 3:1 and from 40 to 440 pounds per hour respectively, with chamber temperatures varied from 1600°-2000°F. A summary of materials tested is shown in Figure 7. Representative emission data for single and double base propellant-water slurries is shown in Figure 8. Propellant/water ratios were 1:3 by weight respectively with a main burner temperature of 1400-1800°F. The results of the rotary kiln pilot plant effort were used to prepare a Design Criteria Package for implementation of a full scale incineration complex to meet the immediate needs of the Army Ammunition Plant at Radford, Virginia.

Hazard evaluation studies were made of the pilot-scale automated incinerator for assessing the initiation, flame transition, and explosive propagation hazard potential for incineration of propellants and the high explosives, TNT, HMX, RDX, and Composition B. The material preparation, grinding and feeding operational phases were assessed. Studies to date support strongly that the potential hazards associated with the incineration of propellant wastes are minimized by use of water as a coolant/diluent. Under normal operating conditions, quantitative hazards analyses of the drum dumpers, conveyor feed hopper, and transfer pumps show safety margins ranging from 1.1 to 4460. The low safety margin of 1.1 was found for impact and friction initiation stimuli applied to nitroglycerin films which are unlikely to be present. Similar analyses of abnormal events such as operator error, entry of hard foreign objects and absence of water coolant show safety margins ranging from none to 61.0. The absence of safety margins in some cases emphasizes the importance of maintaining operator reliability, safety interlocks, the assurance of continuous coolant supply, and good housekeeping in minimizing localized initiation of waste materials.

Normal grinding of propellant and explosive material <0.1 inch to permit slurry suspension for fully dispersed pumping to the incinerator is shown to supply energy levels sufficiently high to induce initiation reactions in the combustibles. These initiations are kept localized by the continuous presence of water as a coolant at a ratio of 10:1 water:waste. In the abnormal situations of coolant supply failures or excessive grinder vibration, e.g., from broken blades, system safety is maintained by an interlock stopping the propellant feed to the grinder by interrupting power to the conveyor and valving-off sluicing water. The grinder was shown to present no critical shaft speed hazards at rotor unbalances up to 10 percent.

Under normal agitation there is no metal-to-metal contact between impeller and suspension tank wall, and hence, no hazard from impact or friction initiation energy. Critical shaft speed analysis shows the design is fully adequate over the operating range to preclude any friction or impact hazard arising from shaft whip. Abnormal conditions arising from loss of the impeller or bending and set of the shaft can release sufficient energy to induce initiation in all combustibles to be incinerated. Again the presence of excess water coolant inhibits growth of the localized initiation into sustained burning. Material bypassing the grinder could permit inadvertent entry of foreign objects capable of damaging pumps and plugging flow lines; this entry should be avoided by screening all materials entering the agitation tank.

The Gulligher Vac-Seal centrifugal pump used to transfer the propellant/water suspension, poses no hazard in transfer of the dispersed combustibles to the incinerator kiln feed pump line under normal conditions, fully suspended in water. The Tri-Clover incinerator feed pump has adequate safety margins under normal conditions. An initiation hazard is introduced in the event this pump is run with dry Sprint propellant present.

Likewise, engineering hazard analyses have shown that the solid explosives and propellants, can be processed safely in the present prototype incinerator. No transition from slow burning to an explosive reaction is predicted for 1:3 solids-to-water dispersions and expected settled material heights for explosive and/or propellant mixtures. Under normal operating conditions, these combustibles are fully suspended as a solids diluent system at a weight ratio of 1:3. This is assured by pumping at high enough rates to secure turbulent flow Reynolds numbers. In the suspended condition, each combustible particle is well surrounded by copious water coolant which prevents any localized initiations from becoming self-sustaining by both heat sink action and thermal insulation effects.

Fluid Bed Incinerator: An advanced incineration technique investigated for future application was the fluidized bed combustor (Figure 9). The ultimate goal for this investigation is to convert the vertical induced draft incinerator to a fluidized bed system to fully demonstrate this technique.

The fluidized bed reactor concept is well-known and has been found to offer economic advantages for many chemical industrial reactions. Gas flows through the distributor plate and can be controlled to any desired rate. At low rates the bed remains in its original "settled" state with the pressure drop across the bed increasing with flow rate until it is equal to the downward force exerted by the solids resting on the plate. The bed begins to expand at this point which is called incipient fluidization, allowing more gas to pass through the bed at the same pressure drop. The bed is now fluidized and has all the properties of a fluid.

Application of this concept to incineration of propellants and explosives offers several advantages over conventional incineration. The violent agitation of the bed particles causes rapid mixing and acts as a large heat reservoir. Their movement throughout the bed keeps it at a constant temperature eliminating the development of hot zones in the bed. When a combustible particle is added to the bed, transfer of energy is rapid and the particle quickly reaches its ignition temperature. The heat of combustion is then rapidly transferred back to the bed. Contact between the burning particle and the oxygen in the gas is excellent reducing the excess air requirements. Combustion can be closely controlled by altering the hazardous waste residence time which is accomplished by increasing or decreasing the fluidizing gas flow. The bed particles can be of any material that will promote chemical or catalytic reactions. For

clarification, the introduction of secondary air embraces a technique called two stage combustion. This concept requires that the total amount of air supplied be broken into two streams and introduced at two separate locations in the reactor. Less than stoichiometric primary air entered the fluid bed at the base of the reactor, and passed up through the distributor grid, while the secondary air entered the bed proper at a point above the distributor grid. This modification for meeting the air requirements of the incinerator had a very significant bearing on the emissions from the incineration process.

To exploit the above fluidized bed characteristics, a small scale unit was designed, constructed and tested* (See Figure 9). The diameter of the fluidized bed was six inches with an overall height of ten feet constructed of a high temperature alloy. Bed material was tabular alumina (Al_2O_3) having a particle size of 500 microns. Combustion air was preheated and propane utilized as fuel. A peristaltic pump was employed to transfer the explosive slurry from a recirculating line to the combustor. A sampling train downstream of the cyclone particulate collector was used to record flue gas analysis for CO, CO_2 , NO, NO_x , HC, and O_2 . A summary of materials incinerated in water slurry form is shown in Figure 10. Average operating conditions were as follows: (1) a fluidized bed temperature of 1600-1800°F, (2) a settled bed height of two feet and a fluidized bed height of five feet, (3) an explosive feed slurry concentration of 10 weight percent, (4) a superficial bed velocity of 3 to 6 feet per second, and (5) theoretical air required to stoichiometrically combust fuel and explosive was varied from 90 to 120 percent.

During the course of the test program, a catalyst was uncovered that drastically reduced NO_x concentrations in the flue gas. It was extensively demonstrated that NO_x emissions could be driven to virtual extinction using the catalyst in the alumina bed while burning in a two-stage mode.

Figure 11 shows the results obtained in the combustion of a 10 weight percent TNT water slurry during 1 stage and 2 stage catalytic and non-catalytic combustion. Of particular interest is the progression that was evident in the exhaust gas analysis as the study progressed through the four combustion modes. The introduction of a catalyst in the single stage mode had a detrimental effect on NO- NO_x emissions, however, when catalyst was used in conjunction with two stage burning, a startling reduction in NO- NO_x , CO and HC concentrations was experienced. Present indications are that the reducing atmosphere created in the fluidized bed by two-stage combustion in conjunction with the catalyst accelerated the reaction of $2NO + 2CO \longrightarrow 2CO_2 + N_2$. NO_x emissions without

*Esso Research & Engineering Company, Linden, New Jersey.

the catalyst range from 1200 to 3500 ppm by volume depending upon the material incinerated in single-stage combustion. Reductions of NO_x emissions of fifty percent could be accomplished by employing the two-stage technique. Using two-stage combustion and the catalyst, representative emission data for explosive slurries were as follows: NO - 47 ppm, NO_x - 57 ppm, CO - 40 ppm, CO_2 - 12%, O_2 - 4% and hydrocarbons - 10 ppm.

In addition to these dramatic results, it was also shown that a soluble form of the catalyst could be transmitted to the combustor via the slurry tank and could be used to remotely activate the bed resulting in immediate NO_x reduction. This could prove invaluable as a means of overcoming any catalyst inhibition without interruption of operations.

To explore these important developments, the vertical induced draft incinerator at Picatinny Arsenal is being converted to a full-scale (8 feet diameter) fluidized bed unit. Figure 12 shows this conversion schematically, in which maximum use will be made of the existing system hardware. Major additions will encompass the compressor, air preheater, plenum chamber and cyclone separator. Revisions to exhaust piping, slurry injection and heat input from the oil burner will be made to effect the change-over to fluid bed operation.

To insure a safe system an engineering development hazards analysis is currently underway. Data available from the rotary kiln incinerator system processes will be used where applicable. In addition, detonation propagation tests of aqueous slurries of explosives and propellants are in progress. This effort was initiated to determine the maximum slurry concentrations, both in suspended and settled conditions, that would not support the propagation of a detonation wave, should one be initiated. Initial tests results (Figure 13) indicate that slurries of TNT, Composition B, and M-9 propellant, at concentrations of 30% (by weight of solids) and below will not support a detonation propagation. This effort has been expanded to include other explosives and propellants.

CONCLUSIONS

The explosive and propellant incineration program has shown that it was possible to safely and cleanly destroy waste explosive material under controlled thermal conditions. The rotary kiln incinerator with scrubbing of exhaust gases can be used to meet immediate needs but has attendant problems of scrubber water treatment. The fluid bed incinerator appears to be a superior system because:

(a) NO_x emission levels significantly below 200 ppm can be achieved without scrubbing.

(b) There are fewer moving parts, and no requirement for a pre-cooler or separate afterburner.

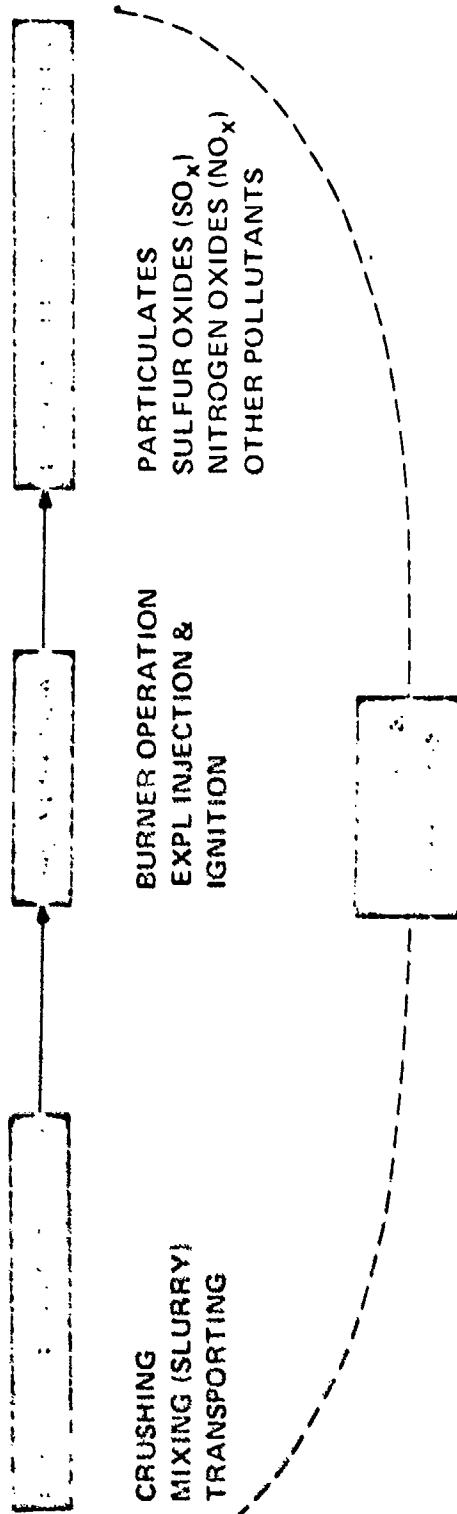
(c) Bed may be readily activated by inclusions of solid catalyst with the solid bed material or by addition of the catalyst in a soluble form in the slurry feed system.

In addition, ancillary procedures of particle size reduction, slurry preparation and transfer and injection have been positively demonstrated with no serious incidents. It is apparent that a safe solution to the problem of open burning waste hazardous materials is attainable.

REFERENCES

1. Santos, Heidelberger, Antman and Bhute, Design Guide for Explosive Waste Incineration, Manufacturing Technology Directorate, Picatinny Arsenal, Dover, New Jersey, Technical Report 4577, October 1973.
2. Kalfadelis, C. D., Development of a Fluidized Bed Incinerator for Explosives and Propellants, Esso Research and Engineering Company, Government Research Laboratory, Linden, New Jersey, October 1973.
3. Petino, Westover, Detonation Propagation Tests on Aqueous Slurries of TNT, Composition B, M-9 and M-10, F & PTD, MTD, Picatinny Arsenal, Dover, New Jersey, Technical Report 4584, November 1973.
4. Carter, Hazards Evaluation of the Prototype Automated Waste Propellant Incineration System Report 3, Hercules Incorporated, Radford Army Ammunition Plant, Radford, Virginia, June 1973.
5. Carter, Hazards Evaluation Summary of the Prototype Automated Waste Propellant Incineration System, Hercules Incorporated, Radford Army Ammunition Plant, Radford, Virginia, March 1973.

FIG-1: EXPLOSIVE WASTE INCINERATION AS A SYSTEM



Reproduced from
best available copy.

PICATINNY ARSENAL INDUCED DRAFT INCINERATOR

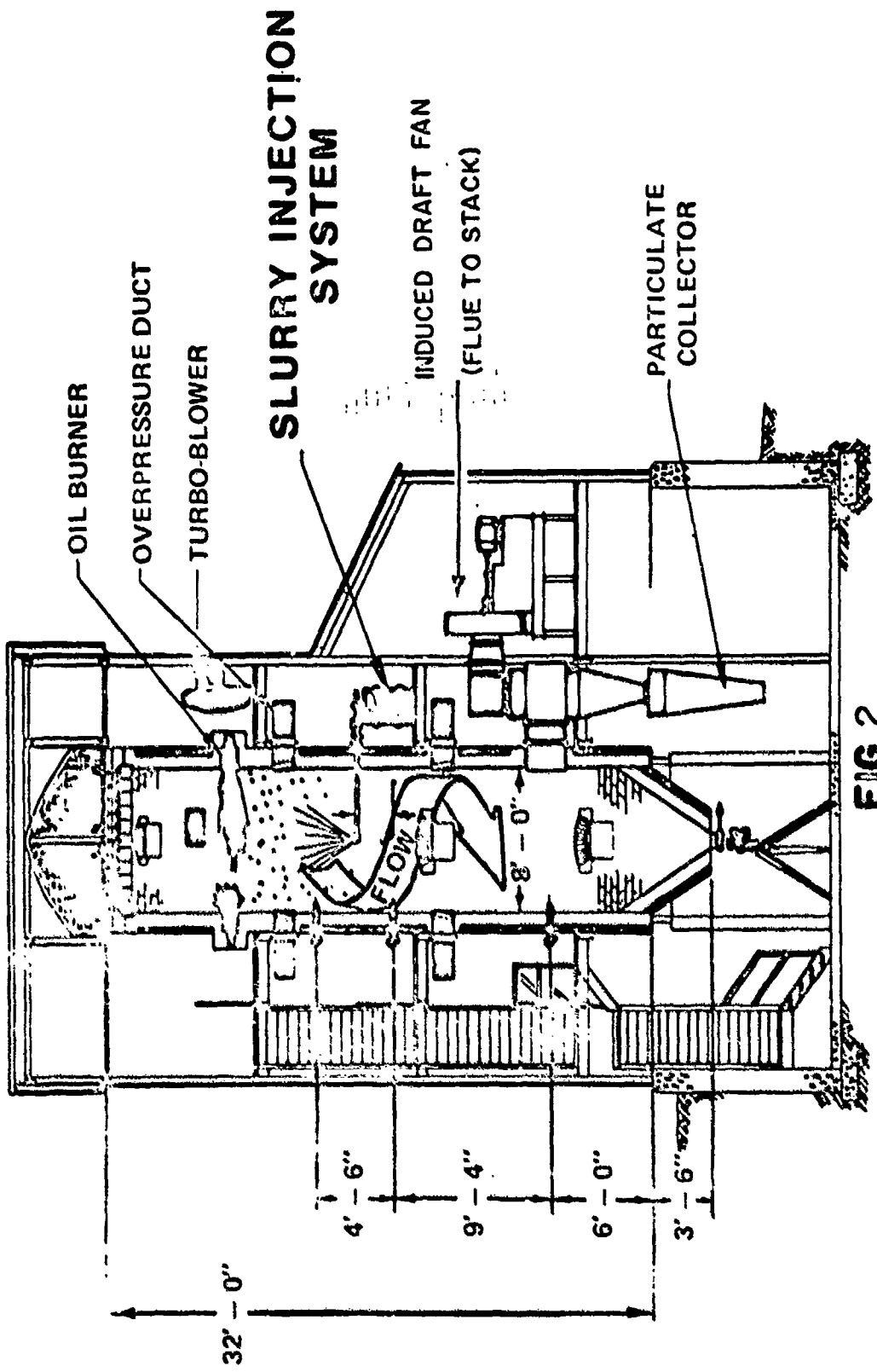


FIG 2

EXPLOSIVE SLURRY PUMP FEED SYSTEM

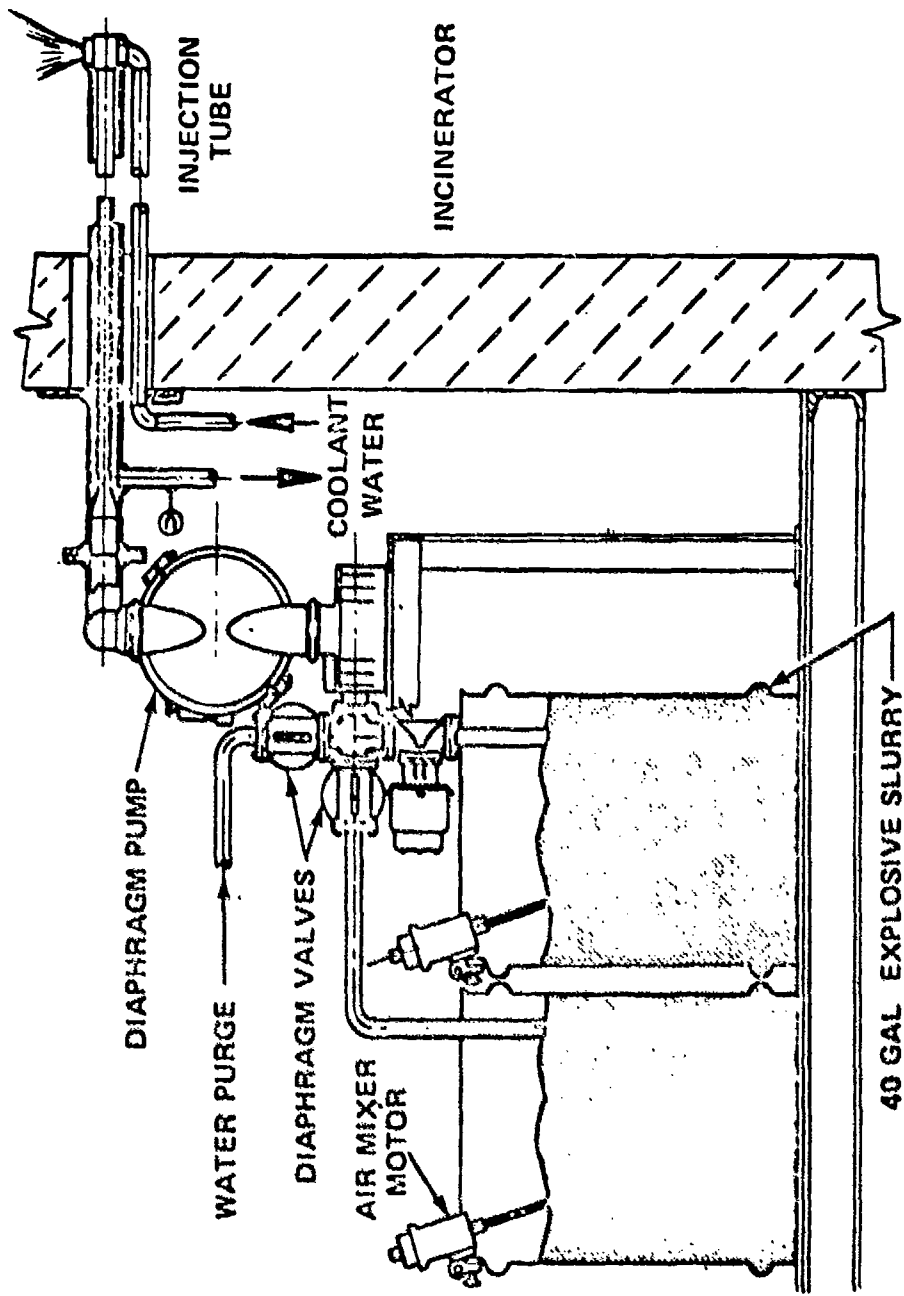


FIG-4: SUMMARY OF INCINERATION TESTS
VERTICAL INDUCED DRAFT INCINERATOR

NOMINAL OPERATING PARAMETERS

BURNING RATE: 250 LB/HR
 DURATION: 21 MIN
 TEMPERATURE: 1600°F — 1800°F
 SLURRY RATIO: 19:1 — 7:1

<u>MATERIAL</u>	<u>NO. TESTS</u>	<u>DURATION</u>
TNT	20	2.5 HR
COMP B	19	2.6 HR
HMX	6	3.5 MIN
RDX	4	2.0 MIN

FIG-5: FLUE GAS ANALYSIS
VERTICAL INDUCED DRAFT INCINERATOR

<u>MATERIAL</u>	<u>PARTICULATE</u> <u>12%CO₂ GR/SCF</u>	<u>%CO₂</u>	<u>%O₂</u>	<u>%CO</u>	<u>NO_x (PPM)</u>
BLANK	.0052	2.6	18.0	.001	33.8
TNT	.081	4.0	16.0	.0075	1110
COMP B	.10	3.4	16.6	.005	1030

FIG-6: ROTARY KILN

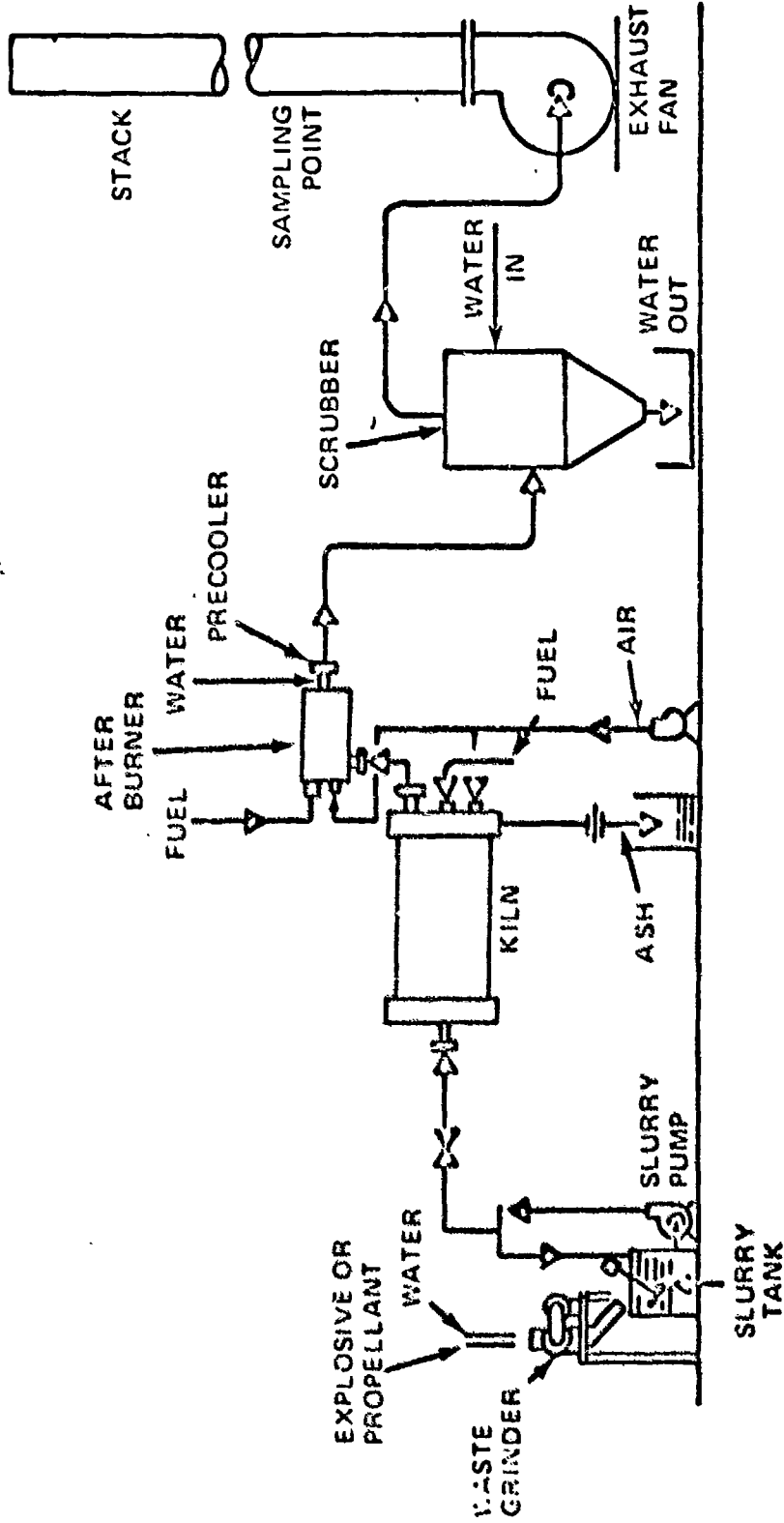


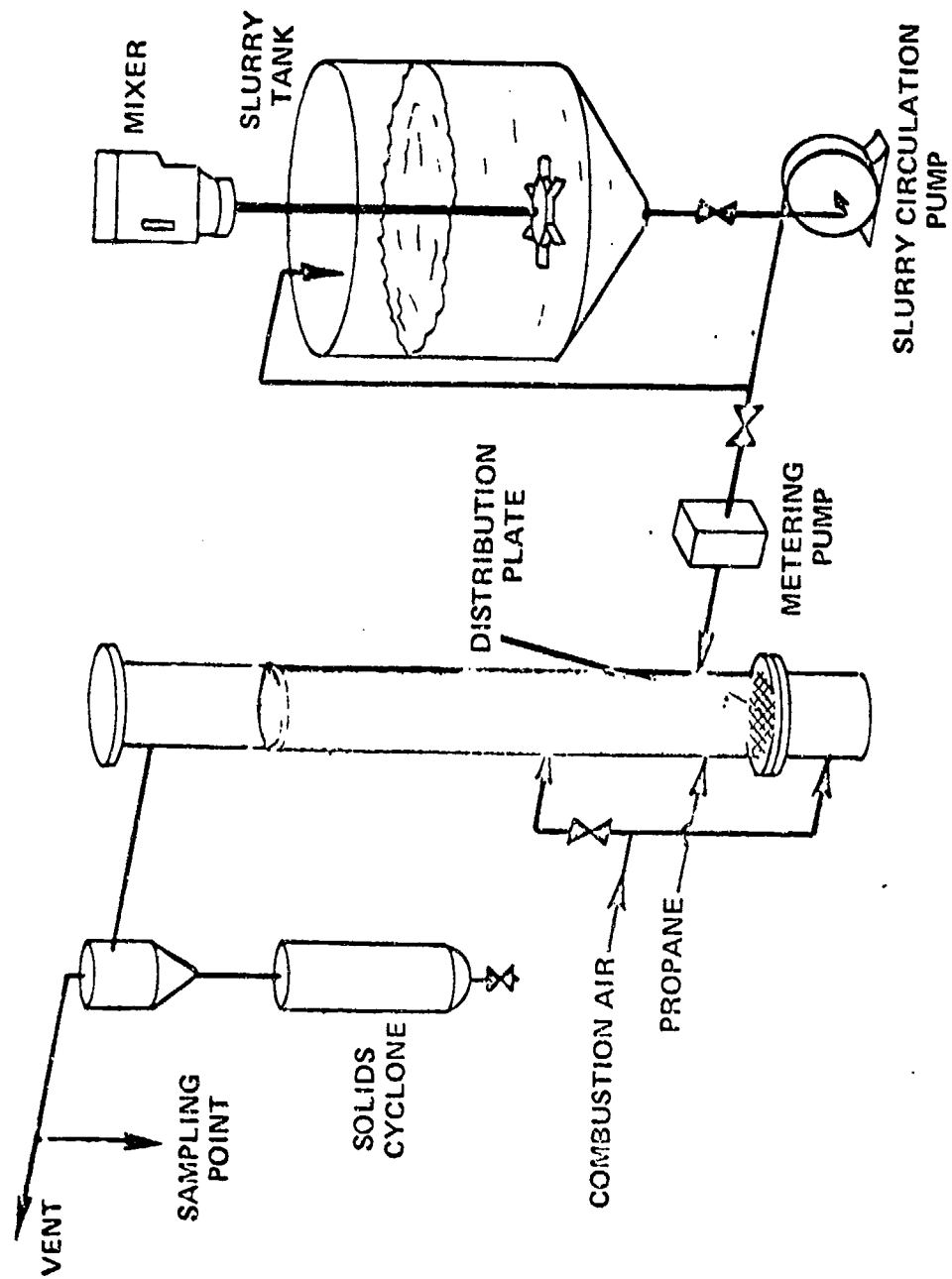
FIG-7: SUMMARY OF INCINERATION TESTS*

TYPE	LIQUID TO SOLID RATIO	FEED RATE (gpm)	NO. OF RUNS	TOTAL TIME (HRS)	TOTAL BURNED (LBS)
IMR	19:1 TO 3:1	1.78 - 2.0	>15	52.4	15600
IMR/EDB	19:1 TO 3:1	1.78 - 2.0	>50	180	45000
EDB	19:1 TO 5.6:1	1.78 - 2.0	>100	120	30000
M1 + INERT	5.8:1	1.78 - 2.0	1	0.88	220
M8	7.5:1	1.78 - 2.0	>4	0.80	200
MS/EDB	7:1 TO 5:1	1.78 - 2.0	3	3.4	855
TNT	12:1 TO 10:1	1.78 - 2.0	10	8.0	2000
2056D	4:1	1.78 - 2.0	3	1.0	250
HMX	10:1 TO 3:1	1.78 - 2.0	15	24.0	6000
COMP A5	3:1	1.78 - 2.0	13	18	4500
COMP B	3:1	1.78 - 2.0	13	18	4500
COMP C-3	3:1	1.78 - 2.0	13	16	4500
BS - NACO	3:1	1.78 - 2.0	1	1.2	300
HOOIE/TOW GR.	3:1	1.78 - 2.0	2	0.4	75/25
M7 LAW STICK	3:1	1.78 - 2.0	1	1.2	300

* AS OF 25 SEPT 1973

FIG-8: INCINERATION TEST RESULTS

TYPE	TEMP	GASES ANALYZED IN PPM							CO ₂ (%)
		HC	H ₂ S	NO	NO ₂	SO ₂			
EDB-IMR	1400	26	32	265	0	6			1.2
	1600		35	208	11	2			1.5
	1600	43	0	198	0	268			2.8
	1800	21	65	205	0	15			2.0
	1400	0	13	146	24	71			2.1
	1600	5	20	190	9	3			2.5
	1800	8	32	101	10	123			2.8
	1500		8	91	0	7			2.1
	1600	0	5	110	4	8			2.6
	EDM-IMR	1600	0	2	180	31	13		



LAB SCALE FLUIDIZED BED COMBUSTOR

FIG-9

FIG-10: SUMMARY OF FLUID BED TEST PROGRAM

MATERIAL	NO OF TESTS	TOTAL DURATION (HRS)
TNT	16	60
COMP B	2	12
RDX	6	20
HMX	7	24
NH_4NO_3	1	6
HNO_3	1	6
CBI (CO%NC)	4	22

Reproduced from
best available copy.



FIG-11: FLUIDIZED BED

CUMBUSTION EMISSION DATA (LB/HR)

PARAMETERS:

- TEMPERATURE: 1600 - 1850°F
- FEED RATE: 7 lb/HR 10% TNT/WATER SLURRY
- VELOCITY: 4.8 - 5.5 FT/SEC
- THEORETICAL AIR: 1 STAGE 2 STAGE
 - PRIMARY 120% 63%
 - SECONDARY 57%

	CATALYTIC		NON CATALYTIC	
	1 STAGE	2 STAGE	1 STAGE	2 STAGE
NO (ppm)	2500	47	1650	800
NO _x (ppm)	2900	57	1750	840
CO (ppm)	250	40	640	650
HC (ppm)	100	10	290	350
CO ₂ %	12.1	12	12	12
O ₂ %	3.8	3.7	5.5	4.0

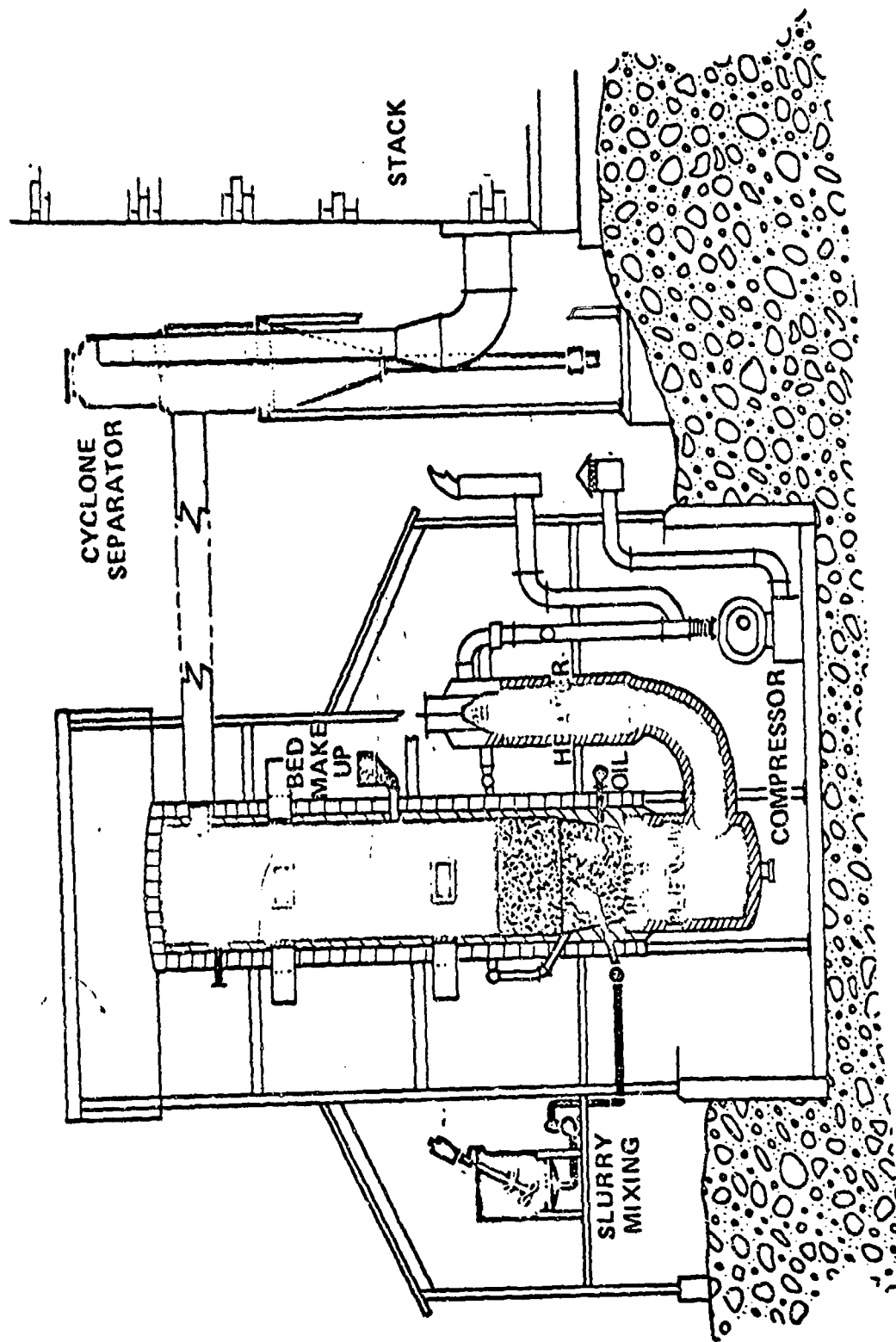


FIG-12: FLUIDIZED BED CONVERSION
PA INCINERATOR

FIG-13: Summary of Detonation Propagation Test Results

Sample Material	Slurry Type	Slurry Concentration (Wt. %) for Propagation		
		No Propagation	Complete Propagation	Partial Propagation
TNT	Gelled	30-40	60(1)	45-55
TNT	Settled	40	55-60(1)	45-50
Comp. "B"	Gelled	30	40(1)	35
Comp. "B"	Settled	30-35	45-50(1)	40
M-9	Gelled	20-40	50(1)	45
M-9	Settled	35-40	50(1)	45
M-10	Gelled	50	70(2)	55-65
M-10	Settled	10-12.5	15-35(1)	45-60
M-10	Settled	-	65(2)	-

(1) High Order Detonation

(2) Low Order Detonation

A PREDESIGN ANALYSIS TECHNIQUE FOR REINFORCED CONCRETE STRUCTURES

Mr. J. O. Davis
Sandia Corporation
Albuquerque, NM

At Sandia Laboratories we endeavor to maintain a high level of safety awareness. In recent years an acute awareness of the need for pressure safety has resulted in the requirement for a pressure safety lab that includes a test cell which permits destructive testing of pressure vessels.

During the design of the pressure cell, it was decided to utilize the HE equivalent of 1.8 pounds of HE. (I am not a firm believer in HE equivalents for pressure vessels, but that is another story.) Energy-wise, this 1.8 pounds of HE represents approximately 1 cu ft of N_2 gas at 20,000 psi.

Since Sandia Laboratories has had negligible experience in the design of blast-resistant cubicles, there was little or no background to either draw upon or to influence our thinking. In effect, we started with a blank piece of paper and had to evolve an analytical solution to the problem.

The technique developed is nothing new analytically but is unique in that it provides computer routines for the "pick and shovel" work of evaluating a generalized design before detailed design is accomplished. Inasmuch as my task was not to design in detail but to provide design criteria to our plant engineering personnel, the technique met this requirement. It permitted the establishment of accurate load criteria without excessive expenditure of analysis time. In establishing accurate load criteria, it is necessary to know the natural period of the structure so that the structural response can be considered.

Before the computerized technique was established, preparation of calculations for one configuration required about 2 days and, owing to constant interruptions, there was considerable doubt as to accuracy. Because the first iteration is generally one of many — unless the designer has ESP or is very lucky — the task is pure drudgery.

After the first iteration, I decided that there had to be a better way.

Since Sandia is blessed with a PDP-10 computer system, a determination was made to go to the computer. A program was written to accomplish the required iterations, thus automating the process. With the routine developed, the requisite answers were available in minutes instead of hours or days.

It should be pointed out that although this routine was set up to handle only the cubicle problem, other types of problems can be computerized following this Sandia format.

Here is a brief resume of the program. It has worked for us and can be made to work for other structures. Since I am not a computer buff and do not program frequently enough to feel confident with Fortran, I wrote the entire program in Basic. Originally, it was felt that after its debugging on the PDP 10, the program would be suitable for any small minicomputer. This proved to be a fallacy. The program will not run properly on less than a 32-bit-word-length computer. When we discuss the equations used, the reason for this restriction will become evident.

In brief, our program works as follows:

1. We input pulse data from TM 5-1300, material parameters, structure dimensions, and wall thicknesses of interest.
2. After some finger counting and contemplation, the computer prints out the pertinent information required for the detail designer. After a maximum of three acceptable configurations are printed, the program is terminated.

Figure 1 is a greatly simplified flow diagram for the computational procedure. Omitted from the program are numerous iteration loops and decision-making steps.

Initially, the program consists of various inputs which require a simple numeric response in predetermined units. Although all units are in the English system at this time, a few constants could be changed to allow metric inputs. The program contains three large iterative loops as follows:

1. Rebar size: 2 to 11 (presently set for 4 to 11)
2. Rebar spacing: 12 to 4 with a step size of -2
3. Wall thickness with range set by the user.

With the appropriate data from the position within the loop parameters, the moment of inertia of the transformed section is calculated. The program calculates two I's, one for the inner and one for the outer layer of steel. The calculated result is for a 1-inch width through the center of the slab.

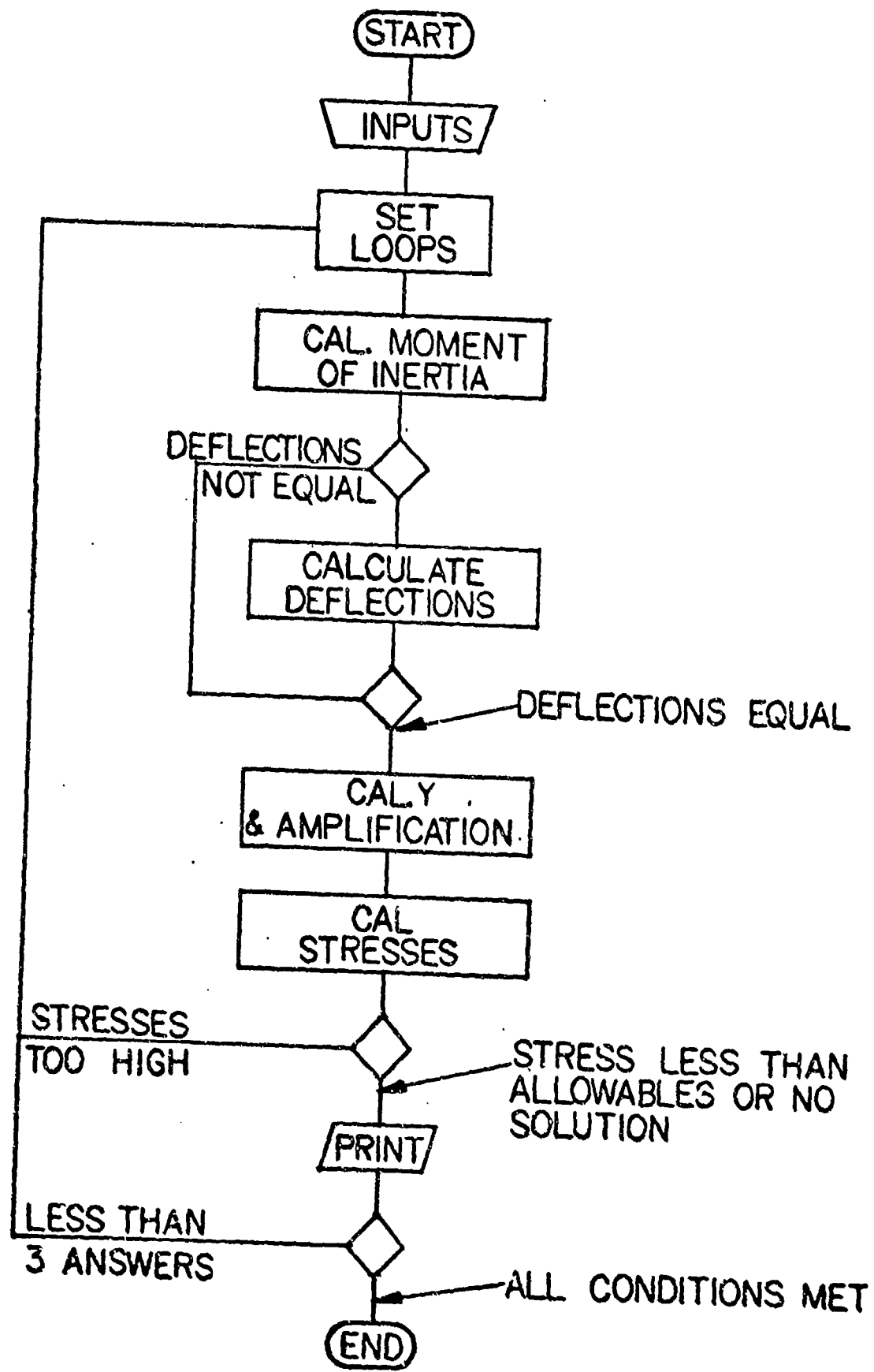


FIG. 1

With these moment of inertia values, the static deflection, δ_{st} , of the structure is calculated by assuming the loading mode encountered during an event. These values are subsequently used to solve for the natural period of the structure. This period is normalized with the pulse duration and compared to a structural response curve incorporated into the program to establish an amplification figure (see Figure 2).

After this amplified loading is calculated, the stress levels are calculated. If stresses are less than calculated allowables, printing occurs. If stresses are greater, the program steps up to the next stronger increment and repeats the procedure. If during the running of the program no acceptable answers are generated, the program prints a diagnostic instruction to reenter with a thicker wall section. It should be noted that no additional entries of material parameters or sizes are required.

Figures 3 and 4 are printouts of typical runs from the program. Figure 3 is a normal run which finds a solution. Figure 4 is a run which does not find a solution but shows the diagnostic printing.

Figure 5 shows the overall structure, with elemental strips cutting through the various slabs. Such use of the individual strips, along with appropriate correction factors for strip interaction, has proved to be a very useful technique in structural analysis.

INITIAL SAWTOOTH

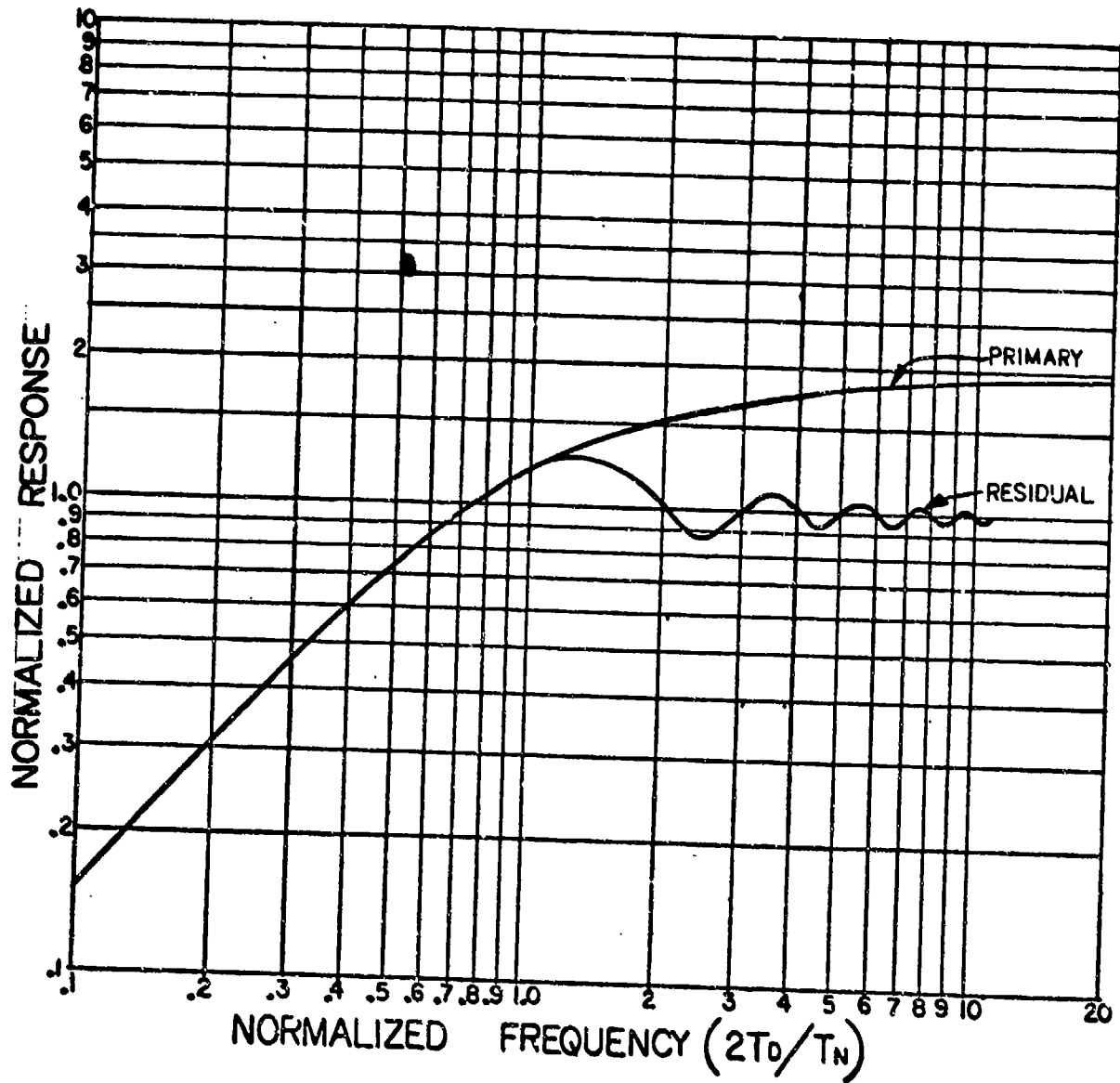


FIGURE 2

READY
RUN

ENGBX

09:12

28-AUG-74

INPUT INSIDE LONGEST DIM. IN INCHES 2144
INPUT INSIDE 2ND LONGEST DIM. IN INCHES 296
INPUT INSIDE SHORTEST DIM. IN INCHES 296
INPUT PULSE PRESSURE IN P.S.I. 240
INPUT PULSE DURATION IN MILLI-SECONDS 76
INPUT OVER-PRESSURE IN P.S.I. 220
INPUT CONCRETE COVERAGE IN INCHES 22
INPUT CONCRETE ULT. IN P.S.I. 23000
INPUT STEEL ULT. IN P.S.I. 290000
INPUT MIN. WALL THICKS. IN INCHES 210
INPUT MAX. WALL THICKS. IN INCHES 212
INPUT WALL INC. IN INCHES 22

*****PROGRAM OUTPUT*****

MAX. AMPLIFIED PRESSURE = 37.086
NATURAL PERIOD= 17.9869
RE-BAR SIZE = 5
DEPTH = 10
STEEL SPACING = 4
EDGE STEEL STRESS CONTROLS
LONG SPAN STEEL STRESS = 17881.6
MARGIN = 1.10618
SHORT SPAN STEEL STRESS = 14277.2
MARGIN = 1.38544
LONG SPAN CONCRETE STRESS = 578.781
MARGIN = 1.29583
SHORT SPAN CONCRETE STRESS = 726.123
MARGIN = 1.03288
LONG SPAN MOMENT OF INERTIA = 26.0276
CENTROID DISTANCE = 5.05371
SHORT SPAN MOMENT OF INERTIA = 21.3881
CENTROID DISTANCE = 2.71379

FIGURE 3A

MAX. AMPLIFIED PRESSURE = 38.7441
NATURAL PERIOD= 16.9119
RE-BAR SIZE = 6
DEPTH = 10
STEEL SPACING = 4
EDGE STEEL STRESS CONTROLS
LONG SPAN STEEL STRESS = 13547.4
MARGIN = 1.46008
SHORT SPAN STEEL STRESS = 11506.
MARGIN = 1.71912
LONG SPAN CONCRETE STRESS = 543.74
MARGIN = 1.37934
SHORT SPAN CONCRETE STRESS = 734.434
MARGIN = 1.02119
LONG SPAN MOMENT OF INERTIA = 33.2332
CENTROID DISTANCE = 4.73286
SHORT SPAN MOMENT OF INERTIA = 25.5481
CENTROID DISTANCE = 3.00164

MAX. AMPLIFIED PRESSURE = 39.1377
NATURAL PERIOD= 16.6553
RE-BAR SIZE = 5
DEPTH = 12
STEEL SPACING = 4
EDGE STEEL STRESS CONTROLS
LONG SPAN STEEL STRESS = 16707.7
MARGIN = 1.1839
SHORT SPAN STEEL STRESS = 13814.
MARGIN = 1.4319
LONG SPAN CONCRETE STRESS = 454.77
MARGIN = 1.64919
SHORT SPAN CONCRETE STRESS = 551.495
MARGIN = 1.35994
LONG SPAN MOMENT OF INERTIA = 44.3046
CENTROID DISTANCE = 6.74121
SHORT SPAN MOMENT OF INERTIA = 37.4873
CENTROID DISTANCE = 3.02147

*** NORMAL TERMINATION ***

TIME: 40.23 SECS.

FIGURE 3B

READY
RUN

ENGR:

09:19

28-AUG-74

INPUT INSIDE LONGEST DIM. IN INCHES 2144
INPUT INSIDE 2ND LONGEST DIM. IN INCHES 296
INPUT INSIDE SHORTEST DIM. IN INCHES 296
INPUT PULSE PRESSURE IN P.S.I. 2200
INPUT PULSE DURATION IN MILLI-SECONDS 26
INPUT OVER-PRESSURE IN P.S.I. 2100
INPUT CONCRETE COVERAGE IN INCHES 22
INPUT CONCRETE ULT. IN P.S.I. 23000
INPUT STEEL ULT. IN P.S.I. 290000
INPUT MIN. WALL THICK. IN INCHES 210
INPUT MAX. WALL THICK. IN INCHES 212
INPUT WALL INC. IN INCHES 22

*****PROGRAM OUTPUT*****

***** NOTE *****

SOME STRESSES ARE HIGHER THAN ALLOWABLES
USE THE INFORMATION OUTPUTTED BELOW AS
GUIDANCE BEFORE PICKING A NEW WALL
THICKNESS AS DIRECTED BY THE PROGRAM

MAX. AMPLIFIED PRESSURE = 181.32
NATURAL PERIOD= 18.5506
RE-BAR SIZE = 11
DEPTH = 12
STEEL SPACING = 4
EDGE STEEL STRESS CONTROLS
LONG SPAN STEEL STRESS = 13996.2
MARGIN = 1.41326
SHORT SPAN STEEL STRESS = 13669.
MARGIN = 1.44708
LONG SPAN CONCRETE STRESS = 789.104
MARGIN = 0.950445
SHORT SPAN CONCRETE STRESS = 1569.73
MARGIN = 0.47779
LONG SPAN MOMENT OF INERTIA = 141.606
CENTROID DISTANCE = 5.0583
SHORT SPAN MOMENT OF INERTIA = 76.0936
CENTROID DISTANCE = 4.52422

NO VALID SOLUTION
RE-RUN PROGRAM WITH LARGER WALL THICKNESS.
INPUT MIN. WALL THICK. IN INCHES 2

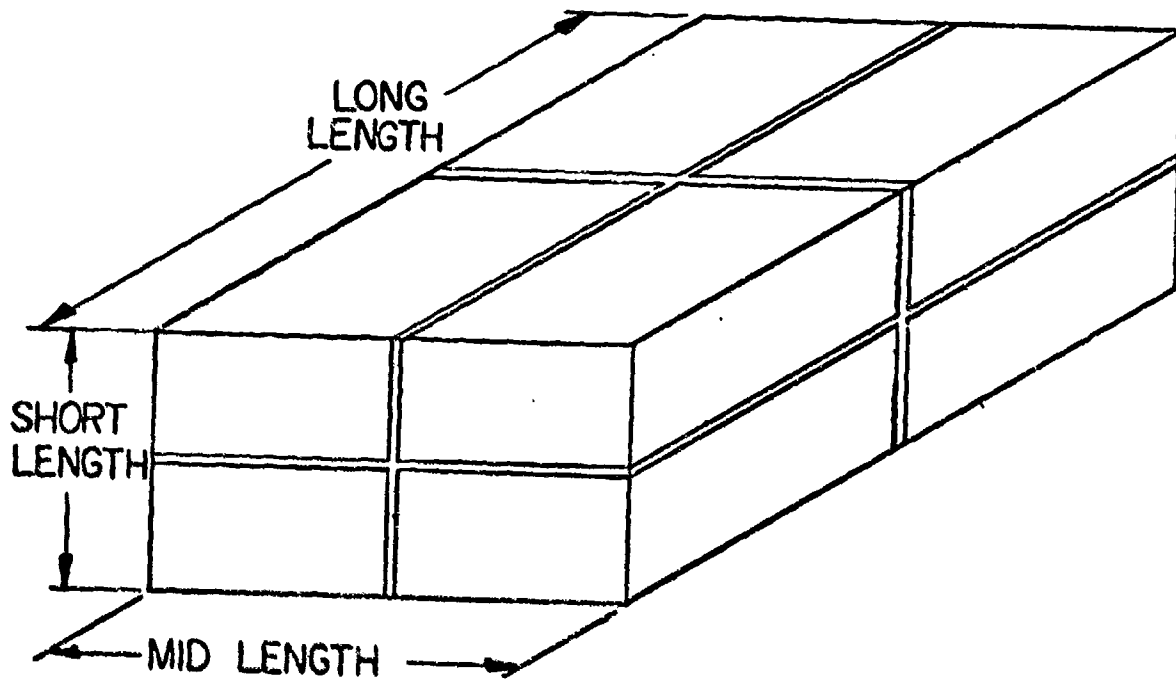


FIGURE 5

We isolate the strips (Figure 6) and assume a uniform loading as shown. Since the strips carry different portions of the load, it is necessary to solve for this distribution. This procedure is accomplished by iteration.

We assume a load for two slabs (normal slab distribution) and then use the equations shown to calculate the third distribution by setting the deflection of the two strips equal in the third. As a matter of interest, we also include the sidewall tension as an additional deflection. We take this calculated value and work on a second slab, then take this second calculated value and work on the third. By incorporating these three loops into another loop, we zero in on the actual distribution. With the final distribution we calculate the deflection on the two smaller slabs, find the minimum, and use it to calculate the period in the structure.

After determining the amplified load, we then calculate moment, again utilizing the strip technique and the largest slab. Moments are taken for both long and short spans and sorted out for the highest stress level. The printout identifies the strip with the highest steel stress and the stress location.

Since the strips are supported by the remainder of the slab, a correction factor must be applied. In our calculation, we did not incorporate a full range of correction figures to reflect a range of length ratios. This could be done as an added refinement, however, in a manner similar to the inclusion of the structural response curve.

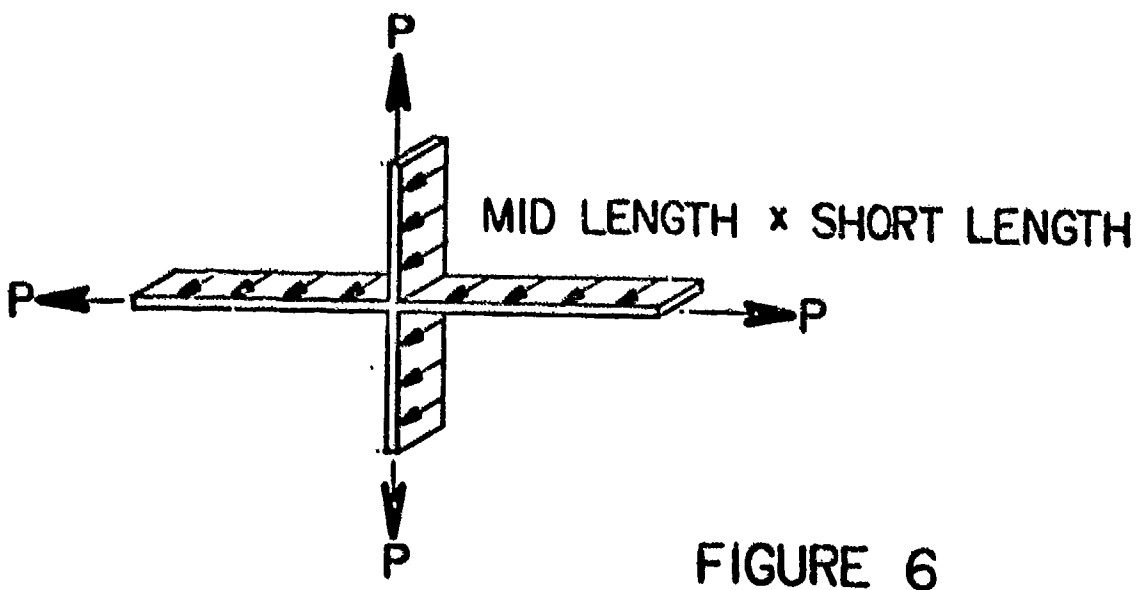
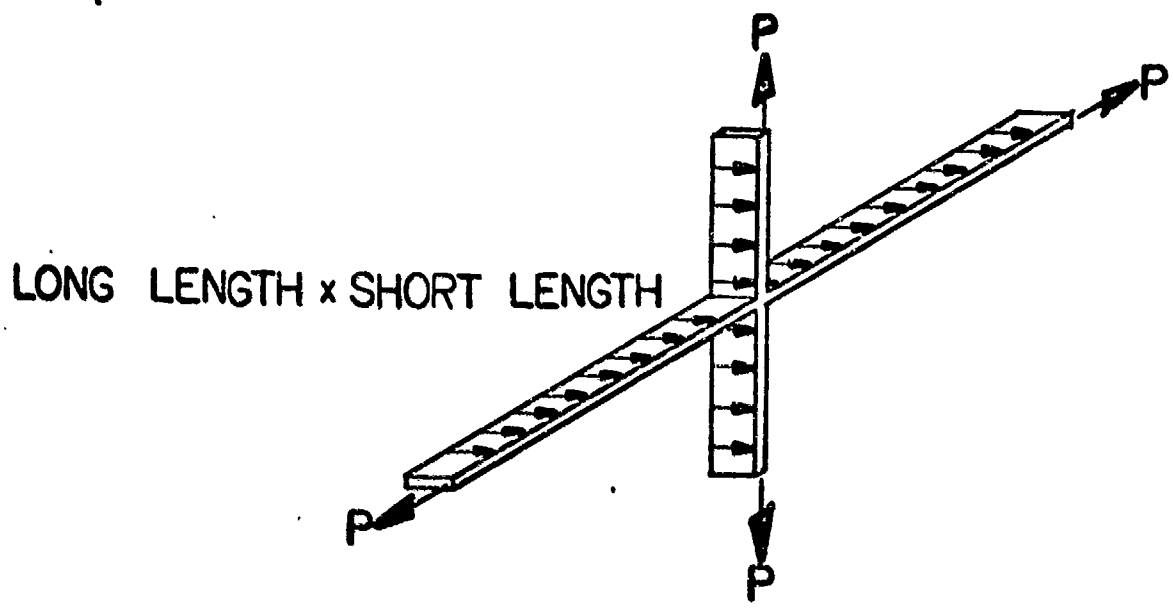
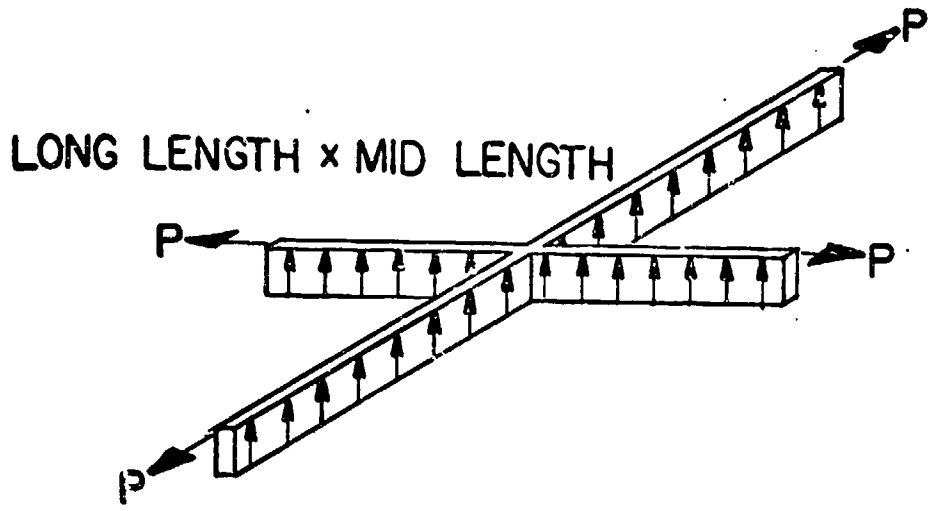


FIGURE 6

In setting up the strips, the following assumptions are made:

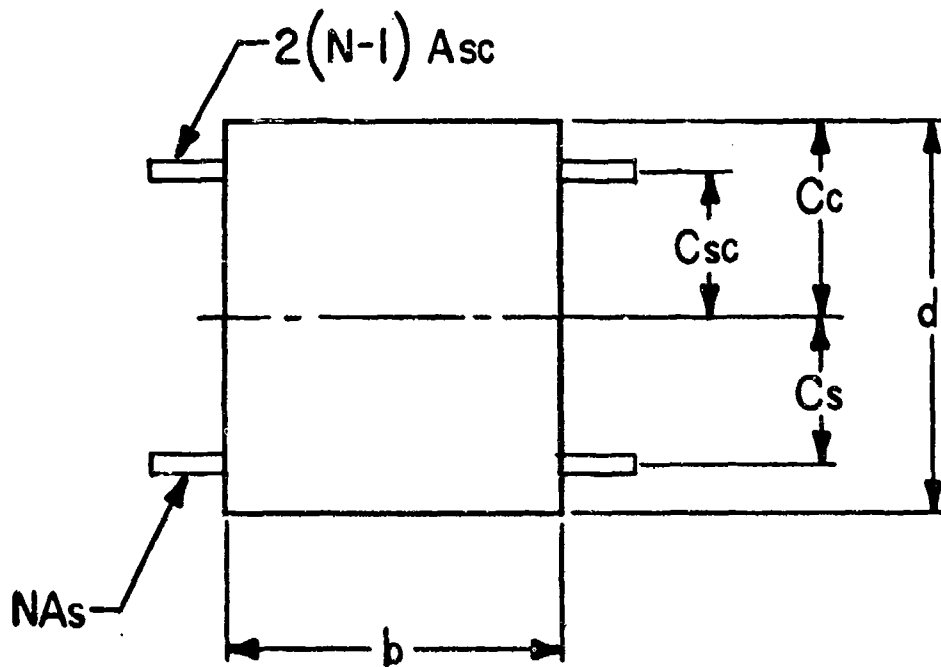
1. The compression steel and the tension steel are identically placed. This is not only a simplifying assumption but also a realistic one, since rebound will reverse all moments.
2. Only one layer of each kind of steel exists. This is a simplifying assumption.

Either of the foregoing assumptions could be negated with more involved programming. In our case, the gain did not seem to be worth the added effort.

Figures 7 and 8 show the equations used during the calculation.

Figure 7 is an illustration of the transformed concrete section and appropriate equation set employed.

In Figure 8 the first of the equations is the culprit on machine size restrictions. As you can see, we subtract a hyperbolic term from 1. Since in our case the hyperbolic is of the order of $1.000XX$, we have a very small number. If the computer has a short word length, no significant digits remain. With our iterative routine, pure

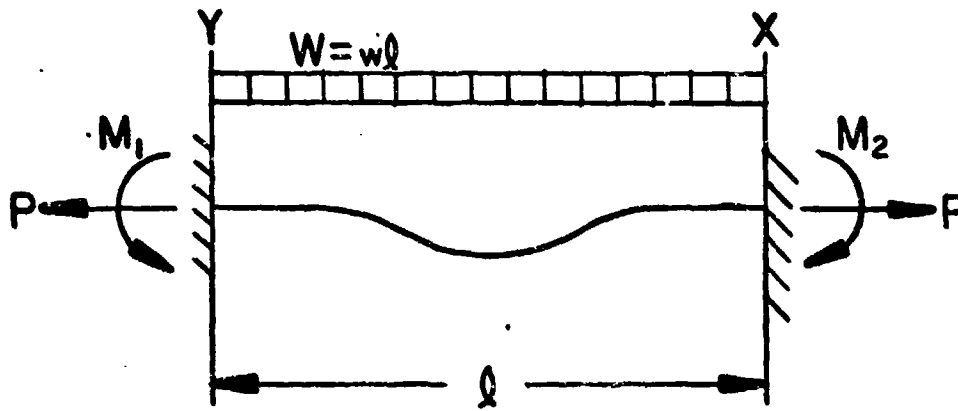


SOLVE FOR C_c :

$$\frac{1}{2} b C_c^2 + 2(N-1) A_{sc} C_{sc} = N A_s C_s$$

$$I = \frac{1}{3} b C_c^3 + 2(N-1) A_{sc} C_{sc}^2 + N A_s C_s^2$$

FIG. 7



$$\Delta y = \frac{-wj^2}{8P} \left[\frac{4u(1 - \text{Cosh } \frac{1}{2}u)}{\text{Sinh } \frac{1}{2}u} + u^2 \right]$$

WHERE : $j = \sqrt{\frac{EI}{P}}$; $u = \frac{\ell}{j}$

FOR THE SIDE WALL TENSION :

$$\epsilon = \frac{Pl}{AE}$$

FIG. 8

nonsense is generated after a few cycles. In some instances we produce a machine error by taking the square root of a negative number. In other instances, answers will result but they are wrong; hence, the computer size restriction. These equations are used to calculate deflection of the beam strips and may be used two ways: (1) Initially to determine the load distribution for the strip and (2) subsequently to determine the static deflection.

The complexity of the equation makes an algebraic solution of the system difficult to solve and hence the load distribution difficult to obtain. In our case, this was done by iteration until a near match was calculated.

In Figure 9:

- (a) This equation solves for the natural period of the structure.
- (b) This equation solves for the moments in the strip at the edge and midpoint of the strip.
- (c) These equations solve for the stresses in the strips at the above locations.

This computerized technique is not only a modern but also an economical approach to our problem and can easily be modified to meet other problems. Any resultant program will prove to be very cost effective in the preparation of design criteria or preliminary cost estimates.

$$\gamma = 2\pi\sqrt{\frac{\delta_{st}}{g}} \quad \delta_{st} = \text{STATIC DEFLECTION}$$

$$M_1 = M_2 = wj^2 \left(\frac{1/2U - \text{TAN} h^{1/2U}}{\text{TAN} h^{1/2U}} \right)$$

$$\text{MAX} + M = wj^2 \left(1 - \frac{1/2U}{\text{SIN}^{1/2U}} \right) \text{ AT } X = 1/2\ell$$

$$\text{CONCRETE STRESS} = MC_c / I$$

$$\text{STEEL STRESS} = NMC_s / I$$

FIG. 9

To give you an idea of the time involved: Our original program was operational in approximately 1 week. This can be contrasted against an initial 2 days for the first iteration alone. As you can see, the first utilization of the program more than justified the time involved.

It should be noted that many short cuts may be taken in the analysis. Inasmuch as a preliminary rather than the final design is being considered, simplifying assumptions are in order but they should be kept on the conservative side.

For those of you who may be interested in our specific program, it is included as an appendix. In the event that this program will not suffice for your explicit problem, it can serve as a skeleton upon which to build your program.

APPENDIX A

10 REM * * * * *
11 REM * ISSUED BY SANDIA LABORATORIES,
12 REM * A PRIME CONTRACTOR TO THE
13 REM * UNITED STATES ATOMIC ENERGY COMMISSION
14 REM * * * * * NOTICE * * * * *
15 REM * THIS REPORT WAS PREPARED AS AN ACCOUNT OF WORK SPONSORED
16 REM * BY THE UNITED STATES GOVERNMENT. NEITHER THE UNITED
17 REM * STATES NOR THE UNITED STATES ATOMIC ENERGY COMMISSION,
18 REM * NOR ANY OF THEIR EMPLOYEES, NOR ANY OF THEIR CONTRACTORS,
19 REM * OR THEIR EMPLOYEES, MAKES ANY WARRANTY, EXPRESS OR
20 REM * IMPLIED, OR ASSUMES ANY LEGAL LIABILITY OR RESPONSIBILITY
21 REM * FOR THE ACCURACY, COMPLETENESS OR USEFULNESS OF ANY
22 REM * INFORMATION, APPARATUS, PRODUCT OR PROCESS DISCLOSED,
23 REM * OR REPRESENTS THAT ITS USE WOULD NOT INFRINGE PRIVATELY
24 REM * OWNED RIGHTS.
25 REM * * * * *
26 REM * THE BASIC REFERENCE DOCUMENT FOR THIS CODE IS:
27 REM * SAND-74-5460 9/3/74
28 REM * * * * *
29 REM * UNLIMITED RELEASE
30 REM * * * * *
31 REM
32 REM DATE OF DOCUMENTATION: 26 AUGUST, 1974
33 REM
34 REM NAME OF PROGRAM: BNGBX
35 REM
36 REM AUTHOR OF PROGRAM: J. O. DAVIS - DIU. 9334
37 REM
38 REM PROGRAM ADMINISTRATOR: W. L. JACKLIN - DIU. 9334
39 REM
40 REM COMPLETION DATE: 23 AUGUST, 1974
41 REM
42 REM RECORD OF CHANGES TO PROGRAM:
43 REM

44 REM BRIEF DESCRIPTOIN: THIS PPROGRAM IS A SEARCH ROUTINE TO
 45 REM PROVIDE PRELIMINARY DESIGN DATA FOR A RE-INFORCED
 46 REM CONCRETE BLAST-RESISTANT STRUCTURE.
 47 REM
 48 REM DETAILED DESCRIPTION: WITH APPROPRIATE BLAST DATA FROM
 49 REM TM 5-1300, BUILDING INSIDE DIMENSIONS, AND
 50 REM MATERIAL PARAMETEPS, THIS PROGRAM WILL PROVIDE
 51 REM THE NECESSARY WALL THICKNESSES AND RE-BAR
 52 REM DISTRIBUTION TO INITIAL SIZE A CONFINEMENT
 53 REM CUBICLE FOR SMALL H.E. BLASTS. THE PROGRAM IS
 54 REM INTENDED TO BE A PRELIMINARY SEARCH ROUTINE TO
 55 REM ASSIST AN ARCHITECT-ENGINEER BY DETERMINING THE
 56 REM STARTING POINT FOR A DETAIL DESIGN.
 57 REM
 58 REM HARDWARE CONFIGURATION REQUIRED: THE PROGRAM WAS DESIGNED
 59 REM TO RUN ON SLA'S PDP-10. REFER TO LANGUAGE NOTE
 60 REM BELOW PRIOR TO IMPLEMENTATION ON SMALLER SYSTEMS.
 61 REM
 62 REM LANGUAGE USED: THE PROGRAM IS WRITTEN IN DARTHOOUTH BASIC
 63 REM AND MAY EASILY BE TRANSFERRED TO ANY OTHER SYSTEM
 64 REM WHICH HAS A BASIC LANGUAGE INTERPPETER, HOWEVER,
 65 REM IT REQUIRES THE ACCURATE EVALUATION OF CERTAIN
 66 REM HYPERBOLIC FUNCTIONS WITH A PRECISION WHICH MAY
 67 REM NOT BE AVAILABLE ON SMALLER (SHORTER WORD-LENGTH)
 68 REM MACHINES.
 69 REM
 70 REM OPERATING SYSTEM: N/A
 71 REM
 72 REM TYPE OF PROGRAM: MAIN WITH INTEGRAL SUBROUTINES
 73 REM
 74 REM CALLING SEQUENCE: N/A
 75 REM
 76 REM SPECIAL ROUTINES USED: NONE
 77 REM
 78 REM FORM OF PROGRAM: PAPER TAPE

```

79 REM
80 REM INPUT: THE PROGRAM ASKS FOR PARAMETERS AND ACCEPTS THEM
81 REM FROM THE TERMINAL IN FREE-FORM.
82 REM
83 REM OUTPUT: MARGINS, STRESSES, AND OTHER INFORMATION REQUIRED
84 REM TO BEGIN DETAIL DESIGN.
85 REM
86 REM KEY WORDS: STRUCTURE, -AL DESIGN, BLAST,BUILDING
87 REM
88 REM TAPES AND FILES: NONE
89 REM
90 REM POSSIBLE AREAS FOR MODIFICATION: MINICOMPUTER IMPLEMEN-
91 REM TATIONS MIGHT BE ATTEMPTED IF THE BASIC SYSTEM
92 REM PROVIDES FOR THE ADDITION OF USER-DESIGNED
93 REM FUNCTIONS OR SUBROUTINES WRITTEN IN MACHINE
94 REM LANGUAGE TO COMPUTE THE HYPERBOLICS IN THE
95 REM RANGE  $10^{-4}$  TO  $10^{-2}$  WITH 8-DIGIT PRECISION.
96 REM
97 REM
98 REM
99 REM
100 REM
105 REM *** LOAD STRUCTURAL RESPONSE DATA ***
110 REM
115 DIM HL(29)
120 DATA .153, .313, .47, .6, .73, .86, .95, 1.05
125 DATA 1.14, 1.2, 1.42, 1.52, 1.6, 1.67, 1.7, 1.72
130 DATA 1.75, 1.78, 1.8, 1.81, 1.81, 1.81, 1.82, 1.82, 1.82
135 DATA 1.83, 1.83, 1.84, 1.84
140 FOR HI=1 TO 29
145 READ HL(HI)
150 NEXT HI
155 REM
160 REM *** LOAD RE-BAR DATA ***
165 REM

```

```

170 DIM RC(10,2)
175 DATA 5.00000E-02,.25,.11,.375,.2,.3,.31,.625,.44,.75
180 DATA .6,.875,.79,1,1,1.128,1.27,1.27,1.56,1.41
185 FOR I=1 TO 10
190 READ RC(I,1),RC(I,2)
195 NEXT I
200 REM
205 REM *** GET USER PARAMETERS ***
210 REM
215 LET X=0
220 LET X5=0
225 PRINT "INPUT INSIDE LONGEST DIM. IN INCHES";
230 INPUT L1
235 PRINT "INPUT INSIDE 2ND LONGEST DIM. IN INCHES";
240 INPUT L2
245 PRINT "INPUT INSIDE SHORTEST DIM. IN INCHES";
250 INPUT L3
255 PRINT "INPUT PULSE PRESSURE IN P.S.I.";
260 INPUT P1
265 PRINT "INPUT PULSE DURATION IN MILLI-SECONDS";
270 INPUT P2
275 PRINT "INPUT OVER-PRESSURE IN P.S.I.";
280 INPUT W9
285 PRINT "INPUT CONCRETE COVERAGE IN INCHES";
290 INPUT J1
295 PRINT "INPUT CONCRETE ULT. IN P.S.I.";
300 INPUT E3
305 LET N1=30000/E3
310 LET N2=2*(N1-1)
315 LET S1=3*10^7/N1
320 PRINT "INPUT STEEL ULT. IN P.S.I.";
325 INPUT E4
330 PRINT "INPUT MIN. WALL THKNS. IN INCHES";
335 INPUT X8
340 PRINT "INPUT MAX. WALL THKNS. IN INCHES";

```

```

345 INPUT X7
350 PRINT "INPUT WALL INC. IN INCHES";
355 INPUT X6
360 LET J3=((X7-X8)/X6+1)*40
365 LET Q=3.14159
370 PRINT
375 PRINT "*****PROGRAM OUTPUT*****"
380 PRINT
385 REM
390 REM ITERATION LOOPS: THICKNESS, SIZE, & SPACING
395 REM
400 FOR T=X8 TO X7 STEP X6
405 FOR S=4 TO 11 STEP 1
410 FOR U=12 TO 4 STEP -2
415 LET X7=0
420 LET L9=L1+T
425 LET L8=L2+T
430 LET L7=L3+T
435 REM
440 REM CALCULATE CENTROIDS & MOMENT OF INERTIA
445 REM
450 LET A1=RES-1,13/U
455 LET A2=RES-1,23
460 LET J2=J1+A2/2
465 GOSUB 2000
470 LET I1=I
475 LET C5=C3
480 LET C4=C1
485 LET J2=J1+3*A2/2
490 GOSUB 2000
495 LET I9=I
500 REM
505 REM SETS WORKING VARIABLES
510 REM
515 LET W=T*150/1728

```

```

520 LET R1=L1/2
525 LET R2=L2/2
530 LET R3=L3/2
535 LET R4=3*L1/8
540 LET R5=3*L2/8
545 LET R6=3*L3/8
550 LET Q7=S1*I1
555 LET Q8=A1*3*10^7*2
560 LET Q9=S1*I9
565 LET O=0
570 LET U8=W*L8^4*I1/(L9^4*I9+L8^4*I1)
575 LET U6=W*L7^4*I1/(L9^4*I9+L7^4*I1)
580 REM
585 REM ESTABLISHES LOAD DISTRIBUTION & DEFLECTION
590 REM
595 GOSUB 6000
600 GOSUB 7000
605 GOSUB 8000
610 LET X7=X7+1
615 IF X7=5 THEN 630
620 IF U>ABS(.02*0) THEN 595
625 IF U<ABS(.98*0) THEN 595
630 IF U8>ABS(1.02*08) THEN 595
635 IF U8<ABS(.98*08) THEN 595
640 IF U6>ABS(1.02*06) THEN 595
645 IF U6<ABS(.98*06) THEN 595
650 IF G1>G2 THEN 665
655 LET Q1=G2
660 GOTO 605
665 LET Q1=G1
670 REM
675 REM ESTABLISHES NATURAL PERIOD & NORMALIZWS
680 REM
685 LET T9=2*0*(SQR(Q1/384))*1000
690 LET T8=2*P2/T9

```

```

695 REM
700 REM CALCULATES AMP. FACTOR & SETS LOAD
705 REM
710 IF T8>.1 THEN 725
715 LET Y=.153
720 GOTO 790
725 IF T8<10 THEN 740
730 LET Y=1.84
735 GOTO 790
740 IF T8>1 THEN 765
745 LET H2=INT(T8*10)
750 LET H4=.1
755 LET H5=H2/10
760 GOTO 780
765 LET H2=INT(((T8-1)/.5)+.5)+10
770 LET H4=.5
775 LET H5=1+((H2-10)*.5)
780 LET H1=H5+H4
785 LET Y=HCH2J+((T8-H5)/(H1-H5))* (HCH2+13-HCH2J)
790 LET H9=0
795 LET W3=P1*Y
800 IF W9>W3*4/5 THEN 810
805 GOTO 830
810 LET W3=W9
815 REM
820 REM CALCULATES MOMENTS
825 REM
830 LET J6=SQR(Q7/(W3*(W-U)/W*R3))
835 LET J7=SQR(Q9/(W3-W3*(W-U6)/W)*R3))
840 LET U1=L7/J6
845 LET U2=L8/J7
850 LET Z1=W3*U8/W*J6^2
855 LET Z2=(W3-W3*(W-U8)/W)*J7^2
860 LET X9=U1
865 GOSUB 3000

```

```

870 LET K4=K2/K1
875 LET M1=Z1*(U1/2-K4)/K4
880 LET M2=Z1*(1-.5*U1/K2)
885 LET X9=U2
890 GOSUB 3000
895 LET K4=K2/K1
900 LET M3=Z2*(U2/2-K4)/K4
905 LET M4=Z2*(1-.5*U2/K2)
910 IF M1>M2 THEN 925
915 LET M9=M2
920 GOTO 930
925 LET M9=M1
930 LET K9=M9*C4/11*.75
935 LET K8=M9*C5*N1/11*.75
940 IF M3>M4 THEN 955
945 LET M9=M4
950 GOTO 960
955 LET M9=M3
960 LET K7=M9*C1/19*.75
965 LET K6=M9*C3*N1/19*.75
970 LET G1=K8+R3*(W3-W3*(W-U)/W)/(2*A1)
975 LET G2=K6+R3*(W3-W3*(W-U6)/W)/(2*A1)
980 IF W9*(W3*4/5) THEN 1035
985 LET E1=E3/4
990 LET E2=E4/4.55
995 LET X5=X5+1
1000 GOSUB 5000
1005 IF G5>0 THEN 1025
1010 IF X5=J3 THEN 1020
1015 IF G5=0 THEN 1325
1020 GOSUB 9000
1025 PRINT "MAX. AMPLIFIED PRESSURE = ",W3
1030 GOTO 1095
1035 LET E1=E3/5
1040 LET E2=E4/5

```

```

1045 LET X5=X5+1
1050 GOSUB 5000
1055 IF G5>0 THEN 1090
1060 IF X5=J3 THEN 1085
1065 IF G5=0 THEN 1325
1070 REM
1075 REM OUTPUT
1080 REM
1085 GOSUB 9000
1090 PRINT "MAX. OVER-PRESSURE = ";M9
1095 PRINT "NATURAL PERIOD=";T9
1100 PRINT "RE-BAR SIZE = ";S
1105 PRINT "DEPTH = ";T
1110 PRINT "STEEL SPACING = ";U
1115 IF G1>G2 THEN 1185
1120 PRINT "SHORT SPAN STRESS CONTROLS"
1125 PRINT "MOMENT OF INERTIA =";I9
1130 PRINT "CENTROID DISTANCE =";C1
1135 IF M3>M4 THEN 1150
1140 PRINT "MID SPAN STRESS CONTROLS"
1145 IF G1>G2 THEN 1180
1150 PRINT "SHORT SPAN STEEL STRESS CONTROLS"
1155 IF M3>M4 THEN 1170
1160 PRINT "MID SPAN STEEL STRESS CONTROLS"
1165 GOTO 1205
1170 PRINT "EDGE STEEL STRESS CONTROLS"
1175 GOTO 1205
1180 PRINT "LONG SPAN STEEL STRESS CONTROLS"
1185 IF M1>M2 THEN 1200
1190 PRINT "MID SPAN STEEL STRESS CONTROLS"
1195 GOTO 1205
1200 PRINT "EDGE STEEL STRESS CONTROLS"
1205 PRINT "LONG SPAN STEEL STRESS =";G1
1210 PRINT "MARGIN =";E2/G1
1215 PRINT "SHORT SPAN STEEL STRESS =";G2

```

```

1220 PRINT "MARGIN =",E2/G2
1225 PRINT "LONG SPAN CONCRETE STRESS =",K9
1230 PRINT "MARGIN =",E1/K9
1235 PRINT "SHORT SPAN CONCRETE STRESS =",K7
1240 PRINT "MARGIN =",E1/K7
1245 PRINT "LONG SPAN MOMENT OF INERTIA =",I1
1250 PRINT "CENTROID DISTANCE =",C5
1255 PRINT "SHORT SPAN MOMENT OF INERTIA ="I9
1260 PRINT "CENTROID DISTANCE =",C1
1265 PRINT
1270 PRINT "*****"
1275 IF X5=J3 THEN 1345
1280 LET X=X+1
1285 REM
1290 REM PROGRAM ROUTING
1295 REM
1300 IF S=4 THEN 1360
1305 IF X=3 THEN 1360
1310 IF U=12 THEN 1335
1315 IF X=1 THEN 1330
1320 IF X=2 THEN 1335
1325 NEXT U
1330 NEXT S
1335 NEXT T
1340 IF X>0 THEN 1360
1345 PRINT "NO VALID SOLUTION ."
1350 PRINT "RE-RUN PROGRAM WITH LARGER WALL THICKNESS."
1355 GOTO 330
1360 PRINT "*** NORMAL TERMINATION ***"
1365 STOP
2000 REM
2005 REM CALC. CENTROIDS & INERTIAS
2010 REM
2015 LET B=2*A1*(N2+N1)
2020 LET C=2*A1*(J2*N1-N2*J2-N1*T)

```

```

2025 LET C1=(-B+SQR(B^2-4*C))/2
2030 LET C2=C1-J2
2035 LET C3=T-J2-C1
2040 LET I=C1^3/3+N2*A1*C2^2+H1*A1*C3^2
2045 RETURN
3000 REM
3005 REM HYPERBOLICS
3010 REM
3015 LET K1=.5*(EXP(X9/2)+EXP(-X9/2))
3020 LET K2=.5*(EXP(X9/2)-EXP(-X9/2))
3025 LET K3=4*X9*(1-K1)/K2+X9^2
3030 RETURN
4000 REM
4005 REM CALC. DEFL.
4010 REM
4015 GOSUB 3000
4020 LET C6=Z1*K3
4025 LET X9=U2
4030 GOSUB 3000
4035 LET C7=Z2*K3
4040 LET C8=ABS(.75*C6)+ABS(Q6)
4045 LET C9=ABS(.75*C7)+ABS(Q5)
4050 RETURN
5000 REM
5005 REM CHECK STRESSES
5010 REM
5015 LET G5=0
5020 IF G1>E2 THEN 5045
5025 IF K9>E1 THEN 5045
5030 IF G2>E2 THEN 5045
5035 IF K7>E1 THEN 5045
5040 LET G5=G5+1
5045 RETURN
6000 REM
6005 REM LOAD DIST. ROUTINE 1

```

```

6010 REM
6015 LET O=U
6020 LET J6=SQR(Q7/(U6*R1))
6025 LET J7=SQR(Q9/(U8*R1))
6030 LET U1=L8/J6
6035 LET U2=L7/J7
6040 FOR U=1.00000E-02*W TO W STEP 1.00000E-02*W
6045 LET Q6=U*R2*R4/Q8
6050 LET Q5=(W-U)*R3*R4/Q8
6055 LET Z1=U*J6^2/(8*U6*R1)
6060 LET Z2=(W-U)*J7^2/(8*U8*R1)
6065 LET X9=U1
6070 GOSUB 4000
6075 IF C8>C9 THEN 6085
6080 NEXT U
6085 LET G1=C8
6090 RETURN
7000 REM
7005 REM LOAD DIST. ROUTINE 2
7010 REM
7015 LET U8=U8
7020 LET J6=SQR(Q7/((W-U)*R3))
7025 LET J7=SQR(Q9/((W-U6)*R3))
7030 LET U1=L9/J6
7035 LET U2=L8/J7
7040 FOR U8=1.00000E-02*W TO W STEP 1.00000E-02*W
7045 LET Q6=U8*R1*R6/Q8
7050 LET Q5=(W-U8)*R2*R6/Q8
7055 LET Z1=U8*J6^2/(8*(W-U)*R3)
7060 LET Z2=(W-U8)*J7^2/(8*(W-U6)*R3)
7065 LET X9=U1
7070 GOSUB 4000
7075 IF C8>C9 THEN 7085
7080 NEXT U8
7085 RETURN

```

```

8000 REM
8005 REM LOAD DIST. ROUTINE 3
8010 REM
8015 LET Q6=U6
8020 LET J6=SQR(Q7/(U*R2))
8025 LET J7=SQR(Q9/((W-U8)*R2))
8030 LET U1=L9/J6
8035 LET U2=L7/J7
8040 FOR U6=1.00000E-02*W TO W STEP 1.00000E-02*W
8045 LET Q6=U6*R1*R5/Q8
8050 LET Q5=(W-U6)*R3*R5/Q8
8055 LET Z1=U6*J6^2/(8*U*R2)
8060 LET Z2=(W-U6)*J7^2/(8*(W-U8)*R2)
8065 LET X9=U1
8070 GOSUB 4000
8075 IF C8>C9 THEN 8085
8080 NEXT U6
8085 LET G2=C8
8090 RETURN
9000 REM
9005 REM DIAGNOSTIC
9010 REM
9015 PRINT
9020 PRINT "***** NOTE *****"
9025 PRINT "SOME STRESSES ARE HIGHER THAN ALLOWABLES"
9030 PRINT "USE THE INFORMATION OUTPUTTED BELOW AS"
9035 PRINT "GUIDANCE BEFORE PICKING A NEW WALL"
9040 PRINT "THICKNESS AS DIRECTED BY THE PROGRAM"
9045 PRINT
9050 RETURN
9999 END

```

READY

**PRIMARY FRAGMENT CHARACTERISTICS
AND IMPACT EFFECTS IN PROTECTIVE DESIGN**

**John J. Healey and Samuel Weissman
Amman & Whitney, Consulting Engineers
New York, N.Y.**

ABSTRACT

Based upon a comprehensive review and critical analysis of available information, the material on primary fragment characteristics and fragment impact effects in the tri-service design manual, "Structures to Resist the Effects of Accidental Explosions" (TM 5-1300) has been updated and expanded. This paper summarizes the results of the study in the areas of fragment design parameters and the effect of fragment impact upon concrete barriers and steel plates. Charts developed to facilitate design calculations are included.

INTRODUCTION

An important consideration in the design of structures for accidental explosions is impact by primary fragments, the relatively small, high velocity fragments produced from the casing of a detonated explosive container. The tri-service design manual, "Structures to Resist the Effects of Accidental Explosions, TM 5-1300," (Ref. 1) contains procedures for treating the phenomena of fragmentation and fragment impact into concrete and composite barriers as they relate to protective structure design.

As part of its overall Engineering Support Program for the U.S. Army Armament Command (ARMCOM), the Manufacturing Technology Directorate of Picatinny Arsenal with the assistance of Ammann & Whitney has undertaken a study to update these design procedures and to expand the treatment to include other structural materials. In order to accomplish this objective, a detailed review and critical analysis of existing data and analytical approaches was performed. Based upon this review, revised and expanded design procedures for protective structures have been developed. The background for and the development of this material is described in Ref. 2. In addition, this reference contains design charts, tables and detailed example problems. The objective of this paper is to summarize the material in two areas, the determination of primary fragment design characteristics and the effect of primary fragment impact on concrete barriers and steel plates.

FRAGMENT CHARACTERISTICS

General

Design for fragment penetration effects requires a complete definition of the probable characteristics of a critical design fragment at its point of impact with the structure. The known data consists of a given explosive in a container of known geometry and material properties at a specified distance from the protective structure. The principal fragment characteristics are random values and include the total number of fragments released and the distribution of their weights, the initial fragment velocity and other physical and geometrical characteristics.

Fragment Weight Distribution

Upon detonation of an explosive container, the casing breaks up into a large number of high velocity fragments with varying weights. Design calculations require that the weight of a so-called critical fragment be defined. A basic equation defining the weight distribution of released fragments has been provided by Mott (Ref. 3), i.e.,

$$\ln N_x = \ln(C^*M_A) - N/M_A \quad (1)$$

where

N_x = the number of fragments with weight greater than the fragment weight, W_f

$C' = \text{fragment distribution constant} = C/(2M_A^3)$

$C = \text{total casing weight (ounces)}$

$N = (W_P)^{1/2}$

$W_P = \text{fragment weight (ounces)}$

$M_A = \text{fragment distribution parameter}$

$= Bc_1^{5/6} d_1^{1/3} [1 + t_1/d_1]$

$t_1 = \text{average casing thickness (inches)}$

$d_1 = \text{average inside diameter of casing (inches)}$

$B = \text{explosive constant (Table 1).}$

The Mott equation assumes that the fragments result from the high-order detonation of a uniform thickness cylindrical casing filled with evenly distributed explosive. Since no procedure is available for a more general configuration, actual explosive containers are usually treated as one or more equivalent cylinders meeting the required conditions.

Equation (1) was derived assuming that the fragmentation process can be described as the two-dimensional break-up of a thin-walled casing. Although there is some evidence that the fragmentation of thick casings ($t_1 > 0.6$ in.) should be considered as a three-dimensional process, the Mott equation has been shown to produce estimates of fragment numbers and weights in substantial agreement with experimental results.

In order to refine the treatment in Ref. 1, formulas were developed, based on Equation (1), for the total number of released fragments, for the average fragment weight and for the design fragment weight in terms of a specified design probability or design confidence level.

The Mott equation can be expressed in the following form:

$$N_x = \frac{C}{2M_A^2} e^{-\sqrt{W_P}/M_A} \quad (2)$$

Hence, the total number of fragments is

$$N_T = \frac{C}{2M_A^2} \quad (3)$$

and the average fragment weight can be found

$$\bar{W}_P = 2M_A^2 \quad (4)$$

The ratio N_x/N_T represents that fraction of the total number of fragments which have a weight greater than W_p . It is interesting to observe that 75.7 percent of all primary fragments generated by the detonation have a weight less than that of the average fragment weight. Hence, the Mott equation predicts the release of a continuous distribution of fragments ranging in size from a large number of lightweight particles to a small number of very heavy casing fragments.

The probability, $1 - N_x/N_T$, that weight W_p is the largest weight fragment released is defined as the design confidence level, CL, and can be expressed as follows:

$$CL = 1 - N_x/N_T = 1 - e^{-N_p W_p / M_A} \quad (5)$$

Equation (5) can then be rearranged to express the design fragment weight W_p as a function of the prescribed probability or design confidence level:

$$W_p = M_A^2 \ln^2(1 - CL) \quad (6)$$

It should be recognized that the Mott equation yields values of W_p exceeding the total casing weight C for values of CL extremely close to one. Although an adjusted equation for W_p was derived which takes into account the finite upper limit of W_p , comparison of this equation with Equation (6) shows that the results are virtually identical except for CL values of the order of 0.9999 and greater. Hence, Equation (6) is recommended for use in all practical design cases.

In order to illustrate the implementation of these relationships in practical design, a step-wise procedure is outlined below. Design charts (Fig. 1, 2 and 3) have been developed to reduce the amount of necessary calculations.

The problem statement and solution can be summarized as follows.

GIVEN: A cylindrical casing filled with a specific explosive, inside diameter of cylinder = d_1 (in.), cylinder wall thickness = t_1 (in.), total casing weight = C (oz.), design confidence level = CL.

FIND: Fragment design weight, W_p . Also, calculate the number of fragments with weight greater than W_p .

- SOLUTION:**
- (1) From Fig. 1, determine M_p/B for known values of d_1 and t_1 . With value of B from Table 1 corresponding to given explosive, determine fragment distribution parameter, M_A .
 - (2) From Fig. 2, determine design fragment weight, W_p , for prescribed CL value and previously determined M_A .
 - (3) From Fig. 3, determine quantity $M_p M_A / C$ for known d_1 and t_1 . Calculate the total number of particles, N_T , for known casing weight C and explosive constant B .

- (4) Calculate N_x , the number of particles with weight greater than the design fragment weight from the following relationship:

$$N_x = N_T(1 - CL)$$

Initial Fragment Velocity

The initial velocity of primary fragments resulting from the detonation of cased explosives is a function of the ratio of explosive charge to casing weight and of the explosive output of the explosive. Gurney (Ref. 4) was able to derive, on a theoretical basis, expressions for the initial velocity of some specific container/explosive configurations. Assuming an even distribution of explosive charge and a uniform casing wall thickness, the following expression was developed for the initial fragment velocity resulting from the detonation of a cylindrical container:

$$V_o = (2E')^{1/2} \left[\frac{E/C}{1 + 0.5E/C} \right]^{1/2} \quad (7)$$

where $(2E')^{1/2}$ = Gurney explosive energy constant (fps) (Table 1)

E = weight of explosive (in design calculations, E = 1.2 times the actual explosive weight)

C = weight of casing

V_o = initial fragment velocity (fps).

Fig. 4 shows the variation of the normalized quantity $V_o/(2E')^{1/2}$ with E/C for this case. Expressions for the initial velocity for other configurations are summarized in Ref. 1.

Although the calculated velocity actually corresponds only to the smaller fragments, the variation of velocity with fragment weight is not well defined and hence, is not considered in design calculations. Instead, the conservative assumption is made that all fragments generated by the detonation travel at the velocity calculated from the Gurney equation.

An alternate fragment velocity expression derived by Mott (Ref. 3) for a cylindrical casing is:

$$V_o = [(E/C)kf]^{1/2} \quad (8)$$

where V_o = initial fragment velocity (fps)

E/C = ratio of explosive weight to casing weight

k = explosive output constant (Table 1)

f = factor defined as follows:

$$f = -0.682 \log_{10} E/C + 0.80 \text{ for } E/C \geq 0.509$$

$$f = 1.00 \text{ for } E/C \leq 0.509$$

Comparison of calculated initial velocities from Equation (7) with those from Equation (8) shows that consistently higher values are obtained with the Gurney velocity equation. An expression can be developed for the ratio of the Gurney velocity to the Mott velocity as a function of E/C:

$$V_G/V_M = \frac{\sqrt{2E'}}{\sqrt{k}} \left[\frac{1}{(1 + 0.5E/C)f} \right]^{1/2} \quad (9)$$

Plotting this velocity ratio relationship for TNT (Fig. 5) shows that for high values of the E/C ratio, the calculated velocity ratio is consistently greater than one; e.g., for TNT, V_G/V_M equals 1.37 for E/C equal to 10. Therefore, for design purposes, it is conservative to base initial velocity calculations upon the Gurney equation. It should be possible to resolve this discrepancy by examining the basic assumptions and ranges of applicability of the two velocity prediction equations.

In addition, the source of variations in measured Gurney constants should be investigated. Reported values of the constant $\sqrt{2E'}$ for a given explosive show variations of up to 12 percent.

Variation of Fragment Velocity with Distance

Since the fragment velocity of interest is the velocity of the fragment when it strikes the protective barrier, the decay in fragment velocity with distance is considered for distances greater than about 20 feet. The variation in velocity is a function not only of the distance but also of the area to weight relationship for the fragment [$A/W_F = 0.78/(W_F)^{1/3}$ for random steel fragments], the drag coefficient ($C_D = 0.6$) and the air density (Ref. 5). The resulting expression for the striking velocity is

$$V_R = V_0 e^{-0.004R/W_F^{1/3}} \quad (10)$$

where V_R = fragment velocity at distance R from detonation (kfps)
 V_0 = initial fragment velocity (kfps)
 R = distance (ft) from detonation to the protective barrier
 W_F = fragment weight (oz).

The variation of the ratio V_R/V_0 over a range of fragment weights for various distances R is shown in Fig. 6.

Primary Fragments - Caliber Density, Shape and Impact Angle

The randomness in fragment characteristics applies not only to their weight and velocity but also to the nature of the fragment surface which strikes the barrier, the relation between weight and diameter and the angle of impact. For design calculations, it is necessary to specify standard fragment characteristics.

The total weight/diameter relationship is usually defined as the caliber density of the fragment

$$D = W_p/d^3 \quad (11)$$

where W_p = fragment weight (lb) and d = fragment diameter (in.). The nose shape factor, N , is defined as

$$N = 0.72 + 0.25\sqrt{n} - 0.25 \quad (12)$$

where n = the caliber radius of the tangent ogive of the assumed fragment nose.

Two possible fragment shapes with their corresponding caliber densities and nose factors are shown in Fig. 7. The shape in Fig. 7(a), the "blunt" fragment, is considered as the "standard fragment" in the penetration design charts presented in the following section. While this fragment shape has a milder nose shape than the alternate shape, it is felt to be appropriate considering the small number of fragments which will strike the structure nose-on and the small fraction of these which will have a more severe nose shape than the standard fragment. Moreover, the length to diameter ratio of these fragments is felt to be more representative of an average fragment configuration.

The angle of obliquity is defined as the angle between the path of the fragment and a normal to the surface of the barrier. In order to design for the most severe condition, normal impact, i.e., an obliquity angle of zero degree, is usually assumed in penetration calculations.

FRAGMENT IMPACT EFFECTS

General

A number of different phenomena are associated with primary fragment impact having different consequences with regard to personnel safety, damage to sensitive equipment and the detonation of additional explosive containers. Since a primary fragment can generally be categorized as a high-speed particle with a mass much smaller than the barrier or target which it strikes, the interaction between local penetration effects and any overall structural response engendered by the impact is not significant. The effects of impact can then be broadly grouped into two classes, namely (1) "front face" effects which include deformation of the missile upon striking the surface, possible shatter or ricochet of the missile, spalling around the point of impact in a more or less conical crater and penetration of the missile into the barrier wall, and (2) "back face" effects including the possible formation of a back face crater with spalling and/or perforation wherein the missile completely penetrates the barriers and exits with a known residual velocity.

The intent herein is to treat those effects which have a critical bearing on the structural design of protective facilities, e.g., depth of penetration, the prediction of residual fragment velocity in the event that perforation occurs and the prediction of spalling of concrete barriers. The emphasis is upon the development of design data rather than a complete description of all the phenomena involved.

The two basic factors affecting the damage inflicted upon the barrier are the characteristics of the fragment (as defined previously) and the properties of the barrier material. The basic equation underlying all penetration formulations is Newton's Second Law of Motion. The case of "mass penetration" wherein the penetration process is treated as the rectilinear motion of a non-deforming fragment through a thick homogeneous material serves as a baseline for which a good deal of test data is available and for which an analytical approach can at least be formulated. However, even for this somewhat simplified case, a complete analytical solution is not available due mainly to a lack of understanding of the exact manner in which the resisting force representing the interaction between the penetrating mass and the barrier varies as the penetrator travels through the barrier.

As a result, missile penetration which has been under serious study since the mid-eighteenth century has remained predominantly an empirical field. This fact is evidenced in the comprehensive review by Robertson of the significant work in this area prior to World War II (Ref. 6), in the summary of the extensive research programs conducted during the war (Ref. 7) and by the orientation of most of the research activity since that time. Empirical study of this subject is also quite difficult due to the degree of scatter exhibited by experimental penetration data and the difficulty involved in comparing experimental data generated by different investigators.

Concrete Penetration

In the development of a design equation for concrete penetration, the "massive penetration" case is considered, i.e., the following conditions are assumed: (a) the angles of obliquity and yaw are zero, i.e., both the path of the missile and the missile axis are coincident with the normal to the surface of the barrier; (b) the missile is an inert non-deforming armor-piercing (AP) projectile or fragment; (c) the barrier or wall constitutes a uniform target of sufficient thickness that this finite dimension does not influence the penetration, i.e., it is assumed initially that back-face phenomena do not influence penetration; and (d) the loss of fragment mass during penetration is not considered. In order to avoid complications introduced by missile and plate hardness effects and non-normal impact, these topics are treated separately as modifications to the basic penetration case.

Under these conditions, the penetration problem essentially involves the one-dimensional motion of a particle with given initial conditions into a target medium which resists the motion. According to the separable force law postulated by Beth (Ref. 8), the force on a penetrator at a given instant is a function of both its current velocity and its current depth of penetration. Adopting this assumption, the basic equation of motion can be solved for the maximum caliber penetration. By including the values of the empirical constants which provide a good representation of observed penetration data (Ref. 8) and by establishing a weighted average value ($6.53/\sqrt{F_c}$) for the concrete penetrability constant (K), the following semi-empirical concrete penetration equation was obtained:

$$G(Z) = \frac{6.53}{\sqrt{F_c}} NDd^{0.2} v^{1.8} \quad (13)$$

where

$$G(Z) = \frac{1Z^2}{4} \text{ for } Z \leq 2 \\ = Z - 1 \text{ for } Z > 2$$

and, to summarize

N = nose shape factor

D = caliber density of the missile, W/d^3 , (lb/in³)

W = missile weight (lb)

d = diameter of missile (in)

V = striking velocity (kfps)

Z = caliber penetration, x/d

x = depth of penetration (in)

f'_c = concrete compressive strength (ksi).

As shown, this equation accounts for the missile nose shape, N, the missile caliber density, D, the effect of the concrete compressive strength, and the scale effect for penetration into concrete, i.e., the observed increase in maximum caliber penetration with increase in projectile caliber for other-wise similar projectiles.

Equation (13) can also be re-arranged in terms of the maximum depth of penetration.

For $x \leq 2d$,

$$x = 2\sqrt{KND} d^{1.1} v^{0.9} \quad (14)$$

and for $x > 2d$,

$$x = KND d^{1.2} v^{1.8} + d \quad (15)$$

These equations were compared with other formulations and experimental data for the normal penetration of reinforced concrete by armor-piercing missiles. Fig. 8 shows the variation of maximum caliber penetration with striking velocity corresponding to Equation (13) and to concrete penetration formulas from Refs. 1 and 9. Also shown are the results of tests on concrete slabs as reported in Ref. 7. The results indicate the following: the penetration equation in Ref. 4 underestimates the experimental data at low striking velocities and overestimates the results at higher velocities. In general, the equation in Ref. 9 and Equation 13 agree quite closely and give conservative estimates vs. the test data. It should be noted that the penetration equation from Ref. 9 does not account for nose factors different from 1.0 and, as the striking velocity approaches zero, the caliber penetration approaches a finite value of 0.5, indicating that the equation gives

overly conservative results at low striking velocities. Finally, Fig. 9 shows an excellent correlation between Equation (13) and a series of test results on concrete slabs described in Ref. 10.

It can be concluded from these comparisons that Equation (13) provides reliable estimates of massive penetration by armor-piercing projectiles into reinforced concrete.

Equations (14) and (15) can be expressed in more convenient form for design against impact by the standard design fragment shown in Fig. 7(a), by substituting the N and D values for the standard shape and assigning the value of 5 ksi to f'_c . The resulting penetration equations in terms of the fragment weight, W_F (oz), are therefore:

For $x \leq 2d$,

$$x = 0.91W_F^{0.37}v^{0.9} \quad (16)$$

For $x > 2d$,

$$x = 0.30W_F^{0.40}v^{1.8} + 0.575W_F^{0.33} \quad (17)$$

Depth of concrete penetration according to these equations for a range of velocities and fragment weights was developed to facilitate design calculations as shown in Fig. 10.

Equations (16) and (17) and Fig. 10 apply to the penetration of 5 ksi concrete by an armor-piercing steel primary fragment. The results can be adjusted for a different f'_c by multiplying by the square root of the ratio of 5 ksi to the f'_c of the concrete in question.

Steel Penetration

In developing a prediction equation for the penetration and perforation of steel plates, it is important to recognize some qualitative differences between failure mechanisms in steel and concrete barriers. The failure mode of primary concern in mild to medium hard homogeneous steel plates subjected to normal impact is ductile failure. In this mode, as the missile penetrates the plate, plastically deformed material is pushed aside and petals or lips are formed on both the front and back faces with no material being ejected from the plate. For plates with Brinell hardness values above about 350, the likelihood of failure by "plugging" increases. In this mode of failure, a plug of material is formed ahead of the penetrating missile and is ejected from the back side of the plate. A third mode of failure is diskling or flaking in which circular disks or irregular flakes are thrown from the back face. This type of failure is mainly of concern with plates of inferior quality and should not therefore be a common problem in the design of protective structures.

An empirical design formula was developed considering the ductile failure mode and subject to the conditions summarized above for massive penetration, i.e., normal impact, non-deforming projectile, etc. An important

difference with steel penetration is that penetration and perforation are treated simultaneously since back face phenomena do not influence the depth of penetration as was the case with concrete. For this reason, most of the steel test data are from perforation tests. The usual criteria of failure considered in such tests are the so-called Navy limit in which the missile completely passes through the plate and emerges with zero velocity and the protection limit criteria in which the missile emerges with sufficient velocity to pierce a thin sheet located a short distance behind the plate. At normal incidence, any differences attributable to these alternate definitions of plate failure are within acceptable limits for the purposes of this study.

Various empirical formulas valid for certain limited ranges and various sources of experimental data are available in the literature. A conservative prediction equation will be determined from these results by evaluating the coefficients in the following semi-empirical equation

$$z = C_1 DV^{C_2} \quad (18)$$

This equation is similar in form to the concrete equation but does not explicitly consider the influence of the missile nose factor or the scale effect since these factors are not significant for steel penetration. It is recognized that due to the relative hardness of the missile and the barrier in the case of steel/steel impact, the likelihood of missile shatter and ricochet is higher than with concrete/steel impact. However, for simplicity and conservatism, these effects are not considered in this design equation.

Steel penetration results from a number of sources (Refs. 7, 11, 12 and 13) were plotted together (Fig. 11) and compared for the assumed condition of penetration of an armor-piercing missile into mild steel. In order to convert the available results to these conditions of missile and plate hardness, it was necessary to develop conversion factors as summarized in the next section of this paper.

A good deal of scatter is apparent in these results. The main source of this scatter is the sensitivity of steel penetration to the relative hardness of the penetrator and the barrier material due to variations in test specimen material properties from their nominal values. To some extent, differences in definition of plate failure, different nose shapes and the scale effect due to the range of projectiles which these results represent, may also be responsible for some of the spread in the plotted results.

The extensive data from the THOR Project essentially represents an upper bound to the results illustrated in Fig. 11. Consequently, in order to provide conservative equations for use in protective design, the empirical coefficients in Equation (18) were essentially determined on the basis of these upper bound results. The following penetration equations were developed:

for AP steel missiles penetrating mild steel plate,

$$z = 2.33DV^{1.22} \quad (19)$$

for mild steel missiles penetrating mild steel plate,

$$z = 1.63DV^{1.22} \quad (20)$$

In order to facilitate the use of these steel penetration equations in design for primary fragment impact, they can be expressed in the following simplified forms:

for AP steel fragments into mild steel plate,

$$x = 0.30W_F^{0.33}V^{1.22} \quad (21)$$

for mild steel fragments into mild steel plate,

$$x = 0.21W_F^{0.33}V^{1.22} \quad (22)$$

where W_F = fragment weight (oz), V = striking velocity (kfps).

A design chart for steel penetration by primary fragments according to Equation (21) is presented in Fig. 12.

Other Influences on Penetration Depth

A. Missile Material

Since most penetration tests and penetration equations apply to steel and particularly to armor-piercing (AP) steel missiles, conversion factors are used to account for the effect of material properties of the given missile according to the following relation:

$$X_{\text{non-AP}} = k_p X_{\text{AP}} \quad (23)$$

where $X_{\text{non-AP}}$ = penetration achieved by a non-armor piercing steel missile

X_{AP} = penetration achieved by identical armor-piercing steel missile.

The k_p factors are determined based on the assumption that the relative penetration achieved by a missile of other than armor-piercing steel can be related to the material density and Brinell hardness number. The k_p factors developed in Ref. 2 and summarized in Table 2 are essentially identical to those found in TM 5-1300 with the exception of aluminum for which the k_p value has been reduced from 0.25 to 0.15. It should be noted that since the projectile material has a reduced effect on penetration at hypervelocities (> 5 kfps), these relative penetrability factors are not strictly applicable and their use in such cases may be unconservative.

B. Steel Plate Hardness

In general, the resistance to penetration of a steel plate increases with increasing Brinell hardness to the point where brittle fracture or plugging type failures occur. In Ref. 11, the penetrations were found to be proportional to the following empirical factor:

$$f_h = \frac{1}{\epsilon \epsilon B^2 + \omega B} \quad (24)$$

where B = Brinell hardness number

$$\omega = 5.41 \times 10^{-3}$$

$$\epsilon = -8.77 \times 10^{-6}$$

This function has a minimum value at a Brinell hardness of $-\omega/2\epsilon$ or about 310 for steel. The function, as shown in Fig. 13, is relatively flat in the region of this minimum. In order to convert data for penetration into steel with a given Brinell hardness to the corresponding penetration into a different type of steel, the following conversion formula can be used:

$$X_{B2} = \frac{f_{h2}}{f_{h1}} X_{B1} \quad (25)$$

where X_{B1} = depth of penetration into steel plate with Brinell hardness B_1

X_{B2} = depth of penetration into steel plate with Brinell hardness B_2

f_{h1}, f_{h2} = plate hardness factors from Fig. 13.

Since the required thickness to provide protection with a plate with a very high Brinell hardness (> 400) may actually exceed the thickness required for a milder steel plate due to the ejection of a plug before the plate is perforated, the use of more ductile plates is advised where deep penetrations are anticipated.

C. Obliquity

It is possible to make a conservative estimate of the effective normal penetration of a missile impacting a target with other than normal incidence. The following relationship provides an upper bound to the penetration achieved normal to the surface of the plate, X_θ :

$$X_\theta = X \cos^n \theta \quad (26)$$

where X = penetration for missile with striking velocity V_s and zero obliquity

V_s = striking velocity

θ = angle of obliquity

$n = 2$ for $V_s \leq 2.5$ kfps

$n = 1$ for $V_s > 2.5$ kfps.

Concrete Spalling

Upon impact of a high velocity fragment with a concrete wall, large compressive stresses are developed and a region of high stress expands spherically toward the back face. When the compressive stress waves reach this free surface, they are reflected and travel back as tension waves. If this disturbance exceeds some critical level, pieces of concrete become separated from and fly away from the back face of the wall, i.e., spalling occurs. Spalling is a factor in protective design in two significant respects:

- a. The release of secondary concrete fragments with significant mass and velocity represent a danger to personnel, equipment or explosives on the back side of the wall;
- b. The spalling of material in the path of the penetrating fragment causes the plate thickness perforated by a given fragment to exceed the equivalent depth of penetration into a massive plate.

The primary approaches to minimizing the effects of spalling are to provide a wall with sufficient thickness such that spalling will not occur or to add steel spall plates to prevent the release of the spalled particles.

Empirical spalling equations for certain test series are available from Refs. 7 and 14. These equations along with some data from Ref. 7 are shown in Fig. 14. The following single expression was developed from these expressions:

$$t_{sp} = 1.222d^{1.1} + 2.12d \quad (27)$$

Thus, upon calculating the caliber penetration into a massive concrete slab for a missile with diameter d , the slab thickness corresponding to the first occurrence of spalling, t_{sp} , can be determined from Equation 27.

Perforation and Residual Velocity

The most critical effect of fragment impact upon a protective barrier is complete penetration or perforation. This criticality is due to the sympathetic detonation of explosives on the rear side of the wall or the serious damage to personnel and equipment which may result if the fragment emerges from the back face with sufficient residual velocity. The basic massive penetration equations are used here also to predict the occurrence of perforation and in the calculation of the residual fragment velocity upon perforation.

Since spalling is not a consideration for penetration into metallic barriers, the penetration equations can be used directly to determine if a finite thickness of plate will be completely perforated. With concrete, however, spalling has a significant influence upon the slab thickness which will be perforated by a given fragment. The perforation thickness can also be related to the equivalent massive penetration based upon the results from Refs. 7 and 14 and as shown in Fig. 15. Based upon this data, the following perforation prediction equation was developed:

$$t_{pf} = 1.132d^{1.1} + 1.31d \quad (28)$$

Thus, the thickness, t_{pf} , of a concrete barrier which will be perforated by a given fragment can be determined based upon the caliber penetration of the fragment into a massive concrete slab.

In cases where a barrier is perforated, it is necessary to calculate the residual fragment velocity in order to evaluate possible effects upon items located behind the barrier.

At the onset of the calculation, the known information will generally consist of the following:

For steel, the calculated fragment penetration, x , is found to be greater than the actual plate thickness, t ;

For concrete, the perforation thickness, t_{pf} , exceeds the barrier thickness, t .

In both cases, an expression is needed for the residual velocity, V_r , in terms of the plate thickness, the striking velocity, V_s and x or t_{pf} .

The basic relationships for determining residual velocity were obtained by relating the velocity value at an intermediate depth of penetration to the striking velocity for the general case of massive penetration.

For concrete penetration, the following residual velocity relationships were developed in this manner:

$$(V_r/V_s) = [1 - (t/t_{pf})^2]^{0.555} \text{ for } x \leq 2d \quad (29)$$

and
$$(V_r/V_s) = [1 - t/t_{pf}]^{0.555} \text{ for } x > 2d \quad (30)$$

For steel penetration, the resulting residual velocity equation is:

$$(V_r/V_s) = (1 - t/x)^{0.82} \quad (31)$$

Equations 29, 30 and 31 are presented in non-dimensional form in Figs. 16, 17 and 18.

TABLE 1
EXPLOSIVE CONSTANTS

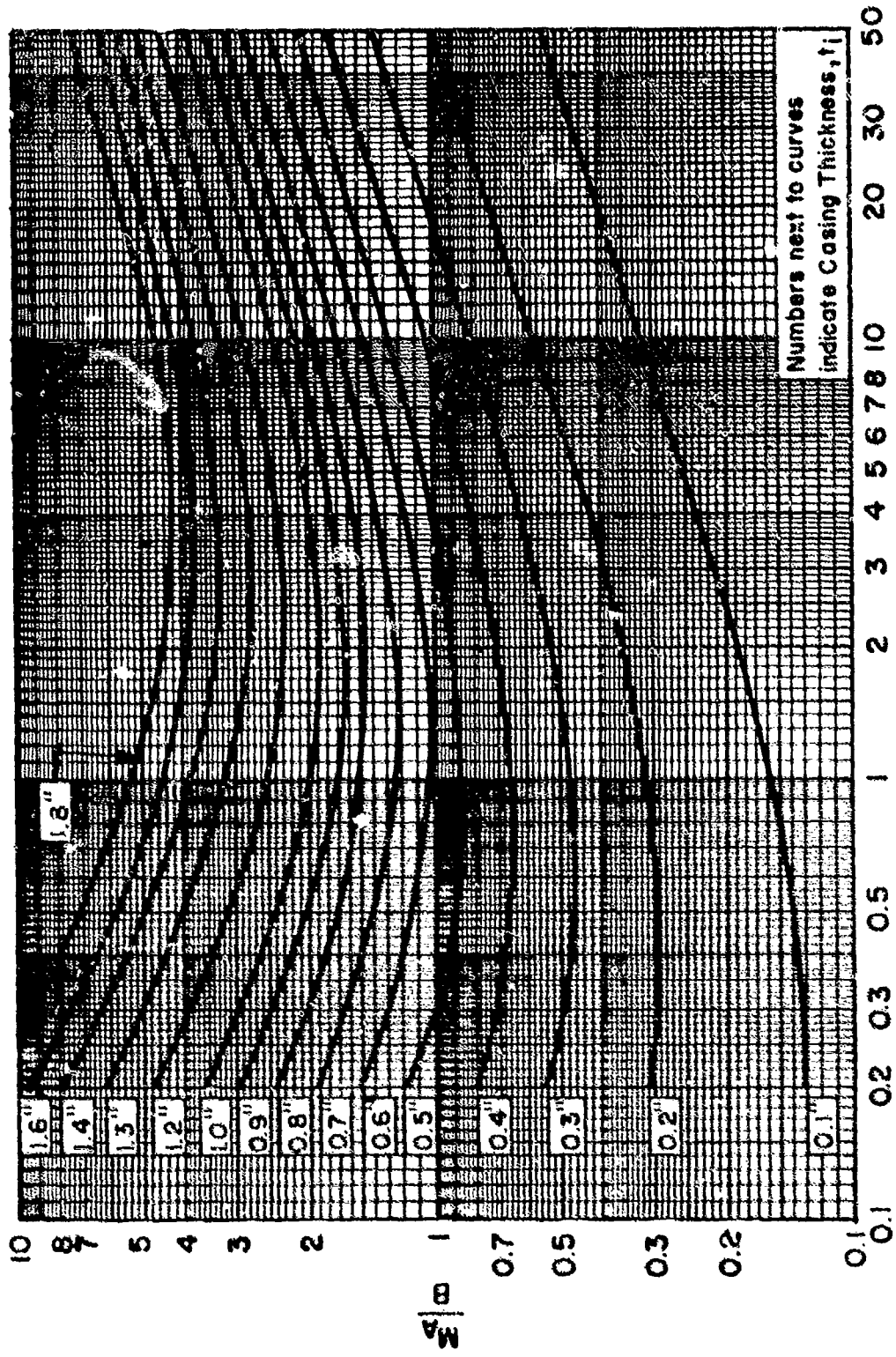
EXPLOSIVE MATERIAL	GURNEY ENERGY CONSTANT $\sqrt{2E^T}$, (fps)	B(Eq. 1) (oz ^{1/2} /in ^{7/6})	OUTPUT CONSTANT (Eq. 8) k
Amatol	6190	0.35	2.7×10^7
Comp. B	7880	-	4.4×10^7
H-6	7710	0.28	-
Hexanite	6850	0.32	3.3×10^7
Pentolite	7550	0.25	-
RDX/TNT (75/25)	7850	-	-
RDX/TNT (70/30)	8380	-	-
RDX/TNT (60/40)	7880	0.27	4.4×10^7
TNT	6940	0.30	3.6×10^7
Tetryl	7460	0.24	5.2×10^7
Torpex	7450	-	-

TABLE 2
RELATIVE PENETRABILITY COEFFICIENT, k_p

MISSILE MATERIAL	DENSITY (lb/in ³)	BRINELL HARDNESS NUMBER (BHN)	PENETRABILITY COEFFICIENT k_p
AP Steel	0.283	285	1.0
Mild Steel	0.283	140	0.7
Lead	0.385	10	0.5
Aluminum	0.098	32	0.15

REFERENCES

1. "Structures to Resist the Effects of Accidental Explosions (with Addenda)", Department of the Army, Technical Manual TM 5-1300, Washington, D.C., June 1969.
2. "Primary Fragment Characteristics and Penetration of Steel, Concrete and Other Materials", Picatinny Arsenal, Technical Report, Draft.
3. MOTT, R.I., "A Theory of Fragmentation", Army Operational Research Group Memo., 113-AC-3642, Great Britain, 1943.
4. GURNEY, R.W., "The Initial Velocities of Fragments from Bombs, Shells and Grenades", Report No. 405, Ballistic Research Laboratories, Aberdeen Proving Ground, Maryland, September 1943.
5. THOMAS, L.H., "Computing the Effect of Distance on Damage by Fragments", Report No. 468, Ballistic Research Laboratories, Aberdeen Proving Ground, Maryland, 1944.
6. ROBERTSON, H.P., "Terminal Ballistics", Preliminary Report, Committee on Passive Protection Against Bombing, National Research Council, January 1941.
7. "Effects of Impact and Explosion", Volume 1, Office of Scientific Research and Development, National Defense Research Committee, Washington, D.C., 1946.
8. BETH, R.A., "Final Report on Concrete Penetration", Report No. A-388, National Defense Research Committee, Office of Scientific Research and Development, March 1946.
9. "Fundamentals of Protective Design (Non-Nuclear)", Department of the Army, Technical Manual TM 5-855-1, Washington, D.C., July 1965.
10. STIPE, J.G., et al., "Ballistic Tests on Small Concrete Slabs", Interim Report No. 28, Committee on Fortification Design, National Research Council, June 1944.
11. "The Resistance of Various Metallic Materials to Perforation by Steel Fragments: Empirical Relationships for Fragment Residual Velocity and Residual Weight", Project THOR Technical Report No. 47, Ballistics Research Laboratories, Aberdeen Proving Ground, Maryland, April 1961.
12. JOHNSON, C. and MOSELEY, J.W., "Preliminary Warhead Terminal Ballistic Handbook. Part 1: Terminal Ballistic Effects", NAVWEPS Report No. 7673, U.S. Naval Weapons Laboratory, Dahlgren, Virginia, March 1964.
13. IPSON, T.W., "Deformation and Reduction in Weight of Compact Steel Fragments Perforating Thin, Mild Steel Plates", NWC TP 4553, Naval Weapons Center, January 1968.
14. "Industrial Engineering Study to Establish Safety Design Criteria for Use in Engineering of Explosive Facilities and Operations", Ammann & Whitney, Consulting Engineers, New York, N.Y., Report for Picatinny Arsenal, Dover, New Jersey, April 1963.



INSIDE DIAMETER OF CASING, d_j (in.)

FIGURE 1 - $\frac{MA}{B}$ VERSUS CASING GEOMETRY

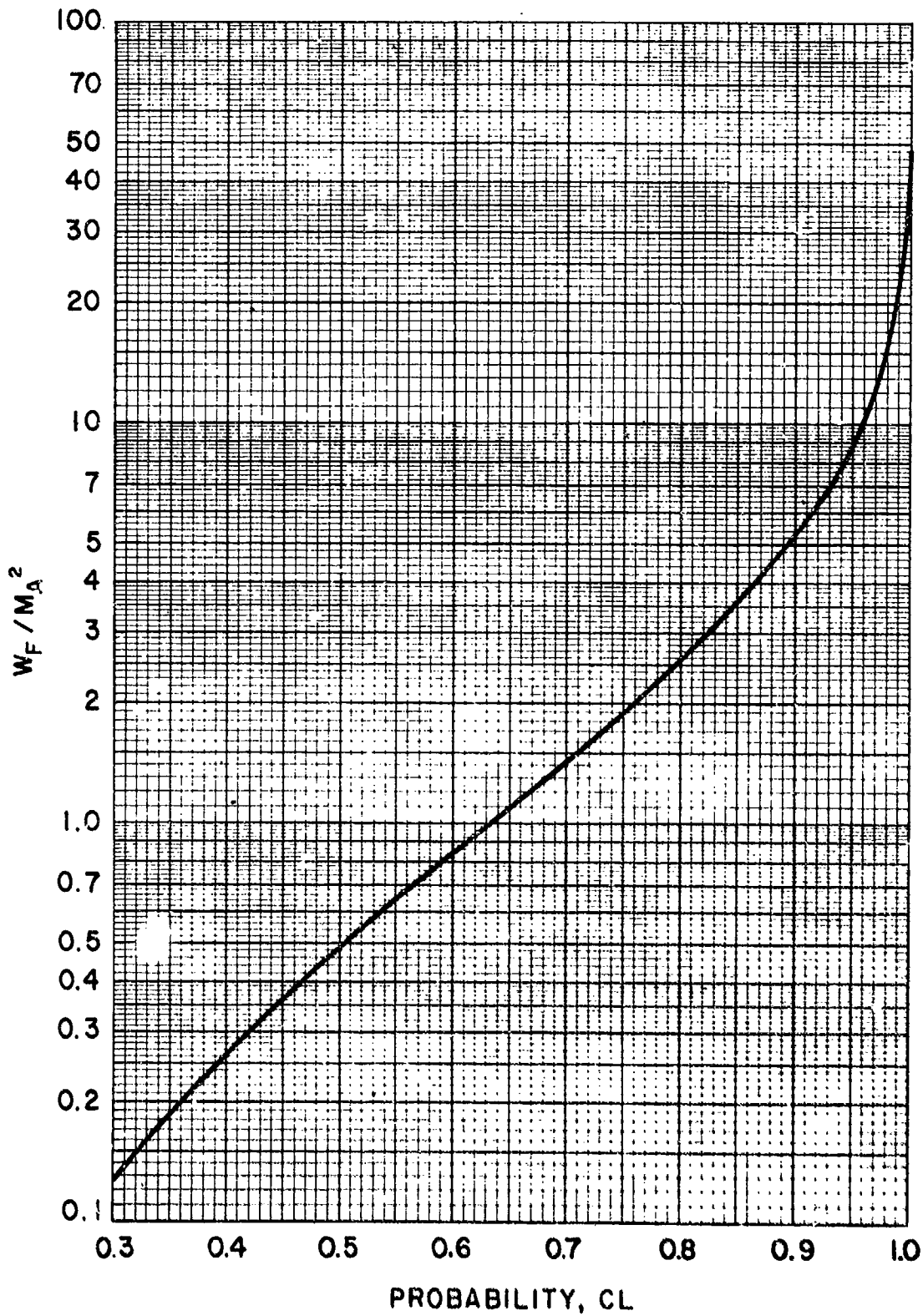


FIGURE 2(a) - DESIGN FRAGMENT WEIGHT VERSUS DESIGN CONFIDENCE LEVEL

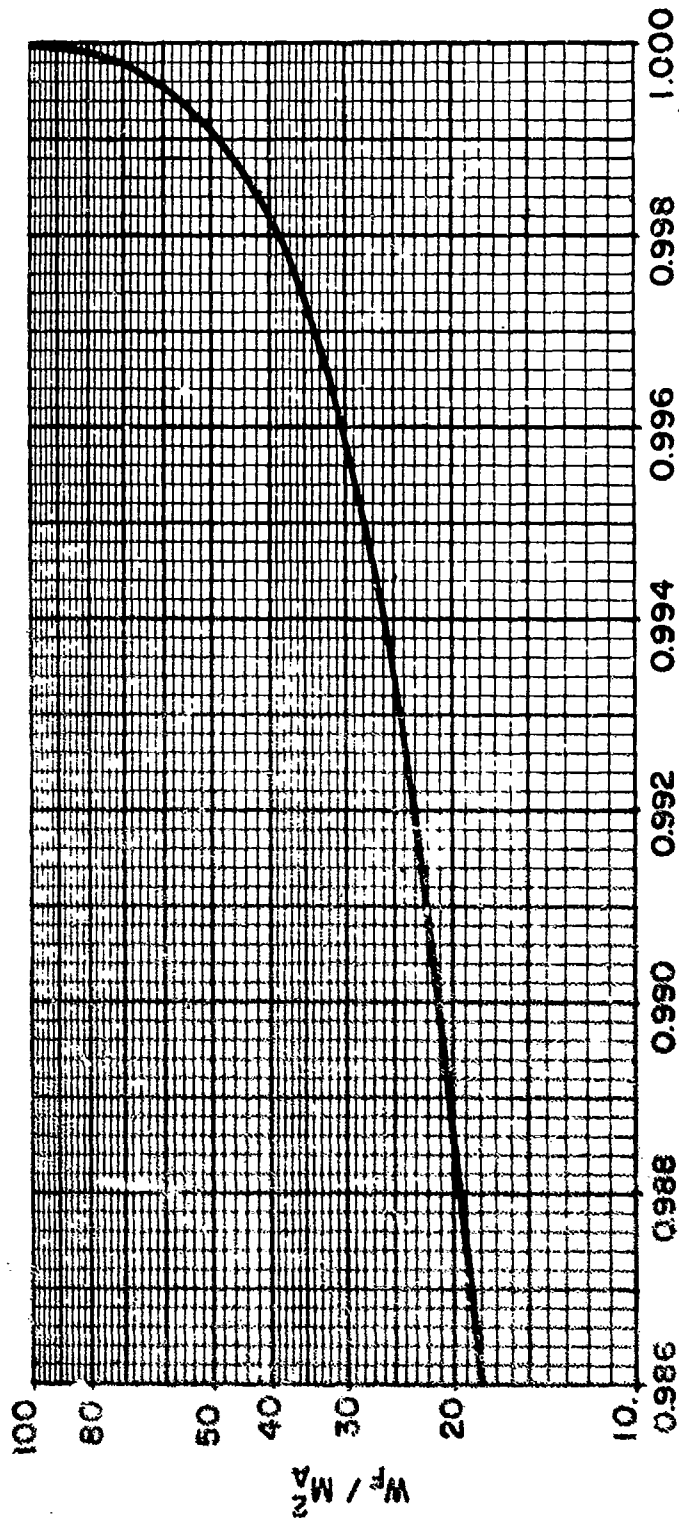


FIGURE 2 (b) - DESIGN FRAGMENT WEIGHT VERSUS
DESIGN CONFIDENCE LEVEL

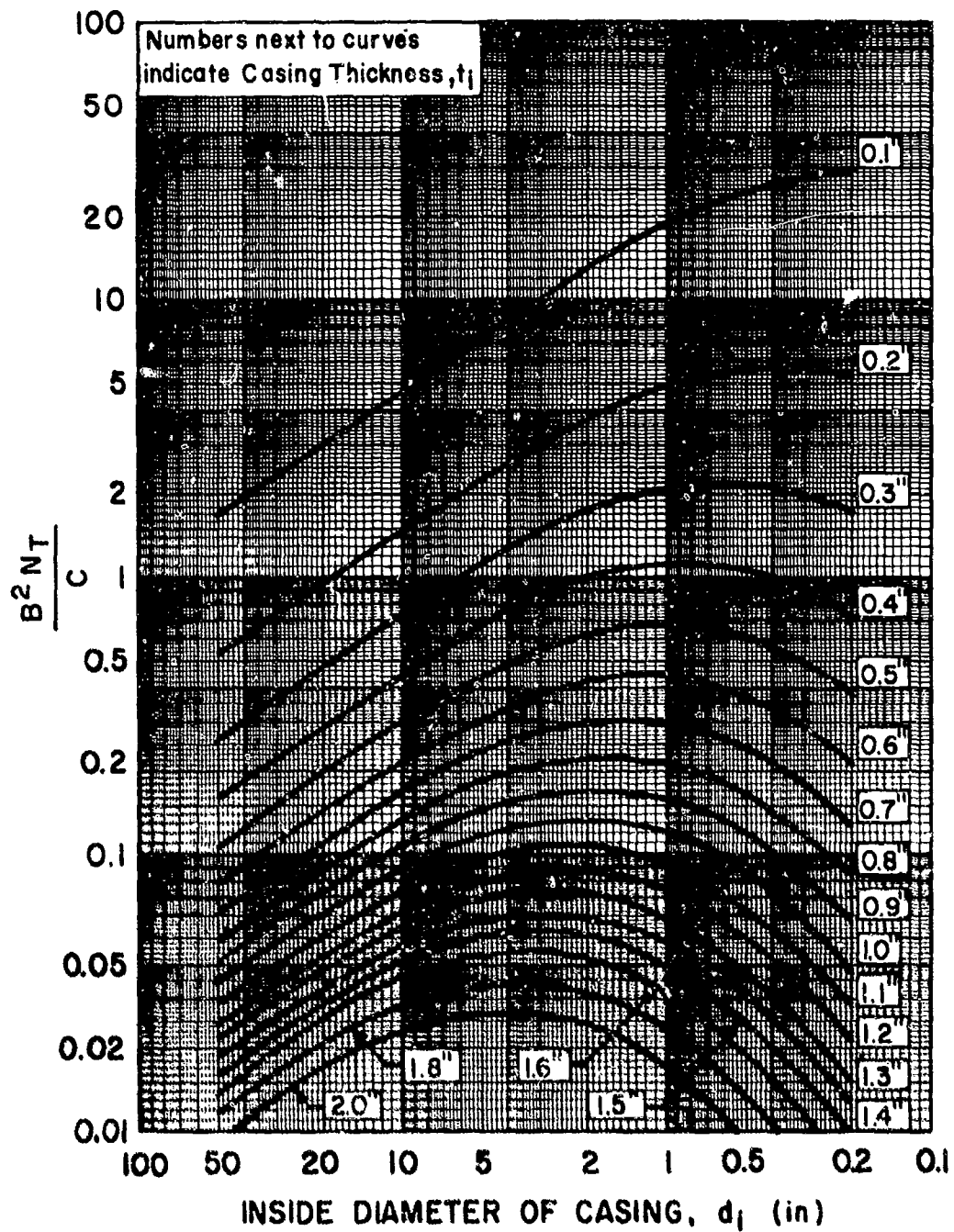


FIGURE 3 - $\frac{B^2 NT}{C}$ VERSUS CASING GEOMETRY

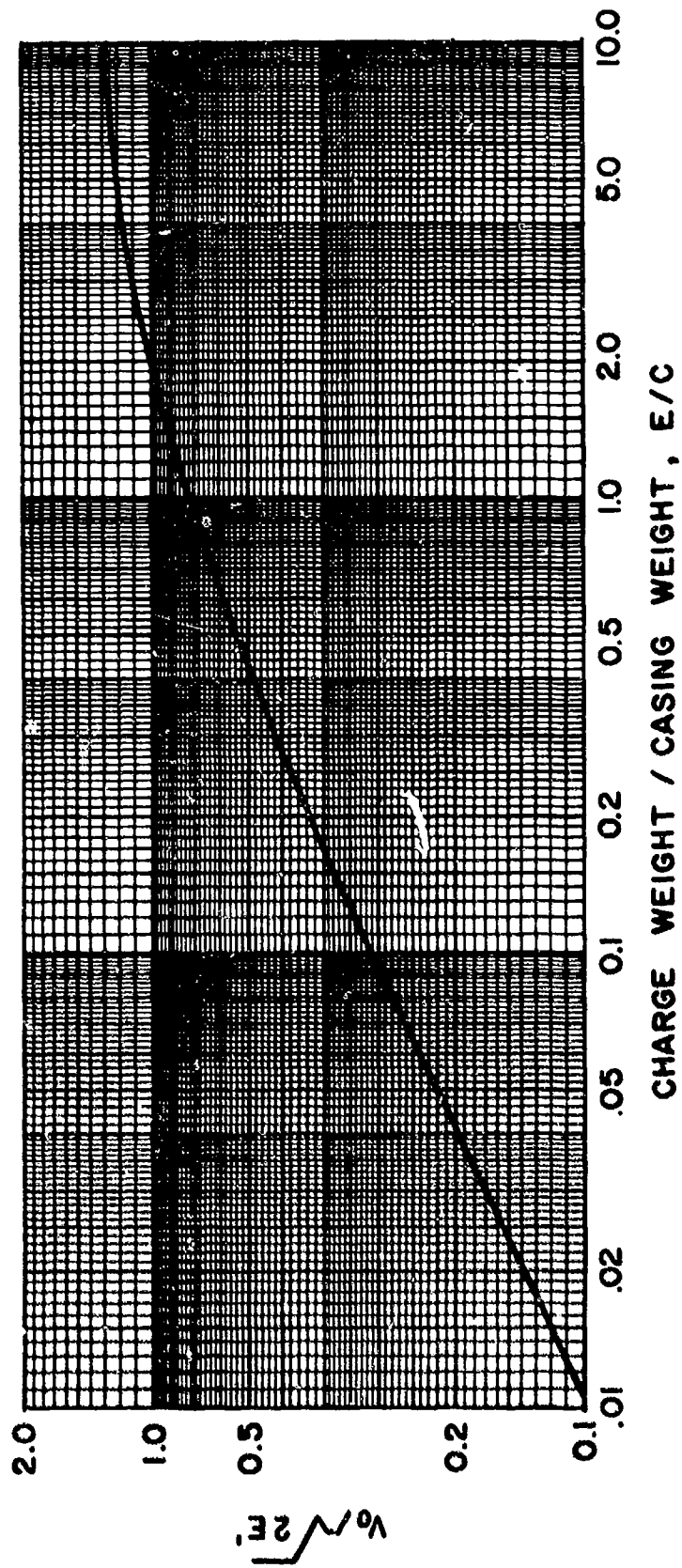


FIGURE 4 - INITIAL VELOCITY OF PRIMARY FRAGMENTS - CYLINDRICAL CASING

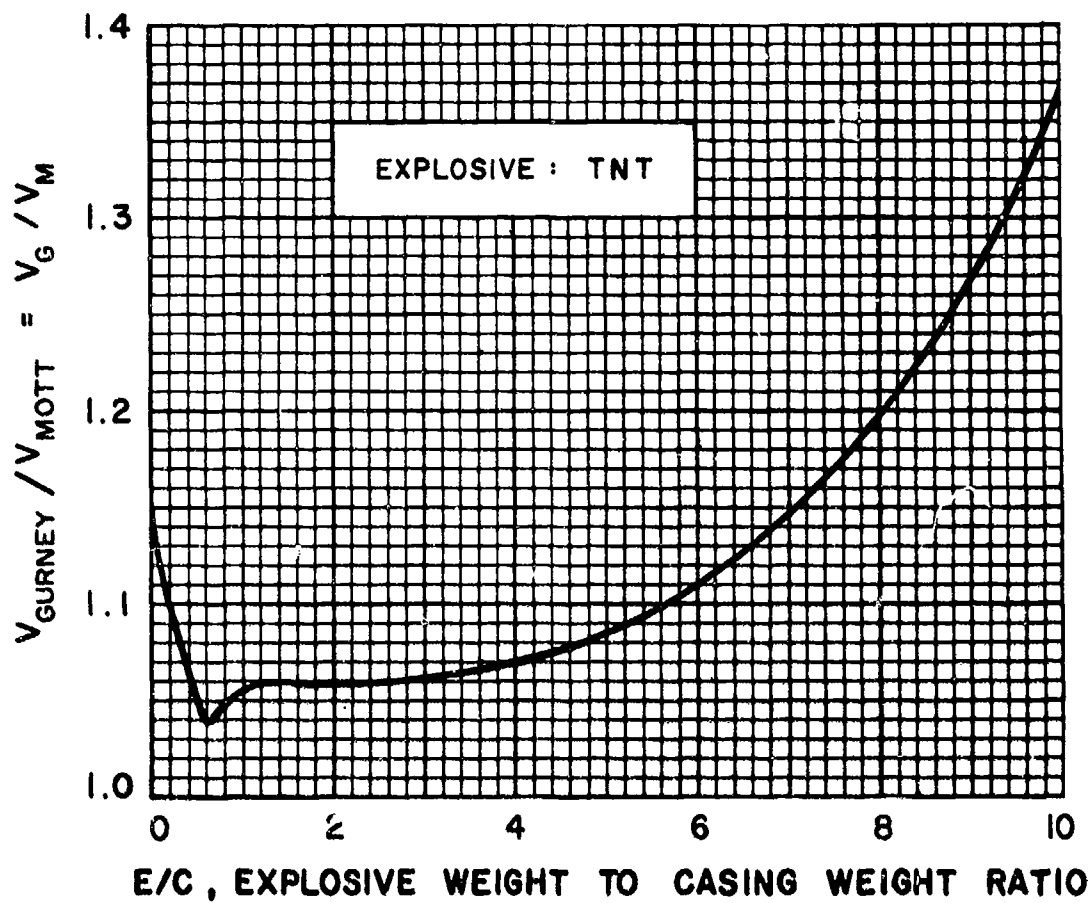


FIGURE 5 - RATIO OF CALCULATED INITIAL VELOCITIES vs. E/C

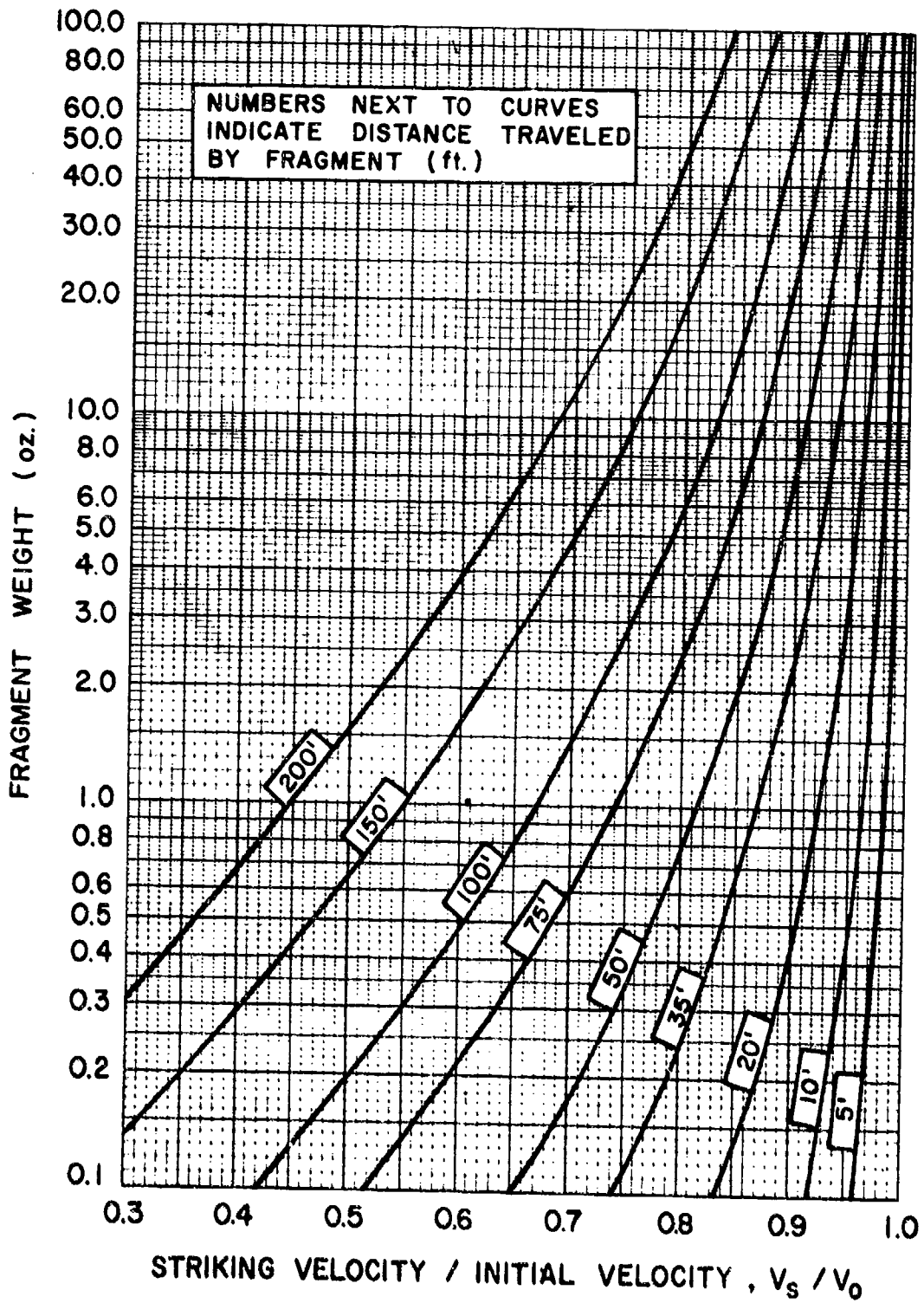
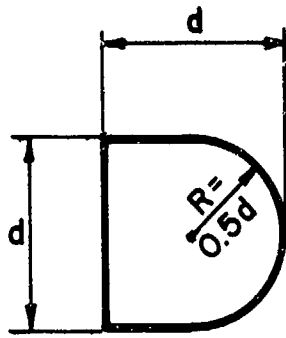


FIGURE 6 - VARIATION OF PRIMARY FRAGMENT VELOCITY WITH DISTANCE



$$n = R/d = 0.5$$

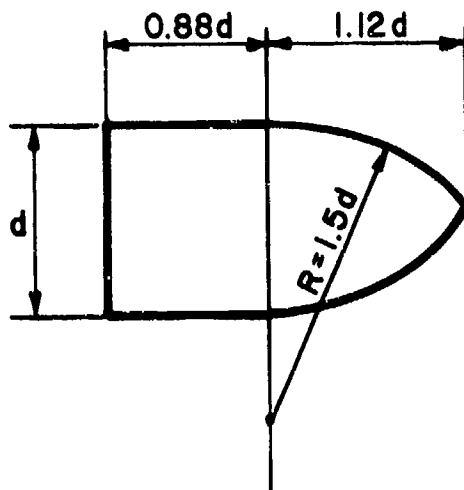
$$N = 0.845$$

$$\text{Volume} = 0.654d^3$$

$$\text{Weight} = 0.654d^3 \gamma = 0.186d^3$$

$$D = 0.186 \text{ lb./in.}^3$$

7(a) STANDARD FRAGMENT SHAPE



$$n = R/d = 1.5$$

$$N = 1.00$$

$$\text{Volume} = 1.2d^3$$

$$\text{Weight} = 1.2d^3 \gamma = 0.34d^3$$

$$D = 0.34 \text{ lb./in.}^3$$

7(b) ALTERNATE FRAGMENT SHAPE

FIGURE 7 - PRIMARY FRAGMENT SHAPES

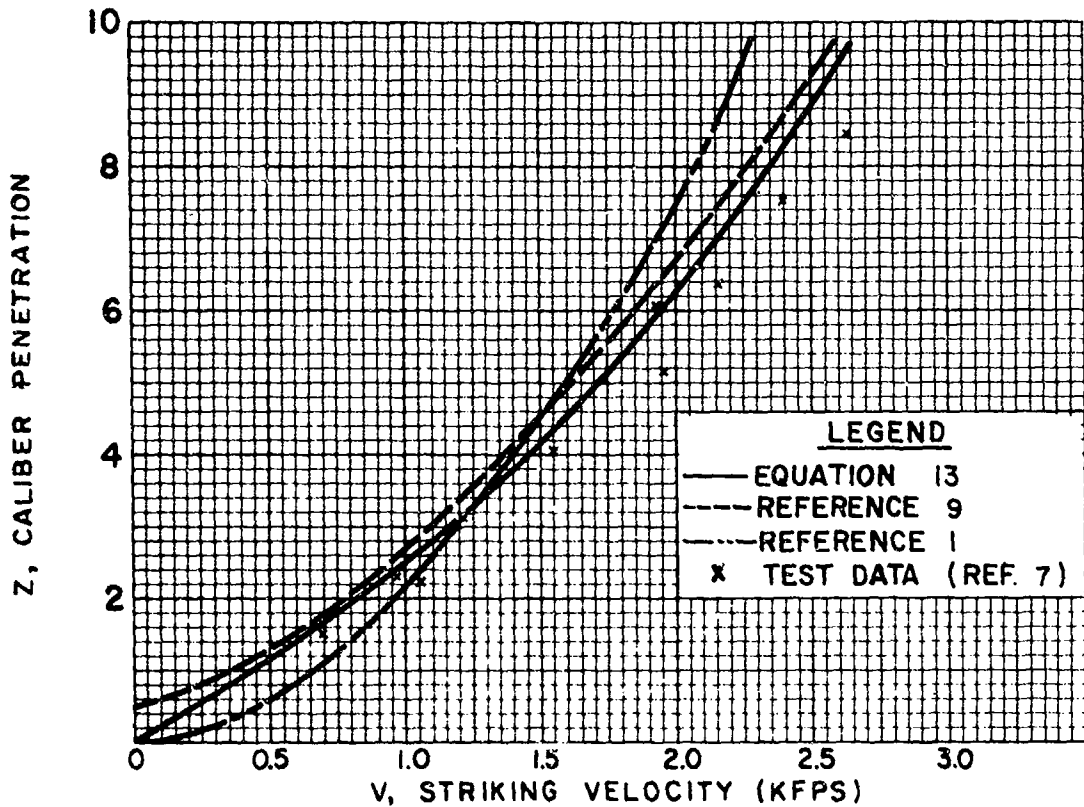


**FIGURE 8 - CONCRETE PENETRATION
EMPIRICAL EQUATIONS VS TEST DATA**

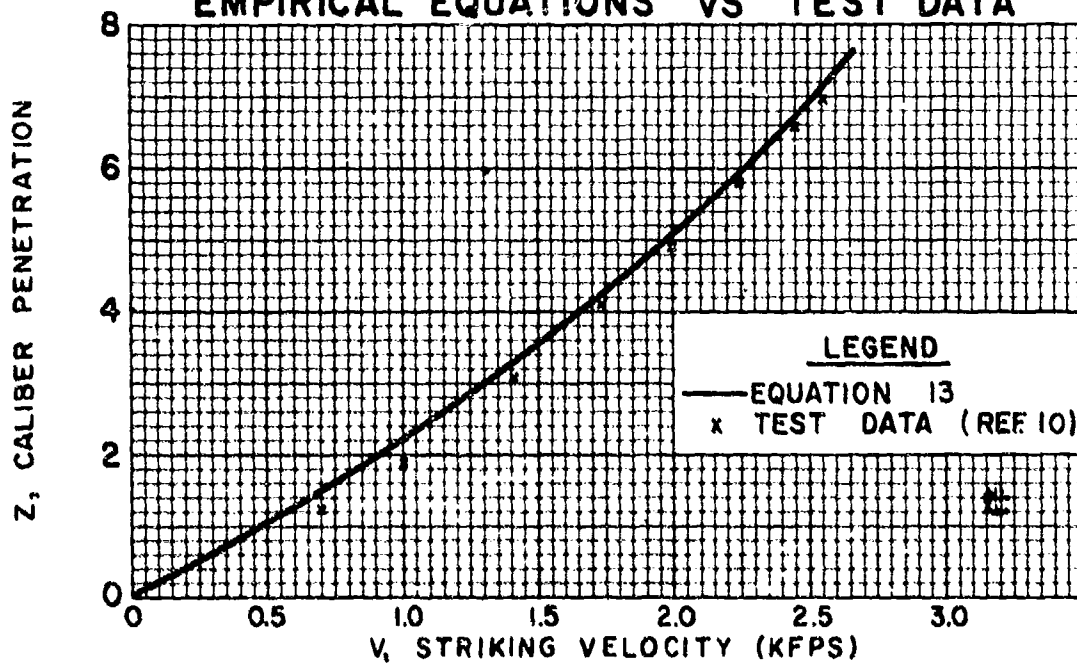


**FIGURE 9 - CONCRETE PENETRATION
EMPIRICAL EQUATION VS TEST DATA**

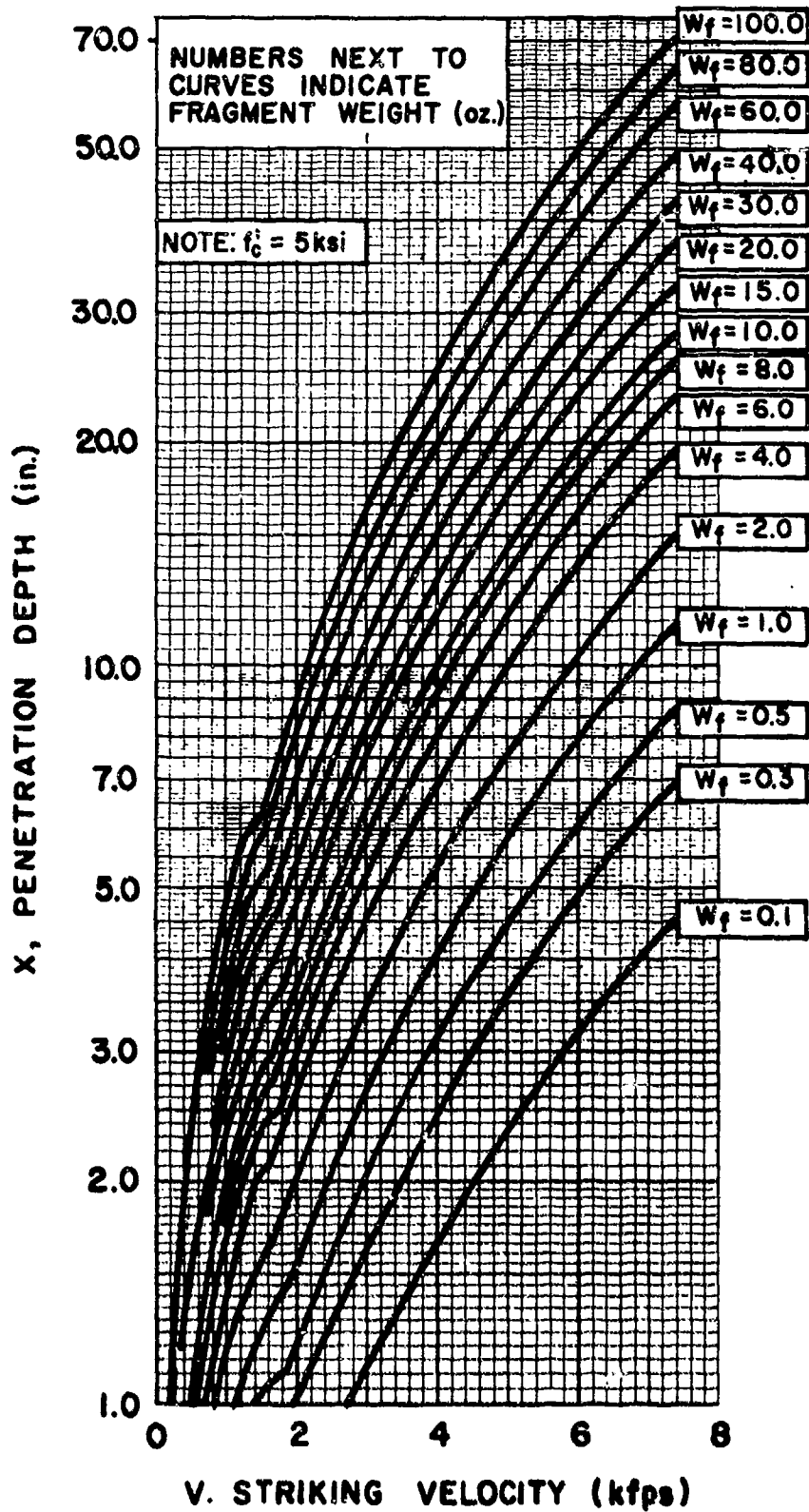


**FIGURE 10 - CONCRETE PENETRATION CHART
(AP STEEL FRAGMENT)**

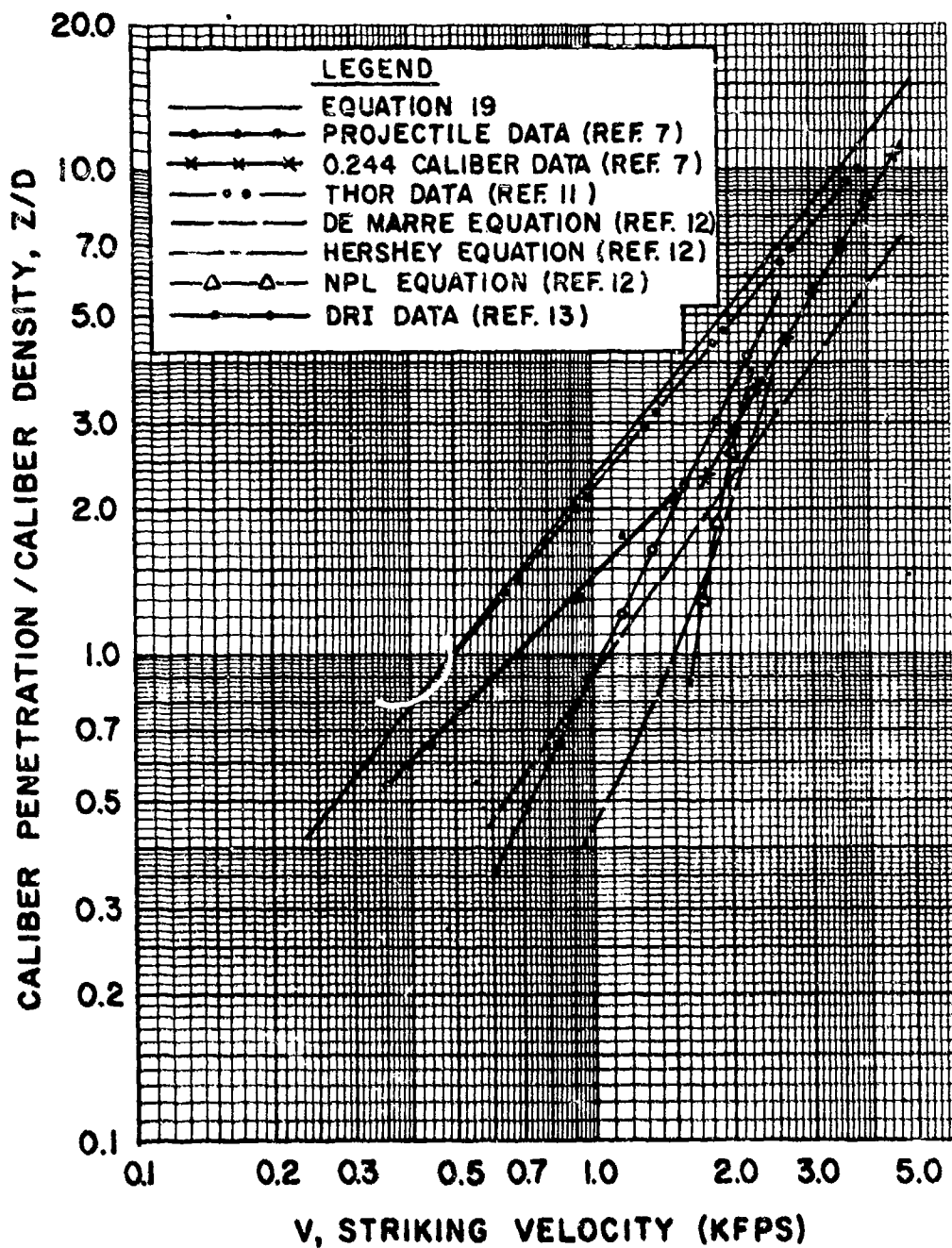


**FIGURE 11 - STEEL PENETRATION
EMPIRICAL EQUATIONS
AP FRAGMENTS INTO MILD STEEL PLATE**

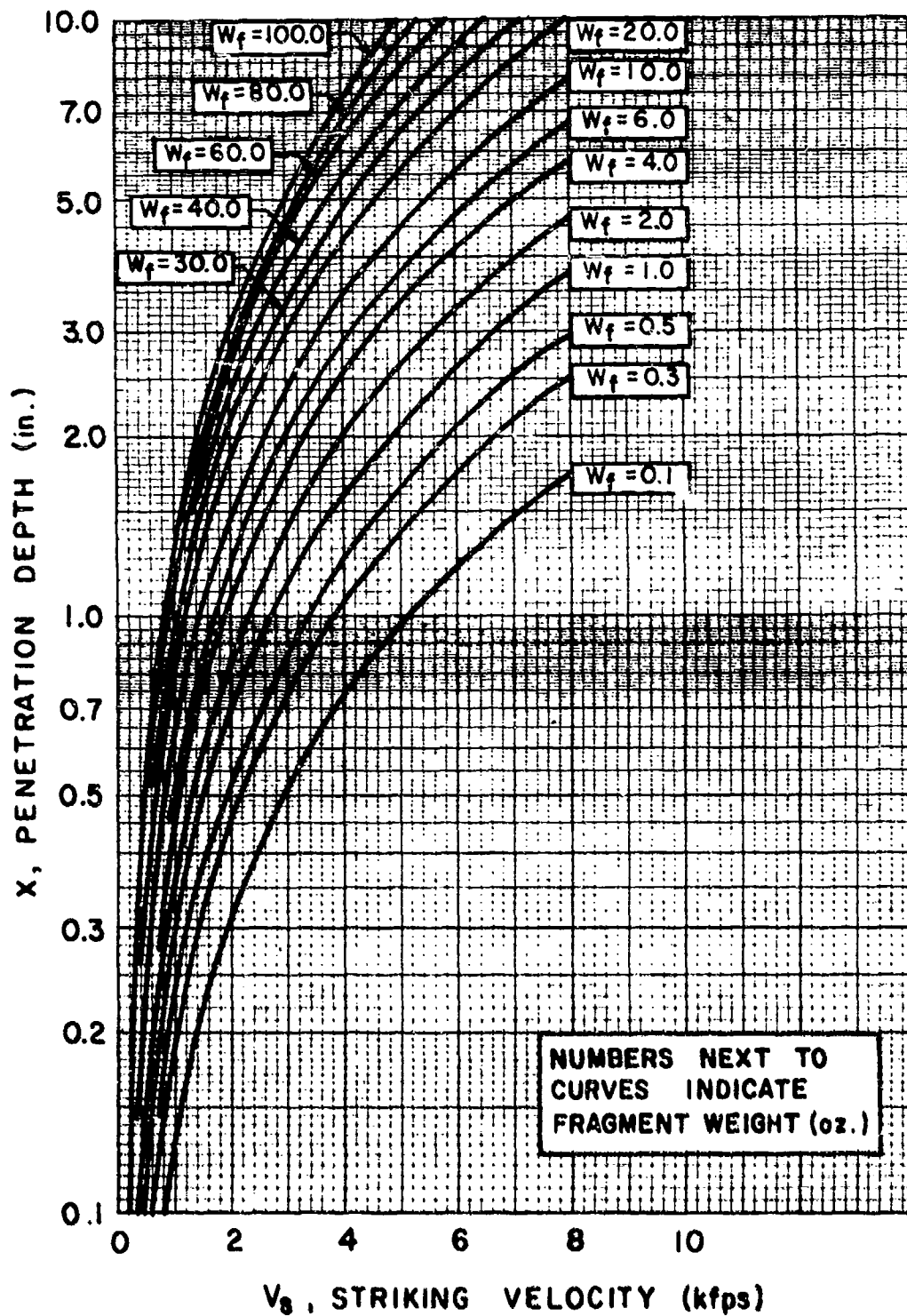


FIGURE 12 - STEEL PENETRATION DESIGN CHART
AP STEEL FRAGMENT - MILD STEEL
PLATE

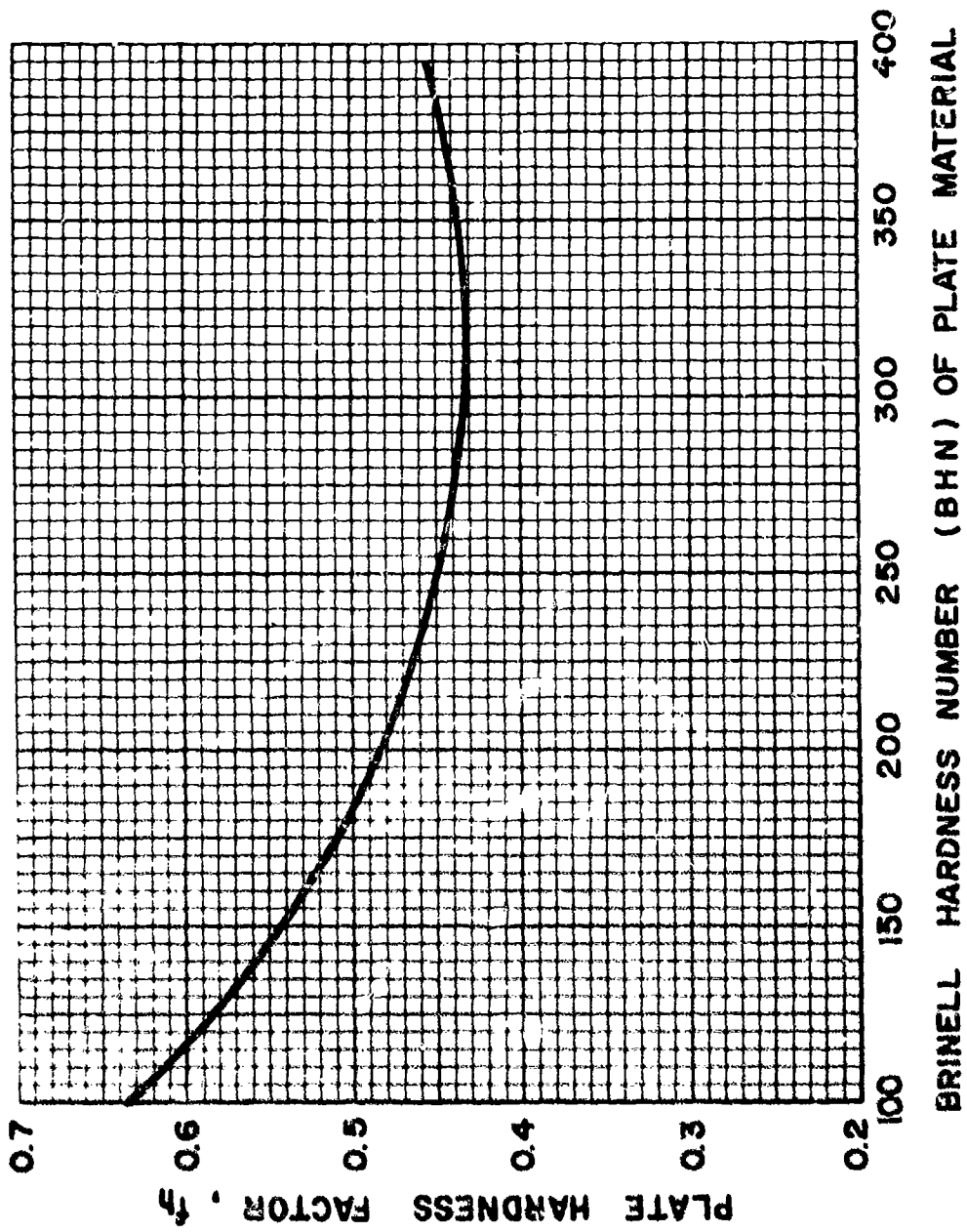


FIGURE 13 - PLATE HARDNESS FACTOR

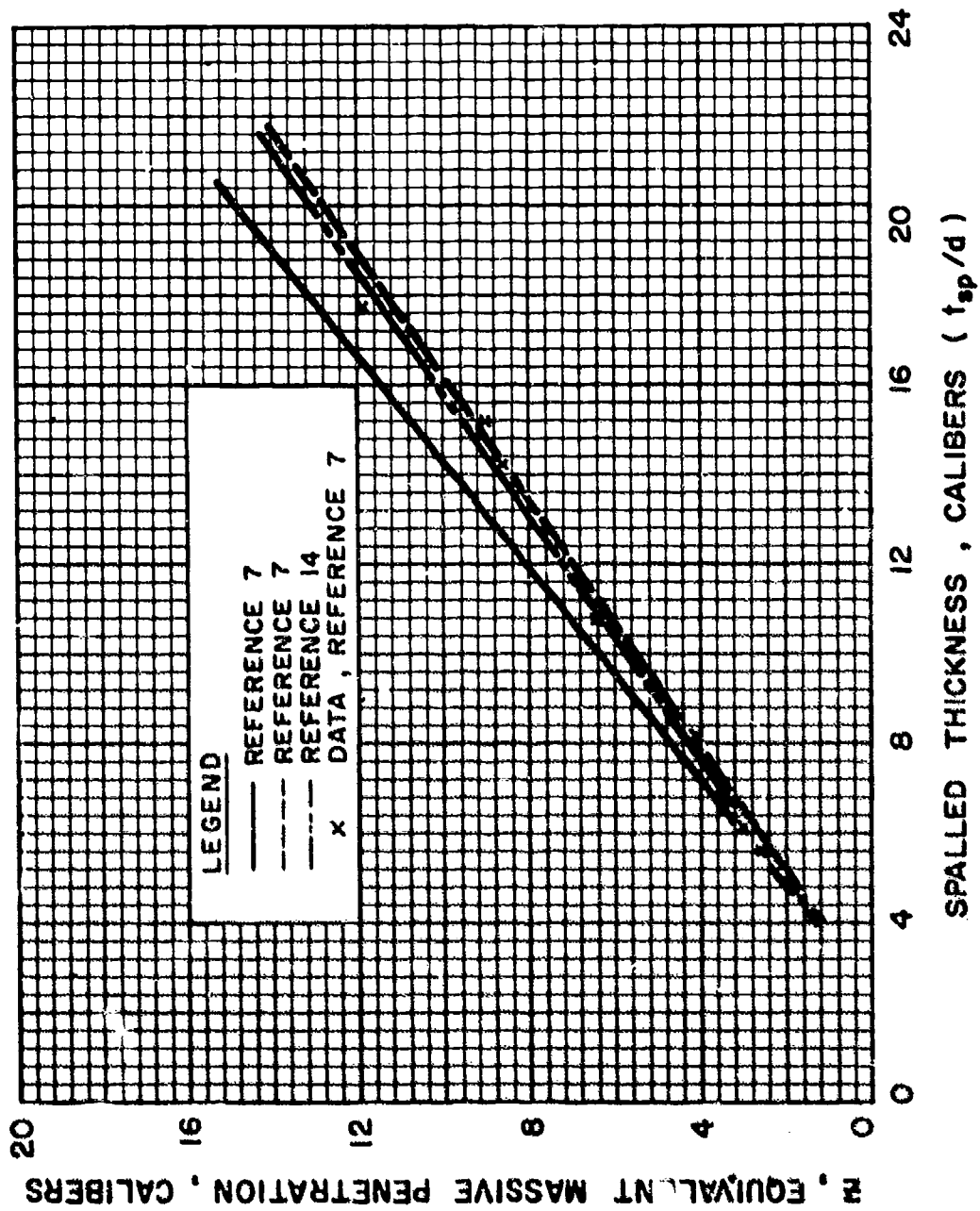


FIGURE 14 - SPALLING PREDICTION EQUATIONS

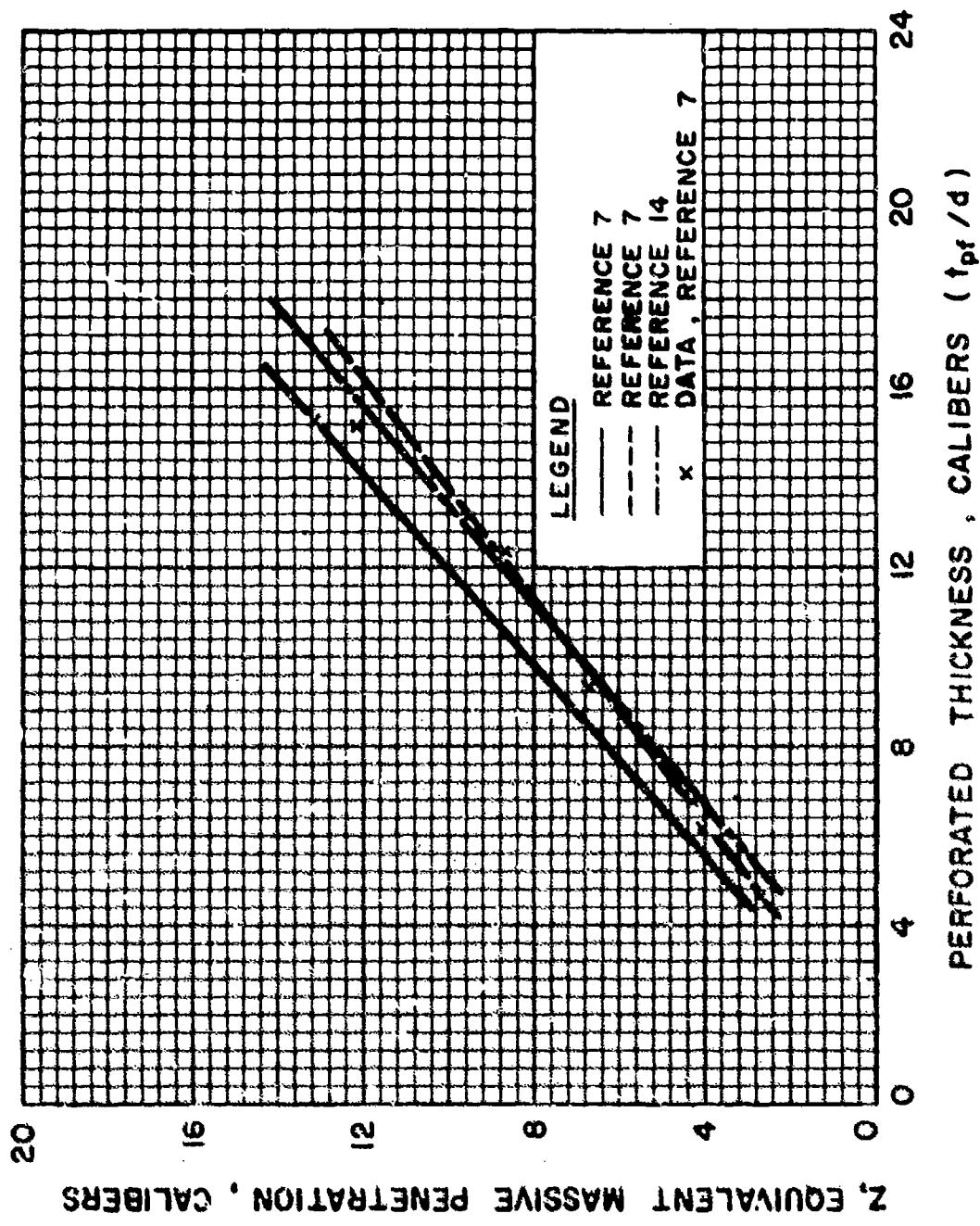


FIGURE 15 - PERFORATION PREDICTION EQUATIONS

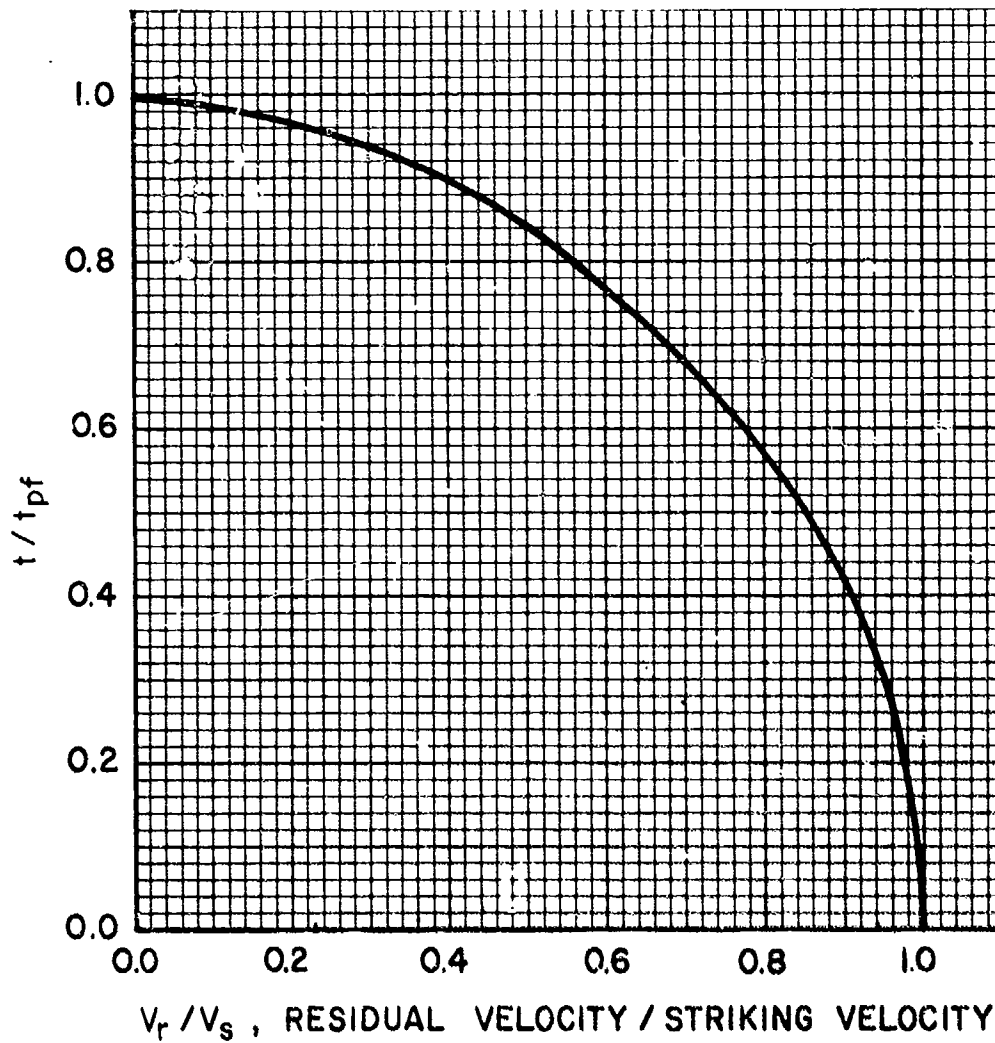


FIGURE 16 - RESIDUAL FRAGMENT VELOCITY UPON PERFORATION OF CONCRETE BARRIERS (FOR CASES WHERE $X \leq 2d$)

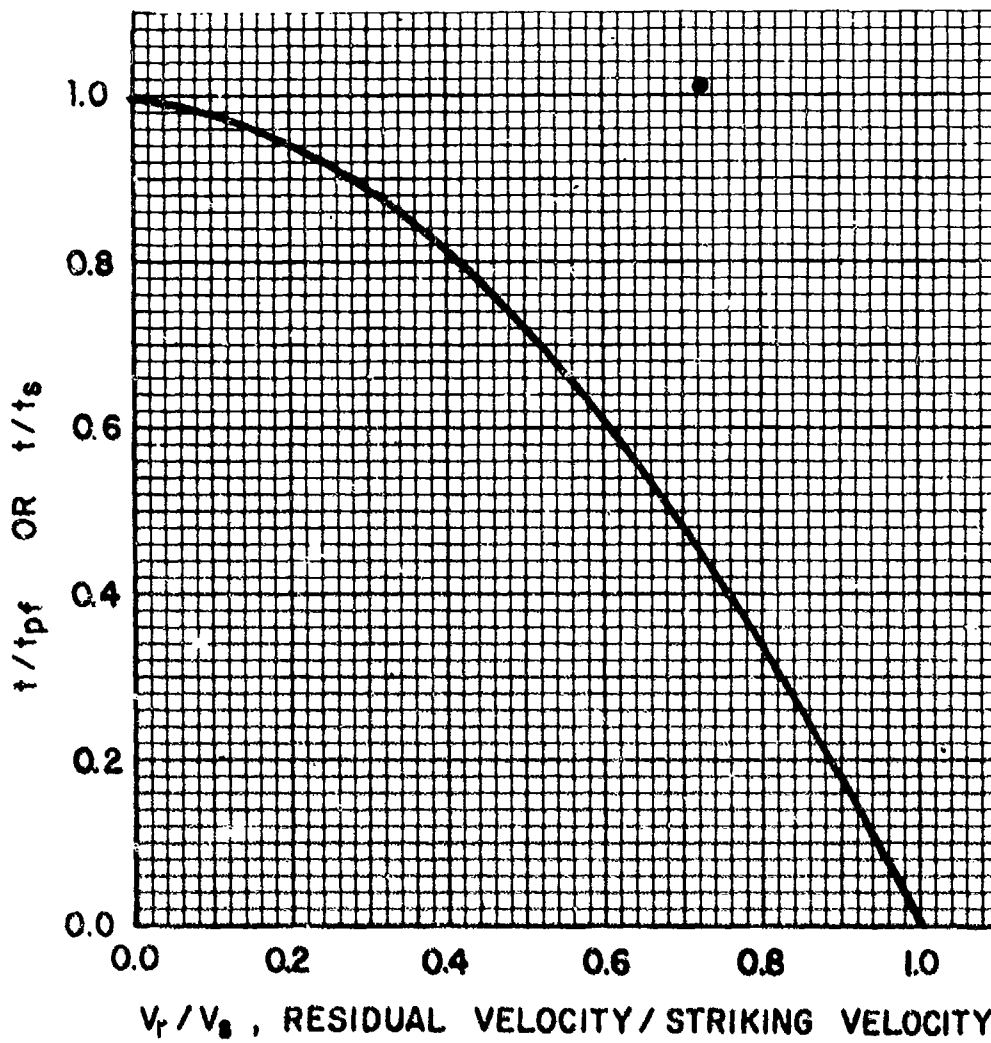


FIGURE 17 - RESIDUAL FRAGMENT VELOCITY UPON PERFORATION OF CONCRETE BARRIERS (FOR CASES WHERE $x > 2d$)

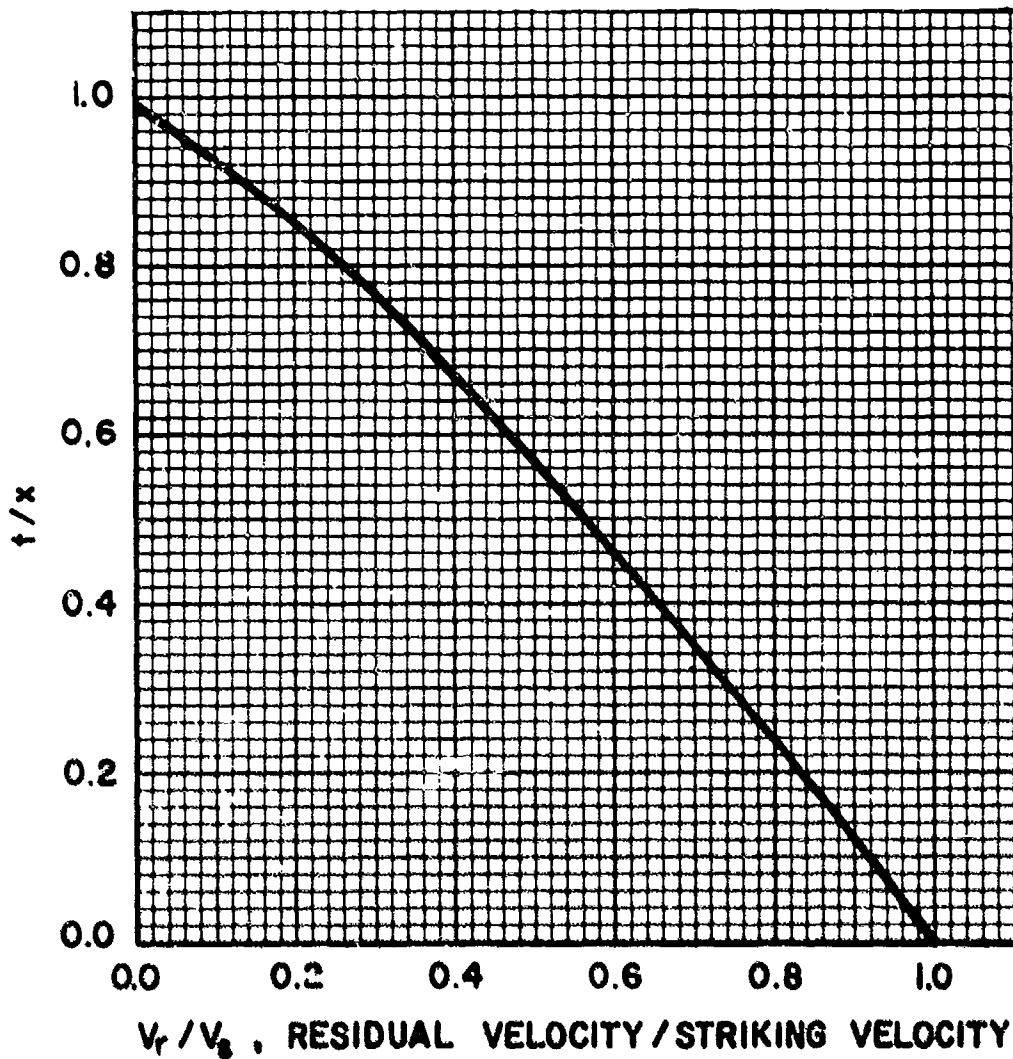


FIGURE 18 - RESIDUAL FRAGMENT VELOCITY UPON PERFORATION OF STEEL PLATE MATERIAL.

STEEL STRUCTURES TO RESIST
THE EFFECTS OF H. E. EXPLOSIONS

By

Paul Price, Picatinny Arsenal
Norval Dobbs, Ammann & Whitney

ABSTRACT

This paper summarizes the recent Picatinny Arsenal reports which delineate procedures for the design of steel structures to resist the effects of high explosive detonations. The data presented herein is similar to that given for reinforced concrete structures in TM 5-1300.

A discussion of the use of pre-engineered buildings as well as procedures used in the design of "Strengthened Frangible Construction" are included. Also discussed are the use of structural steel for both close-in and far range blast effects and economical factors to be considered at various design levels.

Preceding page blank

INTRODUCTION

In conjunction with the design of new and modified Army Ammunition Manufacturing Facilities, a broad requirement for structures which must provide personnel and/or expensive equipment protection in the event of an accidental explosion, has been identified.

At the present time, procedures are available for the design of protective structures for close-in and far-range effects, in the tri-service design manual "Structures to Resist the Effects of Accidental Explosions" (Reference 1). However, this manual is devoted primarily to the design requirements for reinforced concrete structures; the utilization of which at distances away from an explosion (far-range) may result in an uneconomical design.

To remedy this situation the Manufacturing Technology Directorate of Picatinny Arsenal as a part of its Supporting Studies Program for the U. S. Armament Command (ARMCOM), is in the process of developing design criteria for other materials such as structural steel, brick, clay tile, block, and precast concrete. This paper is devoted primarily to the application of structural steel for protective construction. A discussion of the effectiveness of current construction techniques and application of new techniques is presented. Also included is a cursory description of design procedures along with economical considerations related to the use of structural steel.

PRESENT DAY CONSTRUCTION EFFECTIVENESS

Most existing buildings at explosive loading and/or manufacturing facilities, which are located relative to potential explosions at unbarricaded intraline distances or greater, are either wooden structures from the 1942 era or pre-engineered buildings built within the last 10 to 15 years (Figure 1). Both building types provide less than a marginal degree of protection for the personnel and equipment at unbarricaded intraline distance; with damage to both types of structures approaching collapse.

At inhabited building distances, which correspond to blast incident overpressure of approximately 1.2 psi, the wood building frames and sidings will resist the blast pressures without significant damage. However, the doors and windows, which are numerous in the wood buildings (Figure 2), will fail producing debris hazards for the building occupants. On the other hand, failure of the doors and windows permits pressure flow into the structure. This internal pressure, in combination with the increased resistance provided by the relatively more massive timber members, helps to relieve the blast loads on the building exteriors and, therefore, minimizes the damage to the structure as a whole.

It may be well to consider the current practice under which standard pre-engineered buildings are supplied by the various manufacturers. The practice results in efficient and economical structures but does not readily lend itself to meeting the increased requirements of blast protective buildings. In general, a procedure for obtaining such a pre-engineered building is as follows. The designer shows the size and layout of the building and specifies the wind, snow, and earthquake loadings based on the location where the building is to be constructed. The manufacturer then uses this information as input to a design analysis which calculates the size of his standardized building

member components, i. e., wall panels, roofing, purlins, frames, etc. These standard size components are either pre-cut or fabricated through an automated or semi-automated manufacturing system. Under this procedure, only the foundation and architectural designs are required by the architect/engineer to furnish a pre-engineered building.

However, the conventional loadings and the standard component sizes do not cover the range of loads and component sizes required for blast protection. Also the blast load parameters cannot be given as input for the manufacturer's analysis without extensive modification of his current programs and fabricating procedure. Based upon the maximum wind, live and earthquake loads used for the various parts of the country, an estimate of the blast incident overpressure at which the building can be reusable is in the order of 0.2 psi., while an upper limit for the capacity of non-reusable structures is approximately 0.5 to 0.7 psi. The upper limit capacity is a function of the number of doors and windows which will fail and thereby relieve the external blast on the structure. It should be noted that the upper limit of pre-engineered buildings is less than 1.2 psi. or less than the overpressure associated with inhabited building distances.

To illustrate the vulnerability of the use of pre-engineered buildings for blast resistant construction, consider a recent explosive incident where a pre-engineered structure was subjected to a long duration (80 to 100 milliseconds) blast load having an incident overpressure equal to approximately 2.5 psi. The building was approximately 100 feet long by 50 feet wide and with a roof height varying from 16 feet at the edge of the building to 24 feet at the center. These heights were measured above a concrete floor slab which in turn was positioned 4 feet over the ground. Framework consisted of 4 interior, 50 foot long rigid frames spaced at 20 feet on center. The transverse end wall framework utilized columns and beams with diagonal bracing. The

siding and roofing was constructed of corrugated aluminum panels connected to the girts and purlins by 1/4-inch screws. A transverse 8-inch concrete block wall was located at the second and fifth frame from the front (side facing the blast) of the building. Equipment and personnel access doors were located within the side wall of the building.

Figure 3 is a plan layout of the building.

The damage to the building was severe (Figure 4); and was of a magnitude which would produce injury to personnel. The south wall (wall facing the blast), west and north walls and roof failed producing large holes in these surfaces of the structure. The east wall sustained damage but did not fail because of the failure of the doors in this surface which afforded relief for the exterior blast loads. The block wall near the front of the structure remained intact. The pressures penetrated the west wall at the rear of the block wall and relieved the pressures which had penetrated the front wall of the building. On the other hand, relief was not afforded for the rear of the second block wall and the pressures which entered the west side of the building failed this wall. Flying blocks, in addition to the blast pressure, penetrated and deformed the rear wall of the building. Although little damage was sustained by the frames, some of the purlins and girts yielded and buckled. The siding and roof that remained were highly deformed with deflections approaching those that would be formed if the siding acted as a catenary. The minimum damage to the frame was due to the roof failure which considerably reduced the blast loads acting on the framing.

Another pre-engineered building which was closer to the explosion than the above structure, sustained more severe damage than the first structure. The front of this structure was subjected to an overpressure of 3.5 psi. which corresponds to that produced at unbarricaded intraline distance. Here, about fifty percent of the siding and roofing were either dislodged or near dislodge-

ment (Figure 5). It may be noted in Figure 6 that another open ended corrugated steel structure which also was located at the 3.5 psi. overpressure level was virtually undamaged. In this case, both the front (side facing the detonation) and rear of the structure were open. The blast wave passing through the interior of the structure equalized the external blast loads.

DESIGN MANUAL

The manual for the design of steel structures to resist the effects of H.E. explosions is contained in two Picatinny Arsenal reports (References 2 and 3) which will be published in the near future. The first report, titled "Use of Structural Steel in the Design of Structures to Resist the Effects of H.E. Explosions", deals primarily with the analysis of steel elements which can be analyzed as a single-degree-of-freedom system while the methods given in the second report are used for the performance of multi-degree-of-freedom system analyses. The latter report which is applicable to both structural steel and reinforced concrete is titled "Analysis of Frame Structures Subjected to Blast Overpressures".

Included in the first report are the procedures for structural steel design which are similar to the information given for reinforced concrete in TM 5-1300 (Reference 1). Procedures are given for the determination of ultimate strengths of wide flange and standard I - sections, channel elements, structural steel plates and corrugated metal sections (Figure 8). Also contained in this report are static and dynamic properties of steel columns and beams; as well as recommended types of steels and details to be used for blast load design and structural response. In the latter case, permissible deflections of elements are specified for buildings which are either reusable or non-reusable.

In addition to the above, the first report contains a series of charts to simplify the design of beam elements including purlins, spandrels and girts.

Here, required member sizes are specified for various span lengths, spacings and peak blast loads and durations. The charts include solutions for simply supported, fixed, and multi-span elements. The charts have been developed for both reusable and non-reusable structural response conditions.

Figure 9 illustrates a typical design chart. The data presented in the first report is so arranged that it supplements (does not repeat) the data given in References 1 and 4.

The second report describes the solution for performing nonlinear dynamic analysis of one or two dimensional rigid frames. The method of analysis, which has been programmed for solution on a CDC 6600 computer, utilizes a lumped parameter method to represent the masses and stiffnesses of a frame. Solution of the equations of motion is accomplished by a direct integration using the linear acceleration procedure. Nonlinear behavior of the frame is accomplished by using a bilinear stress-strain diagram and by the formation of plastic hinges at the points of maximum moments having values equal to the plastic moments for the cross-section of the member at these points. The combined effects of axial loads and bending is considered to define points of hinge formation or material yielding.

The computer program is capable of analyzing multi-bay and/or multi-story frames and has the following features:

1. The application of dynamic loads in the horizontal and vertical directions; either in combination or separately.
2. The use of either pinned or fixed end conditions for both the beams and the columns.
3. The interaction between axial loads and displacements.

The computer program input data includes the modulus of elasticity of the material of construction, structural geometry (member length, slope, etc.), type of support connection and capacity at yield (axial load and moment) of individual elements and applied loads (time-history relationships). The output data for individual elements includes:

1. Time history of joint and member displacements, accelerations, and velocities.
2. Time history of end shears and moments, and middle span moments.
3. Maximum and minimum displacements.
4. Maximum tensile and compressive axial loads, and associated bending moments and shears.
5. Maximum positive and negative bending moments and associated axial loads and shears.

Call out of the individual output data is optional depending upon the needs of the designer. The above output can be used in combination with the data given in Reference 2 for the design of individual elements of a frame.

APPLICATION OF STEEL DESIGN

As may be expected, structural steel elements designed to resist blast overpressure, will be stronger and heavier than steel elements designed to sustain conventional loads. However, in the event of an explosion within the steel building, the structure will fail with resulting fragments. Therefore, the mass of structural steel elements should be kept to a minimum. Because steel structures must exhibit strength rather than mass, this type of construction is referred to as "Strengthened Frangible Construction" i. e. construction done by materials used for conventional loads which have been strengthened to resist blast loads. Use of strengthened frangible construction is usually practical up to blast overpressure level of approximately 10 psi. At higher pressure levels, the use of reinforced concrete begins to be economical. To illustrate the use of strengthened frangible material consider the following three case studies.

Case Study I (Line Office)

Line offices for many munition manufacturing facilities are located away from the main production line. For the case at hand, the line office is situated at approximately inhabited building distance from the nearest building

containing explosive. Therefore, in the event of an explosion, the line office would be subjected to an incident overpressure of 1.2 psi. with the responding reflected pressure of 2.5 psi.

For this case study, the line office is 62 feet long and 30 feet wide (Figure 10) and has an overall height of approximately 12 feet. Basically, the building is constructed of seven rigid portal frames each of which spans in the short direction of the building (Figure 11). Each member of the portal is 12 W 31.

Exterior walls of the building are constructed of 8-inch concrete blocks. Each horizontal course of the block walls is reinforced with extra heavy Dur-O-Wal; thereby furnishing the necessary strength for the walls to span between the columns of the rigid frames. It may be noted that the 10 ft.-0 inch spacing between the adjacent frames was predetermined by the ultimate strength of the walls. To prevent the walls from collapsing either as a result of rebound and/or negative overpressures, the block walls are connected to the columns supports by anchor straps. Corners of two intersecting block walls are provided with reinforcement to insure continuity between the walls at the corners.

Access into the building is through a series of blast doors constructed of light metal frame and cover plate. Blast doors are discussed later in this paper.

Roof of the building (Figure 12) is constructed of 18 gage corrugated (top hat section with backup plate) metal decking which spans between the spandrels of the adjoining frames. The decking is supported and bolted to spandrel beams of the rigid frames. The bolts provide the continuity for the decking to resist both the positive and negative pressures. The top hat section (with backup plate) metal roof has been selected because of its unique characteristics where the flat (backup) plate portion of the decking provides the necessary lateral restraint to prevent the corrugated portion of the deck-

ing from collapsing intermediate of its supports as a result of the impingement of the blast loads. It may be noted that in this case, the tie-down bolts are located in the valleys of the corrugation to permit placement of insulation and standard roofing over the metal decking.

Case Study II (Process Building)

The amount of structural steel required for buildings designed for blast overpressures will exceed that required for conventional loads. An evaluation of this increased amount of steel is illustrated by this case study.

Plan dimensions of the building are 59 feet long by 46 feet wide. The two shorter end walls are constructed of reinforced concrete. A third reinforced concrete wall positioned parallel to but intermediate of the end walls divides the building into two separate areas. The remainder of the exterior surfaces (two walls and the roof) are constructed of structural steel.

Initially, the steel portion of the building was designed for wind and earthquake loads. The resulting members consisted of light tubular columns and beams which supported a light metal roof decking and wall paneling (Figure 13). The original steel design did not consider the effects of blast loads.

Because the building which will contain personnel is considered vulnerable to a potential explosion in an adjoining building whose operation has been automated, the structural steel portion of the building has been redesigned to resist a blast overpressure in the order of 4.4 psi. (both roof and walls). Although the resulting increased cost of the steel was in the order of 325 percent of that of the conventionally designed steel, the overall cost increase of the structural portion of the building was only approximately 33 percent. Here, the major structural cost was due to the concrete (walls and foundation slab) portion of the building.

Figure 13 illustrates the variation in members required to change from conventional (frangible) construction to strengthened frangible construction.

Case Study III (Process Building)

As may be expected, the cost of construction of blast resistant structures will vary with the magnitude of the blast overpressures. To illustrate this variation, consider the following building layout as given in Figure 14.

This Process Building is 87 feet long, 68 feet wide and has a height of 15 feet. The construction consists of structural steel rigid frame supported on a reinforced concrete mat foundation slab. The roof and walls are covered with structural steel decking. Entrances into and exits from the building are through a series of blast doors.

Figure 15 illustrates the variation in cost as a function of the incident blast overpressure for both the structural steel or "hardened" portion of the building and the overall cost. This latter cost, in addition to the structural steel cost, includes the architectural, HVAC, piping, electrical and the reinforced concrete floor slab and foundation costs.

The percent increase in the cost of the structural steel portion of the building decreases with an increase in the overpressure level as shown below.

OVERPRESSURE (Psi.)	PERCENT INCREASE (%)
0 to 0.5	80
0.5 to 1.0	22
1.0 to 1.5	13
1.5 to 2.0	11
2.0 to 2.5	10

The largest percentage cost increase of the structural steel is realized in the lower pressure range, i.e. between 0 and 0.5 psi. Here, the major cost difference is attributed to the change from conventional construction to the blast resistant construction. Above the 0.5 psi. level, the cost increase

with pressure level decreases rapidly, with the percent increase leveling off to 10 percent at the 2.5 psi. overpressure level. At unbarricaded intraline distances (pressure level of approximately 3.5 psi.), the cost increase is estimated to be about 10 percent above that for the 2.5 psi. level.

Although the above cost variation is typical, the overall cost of structural steel at pressure levels corresponding to unbarricaded intraline distance is three times as high as compared to the cost for conventional construction. However, the overall cost of the blast resistant structure is approximately 33 percent above that of a similar conventional building.

BLAST DOOR

Type of blast doors may be classified based upon the blast pressure levels and fragment environment involved. For relatively high pressure levels and/or where high speed fragmentation will result due to a blast, steel blast doors should be constructed from heavy steel plates. At lower pressure levels (50 psi and less) built-up steel door construction may be used.

The use of steel plate construction is usually applicable where protection is required from the "close-in" effects of relatively small explosive quantities i. e. in order of several hundred pounds of explosives. Use of structural steel for larger quantities usually will not be cost-effective.

One such arrangement for steel plate doors is illustrated in Figure 16. Here, the direct load produced by the blast will be transmitted from the door to its support by bearing whereas reversal action of the door and effects of negative pressures are transmitted to the door supports by a series of reversal bolts. Bolts are provided on both vertical sides of the door in order to eliminate the need for transmitting reversal action through the door hinges. For wider doors the reversal bolts are used at the top and bottom of the door to insure two way action of the plate. The reversal mechanism of steel plate doors should be strong to resist 100 percent of reversal effects.

As previously mentioned, where fragments are not involved and low blast pressures exist, the more conventional built-up door construction may be used. Nevertheless, at low pressures where fragments may occur, plate doors are needed.

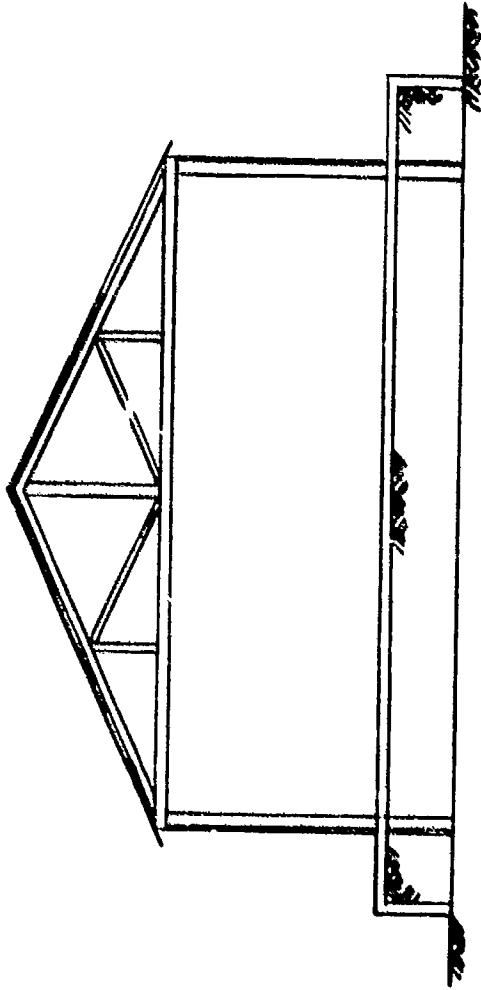
A typical layout of a built-up steel door is illustrated in Figure 16, where the frame of the door consists of a series of channel sections with other channel sections serving as intermediate supports for the "skin" plate of the door. All sections and the plate are welded together. For

personnel doors (3'-0" x 1'-0"), minimum size channels (3 inches in depth) may be used. The thickness of the skin plate will be 1/4 inch or less.

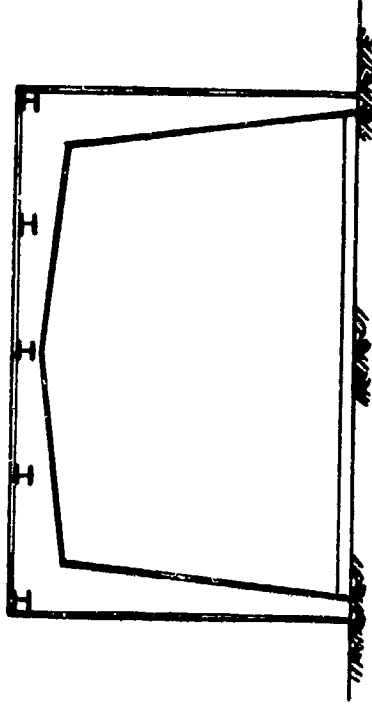
Reversal mechanisms for built-up doors are similar to those used for plate doors except that hinges usually can be designed to serve as the reversal mechanism for one side of the doors.

REFERENCES

1. Structures to Resist the Effects of Accidental Explosions, Department of the Army and the Navy and the Air Force Technical Manual TM 5-1300, June 1969.
2. "Use of Structural Steel in the Design of Structures to Resist the Effects of H. E. Explosions", Picatinny Arsenal Technical Report, Draft.
3. "Nonlinear Analysis of Frame Structures Subjected to Blast Overpressures", Picatinny Arsenal Technical Report, Draft.
4. "Manual of Steel Construction" Seventh Edition, American Institute of Steel Construction, Inc. New York, N.Y.

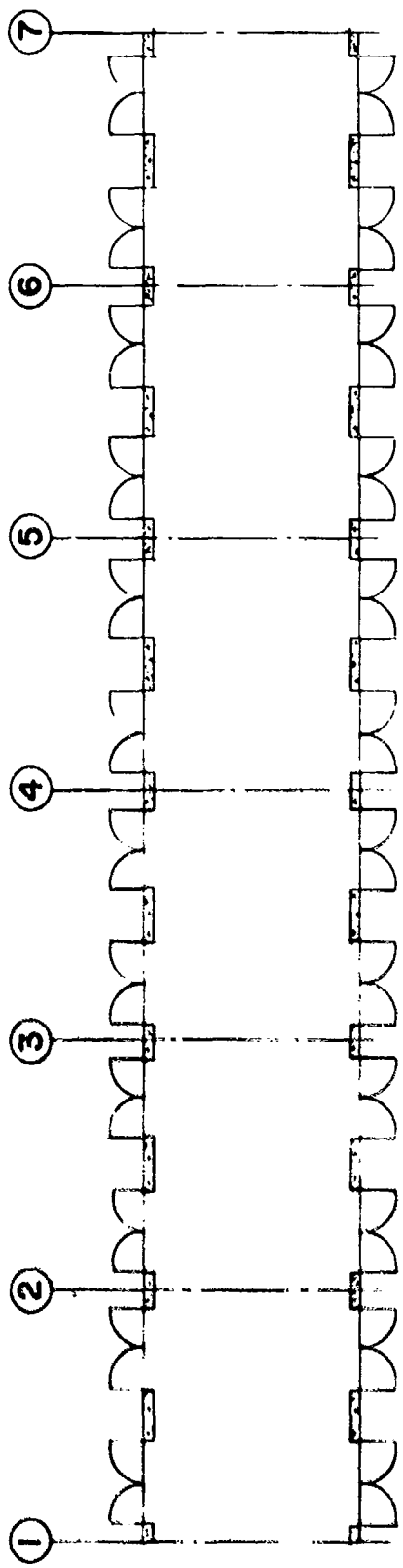


WOOD OR CLAY TILE CONSTRUCTION
(1942 ERA)

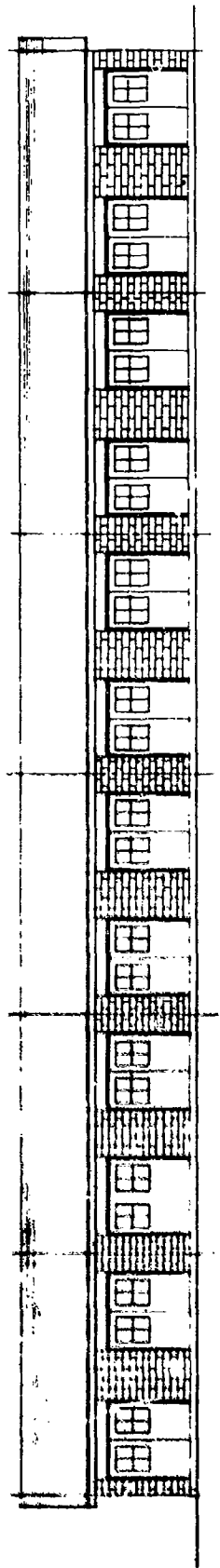


PRE-ENGINEERED BUILDING
(PRESENT TIME)

FIGURE - 1
EXISTING CONSTRUCTION



PLAN



ELEVATION

FIGURE - 2
TYPICAL WOODEN BUILDING

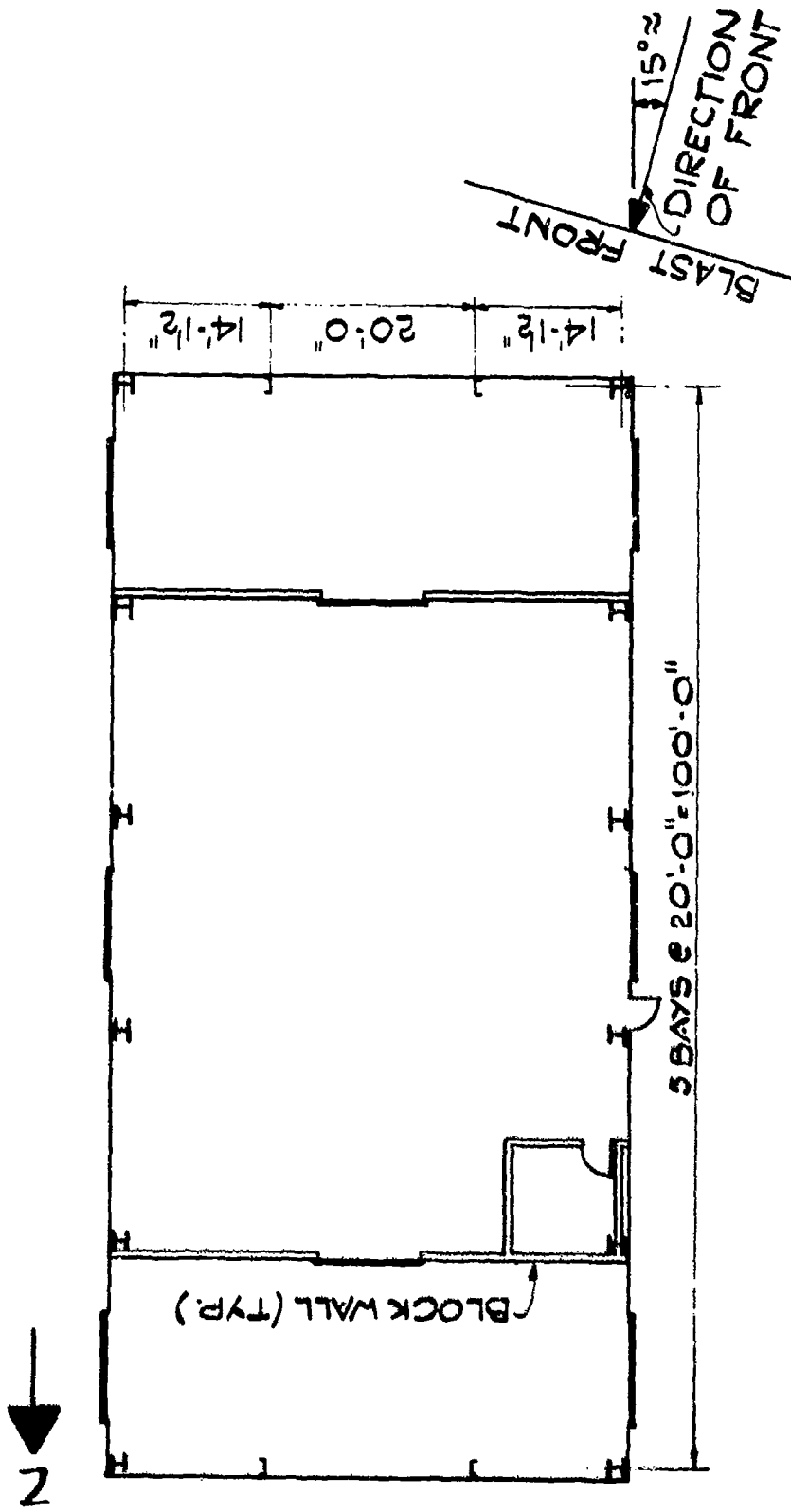


FIGURE - 3
LAYOUT OF BUILDING NO. 1



FIGURE - 4 A
FRONT WALL OF BUILDING NO. 1 (EXTERIOR VIEW)
($P_{30} \approx 2.5 \text{ psi}$)

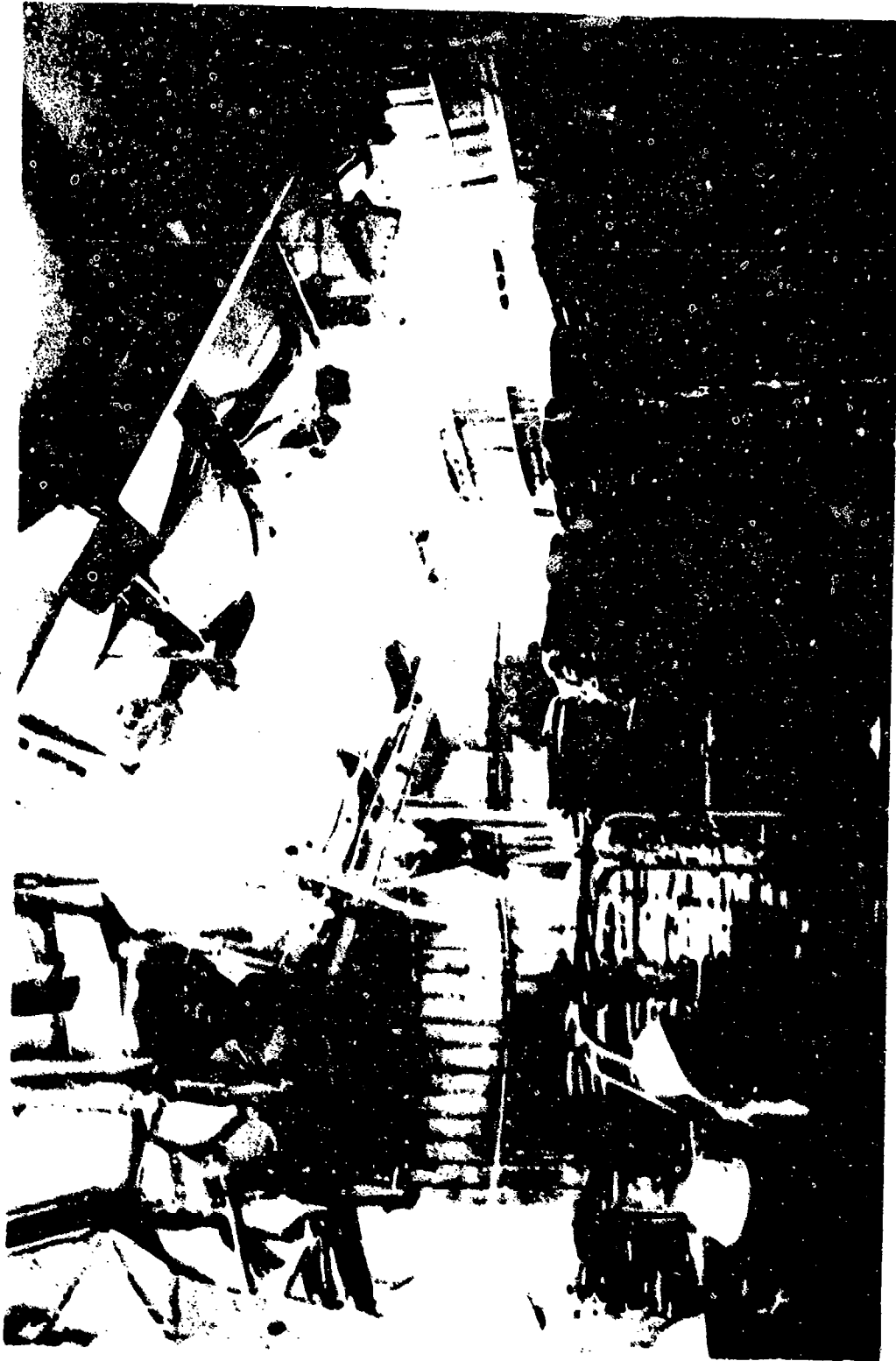


FIGURE - 4 B
REAR WALL OF BUILDING NO. 1 (INTERIOR VIEW)
(Pso \approx 2.5 psi)



FIGURE - 4C
REAR WALL OF BUILDING NO. 1 (EXTERIOR VIEW)
(P₅₀ ≈ 2.5 psi)



FIGURE - 5A
INTERIOR VIEW OF BUILDING NO. 2
($P_{so} \approx 3.5$ psi)



FIGURE - 5B
SIDE WALL OF BUILDING NO. 1 (EXTERIOR VIEW)
(Pso \approx 3.5 psi)

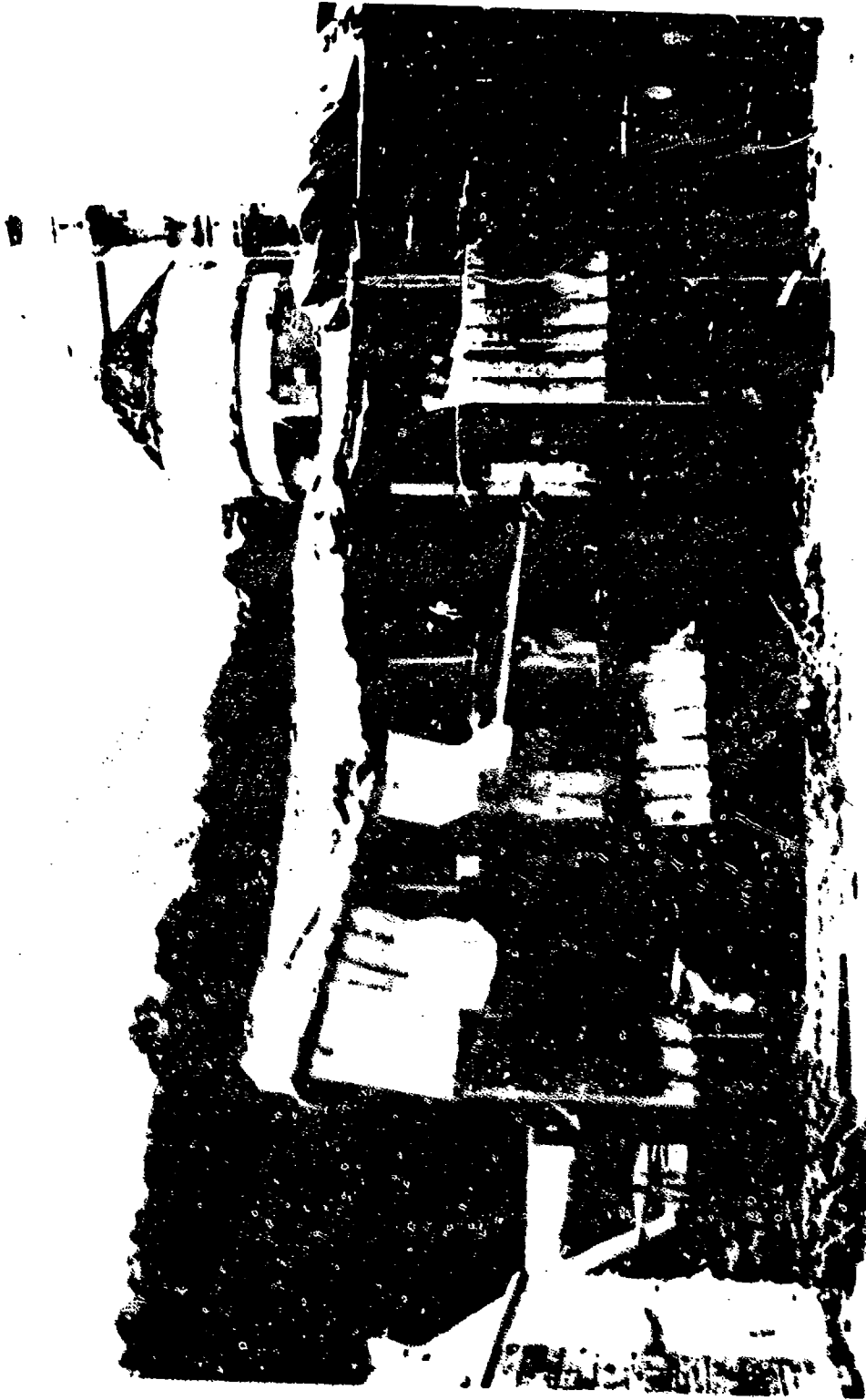
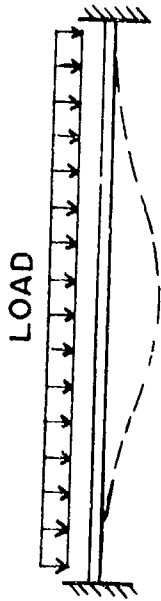


FIGURE -5C
SIDE WALL OF BUILDING NO. 2 (EXTERIOR VIEW)
(Pso \approx 3.5 psi)

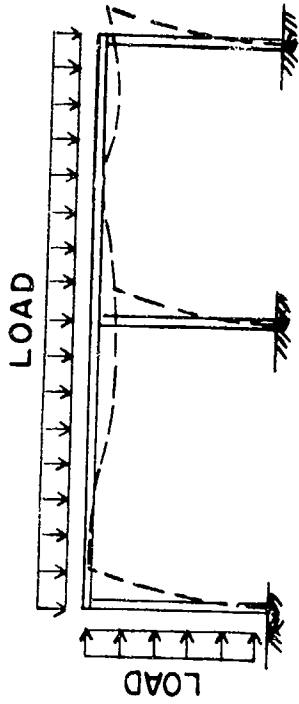


FIGURE - 6
UNDAMAGED BUILDING ADJACENT TO BUILDING NO. 2
($P_{so} \approx 3.5$ psi)



SINGLE DEGREE OF FREEDOM SYSTEM

REPORT NO. 1
 USE OF STRUCTURAL STEEL
 FOR THE DESIGN OF
 STRUCTURES TO RESIST THE EFFECTS
 OF H.E. EXPLOSIONS



MULTI DEGREE OF FREEDOM SYSTEM

REPORT NO. 2
 ANALYSIS OF FRAME STRUCTURES
 SUBJECTED TO
 BLAST OVER PRESSURES

FIGURE - 7
 DESIGN MANUAL



WIDE FLANGE



I - SECTION



CHANNEL



FLAT PLATE



CORRUGATED PLATE

1. Ultimate Strength
2. Static and Dynamic Properties
3. Recommended Steel Type and Detailing
4. Deflection Criteria for Reusable and Nonreusable Structures

FIGURE - 8
TYPICAL STRUCTURAL SHAPES

- CONSTANT VALUES :
- SPECIFIC MEMBER SIZE
 - SPAN / DEFLECTION RATIO

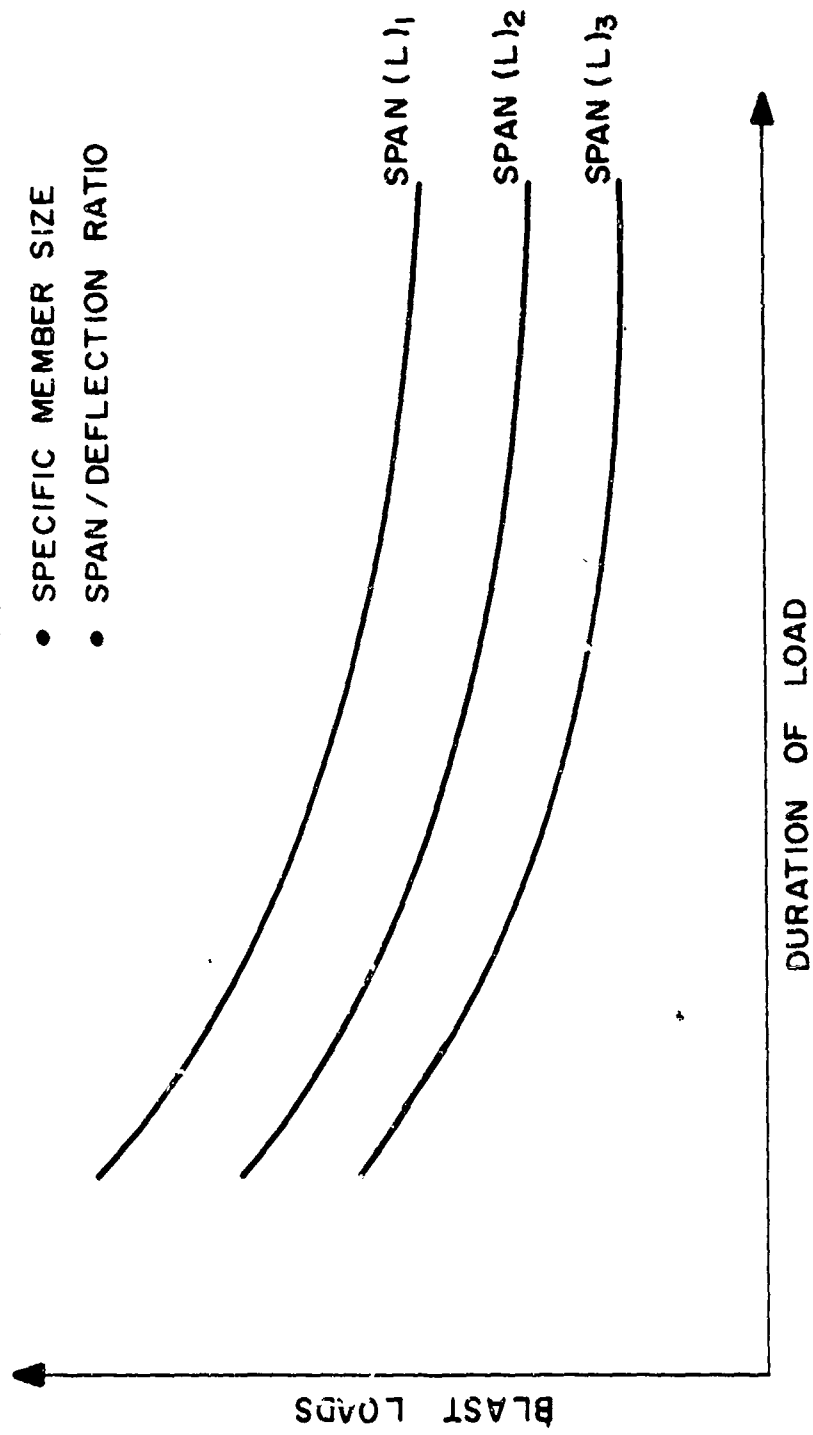


FIGURE - 9
TYPICAL DESIGN CHARTS

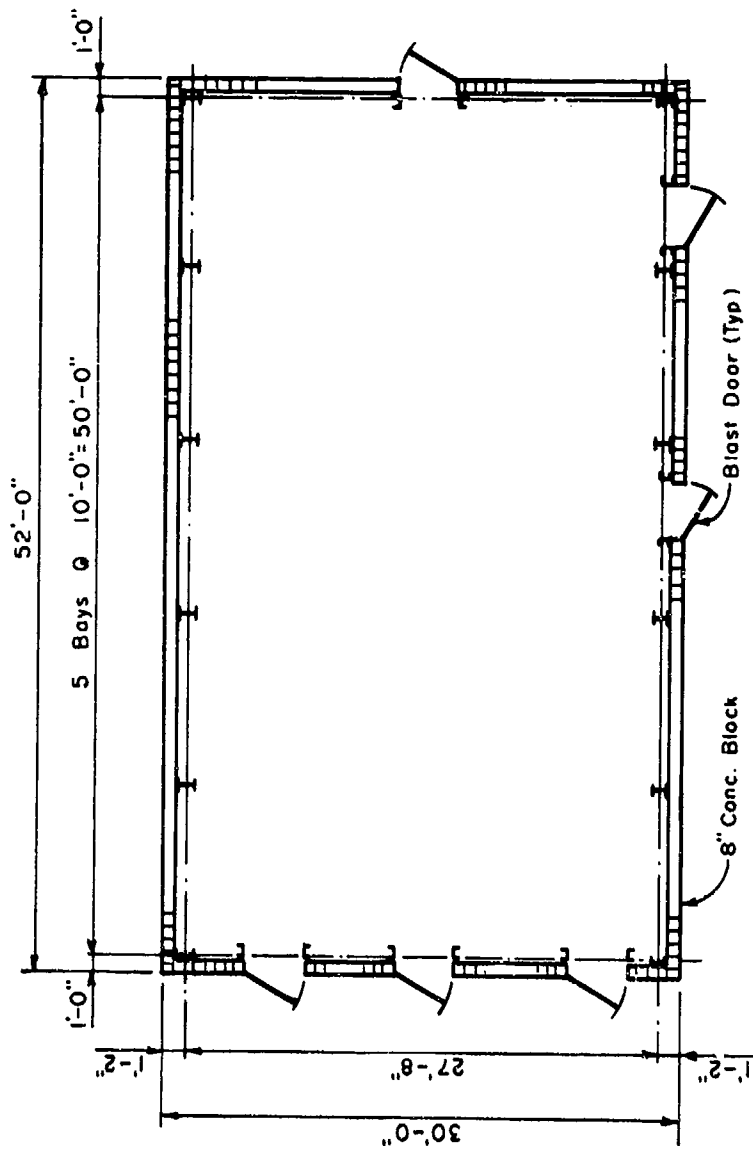
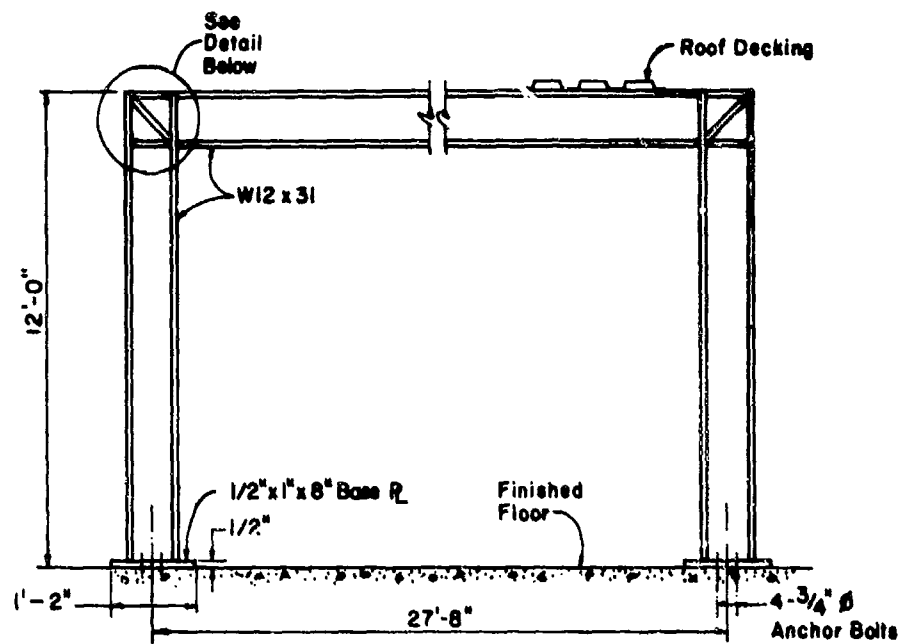
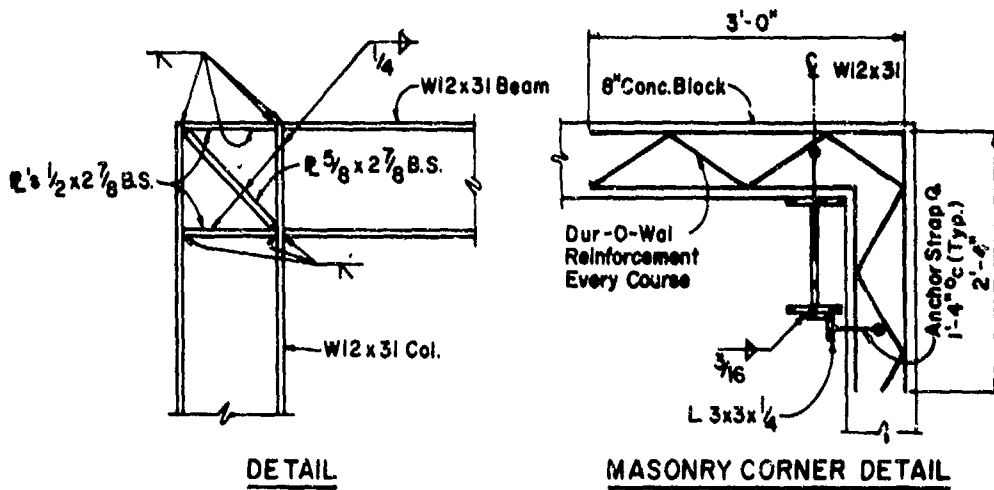


FIGURE - 10
OFFICE BUILDING



RIGID FRAME



DETAIL

MASONRY CORNER DETAIL

FIGURE - II
RIGID FRAME DETAILS

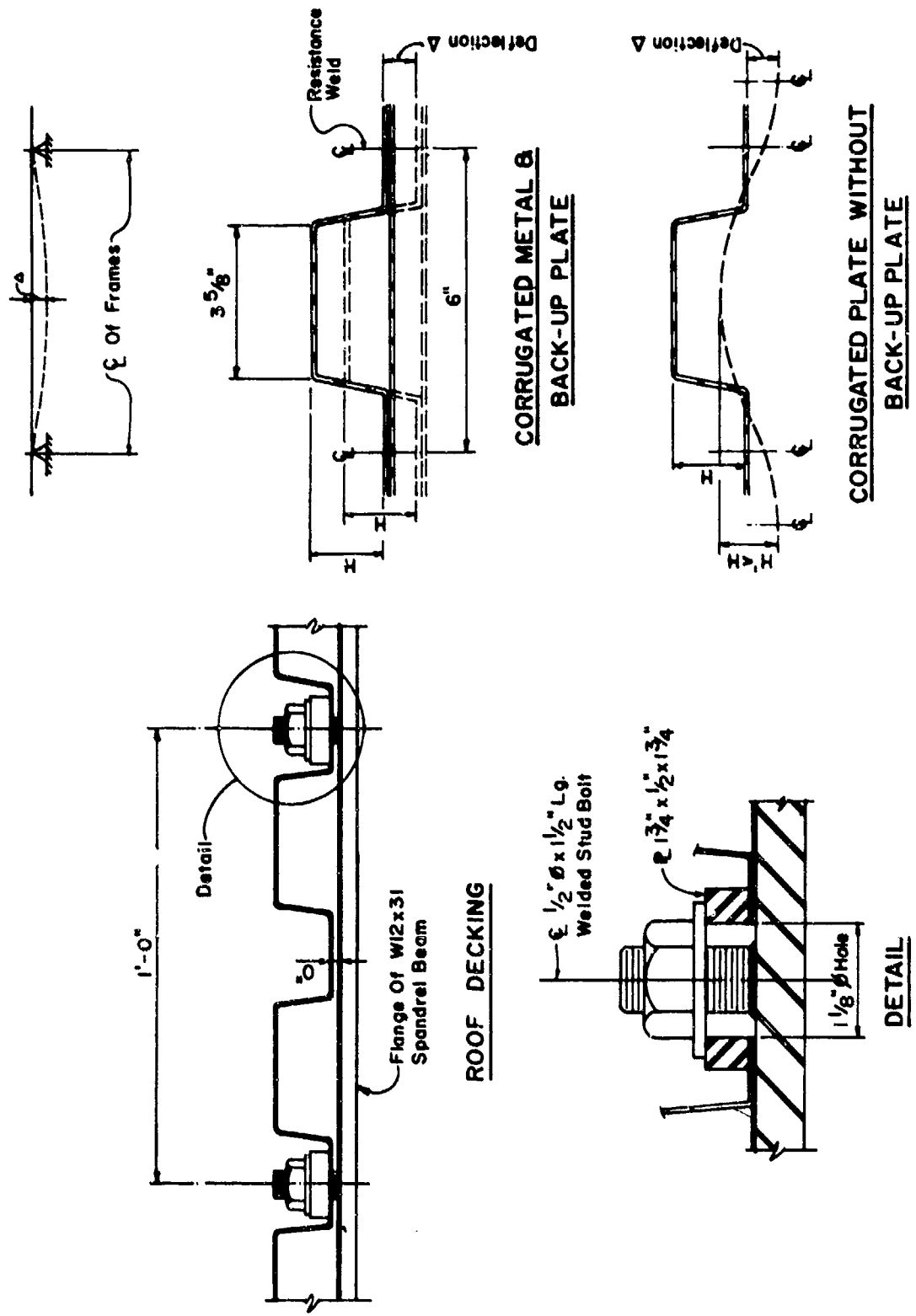
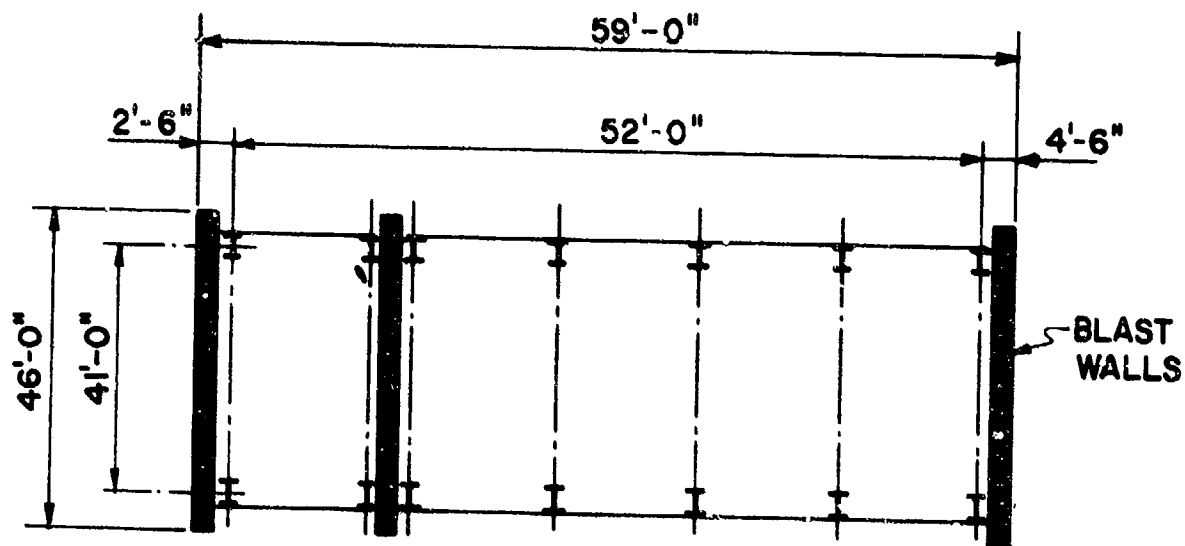


FIGURE - 12
CORRUGATED METAL ROOF DETAILS



ELEMENTS	STEEL DESIGN	
	CONVENTIONAL (P=0.0 psi)	BLAST (P=4.4 psf)
WALL PANELS	20 GA. (2.2 psf.)	UKX-18/18 (4.8 psf.)
ROOF PANELS	DC 4.5 - 18/18 (5.4 psf.)	UKX-18/18 (4.8 psf.)
GIRTS (WALLS)	TS4x6x1/2(12'-9") (15 lbs/Ft)	W8x28(4'-6") (28 lbs/Ft.)
PURLINS (ROOF)	TS4x6x1/4(7'-0") (15 lbs/Ft.)	W8x28(4'-6") (28 lbs/Ft.)
COLUMNS	TS 6x6x1/2 (35 lbs/Ft.)	W18 x 105 (105 lbs/Ft.)
GIRDERS	TS 6x8x1/2 (41 lbs/Ft.)	W24 x 100 (100 lbs/Ft.)

FIGURE-13
 VARIATION OF MEMBER SIZE
 (CONVENTIONAL & BLAST DESIGN)

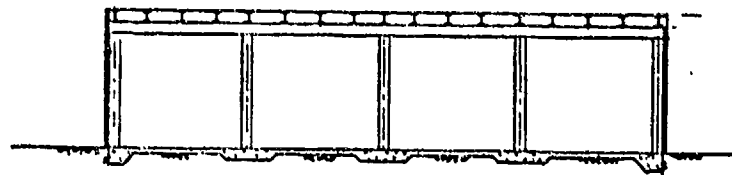
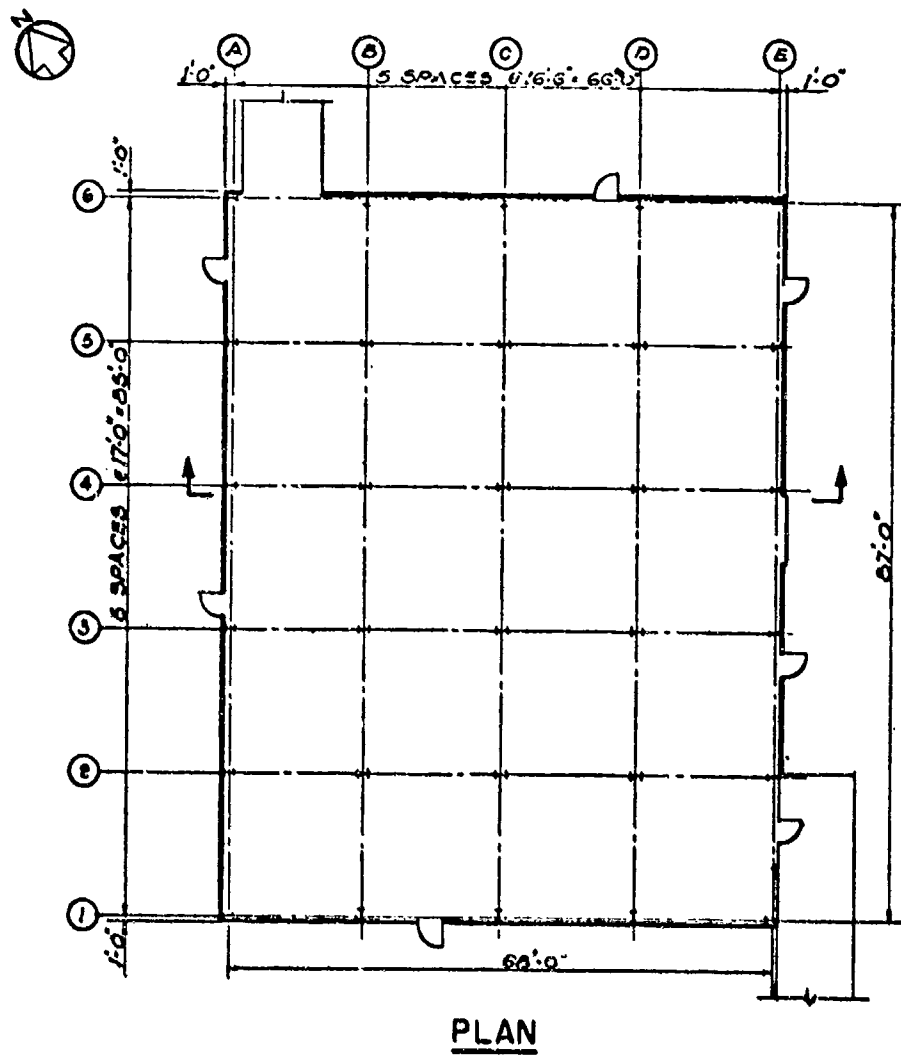


FIGURE-14

PROCESS BUILDING (Case Study III)

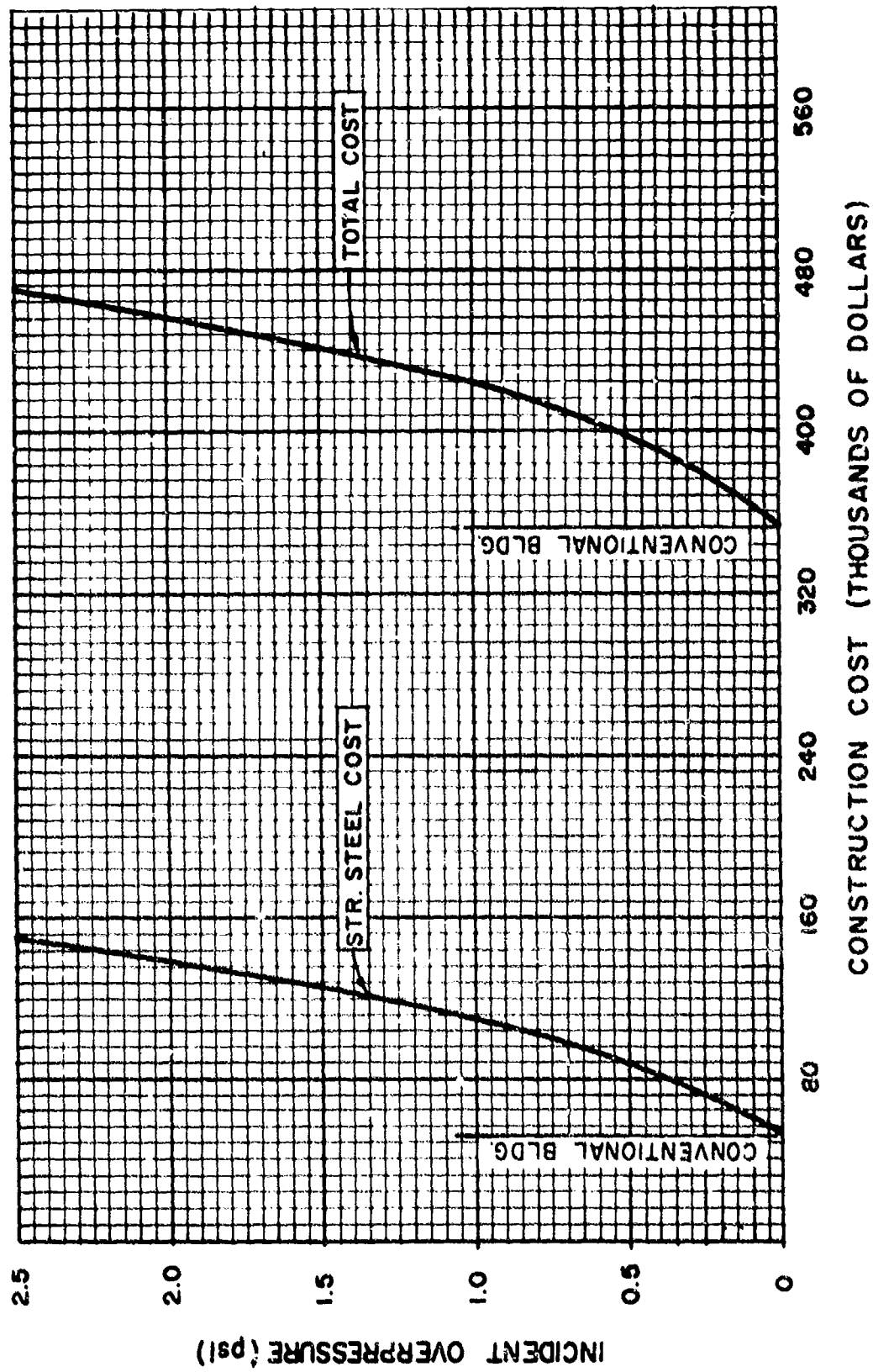


FIGURE - 15
 CONSTRUCTION COST VS. INCIDENT OVERPRESSURE
 (STR. STEEL BLDG.)

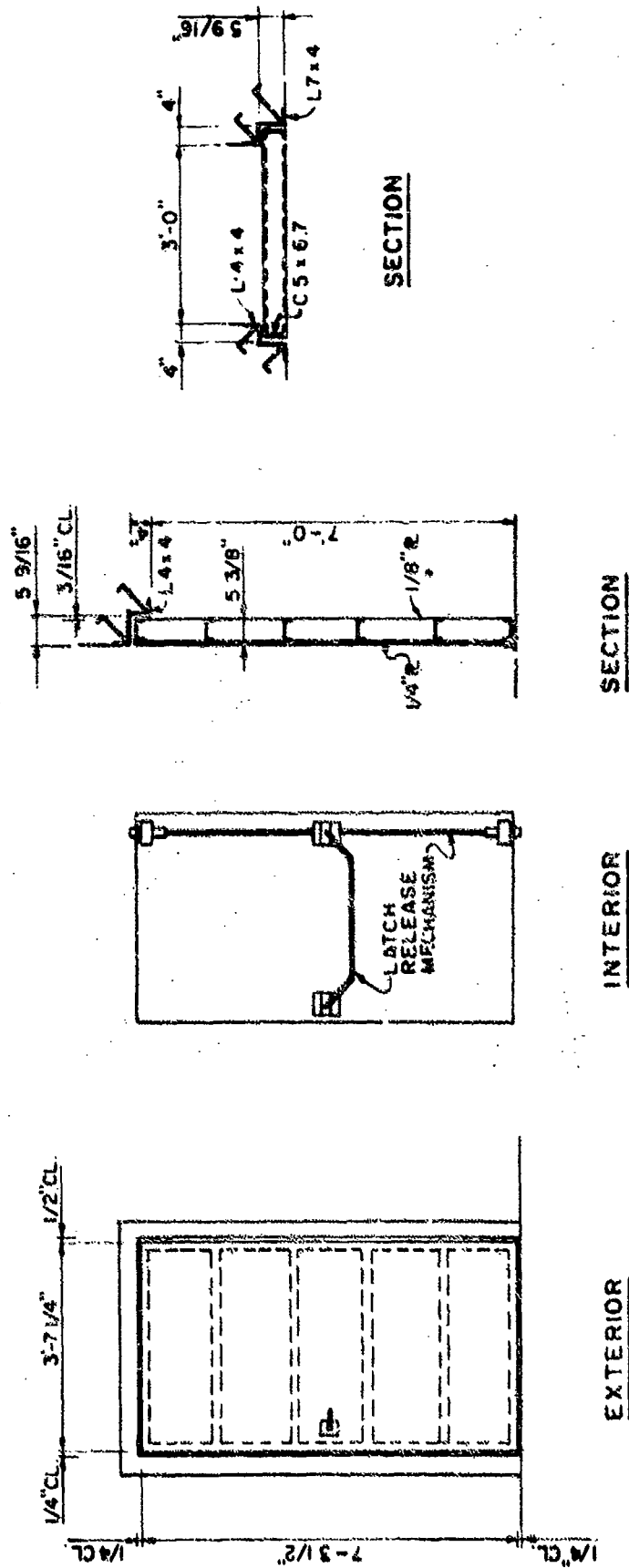
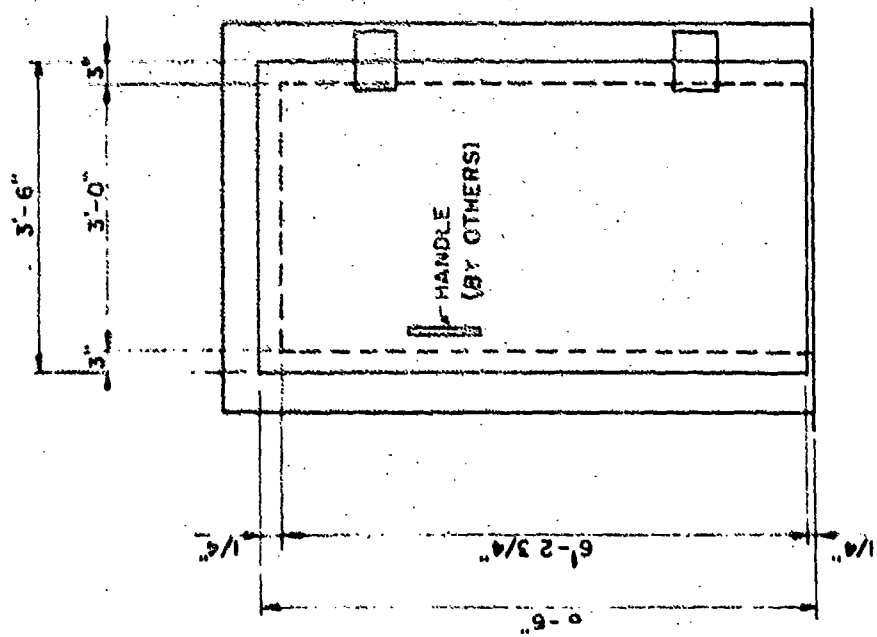
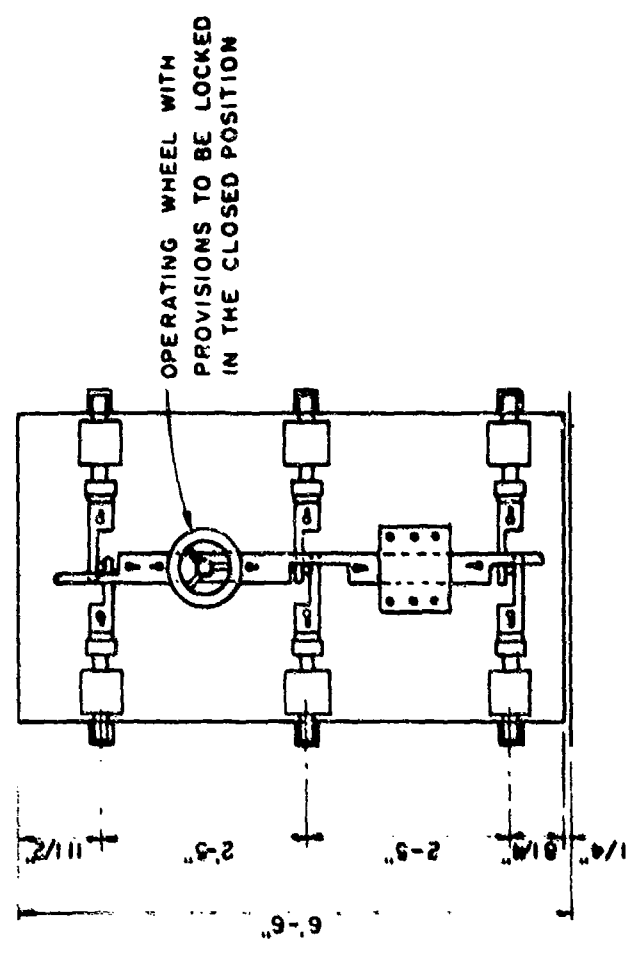


FIGURE - 16A
BUILT - UP BLAST DOORS



INTERIOR



EXTERIOR

FIGURE - 16B
STEEL PLATE BLAST DOORS

EXPLOSIVE-RESISTANT DESIGN
FOR THE
DEMILITARIZATION FACILITY, NAVAL AMMUNITION DEPOT
HAWTHORNE, NEVADA

by

Dirk van Erp, Project Architect, Keller & Gannon
Consultants, Engineers and Planners
and
Frits Fenger, Project Engineer,
Tudor Engineering Company
San Francisco, California

ABSTRACT

This paper reports on an explosive-resistant design project for the Demilitarization Facility of the Hawthorne Naval Ammunition Depot. The design criteria state that, in the event of an incident in one of the ammunition-handling buildings, there shall be no possibility of sympathetic detonation of energetic materials, personnel shall be protected from overpressure and fragmentation, and materials, equipment, and structures shall be protected from disabling damage. The functional arrangement of the facilities was also a consideration. The paper discusses the considerations that impacted the design, as well as the specific design problems encountered and their solutions. Some comments are made concerning NAVFAC P-397, since this is the first time a complete facility has been designed in accordance with this document.

A Demilitarization Facility is presently being constructed for the Navy at the Naval Ammunition Depot, Hawthorne, Nevada. This facility will offer an alternative to previously used but now environmentally unacceptable methods for disposing of obsolete munitions, such as deep-water ocean dumping and open burning. The facility, when complete, will provide the capability for demilitarizing nearly all of the Navy's present inventory of conventional munitions, including gun ammunition for 0.30 caliber bullets through 16-inch projectiles, bombs, mines and depth charges up to 3,000-pound TNT equivalent charge weight, cluster weapons, rocket warheads, grenades, and some pyrotechnics. This facility, which is designed to disassemble large quantities and many varieties of munitions, is the first of its kind. It represents a new concept in the life cycle of ammunition handling -- it is a kind of ammunition factory in reverse, without production quotas but with the goal of safe disposal of obsolete ammunition. The end products of the ammunition down-loading, parenthetically, will provide materials which will have significant reuse or resale value.

The environmental considerations which lead to the need for this facility dictate that ammunition disassembly be accomplished in such a fashion that the environment is not jeopardized by air- or water-borne contaminants resulting from the disassembly process. The elimination of these contaminants has been the subject of intensive study and is being reported on elsewhere in this seminar. ^{1/}

In this paper we are reporting on the structural ramifications of the explosive-resistant design. Ammunition-peculiar design criteria for the project include the following, in order of importance:

^{1/} "Treatment of Explosive-Contaminated Waste Water by Physical-Chemical Means in a 10 GPM Pilot Plant," by James S. Teter, Project Engineer, Tudor - Keller & Gannon.

1. There shall be no possibility of sympathetic detonation from one concentration of energetic material to another, in the event of an incident.
2. Plant personnel shall be protected from overpressure and fragments in the event of an incident.
3. Materials, equipment, and structures shall be protected from disabling damage in the event of an incident.
4. The functional arrangement of the facilities shall be tailored to the demilitarization of ammunition.

The means used to satisfy these criteria are separation of hazards (as established by NAVORD OP-5),^{2/} shielding between hazards (as established by NAVFAC P-397),^{3/} and controlled process flow, as established by the Naval Ammunition Production Engineering Command.

As shown on Figure 1, the facility is located in an ancient lake bed, whose remnants are the present Walker Lake. The average site elevation is 4,020 feet (1,225 meters); the surrounding terrain is undeveloped, sparsely covered desert. All structures accommodating energetic material will be located in a zone at least 2,000 feet (600 meters) from existing unrelated Depot structures and 1,700 feet (500 meters) from Walker Lake.

As shown on Figure 2, the demilitarization facility is a multistructure complex of process buildings, each devoted to a single down-loading procedure.

Material will be delivered to the facility at the Off-Loading Dock by truck and rail. This dock consists of two earth-covered steel arches, separated to prevent sympathetic detonation from one arch to the other. A driverless tractor system will be utilized to move the materials to the Preparation Building.

^{2/} Ammunition and Explosives Ashore, Safety Regulations for Handling, Storing, Production, Renovation and Shipping.
^{3/} Structures to Resist the Effects of Accidental Explosions.

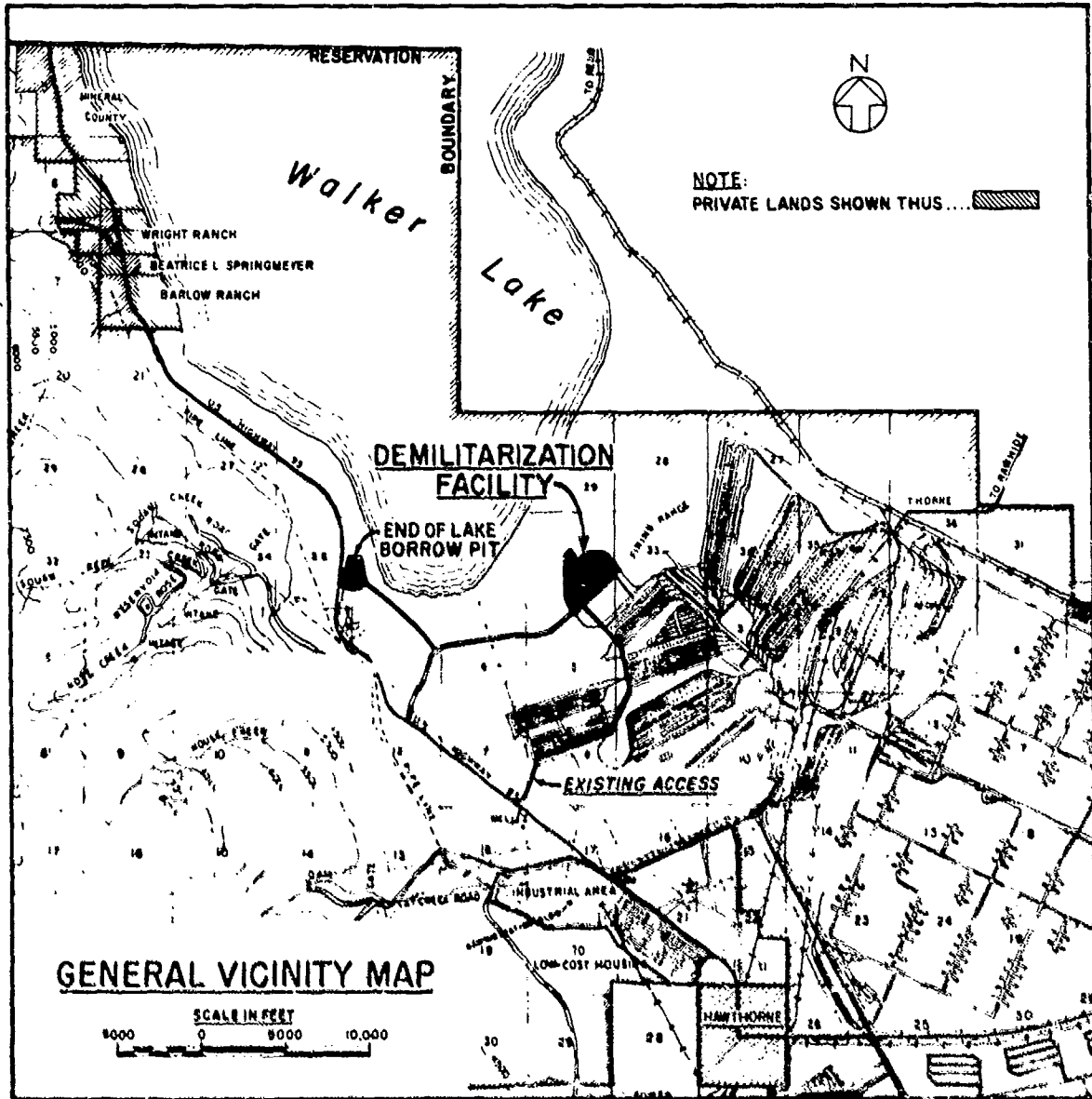
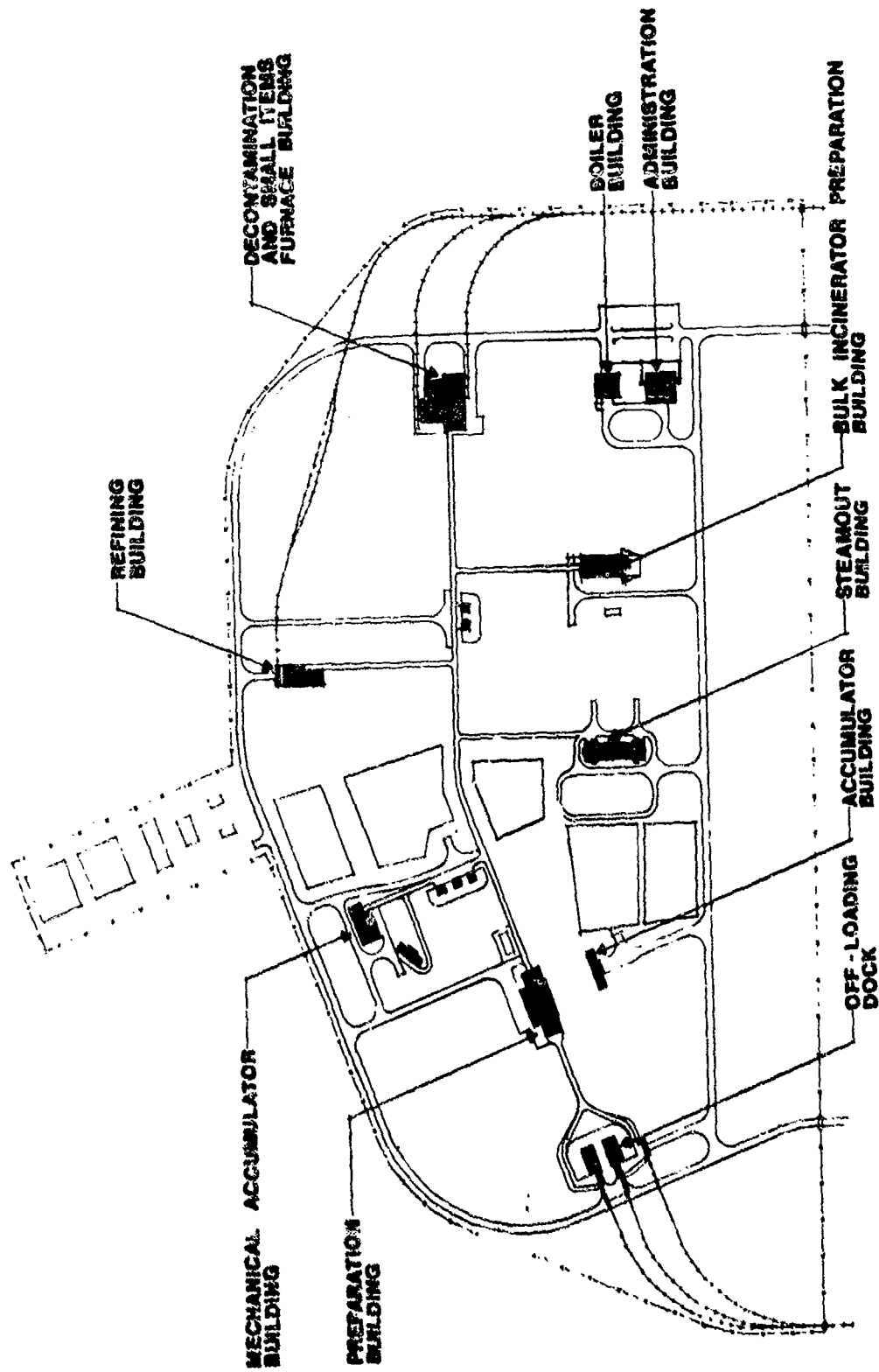


FIGURE 1
Vicinity Map



SITE PLAN

1183

FIGURE 2

Site Plan

In this building uncrating and initial disassembly will be accomplished. It is here that most of the ammunition will be defused in cells by remote-controlled machines. Smokeless powder will be collected at the cells and transferred mechanically to the Accumulator Building for packaging and reuse.

After leaving the Preparation Building, materials can be processed at the Mechanical and Accumulator Building and its ancillary Large Cell Building (where mechanical breakdown of devices will take place), and/or at the Steamout Building, where steam and hot-water melting of the energetic material will take place. At this building, the energetic material will be dried and flaked for either re-processing, direct resale, or destruction.

It is anticipated that energetic material will be refined at the Refining Building for reuse or sale. Energetic material that cannot be recovered will be burned at furnaces fed in slurry form from the Bulk Incinerator Preparation Building.

All metals which have been in contact with the energetic material, and all small arms ammunition, will be flashed or popped in furnaces located at the Decontamination and Small Items Furnace Building. The resulting scrap metal will be sorted and sold for recycling.

Each process building has been assigned a total maximum TNT equivalent explosive loading; each area within each process building has likewise been assigned a maximum TNT equivalent explosive loading. Based on these loadings, interline distances between buildings were established using the criteria given in NAVORD OP-5. The maximum TNT equivalent loading and the minimum distances, both barricaded and unbarricaded, permitted for the process buildings included in the facility are as listed on Table A.

QUANTITY/DISTANCE CRITERIA

FOR

DEMILITARIZATION FACILITY
NAD HAWTHORNE, NEVADA

<u>STRUCTURE</u>	<u>MAXIMUM AMOUNT OF EXPLOSIVE MATERIAL (LBS)*</u>	<u>MINIMUM ALLOWABLE BARRICADED DISTANCES (FT)</u>	<u>MINIMUM ALLOWABLE UNBARRICADED DISTANCES (FT)</u>
OFF-LOADING DOCK	50,000	330	N.A.
PREPARATION BUILDING	6,000	160	320
ACCUMULATOR BUILDING	150	N.A.	N.A.
MECHANICAL ACCUMULATOR AND LARGE CELLS	3,000	130	260
STEAMOUT BUILDING	18,000	N.A.	472
BULK INCINERATOR PREPARATION BUILDING	3,000	130	260
REFINING BUILDING	50,000	N.A.	660
DECONTAMINATION AND SMALL ITEMS FURNACE BUILDING	3,000	N.A.	260
MAGAZINE GROUP A	9,000	160	320
MAGAZINE GROUP B	5,000	130	260

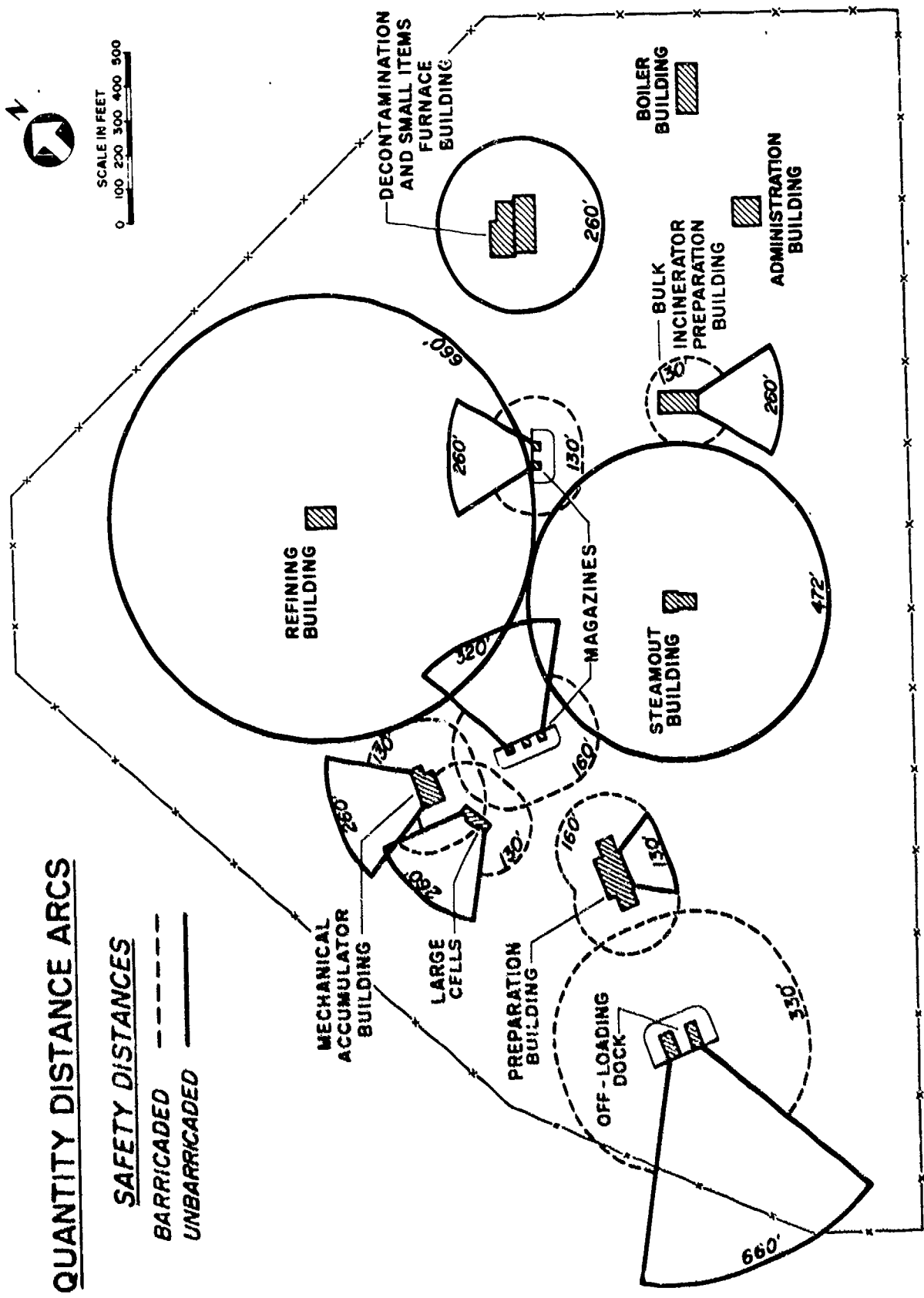
*1 lb. = 0.453 kg.; 1 ft. = 0.305 meter.

The distances delineated in Table A were used to develop the distances between structures as shown on Figure 3. The use of these distances will assure the prevention of sympathetic detonation, should an incident occur.

Although each building has unique functional requirements, the basic structural design solution responding to the problem presented by an anticipated event is typical for each of the process buildings in the complex. The design considerations must be met either for an event occurring in a remote structure or for an event occurring within the structure.

The design of the Preparation Building presented most of the design problems confronted in this project. This building is located more than the required unbarricaded distance from the Large Cell Building and the Steamout Building and at the barricaded interline distance from the Off-Loading Dock.

The Preparation Building will be constructed of reinforced concrete except for the frangible walls and roofs of the cells used for defusing weapons. Figure 4, the floor plan of the Preparation Building, shows the six cells, each of which may contain up to a 300-lb. (135-kg) charge, the work corridor, the off loading and the distribution areas. Figure 5, the building sections show that each cell has a frangible wall and roof to provide an exit for blast forces reducing pressure buildup on the remaining cell walls. The other three walls of each cell are hardened for prevention of sympathetic detonation between cells and for personnel protection in Work Corridor. The floor is slab-on-grade. A Utilities Deck allows an accessible space for the location of the various building systems piping and conduit.



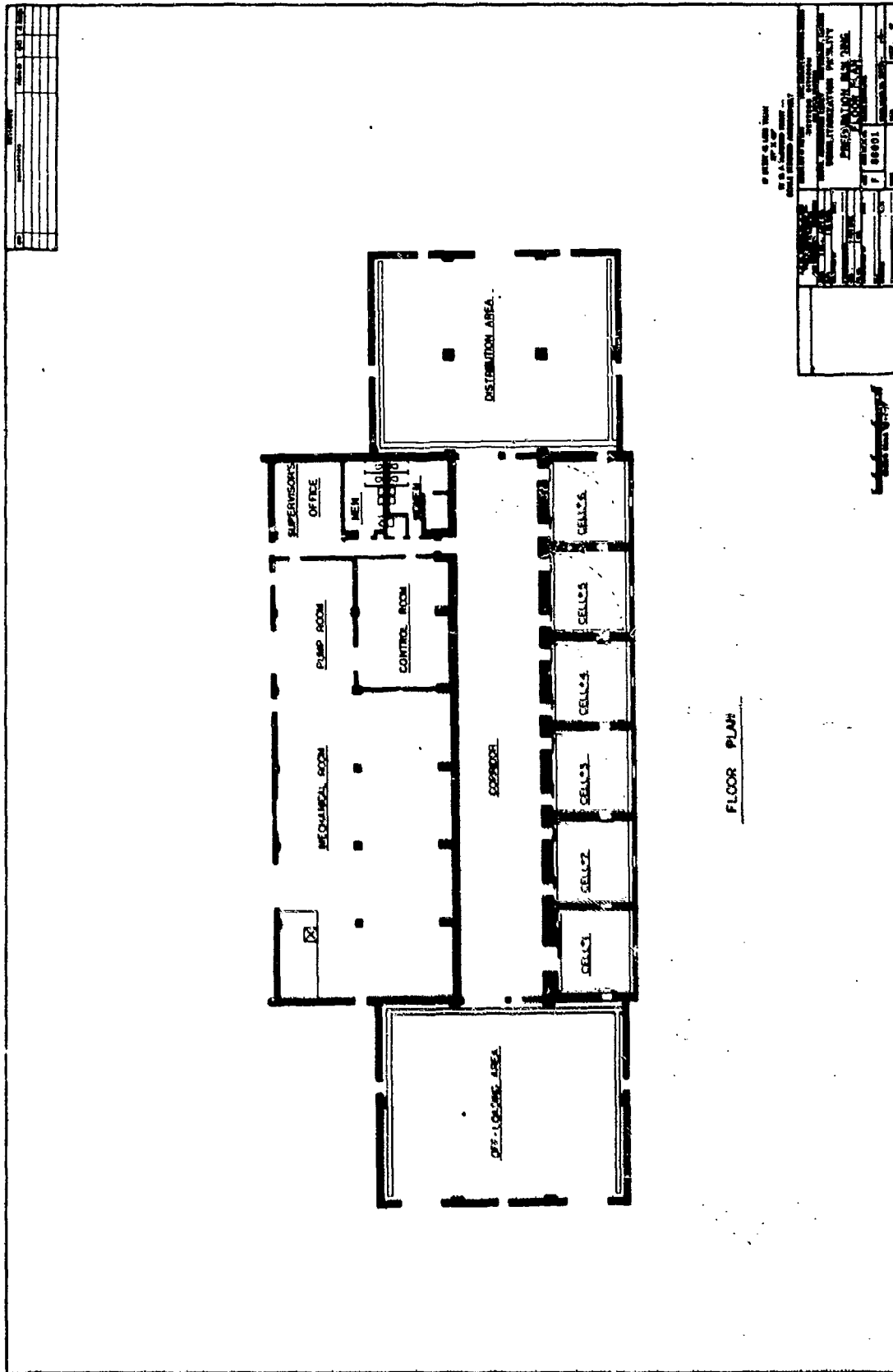
QUANTITY DISTANCE ARCS

SAFETY DISTANCES

--- BARRICADED
 — UNBARRICADED

FIGURE 3

Quantity Distance Arcs



FEDERAL BUREAU OF INVESTIGATION U.S. DEPARTMENT OF JUSTICE 7 88001	
PROJECT NO. 100-100000-100000 DRAWING NO. 100-100000-100000	DATE 10/1/88 SCALE 1/8" = 1'-0"

FLOOR PLAN

FIGURE 4

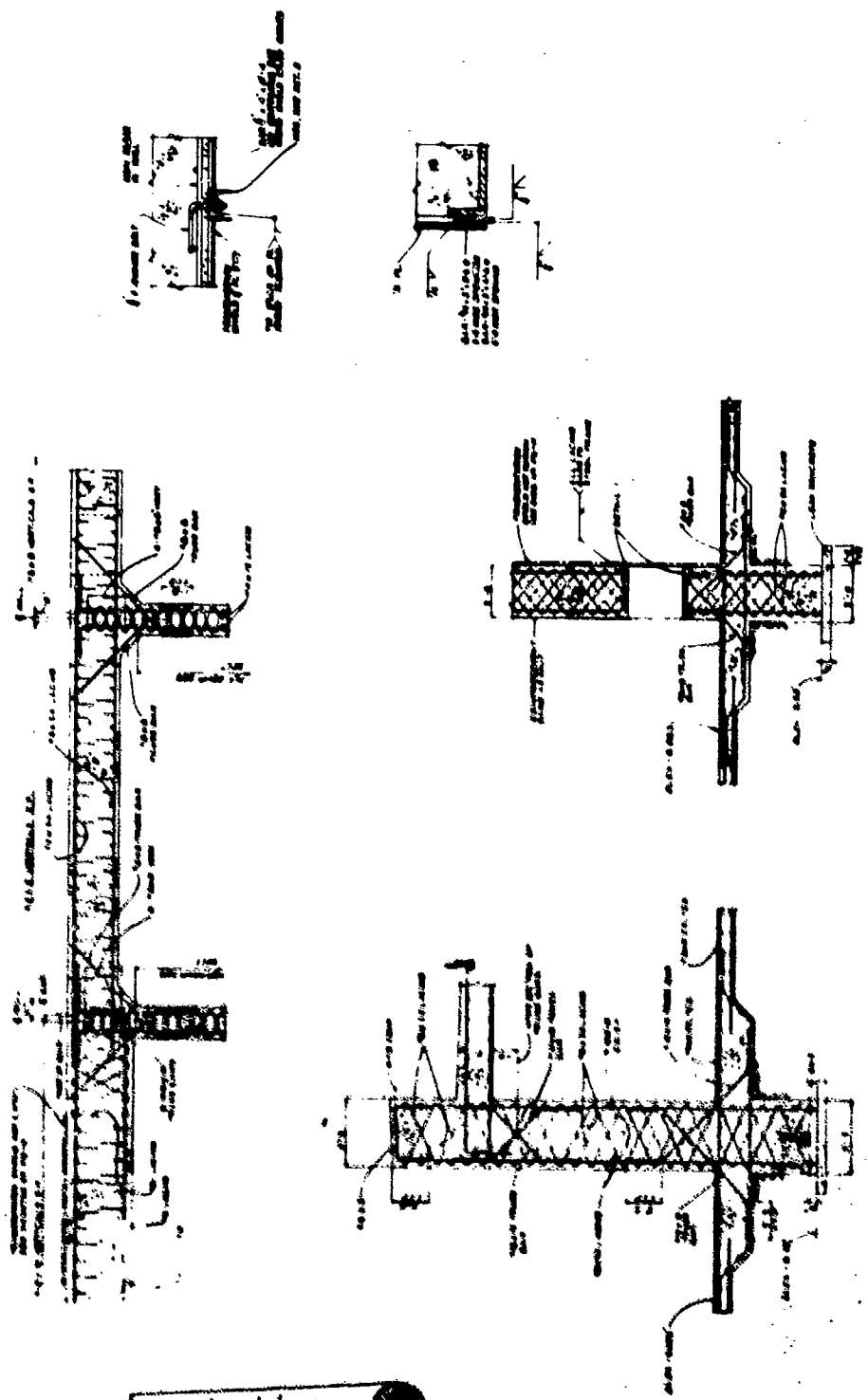
Preparation Building
Floor Plan

The walls between cells are designed to contain an incident involving a charge in a cell with a deformation not exceeding 12° rotation, thereby preventing sympathetic detonation. (A standard reinforced concrete wall would collapse after a rotation of about 2° .) In order to utilize the full ductility of the flexural reinforcing, the reinforcing bars must be tied with continuous diagonal lacing bars as shown on Figure 6. At any particular section of an element, the longitudinal or main tension and compression reinforcement is placed to the interior of the transverse or secondary flexural reinforcing steel around which the diagonal lacing bars are bent. Reinforced in this manner, a concrete wall can rotate up to 12° without losing its integrity. The procedure for analysis is to assume a wall, find the resistance-deflection function, apply the calculated time pressure load function, find the actual deflection, and compare it with the permissible ultimate deflection. In this way a structural element can be designed for flexural strength. It must then be reinforced for shear. The shear reinforcement is a function of the resistance of the element and not applied load.

The cell walls located next to areas in which personnel may be present at the time of an incident were designed to contain an incident involving a charge in a cell with a deformation not exceeding 5° rotation. A fragmentation shield will be attached to these walls to protect personnel from spalling concrete fragments. This shield is designed for a ductility ratio of ten or less.

All other walls and roof slabs were designed against an incident in one of the cells with their support rotation limited to 2° . Beams and columns were designed for the same incidents, but the ductility ratio was kept below unity.

Exterior doors which serve as emergency exits were designed to remain in the elastic range so as to be usable after an incident. All other hardened doors and ports were designed for a maximum support rotation of 15° .



Reproduced from
best available copy.

The blast-resistant design was further complicated by the requirement that each element must be adequate to absorb the kinetic energy of primary fragments without perforation. This requirement often sets a minimum dimension for structural member thickness: in turn, when applied to the blast-resistant design, this leads to smaller deflections and greater forces than those arrived at by purely dynamic design. One effect of this consideration is that the supports must be strengthened. In some cases this strengthening leads to the design of doors of special soft steel. If stronger, standard steel doors were to be used, a design incident would cause the walls to collapse.

All structural elements were investigated to determine the overpressure effects of an incident in any of the other process buildings. This analysis led to a straightforward design of structures for triangular dynamic loads, with the ductility ratio kept below unity.

Since this is the first time a complete facility has been designed in accordance with NAVFAC P-397, it is appropriate to make a few comments on this document. It is a complete and comprehensive manual which is excellently written. The few suggestions which follow are made merely in the hope that an already good manual can be further improved.

On the advice of The Naval Civil Engineering Laboratory, Port Hueneme, we used Fig. 4-63, "Exterior Leakage Pressure vs. Ground Scaled Distance," for large cells, Fig. 4-12, "Shock-Wave Parameters for Hemispherical TNT Surface Explosion at Sea Level," for the smaller cells, and the same figure but with half charges for magazines for the overpressure at one building resulting from an incident in another building. It is hoped that P-397 will be updated to

incorporate information obtained from the Eskimo Series Tests and other tests to eliminate this inconsistency. The method of determination of the overpressure on a roof behind a cell wall requires further tests and clarification.

The method utilized in P-397 depends on graphs for constants. It appears that some of these constants do not apply to walls with several openings or with large openings. Because cell function requires access between cells and between cells and work areas, further data is required to determine the limits of the applicability of these constants.

The Demilitarization Facility will be operational in 1978. From that time forward, it is hoped that the structural design concepts discussed in this paper will not be locally tested in practice.

TREATMENT OF EXPLOSIVE - CONTAMINATED
WASTEWATER BY PHYSICAL - CHEMICAL MEANS
IN A 10 GPM PILOT PLANT

By
James S. Teter
Project Engineer

Tudor - Keller & Gannon
Consulting Engineers
San Francisco, California

INTRODUCTION

In late 1973, the joint venture of Tudor - Keller & Gannon was awarded a contract for design of the structures and site work for the Demilitarization Facility to be located at the Naval Ammunition Depot, Hawthorne, Nevada. This project consists of a complex of industrial buildings which will be utilized to demilitarize, in lieu of deep water ocean disposal, an estimated 800 various types of ordnance items containing various types of explosive materials. Maximum effort will be made in the demilitarization procedure to reclaim explosive materials as well as metallic components.

One of the major components of the Demilitarization Facility is the Steamout Building in which high temperature water and steam will be utilized to remove explosive materials from their casings. Since most explosive materials are water soluble, this procedure will result in a large volume of process wastewater contaminated by the explosive materials with which it has been in contact. Explosive-contaminated wastewater will also result from floor washing and other similar cleanup procedures in the Steamout and other buildings of the Facility. Although detailed design of the washout-steamout equipment had not been completed, it was estimated that this process could produce a continuous flow of wastewater of 120 to 150 gallons per minute (gpm), and that floor washdown and other miscellaneous sources could result in an additional 50 gpm. Little definitive information was available regarding the wastewater characteristics since no similar steamout-washout facility for Naval ordnance is presently in operation. However, it was known that the solubility of TNT, a component of most explosive compounds, in 180°F water is 1,125 milligrams per liter (Mg/L), and therefore concentrations of TNT of at least that value could be anticipated. It was also known that other explosive materials such as ammonium picrate are highly water soluble. Since the Environmental Protection Agency present guideline is that water containing in excess of 1 Mg/L of explosive contaminate not be discharged to either surface water sources or ground water basins, it was obvious the Demilitarization Facility process wastewater must receive treatment prior to discharge.

As Hawthorne is located in one of the most arid regions of the United States, the simplest solution to the waste disposal problem first appeared to be construction of process wastewater evaporation ponds, thereby preventing all waste discharge (This was the method selected for treatment of the sanitary sewage). However, this solution was rejected by Depot personnel who pointed out that when these ponds were in a dry condition the normally strong winds prevailing in the area would blow the explosive material around the countryside, thus substituting air pollution for water pollution. At this juncture another related problem appeared, the Depot water supply which utilizes all available surface runoff as well as groundwater from wells was found to have insufficient capacity to serve the industrial needs of the Demilitarization facility on a continuous basis. It became readily apparent, therefore, that the process wastewater must be treated sufficiently to enable reuse in the steamout-washout process. Navy ordnance personnel set this requirement at 1 Mg/L TNT or other explosive contaminate since the reclaimed process water must be heated to 190°F prior to usage.

Two general types of treatment were given serious consideration for reclaiming the process wastewater (1) biological treatment, and (2) physical-chemical treatment. Most if not all explosives to be handled in the Demilitarization Facility have considerable organic content, and research has shown some success in treating TNT biologically. All biological treatment, however, depends on a nutrient supply, normally contained in the wastewater itself, sufficient to keep the bacteria alive. The Demilitarization Facility, for safety considerations, had been sited many miles from the central Depot area, and thus the only available natural nutrient supply would be contained in the sanitary sewage from the personnel actually working at the Facility, estimated at 100 persons at full capacity. It was anticipated that the nutrients contained in the small volume of sewage discharged by this small number of persons would not be sufficient for the large volume of high-strength process wastewater from the steamout-washout facility, and therefore use of biological treatment was rejected. There was also concern regarding the ability of the bacteria cultivated to adapt to a rapid change in explosive materials being demilitarized, and no knowledge whether materials other than TNT could be successfully treated biologically.

Following selection of the physical-chemical type of treatment, the full scale 200 gpm prototype plant (expandable to 400 gpm) design was completed utilizing the following treatment processes in their sequential order: dissolved air flotation, clarification, cooling, filtration, and carbon adsorption. A storage tank was provided for treated effluent. Sludge basins were designed to provide gravity separation of sludge from the flotator - clarifier unit and filters; the supernatant would later be decanted to evaporation ponds, sludge burned in the Demilitarization Facility bulk incinerator. No facilities for carbon regeneration were provided pending development of applicable technology; initially spent carbon will be burned in the bulk incinerator.

Space was provided for future addition of reverse osmosis equipment for total dissolved solids removal from the treated effluent should this become necessary. Prior to its installation, process water becoming high in TDS will be discharged to evaporation ponds, and replaced with new make-up water.

During the design of the full scale treatment plant, as with any prototype design, a number of questions arose which were at the time unanswerable due to lack of similar treatment facilities. Probably the most important of these was whether the treatment plant proposed would meet the effluent standard of 1 Mg/L explosive material. Obviously the only way these questions could be answered was to construct and operate a pilot plant which would simulate the operation of the full scale plant. This pilot plant was funded by Naval Facilities Engineering Command (NAVFAC) in April 1974. Since the design of the full size plant had been completed with construction bids to be received in June 1974, it was essential that results be obtained from the pilot plant at the earliest possible date.

PILOT PLANT DESCRIPTION

All treatment units in the full scale plant had been designed using standard items of equipment available from manufacturers in the water and sewage treatment industry. Therefore it was relatively simple even on short notice to obtain similar small size units on a rental basis, thereby avoiding fabrication time and probable delays due to steel shortages. It was decided that the plant would be sized for a 10 gpm flow rate, and considered essential that the pilot plant be located in Hawthorne in order to use the same water supply as would constitute the majority of the wastewater. Also, safety considerations regarding transporting and handling of explosive materials precluded siting the pilot plant at a location more convenient for operating personnel. The principle units of the pilot plant are described below in their sequential order:

1. Mix Tank. An existing fabricated aluminum tank at the pilot plant site was used for preparing and storing the explosive wastewater. This tank had a capacity of 2400 gallons. A plywood cover was installed on the tank to prevent exposure to sunlight which would turn the wastewater red in color, a phenomenon commonly known as "pink water".
2. Flotator-Clarifier. This unit was a completely self-contained unit including a 5 foot diameter by 6 foot high flotator tank complete with sludge scrapers and float skimmer, pressurization tank, air compressor, two pressurization pumps, two chemical mix and feed tanks, and two chemical feed pumps.

This unit differed from the full-scale flotator-clarifier in that it did not have the clarification zone for sedimentation exterior to the central flotation zone. A cover was also provided for this unit.

3. Cooling Tower. The mechanical-draft type cooling tower was approximately 3 feet square by 5 feet high, and consisted of an upper spray nozzle system, wet deck, draft fan, and bottom sump.
4. Sand-Coal Filters. These vertical, pressure, downflow type filters were each 2 foot 6 inches in diameter by 6 feet high. The filter media in one unit was 22 inches of anthracite coal over 8 inches of sand; the other unit 15 inches of coal over 15 inches of sand. The units were operated alternately with only one filter in operation at any time.
5. Carbon Adsorption Columns. Two upflow type carbon columns were operated in series. Each column was 28 inches in diameter, and contained a five foot deep bed of granular activated carbon.

In addition to the above main flow stream treatment units, a secondary one gallon per minute flow stream was operated downstream of the cooling tower consisting of the following units:

1. Diatomaceous Earth Filter. The filter itself had a plexiglass case which allowed inspection of the interior, and a stainless steel interior septum with a filter area of 1 sq. ft. The filter was pre-coated and backwashed with accompanying equipment.
2. Polymeric Adsorbent Resin Columns. These 6 inch diameter, plexiglass, downflow type columns were loaded to a depth of 2 foot and 3 feet respectively with Rohm & Hass XAD-4 polymeric resin. The columns were preconditioned and regenerated with methanol.

PILOT PLANT OPERATION

The plant operated for one shift daily for a total operating period of 6 weeks from May 23 - July 3, 1974. This daily start-up and shut-down was intended to simulate the operation schedule of the full scale plant; in addition, sufficient operating personnel were not available to furnish the continuous attention the pilot plant required for monitoring and control to enable a 24 hour per day operation schedule.

Field mobilization and preliminary operation required 4 weeks; demobilization 3 weeks. Thus from the date of notice to proceed on 26 April 1974, the entire pilot plant field operation was completed in 4 months.

Explosive contaminated wastewater of the type anticipated from the steamout-washout process was prepared in the influent mix tank. Hot water (160°F) was provided, and the pH was lowered below 7 with sulfuric acid. Explosive materials were added through a hatch in the top of the tank, with mixing provided by recirculated flow from the flotator-clarifier influent pump. TNT, Comp. A-3, and Picratol were added in dry flake form; HBX-1 and Comp. B were melted in a steam-heated pot and added in molten form. Explosives tested and length of test period was as follows:

<u>Explosive Material</u>	<u>Days Tested</u>
TNT	12
Comp. A-3	3
Comp. B	3
HBX-1	3
Mixture of Comp. A-3, Comp. B, & HBX-1	3
Picratol	3

An extensive sampling and testing program was carried out to monitor the pilot plant performance. Samples were collected of the effluent from each individual treatment unit on a regular basis, typically hourly. Samples were analyzed in the field mobile trailer laboratory for temperature, pH, turbidity, color, and TNT concentration. Composite samples from the daily plant operation were sent to San Francisco for additional analysis, a portion of which were verified by a Navy approved ordnance testing laboratory. Field testing for TNT was performed colorimetrically using sulfite-hydroxide solution; laboratory testing for TNT, RDX, and ammonium picrate utilized vapor phase chromatography.

PLANT RESULTS

Both the 10 gpm and 1 gpm flow streams proved effective at removing explosive contaminants from the process wastewater. Flow Stream No. 1 which contained the carbon adsorption columns accomplished removals of TNT greater than 99.5 percent; the effluent concentration of this flow stream never exceeded 0.5 Mg/L TNT. Similarly, the ammonium picrate concentration from this flow stream never exceeded 1 Mg/L (lowest level measurable by testing procedure), and the RDX concentration did not exceed 0.02 Mg/L. Flow Stream No. 2 which contained the polymeric adsorbent resin

columns was less effective with maximum effluent concentrations as follows: TNT 148 Mg/L, ammonium picrate 368 Mg/L, and RDX 66 Mg/L. A brief summary of the pilot plant performance showing mean effluent values follows:

MEAN EFFLUENT CONCENTRATION IN MG/L

<u>Wastewater Contaminant</u>	<u>Parameter Measured</u>	<u>Flow Stream No. 1 (Carbon Adsorption)</u>	<u>Flow Stream No. 2 (Polymeric Resin Adsorption)</u>
TNT	TNT	< 0.5	62.8
Comp. A-3 *	TNT	< 0.5	4.4
Comp. B	TNT	< 0.5	2.3
HBX-1	TNT	< 0.5	2.6
Mixture **	TNT	< 0.5	3.0
Picratol	TNT	< 0.5	30.5
Picratol	Ammonium Picrate	< 1	132.0
Comp. A-3	RDX	< 0.02	0.62
Comp. B	RDX	< 0.01	25.5
HBX-1	RDX	< 0.02	66.8
Mixture **	RDX	< 0.01	59.0

* Plant treatment units and piping contained residual TNT

** Mixture contained Comp. A-3, Comp. B and HBX-1

From the above it is evident that the carbon adsorption columns produced a much higher quality effluent for all wastewater contaminants tested than the polymeric resin adsorption columns. However, only one type of polymeric resin (Rohm & Hass XAD-4) was tested due to extended delivery times of other resins. A testing program conducted by U.S. Army Labs, Natick, Massachusetts on more dilute wastewater using this same polymeric resin produced somewhat better results.

The flotator-clarifier proved to be an effective treatment unit for removal of suspended solids, grease (wax), and TNT during periods when a floc could be formed in this unit. Due to the long delivery time for bulk quantities of most types of organic coagulants, it was necessary to order the polymer to be utilized prior to start-up of the plant. Preliminary jar tests indicated a cationic polymer (Hercufloc 815.3) to produce a good floc, and therefore this material was used throughout the pilot plant operating period. Under actual operating conditions, however, this polymer was found to produce only a poor to fair floc with TNT wastewater, and virtually no floc with Comp. A-3, HBX-1, Comp. B, and picratol.

Due to this poor floc formation, a series of secondary jar tests were performed using various types of polymers. For the mixture (Comp. A-3,

Comp. B and HBX-1) a nonionic polymer, American Cyanamid 905N, was found to form an effective floc while all anionic and cationic types tested were ineffective. For picratol wastewater only high concentrations of an anionic polymer, Magnifloc 837A, formed a good floc. Testing of TNT wastewater indicated both nonionic and anionic polymers to be generally more effective than the cationic type used throughout the pilot plant study. The performance of almost all of the polymers tested was greatly enhanced by the addition of alum (aluminum sulfate). Alum was not utilized as a coagulant in the full scale plant since it would make the sludge more difficult to incinerate, and might have a deleterious effect on the explosive materials themselves making their reuse more difficult.

The flotator-clarifier in the full size plant can be expected to perform more effectively than that in the pilot plant due to (1) better floc formation resulting from availability of various types of polymers (2) increased suspended solids removal achieved in the sedimentation zone of this unit which was not present in the pilot plant and (3) increased cooling due to greater detention time.

Both the sand-coal filters and diatomaceous earth filters proved effective in removing suspended solids from the wastewater, with almost no difference regarding their removal efficiency. However, the sand-coal filters provided longer filter runs before backwashing was required, especially for the wastewater mixture (Comp. A-3, Comp. B, and HBX-1) and picratol. Difficulties were encountered in backwashing the diatomaceous earth filters as the material stuck to the septum requiring removal by scraping. No operating difficulties were encountered with the sand-coal filters.

The cooling tower which reduced wastewater temperatures about 50 to 60°F provided effective removal of TNT due to the lower solubility (1,125 Mg/L at 180°F versus 130 Mg/L at 68°F) of this material in lower temperature water. However, severe operating problems were encountered with this particular type of cooling tower since the TNT dropped out of solution tended to plug the spray nozzles and incrust on the interior walls. Constant maintenance was required. Similar serious incrustation occurred on the interior walls of the plant PVC piping.

The effectiveness of the carbon adsorption and polymeric resin columns is visually illustrated in the preceding table of plant effluent concentrations. In summary the effluent from the carbon columns consistently met or exceeded the plant requirements while that from the polymeric resin tested did not. In addition, frequent regeneration of the resin columns with methanol was required when breakthrough was observed. The carbon columns operated throughout the entire test period without breakthrough or need of regeneration; observation of ring demobilization indicated that all removals

had been accomplished in the first half of the column.

CONCLUSIONS AND RECOMMENDATIONS

1. Explosive material-contaminated wastewater (at least those having constituents contained in TNT, Comp. A-3, HBX-1, Comp. B and Picratol) may be successfully treated by physical-chemical means to an effluent concentration less than 1 Mg/L.
2. Flow Stream No. 1 of the pilot plant, a 10 gpm model of the full scale plant now under construction, demonstrated that the full-scale prototype plant will produce an effluent suitable for recycling back to the steamout-washout facility.
3. Coagulation using organic polymers can be accomplished, but is greatly enhanced by addition of alum.
4. Assuming good coagulation, significant removal of suspended solids can be effected in a flotation-clarification unit, thus lowering the loading rate and extending the useful life of the carbon adsorption columns.
5. Cooling of wastewater saturated with TNT will accomplish significant TNT removal since the solubility of this material is highly temperature dependent. However, the type of cooling device must be carefully selected to permit cleaning since the TNT tends to incrust on the walls of the unit.
6. Piping carrying explosive-contaminated wastewater must be designed to permit flushing with hot water and chemical solutions as the contaminants incrust heavily on the interior pipe walls.
7. Either diatomaceous earth or sand-coal filters can effectively remove suspended solids from the wastewater if preceded by proper coagulation. However, shorter duration filter runs were experienced with the diatomaceous earth filter with certain explosive materials, and this filter could not be back-washed automatically without hand cleaning due to material sticking on the filter septum.
8. During the operation of the pilot plant, the effluent from the carbon adsorption columns was consistently at or below the recommended value of 1 Mg/L explosive contaminate while that from the polymeric adsorption columns was normally above this value, although other studies have shown polymeric resins to produce an effluent below the 1 Mg/L value.

SECRETARY OF LABOR v. GEARHART-OWEN INDUSTRIES, INC.

D. E. Ray, Esq.
U.S. Army Armament Command
Rock Island, IL

Thank you Larry, and good afternoon (ladies and) gentlemen. I am employed at the Army Armament Command Legal Office, located in Rock Island, Illinois. As you may know, the mission of the Armament Command involves procurement of most types of conventional ammunition for all the Armed Services and for many foreign allies. Naturally, this includes the procurement of explosive and propellant materials. Our procurement responsibilities are accomplished through some twenty odd Government-owned contractor-operated plants commonly known as GOCO's, and by direct procurement from private industry using their own facilities. Most of our procurements from private industry involve ammunition metal parts; but some of these also include explosives, either as an end product or as a part of the item being purchased. Many of our procurement activities since 1971 have been either directly or indirectly affected by the enactment of Public Law 91-596, the Williams-Steiger Occupational Safety & Health Act. There has since that time been a great deal of discussion and debate within Army circles as well as involving other agencies and private firms, as to just how the provisions of OSHA should be carried out so as to be most harmonious with the job we have to do. In at least one area of activity, that is, in procurements involving explosives, it has long been debated as to whether OSHA actually applies at all. Generally speaking, within the Federal Government it has been the Army maintaining the inapplicability of OSHA in such cases. As you can imagine, the expenditure of large sums of money is at stake. It is not news for me to tell you that compliance with OSHA involves spending a great deal of money, especially when we speak in terms of a procurement program of nearly three billion dollars per year.

My purpose here today is not to rehash the Act itself; most of you may know more about its technical intricacies than I do. Instead, I would like to suggest to you the potential impact on Army programs of a relatively recent case, namely, that of the Secretary of Labor v. Gearhart-Owen Industries, Inc. (OSHRC No. 4263), decided on 15 March 1974. I have just mentioned the high cost of compliance with the Act, though this is not to say that the objective of this Act, or any other safety program, is not worth far more than the cost in dollars of achieving it. But perhaps the general magnitude of cost itself might interest you as a taxpayer, even if you are not directly involved in whatever it is that eventually evolves out of the Gearhart-Owen decision.

Firstly, for the benefit of those here who may not have heard of the case, or who are perhaps a bit forgetful of the details, let me briefly refer to the decision and some of the events leading up to its becoming a matter of controversy. In fact, the decision itself is short. Let me read it to you to give you a bit of insight into the legal arguments made on behalf of the respondent, Gearhart-Owen, with which the Judge of the Department of Labor's Occupational Safety and Health Review Commission was in agreement.

Being captioned an Order of Dismissal, the decision reads substantially as follows:

"Order of Dismissal

"On August 15, 1973, complainant issued three citations to respondent, a manufacturer of munitions, alleging violations of Section 5(a)(1) of the Occupational Safety and Health Act of 1970 (29 USC 651 et seq., hereinafter called the Act). Penalties totalling \$20,700 were proposed. In due course respondent made known its intent to contest the citations, and a complaint and answer were filed.

"Following a prehearing conference the parties entered into a limited stipulation of facts, and respondent filed a motion to discuss charges under the Act on the basis of Section 4(b)(1) of the Act, which provides as follows:

'Nothing in this Act shall apply to working conditions of employees with respect to which other Federal agencies exercise statutory authority to prescribe or enforce standards or regulations affecting occupational safety or health.'

"Specifically, respondent maintains that its workplace is operated in accordance with safety regulations promulgated by the Department of Defense pursuant to statutory authority, thereby bringing Section 4(b)(1) into play. Review of the stipulation and the documents attached to it substantiates respondent's position. It was awarded a contract to manufacture certain hand grenade fuzes for the United States Army in accordance with an invitation to bid which incorporated by reference portions of the Armed Services Procurement Regulation (ASPR) dealing with 'Safety Precautions for Ammunition and Explosives'. The ASPR is considered to be a regulation of the Secretary of Defense promulgated pursuant to applicable statute.

"The safety precautions for ammunition and explosives clause of the ASPR requires compliance with Department of Defense Manual 4145.26M, a safety manual for DOD contractors. This is a detailed and lengthy book of instructions in safety matters, pertinent portions of which were, as appears in the stipulation, followed by respondent in performing the work which gave rise to the allegations contained in the citations referred to above.

"On these facts the undersigned must find that jurisdiction under the Act does not lie with respect to the work being performed in respondent's workplace under the contract referred to in the preceding paragraphs. It is therefore ordered that the citations dated August 15, 1973, be dismissed and that the proposed penalties be vacated.

Dated: Mar 15 1974

WILLIAM J. RISTEAU
Judge"

Section 4(b)(1) of the Act cited by the attorney for respondent and quoted in the decision has, of course, been the basis for the Army's argument that OSHA does not apply to its procurement of explosives. Not only is the Armed Services Procurement Regulation promulgated pursuant to a statute which is encoded in Chapter 137 of Title 10 of the US Code, the DOD Safety Manual prescribed for use by the ASPR clause entitled, "Safety Precautions for Ammunition and Explosives," is promulgated by the same Department of Defense Explosive Safety Board which is sponsoring this seminar. That Board is itself established by another Federal statute, 10 US Code Section 172.

The latest information available to me is that the decision of the Judge of the Occupational Safety and Review Commission in the Gearhart-Owen Case has been ordered for review by the full commission in accordance with established rules, and is still pending decision by the full commission. The law provides that any person adversely affected or aggrieved by the order of the commission may obtain a review in the US Court of Appeals for the circuit in which the alleged violation occurred, with several alternative appellate courts available as well, by filing within 60 days of the entering of the order. Since there does not appear to be any limit on the time in which the commission must make its decision and enter the order, and considering the backlog of work in the various courts of appeal to which any request for review might be directed, you can see that it could be a very long time before we see the final result of Gearhart-Owen. Perhaps one side effect of the decision which in my view would be desirable, will be that the various Federal agencies may come to a mutual agreement long before the case itself might otherwise be finally determined, as to where OSHA shall apply and where it shall not, in those areas where the law itself does not take care of the issue.

It is interesting to note that the Assistant Secretary of Labor, in a memorandum to the Department of Defense dated 2 July 1973, and thus much prior to Gearhart-Owen, took the position that insofar as Army material facilities are concerned, OSHA standards were not applicable. He observed that the Department of Defense Explosive Safety Board functions under the type of express statutory authority contemplated by Section 4(b)(1) of the Act. The provisions of 10 USC 172 set forth the unique grant of express authority to the Explosive Safety Board to prevent hazardous conditions from arising to endanger life and property inside or outside of military storage reservations. He stated that the exercise of this express authority through the promulgation of standards relating to explosives creates a situation to which the provision of Section 4(b)(1) must be applied. Therefore, he continued, we conclude that in order to avoid unnecessary duplication of effort, the Department of Defense regulations relating to explosives should be applied in Army Materiel facilities rather than the OSHA standards.

We very much agree that this duplication of effort of which the Under Secretary speaks should be eliminated. Safety in operation is and has been of primary importance to our procurement activities, but to do the same thing twice, as would be required if both OSHA and DOD standards were made to apply in a given instance, simply does not make sense unless the end result would be that our operations become doubly safe. That is not the case.

For reasons not known to me, the Under Secretary of Labor's memo I just mentioned has not entirely been adopted and put into practice by the Department of Defense, or at least not in the Agency for which I work. For example, plans have been made and are being carried out to one degree or another to conduct OSHA compliance reviews at our GOCO plants. No doubt one reason we have gone ahead with OSHA compliance reviews, notwithstanding the memo, is that while OSHA has not promulgated explosive safety standards to the degree the DOD has, it has promulgated industrial safety standards for the work place that could be applied to significant portions of our GOCO plants. A problem arises, however, because the DOD has also established industrial safety standards, and has enforced its own standards for many years, thereby compiling an excellent safety record. Must we now make costly changes to comply with OSHA in places that are already safe by our own high standards? This the Under Secretary of Labor did not clearly resolve, but hopefully it will be decided one way or the other by the Gearhart-Owen case when it is ultimately decided, if the agencies involved do not mutually agree to the now unsettled matters beforehand.

I have dealt fairly exclusively with GOCO operations in this talk, because that is where I believe the chief potential impact of the Gearhart-Owen decision lies. However, it should be borne in mind that that case involved a privately owned plant. Thus if it is upheld in its ultimate review, OSHA would not be applicable to any of our contracts which properly include the ASPR Ammunition Safety Clause discussed before. This would mean that our contractors would not have to spend additional moneys to comply with OSHA in order to perform our contracts, and thus would not be passing that cost along to the Government as part of the contract end item price. Additionally, the Government would not be required to spend additional money to bring its own equipment, which is often furnished to private contractors at their plants to be used in performing Government contracts, to bring that equipment into compliance with OSHA standards. I make no particular assessment of the value of this from an overall safety standpoint, but I do suggest to you that specific and stringent safety standards have long been an important requirement of Army contracts, for munitions as well as other items, and thus the absence of OSHA would not create a void in those cases.

You probably have noted that 10 US 172 and the ASPR clause mentioned before relate specifically to explosive safety, and it is obvious that most munitions plants, even the ones which produce only the explosive

itself, involve plenty of operations which have nothing directly to do with the explosive, but which could create safety hazards. This is especially the case with some of our GOCO plants which load the explosive into the round, assemble it, and pack it for shipment and storage. In fact, we have one GOCO plant which produces TNT on one side of the installation and has a LAP operation on the other, both operated by one contractor under a single contract containing the Ammunition Safety Clause. Plenty of room for both OSHA and the DOD Explosive Safety Standards at that plant, you might say.

But let us look again at the Gearhart-Owen decision. The Judge specifically found that "jurisdiction under the Act does not lie with respect to work being performed in respondent's workplace under the contract referred to in the preceding paragraphs." He was talking about a contract for the manufacture of grenade fuzes, a process that requires considerable effort other than handling the explosive itself. Yet he did not limit his ruling to that part of performance which required explosive handling, he applied it to the contract as a whole. Thus if the case is upheld, OSHA would not apply to any of our contracts containing the critical clause, regardless of multiplicity of operations not directly related to explosives. Once again, this would not create a void. We have the statute (10 USC 172), the ASPR Safety Clause, the DOD contractor's safety manual which is incorporated by reference in all our contracts, and the necessary expertise to inspect to insure compliance therewith.

Without going into great detail, I again refer to the duplicative efforts which would be required in many of our operations if both OSHA and DOD standards are made to apply. Different formats of the same reports would be required to be made through separate channels to different agencies. Duplicate investigations of the same incident made by different investigating bodies would result, likely with divergent conclusions in many cases. In addition, there would be the inevitable cases of direct conflict between the two standards which would cause unnecessary and troublesome problems to be resolved.

I am aware that as a general rule, the labor force and especially labor unions favor OSHA, perhaps over DOD standards at least in the area of industrial safety outside of explosive handling. If Gearhart-Owen is upheld, the reasonable objections of the work force to present safety practices must be met and corrected. One area which is specifically covered by OSHA, is the reporting of unsafe conditions without fear of retaliation. OSHA provides assurances that there will be none, and if Gearhart-Owen prevails as decided, we must remove any obstacles, real or imagined, to the reporting of hazardous conditions at all our plant as well as in private facilities where Government contracts are being performed.

In the event Gearhart-Owen is reversed on appeal, then somehow we must work out the problems discussed before which will exist under those conditions.

In my view our explosive procurement operations will be exempted from OSHA under Section 4(b)(1) of the Act, notwithstanding the possibility of such reversal. However, the remaining gray areas will take years to resolve, and a great deal of effort will be wasted in the administration of our safety programs, unless reasonable compromises can be worked out expeditiously.

This concludes my presentation. I thank you for your attention.

A NEW METHODOLOGY FOR WOUNDING AND SAFETY CRITERIA

William Kokinakis
U.S. Army Ballistic Research Laboratories
Aberdeen Proving Ground, Maryland

For the next half hour I will be discussing a new approach to wound assessment and the methodology developed to address this area. In the past years we have attempted to conduct a wound ballistics program which was a balanced effort between research in physiological damage mechanisms and penetration mechanics. Early last year it was decided to shift nearly our entire effort to one of simulation, and in particular to mechanical simulation. My presentation will center on the simulation aspects of the modeling of the wounding or vulnerability process, as well as the development of safety criteria.

Before continuing let me say a few words in the way of background information for a sample calculation which I will use to illustrate the modeling. The calculations are being conducted by BRL to provide a criteria for the selection of an optimum handgun/ammunition combination for use by law enforcement agencies, and this portion of our program is being funded by the Department of Justice.

To quantify the effects of a wound we must first have a consistent description of the target we intend to evaluate. This is represented by a cadaver which has been sliced into horizontal cross sections, ~2 cm thick, and coded for storage on a computer, as shown on Viewgraph 1. This computer representation of the human body is called the BRL Computer Man. On Viewgraph 2 we see a sample cross section thru the shoulder and the rectangular grid used to locate tissue types.

In the past, trajectories (horizontal only and uniformly random), were traced by a computer program through the Computer Man body to determine the type and location of tissue cells intersected. In an attempt to upgrade and make our analysis more general, we are replacing the tissue coding as used in the past with a numerical designation to signify the relative importance of a given cell to the overall survivability of the man, based on some specific injury criteria. The previous cross section is shown on Viewgraph 3 with the appropriate numerical codes for each cell. The vulnerability numbers shown were determined by the doctors at the University of Maryland Shock Trauma Unit. For the particular set of numbers shown, the doctors were asked to rate each of the cells on a relative

scale from 0 to 10. Their criterion was to estimate the importance of a given cell relative to lethality if it was suddenly removed and there was no following medical treatment. The same type of cell ranking will be accomplished for any injury or incapacitation criterion we need to develop, including the establishment of safety criteria. I will have more to say on this matter later in my presentation.

To date we have asked our medical team to evaluate six different criteria, three lethal and three incapacitation oriented, as defined on Viewgraph 4. Each of these six criteria have been evaluated by three different medical assessors. The three incapacitation type criteria also require the establishment of a definitive scenario to which the medical assessor can estimate a performance decrement. An example of how these criteria are defined is shown on Viewgraph 5 for the case of immediate incapacitation. The criteria is presented to the doctor in such a way as to explain its purpose or objective, describe a general scenario which defines the tactical situation, and request the doctor to identify those portions of the body which will produce a given probability level of achieving the defined objective. It should be pointed out that we are assessing wounds in humans, rather than interpolate from wounds in animals to their effect in humans, as was the procedure in the past. With a complete set of these numbers we now have our new target description, the revised Computer Man.

The next step in the process of determining the vulnerability of personnel to injury, is to determine a vulnerability index as a function of projectile or missile penetration. With the revised Computer Man, we have a three-dimensional mapping of the areas of the body in terms of their vulnerability. For any given weapon though, these areas (or the individual computer cells), do not have equal likelihood of being encountered. For example, if a hand grenade is the attacking weapon, it will be primarily a ground burst munition, which, because of increased hit probability, would dictate that computer cells in the lower extremities be weighted higher than those in the upper body. This then brings us to the second input into the vulnerability index as a function of penetration, the hit distribution.

What is desired of the hit distribution is a technique for characterizing the spatial distribution of possible trajectories of projectiles for a given weapon. Again going back to the example of handgun effectiveness, the weapon can be characterized by the range of the target and the aiming error or standard deviation of shot about the aim point. Using the standard deviation about an aim point, we can then use monte carlo techniques to conceptually fire trajectories at the Computer Man. The purpose here is to generate the average vulnerability of the body. To make this a little more clear, an example calculation is shown on Viewgraph 6. Again, using our example based on small arms, characterized by the range and aiming error, a set of random trajectories are traced through the Computer Man. Keep in mind that while the slide is two-dimensional, the actual computer tracings are done in three-dimensional space. To determine the average vulnerability of the body (i.e., vulnerability index, V_1 , as a function of penetration, X), we compute the average cell value at each increment of penetration for all trajectories. For example, for the vulnerability index at five centimeters shown in the calculations, the trajectories which miss the man are also counted. We now have generated the situation where the vulnerability of personnel is no longer independent of hit probability. Based on this methodology, the "more accurate" weapons are given greater importance than before. When this incremental calculation is performed at each increment of penetration depth, the resultant vulnerability index versus depth of penetration curve on Viewgraph 7 is generated. This plot is based upon 500 trajectories and shows, again for the handgun criteria, the average importance of the body in terms of vulnerability as a function of depth of penetration along the average trajectory. It is important to note at this time the following:

1. This function is dependent on the weapon and if a different weapon is used the function may change.
2. No mention has been made of the projectiles given off by the weapon. We have only considered to this point the directions in which the projectiles travel. This is intentional because it allows weapon and projectile design to be optimized or evaluated separately as to their effects on personnel vulnerability.

At this point we will begin to consider how projectiles effect vulnerability. Given the V_i versus X curve, then the logical questions to ask are what does it mean and how should it be used? With regards to its interpretation, the V_i versus X distribution implies that, if damage to the body is caused by projectile penetration, then ideally, the mechanical damage to the body as a function of depth should match the vulnerability index as a function of penetration depth. This suggests applying the V_i versus X distribution as a weighting function to determine the importance of causing damage at a given depth. It should be noted here that we are attempting to generate a measure of expected damage, and here the emphasis is on measure. We are not trying to predict the physiological response of an individual to wounds.

In our model we assume that the body material is homogeneous and can be approximated by 20% gelatin. This is not new. Twenty percent gelatin has been used as a tissue simulant for over a decade. But we are doing several things in developing our new Wound Ballistics Methodology which are new:

1. We are examining in detail the material properties of gelatin.
2. We are looking at the comparison between gelatin and animal tissues in terms of their response to projectile impact.
3. We are investigating the effects of projectile geometry or shape, orientation on impact and during penetration, construction and how it effects break-up and deformation, and lastly, the effect of changing striking velocity.

In order to apply the vulnerability index as a weighting function we needed a measure of the mechanical damage produced in the gelatin as the projectile slows down. The measure chosen was the maximum temporary cavity (MTC) formed in the gelatin, that is, the maximum radius of expansion of the gelatin in each point along the trajectory of the projectile. At present this MTC can be determined in one of two ways: experimentally, by observing the cavity growth by high-speed photography or flash x-ray, or computationally, based on a model as to how these cavities are actually formed. Although at this time our model has limited predictive

capabilities, it does provide a mathematical description of temporary cavity envelopes for any projectile whose drag history is known. For example, the model was used to generate a cavity envelope for a sphere, a soft bullet and a pistol bullet, as shown on Viewgraph 8.

The cavity envelopes for the three projectiles are plotted as damage radii versus penetration. The M193 bullet is the Cal 0.23 used with the M16 rifle and the M1911 is the Cal .45 bullet used with the M1911A1 pistol. For the purpose of this example, all projectiles were assumed to strike the target at 500 meters/second. This velocity is approximately twice the muzzle velocity of the Cal .45 pistol, so the reader is cautioned not to draw inference on comparative effectiveness among the projectiles used in this presentation. Also shown on this viewgraph is the vulnerability index shown on the previous slide.

We now have the two pieces necessary to provide a figure of merit for the weapon/projectile combination, that is:

1. Vulnerability versus depth.
2. Damage versus depth.

The convolution of these two curves yields a single number for a figure of merit defined as the lethal volume. On Viewgraph 9 is shown the product curve and the integrated lethal volume values for each projectile. Note the low value of lethal volume for the M193 bullet. It ranks low on a relative basis because its energy is not dissipated efficiently within the target medium. The peak on the curve for this projectile represents the start of tumbling which occurs after 15 cm of penetration or well after it perforates the most important vital organs. The Cal .45 pistol bullet is an efficient penetrator, even though the velocity used in this example is about twice muzzle velocity. This is attributable to the projectiles large mass and cross sectional or presented area, and the fact that velocity does not decay appreciably as the projectile penetrates the target medium. Finally, as mentioned, lethal volume is the measure we intend to use to compare and rank competitive projectiles and weapon systems. This measure, along with a graphic representation of how the missile behaves in the target and the effect of this behavior, will make

available new tools to weapons designers, ballisticians and weapons systems analysts.

Now let me attempt to show how the methodology just presented is being used to generate safety criterion for low density fragments. At the 13th Annual Explosives Safety Seminar in September 1971, I presented a simple first approximation model which related the ballistic limit of clothing and skin to the area to mass ratio of steel fragments. Those relationships, shown on Viewgraph 10, established criteria which have been used by the services to establish safety limits for friendly troops during field exercises and tactical training where fragmenting live munitions are employed. More recently the Army has requested quantification of the hazard to friendly troops from low density plastic fragments that merge from breakup of the sabot used to launch a variety of small and large caliber projectiles. Another area of interest concerns that of the breakup of plexiglass windows in helicopters and the ensuing hazard to crew personnel.

The dots on the Viewgraph 10 represent steel fragment data penetrating skin, and the stars represent the ballistic limit of some representative end on plastic sabot fragments penetrating one centimeter of 20% gelatin (only end on hits were evaluated because they represent the most severe threat to personnel). As one centimeter thick slabs of twenty percent gelatin were found to ballistically simulate isolated human skin, it can be observed that the ballistic limits of the end on plastic fragment hits generally agree with those for steel fragments. Thus, we now also have a conservative criteria for troop safety for plastic sabot fragments.

In considering incapacitation or injury criteria, however, it is evident that the penetration characteristics of low density fragments in the human body differ considerably from those of dense chunky projectiles. Thus maximum temporary cavity data for low density fragments penetrating the gelatin simulant should be determined either experimentally, by observing the cavity growth, or computationally, based on a model as to how these cavities formed. However, because of other urgent and high priority requirements we have not as yet been able to pursue these efforts, except

for some limited experimental work which related striking velocity and maximum penetration depths for the plastic fragments represented on this viewgraph.

As previously pointed out, our methodology requires a measure of the vulnerability of the human body as low density fragments perforate, in addition to the measure of the mechanical damage. Fortunately, the Lovelace Foundation for Medical Education and Research recently completed work on plexiglas fragments, under contract for BRL, which become the basis for our developing an interim vulnerability index for low density fragments. Lovelace fired four weights of plexiglass fragments, obtained from blast impingement on helicopter windshields, point first into various anatomical locations of anesthetized shorn sheep. The penetration of the skin and the body wall were related to fragment mass and velocity by probit analysis. The BRL is having the same plexiglass fragments fired into gelatin in order to correlate Lovelace's animal experimental data with gelatin penetration, again by probit analysis. This analysis will quantify two relative measures of injury, a non serious wound and a serious wound. Quantification could be further extended, through medical assessment, by numerically ranking the consequences of skin and body wall penetration as a function of location of hit on the various parts of the anatomy. From this would be generated a vulnerability index for each cross section of the anatomy. As a first approximation, the cavity envelope could simply be the diameter times the width of the cut as a function of penetration depth, as little or no cavitation occurred for velocities associated with Lovelace experiments. The correlation of these two inputs would produce a figure of merit as discussed earlier for the fragment-bullet example.

In conclusion, I have presented a new methodology for addressing research in wound ballistics. The key to our approach requires maximum emphasis on engineering principles, the development of models which quantify relations between projectiles and their dynamic behavior in a tissue simulant, gelatin, and the development of computer codes, which simulate mechanics of penetration. New incapacitation/injury criteria

were developed and integrated into an updated 3-D Computer Man target description. Vulnerability data obtained by simulation with the Computer Man were coupled with modeled projectile cavity contours to obtain a single number as a figure of merit for ranking weapon systems, the lethal volume.

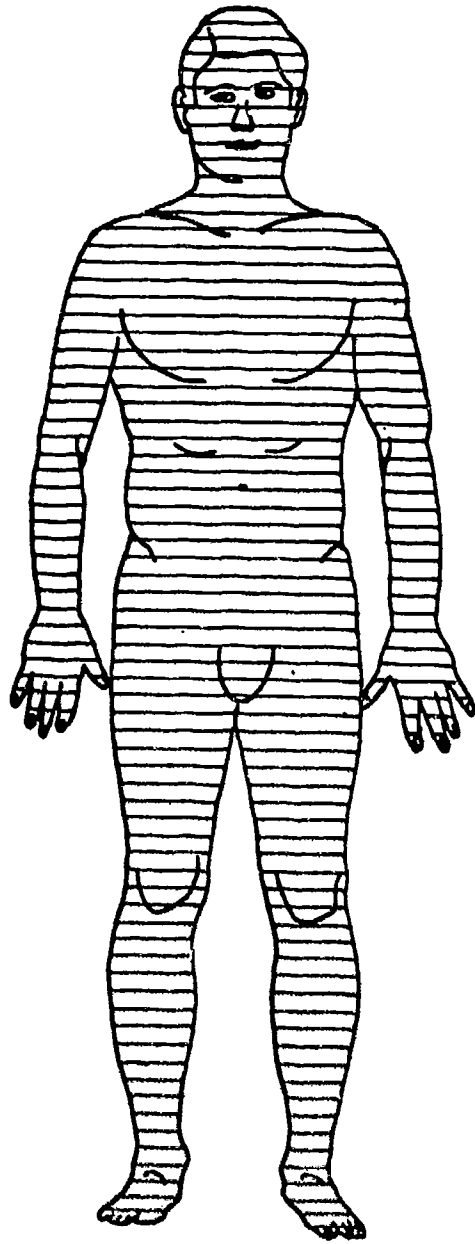
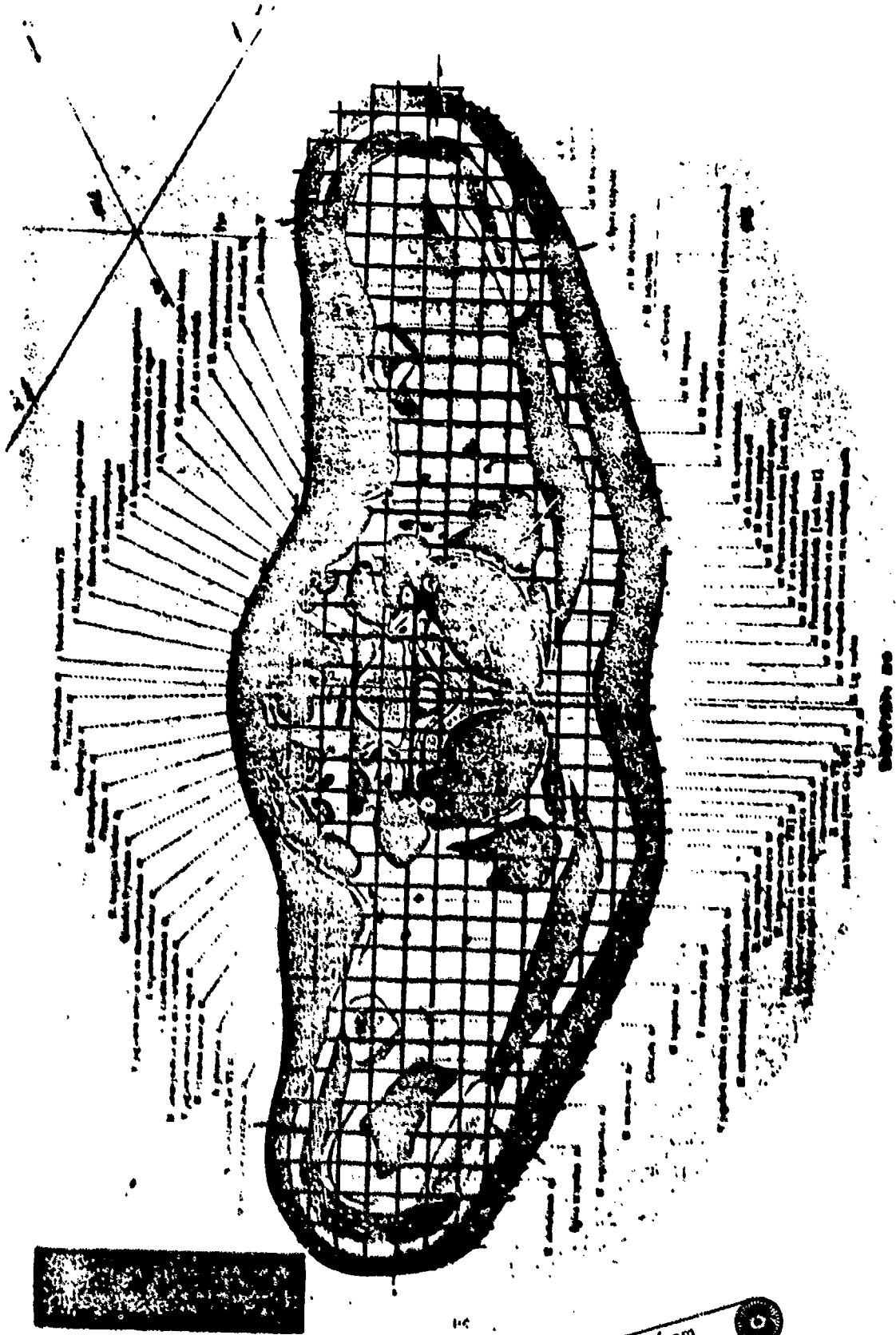


Figure 1.



1218

Reproduced from
best available copy. 6

Figure 2

CURRENT INJURY CRITERIA UNDER CONSIDERATION

Probability of Lethality:

- No treatment
- Treatment after 6 hours
- Treatment after 1 hour

Probability of Incapacitation:

- Immediate
- Within 30 seconds
- Within 5 minutes

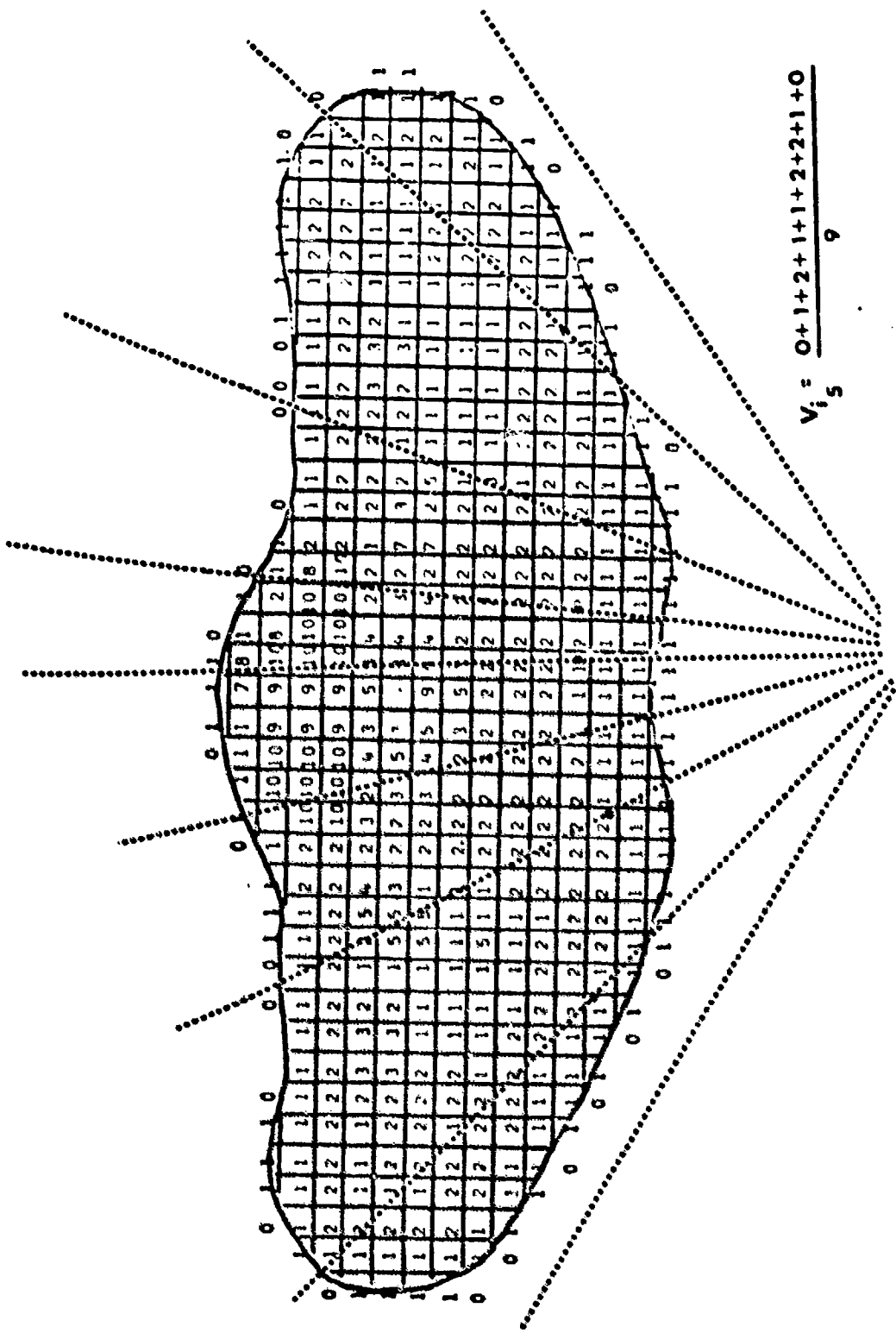
Figure 4.

IMMEDIATE INCAPACITATION:

Purpose: Identify those areas of the body which when rendered non-functional will produce an immediate incapacitation, i.e., no retaliation by an assailant is permitted.

Example of organs/tissues which will result in a 95% decrement:

- Skull
- Brain
- Upper Face
- Cervical Spine
- Brachial Plexus
- Median, Radial, Ulnar Nerves
- Elbow Joint



$$V_i = \frac{0+1+2+1+1+2+2+1+0}{9}$$

Firing Point ~ range, σ

Figure 6

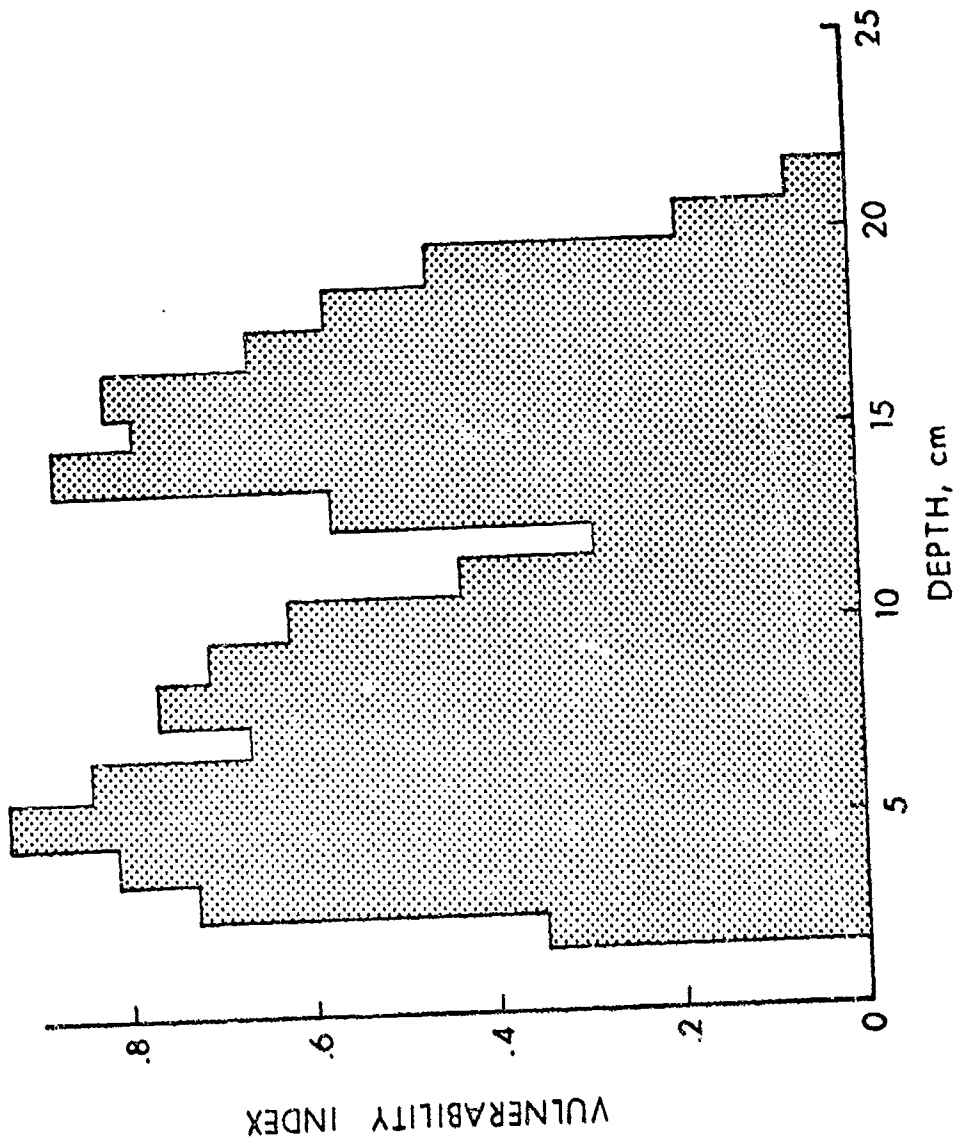


Figure 7.

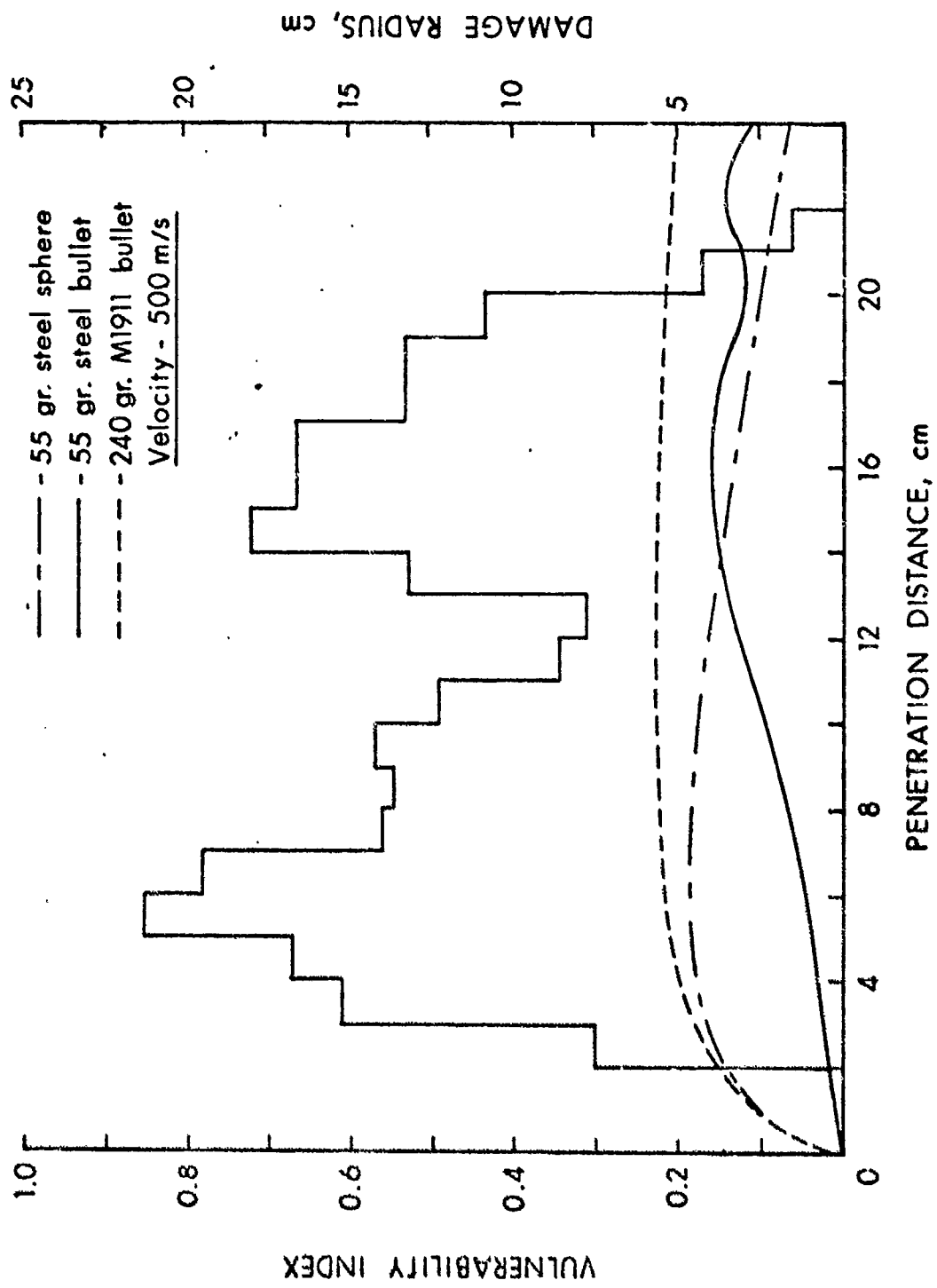


Figure 8

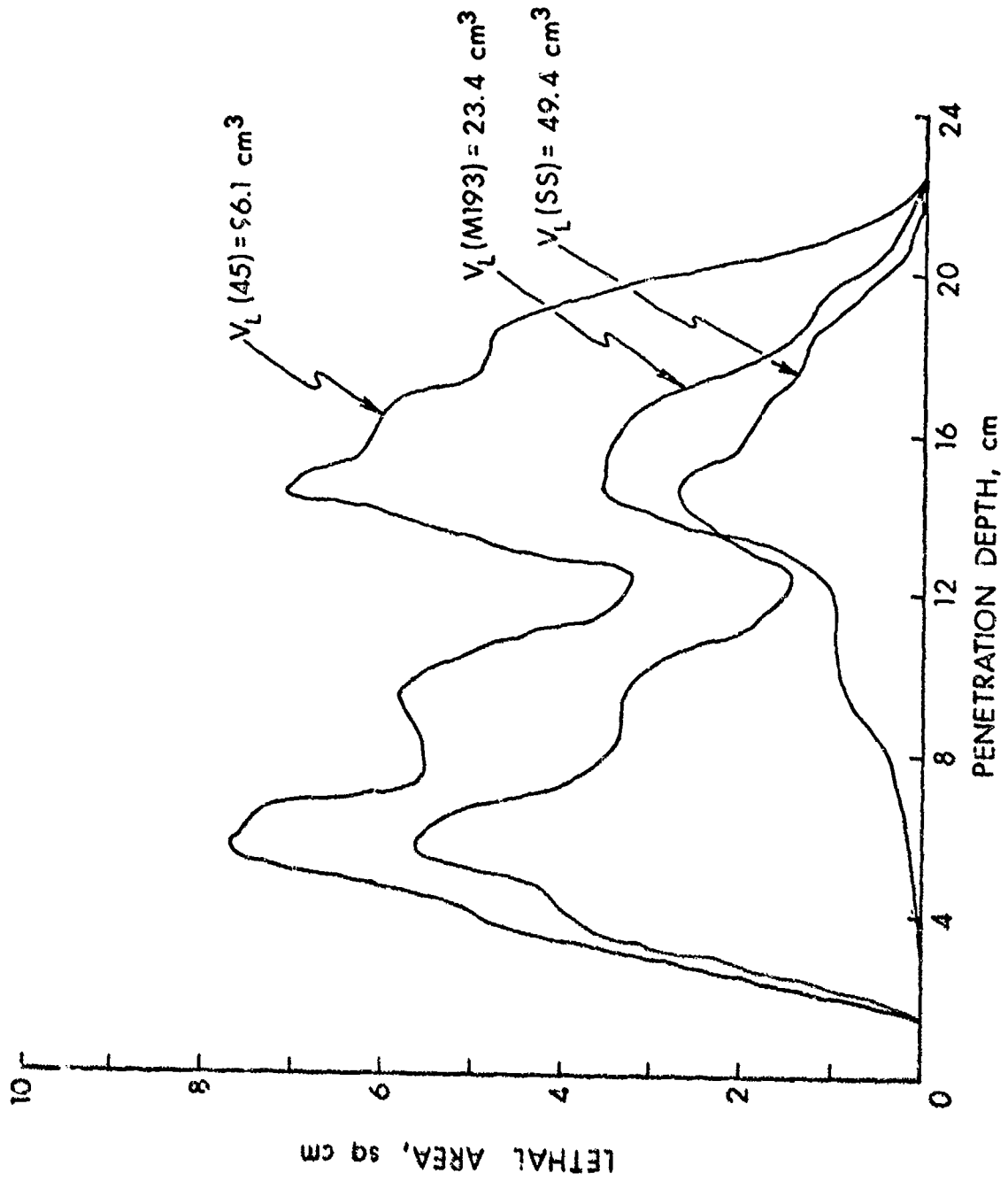


Figure 9.

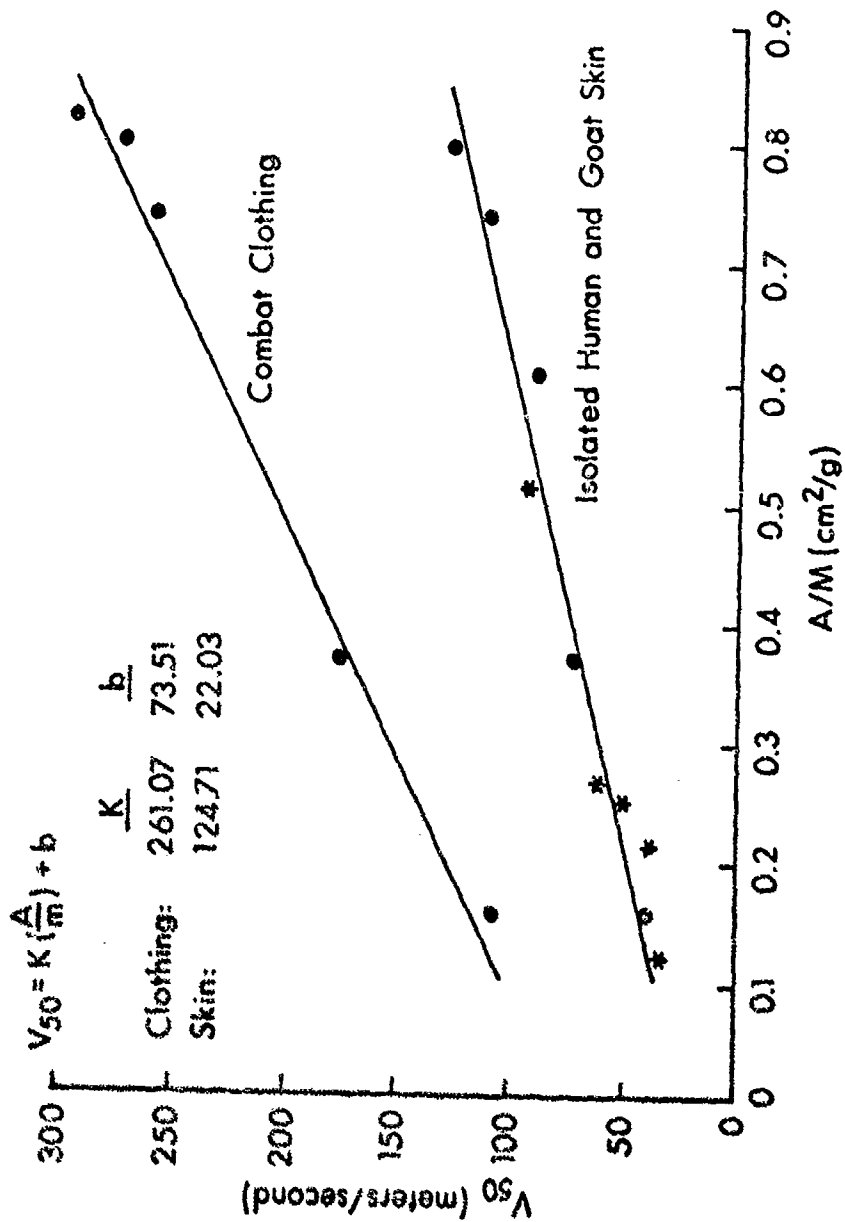


Figure 10.

ELECTRONIC INITIATION OF ENERGETIC SOLIDS

Thaddeus Gora
David S. Downs
Harry D. Fair, Jr.

Solid State Branch
Explosives Division
Picatinny Arsenal
Dover, N.J. 07801

INTRODUCTION

Explosives are members of a class of materials which can exist at normal temperature as pseudostable solids. They undergo decomposition into more stable compounds by rapid self-sustaining decomposition, deflagration, or detonation. They are pseudostable because initiation of the reaction requires that some activation energy be supplied by an external stimulus as illustrated in a reaction coordinate diagram (Fig. 1). R is a generalized reaction coordinate describing the chemical state of a system and can represent, for example, the distance between atoms in a molecule or solid. The effective potential energy (V_{eff}) of an explosive or energetic solid in a pseudostable state is located at a local minimum corresponding to R_1 in Fig. 1. If the system receives the activation energy E_a , chemical reaction takes the system to the state represented by R_2 with the release of chemical or explosive energy E_r .

Any given explosive has a number of reaction coordinates and reaction paths of the type shown in Fig. 1. The quantity of energy required to initiate the explosive reaction, E_a , is different for each explosive and is in general different for each reaction path for a given explosive. This leads to differences in observed activation energies depending on the explosive material, the stimulus, and the effective localization of energy input. Materials with small activation energies may be easily initiated and are classified as sensitive or primary explosives. For some materials, the activation energy may be appreciable (secondary explosives), requiring the use of strong shock waves from sources such as primary explosives to supply the necessary energy for initiation.

It is almost universally (1) assumed that the stimulus supplying the activation energy is first converted into heat, no matter whether it was initially mechanical, electronic, or thermal in origin. The horizontal lines in Fig. 1 represent excited vibrational states of the molecule or solid. Thermal initiation corresponds to raising the local temperature, increasing the excursions of the atomic vibrations, or populating higher excited vibrational states until the activation energy is supplied.

It has been postulated that initiation of reaction and of detonation could arise from purely photochemical processes or by direct excitation of the electrons within the explosive molecules or solid (2). Demonstration of this speculation has been lacking due to the absence of a strong theoretical basis and the ambiguity of much of the experimental evidence.

A general theory relating electronic structure to chemical instability was developed by Williams (3) and is given in Appendix A. Briefly, the quantum-mechanical Hamiltonian governing the motion of the nuclei (atoms and/or molecules) in a solid contains an effective potential in terms of internuclear distance R .

$$V_{\text{eff}}(R) = V(R) + E_{e1}(R);$$

where $V(R)$ is the interaction potential between nuclei, and $E_{e1}(R)$ contains the dependence of electronic energies on internuclear separation. As the latter term can vary strongly from one electronic state to another, the internuclear forces governing chemical reactions and therefore decomposition processes can be strongly affected by populating excited electronic states, as shown in Fig. 2.

Excited electronic states in a solid may differ substantially from the excited states of its constituent atoms or molecules, and in some cases are spatially delocalized over hundreds of atomic or molecular volumes. These states can be excited by optical irradiation of appropriate energy, or by charge injection from appropriate contacts. They may be involved in long-term energy storage. And, perhaps most importantly, the excited electronic states may be mobile in the solid; if they involve charge carriers, external electric fields can influence energy transport, and perhaps lead to avalanching effects.

FUNDAMENTAL ELECTRONIC PROPERTIES

The electronic energy levels of a solid are arranged in a fashion similar to their arrangement in the free atoms or molecules which comprise the solid with several critically important differences. In the solid all of the electronic particles interact, perturbing the atomic or molecular electronic states so that they appear as energy bands rather than discrete levels of energy (4). The bands of energy are separated by energy regions for which no electron energy states are allowed; such forbidden regions are called energy gaps or band gaps. The highest energy band filled with electrons is called the valence band and the next higher band (which is not completely filled) is called the conduction band. Electrons excited to the latter band may move under the influence of an electric field, giving rise to electronic conduction.

The widths of the energy bands, the band gap separation between them, and other features of the bands are referred to as the electronic band structure or the electronic energy level structure. Relatively small differences in the electronic energy level structure can lead to quite marked differences in the behavior or properties of solids. For example, the distinction between insulators, semiconductors, and metals can be made solely on the basis of energy band gap widths and on the distribution of electrons within the band structure. A detailed knowledge of the band structure and of the transport properties of electrons in such semiconductors as germanium and silicon has led to the development of new semiconducting materials and devices. The critical question is whether a similar understanding of the electronic structure of explosive solids can be exploited for discovering equally new and important applications.

Information about the electronic structure is obtained by measuring the spectral response of optical absorption and photoconductivity. These results can often be correlated to provide a basis for understanding the electronic processes involved. Typical results for lead azide are shown in Fig. 3.

The energy states involved in the transitions giving rise to absorption and photocurrents are the lowest and most conveniently accessible excited states and correspond roughly to the band gap of lead azide.

What our investigations have shown is that a combination of a low intensity static electric field and optical excitation in the particular spectral regions corresponding to strong absorption and photoconductivity result in initiation (the photoelectronic initiation or PEI effect). Neither stimulus alone (at the intensities used) produces initiation, and the effect cannot be explained by purely thermal processes (See Appendix B).

This solid state initiation mechanism has been studied in some detail on lead azide (5). In the following we discuss how this result was obtained and the subsequent experiments being performed in an attempt to understand this phenomenon.

Photo-Electronic Initiation (PEI)

The apparatus for the original initiation experiments is shown schematically in Fig. 4. Desired wavelengths were selected by either appropriate filters or by a grating monochromator from a 200 watt Xenon lamp. Threshold electric fields to initiate production-grade lead azide pellets without illumination were 30 kV/cm using silver paint electrodes separated by 1mm. The current-voltage characteristics were found to be ohmic up to the point of initiation, and the typical resistance was 10^{13} ohms (2 orders of magnitude higher than in crystals). Illumination of the area between the electrodes with 400 m μ light (corresponding to the fundamental absorption edge) reduces the threshold voltage for initiation slightly; however, due to the low photoconductivity, the reduction is not spectacular. On a microscopic scale, the pellets are made up of tiny crystallites, and as a consequence the conductivity and electric field distribution is expected to be very inhomogeneous.

For single crystals, threshold average electric fields for initiation without illumination were as high as 15 kV/cm. Applying electric fields of 6-7 kV/cm for long periods of time produced no detectable decomposition of lead azide crystals. The current-voltage characteristics displayed a non-ohmic region at fields just below initiation, a phenomenon not found in pressed pellets.

The photocurrent maximum in lead azide crystals is 1000 times greater than the dark current for the relatively low light intensity used. Thus the population of excited electronic states is considerably increased, enhancing the conditions for instability. With field strengths below the threshold value, no initiation was observed with low light intensity (10^{15} photons/cm²/sec) in the red region of the spectrum. However, as the wavelength of the light was decreased at constant light intensity, lead azide crystals were observed to detonate with approximately 400 m μ irradiation. There is some evidence for current oscillations just prior to the initiation; the time between

the application of light and the initiation of detonation is generally on the order of a few seconds. The threshold electric field for photoelectronic initiation for 400 m μ irradiation is on the average 1/2 that required with no irradiation. Care was taken to exclude heating effects from stray infrared irradiation, and in fact the PEI effect in lead azide was observed at 77°K. In addition, photoelectronic initiation has been observed in silver azide crystals and most recently in crystals of thallos azide.

The apparently non-thermal (see Appendix B) nature of the PEI effect, its dependence on the wavelength of optical irradiation, and its non-ohmic I-V characteristic below the initiation threshold electric field all suggest a direct electronic mechanism.

Electric Field Effects

To gain an understanding of the effect of the electric field in the absence of photo-effects a detailed study of the current-voltage characteristics and thickness dependence was made. Gold electrodes were applied to both sides of single crystal lead azide plates by vacuum evaporation. These gold electrodes were then contacted by gold wires using dots of silver paint. Sample thickness varied from .019 to .076 cm in this series of experiments. The electrode diameter, 2.36mm, was the same on all samples. By keeping the evaporated electrode diameter large compared to the sample thickness, the results can be analyzed on the basis of one-dimensional planar current flow (6). An advantage of the sandwich-type electrode configuration is that surface currents can then be essentially eliminated. The samples were potted in RTV, a polymeric electronic potting composition, which aids in prohibiting current flow by any path other than through the bulk of the sample. This is shown in Fig. 5.

An inherent procedural difficulty arose because of the possibility that lead azide crystals subjected to high electric fields may experience localized decomposition or other damage prior to detonation. This could act as a memory of previous treatment and might influence both the conductivity and critical voltage for detonation. One solution would be to use a fresh crystal for each value of applied voltage. However, this procedure would require an unrealistic number of samples with accurately controlled thickness. To minimize memory effects, each sample was subjected to the same voltage history. Our procedure consists of one-minute-on, one-minute-off application of voltage, increasing the voltage in 100V increments. The procedure was continued until the sample detonated, with current being monitored continuously.

Seven samples of varying thickness were investigated in this manner. The voltage at which detonation occurred, (V_{DET}), is shown in Table I along with the current just prior to initiation, I. It should be noted that the detonation does not generally occur immediately upon application of the voltage. The delay time was observed to vary. Typical current-voltage characteristics are shown in Figs. 6 and 7 and reflect the non-ohmic nature of the Au/lead azide system.

The voltage applied to a crystal can under some circumstances produce a constant electric field throughout the sample given by V/L , where L is the sample thickness. That is, the contacts to the crystal do not affect the field distribution in any way (the contacts are ohmic). On the other hand, it is possible that the contacts to the sample are non-ohmic and restrict the flow of current. This kind of contact is called a blocking or rectifying contact; and, because it can present more resistance to current flow than the bulk resistance of the sample, the field distribution may be altered considerably. Gold forms a non-ohmic contact with lead azide (7). The effectively higher resistance of the Au/lead azide interface can result in a significant voltage drop across this region, with considerably less voltage actually applied across the bulk of the sample.

The average field for detonation, calculated for each crystal from V_{DET} divided by the sample thickness L, ranges from 3.02×10^4 - 4.21×10^4 V/cm. Thus there is a threshold in this average field range at which detonation occurs. The scatter in values could be accounted for by differences in the crystal-electrode interfaces or differences due to crystal orientation. The threshold field values for the four thinnest samples (.049 - .025 cm) are all higher than those for the thicker samples (.043 - .076 cm). This would be expected if effects resulting from exposure to electric fields tend to lower the field threshold since the thicker samples experienced longer cumulative exposure times to electric fields.

MODEL FOR THE PHOTOELECTRONIC INITIATION EFFECT

The photoconductivity and electric field studies have led to a number of specific and general conclusions on the individual phenomena investigated. Our purpose, however, was not only to understand the separate phenomena but to relate them to understand the nature of the more complex PEI effect. It is now possible to infer a mechanism for the PEI effect.

We first review the evidence pertinent to the mechanism. Neither the field alone nor the light alone, at the intensities used, can produce initiation by simple thermal effects. Similarly, the combination of light and electric field intensities used in the PEI effect are not sufficient to lead to initiation thermally. Even if all of the energy released by exothermic photodecomposition reactions is taken into account, the magnitude of the efficiency for photodecomposition is far too small to provide sufficient thermal energy to initiate fast decomposition. The exciting light does lead to the production of nitrogen gas and to the formation of lead colloids (8,9). The resulting decomposition may produce energy states which enhance reaction. In addition, the exciting light produces large changes in the electrical conductivity (up to four orders of magnitude) by the production of photocarriers (5). Initiation clearly occurs in response to an applied electric field, and an average field value has been determined experimentally.

In order to initiate lead azide by light alone, an intensity six orders of magnitude greater than that used in our experiments is required (Appendix B). However, with the low light intensity used in the PEI effect, the value of the applied voltage is of the order of half that required to initiate with electric field alone. Therefore the primary effect of the exciting light combined with the applied electric field is to change the electric field distribution in the lead azide. This accounts for the factor of two or more decrease in average electric field necessary to achieve initiation with light. Figure 8 depicts a uniform voltage drop, which by Maxwell's equations predicts a constant electric field and overall zero net charge. This approximates conditions in the bulk of the crystal in the absence of light, and is generally correct independent of the nature of the contact/sample interface. When the light is turned on, charge carriers of both signs are produced, either directly or through the intermediate step of exciton formation. The original applied electric field separates charge carriers of opposite sign. The resulting charge distribution alters the electric field distribution. The nature and degree of the charge separation are related to the carriers' conductivity properties, the intrinsic defect structure of the crystal, and possibly to the photo-produced defects. In addition, the charge distribution can be strongly affected by the presence of blocking contacts which prohibit the flow of charge into and out of the sample. Charge can accumulate at the interface, producing high fields across the contact region, and considerably altering the field in the bulk. For example, the arbitrarily chosen charge distribution shown in Fig. 9 leads to the indicated voltage and field distributions. The important point is that upon illumination, the resulting photo-induced charge distribution leads to an increase in the electric field

at some point in the sample by a factor of two or more above that which it had in the nonilluminated case. This increase in internal electric field is sufficient to produce initiation.

Although there is not yet a clear understanding of why a threshold electric field at a given region of the sample causes initiation, one plausible explanation is that the electric field produces an avalanche multiplication of charge carriers. This results in a region of dense electronic excitation leading to an ultimate exothermic process. This is further supported by the fact that low-intensity light alone does not produce these regions of dense electronic excitation.

CONCLUSIONS

Our theoretical studies (5) indicated the possibility of initiating decomposition and detonation by several radically new mechanisms. The photoelectronic initiation effect in lead azide was the first experimental observation of the initiation of detonation by purely non-thermal electronic processes. To understand this phenomenon, techniques were developed to grow, cut and polish large pure single crystals of lead azide. The separate effects of light and electric fields on lead azide single crystals were studied to determine the detailed mechanisms of the interactions. These were related to develop an understanding of the PEI effect in terms of threshold average electric fields. Illumination creates photo-carriers which change the electronic charge distribution within the lead azide, raising the electric field to the threshold for initiation. These results provide the understanding to apply the photoelectronic initiation effect to other technologically important explosives, and provide the rational basis for pursuing related new mechanisms for initiation.

APPENDIX A

Williams (3) has considered from a general theoretical point of view the relationship between the electronic energy states or the electronic structure and chemical instability or initiation.

According to quantum mechanics, all information about a physical system is contained in its wavefunction $\psi(\underline{r}, \underline{R})$. The coordinate \underline{r} stands for all the electronic coordinates while \underline{R} represents the coordinates of the nuclei. This wavefunction satisfies the Schrödinger equation:

$$H \psi(\underline{r}, \underline{R}) = E \psi(\underline{r}, \underline{R}),$$

where H is the Hamiltonian operator containing the kinetic energies of all the particles (nuclei and electrons) and all the potential interactions and E is the energy eigenvalue. From the difference in mass of the electrons m and the nuclei M_j and from equipartition of energy, it is evident that the electrons move much more rapidly than the nuclei. Thus at each instant, the motion of the electrons or the electron distribution can be determined as though the nuclear positions or coordinates were fixed. The electronic motion can then be determined parametrically as a function of the nuclear coordinates since the electrons exist in separable, approximate stationary states that are smoothly modified by the motion of the nuclei. This is the adiabatic approximation of Born and Oppenheimer (10). In accordance with the adiabatic approximation, the wavefunction can be put into the following form:

$$\psi(\underline{r}, \underline{R}) = \phi_{\underline{R}}(\underline{r}) \chi(\underline{R});$$

$\chi(\underline{R})$ describes the state of the nuclei and $\phi_{\underline{R}}(\underline{r})$ the state of the electrons about fixed nuclear coordinates \underline{R} . The stationary electronic states are determined from the following Schrödinger equation where the nuclei are taken to be fixed:

$$H_{el} \phi_{\underline{R}}(\underline{r}) = E_{el}(\underline{R}) \phi_{\underline{R}}(\underline{r}),$$

where H_{el} is that part of the total Hamiltonian operator containing the electronic coordinates only, $E_{el}(\underline{R})$ are the electronic eigenvalues or electronic energy levels, and \underline{R} specifies the fixed nuclear positions R_1, \dots, R_n . The equation describing the motion of the nuclei is approximately:

$$\left(- \sum_j \frac{\hbar^2}{2M_j} \nabla_{\underline{R}_j}^2 + V(\underline{R}) + E_{el}(\underline{R}) \right) \chi(\underline{R}) = E \chi(\underline{R}),$$

where the first term represents the kinetic energies of the nuclei and $V(\underline{R})$ the potential interactions between nuclei. The validity of the approximations used in deriving this equation, particularly for large excursions in \underline{R} occurring during chemical reactions, has been discussed by Williams (3).

Assuming the approximate validity of the preceding equation, it is clear that the motion of the nuclei is determined by the effective potential

$$V_{\text{eff}}(\underline{R}) = V(\underline{R}) + E_{\text{el}}(\underline{R}).$$

Thus the important conclusion is that the motion of the nuclei depends not only on the internuclear interactions but depends, in addition, explicitly on the electronic state of the system, $E_{\text{el}}(\underline{R})$. A schematic presentation of this concept appears in the reaction coordinate diagram, Fig. 2. The shape of V_{eff} can be quite different for the electronically excited state E'_{el} than for the electronic ground state E_{el} with a lower activation energy. For other electronically excited states such as that represented by E''_{el} in Fig. 2, a substance when excited to this electronic state would be completely unstable since there is no activation energy required to lead to the lower decomposed state. Thus even at low temperatures, characterized by small atomic vibrations, it would be possible in this system to initiate decomposition purely by excitation to this excited electronic state.

Thus in general, states of electronic excitation in a chemical system can determine the manner in which chemical reaction proceeds. When the chemical system is an explosive, radically different modes of initiation of reaction are possible. Specific initiation mechanisms will depend on the excited electronic states or on the fundamental electronic properties of particular explosive substances.

APPENDIX B

Non-Thermal Nature of the Photo-Electronic Initiation Effect

The important question of whether the photoelectronic initiation effect is a thermal or non-thermal mechanism may be answered by considering the threshold energy densities required for the initiation of single crystals of explosive azides by intense light flashes. In these materials, for strongly absorbed light pulses of 1-10 microsecond duration, threshold light energy fluxes of 0.1 cal/cm^2 are sufficient to initiate detonation (11). For flashes lasting near 1 millisecond, threshold energy fluxes are about ten times greater. It has been assumed that the energy from these intense light flashes rapidly degrades to heat and that flash initiation is caused by a thermal mechanism. The energy fluxes involved then serve as a useful lower limit for energy densities necessary to initiate detonation thermally in single crystals for energy vs distance profiles similar to the ones in our photo-electronic initiation experiments. To be specific, we assume throughout this discussion that all radiation being considered falls in a spectral region corresponding to an absorption coefficient of 10^5 cm^{-1} , rather strong absorption. Then, as depicted in Fig. 10, the bulk of the irradiation is absorbed in a surface layer 1000\AA (10^{-5} cm) deep. This gives a threshold absorbed energy density of 10^4 cal/cm^3 for flash-induced initiation or a power density of $10^{10} \text{ watts/cm}^3$ for a 1 μsec flash duration.

In the photo-electronic initiation experiment, two sources of external thermal energy input are present: degradation of absorbed light energy into heat and joule heating due to photocurrents. The light intensity used here corresponds to a power flux of $10^{-1} \text{ watts/cm}^2$ (10^4 watts/cm^3 in the surface layer), a factor 10^6 smaller than the light power density used for flash initiation. In the absence of any heat flow, the present irradiation has to continue for about 1 second to reproduce the energy densities achieved in the flash initiation experiments. But in point of fact, it can be shown that a heat pulse applied uniformly at the surface will diffuse over a surface layer $10,000\text{\AA}$ (10^{-4} cm) deep in 1-10 microseconds even for poor thermal conductors. Thus initiation in these azide materials is not expected for such low light intensities applied without an electric field. This expectation is indeed borne out experimentally: decomposition can occur at these intensities but not the initiation of detonation.

The second source of thermal energy mentioned was joule heating due to photoconductivity. Because the photoconductivity is so much stronger than the dark conductivity, it is clear that almost all the photocurrent flows in the thin 1000A layer at the surface where the absorption is strong (Fig. 10). Estimating the power absorption density in different regions of the surface layer depends on the electric field distribution and on whether the current flows over the entire surface area or in a thin filament connecting the electrodes. For a uniform field distribution, the joule heating power density for currents measured just below threshold is 10 watts/cm³, 1000 times less than that due to the light irradiation alone. It is not possible to exceed the power density input of the light by considering that most of the voltage drop takes place over a small fraction of the inter-electrode distance because the resulting fields would be in the dielectric breakdown range (about 10⁶ V/cm). Although dielectric breakdown cannot be discounted as an initiation mechanism, it is not a strictly thermal mechanism. Further, even under the most extreme assumptions, thermal initiation requires all the photocurrent to be carried by a filament less than 1000A (10⁻⁵ cm) in diameter with local fields approaching the dielectric breakdown limit. The formation of filaments of this nature could not be explained by simple thermal arguments.

Thus we see that the thermal energy densities achieved in our photo-electronic initiation effect are far too small to explain the effect by simple thermal arguments. It would appear that detonation is instead initiated by an electronically excited state of the crystal (which is itself a result of the combination of electric field and light) as the general theoretical argument predicts.

REFERENCES

1. A. Macek, *Chem. Rev.* 62, 41 (1962).
2. F. P. Bowden and A. D. Yoffe, Fast Reaction in Solids, Chapter VI (Academic Press, New York, 1958) and Explosives Division Semi-annual Reports 1965-70.
3. F. E. Williams in Chemical Dynamics, J. O. Hirshfelder and D. Henderson, Eds. (Wiley-Interscience, New York, 1971), p. 289.
4. See, for example, C. Kittel, Introduction to Solid State Physics (John Wiley & Sons, Inc, New York, 1967).
5. H. D. Fair et al, PATR 4607 (1973).
6. M. Lampert and P. Mark, Current Injection in Solids (Academic Press, New York, 1970).
7. D. S. Downs, PATR (in publication).
8. W. Garret in High Energy Chemistry: Physics and Chemistry of the Inorganic Azides, H. D. Fair, Ed. (Plenum, New York, in publication).
9. D. A. Wiegand, PATR 4080 (1970).
10. M. Born and J. R. Oppenheimer, *Ann. Phys.* 84, 457 (1927).
11. F. P. Bowden and A. D. Yoffe, Fast Reactions in Solids (Academic Press, New York, 1958), pp. 88-112.

TABLE I
ELECTRIC FIELD EFFECTS ON LEAD AZIDE

Sample	Thickness L(cm)	Current at Detonation (amp)	Voltage at Detonation V_{DET}	Threshold Field V_{DET}/L (Volts/cm)
3-72-30	.019	1.2×10^{-9}	800	4.20×10^4
3-72-31	.024	6.9×10^{-8}	1000	4.17×10^4
3-72-32	.022	7.0×10^{-9}	800	3.60×10^4
3-72-33	.043	1.6×10^{-8}	1300	3.02×10^4
3-72-34	.025	1.4×10^{-8}	1000	4.00×10^4
3-72-35	.076	5.5×10^{-9}	2700	3.54×10^4
3-72-36	.073	1.1×10^{-8}	2400	3.26×10^4

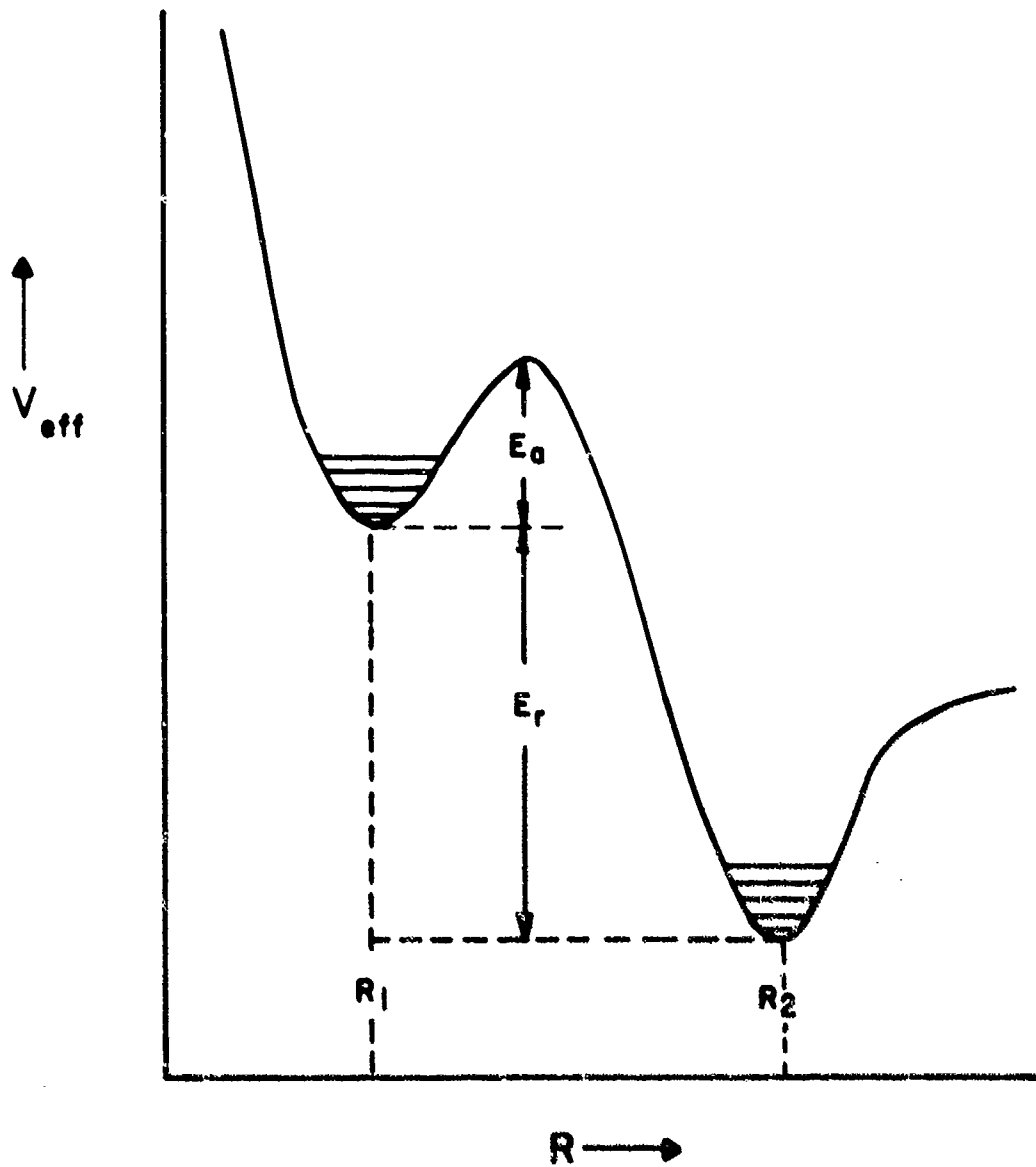


FIGURE 1 - Reaction Coordinate Diagram Depicting the Metastable Character of Reactive Solids

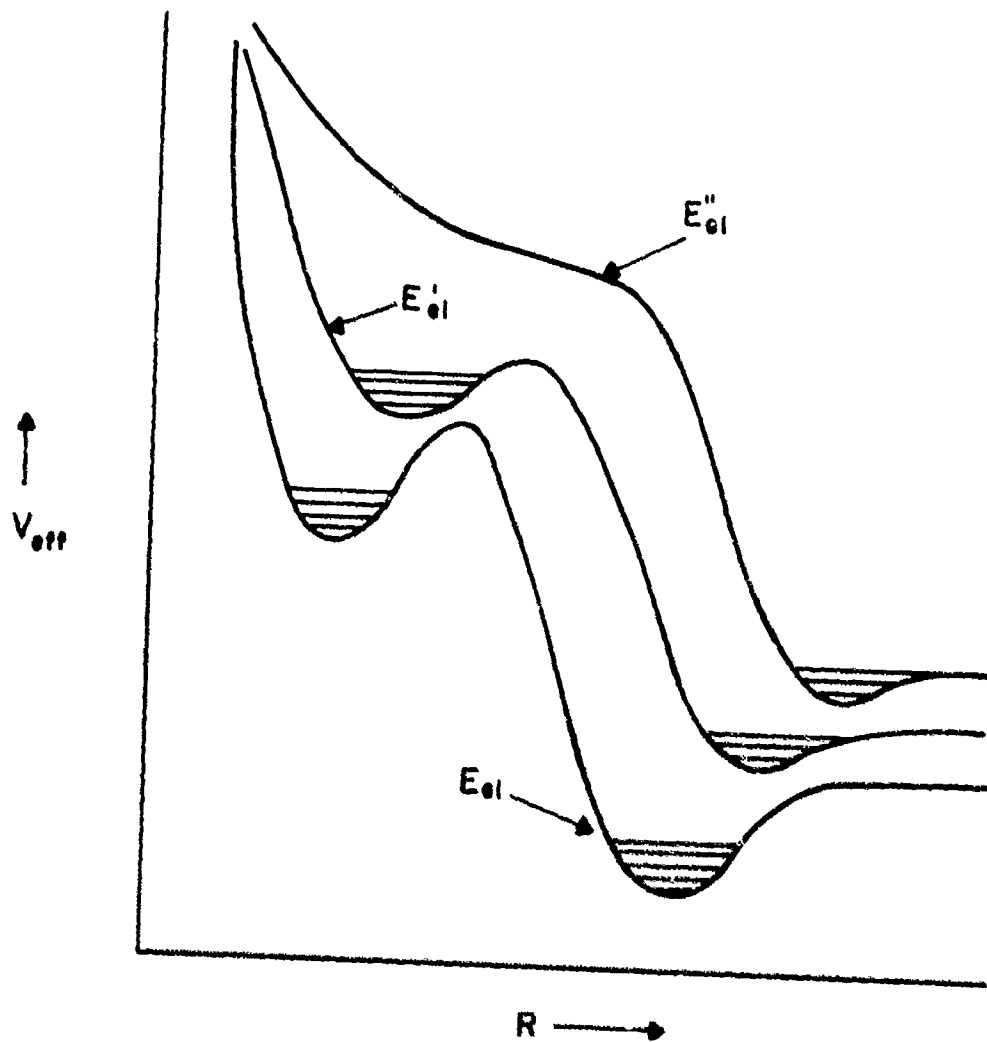


FIGURE 2 - Reaction Coordinate Diagram Depicting Possible Changes in Activation Energy Due to Excited Electronic States

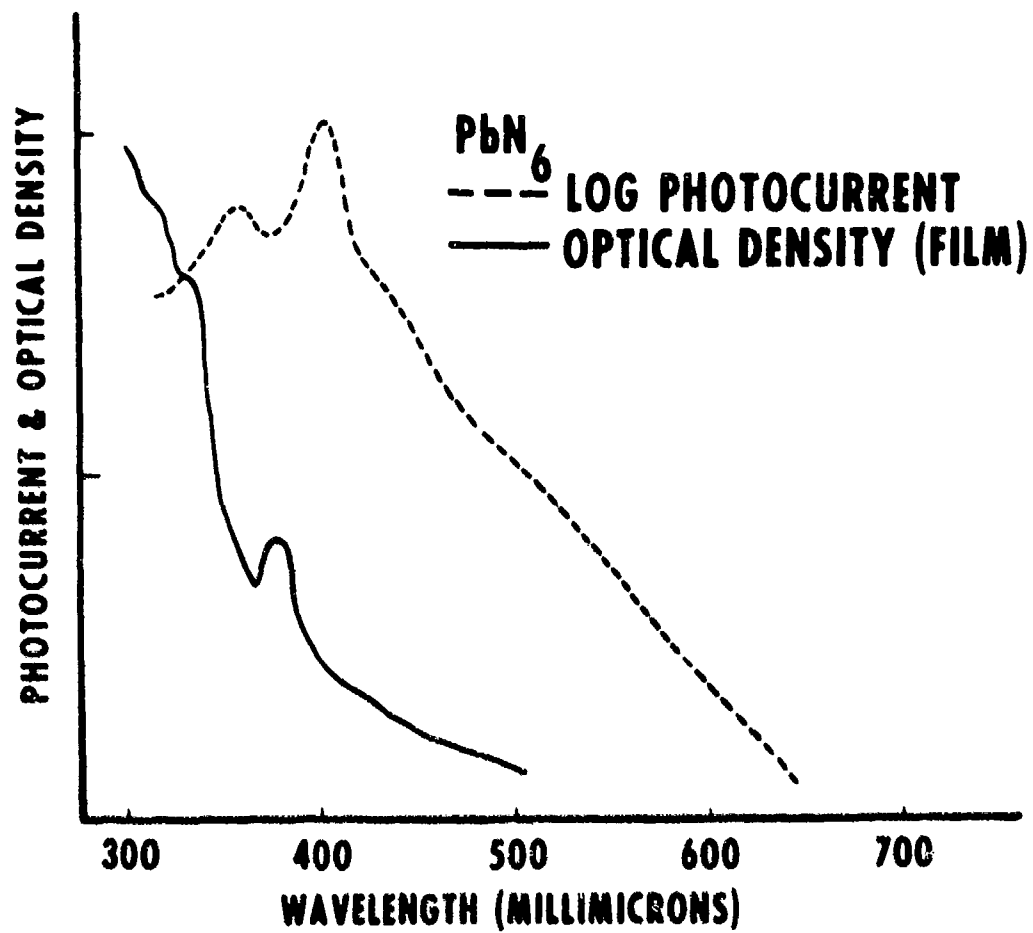


FIGURE 3 - Spectral Response of Optical Absorption (—) and Photo-Current (---) in Lead Azide

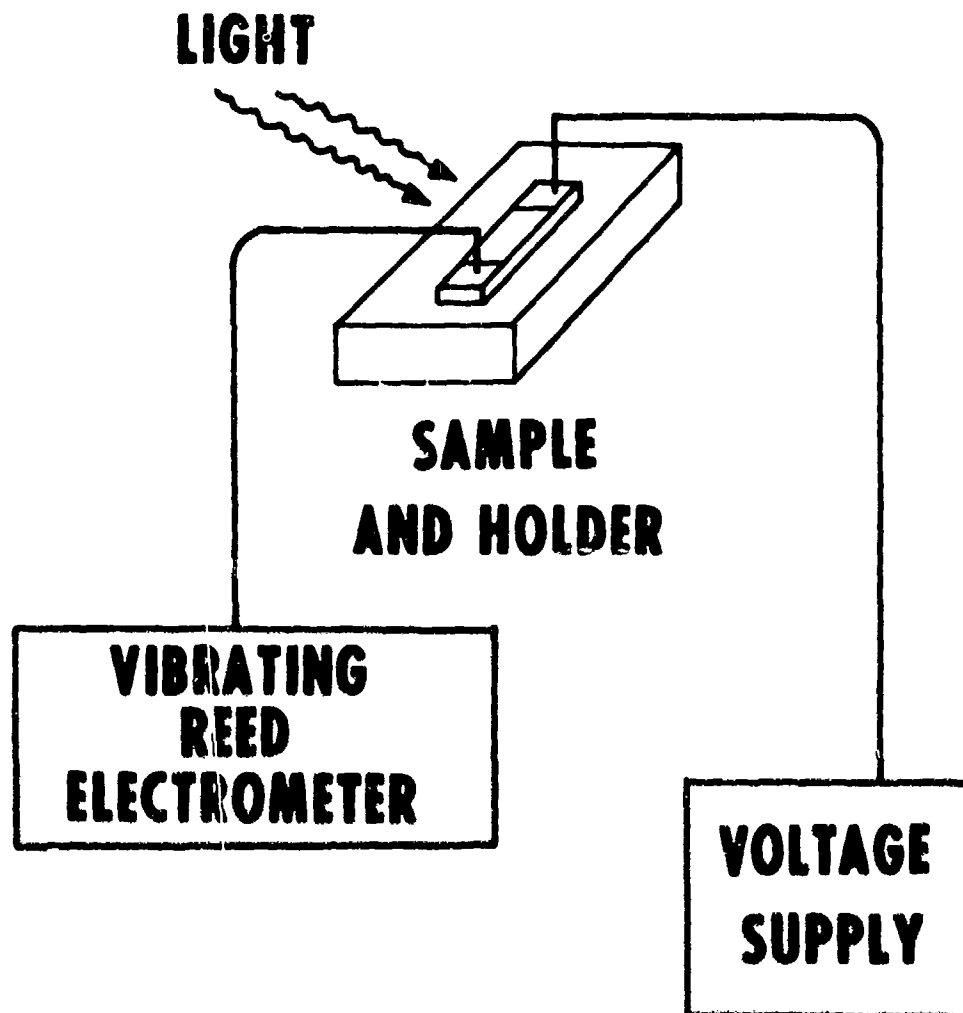


FIGURE 4 - Experimental Arrangement for Investigation of the Photo-Electronic Initiation Effect

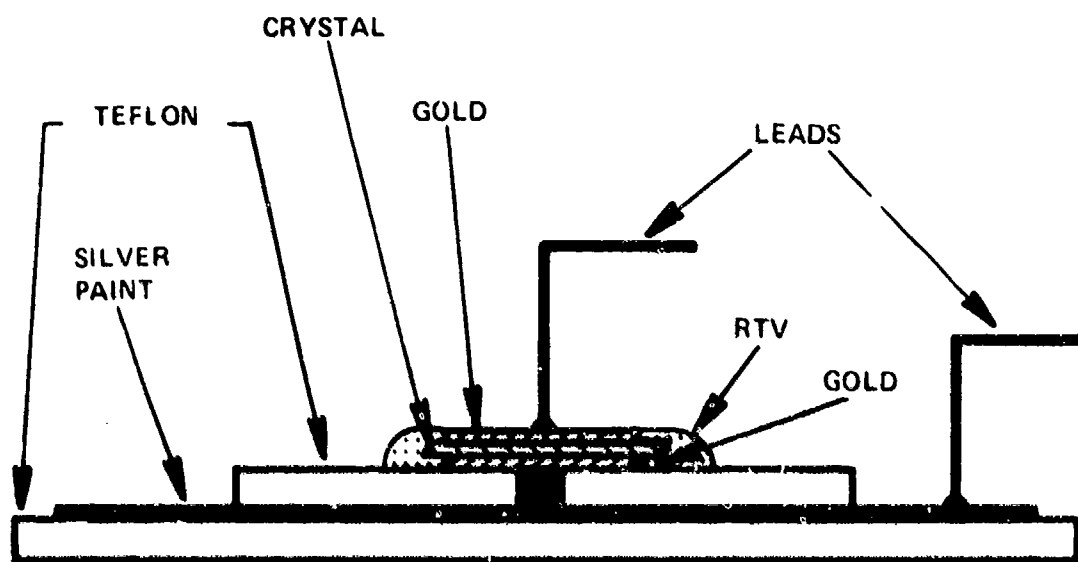


FIGURE 5 - Sample Mounting for Investigation of Electric Field Effects

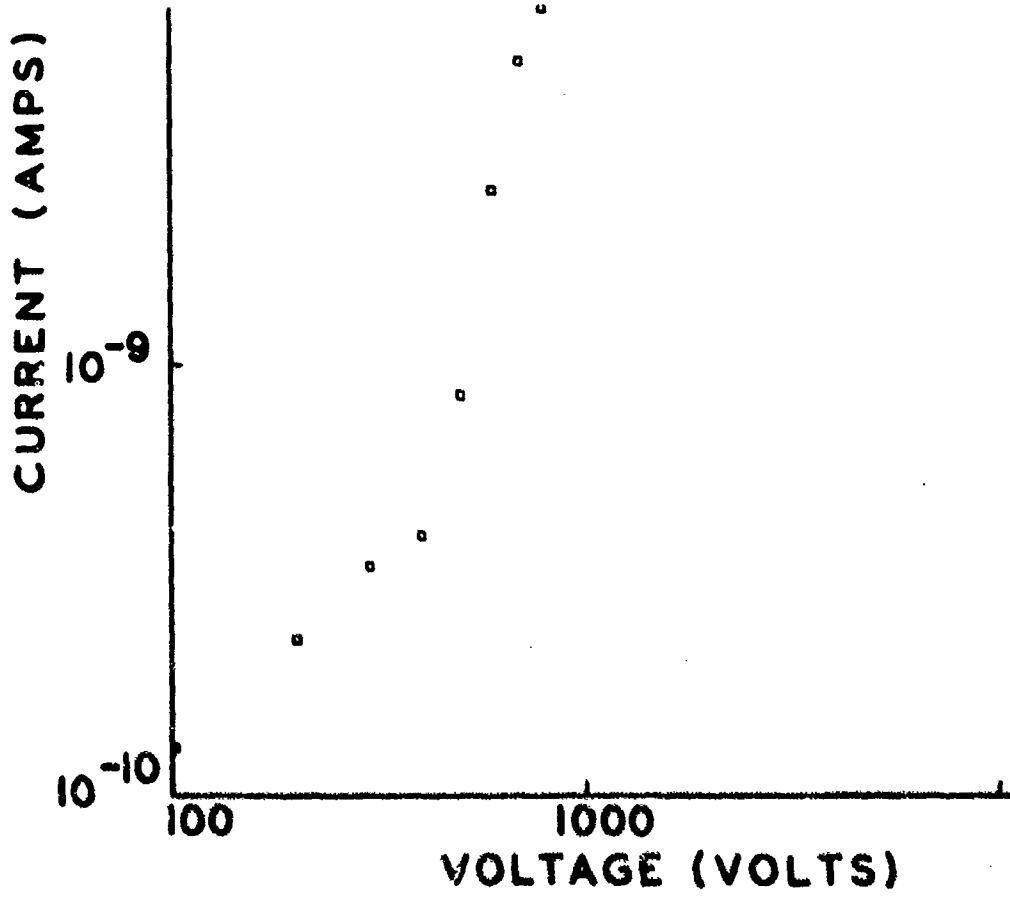


FIGURE 6 - Current-Voltage Characteristic for .025 cm Thick Lead Azide Crystal with Gold Electrodes

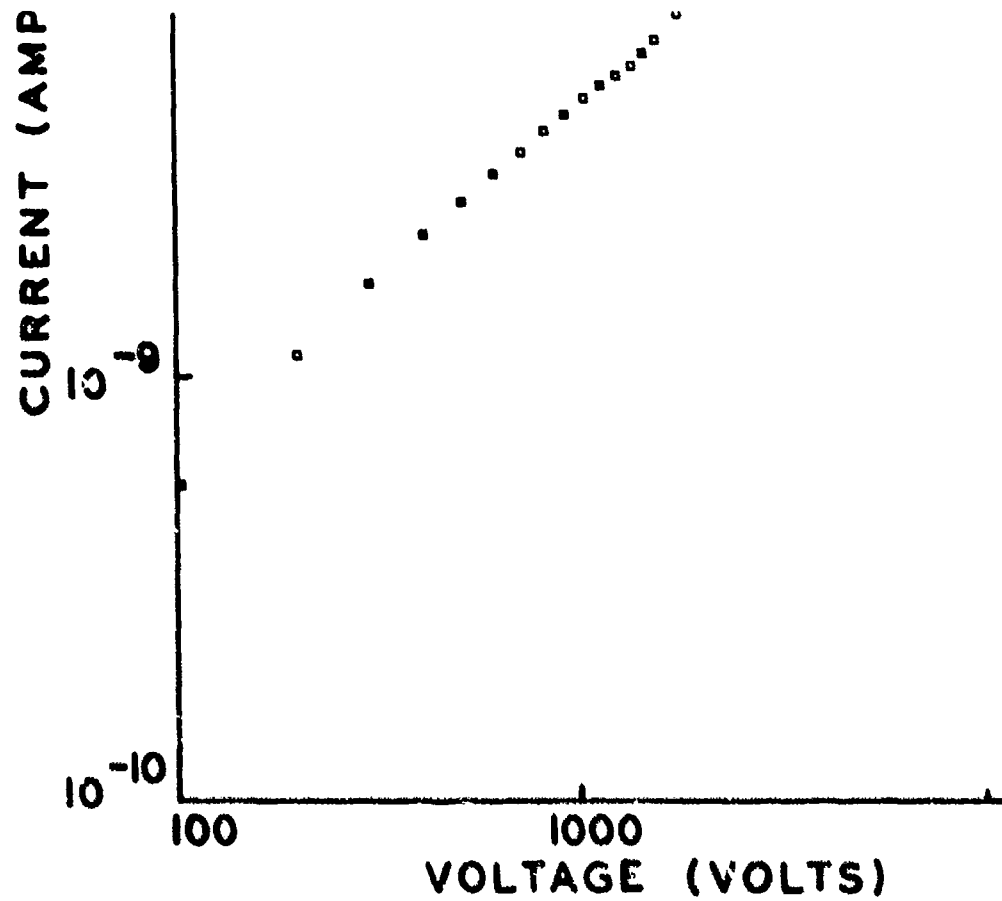


FIGURE 7 - Current-Voltage Characteristic for .073 cm Thick Lead Azide Crystal with Gold Electrodes

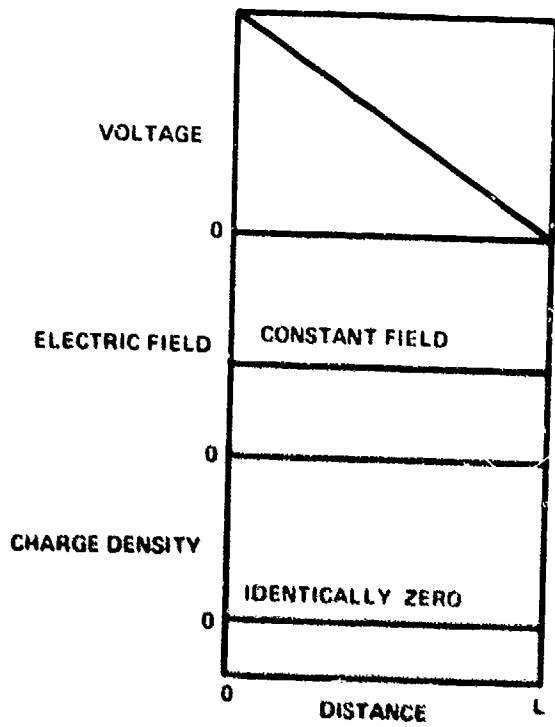


FIGURE 8 - Voltage and Charge Profiles for the Constant-Field Case

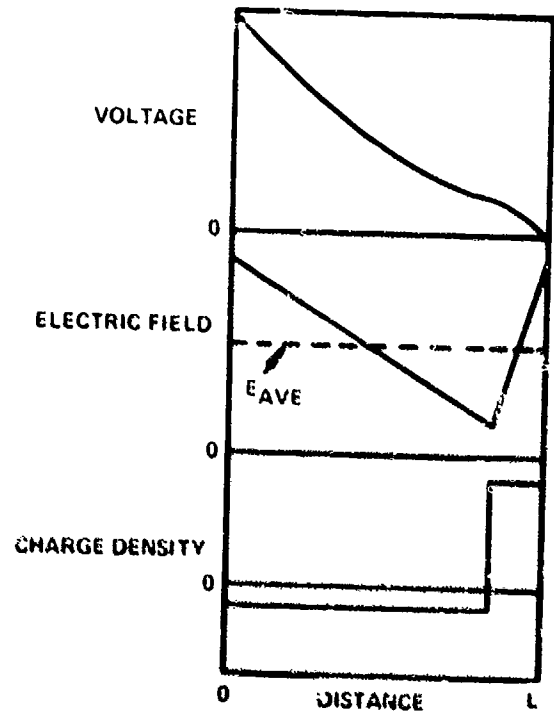


Figure 9 - Voltage and Field Profiles Resulting from a Non-Uniform Charge Distribution E_{ave} = Applied Voltage/L.

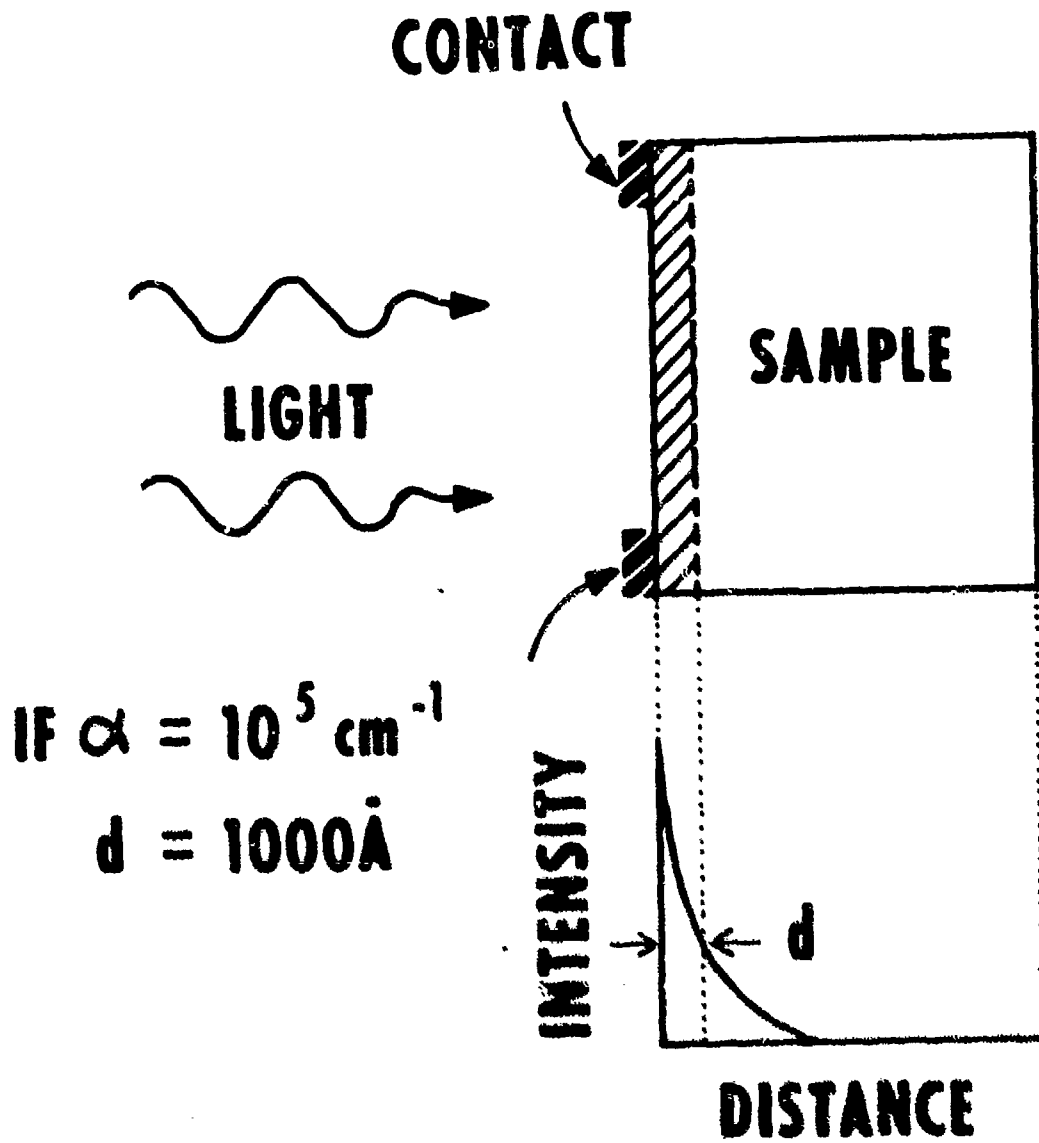


FIGURE 10 - Effective Volume of Photo-Electronic Excitation for Direct Initiation

GENERATION AND DISSIPATION OF ELECTROSTATIC CHARGES
ON EXPLOSIVE POWDERS

Bernard D. Pollock
Explosives Division, FRL
Picatinny Arsenal, Dover, NJ 07801

ABSTRACT

The charging of explosive powders was investigated by means of a vibrating trough apparatus in which the predominant mechanisms, contact and induction, could be simultaneously observed. Graphite-coated propellant is an example of an inductively charge powder, RDX is an example of contact charge powder, and lead azide is a "hybrid".

Charge relaxation on representative primary explosives was investigated by charging small amounts of a powder by a corona discharge and observing the decay of charge by means of a sensitive electrometer. This provided a method of measuring relative resistivities of powders. Photoconduction was clearly evident in lead azide and tetracene, though not in lead styphnate. Decay rates could be increased appreciably by addition of 0.1 to 0.2 wt.-% of antistatic agents, but were very much more markedly influenced by changes in relative humidity.

I will describe our work on the electrification of explosive powders and on the relaxation of charges. Because of the sensitive nature of these powders, the techniques and procedures used in this work may be of interest.

I will begin with the charging work. There are two mechanisms by which powders are electrified during handling. The first is by contact, and the other is by induction. Contact charging can occur when two different substances, at least one of which is a non-conductor, come into intimate contact and are then separated. Charging by induction can occur when two conductors are placed in an electric field and then separated. In most of the previous work on powders, the mechanism involved has been contact charging, and the usual method of investigation has been to allow a mass of powder to slide down a chute or tube, usually under the influence of gravity. The apparatus used in this work consisted of a metal trough "driven" by a small vibratory motor of the type used to move powder or small parts, a Faraday cage and an electrometer. A 1/8" diameter rod was positioned above the trough and was insulated from it. The rod could be grounded to provide electrostatic shielding, or could be connected to a source of voltage to investigate the influence of an applied electric field. Figure I is a schematic representation. The Faraday cage, you may recall, is no more than a special form of capacitor, which consists of a

pair of concentric containers insulated from one another and in operation it is charged by putting something that is charged into the inner container. The voltage that is thus induced is measured by means of an electrostatic voltmeter or in our case, by a sensitive electrometer. This permitted using quite small amounts of powder. Many of these experiments were performed with 5 or 10 mg, though the amounts ranged from 0.3 to 35 mg in some series of experiments. The advantage of the vibratory motor was that it gave good, controllable contact between the powder and metal.

Most of the work was done with various commercial types of lead azide, but some experiments were made on graphite-coated propellant, a highly conductive powder in electrostatic terms, and on RDX, a non-conductor, in order to clearly illustrate two types of charging.

Among the parameters investigated were trough metal, type of powder, and manner of feeding the powder into the trough. However, the experiments, in which particle size, amount of powder and electric field were varied, were the most informative⁽¹⁾. The family of curves in Figure 2 illustrate the dependence of charge on quantity and on particle diameter. From the slopes on the log-log plots we can see that the charge is approximately proportional to the square root of amount. Also the charge per unit mass at a given sample size increases with decreasing particle diameter.

In a separate series using 5 or 10 mg samples of powder having narrowly defined particle diameters, it was found that for a given lot of powder, the charge per unit weight was inversely proportional to the first power of the particle diameter. One can infer that the charging would be proportional to the number of contacts between a particle and the metal.

In the next figure, Figure 3, the influence of an electric field on the charging of lead azide is shown. The linearity - up to a point - is evident. The intercept with the ordinate, i.e. at zero applied field, corresponds to contact charging. Note that it is possible to compensate for this by applying an external field of appropriate direction and magnitude. The curvature in the left side, with negative voltage on the upper electrode, was due to electrostatic attraction, which caused the particles to be picked up, charged in the opposite sign, and then be repelled away from the upper electrode. Most of the particles were thrown away from the apparatus. Incidentally this effect did not cause any initiations.

The behavior of a conductive powder, (graphite-coated propellant) and of a non-conductive powder (RDX), is compared with that of lead azide in Figure 4. The curves are for 25 mg samples in all cases, and in the case of the RDX and lead azide, the particle sizes were comparable. That for the propellant was considerably larger. The propellant shows charging by induction only, while the RDX shows

essentially contact only, at least within the time scale of the experiment. The lead azide shows both mechanisms. If the size of the propellant particles had been comparable, the slope of that curve would have been much greater, by a factor of about eight.

Now I want to describe the relaxation work. Although it is not difficult to measure magnitude of charging or to determine which charging mechanisms are important in a given powder, it was felt that measurements of relaxation times of charges would be a more useful approach. Not only does this quantity give a direct measure of the retention of a charge, but it also gives a measure of resistivity, which in turn is important in determining the nature of the charge mechanism. The resistivity is related to relaxation time by the expression

$$\tau = \epsilon \epsilon_0 \rho \quad (1)$$

where τ is the relaxation time in seconds, ϵ is the dielectric constant, ϵ_0 is the permittivity of free space (0.885×10^{-13} Farad/cm) and ρ is the resistivity in ohm-cm.

The experimental method chosen^(2,3) is illustrated in the schematic drawing of Figure 5 and a prototype of the principal parts is shown in Figure 6. The method is based on charging a small amount of powder by means of a corona discharge, and then observing the decay of the charge with an electrometer and recorder, or with an oscilloscope. In operation, 10 to 20 mg of powder is spread out so as

to cover 1/2 to 1 cm² near the periphery of the turntable, the turntable electrometer, recorder and power supply are turned on and when the recorder shows that the powder has come to a steady state of charge, the power supply is turned off. The decay is then followed by the electrometer and recorder. Figure 7 shows representative decay records for three powders, lead azide, basic lead styphnate and tetracene. The rates are quite clearly different.

To obtain a decay rate from the recording, the readings may be plotted on semi-log paper (Figure 8). In the case of an exponential decay, the plot gives a straight line the negative reciprocal of the slope of which gives the decay time. It was found, however, that initial rates were high, as illustrated for lead azide in Figure 8, the curves approaching a steady state asymptotically. This was attributed to a polarization effect⁽⁴⁾ and was most noticeable in the faster rates which were associated with high humidities. In practice, it was faster and more convenient, in such cases, simply to disregard the first third or half of the decay curve and to read off the time required for the next drop of 63%. This procedure, it is felt, gave conservative (longer) time constants. In those samples in which decay was too slow to use this procedure - as for the tetracene and lead styphnate - the time constants were obtained by use of the equation

$$\ln(V_2/V_1) = 1/\tau(t_2 - t_1) \quad (2)$$

Representative data for ambient conditions are shown in the Table 1. The resistivity values were obtained from the experimentally determined relaxation times and by use of the equation (1). In using equation (1), the product $\epsilon\epsilon_0$ was taken to be approximately 2×10^{-13} . The values of resistivity, it should be noted, are only empirical, but they do serve for comparative purposes. The values in parentheses were obtained at a time when sunlight was entering the hood where the experiments were being done. These show that lead azide and tetracene are photoconductive.

The marked dependence of relaxation times - or if you prefer resistivity - on humidity is shown in the next pair of photographs, Figures 9a and 9b. These were obtained using a later version of apparatus with a storage oscilloscope and charge amplifier. In the first, the relative humidity was 66%; in the second, the powder was allowed to equilibrate for an hour with Drierite. The humidity in the chamber was estimated to have been 10%.

During this work one of the investigations undertaken was to evaluate the effect of small amounts of antistatic agents. For this purpose, samples of commercial anti-static agents were dissolved in alcohol at concentrations such that two drops of the solution would leave 0.1 to 0.2 wt.-% in about 35 mg of the explosive, after drying. Although decay rates were increased detectably in some cases,

results were sensitive to small amounts of residual alcohol, and were not very marked at the additive levels used. The effect of humidity was much greater.

This concludes my description of the relaxation work.

I would like now to make a few observations concerning the applicability of charging and relaxation measurements such as those described here. First, it is general practice, in order to control electrostatic hazards, to eliminate or to get rid of charges as soon as possible. The methods described are safe and do give reliable methods of indicating probability of charging by a given method but also permit quantitative evaluation of amount of charge and the effectiveness of steps taken to rectify a given hazardous condition.

A second point: it is well known that powders do in fact become charged in handling. Even powders through which highly insulating liquids are passed as in a filter bed, can become charged. However, there has so far been no way to answer the question "Yes, but how dangerous are these charges?". One way to give a quantitative answer is to compare the amount of charge available, with that needed to initiate. The experiment to determine the latter still needs to be done, but we can determine "how much is there?".

REFERENCES

- (1) B. D. Pollock, W. B. Zimny and C. R. Westgate, "Electrification of Lead Azide Powders Under Ambient Conditions", PATR 4214 (June 1971).
- (2) L. W. Zabel and R. Estcourt, J. Appl. Polymer Sci. 13, 1909-19 (1969).
- (3) L. L. Spiller, Journal of Paint Technology 19, 98-105 (1972).
- (4) J. E. Lawver and J. L. Wright, Proc. AIME 244, 78-82 (March 1969).

FIGURE 1

VIBRATING TROUGH APPARATUS

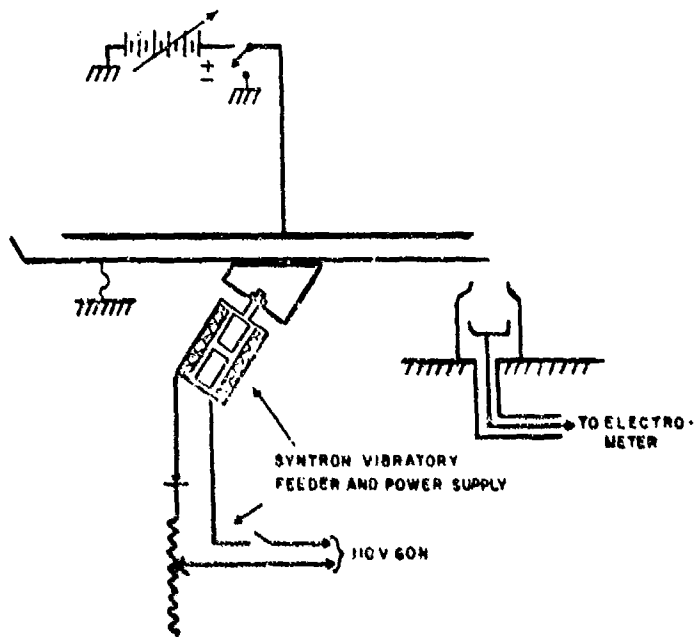
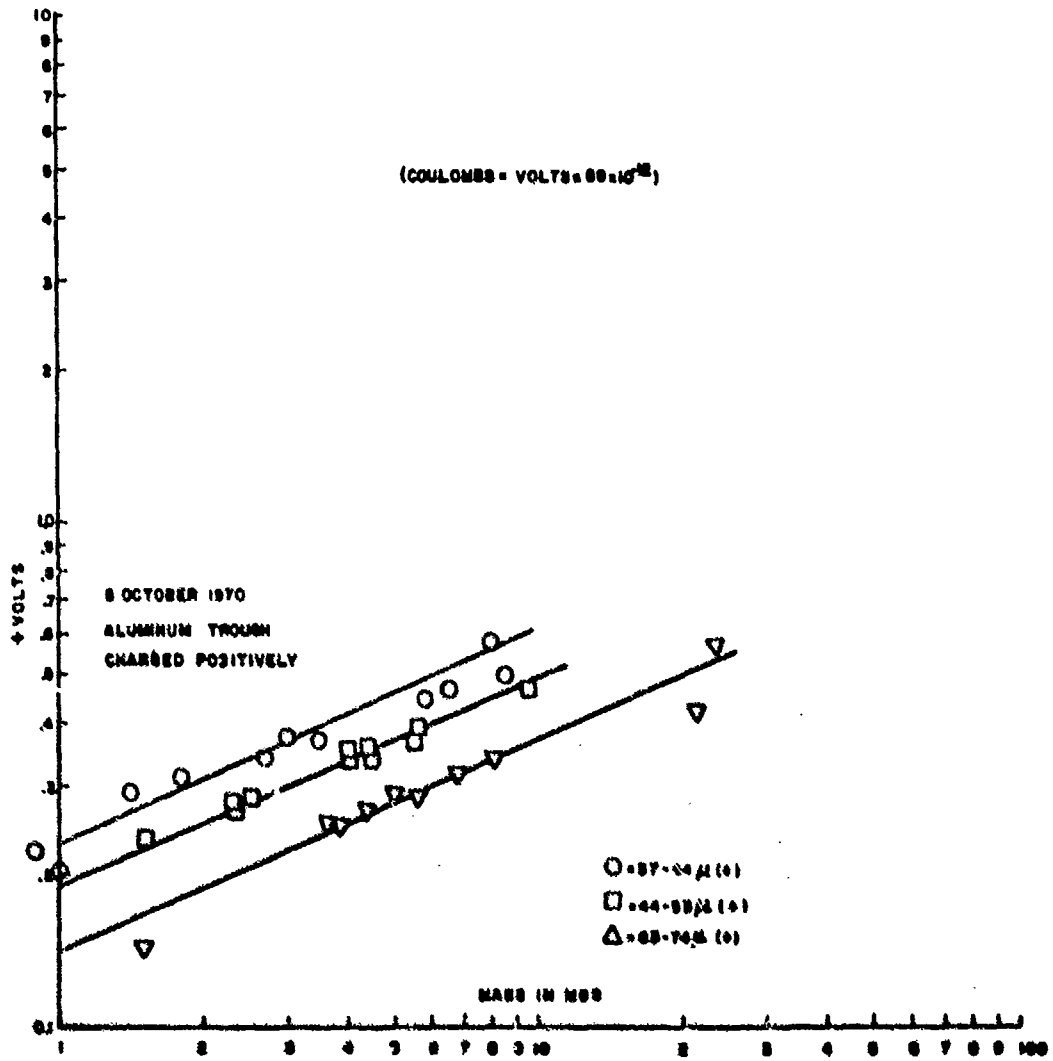
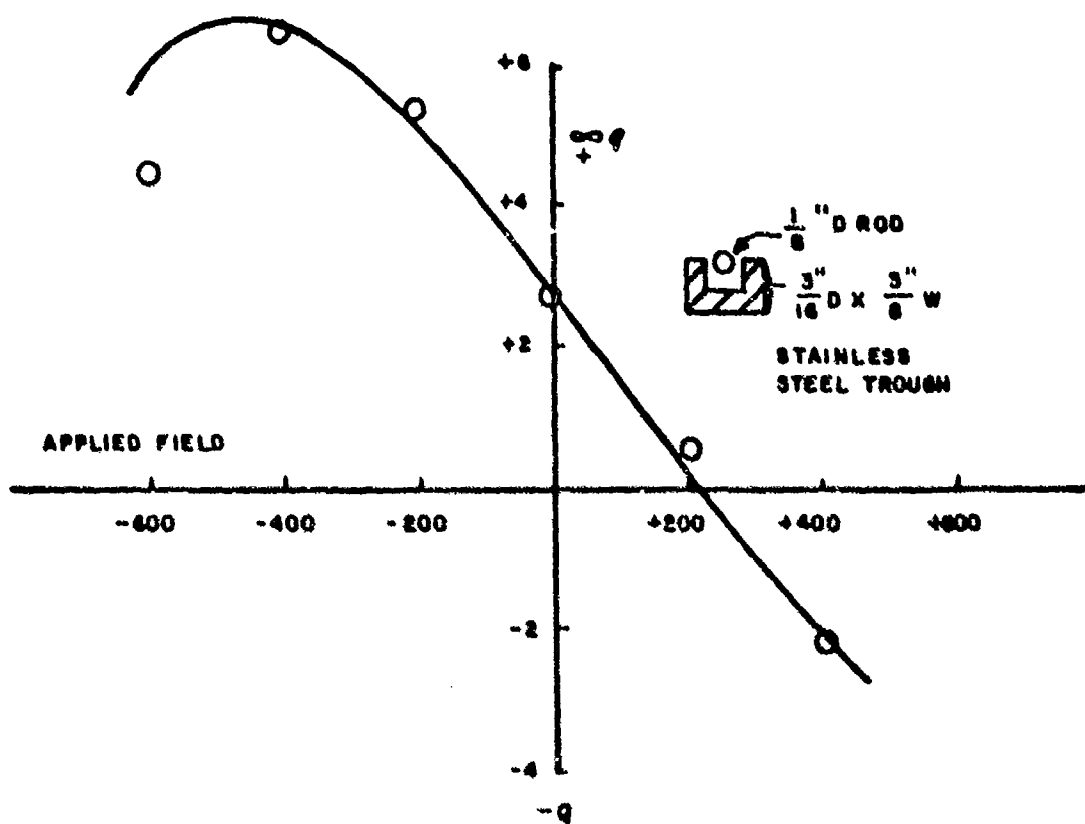


FIGURE 2

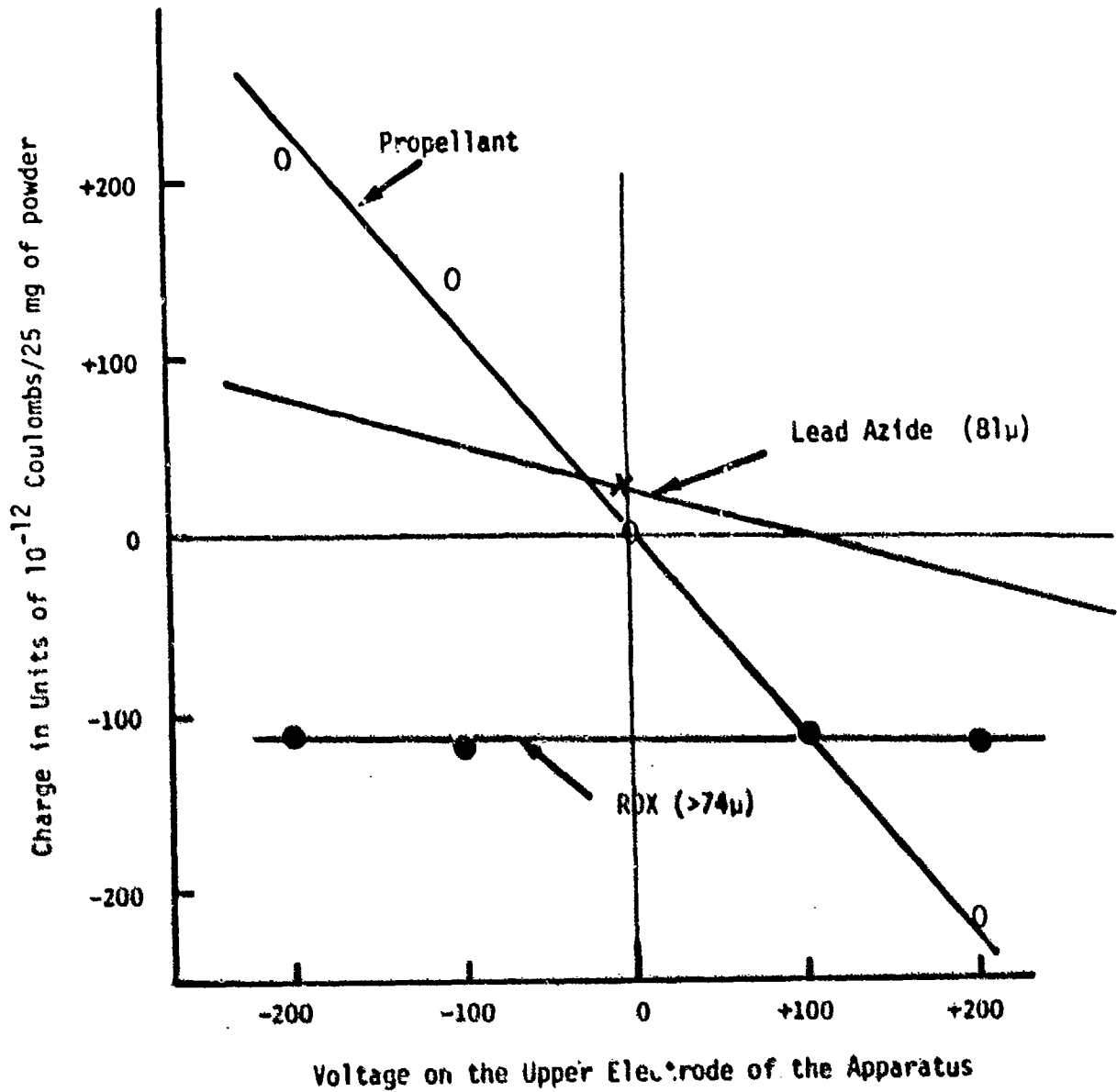
DEPENDANCE OF CHARGE ON SAMPLE SIZE AND PARTICLE DIAMETER



EFFECT OF AN ELECTRIC FIELD



ELECTRIC CHARGES INDUCED ON POWDERS AS A FUNCTION OF APPLIED FIELD IN A VIBRATING TROUGH APPARATUS



*Data for plot of Lead Azide curve was extrapolated from data in Figure 4, and from information regarding "Effect of Applied Field" and derivation in Appendix C, of PATR 4214.

Figure 3

FIGURE 5
CORONA CHARGING APPARATUS; SCHEMATIC

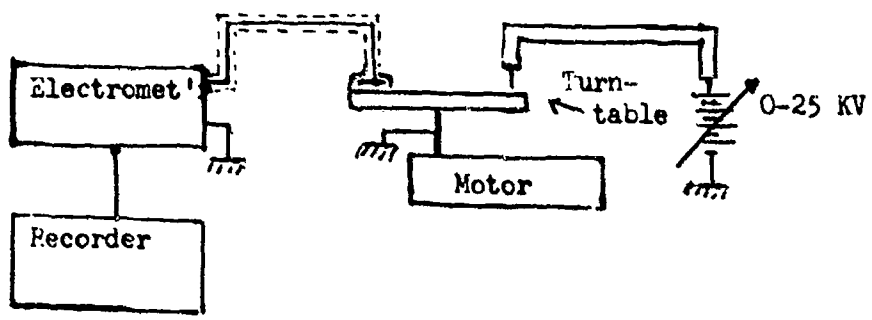


FIGURE 6
CORONA CHARGING APPARATUS; TURNTABLE

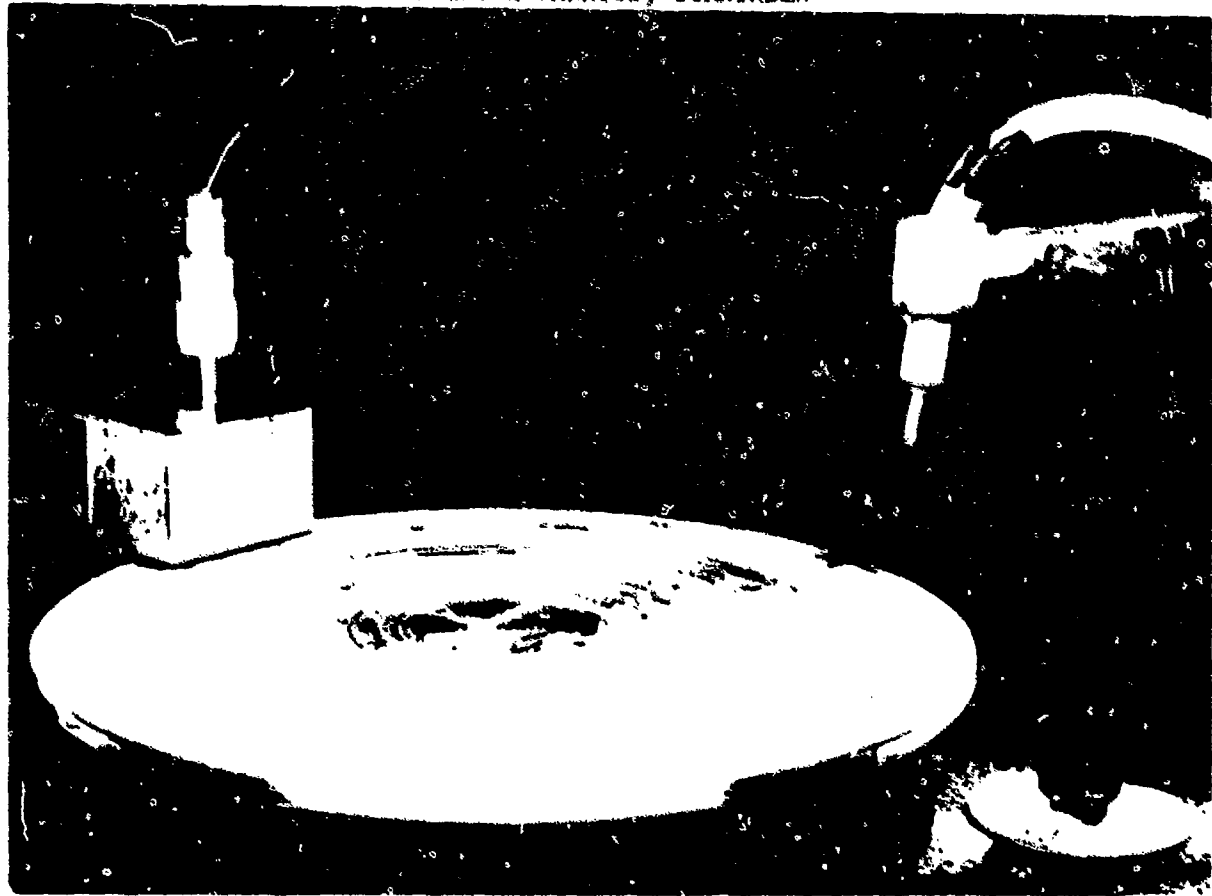
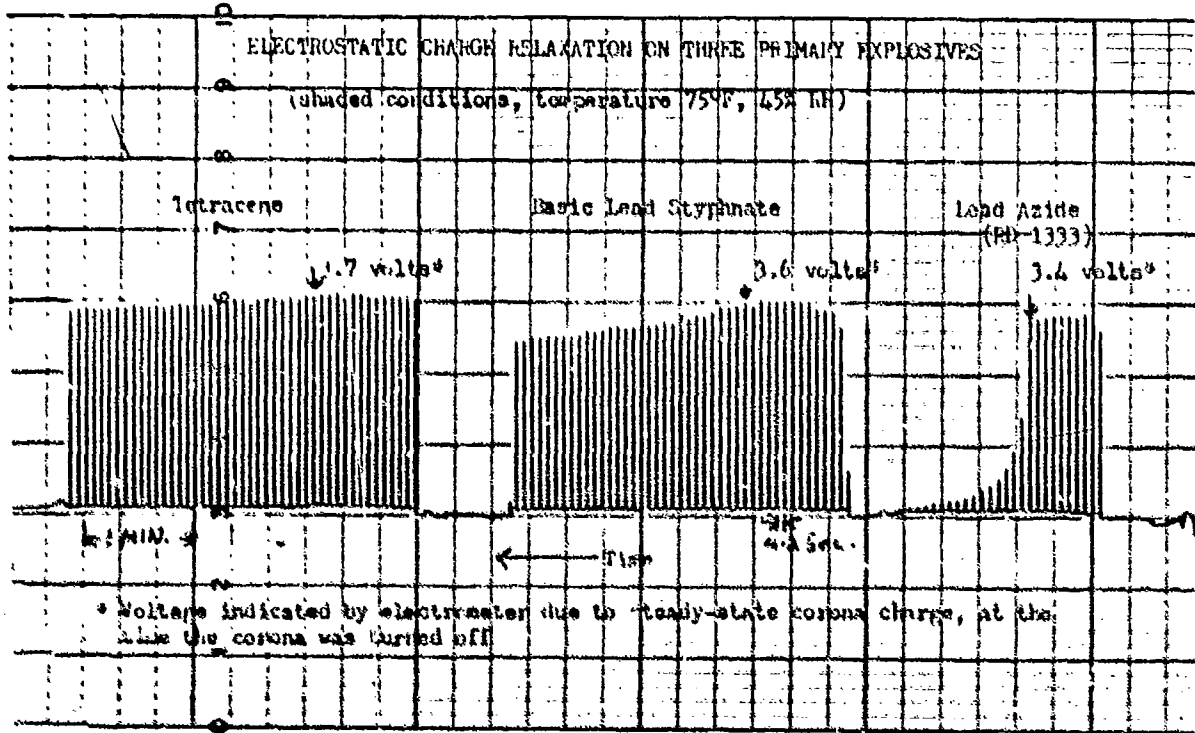


FIGURE 7

KEITHLEY INSTRUMENTS, INC. CLEVELAND OHIO, U.S.A.



3/28/73 AM.

SEMI-LOG PLOTS OF CHARGE vs TIME

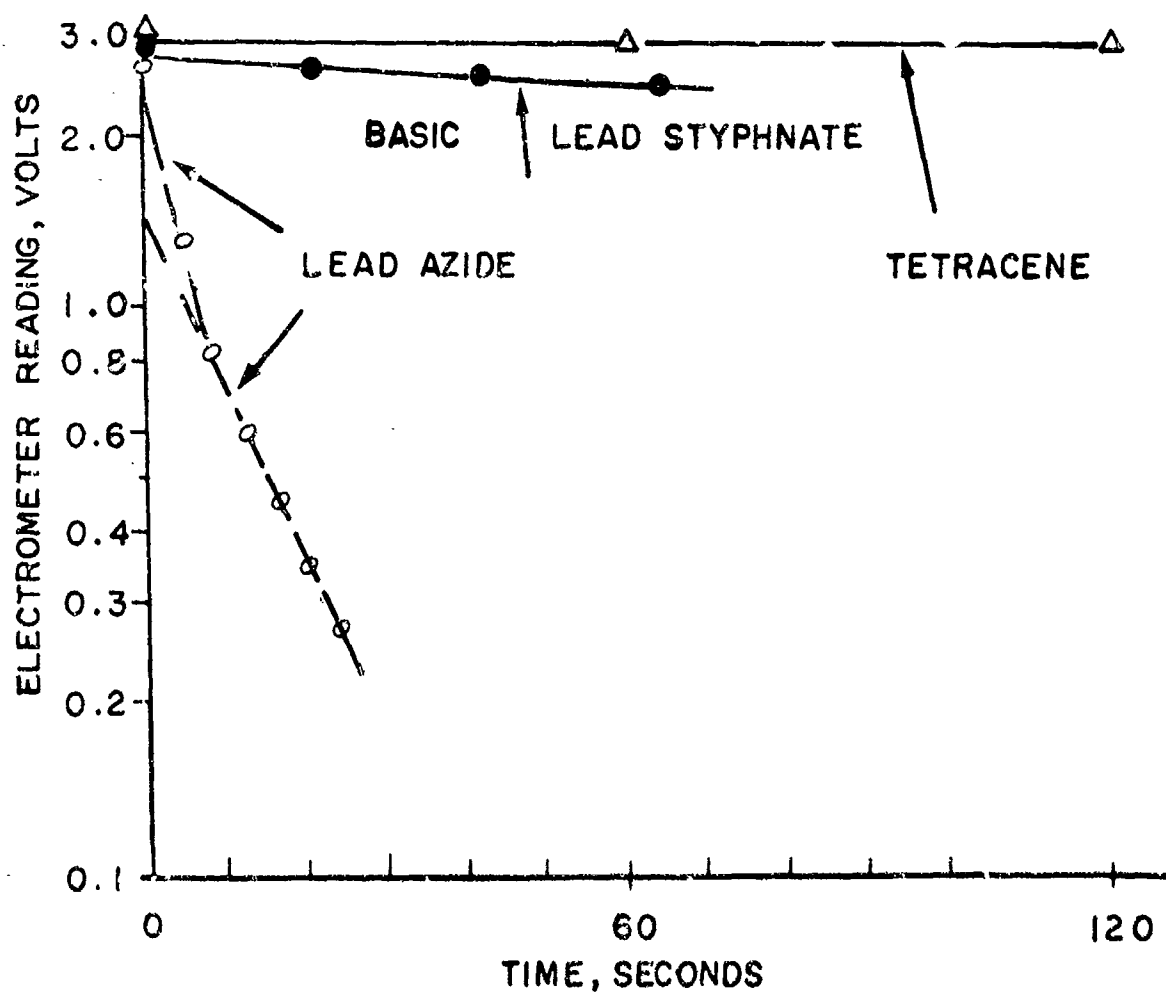
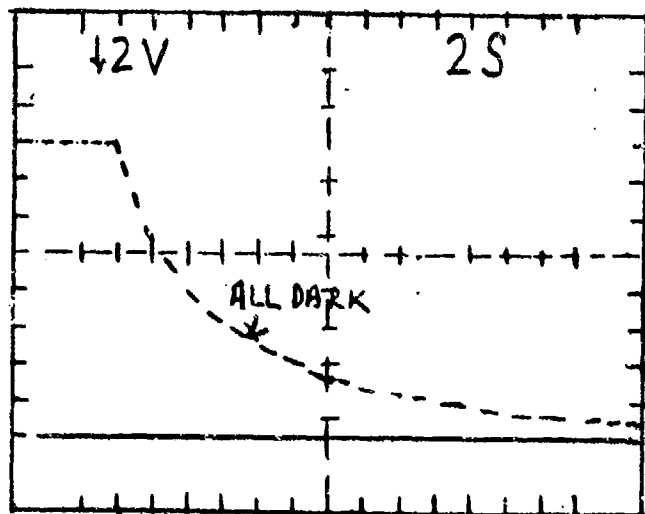
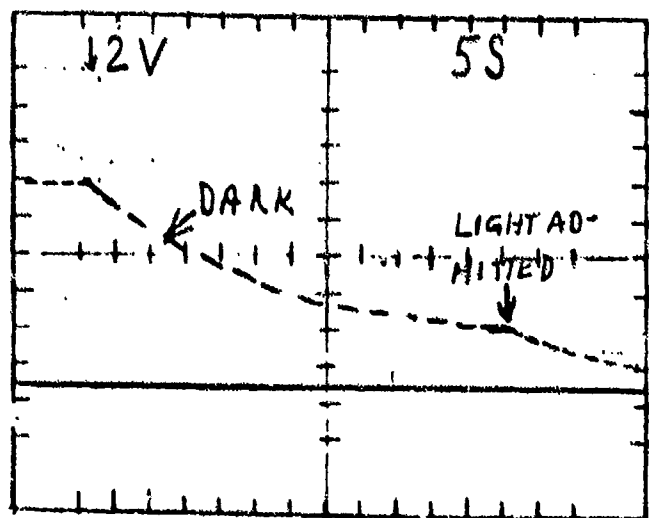


Figure 8

Figure 9
 EFFECT OF RELATIVE HUMIDITY ON CHARGE RELAXATION ON
 LEAD AZIDE AS FUNCTION OF HUMIDITY



A. LA; EQUILIBRATED AT 66% RH; DARK



B. LA; WITH DRIERITE (~10% RH)

Note: the original photographs are not well reproduced on the Xerox machine. In this sketch, only the envelope of the traces are shown to illustrate the effects.

TABLE 1

CHARGE RELAXATION TIMES OF EXPLOSIVES

SAMPLE	RELAXATION * TIME (Sec)	RESISTIVITY (Ohm-cm)
(Pow ders Used in Electrification Studies)		
PROPELLANT FOR Cl MM MORTAR	—	10^5
RD 1333 LEAD AZIDE (OMC 2-2)	17(6)	10^{14}
RDX (Cl B, Type A)	1980	10^{16}
(Other Explosives)		
FVA LEAD AZIDE (OMC 69-1)	29(13)	10^{14}
LEAD AZIDE WITH 0.1% anti-static agent	1	$10^{13} - 10^{12}$
BASIC LEAD STYFNATE	275	10^{15}
TETRACENS	2400(150)	10^{16}

* VALUES IN PARENTHESES ARE FOR SAMPLES ILLUMINATED BY
UV LIGHT AND ARE INDICATIVE OF PHOTOCONDUCTION

CLOTHING MATERIALS AND STATIC GENERATION

by
Frank J. Rizzo
U. S. Army Natick Laboratories

To those individuals involved in some way with hazardous or sensitive materials the word 'static' conjures up thoughts of explosions, fires, death and injury and even of general devastation. This conference attests to the concern that exists among one discipline group whose involvement is with materials of this nature. Our purpose here today is to cast the revealing light of verified fact on the subject with reference to the role that may be played by clothing in a system that consists of the clothing, the hazardous or sensitive materials and a particular set of conditions. We do not intend to promote relaxation of attitude or lack of concern about the possible adverse effects of electrostatic discharge but rather to identify the proper measures that may be taken in a given situation, to explain the purpose for these measures and to assess the degree to which they may apply under a specified set of conditions.

In order to set the stage for the analysis of the levels of hazard that can exist as well as the means that can be taken to deal with the problem as it relates to clothing, we need first of all to have before us an understanding of the origin, the controlling factors and the general behavior of electrostatic charges on textile and related polymer surfaces. Thus, the first point that needs to be made is that static is of electronic origin related to polymer structure. It is the electronic configuration

of the component atoms and molecules and the nature and completeness of the molecular bonding in the establishment of structure and order in the polymers that in fact underlie the phenomenon of static electrification.

If a perfect electronically-neutral system could be realized, no electrostatic properties of any consequence would exist. Such fibers would be electrophobic ⁽¹⁾. Unfortunately, for the area of our concern polymer structure does not achieve the degree of perfection in order and molecular coupling that would provide this ideal, and aberrations and discontinuities are generated within and between the molecular chains of these polymers. These structural features form the loci of free electrons and/or positive charges, generally referred to as electrons and 'holes'. They impart to the material an ability to release or to attract charges from any medium within its environment to achieve the lowest energy state possible. With textile materials these occur by acquisition of ions during wet processing as well as from the atmosphere. Thus what exists on a fabric surface under normal conditions are ion pairs.

The charges associated with the several aberrations and discontinuities (many of these are chain ends at the surface) are not all of the same electrical state; some lie deeply in the polymer structure or are quite strongly bound (deeply trapped) some are weakly bonded; (in shallow traps). Around each of these free charges is an electrostatic field. If the fields of any two opposing charges overlap, we have internal neutralization. If the fields are far apart, so that interaction

between fields is not possible, then the movement of the charges becomes necessary in order to achieve neutralization. This implies a degree of mobility for the charge and a restraint to movement of the charges along the polymer surface. Specifically defined, the mobility of a charge depends on the strength of the bond with the polymer structure, (i.e., the depth of the trap), the electrical conductivity of the medium and the path length between opposing charges, and the temperature. The electrical conductivity of the medium measured at the surface of the material or through the volume is recorded as surface or volume resistivity or as specific resistance, measures on the one hand of the strength of the bonding and on the other hand of the height of the barrier to motion across the material.

Textile fibers vary intrinsically in specific resistance relative to each other, a characteristic that is related to their dielectric constants as seen in Table I utilizing data reported by Hearle⁽²⁾. There is also thereby a relationship to the moisture content. The general order of arrangement of different materials in this table is quite similar to that achieved from an examination of the charges found on these same materials when rubbed against one common material surface. This ranking is called the triboelectric series providing a qualitative placement of these materials ranging in strength of polarity from strongly positive to strongly negative. Two such series are shown in Table II. The order of placement of materials in any such series obtained by rubbing of one surface upon another is highly dependent upon the severity of the rubbing and the degree of intimacy of surface contact

TABLE I

DIELECTRIC CONSTANTS AND LOGARITHMS OF MASS SPECIFIC
RESISTANCES (R_s) OF VARIOUS FIBROUS MATERIALS

	<u>Dielectric Constant at 65% R.H. + 1 Kc/S</u>	<u>Log 10 R_s at 65% R.H.</u>
Cotton	18.0	6.8
Viscose	15.0	7.0
Wood	5.5	8.4
Fiberglass	4.4	---
Polyamide	4.0	9-12
Acetate	4.0	11.7
Polyvinylchloride	3.0	---
Vinylidenechloride	2.9	---
Polyacrylonitrile	2.8	14.0
Polyester	2.3	14.0

TABLE II

TRIBOELECTRIC RANKING OF FIBROUS MATERIALS

<u>Hersh and Montgomery</u> (3)	<u>Lehmicke</u> (4)
+	+
Wool	Glass
Nylon	Human Hair
Viscose	Nylon
Cotton	Wool
Silk	Silk
Acetate	Viscose
Lucite	Cotton
Polyvinylchloride	Ramie
Dacron	Steel
Orlon	Rubber (Natural)
Dynel	Acetate
Velon	Rubber (Synthetic)
Polyethylene	Saran
Teflon	Orlon
	Polyethylene

that is achieved. Charge reversal can occur. When this is found, it has been generated by evaporation of adsorbed moisture (this occurs with cotton at high voltage gradient levels) or to the movement of matter from one surface to the other by which additional structural aberrations have been produced during the rubbing.

The relative polarity differences seen in a triboelectric tabulation theoretically could provide a possible approach to limiting the amount of the charges that can develop on a material. In point of fact, this does occur so long as the blend of the two fibrous materials is sufficiently intimate and the proportions of each in the blend are related to polarity strength differences. However, in a clothing assembly on an individual in a layer separation situation, the electrostatic properties of the separated layers and of other elements of the clothing and the characteristics of the physical environment of the suspected hazardous or sensitive situation are generally the ultimate determinants of the charge density on the individual.

Our attention to the properties of the materials and to the circumstances of the hazard scene is appropriate because as can be deduced from the foregoing, it is the relative materials properties that lead to the nature and density of the charges on the layers in a separation situation. The clothing elements in isolation are not a threat. Removal of an outer-garment from a clothing system on a manikin having the capacitance of a human but a skin surface of very high specific resistance, does not pose a threat to anyone or to anything, even though a charge equal to that on the residual outer layer of the clothing has been induced on the manikin.

In this case, the barrier to charge movement is so high that charges have no place to go. They do not move from the manikin, even to a grounding element, unless that element is all encompassing and achieves over-all intimate contact.

With a human subject, who is both a capacitor and a conductor, a similar condition is realized in an isolated-from-ground situation, although unlike his inanimate image he does represent a threat in a grounding situation. Thus, as soon as he can contact either a material or surface of lower capacitance or a conductor, charge release occurs. A spark is observed when the voltage on the individual exceeds the breakdown voltage of the air gap between the individual's finger and the receiving surface, and only at the proper gap distance.

When a spark is generated and released, we are dealing with an energy factor. It is the amount of this energy, the rate of its release and the energy and time constant requirements of the hazardous or sensitive material that must be equated to establish the probability for the occurrence of an event. The relationship of energy (E) in joules to capacitance (C) in farads and to potential (V) in volts is:

$$E = 1/2 CV^2$$

In Figure 1, are plotted E_{mj} in millijoules for a 200 picofarad human at different induced potentials, within the range of voltages normally realized in a human whose clothing is in equilibrium with an atmosphere containing 30% R.H. or less.

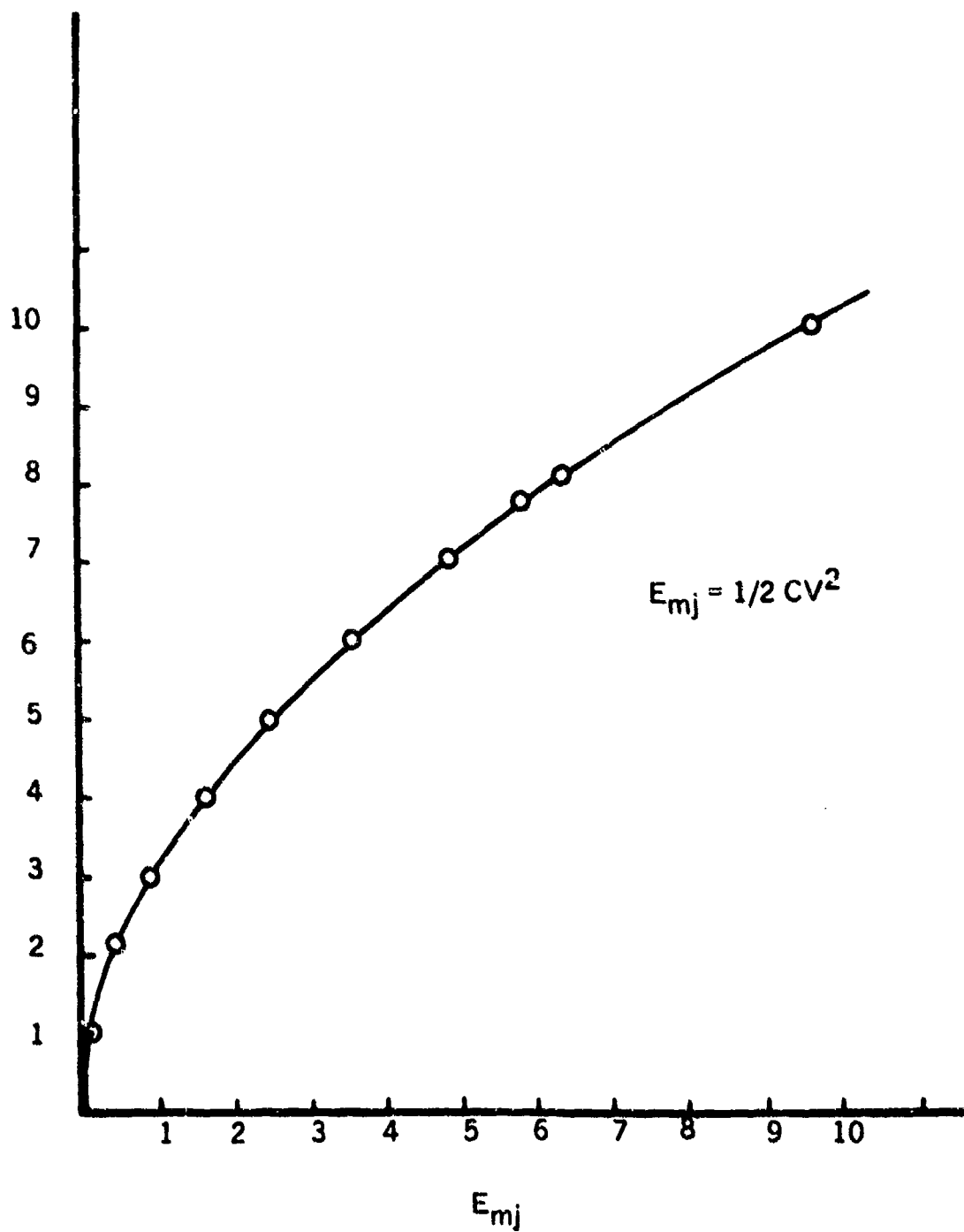


FIGURE 1.
SPARK ENERGY FROM HUMAN SUBJECT
AT DIFFERENT ELECTROSTATIC POTENTIALS

In Table III, are data after Silsbee⁽⁵⁾ and Lewis and Von Elbe⁽⁶⁾ for several sensitive or hazardous materials.

TABLE III
IGNITION ENERGIES OF SELECTED SENSITIVE OR
HAZARDOUS MATERIALS

	<u>Silsbee Data</u>	<u>Lewis & Von Elbe Data</u>
Methane/Air	0.50	0.29
Gasoline/Air	0.80	----
Diethyl/Ether/Air	0.20	0.20
Propane/Air	----	0.25
Propane/Oxygen	----	0.002
Cyclopropane/Air	0.20	----
Heptane/Air	----	0.23
Benzene/Air	0.50	0.20
Hydrogen/Air	----	< 0.014
Acetone/Air	0.60	----
Cu-Acetylide	0.002	----
Pb-Azide	0.04	----

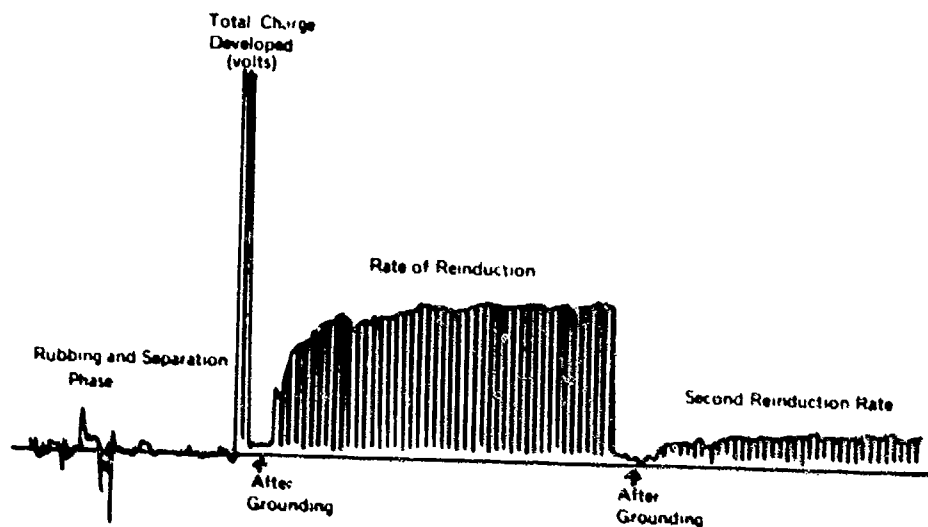
While differences exist due to the differences in methodologies used in attaining the data, the fundamental fact is that either set of values are readily attainable from a clothing-human system.

Several considerations emerge from the immediate foregoing. One is the role of moisture in controlling static generation; a second is that there is enough energy in a spark released by a human with power exceeding that required by many sensitive or hazardous materials; a third is that there is a relationship between rate of delivery of the

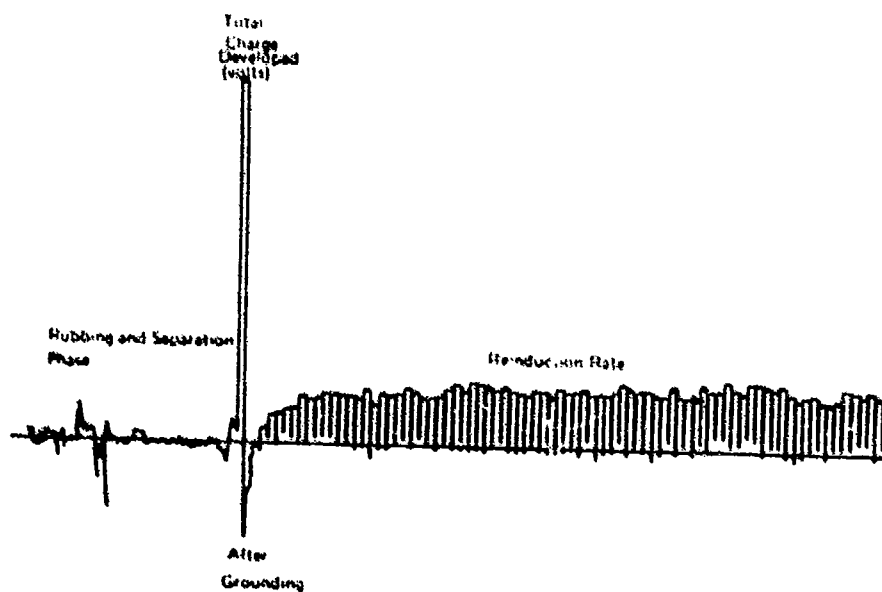
energy and its ability to create a problem. There are others.

The role of moisture is most significant because it is the medium for ionization and for electrical conductivity or ionic transport, once the moisture content exceeds a monomolecular layer ⁽⁷⁾⁽⁸⁾. Keggin ⁽⁹⁾ et al have also shown that moisture influences the extent of the residual charge after a discharge. This matter of a residual charge is related to charge mobility in the external layers of the clothing system and more particularly on the manner of discharge. When physical contact between the human and a grounding element is not achieved, the amount of the charge that transfers through a spark is that required to balance what are essentially two capacitances. Here, only a part of the total charge on the subject is released. In a physical contact situation with a grounded element, the human is completely discharged but the clothing can retain its charge in relation to charge density and barrier height. We have shown that this can result in a reinduction of charge ⁽¹⁰⁾ once connection with ground is broken. This is shown in Fig. 2 for two specific conditions.

On theoretical grounds alone, it becomes obvious that relaxation and dissipative forces in the receiving material of an energy input determine whether a particular reaction proceeds and at what rate. This reasoning applied to electrostatic discharge will show that the rate of energy input as well as the availability of the required amount of energy will determine whether anything happens. Orner ⁽¹¹⁾ has shown by data reproduced in Table IV that the rate of doffing of an outer garment makes a difference in the voltage induced on the individual.



REINDUCTION OF CHARGE FOLLOWING GROUNDING
 WOOL UNIFORM RUBBED WITH NOMEX FABRIC
 METHACRYLATE PLATFORM



REINDUCTION OF CHARGE FOLLOWING GROUNDING
 WOOL UNIFORM RUBBED WITH NOMEX FABRIC
 GROUNDED METAL PLATFORM

FIG. 2. Reinduction of Charge

TABLE IV

EFFECT OF RATE OF OUTER LAYER SEPARATION ON INDUCED
POTENTIAL POLYESTER/COTTON POPLIN JACKET OVER NYLON/COTTON

TWILL JUMPER

33% R.H. - 69°F.

<u>Removal Time</u> (Secs.)	<u>Potential on Human Subject</u> (In KV)
< 1	5.5
2.5	6.3
3.0	5.7
4.0	4.0
6.0	3.0
8.0	2.6

Obviously, as resistance to charge motion increases, this effect is reduced eventually attaining a high steady state potential value.

Another factor limiting the level of charge on the individual is the degree of intimacy of contact of the garment layers prior to separation. Since ion pairs are elements in the redistribution of charges on the two outermost layers of a clothing assembly during separation, the layers must have come in sufficiently close contact with each other previously so that their electrical fields were able to interact. In a normal clothing system the degree of intimacy of contact is sporadic. In addition, as Bertein⁽¹²⁾ has shown there exist islands of charges of different polarities on the same surfaces as a normal situation and by implication there must be charge-free areas as well. Thus, even in the highest barrier conditions (highest specific resistance) the maximum

charge density possible is not realizable. On the other hand, where charge mobility is high, as it is with cotton at normal to high R.H. levels, the charge mobility factor can compensate for the lack of complete surface-to-surface contact, and lower levels of residual charge density result. Accordingly, it is advantageous to have high conductivity in the fabric layers to reduce the amount of the residual charge. Several approaches exist as seen in Table V.

TABLE V
METHODS FOR REDUCING ELECTROSTATIC CHARGE
BUILDUP IN TEXTILE MATERIALS

<u>Materials</u>	<u>Functioning</u>	<u>Durability</u>
Humectants	Enhance charge mobility	Regenerate after each laundering
Ionic compounds and salts	Electrical conduction	Regenerate after each laundering
Curable ionic polymers	Electrical conduction	Up to 30 laundering (min.)
Graft Functionalities on Fibers	Electrical conduction	Durable in soft water washing. Fail in hard water
Metallic Fiber in Blend (Brunsmet)	Dipole - Dipole Smearing of Fields	Lifetime
Epitropic Fibers (conducting carbon on surface of fiber)	Electrical conduction	Lifetime

Treatment of the fabrics is obviously beneficial, but whether the individual acquires a charge of potentially hazardous dimensions depends upon the system, as previously mentioned, and significantly upon whether he is grounded or isolated from ground by virtue of footgear or the platform on which he stands. We alluded to this earlier and illustrated the

effect by Fig. 2. In Tables VI and VII, we repeat data previously
reported ⁽¹⁰⁾ achieved with several combinations of materials on a hu-
man subject at two different R. H. conditions. The differences are
certainly impressive. They suggest that one of the several ways to
avoid problems is to ground the individual at all times while in the
performance of his duties. Another approach is to completely isolate
him from ground, but this has the element of human failure. A further
suggestion has been made ⁽¹³⁾ for the attainment of an equipotential
state by constant release of charge from fine points. This would be a
useful concept if there were an easy way to achieve it. Needle points
like 'spurs' on a rider's ankles in direct contact with the skin by
bleed-off of corona discharge may accomplish this. This is being studied.

Finally, the nature of the discharge point has been an area of
controversy. With the human, the finger tips are generally the release
points. Heidelberg, in a discussion following a paper by Bertein ⁽¹²⁾
previously mentioned, reported that the larger the radius of the electrodes,
the lower the probability of danger from electrostatic discharge in the
presence of explosive mixtures even of hydrogen and air. Recent work
by Orner ⁽¹¹⁾ using a propane/air mixture at room temperature and pressure
produced ignition with brass needles of the order of 0.05 mm. Increasing
the electrode radii led to increases in the energy levels required to
achieve ignition of this gaseous mixture. Our most recent efforts with
Avgas vapor mixtures with air well in the explosive range undertaken
for the USAF failed even with fine pointed electrodes. The voltages were
generated by personnel wearing Polyester/Cotton Durable Press fatigues

TABLE VI

EFFECT OF PLATFORM MATERIAL AND FOOTWEAR CHARACTERISTICS
ON VOLTAGE GENERATED ON CLOTHED INDIVIDUAL

21°C - 20% R.H.

Rubbing Fabric - Polyester Plain Weave

	METHACRYLATE PLATFORM		GROUNDED COPPER PLATFORM	
	Initial Voltage	Voltage After 1 Min.	Initial Voltage	Voltage After 1 Min.
1. UNTREATED NOMEX LAYER OVER:				
A. Antistatic Nomex Layer	1250	1250	2375	625
B. "A" - Washed	1000	800	0	----
C. Cotton Fatigues	1150	125	0	----
D. Wool Field Uniform	1250	1250	0	----
2. NOMEX W/1% STAINLESS STEEL FIBER OVER:				
A. Antistatic Nomex Layer	1875	1250	0	----
B. "A" - Washed	1250	1000	0	----
C. Cotton Fatigues	1875	1125	1875	2000
D. Wool Field Uniform	2700	750	100	100
3. DIRECT RUBBING ON:				
A. Antistatic Nomex Layer	2570	1750	2500	1000
B. "A" - Washed	2250	1525	900	450
C. Cotton Fatigues	2875	2690	2500	1250
D. Wool Field Uniform	2800	2250	1250	350

TABLE VII

EFFECT OF PLATFORM MATERIAL AND FOOTWEAR CHARACTERISTICS
ON VOLTAGE GENERATED ON CLOTHED INDIVIDUAL

21°C - 50% R.H.

Rubbing Fabric - Polyester Plain Weave

	<u>METHACRYLATE PLATFORM</u>		<u>GROUND COPPER PLATFORM</u>	
	<u>Initial Voltage</u>	<u>Voltage After 1 Min.</u>	<u>Initial Voltage</u>	<u>Voltage After 1 Min.</u>
1. UNTREATED NOMEX LAYER OVER:				
A. Antistatic Nomex Layer	1000	1000	2500	0
B. "A" - Washed	1625	625	0	340
C. Cotton Fatigues	1400	1180	1300	
2. NOMEX WITH 1% STAINLESS STEEL FIBER OVER:				
A. Antistatic Nomex Layer	875	325	50	0
B. "A" - Washed	2125	1050	0	
C. Cotton Fatigues	625	75	175	50
3. DIRECT RUBBING ON:				
A. Antistatic Nomex Layer	1650	1250	650	25
B. "A" - Washed	300	275	0	
C. Cotton Fatigues	475	125	120	25
D. Wool Field Uniform	550	525	0	

TABLE VIII

POTENTIAL DEVELOPED ON BODY
OF
INDIVIDUAL WEARING AF CLOTHING

Uniform	Removed Layer	Touches Electrode to Chamber, Then Touches Sensing Device		
		70°F RH	86°F 39% RH	86°F 5% RH
<u>Uniform, M-1, Man's, P/C, D.P.</u>				
Shirt, Long Sleeve, Blue 1577	None	375	250	250
Trouser, Blue 1577	Utility Jacket	125	125	125
	Flying Jacket	1400	1125	1250
	Nomex Jacket	1250	1125	2000
	Nylon Jacket	1375	625	1500
<u>Uniform, W-3, Woman's, P/C, D.P.</u>				
Shirt, Blue 1577	None	750	625	500
Slacks, Blue 1577	Utility Jacket	125	750	750
	Flying Jacket	1125	750	375
	Nomex Jacket	750	875	1125
	Nylon Jacket	875	625	500
<u>Uniform, W-2, Woman's</u>				
Shirt, Flannel, 8% Wool, 15% Nylon, OG	None	1000	1125	1000
Slacks, Serge, Wool, OG	Utility Jacket	250	375	375
	Flying Jacket	> 5000	> 5000	> 5000
	Nomex Jacket	3625	4250	4750
	Nylon Jacket	5000	1625	3750

TABLE IX

SURFACE RESISTIVITY VALUES FOR AF CLOTHING
70°F - 30% R.H.

<u>Garment/Layer</u>	<u>Surface Resistivity</u> ohms/sq
Shirt, Women's, Utility, P/C, Blue 1550	3.3×10^{12}
Slacks, Women's, Utility, P/C, Blue 1577	7.0×10^{12}
Shirt, Women's, Wool Flannel, Field, OG-108	3.3×10^{13}
Slacks, Women's, 85% Wool, 15% Nylon, Field, Serge, OG-108	$>10^{13}$
Shirt, Women's, Long Sleeve, 50/50 P/C, Precured, Blue 1577	2.7×10^{12}
Slacks, Women's, 50/50 P/C, Post Cured, Blue 1577	5.5×10^{12}
Shirt, Men's, Long Sleeve, 50/50 P/C, Post Cured, Blue 1577	3.3×10^{12}
Shirt, Men's, Short Sleeve, 50/50 P/C, Post Cured, Blue 1577	5.7×10^{12}
Trousers, Men's, 50/50 P/C, Post Cured, Blue 1577	9.3×10^{12}
Jacket, Men's, Utility, 50/50 P/C, Precured, Blue 1577	7.3×10^{11}
Lining of Jacket, 50/50 P/C, Post Cured, Blue 1577	4.7×10^{12}
Flying Jacket, Men's, AF, Nylon Twill - Outer Shell	$>10^{13}$
- Lining	$>10^{13}$
- Fur	$>10^{13}$
Nomex Jacket (used as separation layer)	$>10^{13}$
Nylon Jacket (used as separation layer)	$>10^{13}$

under nylon flight jackets. Tables VIII and IX show the resistivity and voltage data for these systems. When oxygen replaced air in these mixtures, explosions were readily realized with all electrode systems used.

What then does all of the foregoing tell us with respect to the hazardous situation stemming from the materials and end items of concern to this audience? If we review the possible ways in which to control the charge development on the clothing system, as we have in Table X,

TABLE X

POSSIBLE WAYS TO CONTROL CHARGE
DEVELOPMENT ON CLOTHING.

Achieving a higher degree of purity in the substrate.

Using additives that will lower the energy barriers and increase electrical conductivity of the material.

Using additives that will provide a new surface on the material with electronic configurations having smaller energy gaps.

Modifying the polymer structure to achieve a molecular orbital configuration with a high π -electron cloud or ionic strength.

we conclude that in a practical sense all that we can do is what we show in Table XI. We can insist on using only all cotton clothing which most individuals consider as a standard of reference including us, as seen in Table XII. This is based on experience over many years when everything a person wore was either cotton or wool. What

TABLE XI

PRACTICAL WAYS FOR CONTROLLING CHARGE
DEVELOPMENT ON CLOTHING

Blending of fibers from opposing positions in the triboelectric series.

Applying antistatic finishes.

Admixing of organic and metallic fibers.

Grafting ionizing functional groups on existing fibers.

TABLE XII

STANDARD LEVELS OF SPECIFIC
RESISTANCE FOR MATERIALS

<	- 10^9	safer than cotton
10^9	- 10^{11}	practical safe levels - as safe as cotton or better
10^{11}	- 10^{12}	marginal for safety
>	- 10^{12}	progressively unsafe

do we do then when we have conditions such as we have seen in Table XIII? What we are left with is our best intuition after careful scrutiny and analysis of the technical evidence at hand. This evidence tells us that the problem of hazard really is a probability function and our experience is that overall it is quite low. Further analysis tells us that it is low because of the many factors involved that must operate in consonance and in proper time and with sufficient

TABLE XIII

LOG₁₀ R PER UNIT AREA FOR FIBERS AT DIFFERENT
TEMPERATURE - R.H. CONDITIONS

	<u>2% R.H./</u> <u>-1°C</u>	<u>2% R.H./</u> <u>0°C</u>	<u>2% R.H./</u> <u>50°C</u>	<u>50% R.H./</u> <u>24°C</u>	<u>70% R.H./</u> <u>0°C</u>
Cotton	15.5	15.5	14.5	10.3	10.0
Wool	15.5	15.7	16.0	12.3	12.5
Nylon	15.5	15.7	14.9	14.3	13.0

energy, a situation that does not seem to develop with a high level of incidence. We can, as we have seen, attain sufficient energy but to achieve a proper level of assured safety, our judgment is that both of the outer layers of a clothing system need to have some kind of charge dissipating quality about them. We have shown that there are several ways in which this can be done but it all comes down to this type of action plus insuring that there is a constant grounding of the individual at all times while he is performing the potentially hazardous activities.

References

1. Inokuchi, H. and Akamata, H., Solid State Phys. 12, 93 (1961)
2. Hearle, J. W. S., Tex. Res. J. 24 (4) 307 (1954)
3. Hersh, S. P. and Montgomery, D. J., Tex. Res. J. 25 (4) 279
4. Lehmicke, D. J., Am. Dyes. Rptr., 38 (24) 853 (1949)
5. Silsbee, R. B., NBS Circular C-438, US Department of Commerce (1942)
6. Lewis, B. and Von Elbe, G., Combustion, Flame and Explosions of Gases, 2nd Edition, New York Academic Press (1965)
7. Sereda, P. J. and Feldman, R. R., J. Tex. Inst. 55, T288 (1964)
8. Crugnola, A. M. and Robinson, H. M., Tex. Series Rpt. #110 (1959) QMR&E Command
9. Keggin, J. F., Morris, G. and Yuill, A. M., J. Tex. Inst. 40 (10) T702 (1949)
10. Rizzo, F. J., USA Natick Labs. Rpt. 74-2-CB (1973)
11. Orner, G. M., Navy Clothing and Textile Research Unit, Tech. Rpt. #109, (1974)
12. Bertein, H., Conf. Proc. Static Electrification, 11, Inst. of Phys. and Phys. Soc. London (1967)
13. Wilson, L. G., Canadian Defence Res. Establishment, Private Communication

RENOVATION OF OLD CONDUCTIVE FLOORS

Mr. I. T. Cruz
Naval Weapons Station, Yorktown, VA

Navy Safety Regulations (OP 5, Volume I, Third Revision) require a conductive floor for operations where there are open explosives and/or sensitive ordnance devices that could possibly be affected by static discharges. In other words, conductive floors with positive grounding are mandatory in areas where personnel work with or, are in contact with:

1. Open explosives or explosive mixtures that are sensitive to static discharge.
2. Solvents and other flammable chemicals
3. Electro-explosive devices

Examples of 1 are open melts, castings, incendiary, primer and pyrotechnic mixtures. Examples of 2 are ethyl ether, ethyl alcohol, ethyl acetate, acetone, gasoline, benzine, and naphtha. Examples of 3 are primers, initiator, detonator, igniter, and tracer. Op 5 further states that the electrical resistance must be measured at least semi-annually, and that the resistance measured between ground and five square inches of floor area must not exceed 250,000 ohms.

During the fall of 1972, several conductive floors in the explosive pouring plants at the Naval Weapons Station, Yorktown, Virginia, were found to have very high and unsatisfactory floor resistance readings. Some readings were in the million ohms while the acceptable reading at that time was "not to exceed 250,000 ohms." Since then, this regulation was changed in September 1973 to read "not to exceed one million ohms."

Preceding page blank

Several methods were used to clean the conductive floors; they were steam cleaning, scrubbing with approved cleaning agents and the use of dry grinding machines to attempt to clean the floor; however, none of these methods gave a satisfactory result,

Since cleaning had been unsuccessful, it appeared that perhaps the best solution would be for a new conductive floor to be laid over the old floor. The method described in NAVFACSPEC TS-9F15a with change one, was one of the new floors considered. However, refinishing in accordance with this specification requires a minimum of sixty days curing time. The curing time when added to the cleaning, preparation, and the application time dictated the consideration of some other method.

The kettle deck of Mine Filling Plant Three was chosen to be the pilot test for laying of a new conductive floor, with an area of approximately 1,420 square feet. A new floor cost approximately \$9, per square foot -- making an approximate total cost of \$12,780.

The writer of this paper was not completely satisfied that laying a new floor was the best solution -- considering the cost and the sixty days curing time as required by NAVFACSPEC TS-915a with change one. Therefore, a re-examination of the old conductive floor of the kettle deck of Mine Filling Plant Three was made as follows:

1. The floor was constructed/poured in 1945. A typical cross section of the floor is similar to figure 1. It consisted of approximately eight inches of reinforced concrete plus one inch of conductive floor consisting of a network of copperwiring and metal filings sprinkled generously throughout to provide continuous electrical conductivity.

2. Through the years, dirt and wax filled the porous surface of the conductive floor. In checking with one of the contractors who provided the waxes in accordance with specifications, it was revealed that non-conductive waxes were used instead of conductive ones.

3. The use of steam cleaning just removed dirt and wax on the surface but did not remove those imbedded within the concrete pores.

4. The use of dry grinding machines imbeds the dirt and wax deeper into the concrete pores. In many cases the resistance readings were higher after the dry grinding operations.

It was then decided to use another type of grinding machine. An electric terrazzo grinder as shown in figure 2, was chosen because this machine uses a large amount of water during the stone grinding operations on the concrete deck. It proved to be a most successful operation. Floor resistance readings in the mega ohms were recorded before grinding. After using the terrazzo grinder the metal filings could be readily seen all over the floor and the resistance readings dropped in most areas to between 10,000 and 100,000 ohms -- well within the 250,000 ohms limit.

The advantages of renovation of old conductive floors in lieu of a new layer of conductive floor are as follows:

1. There is no preparation, cleaning, or application and curing time involved.

2. There is no added weight of the additional floor.

3. It is more economical. The estimated saving for the kettle deck alone on Mine Filling Plant Three is as follows:

a. New floor - 1,420 square feet at \$9, per square foot \$12,780.

- b. Terrazzo grinding - 1420 square feet at \$0.35 per square foot (Done by private contractor through a service contract), 497,00
- c. Saving reflected \$12,283.00

Upon completion of this experiment in 1972, the Naval Weapons Station Yorktown, Virginia procured its own terrazzo grinder machine. Since then several other conductive floors have been successfully renovated using this machine,

NOTE: Mr. Ignacio T. Cruz is the Safety Director, Naval Weapons Station, Yorktown, Virginia. In 1972, when the experiment of renovating the conductive floors was being performed, Mr. Cruz was the Maintenance Control Director of the same command.

2" ROUND OR SQUARE HARDWARE CLOTH, BRAZED TO STUD

CUP-SHAPED POCKET AROUND HARDWARE CLOTH

DUSTED-ON SURFACING

3/4" MIN. ϕ

1" TOPPING

BASE SLAB

CONNECT STUD TO SLAB REINFORCING WITH BRAZED STRAP.

SLAB REINFORCING.

1/2" DIA. GROUNDING STUD.

SECTION

METALLIC-TYPE STATIC-DISSEMINATING AND SPARK-RESISTANT FLOOR FINISH

(FOR SUPPORTED FLOOR SLABS)

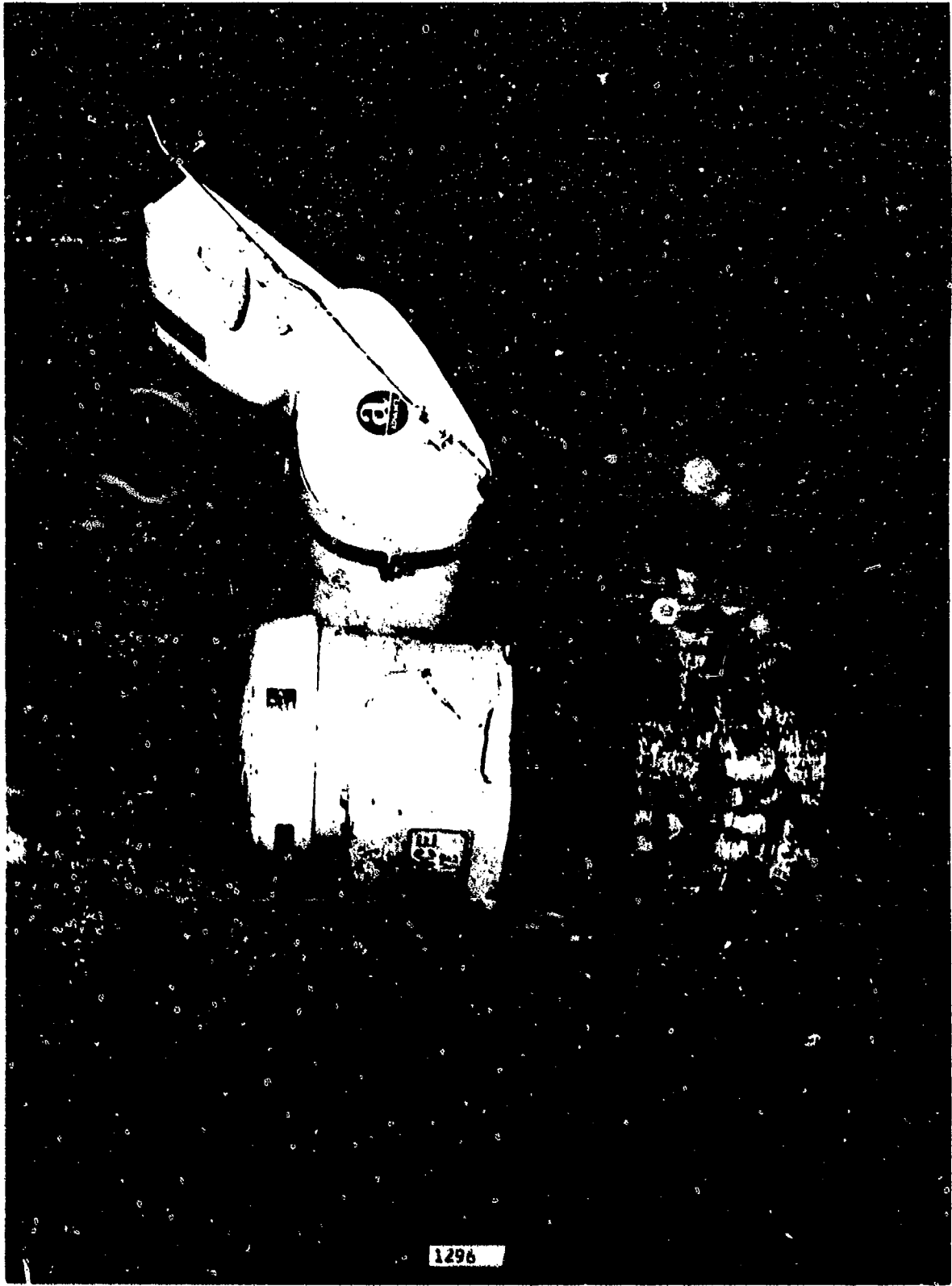


FIGURE 2

1296

NAVSEA SYSTEMS SAFETY GUIDELINES

T. M. Leach
Manager, Systems Safety Programs Division
NAVSEA Safety School Department
NAD Crane, Indiana

I would like to discuss some of the new strides which are taking place in the area of Systems Safety within the Naval Sea Systems Command in the form of OD-44942.

First, I think it is important that we realize the overall purpose of performing System Safety Analysis, and that purpose is to acquire information about a specific system. All that we can hope to achieve from analysis is information. Hopefully, we will use that information to make informed management decisions, and make them before we have accidents.

It should be pointed out that the analysis will not make any decisions, but only give us information from which decision can be made. The question may be asked, is this information gathering process, system safety analysis, worthwhile? Our contention is "yes," because of consequence factors such as: accident cost, property damage, personnel injury and death, and public notoriety. It is important to acquire as much information as possible about our systems so the disaster such as these (Slides 1 and 2) may be avoided in the future.

To help accomplish this task NAVSEASYS COM has developed the Weapon System Safety Guides, OD-44942, Parts I-IV. The OD's are



SLIDE 1.



SLIDE 2.

designed to cover the entire life cycle of a weapon system. Part I is the System Manager's Guide. Part II covers the responsibilities of the Principal for Safety; Part III the responsibility of the Safety Engineer at the program level, and Part IV covers the Explosives Ordnance Production evolution.

For the purpose of this presentation, I would like to discuss Part IV; the types of operations encompassed and how a typical system safety program may function at a production activity.

The purpose of OD-44942, Part IV, is to provide guidelines for the application of system safety techniques to the control of explosive hazards encountered during the production and certain ordnance life cycle operations.

These operations include:

- Manufacturing
- Explosives Loading
- Component, Sub-Assembly Build-Up
- Renovation
- Demilitarization
- Routine Disposal

Routine disposal does not encompass explosive ordnance disposal (EOD) operations.

LIFE CYCLE INTERFACES

The relationship of the Weapon System Life Cycle and the Production Life Cycle can be seen in Slide 3. The Production Phase can be extracted from the weapon system cycle described in Parts I, II, and III and expands the phase into the explosive ordnance production life cycle. To define the responsibilities for the performance of system safety tasks in each phase of the production cycle, the function of and interfaces between, the Naval activities and personnel involved must be considered.

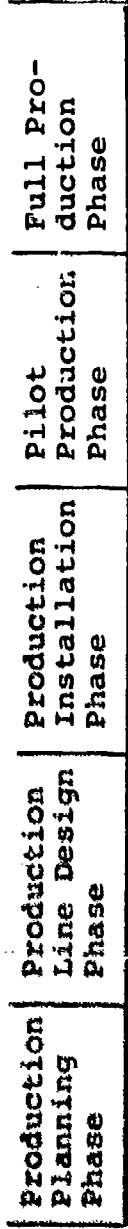
The functional responsibilities of each of the activities can be illustrated in the following slides (Slides 4 and 5). The procuring activity must require and provide funding for a system safety program in accordance with MIL STD 882 whenever it issues a work request for production of explosive ordnance. This includes start-up of an inactive existing line, design and development of a new production line, or modification of an existing production line.

The Liaison Agent serves as the coordinator between the outside activities (engineering agents, process developer, production planners, facility designers, equipment designers, and procedure developers at other government activities or contractor's plants) and the production activity.

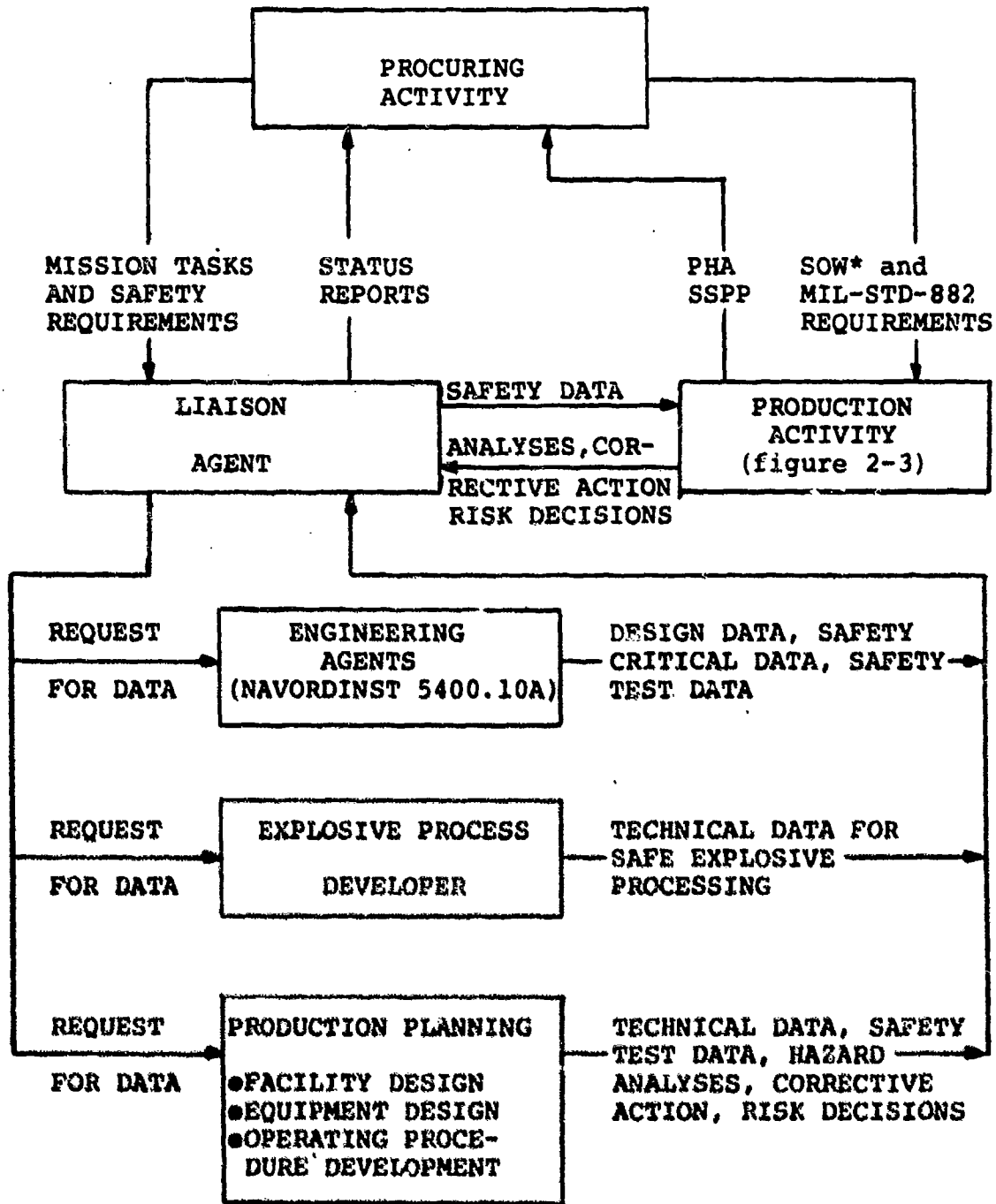
**WSSG Part I, II
and III Weapon
System Life Cycle**



**WSSG Part IV
Production
Process
Life Cycle**

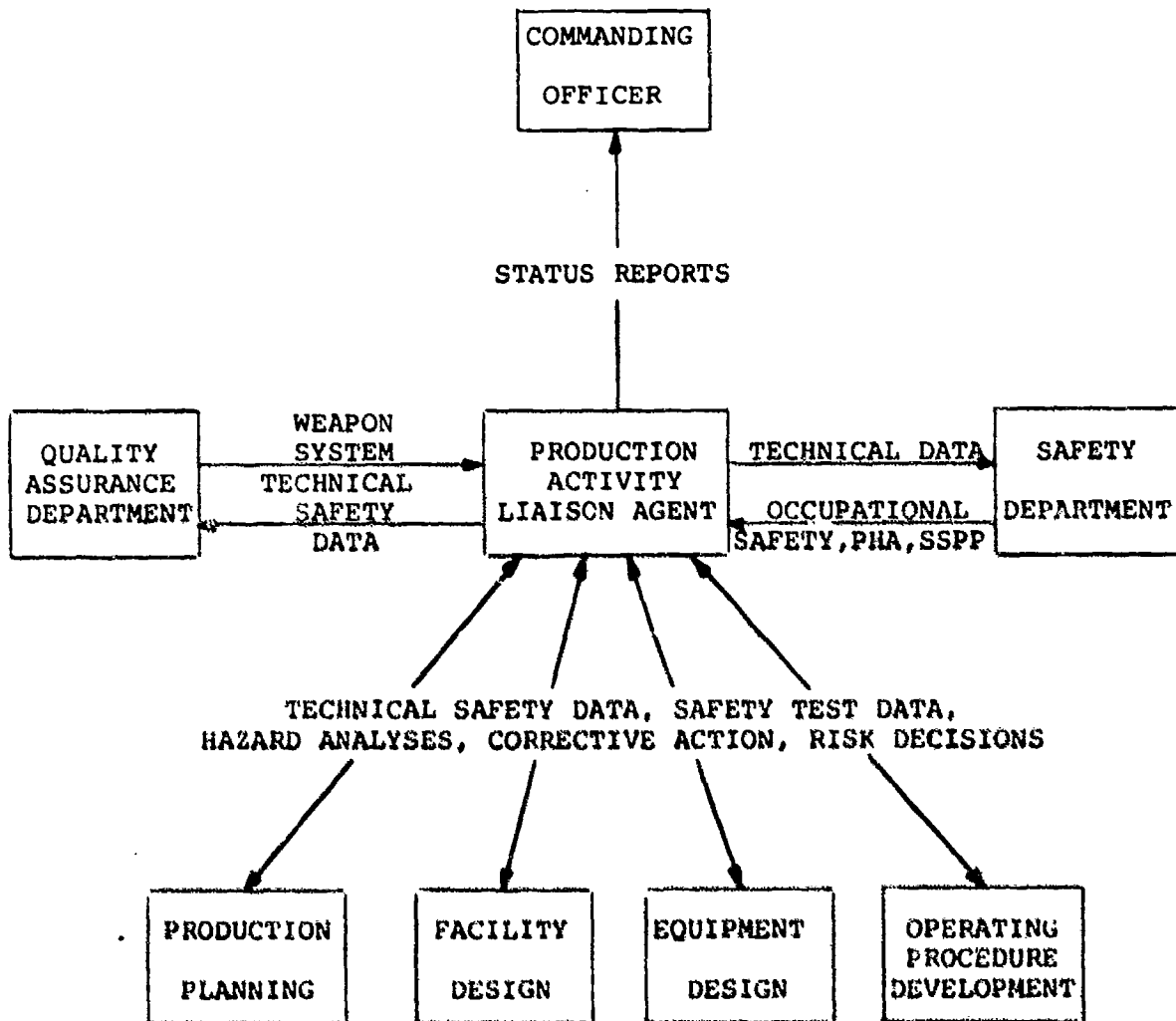


SLIDE 3. PRODUCTION PHASE LIFE CYCLE



* SOW = Statement of Work

SLIDE 4. PRODUCTION SYSTEM SAFETY INTERFACES



SLIDE 5. PRODUCTION ACTIVITY SYSTEM SAFETY INTERFACES

The Liaison Agent receives the mission tasks and safety requirements from the procuring activity and passes them on to all other activities. He in turn provides the procuring activity with status reports on the system safety hazard analysis results. In essence he assumes responsibility for coordinating the SSPP* requirements, hazards analyses results, safety critical data, etc., between the production activity and all other outside activities to insure that, from the safety standpoint, no interfaces are ignored or areas of required analysis are overlooked.

The production activity in response to the work request must prepare a PHA** of the proposed production process, and from the results of this analysis prepare a SSPP. To prevent a proliferation of unnecessary paper work, it is recommended that each production activity prepare a station instruction entitled System Safety Program Policy which contains an all inclusive sample SSPP which is readily adaptable to any production process. This SSPP should be adaptable to those production cycles carried out completely on station as well as those requiring other government activity and/or contractor assistance. Slide 6 provides an outline of a typical SSPP. In order to provide continuity, efficiency, timeliness and overall effectiveness it is advisable to train specific individuals for preparing PHA's and SSPP's for all production

-
- * - SSPP - System Safety Program Plan
 - ** - PHA - Preliminary Hazard Analysis

lines. At the discretion of the Commanding Officer, this individual could be located in the Safety Department, Ordnance Department, or Resources and Planning Department. For example, the PHA and SSPP may be prepared by the production activity Ordnance Department. However, the PHA can only be conducted with inputs from the Safety Department and operating procedure preparer. In addition, the Quality Assurance Department must conduct and integrate with the Ordnance and Safety Departments a PHA to ensure that design safety of the weapon system is not degraded during the production process and must recommend corrective action to preclude such an occurrence. Oftentimes, tests must also be conducted or test data obtained from engineering agents, process developers, etc., to determine requirements for safety devices, safe distances, etc.

After the Safety Department has reviewed and approved the completed PHA and SSPP and risk decisions have been made by the Station Commanding Officer or his representative and/or the procuring activity, Subsystem Hazard Analyses (SSHA) are conducted on high risk work areas, equipment, and facilities/utilities. High risks are determined as a result of the PHA. SSHA's and corrective action are to be completed by those responsible for production planning, facility/utility design, equipment design and operating procedure development.

The original PHA is also updated by the Ordnance Department to insure no additional hazards are involved in the areas not covered by the SSHA's and to integrate the results of the SSHA's into the overall system analysis. When the equipment and facility drawings are available, the SSHA's are completed and the PHA updated, they are utilized by the preparer of the operating procedures in order to conduct a System Hazards Analysis (SHA) during the time he is writing the operating procedures.

Corrective action will be taken preferably through design changes or through procedural changes when design change is impractical. The SHA may be in a narrative format, columnar format or a fault tree, any of which often reduces to a detailed update of the PHA. With completion of the SHA, actual safety inspection of the line is conducted during a dry run using inert materials wherever possible.

During pilot line production an Operating Hazards Analysis (OHA) must be conducted with specific emphasis placed on experience gained from observing the man-machine/machine-machine/machine-facilities interface. Results of the OHA are to be utilized to improve equipment and procedure safety through design changes or operating procedure changes. The OHA should generally be a combined effort of the Safety Department, operation procedures

preparer, and Ordnance Department and Quality Assurance.

Particular emphasis should be placed on analysis of interfaces between different equipments and between people and equipment during all stages of design since most hazards often are caused by an improper interface.

Prior to start-up of full production, arrangements must be made for a safety inspection conducted by independent safety observers (e.g. NAPEC and the Naval Sea Systems Support Offices or the station Safety Department). Upon satisfactory completion of this inspection, the full production start-up is approved.

During line operations, updates of the OHA are required whenever any changes are to be made to the production process.

An example of a System Safety Program responsibilities can be seen in the next slide (Slide 7). It should be noted that risk decisions are required after each hazard analysis. Most routine risk decisions are made as the result of agreement between the hazard analyst and the designer. However, where the risk decision requires the expenditure of considerable funds the use of a risk panel comprised of representatives from the Ordnance Department, Safety Department, and all others involved may be in order.

The control of the hazards identified by the analysis must be controlled in accordance with the following order of precedence:

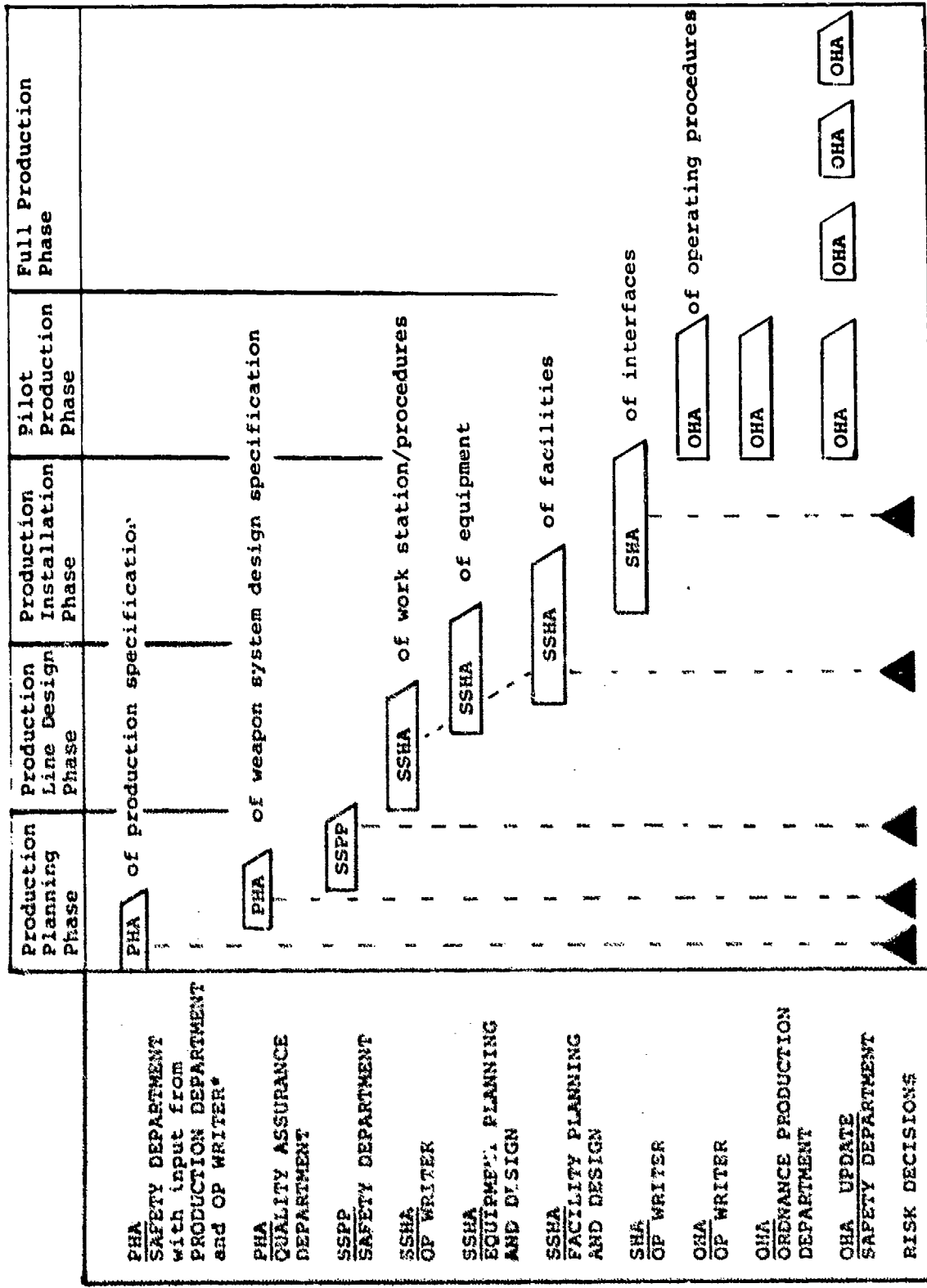
- Design for minimum hazard.
- Use Safety Devices - hazards which cannot be eliminated through design selection will be reduced to an acceptable level through the use of appropriate safety devices.
- Warning devices - where it is impossible to eliminate a hazard, warning devices will be employed to provide timely detection of the hazardous condition and will generate an adequate warning signal. Warning signals will be designed to prevent incorrect personnel reaction to the signals and will be standardized throughout the production activity.
- Special Procedures - where it is not possible to reduce the hazard through design or the use of safety and warning devices, special procedures will be developed. Precautionary notations and signs will be standardized throughout the production activity.

It is the hope of NAVSEASYSKOM that by acquiring more information through the use of System Safety techniques, more effective safety risk decisions will be made. This information can be used to bring our production, disposal, and rework operations into the area of acceptable levels

of risk. This will not eliminate all hazards or accidents,
but it is felt that the use of system safety techniques is
a step in the right direction.

TYPICAL PRODUCTION SSPP TOPIC OUTLINE

1. Scope
2. Production activity organization
3. Systems Safety program milestones
4. Extra-activity organizational interfaces and responsibilities
5. Systems Safety (general requirements and controls)
6. Hazard Analyses
7. Training
8. Systems Safety Program audit



SLIDE 7. ANALYSIS PROGRAM SEQUENCE AND RESPONSIBILITIES

**Safety and Hazards Analysis
of the
Automated Production System
for
155MM and 8" Propelling Charges**

**K. K. Arora
General American Transportation Corporation
Niles, Illinois**

**J. S. Chiappa
Picatinny Arsenal
Dover, New Jersey**

ABSTRACT

This paper presents a quantitative hazards analysis of the concept design of the Automated Production System for 155 mm and 8" Propelling Charges. The system is being designed and developed by General American Research Division of General American Transportation under a contract with Picatinny Arsenal, Dover, New Jersey. The Automated Production System will be installed at Indiana Army Ammunition Plant, Charlestown, Indiana.

A preliminary hazards analysis was performed to identify inherent safety hazards in equipment operation, design, or operating procedures which endanger life, property, or the environment. This was accomplished as part of Phase I of the program. In Phase II, an engineering analysis was conducted to determine the in-process potentials associated with the various forces and/or stimuli that can give rise to hazards such as fire or explosion. Based on the estimated in-process potential and sensitivity initiation data for M1 propellant, the safety margins were evaluated.

Results presented in this paper refer to the conceptual design phase of the Automated Production System for 155 mm and 8" Propelling Charges.

Preceding page blank

1. INTRODUCTION

The introduction of an automated production system to assemble 155 mm and 8 inch propelling charges is a further step in the overall ammunitions facilities modernization program. In order to ensure that the design of the system is acceptably safe from both personnel and facility standpoint, a safety and hazard analysis study must be conducted.

A safety and hazards analysis provides quantitative data for making decisions to optimize the process, production rates, production quality, and costs by showing the quantitative relationship and balance between factors of safety, production rates, production quality and costs. In addition, it identifies specific potential or existing hazards of the system and presents alternative design modifications for the elimination and/or control of these hazards. It is essentially an accident investigation before the accident happens. Generally, this involves a determination of:

- 1) The degree of the hazard
- 2) Whether the precautions to prevent initiation or explosion are sufficient
- 3) Whether the protection of personnel and facilities is adequate in the event of initiation or explosion.

These considerations must be balanced against the original justification for introducing the material or process, whether for reasons of economy, quality, or performance.

The complete safety and hazard analysis study for the designed process was accomplished in the following two phases:

Phase I - In this phase, an analytical engineering study was performed to properly define the system and the boundaries of investigation. The preliminary hazards analysis and faults hazard analysis were performed to identify inherent safety hazards and/or failure modes in equipment operation and design. A logic model of the entire process line was developed.

Phase II - This phase consisted of conducting an engineering analysis and hazard evaluation to determine how the in-process material, MI propellant and equipment will react to the modes of failure and environmental conditions established in the previous phase and establishing the quantitative safety margins associated with the various process equipments that can cause plant shutdown, through mechanical or electrical failures, fires or explosions.

2. SYSTEM DESCRIPTION

The Automated Production System for 155 mm and 8" Propelling Charges is an improved process to load, assemble, and pack-out the five (or three) increments required for the M4A2 and M3A1 propelling charges for the 155 mm howitzer, and M2 and M1 propelling charges for the 8 inch howitzer. The process differs from the present manufacturing system in the sense that it provides:

- o Reduced line personnel
- o Reduced line personnel exposure to explosive hazards
- o Reduced direct and indirect labor cost
- o Higher efficiency in building space utilization
- o Increased ability for product quality control
- o Increased product uniformity
- o Commonality of equipment for variant charge assemblies.

The system provides capability for production of an "end-of-line" average rate of 20 assemblies per minute. The system consists of the following four sub-systems:

- 1) Loading Booth Sub-system
- 2) Hall Conveyor Sub-system
- 3) Charge Assembly Sub-system
- 4) Charge Packing Sub-system.

These sub-systems are described in brief in the following paragraphs.

Loading Booth Sub-system

The operations to be performed at this sub-system are bag filling, sewing, weighing, and inspection. The layout of the sub-system is shown in Figure 1.

Operator #1 will take an empty bag from the bag supply box and place it on the platform of scale #1. The bag will be weighed and upon completion of the weighing, the bag will be alternately swept by an arm into the pick-up tray for operator #2 or #3. Each operator will place a bag on a loading device pertaining to his particular station of the carousel.

Each station will be color-coded, using a two-color code to designate the station each operator will load with a bag. Mounted on the carousel will be fourteen loading stations. After the placing of a bag by either operator on the loading device of one of their designated stations, the bags will proceed through the filling and sewing operations and will be discharged on a conveyor which carries each filled and sewn bag and places it on scale #2 where the total weight is determined. The previous weight will then be subtracted from the total weight to determine the propellant weight. If the propellant weight is acceptable, the gate, normally in the reject mode, will be rotated to allow the filled bag to travel on to the transfer conveyor.

If the propellant weight is unacceptable, the gate will remain in the reject mode and divert the bag into the reject box. The acceptable bag will be conveyed to operator #4 where it will be visually inspected for sewing defects and tears. If acceptable, the bag will be placed on the hall conveyor leading to the assembly room. If the bag is rejected during this visual inspection, it will be placed by operator #4 into the reject box.

Hall Conveyor Sub-system

The configuration of hall conveyors for the total system employing five operating booths and a spare capable of supplying any increment in the event of single booth failure is shown in Figure 2. All increments with exception of base charges maintain vertical orientation. The hall conveyor sub-system transports increments from loading rooms to the charge assembly room. Each of the supply lines consist of three conveyor sections: a right-angle turn out of the booth, a straight section parallel and adjacent to first section and a third section. The third section also consists of a right-angle turn into the assembly area. The sections are individually driven by a solid state direct current fractional motor drive, electrically linked for simultaneous speed regulation. For considerations of the overall system control, the conveyor system is considered an extension of the loading booth and will vary in speed proportionately to increment output.

Charge Assembly Sub-system

The operating characteristics and the overall layout of the Charge Assembly Machine are presented in Figures 3 and 4, respectively. The two figures can be compared to see the physical position of components as they relate to a specific function.

Charge Packaging Sub-system

The Charge Packaging Area consists of all machinery between the output of the assembly area and the removal conveyor for the completed canisters. A plan view of the packaging area is presented in Figure 5. This area of the automated production system differs from the rest of the equipment in that it is comprised substantially of commercially available machinery.

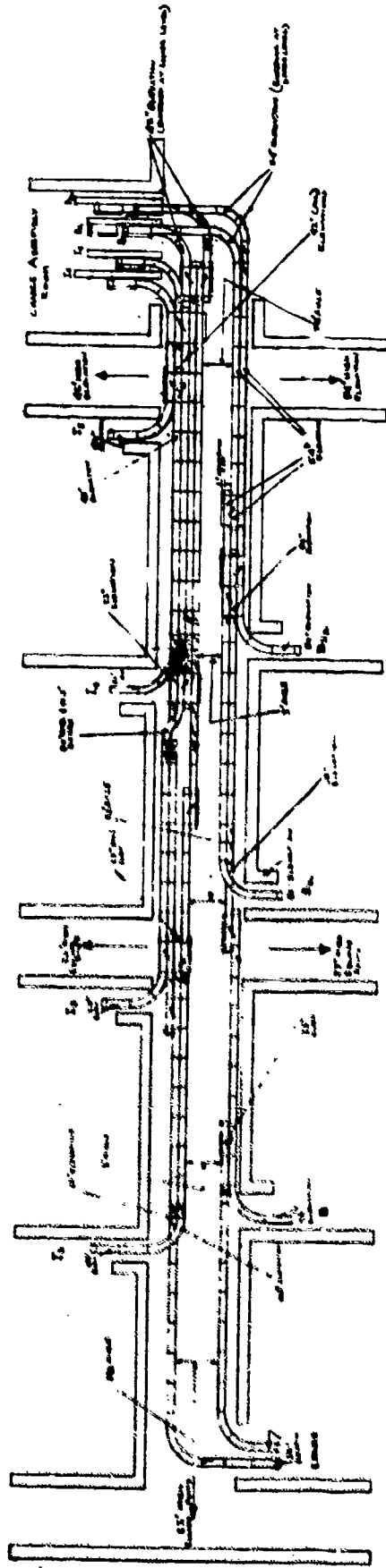


Figure 2 HALL CONVEYOR SUB-SYSTEM LAYOUT

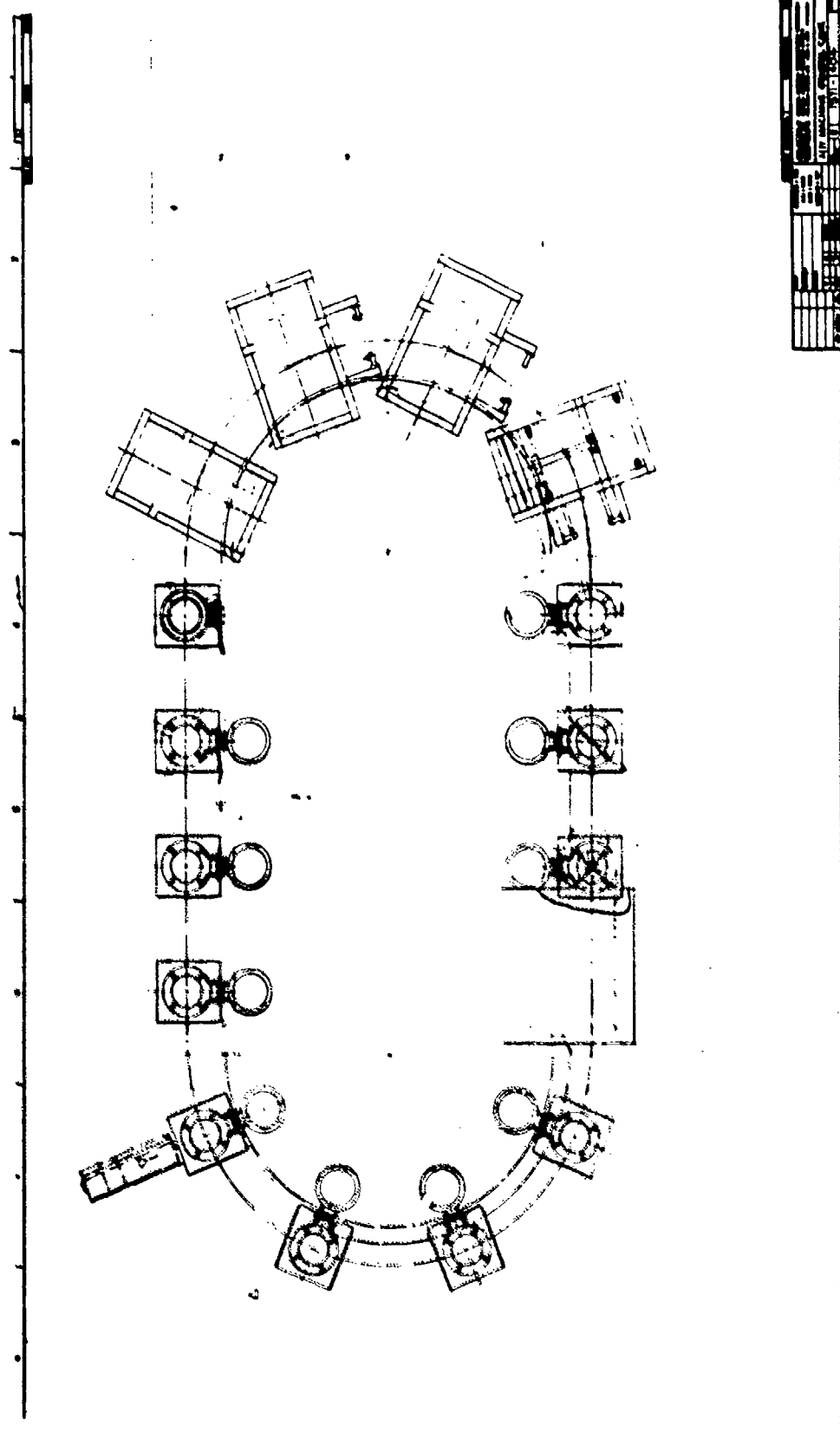


Figure 4 CHARGE ASSEMBLY MACHINE LAYOUT

3. SAFETY AND HAZARD ANALYSES

The safety and hazard analyses were performed to identify hazardous conditions and determine any needed corrective actions. These analyses are qualitative in nature and provide a technical assessment of the relative safety of the automated production process design. The descriptions of these analyses are presented in the following subsections.

Preliminary Hazard Analyses (PHA)

This analysis was performed as the initial investigation to identify inherent safety hazards in the design approach used in developing the Automated Production System for 155 mm and 8" Propelling Charges. The outcome of this analysis provided back-up data for subsequent analyses and established safeguards and design considerations to eliminate and/or control hazards. For purposes of this analysis, the automated production system was divided into four sub-systems as listed earlier in Section 2.

A sample worksheet used in conducting this analysis is presented in Figure 6. The format provides space for recording gross information concerning the hazards at sub-system/system level, the effects of these hazards, and finally, the safeguards and design considerations required to remedy the situation. The following descriptions are indicative of the information required for each category in the format:

- a) End Item - Identifies a finished in-process item within the sub-system under study.
- b) Causative Hazard - Identifies the condition which has the capability of producing a hazard.
- c) Resultant - The potential accident which could result from the hazard.
- d) Class - Qualitative measure of hazards stated in relative terms.

For purposes of this study, the following hazard levels were established:

Hazard Class I - Negligible - Conditions such that personnel error, environment, design characteristics, procedural deficiencies, or operational failure does not result in personnel injury or system damage. These operations are considered inherently safe or have identifiable hazards that are readily eliminated through design and operator training.

Hazard Class II - Marginal - Conditions such that personnel error, environment, design characteristics, procedural deficiencies

PRELIMINARY HAZARD ANALYSIS FORM

Sheet No. 1 of 4

Date _____ System AUTOMATED PRODUCTION SYSTEM Subsystem LOADING BOOTH

END ITEM	CAUSATIVE HAZARD	RESULTANT	HAZARD CLASS	SAFEGUARDS & DESIGN CONSIDERATIONS	REMARKS
Propellant Bucket (Individual)	Static discharge	Fire	II	Provide static bonding and grounding, minimize use of materials, which generate or build up charge. Control moisture in room. Positive powder drainoff system.	Backup with Hi-Deluge system. Periodic inspection.
	1. Equipment				
Propellant Bucket (Multiple)	2. Propellant	Fire	II	Provide guard rails, use impact-reducing equipment and surfaces.	"
	Impact				
	- on ground				
	- against one another				
Sparks	Overheating	Fire	II	Non-sparking metals (stainless steel, aluminum). Eliminate heat-producing operations, protect high friction areas.	"
Same as above.	Same as above.	Fire	II	Provide guards at pinch points. Maintain safe spacing. Prevent critical buildup. (Limit buffer size) Prevent confinement.	"

Figure 6 SPECIMEN PRELIMINARY HAZARD ANALYSIS FORM

or operational failure can be counteracted or controlled without injury to personnel or major system damage. These are operations where hazards can be eliminated or controlled to an acceptable limit to not seriously injure personnel or cause major system damage.

Hazard Class III - Critical - Conditions such that personnel error, environment, design characteristics, procedural deficiencies, or operational failure will cause personnel injury or major system damage, or will require immediate corrective action for personnel or system survival. These operations present hazards that cannot be eliminated, but can be reduced by rigid control of procedures, operator training in safety and redundant controls or interlocks. Resultant incidents may cause severe personnel injury or major system damage.

Hazard Class IV - Catastrophic - Conditions such that personnel error, environment, design characteristics, procedural deficiencies, or operational failure will cause death or severe injury to personnel, or system loss.

- e) Safeguards and Design Considerations - This category is reserved for listing those safeguards and design considerations necessary to eliminate or control identified hazardous conditions.
- f) Remarks - This category is reserved for making general comments with regard to the control and/or elimination of the hazardous condition.

The results of this analysis were amplified in the fault hazard analysis which followed. This analysis is described next.

Fault Hazard Analysis

Based on the information obtained from preliminary hazard analysis a fault hazard analysis was performed. Some of the worksheets used in conducting this analysis are presented here. The format provides space for recording particular information concerning the identity of hazards, their cause, the effects of these hazards on the system, and finally, the corrective measures required to remedy the situation. The following descriptions are indicative of the information required for each category in the format:

- a) Function - The particular sub-operation being analyzed.
- b) Mode - identifies the system phases which are applicable.
- c) Hazardous Element - identifies the elements, in the hardware of the function being analyzed, which are inherently hazardous.
- d) Hazardous Condition - the condition which has the capability of causing an accident.

FAULTS HAZARD ANALYSIS FORM

Date _____ System AUTOMATED PRODUCTION SYSTEM Subsystem LOADING BOOTH

FUNCTION	MODE	HAZARDOUS ELEMENT	HAZARDOUS CONDITION	TRIGGERING EVENT	POTENTIAL FAILURE	EFFECT	HAZARD CLASS	CORRECTIVE ACTION
Tray Conveyor	Buffer standby	Tray door	Tray door distorted	Door snagged by conveyor	Door opens Prop.spills	Fire	II	P.I.
Filling	Tray insertion	Tray guides	Tray cannot be inserted	Tray guides plugged, flange distorted	Tray crushed Prop.spills	Fire	II	P.I., control max. air pres. Ensure completion of air cycle
"	Tray door open	Tray door lock mechanism	Latch Mech. does not open doors	Worn or binding parts	Prop.spilled on refill	Fire	II	P.I., lub, reduce opening force

FAULTS HAZARD ANALYSIS FORM

System AUTOMATED PRODUCTION SYSTEM Subsystem LOADING BOOTH

FUNCTION	MODE	HAZARDOUS ELEMENT	HAZARDOUS CONDITION	TRIGGERING EVENT	POTENTIAL FAILURE	EFFECT	HAZARD CLASS	CORRECTIVE ACTION
Bag Weighing (Base Charge)	Scale sweep	Sweeping arm	Excessive speed	Speed control fails	Avail. impact energy greater than threshold sensitivity	Fire	II	Limit/Control sweep speed
Bag Insertion	B.O.D.*	Opening device	Bent or distorted BOD	BOD sensor indicates open bag	Funnel cannot be inserted properly	Fire	II	P.I./strong BOD, proper operator training, W/Changes I
"	Needle, insertion	Air cyl. actuator	Bag is unsupported	Air cyl. not actuated	Prop. spills during loading	Fire	II/III	P.I., sensor
Bag Loading Transfer Out	Bag O.D. Rotation	Cam and follower	Prop. on cam follower from previous operation	Cam crushes prop.	"	Fire	II	Provide guards over cam
"	Needle, insertion	Needles	Bag unsupported by needles	Needles dull, distorted, bent	Could cause prop. to spill at filling sta.	Fire	II/III	Sensor, P.I.**

* B.O.D. = Bag Opening Device
 ** P.I. = Periodic Inspection

FAULTS HAZARD ANALYSIS FORM

FUNCTION	MODE	HAZARDOUS ELEMENT	HAZARDOUS CONDITION	TRIGGERING EVENT	POTENTIAL FAILURE	EFFECT	HAZARD CLASS	CORRECTIVE ACTION
Sewing	Plowing	Guides	Static elec.	Grounding fails	Threshold sensitivity level exceeded	Fire	III	Grounding redundant, W/Changes, II
	"	"	Spilled prop. on cam	Torn bag	"	Fire	III	P.I.*
	Stitching	Cam Follower	Interference	Spilled prop.	"	Fire	III	Protective covers on follower, W/Chges II
	"	"	Excessive heating Sparks	Cam follower breaks	Bag tears	Spilled prop.	III	P.I., Lub.
	"	Hot needle	Overheating	Needle mis-aligned	Thres. temp exceeded	Fire	III	P.I., sensor
	"	Needle	Excessive friction/spark	Lub inadequate	"	Fire	III	Use non-sparking material
	"	Lubricated Joints	Galled or rough surf.	Overheated surface	Temp > T.S.**	Fire	III	Use non-flam oil, monitor oil level
	"	Feed foot	Chain breaks and/or slips	Snags, tears bag	Spilled prop is ignited	Fire	III	Redesign or P.I., use non-sparking mtg and/or heat sensor unit. P.I.
	"	Chain drive surface	Binding	Loose chain	Poorly stitched bag spilled prop Unstitched bag	Fire	II	P.I.
	"	Counter-weight		Dirt, burr	Spill'd prop	Fire	III	Sensor on counterwt.

* P.I. = Periodic Inspection.
 ** T.S. = Threshold sensitivity.

FAULTS HAZARD ANALYSIS FORM

FUNCTION	MODE	HAZARDOUS ELEMENT	HAZARDOUS CONDITION	TRIGGERING EVENT	POTENTIAL FAILURE	EFFECT	HAZARD CLASS	CORRECTIVE ACTION
Base Increment Loading	Supply	Belt/Hallway conveyor interface	Pinching of increment	Poor conveyor alignment	Threshold sensitivity level exceeded	Fire	II	Periodic inspection
"	"	Belt conveyor	Excessive friction with increment	Excessive belt speed	"	Fire	II	Reduce coefficient of friction Limit belt speed Provide cooling devices
"	"	Pier Gate	Excessive build-up of increments	Malf. of pier gates	Build-up and ignition of critical size charge	Fire	II	Sensors on supply Sensors on gates
"	"	Belt conveyor	"	Frayed belt	"	Fire	II	Sensor for conveyor operation Highly reliable belt and drive ass'y.

* Charge Assembly Machine Area will be equipped with a Hi-DeLuge System.

FAULTS HAZARD ANALYSIS FORM

Date _____ Sheet No. 3 of 5

System AUTOMATED PRODUCTION SYSTEM Subsystem CHARGE ASSEMBLY

FUNCTION	MODE	HAZARDOUS ELEMENT	HAZARDOUS CONDITION	TRIGGERING EVENT	POTENTIAL FAILURE	EFFECT	HAZARD CLASS	CORRECTIVE ACTION
Increment Loading	Picking	Picker	Picker drops increment	Inadequate grip	Increment impacts machine/floor	Spilled prop.	II	Redesign picker if required Ascertain reliability of operation, P.I.
"	Shuttle	Base doors	Increment fails to be released	Malf. of doors	Subsequent increment interface with machine	"	II	High reliability components, ascertain reliability of operation, P.I.
"	"	Shuttle	Increment protruding from fixture	Straps prevent base charge from moving down	Threshold sensitivity level exceeded	Fire	II	Sense position of preceding increments, ascertain reliability of operation
"	"	Shuttle cup	Increment fails to fall into fixture	Poor alignment of cup and fixture	Return motion of shuttle increment with fixture	Spilled prop.	II	High reliability components, ascertain reliability of operation, P.I.
"	"	"	"	Picker/cup misalignment	"	"	II	"

FAULTS HAZARD ANALYSIS FORM

Sheet No. 1 of 4

Date _____ System AUTOMATED PRODUCTION SYSTEM Subsystem _____ PACKING AREA*

FUNCTION	MODE	HAZARDOUS ELEMENT	HAZARDOUS CONDITION	TRIGGERING EVENT	POTENTIAL FAILURE	EFFECT	HAZARD CLASS	CORRECTIVE ACTION
Charge Transportation	Automatic discharge inspection station	Movable Guide	Crushing, impact	Failure of press. sens/regulator	Threshold level exceeded	Fire	II	Redundant pres. sensors & regulators, W/Changes I P.I., provide grounding backup
Charge Transportation	Conveying	Tie straps	Bag torn open	Snagged strap	Spilled prop.	Fire	II	Ascertain reliability of conveyor, use low friction material
"	Transfer of charge from one conveyor to other	Transfer plate	Pinching	Plate snags bag	Threshold initiation level exceeded	Fire	II	Ensure smooth transition of charge from one conveyor to another
"	"	Conveyors	Buildup of static charge	Ground malf.	"	Fire	II	Provide grounding
"	Diverging charge to floating supply chute	Charge Diverter Gate	Impact	Malf. of diverter gate/sensor	Threshold level exceeded	Fire	II	Redundant sensor, P.I.

* Packing Area will be equipped with: 1) a Fire Wall located at Floating Supply Area and 2) a Hi-DeDuge system.

- e) Triggering Event - that element which could initiate (trigger) the hazardous condition into becoming a potential accident.
- f) Potential Failure - the potential failure (accident) which could result from the hazardous conditions.
- g) Effect - the possible result of the potential accident.
- h) Hazard Classification - this category provides a qualitative measure of the hazards effect and is categorized as listed in the previous section.
- i) Corrective Action - this category is reserved for listing those control measures necessary to eliminate or control the identified hazardous condition.

This analysis provided a source of data for corrective action (procedure or hardware changes).

4. ENGINEERING ANALYSIS AND HAZARD EVALUATION

Analysis Approach

In order to assess the hazards that are associated with the automated production process, a quantitative hazards evaluation involving engineering analysis was performed utilizing sensitivity data.

The potential hazards and the initiation modes that could give rise to a hazard were compiled for the complete process from bag loading to the final pack-out of the assembled charges. For the purposes of this analysis, the plant was divided into its operating areas, namely: Loading Booth Area, Hallway Conveyor Area, Charge Assembly Machine Area, and the Charge Packing Area. In performing the engineering analysis and hazard evaluation, the major task was to calculate the process energy generated by friction, pinching, crushing, impact, and electrostatic discharge. The calculations to determine the in-process potentials are based on establishing thresholds that would be generated if the worst possible conditions exist during a particular process. For example, a hopper containing electrostatically charged material is unsafe only if the grounding and bonding system for the hopper fails. Thus, calculations to determine the electrostatic energy buildup will pertain to this worst condition, i.e., an ungrounded hopper system. The computed in-process potentials for the potential hazards in the process were compared with the threshold initiation level (TIL) for the process material, MI propellant, to give the safety margin for the process. In the cases where the in-process potential exceeds the threshold initiation level such that the safety margin is less than 1, rigid conclusions regarding the unreliability of the process can be drawn, (only when the initiation mode is realized in the system failure).

Safety Margin Summary

Partial results of the engineering analysis and hazard evaluation study for the automated production process plant are presented in table 1 through 4. For each operating area in the plant, the columns in the Tables shown

HAZARDS ANALYSIS FORM

Date _____ System AUTOMATED PRODUCTION SYSTEM Subsystem LOADING BOOTH AREA Sheet No 3 of 4

Potential Hazard	Initiation Mode	In-Process Potential (Analysis)	Threshold Initiation Level (Sensitivity Test Data)	Conclusions	
				Hazard	Safety Margin
Propellant Grains Trapped in Bucket Conveyor Mechanism	ESD from propellant to metal on moving V-belt rollers <u>Thermal Buildup</u> due to friction between trapped propellant and rollers	0.02 Joules 428 psi @ 2 ft/sec 27°C/sec	5 Joules 80,000 psi @ 8 ft/sec 263°C (5 sec)	No No	250 187 1.94
Bag Weighing (Igniter and Flash Reducer)	<u>Impact</u> by sweeping arm	.12 ft-lbs/in ²	17.4 ft-lbs/in ²	No	145
Filling of Funnel Ass'y. (Bucket Doors Open)	ESD due to grounding loss from propellant flow (free-fall) <u>Electrostatic Charge Generation</u> in funnel due to grounding loss	0.005 Joules 0.006 Joules	5 Joules 5 Joules	No No	1000 833
Vibrator (on Clam Shell)	<u>Thermal Energy Buildup</u> due to excessive vibration of bag	12.2 ft-lbs/in ² 500 psi @ .65 ft/sec	17.4 ft-lbs/in ² 80,000 psi @ 8 ft/sec	No No	1.5 160

HAZARDS ANALYSIS FORM

Date _____ System AUTOMATED PRODUCTION SYSTEM Subsystem LOADING BOOTH AREA Sheet No. 4 of 4

Potential Hazard	Initiation Mode	In-Process Potential (Analysis)	Threshold Initiation Level (Sensitivity Test Data)	Conclusions	
				Hazard	Safety Margin
Sewing Machine - Needle - Lubricated Joints	Thermal Energy Buildup due to excessive heating of needle	750 psi @ 26 ft/sec 53°C/sec	80,000 psi @ 8 ft/sec 263°C (5 sec)	No	106.67
	Thermal Energy Buildup due to inadequate lubrication of joints			Yes	NONE
Cut Chain Stitch - Blades Overheated	Thermal Energy Buildup due to excessive friction between treadle and base	.22°C/sec	263°C (5 sec)	No	239
	ESD due to grounding loss sewing machine	0.001 Joules	5 Joules	No	5000
	Thermal Energy Buildup due to bindings/misalignment of cutting blades	0.008°C/sec	263°C (5 sec)	No	6575

HAZARDS ANALYSIS FORM

Sheet No. 1 of 2

Date _____ System AUTOMATED PRODUCTION SYSTEM Subsystem CHARGE ASSEMBLY MACHINE

Potential Hazard	Initiation Mode	In-Process Potential (Analysis)	Threshold Initiation Level (Sensitivity Test Data)	Conclusions	
				Hazard	Safety Margin
Poor Conveyor Alignment (Belt/Hallway Conveyor Interface)	<u>Thermal Energy Buildup</u> due to pinching of increment	6.4 psi @ 3 ft/sec	80,000 psi @ 8 ft/sec	No	12,500
Belt Conveyor	<u>Thermal Energy Buildup</u> due to excessive friction between belt and increment	.02°C/sec	263°C (5 sec)	No	2,630
Spilled Propellant (Bag Leaks)	<u>Thermal Energy Buildup</u> due to propellant trapped in conveyor mechanism	.50 psi @ 1 ft/sec .02°C/sec	80,000 psi @ 8 ft/sec 263°C (5 sec)	No	160,000
	<u>ESD</u> due to grounding loss in conveyor	0.010	5.0 Joules	No	500
Base Charge Loading	<u>Impact</u> of charge against ramp stop	1.8 ft-lbs/in ²	70 ft-lbs/in ² (Igniter)	No	39
Transfer of Base Charge to Operator #2	<u>Impact Energy Buildup</u> due to base charge sliding off the work table	1.8 ft-lbs/in ²	17.4 ft-lbs/in ²	No	10

HAZARDS ANALYSIS FORM

Date _____ System AUTOMATED PRODUCTION SYSTEM Subsystem CHARGE ASSEMBLY MACHINE Sheet No. 2 of 2

Potential Hazard	Initiation Mode	In-Process Potential (Analysis)	Threshold Initiation Level (Sensitivity Test Data)	Conclusions	
				Hazard	Safety Margin
Base Charge Insertion	<u>Impact of base charge with clamp ring (base charges not fully inserted)</u>	.3 ft-lbs/in ²	17.4 ft-lbs/in ²	No	58
Spilled Propellant on Clamp Flange	<u>Impact of material with clamp ring</u>	15 ft-lbs/in ²	17.4 ft-lbs/in ²	No	1.2
Increment Loading	<u>Picker drops increment. Increment impacts machine/floor</u>	7.8 ft-lbs/in ²	17.4 ft-lbs/in ²	No	2.25
Spilled Propellant	<u>Thermal Energy Buildup due to material trapped between moving parts</u>	50,000 psi @ 1 ft/sec	80,000 psi @ 8 ft/sec	No	1.6
Increment Loading	<u>Increment fails to be released. Crushing of increment by shuttle</u>	.1 ft-lbs/in ²	17.4 ft-lbs/in ²	No	174
Control Ring Opens	<u>Pinching of loose propellant</u>	5 ft-lbs/in ²	17.4 ft-lbs/in ²	No	3.50
Jaws Open & Fixture Lifted. Loose propellant on cam follower	<u>Excessive stress due to pinching of propellant by cam surface</u>	50,000 psi @ 1 ft/sec	80,000 psi @ 8 ft/sec	No	1.60
Sudden Release of Tension during Knot Tightening	<u>Pinching of loose propellant</u>	1.06 ft-lbs/in ²	17.4 ft-lbs/in ²	No	16.5

represent the following items:

Potential Hazards

Initiation Modes

In-Process Potentials

Threshold Initiation Levels (TIL)

Conclusions $\left\{ \begin{array}{l} \text{Hazards} \\ \text{Safety Margin} \end{array} \right.$

Engineering Calculations

The in-process potentials were calculated for each process and/or item of equipment and consisted of determining the forces arising from pinch forces, impact loading, the heat release due to friction, and electrostatic charge buildup.

The in-process potential has been evaluated on the basis of available sensitivity data. These data are based on the standard test methods as outlined in TM 9-1300-214, and include such tests as impact, friction pendulum, and electrostatic discharge tests. In addition to these standard tests, additional sensitivity test data are available as a result of special testing on previously analyzed systems to more closely duplicate special in-process operations and/or hazards. When such data are available, i.e., data which more closely simulates the actual in-process operation, these data have been used.

5. CONCLUSION

The safety and hazard analysis of the automated production system for 155 mm and 8" propelling charges consisted of (1) data acquisition and (2) analytical phase. The analytical phase of the program consisted of conducting engineering studies to identify inherent safety hazards and establish safety margins.

The results indicate that the hazards which may occur in the automated production process can be broadly classified as: (1) Fire, (2) Explosion. The category of "fire" could be further classified as: (a) fire due to in-process material, and (b) fire due to spilled propellant. The spilled propellant by itself is not hazardous unless accompanied by an ignition source and a means of propagation. The two major hazard potentials throughout the plant as indicated by the various hazards analysis that were performed, are associated with the possibility of electrostatic discharge and heating of trapped propellant grains/dust in moving parts, cracks, cavities, etc. of the machine system.

Friction and impact potentials were in general found to be lower than electrostatic hazards, except in the case of the sewing operation in the loading booth area. The continuous operation of the sewing machine at the rate of 5000 stitches per minute can cause excessive heating of the needle/looper mechanism. In order to eliminate and/or control this potential hazard it is recommended that a cooling device be provided to control the heating. Other hazard-prone areas in the automated production system process are listed below.

Conveyor System - The design of the plate conveyor system used in the loading booth and hallways has many potential pinch and friction points. Loose propellant can become lodged in these areas and possibly ignited unless certain precautions are taken (e.g., shields, deflectors). Very little information is available regarding the electrostatic charge build-up due to the plastic plates rubbing against the metal wear strips. Additional information is required regarding this hazard. Many areas exist for accumulation of dust and granules of propellant. Grease and/or oil on the chain and drive mechanism should be held to a minimum as they tend to attract and retain any dust or loose granules. On the curved sections of the conveyors the plates may pinch or snag the increments. Again, operational testing is required to evaluate this hazard.

Funnel System - A potential hazard exists in the loading booth if the propellant flow through the funnel is either choked or is excessively restricted. In either case, the propellant will spill and could lead to a hazardous condition. It is understood however that a test program is in progress to evaluate this potential and to incorporate design changes as required. In addition, the funnel extension offers potential hazards. Granules of simulated propellant were observed to adhere and stick in the folds of the extension. These granules subsequently loosen and fall to the floor. Further, the continuous operation of the funnel extension may introduce fatigue openings in the extension and resulting spillage. Operational testing will be required to evaluate this hazard, although periodic inspection may suffice.

Air Cylinders - The air cylinders used throughout the system have an inherently low reliability. This is offset however by their non-electrical operation (and therefore safer from an ignition source potential) and the incorporation of a fail safe mode, i.e., if failure occurs the valve or mechanism is in a safe operating position. The low reliability can be overcome by periodic inspection. Therefore for these and other critical components, periodic inspection is considered essential for a safe operation.

Shuttle Mechanism - The shuttle mechanism used in the assembly area has not been finalized and therefore introduces many unknowns with regard to the reliability of the operation. The shuttle assembly must be brought up to the speed of the moving fixture in a short distance and the increment precisely released. Interference and resulting spillage can occur in this operation. However, because of the unique nature of this design, operational testing will be required to evaluate these hazards.

Clam Shells - Ejection of the increments in both the bag loading and assembly areas depend on the operation of a clam-shell type fixture. The doors rotate to open and at the same time push the increment from the rear. For the bean-bag type configuration of the increments this method may not provide for positive ejection. If the increment is not ejected, subsequent closure of the shells may ignite or tip the bag. As with many of the other items in the design, operational testing will be required to evaluate this hazard.

In general, propellant spills are not considered a major hazard with these particular propellants for the following reasons:

1. In addition to a spill, an ignition source must be available at that point.
2. In order for the fire to spread, a path of propellant must be available to propagate the flame.
3. Preliminary tests indicate that unconfined propellant will not explode.
4. Periodically the machines and areas are washed down to remove spilled propellant and powder dust.

In order to reduce the electrostatic discharge initiation hazards of in-process material to very low levels the following actions are recommended:

1. Ensure positive grounding and bonding between all equipment and items in the individual rooms, between the rooms, and between the hallway and rooms.
2. At least once a week on a regular basis all equipments shall be checked for adequacy of grounding and bonding. Resistance values shall conform to the requirements of AMCR 385-100, Section 7-4.
3. Provide humidity control in all rooms and areas where in-process propellant is present. As indicated in AMCR 385-100, Section 7-8, humidification for preventing static electricity accumulations and subsequent discharges is usually effective if the relative humidity is above 60 percent.
4. Static detectors should be used in the plant to measure and monitor electrostatic charge. These include electrometer amplifiers, electrostatic voltmeters, neon lamps, etc.
5. In order to prevent dust formation, an effective dust monitor and dust collecting system, employing a wet type collector should be used. Explosive dust should be removed periodically from the collector chamber to eliminate unnecessary and hazardous concentrations of propellant dust. The dust collector system itself should be periodically washed.

The high deluge system should serve to both extinguish the fire and render inert the propellant that is not yet engulfed in flame. The deluge system should not only be capable of extinguishing fires in each of the operating rooms in the plant, but should also prevent

the propagation of fire or explosion between rooms. The overall response time (from sensor functioning to delivery of water to material) of the deluge system is of paramount importance since, with a reduction in overall response time there is the opportunity to effect extinguishment and significantly reduce the damage within a plant. In order to design the fastest feasible arrangement of the high deluge system, it might be necessary to make a mock-up of the equipment and run tests to determine the most effective location, discharge pattern and piping arrangement.

All electrical motors and control equipment to be used in the plant shall be Class I, Group C and D, and Class II, Group E, F, and G in accordance with the requirements of the National Electrical Code, 1972-73, of the National Fire Protection Association, Chapter 5, Article 500 - Hazardous Locations. In areas where electrical installations may create an undue hazard, it may be necessary to exceed the requirements of the code.

The task of acquiring the sensitivity data for MI propellant involved collecting the information concerning initiation sensitivity, explosibility characteristics, critical height to explosions, and propagation characteristics of MI propellant. This was accomplished by reviewing the work done by GARD and other appropriate sources in the past. No data was found with regard to the propagation characteristics of MI propellant on configurations that simulate assembly plant environments. The preliminary tests conducted by another firm under a different program showed that in a container filled with increments, fire propagation was from one increment to another as opposed to the entire contents bursting into flame. In another test run with a hopper full of MI propellant, the ignited propellant spewed fire vertically with little effect on the container itself and only scorched a newspaper lying nearby. More detailed testing is required to backup these statements with a high degree of confidence. The separation distance between cannisters is an unknown and requires additional experimentation and analysis.

The hazard evaluation study has shown that the in-process energy levels are not of sufficient magnitude for initiating MI propellant dust layers or granules during manually performed/mechanical equipment operations. Adequate margins of safety are present for impact, friction, electrostatic discharge, impingement, and metal sparking attributable to humans, the equipment or the propellant itself. This statement is based on the fact that the sensitivity data acquired from the various sources is correct and reliable.

Calculated in-process potentials for the various mechanical type operations have been computed on the basis of the severest combinations of operating conditions. For example, the pressure on propellant in gear meshing operations is assumed to be the maximum contact stress and the maximum sliding velocity between the mating teeth. In the real situation, the propellant on the teeth would tend to distribute the load more uniformly (thereby reducing the peak pressure) while the

maximum sliding velocity would only occur at one particular time during tooth contact. Therefore, the computed safety factors are considered conservative.

Humidity plays an important role in electric charge build-up on the surface of nonconducting solid materials. It increases the conductivity of the solids. Information relating to the variation of the conductivity of MI propellant granules with changes in humidity levels was not available. Bulk conductivity and dielectric constant evaluations should be conducted on samples of in-process material to characterize its electrical charging and bleed-off abilities.

At the time the present study was performed, the design of the Automated Production System for 155 mm and 8" Propelling Charges was at the concept stage. The study will be updated during the prototype debugging, final design and final debugging phases of the design program.

REFERENCES

1. Encyclopedia of Explosives and Related Items, PATR2700, Volume 2, Picatinny Arsenal, Dover, N.J., 1962.
2. Military Explosives, TM9-1300-214/T011A-1-34, Departments of the Army and the Air Force, Washington, D.C., November 1967.
3. "Hazards Analysis Study of Building 1813 Preblending Incident", Hercules Incorporated Report, for Radford Army Ammunition Plant, dated September, 1972.
4. "Hazards Analysis Studies Pertaining to the Automated Single-Base Program", Report No. 1, Prepared by Hercules Incorporated for Radford Army Ammunition Plant, dated October 31, 1972.
5. "Determination of Critical and Safe Height of M1 Propellant", Results as of December 5, 1973, Interim Report Prepared by IITRI for Picatinny Arsenal, Dover, N.J.
6. Firenze, R. J., "Applying Systems Analysis to Ordnance Production Systems", 12th Explosives Safety Seminar, Armed Service Explosives Safety Board, Washington, D. C.

AN ANALYTICAL MODEL TO PREDICT EXPLOSION PROPAGATION

by

James M. Dobbie and Donald S. Allan

Arthur D. Little, Inc.
Cambridge, Massachusetts 02140

ABSTRACT

This paper describes an analytical model for predicting the spacing required between adjoining explosive projectiles to obtain a high probability that a detonation will not propagate from one to another. It also describes experiments that were conducted to obtain data for comparing with the analytical model. The model was constructed by Arthur D. Little, Inc., under the direction of the Manufacturing Directorate, Picatinny Arsenal.

The general procedure is as follows: from fragmentation data and empirical equations obtained from such tests estimate the mass and spatial distributions of fragments relative to the donor. Also, estimate the initial velocities of the fragments issuing in various polar zones. Use geometrical relationships and drag laws, if the spacings are large, to estimate the distribution of mass and striking velocity of fragments on various zones of the receptor. Next, use sensitivity data and empirical equations obtained from such tests to determine the effects of fragment impacts, in particular, the probability of high-order detonation. Finally, use simple probability arguments to compute the probability that the receptor will receive at least one high-order impact, thereby obtaining the probability of propagation as a function of the spacing. Then solve the set of equations, by iteration if necessary, to obtain the spacing required

for a given probability of propagation.

The purpose of this presentation is to describe the model, summarize the results of the experiments that were made to develop and test the model, and to indicate analytical and experimental work that is needed to improve the model.

1. The Propagation Model

1.1 Background

The spacing necessary to prevent the propagation of an explosion between two or more adjoining projectiles is of prime concern in the design and layout of ammunition plants. Knowledge of the required spacing may also aid in achieving improved safety both in the storage and field use of projectiles.

The usual method of determining "safe" separation distances between explosive items is to conduct propagation tests at selected spacings, using sufficient receptors to obtain a small confidence interval for the confidence level of interest. This method is slow and expensive. Also, it yields little insight into the propagation process and the factors that are critical.

Recently Arthur D. Little, Inc., under a contract with Picatinny Arsenal, undertook the development of an analytical model with which to predict the probability of detonation for a given spacing and orientation of the donor and receptor, and to estimate the spacing required to obtain a given probability of propagation. Such a model can be used not only for determining safe separation distances of current projectiles, but also for estimating the effects of shields and deflectors, and the effects of changes in case thickness, charge composition, charge-to-metal weight ratio, etc.

The type of detonation of primary interest is a high-order detonation, similar to that produced by the firing of a fuze. If detonation

of this type is initiated at one or more positions along the lateral surface of the receptor, it is expected that the detonation wave will propagate throughout the charge and the receptor will detonate high-order. This type of detonation might be called domino detonation, since fragments from the receptor could detonate a third projectile at the same spacing. Low order detonations, while not negligible, are of secondary interest.

The basis for the model is the knowledge that propagation of a detonation between explosive projectiles of interest is caused by primary fragment impact. The sensitivity of the acceptor projectile to detonation is determined by the presented area of the fragment, its velocity at impact, the angle at which it impacts, the casing thickness, and the explosive loading of the acceptor. Some sensitivity data and empirical relationships are given by Slade and Dewey⁽¹⁾. The sensitivity results and analyses that have been performed by Picatinny Arsenal⁽²⁾ and by Arthur D. Little, Inc.⁽³⁾ for both the Arsenal and the Department of Defense Explosives Safety Board⁽⁴⁾ provide a reasonable basis for the development of an analytical model.

1.2 Fragment Properties and Distributions

Data have been obtained on the properties of fragments that are produced in the detonation of projectiles. These properties include initial velocities and various measures of fragment size. Measurements have been made of the distribution of fragment mass, the spatial distribution of ejected metal, and the variation of mass distribution with the polar angle measured from the nose of the projectile. Measurements have been made of the initial velocity of fragments and the variation of velocity with polar angle. The results of these measurements have been used to obtain various empirical equations from which the fragment properties can be estimated from the dimensions of the projectile, the composition of the charge, and the composition of the case. References (5), (6) and (7) contain equations of this type and discussions of other properties for which empirical equations have not yet been developed.

From scaled drawings of the donor estimate the average outside diameter and case thickness over the middle third of the projectile. From these quantities and the densities of the charge and metal compute the corresponding charge-to-metal ratio, the initial velocity V_0 , and the average mass m_0 of fragments from well-known equations. The one-third rule has been observed to yield accurate estimates of V_0 for the central 10 degree polar zone. Accurate estimates of m_0 for the central zone required a change in a parameter K_0 from the value that applied to all fragments to a smaller value.

In general, the maximum initial velocity is obtained in the central polar zone. The variation of the initial velocity with polar angle depends on the projectile. Let the initial velocity at polar angle ϕ be $V_0 F_V(\phi)$. The values of $F_V(\phi)$ for a typical nose-fuzed projectile are approximately as follows:

ϕ (degrees):	60	70	80	90	100	110	120
$F_V(\phi)$:	0.6	0.7	0.9	1.0	0.7	0.6	0.5

The distribution of fragments with polar angle also depends on the projectile. For a typical nose-fuzed projectile the fraction $F_M(\phi)$ of the fragment mass that is ejected in a polar zone of 10 degrees centered at polar angle ϕ varies as follows:

ϕ (degrees):	60	70	80	90	100	110	120
$F_M(\phi)$:	0.05	0.10	0.10	0.15	0.45	0.05	0.05

The accuracy needed for the $F_V(\phi)$ and $F_M(\phi)$ factors depends on the particular application of the model. The spacing required for a small probability of a high-order detonation of a receptor is large enough that the fragments that can strike the receptor are limited to those that issue from the donor in a small polar zone. Hence, only the factors that apply to that zone are needed. For example, when the receptor and donor

are parallel, as in Load-Assembly-Pack operations, only the factors for the 10 degree zone centered at $\phi=90$ degrees are needed. On the other hand, spacings that yield propagation probabilities near 50 percent are small enough that several 10 degree polar zones are involved.

We also need the distribution of fragment sizes in the relevant polar zone. Here we used an empirical distribution function that has been found to yield a fair fit to the observed distribution of all fragments. The fit is good for small and medium sizes, but not for large sizes. The critical fragment size for explosive propagation is in the region where the fit is good when the spacing is small. For small probabilities of propagation the spacings may be large enough for some projectiles that the assumed distribution function is not adequate. When work on the model is resumed we expect to re-examine this question in an attempt to obtain a more appropriate distribution function, one that applies to fragments in the relevant polar zones and to all critical sizes.

At large spacings the striking velocity may be significantly less than the initial velocity. We estimated striking velocities from the square drag law, using a shape factor for random steel fragments. The drag factor depends on the fragment mass, as well as the spacing.

1.3 Sensitivity Properties

The sensitivity equation gives an estimate of the striking velocity that is required for high-order detonation of the receptor. This critical striking velocity depends on the sensitivity of the charge, the thickness of the casing, the size of the fragment, and the impact angle θ to the normal.

Most of the available data consist of the critical (50 percent) detonation velocities obtained in sensitivity tests with cylindrical fragments of known size, orientation, and impact angle. Slade and Dewey⁽¹⁾ give results and empirical equations for tetryl and Composition B with

bare charges and with charges covered by plates.

Most of the data for cylindrical fragments were obtained at zero impact angle, with the circular face parallel to the surface of the charge or plate. To use the corresponding sensitivity equations it is necessary to change from cylindrical fragments to irregularly-shaped fragments and from zero impact angle to the variations of impact angle that occur on the receptor.

The results reported in reference (1) and in some classified reports indicate that the critical measure of fragment size for cylindrical fragments in the orientation described above is the area of the striking face. We used the shape factor for irregularly-shaped fragments to make the conversion from average presented area to the mass m . Since an irregularly-shaped fragment of given presented area will not be as effective in producing detonation as a cylindrical fragment of the same presented area, we introduced a factor F_A to account for this difference. This factor is the fraction of the presented area of the irregularly-shaped fragment that is as effective in producing detonation as a cylindrical fragment having a circular face equal to that area. The value of F_A is not known; it probably lies in the interval (0.5, 1.0).

When the transformation described above has been made the sensitivity equation gives the striking velocity V required at normal impact in terms of the mass m , for a given explosive composition and case thickness. It also may be regarded as an equation that determines the critical mass as a function of striking velocity. If the drag is significant, the relationship is complicated, since the drag factor also depends on the mass.

In practice it was found that the drag factor could be handled by iteration, starting with the assumption that the drag is negligible. After the critical mass and corresponding spacing are computed, the drag factor can be estimated and new values computed for the critical mass

and spacing, etc. It was found that only a few iterations are needed to obtain the spacing to within one percent.

The sensitivity equation was solved for the critical mass m in terms of the striking velocity V , which is determined from the initial velocity V_0 in the central zone, the $F_V(\phi)$ factor in the relevant ϕ direction, and the drag factor. The mass distribution function and geometric relationships then were used to estimate the number of fragments with more than critical mass that would strike the receptor.

1.4 Effect of Non-Normal Impact

Since most fragments will not strike at normal impact, the computed number of supercritical fragments for normal impact is multiplied by an impact factor F_I . Its value depends on how the effective component of striking velocity varies with the impact angle. The value of F_I is not known accurately and probably depends on the charge composition. For composition B it is estimated to be in the interval (0.2, 0.4), as described below.

Relatively few sensitivity tests have been made at impact angles different from zero. Results of some tests at small angles from the normal are reported in reference (1) for tetryl and composition B. We used these results to get a rough estimate of the effect of non-normal impact.

We assumed that the effective velocity at impact angle θ is $V(\cos \theta)^j$, where V is the striking velocity. Figures 8 and 9 of reference (1) indicate that j is at least 2 for $\theta \leq 30$ degrees. For bare Comp B there is an anomalous value at $\theta=8$ degrees, while the critical velocity at $\theta=20$ degrees is approximately 1.45 times the critical velocity at $\theta=0$, which corresponds to a value of j of approximately 6. For convenience, we used $j=2$ and $j=5$ as limiting values.

We replaced V in the sensitivity equation by $V(\cos \theta)^j$, computed

the corresponding critical mass $m(\theta)$ and the fraction $f(\theta)$ of the fragments that are supercritical. From geometric relationships we determined the range of θ and computed the average \bar{f} of $f(\theta)$. The factor F_I is the ratio $\bar{f}/f_1(0)$ of the average to the value at impact angle $\theta=0$. For typical projectiles the value of F_I was found to be approximately 0.4 for $j=2$ and 0.2 for $j=5$.

1.5 Probability of Detonation For a Given Spacing

We assume that the donor and receptor are parallel with center-to-center spacing S , the bases of the projectiles are in the same plane, and no shielding is between them. The probability P that the receptor will detonate (high-order) was computed from the following steps:

(a) On a scaled drawing with the donor and receptor spaced S inches center-to-center lay off the dividing rays for polar zones of 10 degrees. Determine the polar zones in which fragments from the donor can strike the receptor. For each zone estimate the average outside diameter and case thickness and the fraction of the zone over which the vulnerable section of the receptor extends.

(b) For each zone estimate the striking velocity from V_0 and the $F_v(\phi)$ factors; then compute the corresponding critical mass for normal impact.

(c) Estimate the fraction of the striking fragments in each zone that have sufficient mass to produce detonation of the receptor charge. This quantity is the product of two factors. The first factor is the fraction of fragments that have mass exceeding the critical mass for normal impact. The second factor is the impact-angle factor F_I .

(d) Estimate the total number of fragments in each zone. Use geometric probability to estimate the fraction of these fragments that strike the receptor.

(e) Combine the results from (c) and (d) to obtain the expected number of fragments that strike the receptor and have sufficient mass and velocity to detonate the receptor.

(f) Compute the probability that the receptor receives at least one supercritical hit. This is the probability P that explosive propagation will occur when the donor detonates at spacing S from the receptor.

1.6 Computation of the Required Spacing

The spacing S for a given probability P is obtained by solving the equations described in Section 1.5 for S when P is given. The solution is difficult to obtain directly. Iterative procedures have been developed for two important cases, while trial values and interpolation can be used in all cases. The procedures are described below.

a. Procedure for Large Spacings

This procedure is based on the assumption that S is large enough that all fragments that can strike the receptor are in the central 10 degree zone. The assumption is valid for all the projectiles involved when P is small and is valid for projectiles larger than 155 mm when $P=0.5$.

At the large spacings for which the assumption is valid the air drag on the fragments decreases the striking velocity significantly. Except for this fact the relevant equations can be solved analytically for S in terms of P . Hence, S can be computed by an iteration that starts with the estimate S_1 obtained by ignoring the drag. Then S_1 can be used to estimate the drag for the second estimate, which usually is accurate to the nearest inch. Another iteration yields a very accurate estimate of S .

b. Procedure for Small Spacings

This procedure is based on the assumption that the receptor is close enough to the donor to subtend the entire polar zone over which

supercritical fragments may issue, except for the base and nose fragments. Then the drag can be ignored and the spacing S can be computed by another iterative procedure. This procedure starts with an estimate S_1 that is obtained by using the average case thickness and outside diameter over the entire vulnerable section of the receptor for all polar zones. With the initial value S_1 estimates are made of the average case thickness and outside diameter for each zone, which yields a more accurate value S_2 . Iteration is continued until a stable value is obtained.

c. Procedure for Intermediate Spacings

If neither of the above assumptions is found to be valid, the spacing S can be found by using trial values and linear interpolation until a value of S is obtained that yields the probability P by the method described in Section 1.5 above.

2. Description of Experimental Tests

2.1 General

Two types of tests were performed; the first being the primary tests to establish projectile separation distances over which an explosion would propagate 50 percent of the time, and the second being tests to obtain information on the fragmentation characteristics of the three projectile designs employed in the explosive propagation experiments. All of the experimental work was conducted by the Space Research Corporation (SRC), North Troy, Vermont under the supervision of ADL personnel.

2.2 Explosive Propagation Tests

Three series of tests were conducted to obtain data on the spacing which would result in a 50 percent probability of propagation of an explosion between the donor and receptor projectiles. Each series of tests was devoted to a different projectile design. That is, three different projectiles were employed; 81 mm, 105 mm and 175 mm, all Comp B loaded.

The test arrangement was essentially the same for each series of tests. Three projectiles were used in each test; one, the donor, was placed between two receptors. They were placed side by side so that their longitudinal axes were parallel to the ground and their bases located all in the same plane. The projectiles were held at the same height above the ground by individual wooden supports. The spacing between the donor and each receptor was the same in each test but was varied from test to test according to a specific test design.

A number of possible test designs described in reference (9) were carefully reviewed and a modification of the Kesten design, which is a variation of the Robbins-Monro design, was selected. In the Kesten design the spacing between projectiles is changed in the appropriate direction by a fixed amount until a straddle is obtained. The amount by which the spacing is changed is reduced each time a straddle is obtained, thereby generating a sequence of spacings converging to the 50 percent spacing.

We modified the Kesten design in two ways. First, we adjusted the procedure to account for the fact that two receptors are used in each trial, rather than the one receptor assumed in the Kesten design. Second, we changed the assumption of a normal distribution for the initial estimate of S , on which the Kesten design is based, to the more reasonable assumption that this estimate is lognormally distributed. We believe that the modified design is significantly better than the Kesten design, particularly in tests for which the initial estimate may contain a large error.

An initial estimate of the 50 percent spacing is used on the first trial. The spacing on a subsequent trial depends on the outcomes on the preceding trials. If no detonation is obtained on a trial, the spacing on the next trial is reduced by a fraction of the previous spacing. If two detonations are obtained, the spacing on the next trial is increased by a fractional amount. If one detonation is obtained, no change is made in the spacing.

The fraction that is used to change the spacing initially depends on a measure of the errors that are likely to occur in the initial estimate of the 50 percent spacing. This fractional change is used until a straddle or a match is obtained. A match is defined to be the outcome on a single trial in which one receptor detonates and the other receptor does not. A straddle is defined to be the outcome on two consecutive trials in which opposite results are obtained, that is, two detonations followed by no detonations, or conversely. At the first occurrence of a match or straddle, the fractional change is reduced to half the initial fraction; at the second occurrence it is reduced to one-third; etc.

In the conduct of the tests the detonation of the receptors was established by observing their condition after the test was completed. There were three primary cases observed; one in which no reaction of the explosive was observed (no detonation); the second in which reaction of the explosive was noted, but either or both unreacted explosive or very large fragments were observed (low-order detonation); or the third in which the projectile was completely fragmented and all of the explosive was consumed (high-order detonation). All projectiles that did not detonate (either high or low order) were photographed on the side exposed to fragments from the donor.

2.3 Results of Propagation Tests

It was necessary to make initial estimates of the 50 percent spacings to start the test procedure described above. These estimates were made from a preliminary model early in the development, since the test program could not start without them. The preliminary model did not contain the factor F_A for the effective area of irregularly-shaped fragments, and the impact factor F_I was chosen before the analysis described in Section 1.4 had been made. For these and other reasons the initial estimates were much too large.

TABLE 1
SPACINGS FOR 50 PERCENT PROBABILITY OF DETONATION

	<u>Spacings in Inches</u>		
	<u>81 mm</u>	<u>105 mm</u>	<u>175 mm</u>
Initial Estimates	24	38	155
Experimental Values	10.5	10.5	80.5

The initial estimates and the experimental values are listed in Table 1. Despite the fact that the initial estimates were much too large, the test procedure described in Section 2.2 converged rapidly towards the final values. For all three projectiles the test spacings had converged to values within about 10 percent of the final values in 8 tests, and then made small oscillations during the remaining 8 tests.

2.4 Fragmentation Tests

Two fragmentation tests were conducted with each of the projectile designs used in the propagation tests. The purpose of these tests was to obtain data on the spatial distribution of the fragments of the donor projectile. The number and size of the fragments projected in angular zones around the projectiles were determined.

In each test the projectile was held with its long axis parallel to and about 4 feet above the ground. Plywood panels placed vertically in a semicircle around the projectile with a radius of from 10 to 35 feet (increasing with projectile size) were used to intercept the fragments projected by the projectile.

After each test the plywood panels were photographed and the photographs analyzed to provide data on the spatial distribution of the fragments.

3. Estimates of Required Spacings

3.1 Parameter Values

Average values of case thickness and outside diameter were obtained by measurement from the drawings listed in reference (10). Additional measurements were made for particular spacings. Also, the length of the vulnerable section of the receptor and the total weight of metal fragments from the donor were obtained.

Two parameters that have a large effect on the estimates of spacings are F_A and F_I . The area factor F_A is the fraction of the average presented area of the irregularly-shaped fragment that is effective in producing high order detonations. It was omitted in our initial computation of the 50 percent spacings, which is equivalent to using $F_A=1.0$. We have no data from which to estimate the value of F_A . Sensitivity tests with irregularly-shaped fragments are needed for this purpose.

The impact-angle factor F_I accounts for non-normal impacts. It can be interpreted as the fraction of the area presented by the charge of the receptor to the fragment stream that is vulnerable to attack. The value of F_I is approximately 0.4, if the effective component of striking velocity varies as $(\cos \theta)^2$, where θ is the impact angle; and is approximately 0.2, if the effective component varies as $(\cos \theta)^5$. For composition B values near 0.2 appear to be more likely for F_I than values near 0.4, from the meager data available on non-normal impacts.

3.2 Estimates of 50 Percent Spacings

Estimates of spacings required for $P=0.50$ and for $P=0.02$ for projectiles that are loaded with composition B explosive are listed in Table 2 in the order in which they were obtained. The original 50 percent spacings were made early in the development of the model, since they were needed to start the experimental tests. The value of $K_0=5500$ used

there applies to all fragments, whereas the value $K_0=4500$, used in later computations yields a more accurate estimate of the average mass for those fragments that strike the receptor. As stated above in Section 3.1, the area factor F_A was omitted from the original model and added later in refining it. The impact-angle factor $F_I=0.4$ was chosen before the analysis of the effects of the impact angle was made. At that time it was little more than a guess, based on the estimate in Figure 34 of reference (8) that the width of the effective strip for the 155 mm projectile is about 2 inches.

The experimental results listed in Table 2 were obtained by a procedure described in Section 2.2. Since the estimates from the experiments are much smaller than the original estimates from our model, the model was reexamined and some revisions were made. In addition to changing K_0 to 4500 and F_I to 0.2, for reasons given above, the area factor F_A was introduced. The value, $F_A=0.75$, used in the revised parameters is a fortuitous guess that happened to yield estimates of S that are very close to the experimental values when used with the revised values of K_0 and F_I .

The fitted parameter values, $F_A=0.58$ and $F_I=0.38$, were obtained by finding the values of F_A and F_I that would yield estimates of $S=10.5$ inches for both the 81 mm and 105 mm projectiles, as had been obtained in the experimental tests. The corresponding value of 84 inches for the 175 mm projectile is close to the experimental value of 80.5 inches, although not as close as that obtained with the revised parameter values.

3.3 Comparison of 50 Percent Spacings

The experimental values listed in Table 2 are those obtained for the 50 percent spacing with composition B loaded projectiles by an efficient test design described in Section 2.2, using approximately 32 receptors for each of the three projectiles listed. The corresponding spacings that are obtained for composition B by computation from our model when the revised parameter values are used are almost equal to the

experimentally-determined values. Thus, the experimentally determined spacings are 10.5, 10.5, and 80.5 inches for the 81 mm, 105 mm, and 175 mm projectiles respectively, while the computed spacings are 9.9, 11.1, and 80 inches respectively.

We have also examined experimental data reported in reference (8) for the 155 mm (M107) projectile. In these tests the projectiles were mounted either vertically or horizontally on test stands. The results are reported in terms of the case-to-case separation distance, which is S-D in our notation. Hence, we add D, which is approximately 6 inches, to obtain the corresponding center-to-center spacing. In the vertical orientation 4 of 4 receptors detonated (high-order) at S=30 inches, 3 of 4 at 54 inches, 2 of 4 at 78 inches, 0 of 12 at 90 inches, and 0 of 4 at 102 inches. In the horizontal orientation 1 of 2 detonated at 54 inches, 2 of 8 at 66 inches, and 0 of 2 at 78 inches.

Unfortunately there were insufficient experimental data to allow a reasonable statistical estimate to be made for the 50 percent spacing. Our model, however, using the revised parameter values, predicts a 50 percent spacing of approximately 42 inches. The experimental data for the 90 inch spacing does allow a limited statistical comparison to be made with model predictions. For the 0 out of 12 detonations a confidence interval on the true probability, p , for 95 percent confidence probability is, from the theory of Bernoulli trials used to obtain Figure 31 of reference (8), $0 \leq p \leq 0.27$. The probability of detonation at S=90 inches computed from the model described in Section 2 is $p=0.14$, which is approximately at the midpoint of the confidence interval. The estimated p falls within the confidence interval for all values of the confidence probability greater than 0.67.

A total of 12 detonations were obtained with the 38 receptors positioned at different spacings and orientations. Taking the spacings into account our model predicts 10 detonations for 38 receptors, which is in good agreement with the observed number.

3.4 Predicted Spacings for Small Probabilities

As indicated above, the spacings required for small probabilities of detonation can be predicted from the model described in Section 1. The accuracy of these predictions depends upon the validity of the model, particularly on the variation of the probability of detonation with the spacing.

The spacings required for 2 percent probability of detonation were computed by using the revised parameter values and by using the fitted parameter values. These estimates are listed in Table 2. For a given projectile the required spacing for 2 percent probability is much larger than that for 50 percent probability.

3.5 Some Limitations on the Model

More experimental data are needed to test the model before it can be used with confidence to predict required spacings for small probabilities of detonations. We have examined potential areas of uncertainty in our model in terms of its ability to accurately predict spacings for small probabilities.

Some possible sources of error are: (a) uncertainties concerning the parameter values, such as F_A and F_I ; (b) validity of the empirical equations used in the derivation, such as the fragment distribution and the drag law; and (c) possible discrepancies between the conditions that existed in the propagation tests and the corresponding assumptions made in developing the model. These likely sources are discussed briefly below.

The model predicts that the expected number of supercritical hits decreases as the inverse square of the spacing from geometric considerations, and also decreases in a complex way from the decrease in striking velocity, as the spacing increases. We assumed the usual square drag law in computing the striking velocity. The corresponding effect on the expected number of supercritical hits depends on the variation of the

required mass with striking velocity from the sensitivity equation, and the fragment mass distribution. The empirical equations involved here are open to question. The transformation of the sensitivity equation to make it applicable to irregularly-shaped fragments needs to be checked. Also, the empirical distribution function for fragment mass is questionable, especially the tail of the distribution for large masses in the central 10 degree zone. We used the usual exponential distribution function for the probability that a fragment has mass exceeding m . This distribution appears to be good for small values of m , but not for large values of m . Since one dimension of a fragment is limited to the case thickness and the total amount of metal in the central 10 degree zone is limited, a distribution with an upper limit is more appropriate.

Another possible source of error is that some of the assumptions made in developing the model are not in agreement with the conditions that existed in the experiment. For example, the fragment distribution of the 155 mm projectile may have been distorted by the supports.

The ultimate objective of the experimental tests and model construction is to obtain a procedure for estimating separation distances for a given probability of explosive propagation under the conditions that exist in Load-Assembly-Pack (LAP) operations. If the conveyors that support the projectiles in LAP operations distort the fragment distributions and velocities, as appears likely, the distributions and velocities in our models should be modified accordingly when information on these effects becomes available.

TABLE 2 - ESTIMATES OF REQUIRED SPACINGS FOR PROJECTILES WITH COMP. B LOADING

<u>NO.</u>	<u>CONDITIONS</u>	<u>P</u>	<u>S-inches</u>					<u>8 in.</u>
			<u>81 mm</u>	<u>105 mm</u>	<u>155 mm</u>	<u>175 mm</u>		
1	Original parameters	0.5	24	38	90	155	160	
2	Experimental values	0.5	10.5	10.5	--	80.5	--	
3	Revised parameters	0.5	9.9	11.1	41.5	80	73	
4	Fitted parameters	0.5	10.5	10.5	--	84	--	
5	Revised parameters	0.02	75	105	208	349	333	
6	Fitted parameters	0.02	79	104	212	360	343	

Original parameters: $K_0 = 5500, F_A = 1.0, F_I = 0.4$

Revised parameters: $K_0 = 4500, F_A = 0.75, F_I = 0.2$

Fitted parameters: $K_0 = 4500, F_A = 0.58, F_I = 0.38$

REFERENCES

1. Slade, D.C. and Dewey, J., "High Order Initiation of Two Military Explosives by Projectile Impact", BRL Report No. 1021, July 1957, UNCLASSIFIED.
2. Rindner, R.M., "Response of Explosives to Fragment Impact", Annals of New York Academy of Sciences, Vol. 152 Art. 1, Oct. 28, 1968.
3. McLean, D.G. and Allan, D.S., "An Experimental Program to Determine the Sensitivity of Explosive Materials to Impact by Regular Fragments", Final Report to Picatinny Arsenal by Arthur D. Little, Inc., Contract DA-19-020-ORD-5617, Dec. 26, 1965.
4. Allan, D.S. and Meyers, S., "Development of a Weapons' Sensitivity Handbook" (J), Final Report (Phase I and II) to Department Defense Explosives Safety Board by Arthur D. Little, Inc. Contract DAAH-CO4-70-C-0042, Feb. 28, 1971.
5. Gurney, R.W., "The Initial Velocities of Fragments from Bombs, Shells, and Grenades", BRL Report No. 405, September 1943, UNCLASSIFIED.
6. Heppner, L.D., "Fragmentation Test Design, Collection, Reduction and Analysis of Data", APG Misc. Report No. 306, September 1959, UNCLASSIFIED.
7. Giere, A.C., "Calculating Fragment Penetration and Velocity Data for Use in Vulnerability Studies", Naval Ordnance Report No. 6621, Oct. 1, 1959, UNCLASSIFIED.
8. Anderson, C. and Rindner, R., "Separation Distances Tests of 155 mm (M107) Projectiles", Picatinny MTD Technical Report No. 4425, Jan. 1973, UNCLASSIFIED.
9. Rocketdyne Report R-6152, "The Design and Analysis of Sensitivity Experiments", NASA CR-62026, May 1965, UNCLASSIFIED.
10. Specification Drawings of Part No. 10543028 (81 mm M374 Projectile), Part No. 1053878 (105 mm M1 projectile), Part No. 75-4-99 (155 mm M107 projectile), Part No. 10520195 (175 mm M437), and Part No. 10534911 (8 inch M106), UNCLASSIFIED.

SAFE SEPARATION AND SECONDARY FRAGMENT IMPACT STUDIES

BY

Richard M. Rindner

Robert S. Kukulka

Manufacturing Technology Directorate
Picatinny Arsenal
Dover, N.J.

SUMMARY

A continuing experimental program on explosives sensitivity is underway as part of the Picatinny Arsenal Safety Engineering Project. This program provides support to the Modernization of the Army Munition Manufacturing Facilities. Its purpose is:

a. To determine the safe separation distance for ammunition end-items and in-process explosive materials at various stages of their manufacture.

b. To determine the sensitivity of explosives and explosive end-items to impact by secondary fragments (such as concrete pieces) in order to establish the mass-velocity relationship below which no detonation propagation will occur under any realistic condition.

The safe separation distances with or without shielding on a conveyor which were established for several end-items were: 155mm Comp B loaded projectiles, 2.75" Rockets and M18A1 Mines (presented at the 14th Safety Seminar) as well as 81mm projectiles and HE cartridges. Also, safe separation distances were established for 55 lbs TNT boxes, 60 lbs Comp B boxes and buckets, and 35 and 50 lbs Comp C₁ buckets. Other tests, which will have a major bearing on the plant modernization program (and which are discussed in this paper) are presently underway.

Explosive sensitivity tests using secondary (concrete) fragments were performed in which 155mm projectiles, RDX slurry and Black Powder were impacted with concrete fragments of various sizes at different velocities. No reaction occurred with 155mm projectiles and RDX slurry and thus it appears that they are insensitive to impact by concrete fragments. A series of go/no-go situations resulted from the experiments with Black Powder and, therefore, a sensitivity profile (weight/velocity combination) was established for Black Powder. At present work is in progress to establish impact sensitivity of molten Comp B in shells and in the melt-kettle.

INTRODUCTION

The modernization of its munition manufacturing facilities and load, assemble and pack operations is of prime importance to the Army. The

installation of new, complex systems including processes, handling equipment, buildings and barricading requires an ultimate effort in safety engineering technology.

Picatinny Arsenal, with Army Materiel Command guidance and under the direction of the U.S. Armaments Command, is providing this technology. Under its broad project titled "Safety Engineering in Support of Ammunition Plants", Picatinny is rendering safer, more economic and realistic design data in support of the Modernization Program. This information is provided to the Government owned, contractor operated plants, the Corps of Engineers and others actively engaged in design and construction of the new munitions facilities.

A segment of the overall "Safety Engineering Project" includes the testing and analysis dealing with the sensitivity of explosives and explosive-end-items. The information presented in this paper deals with this subject.

The objectives of the explosives sensitivity task are two-fold,
Figure 1:

1) Determination of the safe separation distance (non-propagating) of ammunition end-items and of explosive materials at various stages of their manufacture (in-process conditions).

2) Establish the mass-velocity relationship below which no detonation propagation will occur to explosives and explosive end-items when impacted by secondary fragments (concrete pieces).

It should be stressed at this point that the work already completed to-date has resulted in either major savings in space requirements or in establishing the minimum distance for separation that is safe between ammunition items where this information was not covered by present safety regulations. As the work has progressed, it has become obvious that a great deal remains to be done as a result of previous limited testing carried out in this area and the Army has reinforced its efforts in this regard. The ultimate goal of the results achieved by these test programs will be supplementation and/or modification of the present Safety Manual ANCR 385-100.

SAFE SEPARATION DISTANCE TESTS

GENERAL:

The purpose of these tests was to determine spacing and/or shielding requirements to prevent propagation between ammunition items and explosives being transported on a conveyor.

Several ammunition end-items individually and on pallets as well as in-process explosive materials were tested at the Tooele Army Depot, Sierra Army Depot and Dugway Proving Grounds and are presented in Table 1.

The test series consisted basically of three parts (although not all of them were applied to each item tested).

Part 1 dealt with establishment of safe separation distances (without shields) on a conveyor.

Part 2 dealt with the establishment of safe separation distances using some kind of a shield between the donor and acceptors.

Part 3 dealt with performing confirmatory tests at the acceptable confidence level and reliability based on results produced in Parts 1 and 2.

Several test results which resulted in establishment of safe separation distances for ammunition end-items and explosive in-process materials such as individual 155mm Comp B projectiles, 2.75" Rockets, M18A1 mines and 55# TNT boxes were discussed during the 14th Explosive Safety Seminar and are shown in Table 1.

TEST SET UP

81mm Projectile & HE Cartridge Tests

Tests with 81mm projectiles and 81mm HE Cartridges were performed to confirm previously established distances (8.8^{ft}) between the rounds with interrupters simulating the facing operation which is considered to be the most hazardous operation during the projectile assembly.

In this test simulated drill fixtures were inserted in the acceptor's fuze well cavity. The transfer pallets were mounted on standard roller-type conveyor approximately 36" from the ground. Figure 2 illustrates the test arrangement, the center projectile being the donor, with the acceptor projectiles each containing drill fixtures for these tests.

60 lb Comp B Boxes

The 60 lb Comp B boxes test set-up was similar to the previously conducted tests with 55 lb TNT boxes. Three boxes were placed in a straight line on salvaged sections of roller conveyors (see Figure 3). The center box was the donor while the end boxes simulated the acceptors. The test items were supported by wooden stools at the height of 30 inches which simulates the approximate height of a conveyor used in production lines. The entire assembly was then enclosed with 3-ten foot long 24-gauge aluminum hoods. These covers are analogous to those existing in an actual production line and will be used in future conveying systems.

60 lb Comp B Buckets

The 60 lb Comp B bucket tests simulated buckets being transported through a tunnel via an overhead pendent-type conveyor.

The buckets were suspended from a 3 X 2 3/8" steel "I" beam and oriented longitudinally within the tunnel at a distance of 5 ft. from the ground as shown in Figure 4. The tunnels were fabricated from welded 2 X 2 X 1/2" structural steel angle and covered with 24 gauge corrugated steel sheeting in order to closely simulate the actual plant conditions. The buckets used in the test were 1/8" molded Phenolformaldehyde plastic and were 16" in dia X 14" deep.

35 lb & 50 lb Comp C₄ Buckets

This test series was conducted to simulate a material handling system for extruder operations.

The test set-up for this test series is shown in Figure 5. The tunnels were fabricated from 2 X 4 lumber and covered with 26 gauge corrugated steel sheeting. They were 8 ft wide by 10 ft high. The total length of each tunnel was approximately 56 ft. The aluminum buckets (containing Comp C₄) were suspended longitudinally from the roof structure at a distance of 7 ft from the ground. The same size buckets (14" dia X 20" deep) were used for both 35 lb and 50 lb Comp C₄ separation tests.

105 mm M1 Comp B. Projectiles on Conveyor Carriages

The purpose of this test program, which has been recently initiated and is presently underway, is to establish safe separation distances between carriages containing 16-105mm Comp B loaded projectiles on a conveyor. This test series is being performed in support of several GOCO plant modernization programs.

Sixteen projectiles spaced approximately 1" apart on a carriage will be transported by conveyor within and out of the melt-pour area. Preliminary tests have been performed with and without pouring funnel and with and without blast interrupter bars. The fixtures and carriages used in these tests (aluminum alloy 6061-T6) are comparable to those used in actual operating conditions (see Figure 6).

Two carriages - one serving as a donor, the other as an acceptor - each containing 16 vertically oriented projectiles were placed on 18" X 5 ft long sections of salvaged steel roller conveyor and spaced apart at various distances from each other. These assemblies were supported by wooden horses at 33" above the ground which simulates the approximate height of plant conveyor systems.

TEST RESULTS

Except for the 105mm carriage test, all tests discussed above were completed. After performing exploratory type tests in order to establish a minimum safe distance and/or shielding between the donor and acceptors, confirmatory tests were conducted at which no detonation propagation occurred.

81mm Projectiles & HE Cartridges

In the case of the 81mm projectile tests, although cracking and splitting did occur to the acceptor projectile, no penetration of the acceptor projectiles was caused by primary fragments emitted from the donor. Since the prime objective of the test was to determine the effectiveness of the shield in preventing detonation propagation, the degree of indentation and cracking was not considered relevant.

105mm Projectiles in Pallets

The preliminary tests with 16-105 mm projectiles on a transfer carriage (pallets) indicated, however, that the present regulations concerning safe spacing of these pallets are grossly inadequate.

These tests, which will be continued shortly, indicated that a total propagation between pallets occurred at a clear separation distance of 170 in. As of now, no safe separation distance was established between the pallets. Present regulations, however, (as spelled out in Safety Manual AMCR 385-100) call for 109" separation between pallets containing 32 projectiles.

A summary of the results of all safe separation tests with explosive end items discussed in this paper and planned shortly is presented in Table 2.

Comp B Boxes

Tests performed with Comp B boxes indicated that no propagation occurred at a clear separation distance of 9 ft.

In view of the above, 25 confirmatory tests involving 50 acceptors were performed at 12 ft clear separation between the donor and the acceptors. No detonation propagation took place in any of these tests. However, burning of both acceptors in some tests was observed.

Comp B Buckets

Ten tests (20 acceptors) performed at 12 ft separation distance with Comp B buckets resulted in no propagation into the acceptor buckets. Although the steel angle frame and the tunnel sections were severely damaged, no fragments were emitted by the steel framing or "I" beam (see Figure 7). All acceptor buckets were torn apart and Comp B was scattered to within 100 ft from its original location. No burning of the plastic bucket debris was evident. Only one small Comp B acceptor fire was observed and this was attributed to a burning piece of wood from a tunnel base support.

Comp C₄ Buckets

A total of 20 tests were performed (10 each) with 50 lb and 35 lb buckets containing Comp C₄. The safe separation distance of 35 lb & 50 lb buckets was established at 20 ft. and 25 ft respectively. In all tests conducted, no propagation into the acceptor bucket occurred (see Figure 8). The steel corrugated sheeting was torn apart or deformed and strewn about the test site. In all cases the acceptor buckets sustained only minor deformation with no penetration. No fires were produced in the acceptors.

Table 3 summarizes the test set-up and results of all tests conducted to date and planned for the near future with the explosive in-process materials.

SECONDARY FRAGMENT IMPACT TESTS

A series of experiments were conducted at the IIT Research Institute Test Facility to determine explosive sensitivity to impact by concrete fragments. Figure 9 simulates a situation where wall fragments resulting from donor detonation impact the acceptors.

The concrete used in this program was launched from a 12 in. air gun facility (Figure 10). The gun is capable of launching a wide range of missile weights at varying velocities.

These tests utilized two types of concrete fragments:

- a. Solid concrete cylinder
- b. Containers filled with concrete rubble.

To prevent scoring of the air gun barrel, it was necessary to place the concrete fragments in some type of soft container. The container had to be strong enough to support the weight of the fragment, yet have minimal influence on the impact of the projectile with the target (See Figure 11).

155mm Projectile Experiments

Twenty experiments were performed on 155mm Comp B loaded projectiles subjected to impact by concrete fragments. Of these, 12 shots were made using solid concrete projectiles with weights ranging from 55 - 480 lbs. Eight experiments used concrete rubble filled containers weighing from 125 - 250 lbs. High speed and normal speed cameras recorded the results. The direction of fragment impact in all experiments was approximately normal to the 155mm projectile axis. The 155mm projectiles were placed on steel witness plates and then positioned such that the projectile's axis was normal to the expected line of flight of the concrete fragment (see Figure 12).

Post test inspection of the 155mm projectiles showed a varying degree of deformation to the projectile casing. In several tests, the lifting eyebolt ring was sheared from the projectile assembly. None of the tests resulted in any Comp B reaction. A summary of the test results is given in Table 4.

RDX Slurry Experiments

Fourteen experiments were conducted employing RDX Slurry as the target. The RDX was type B1 Class E. For these experiments the same type of fragments as described before in this paper were employed. The experimental configurations, along with the weight of the slurry and its mode of confinement are given in Figure 13. The direction of impact between the concrete projectile and the target was approximately 75 degrees.

Failure of the slurry to react to impact necessitated the number of different experiment configurations. As each configuration was tried, and failure to produce a reaction occurred, a new setup was instituted.

Sixteen additional experiments were performed by firing 30 caliber bullets from a rifle into RDX slurry. The purpose of these experiments was to observe if a reaction to the RDX slurry by bullet impact would occur. Both armor piercing and copper ball bullets were used. For both types of bullets, the target velocity was approximately 2,500 ft/sec. In each of these experiments, where a 5 gallon container was used as the target, the canister was either badly damaged or destroyed by the kinetic energy of the projectile. The water tanks employed as the environment for the slurry container were split apart at the seams. In every case, RDX slurry was scattered about the test area.

Table 5 summarizes the results of these experiments. The fragment velocities ranged from 200 - 1,270 ft/sec. The projectile weights ranged from 55 - 480 lbs. In none of these experiments, regardless of fragment size or velocity, did an explosion-type reaction occur.

No reaction of the slurry was produced in the series of slurry bullet experiments. However, the box containing RDX slurry had been blown away from the area of impact.

Black Powder Experiments

For this series of 20 experiments, in which Black Powder was subjected to fragment impact, a single configuration was maintained. (see Figure 14). A single 25 lb cylindrical metal shipping container of Black Powder was placed on a steel witness plate with the length of the container in line with the line-of-flight of the fragment. Impact direction was approximately 15 degrees off normal to the side of the container. The witness plate was placed on hard packed soil. The shipping container had a thickness of 0.013 in.

The same type concrete fragments were used as before and are described in Table 6. Only 1 out of 20 experiments used concrete rubble. The size of fragments ranged from 55 - 480 lbs; their velocities from 100 - 1055 ft/sec.

The results of this test series are presented in Table 6. The magnitude of the reaction varied from no reaction to slow burning to intense reactions with accompanying fireball. Since no instruments were used in this series, no measurements of the degree of reaction (explosion) were possible. Where the shot resulted in no reaction, a post test survey showed Black Powder to be scattered about the test area. In each test (except one) the target canister was destroyed. Based on the test data obtained, an attempt was made to plot a go/no go profile of confined Black Powder as a function of projectile velocity and its weight. Figure 15 is a graphical presentation of these data.

Because only camera coverage of these tests was used as the basis for determining reaction intensity level, it is anticipated that a limited number of tests will be conducted in the future using airblast measuring devices. This will provide a quantitative assessment of the reaction intensity level.

CURRENT AND FUTURE WORK ON FRAGMENT IMPACT

Currently, we are determining the impact sensitivity of molten Comp B and TNT in various in-process stations of the production of the 155mm shell. Specifically, sensitivity of the following configurations are being evaluated:

1. The melter-kettle, which will hold 40 lbs of either Comp B or TNT in a molten state.
2. The Comp B filled 155mm shell with the explosive at approximately 155° F (its temperature during the facing operation).
3. The Comp B 155mm shell - "just filled condition", i.e. with the loading funnel in place and the explosive at approximately 200° F.

Work has started in evaluating these configurations. Preliminary results indicate that the Comp B at elevated temperature is significantly more sensitive to impact by secondary fragments. The fragments (both rubble and solid concrete) ranged in weight from 40 - 500 lbs and impacted at the target at velocities from 360 to over 1000 ft/sec.

Figure 16 is a summary of the work either in progress or planned in the near future.

CONCLUSIONS

The safe separation tests conducted to date and currently in progress have demonstrated the following:

1. The present requirements and direction for safe separation of explosive end-items and in-process materials are inadequate.
2. Major savings in space requirements and safe separation distances on a conveyor can be achieved.
3. An urgent need exists for additional work in this field in order to accomplish effective facility design.

The outcome of the secondary fragment impact testing may result in less stringent design requirements for dividing wall construction in new facilities and thus, a cost savings. Experiments of this type could also make the redesign of existing walls in many instances unnecessary. Utilization of the air gun technique in simulating wall fragment impact of explosive munitions appears to be quite effective.

SENSITIVITY STUDIES

- SAFE SEPARATION DISTANCE
- END ITEMS
- IN-PROCESS MATERIALS
- SECONDARY CONCRETE FRAGMENT IMPACT

COMPLETED SAFE SEPARATION TESTS

ITEM	DISTANCE/SHIELDING
155MM, M107 PROJECTILE	18 INCHES WITH SHIELDING ROD— (½ IN. STEEL OR 1 IN. ALUMINUM)
2.75 IN. ROCKET WARHEAD	9 IN. CTR TO CTR, WITH 2 IN STEEL ROD
M18A1 MINE	10 INCHES
COMP C4 BLOCKS	10 INCHES
COMP C4 BUCKETS	35 LBS — 20 FEET 50 LBS — 25 FEET
50 LBS TNT BOXES	12 FEET
60 LBS COMP B BOXES	12 FEET
60 LBS COMP B BUCKETS	12 FEET
81MM HE M374A2E1 CARTRIDGE	8.8 IN. (WITH ¼ IN. THICK X 6 IN. HIGH LEXAN SHIELD)
81MM HE M374 PROJECTILE	8.8 IN. (WITH 2 IN. X 4 IN. X 14 IN. ALUM BAR

TABLE 1

TEST SET UP - 81 MM PROJECTILE

PROPAGATION TEST
81 M/M M374A2E1
FIXTUREM-913-200

TEST NO. 1-72

OCT. 1973

FIG 2

TEST SET UP-60 LB COMP B BOXES



**COMP B
BOXES
TEST NO. 2**

FIG 3

TEST SETUP-60 LB COMP B BUCKETS



FIG 4

TEST SET UP - COMP C4 BUCKETS

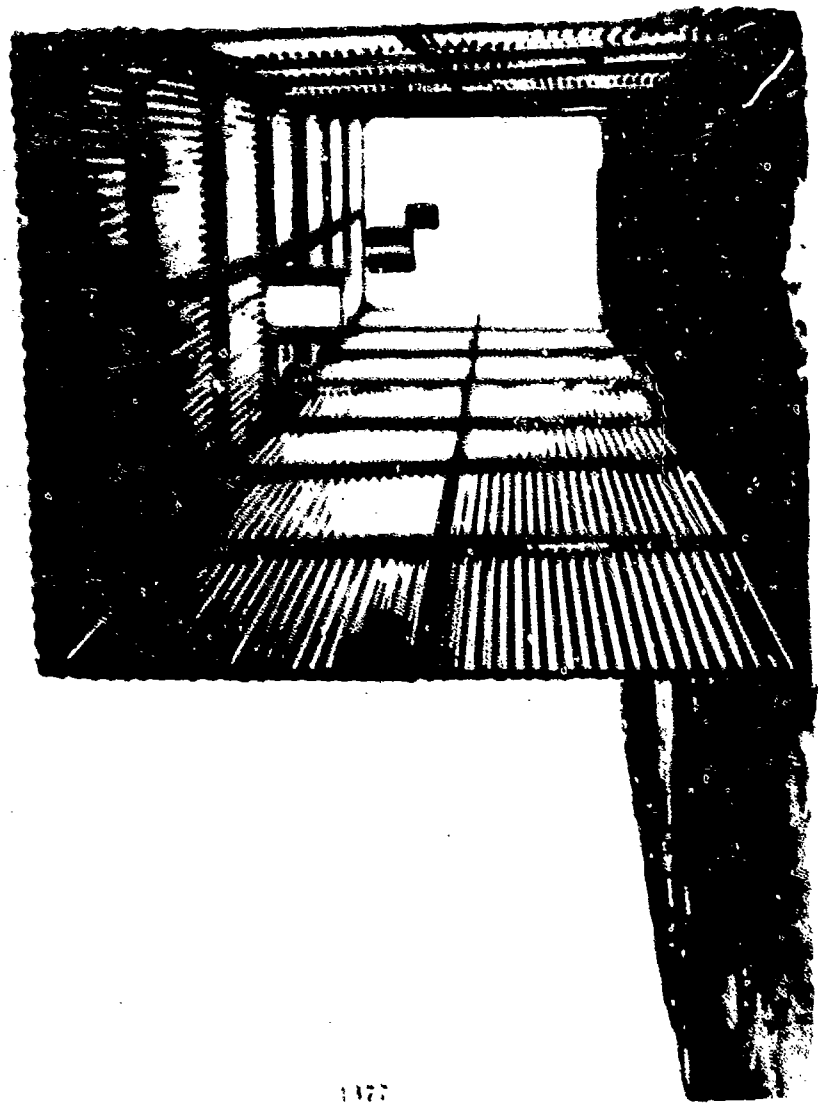


FIG 5

TEST SET UP - 105 MM PROJECTILES (16/CARRIAGE)



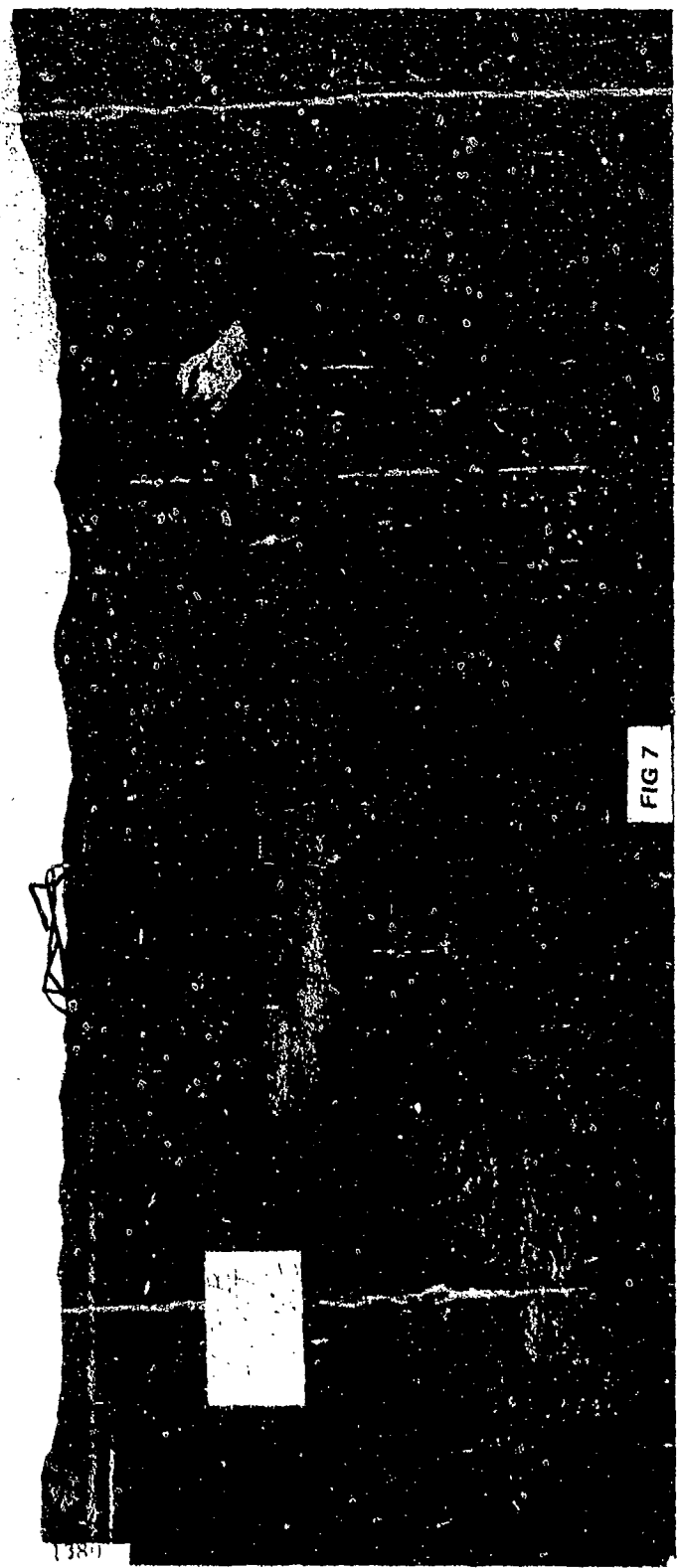
FIG 6

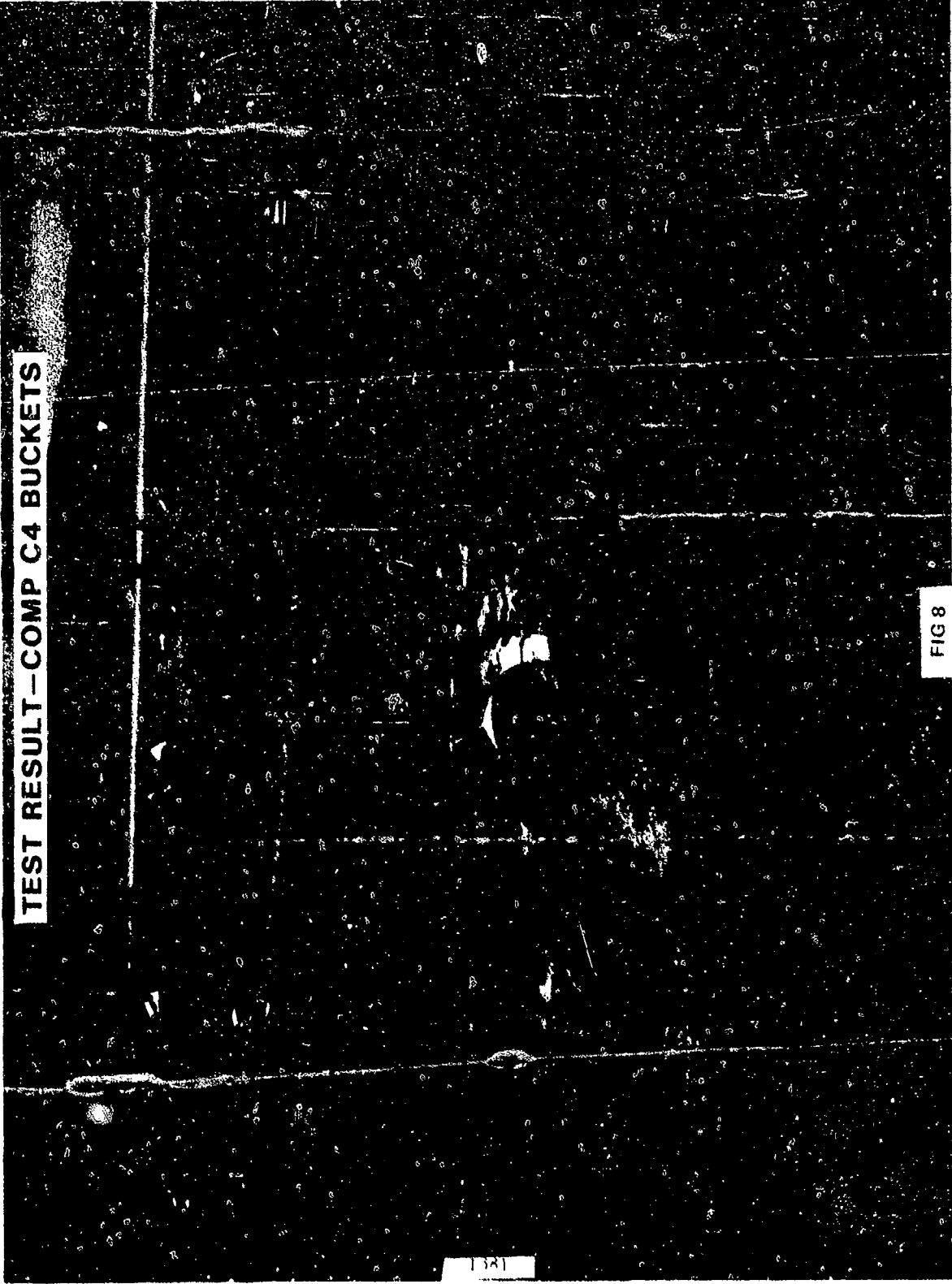
SAFE SEPARATION DISTANCE TESTS - END ITEMS

(STORAGE & IN PROCESS)

ITEM	TEST SETUP (ON CONVEYOR)	RESULTS/STATUS
81MM MORTAR a. HE M374 PROJECTILE b. HE M374A2E1 CARTRIDGE	2"x4"x14" ALUM PLT 1/4"x6" LEXAN SHIELD ON HOUSING	COMPLETED. 8.8" SAFE DISTANCE ESTABLISHED. REPORT BEING FINALIZED
105MM (M1) PROJECTILE	16 ITEMS/CARRIAGE W & W/O FUNNELS & W & W/O BLAST SHIELDS	IN PROGRESS. INITIAL RESULTS INDICATE EXCESSIVE SAFE DISTANCES
155MM PROJECTILE M107 & M549	SINGLE ITEMS W & W/O FUNNELS & W & W/O BLAST SHIELDS & 4/ CARRIAGE	PRELIM TESTS CONDUCTED. ADDITIONAL TESTS PLANNED
8" PROJECTILE (M106) TNT & COMP B	SINGLE ITEMS	PRELIM TESTS CONDUCTED. ADDITIONAL TESTS PLANNED
155MM PROJECTILE (M107)	24 ITEMS/PALLET	PLANNED

TEST RESULT-60 LB COMP B BUCKETS





TEST RESULT - COMP C4 BUCKETS

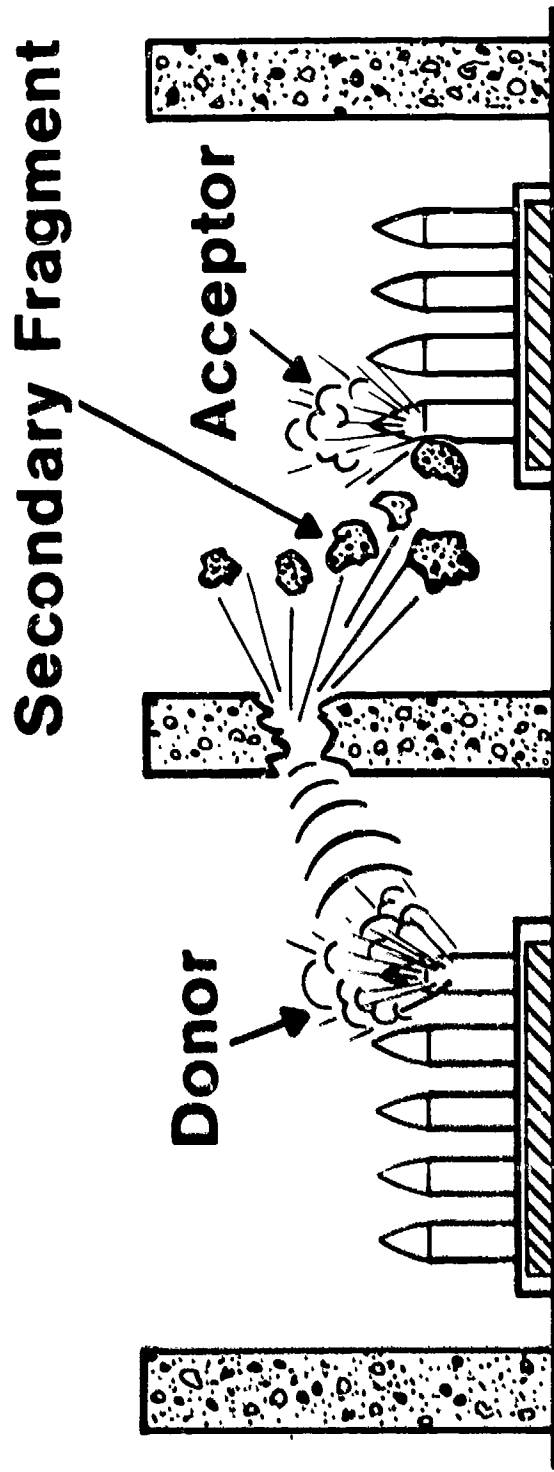
FIG 8

1321

SAFE SEPARATION DISTANCE TESTS - IN PROCESS EXPLOSIVES

MATERIAL	TEST SETUP	RESULTS/STATUS
COMP B (60 LB BOXES)	ON CONVEYOR IN TUNNEL	COMPLETED. 12' SAFE DISTANCE ESTABLISHED. TR4622 DISTRIBUTED
COMP B (60 LB BUCKETS)	PENDENT CONVEYOR IN TUNNEL	COMPLETED. 12' SAFE DISTANCE ESTABLISHED
COMP C4 a. 35 LB BUCKETS b. 50 LB BUCKETS	PENDENT CONVEYOR IN TUNNEL	COMPLETED { 20' SAFE DISTANCE 25' SAFE DISTANCE
COMP A7 (165 LB TOTE BIN)	ON CONVEYOR IN TUNNEL	IN PROGRESS
COMP B (FLAKE)	ON CONVEYOR	PLANNED

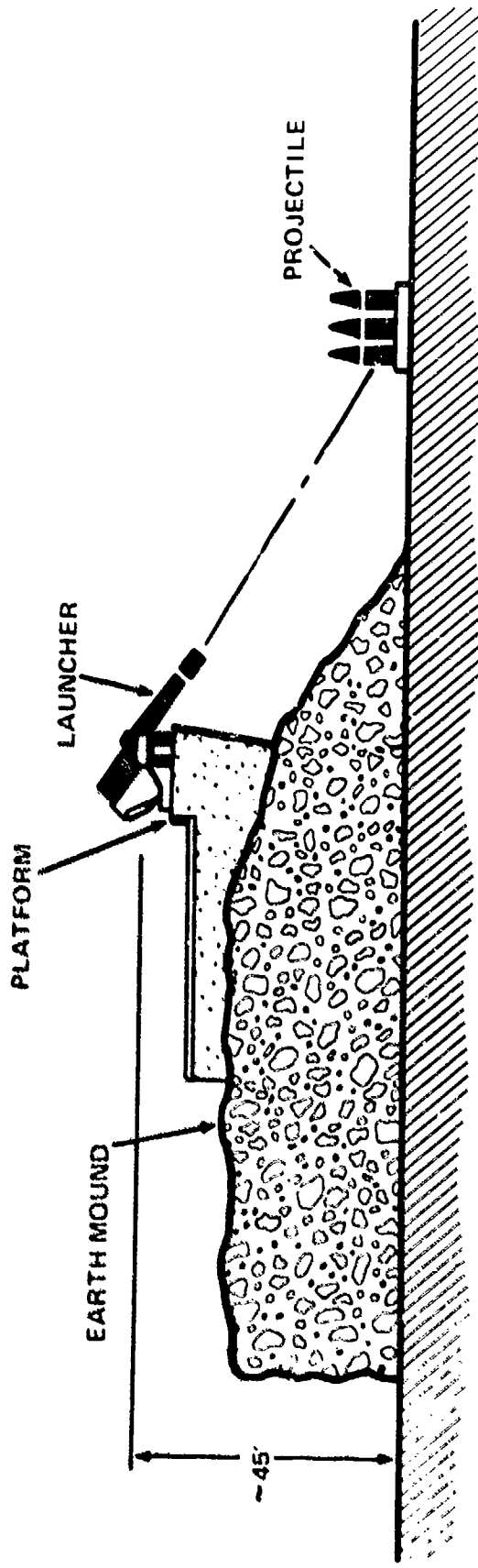
SECONDARY FRAGMENT EFFECT



1383

FIG 9

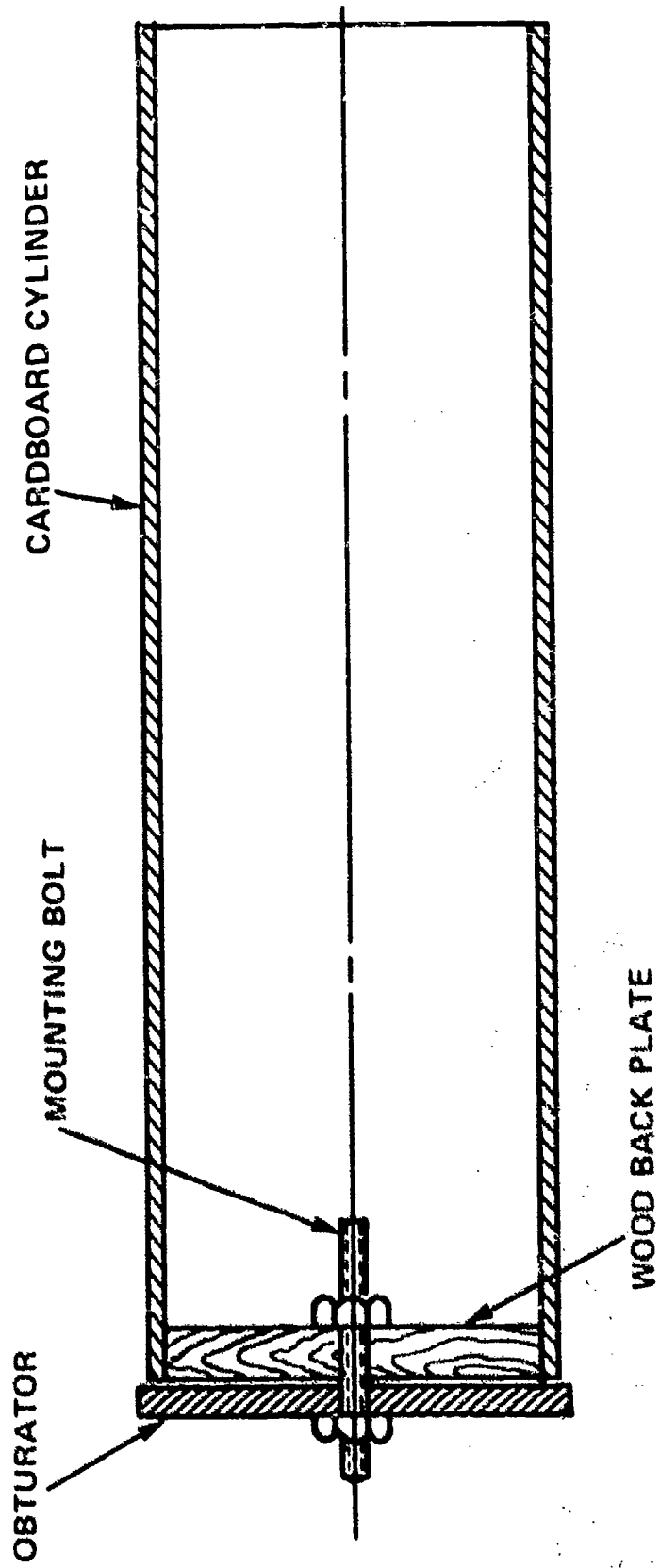
SECONDARY FRAGMENTS IMPACT TEST AGAINST 155MM PROJECTILE



1384

FIG 10

CONCRETE FRAGMENT CONTAINER



1385

FIG 11

INITIAL 155MM PROJECTILE CONFIGURATION

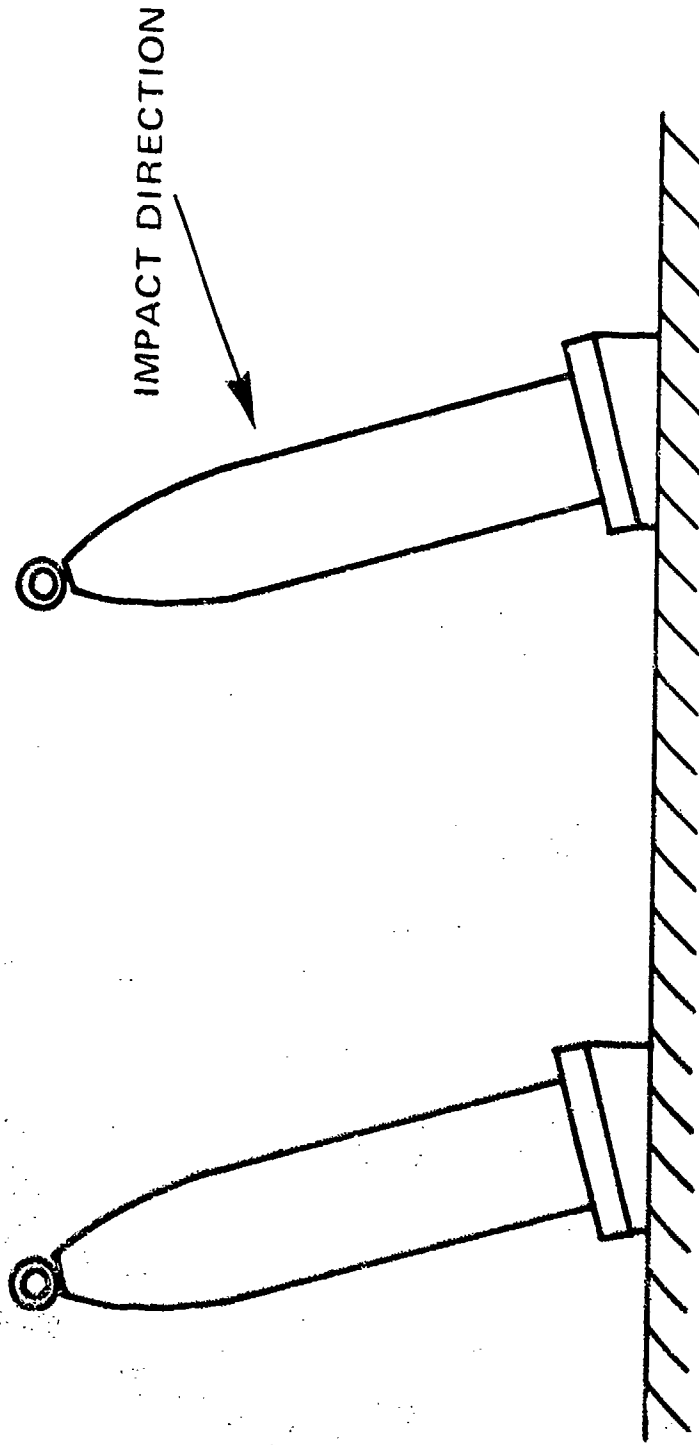


FIG 12

Table 4
155 MM PROJECTILE RESULTS

Test No.	Projectile Description				Results
	L/D	Type	Weight (lbs)	Velocity (fps)	
S-1	4	Solid	380	500	Glancing Impact - No Visible Damage
S-2	4	Solid	380	425	No Damage
S-3	2	Solid	180	560	No Damage
S-4	2	Solid	180	555	Small Deformation of Projectile Case
S-5	2	Solid	188	560	Small Deformation of Case
S-6	1/2	Solid	55	1170	Deformation of Casing
S-7	1/2	Solid	55	1170	Deformation of Casing
S-8	4	Solid	380	545	Slight Damage
S-9	4	Solid	380	550	Slight Damage
R-1	4	Rubble	250	600	Small Crack in Casing Near Lifting Eye
R-2*	4	Rubble	250	540	Slight Damage to Casing
R-3*	2	Rubble	125	675	Slight Damage to Casing
R-4*	2	Rubble	125	680	Sheared off the Lifting Ring
R-5*	3	Rubble	190	525	Slight Damage to Casing
R-6*	3	Rubble	190	540	Sheared off the Eyebolt
R-7*	3	Rubble	190	560	Slight Damage to Casing
R-8*	3	Rubble	190	570	Slight Damage to Casing
S-10*	5	Solid	480	350	Dented Casing
S-11*	5	Solid	480	360	Sheared off the Eyebolt
S-12*	5	Solid	480	350	Sheared off the Eyebolt

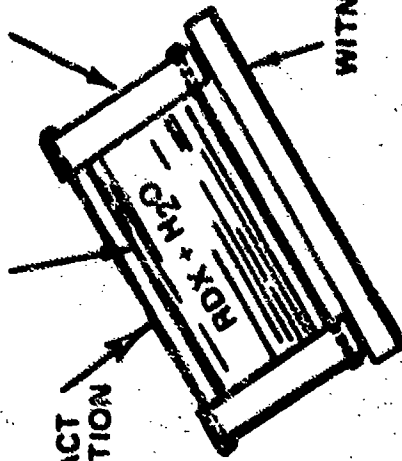
*Witness plate placed on concrete pad.

RDX SLURRY EXPERIMENT CONFIGURATIONS

7" DIAM x 1' ± 3/16"
STEEL TUBING

1/2" STEEL PLATE
BOTH ENDS

IMPACT
DIRECTION

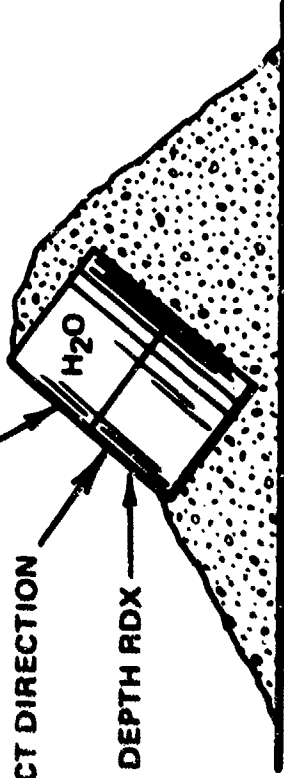


18 LB RDX

5 GAL COVERED CONTAINER

IMPACT DIRECTION

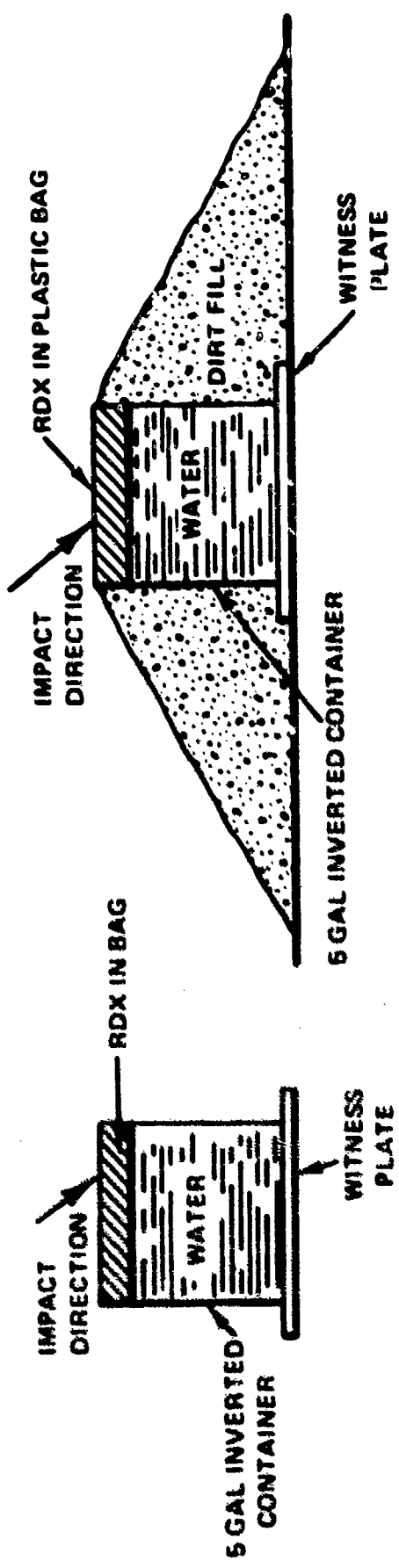
8" DEPTH RDX



35.5 LB RDX

FIG 13

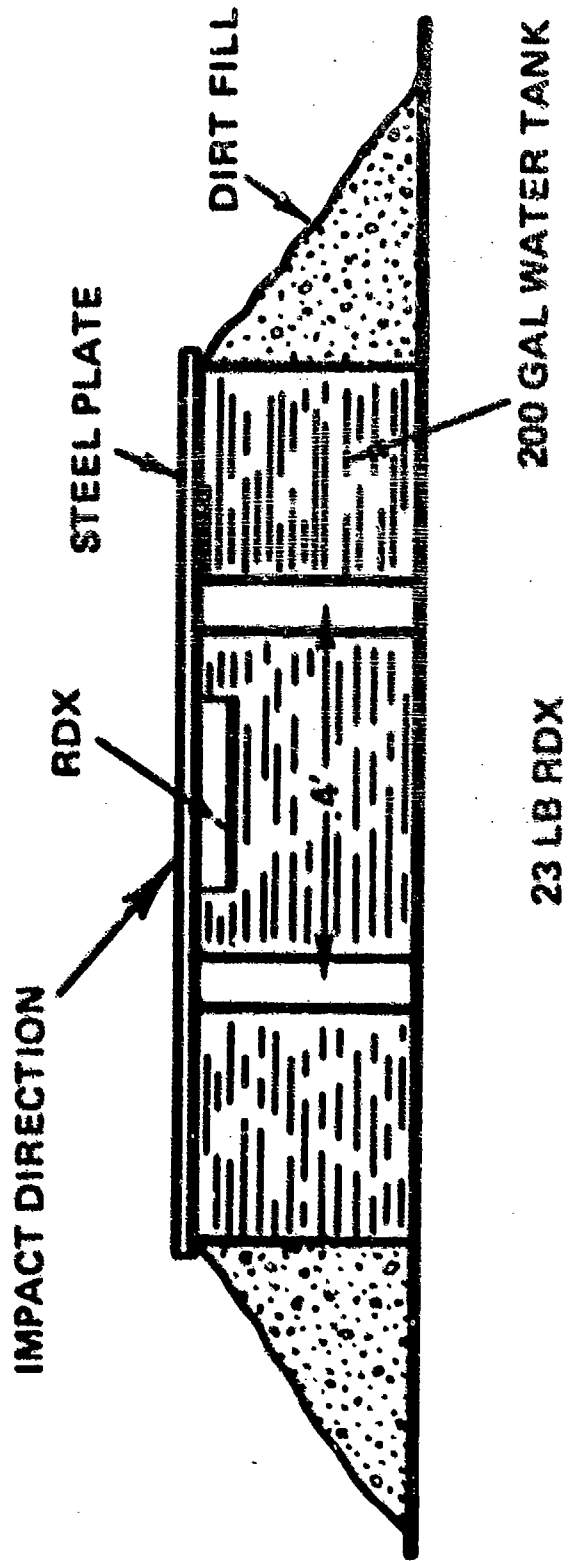
RDX SLURRY EXPERIMENT CONFIGURATIONS



15 LB RDX

FIG 13 (CONT'D)

RD_X SLURRY EXPERIMENT CONFIGURATION



1390

FIG 13 (CONT'D)

Table 5

RDX SLURRY RESULTS

Test No.	Projectile Description			Velocity (fps)	Results
	L/D.	Type	Weight (lb)		
X-1	5	Solid	480	370	No reaction. Tank split at riveted seams. RDX scattered over area.
X-2	5	Solid	480	370	No reaction. Canister split at seam. Bottom found in crater.
X-3	0.5	Solid	55	1220	No reaction. Top and bottom of can in good condition. RDX found in area posttest.
X-4	0.5	Solid	55	1270	No reaction. RDX found in area after test.
X-5	0.5	Solid	55	1270	No reaction. RDX in area posttest. Canister was split.
X-6	0.5	Solid	55		No reaction. RDX scattered about area.
X-7	5	Solid	480	470	No reaction. RDX strewn over area. Two feet of projectile left in one piece.
X-8	0.5	Solid	55	1200	Miss. Nicked lower corner. Pipe found in area after test.
X-9	0.5	Solid	55	1230	No reaction. Pipe split apart. Most of pipe recovered in test area. Projectile completely smashed.
X-10	5	Solid	480	470	No reaction. Pipe split apart. Recovered two pieces of pipe with RDX trapped between them. 18 inches of projectile recovered. RDX scattered about area.
X-11	5	Solid	480	200	No reaction. RDX scattered over area. 3 ft of projectile left in one piece.
X-12	0.5	Solid	55	500	No reaction. Recovered tube flattened out. RDX scattered over area and on tube.
X-13	5	Solid	480	200	No reaction. Hit top of tube. Most of tube found in one piece.
X-14		Rubble	135	850	No reaction. Some bolts and nuts found in hole. RDX scattered about area.

BLACK POWDER EXPERIMENT CONFIGURATION

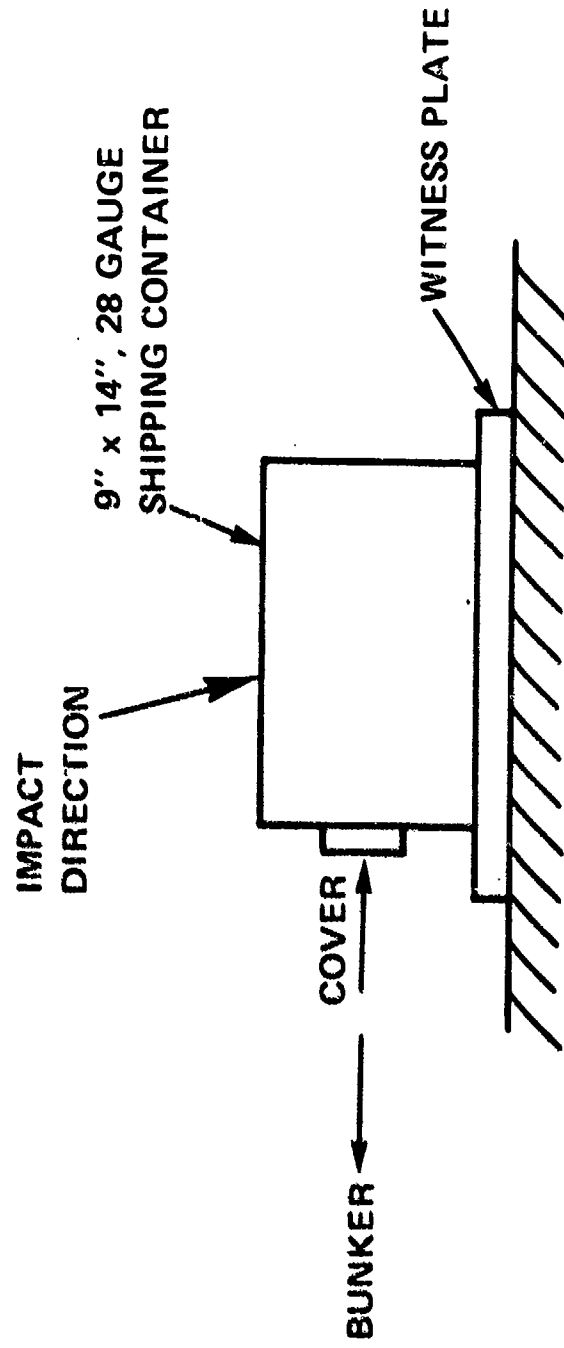


FIG 14

Table 6

BLACK POWDER RESULTS

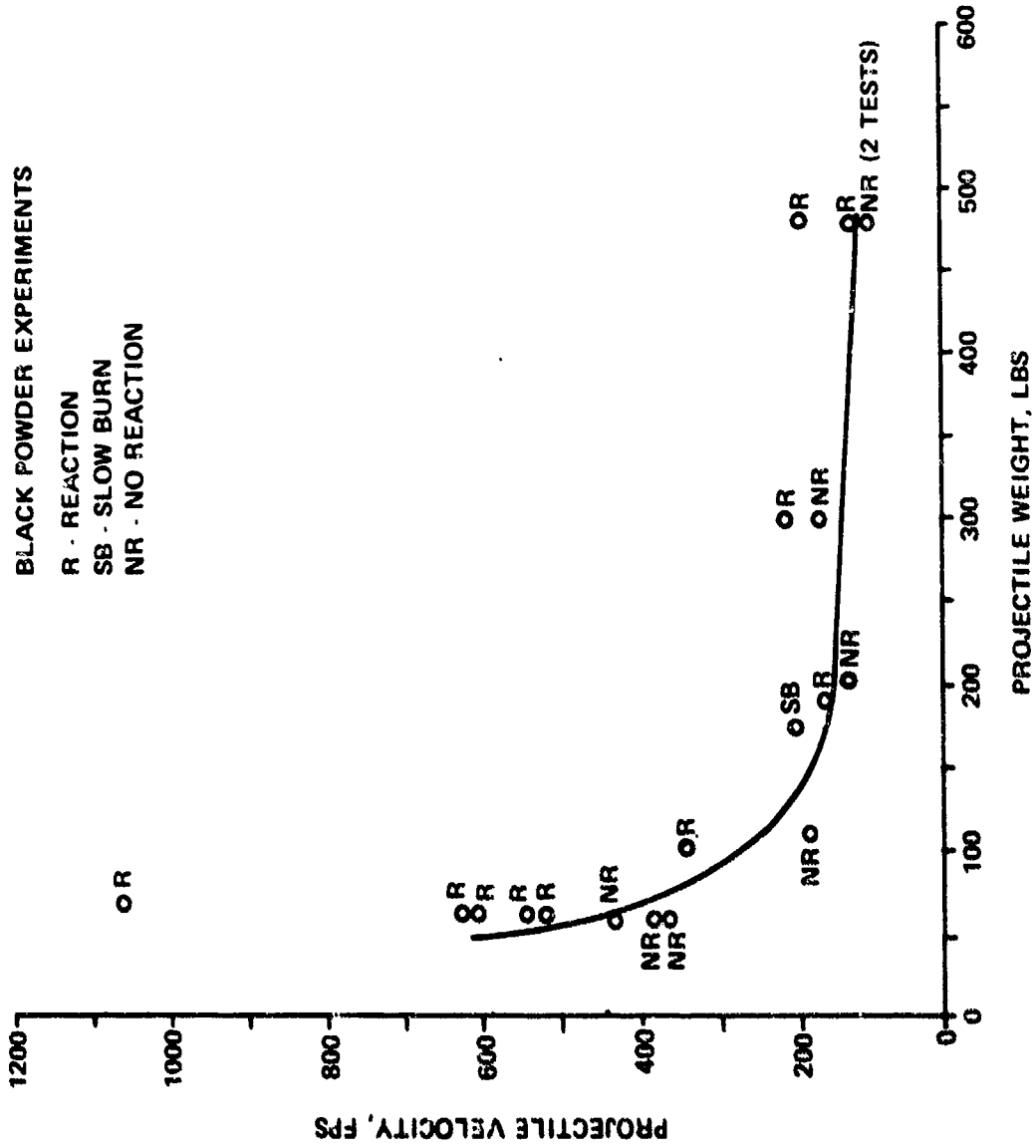
Test No.	Projectile Description			Results	
	L/D	Type	Weight (lbs)		Velocity (fps)
BP-1*	0.5	Solid	55	1055	Reaction. Small fragments of container found.
BP-2*	0.5	Solid	55	621	Reaction. Recovered most of container in three pieces.
BP-3	0.5	Solid	55	606	Reaction. Container destroyed. Pieces of container recovered
BP-4	0.5	Solid	55	377	No reaction. Recovered container in four pieces. Black Powder strewn over area. Projectile in one piece.
BP-5	0.5	Solid	55	538	Reaction. Most of container recovered in one piece. Projectile broken up.
BP-6	0.5	Solid	55	514	Reaction. Container split at seams. Projectile broken up.
BP-7	0.5	Solid	55	434	No reaction. Container recovered. Black Powder strewn about.
BP-8	5	Solid	480	185	Reaction. Small pieces of container recovered; Projectile broken into three pieces. Impact end slightly damaged. Projectile fragments found in area.
BP-9	5	Solid	480	114	Reaction. Fireball. Most of container found in hole after test. Projectile found almost intact.
BP-10	5	Solid	480	100	No reaction. Impact with container doubtful.
BP-11	5	Solid	480	100	No reaction. Container impaled on end of projectile. Black Powder strewn about area.

* Class 6, all other experiments are for Class 1 Black Powder.

Table 6 (Concluded)
BLACK POWDER RESULTS

Test No.	Projectile Description			Results	
	L/D	Type	Weight (lbs)		Velocity (fps)
BP-12	2	Solid	175	187	Slow burn. Container split apart at seams. Burn marks on projectile cover.
BP-13	0.5	Solid	55	365	No reaction. Container recovered in part with top torn away. No visible damage to concrete projectile.
BP-14	2	Solid	190	150	Reaction. Container recovered in five pieces. Projectile in one piece.
BP-15	2	Solid	205	125	No reaction. Projectile hit end of container. Black Powder crushed inside container. Projectile broken into many small fragments.
BP-16	3	Solid	300	154	No reaction. Container split apart. Black Powder strewn about area. Projectile not broken.
BP-17	3	Solid	300	201	Reaction. Parts of container found in area posttest. Concrete projectile broken up.
BP-18	1	Solid	100	336	Reaction. Fragments of container found in area. Projectile found basically in one piece.
BP-19	0.5	Rubble	40	266	Reaction. Container split apart and found in area posttest. Black Powder found in area. Rubble strewn about.
BP-20	1	Solid	110	173	No reaction. Black Powder strewn over area. Projectile in one piece.

GO/NO-GO REGIONS AS A FUNCTION OF PROJECTILE VELOCITY AND PROJECTILE WEIGHT



FUTURE WORK (SECONDARY FRAGMENTS)

- 155MM PROJECTILES WITH FUNNEL (SIMULATING COOLING BAY)
- SIMULATED MELT KETTLE-COMP B & TNT
- 105MM PROJECTILES
- 81MM PROJECTILE



END ITEM & IN-PROCESS

EXPLOSIVE LOAD RESPONSE TO NAVAL GUN SYSTEMS ENVIRONMENT

AND

ITS RELATIONSHIP TO IN-BORE SAFETY AND PERFORMANCE

M. C. Shamblen and J. S. O'Brasky
Naval Weapons Laboratory, Dahlgren, VA

ABSTRACT

The dynamic mechanical loading to which projectile fillers and fuze explosive trains are subjected during gun launch can be of sufficient magnitude to cause structural failure of the explosive load leading to load movement and occasionally thermal ignition. Low level (1 Kb) shock inputs can cause thermal ignition of the projectile filler. The low energy shock environment can cause the operation of fuze explosive train components resulting in duds if the fuze is properly assembled and detonation of the projectile if it is not.

This paper will treat the nature of such inputs as those described above, their measurement and laboratory simulation. The structural and sensitivity response of Composition A-3 and Explosive D projectile fillers to such inputs will also be described.

INTRODUCTION

The Navy has sponsored programs to improve the safety characteristics of its ammunition for many years. Each phase of the development, production, deployment and use cycle has received some attention. Between October 1970 and July 1974, five major gun ammunition malfunction investigations were conducted under the sponsorship of Naval Ordnance Systems Command. The Naval Weapons Laboratory participated in each investigation as the principal experimental facility. In five of these investigations involving three weapons systems, the dynamic responses of projectile components to ballistic environmental inputs were of sufficient magnitude to cause structural failure or thermal initiation of the explosive fillers and shock initiation of fuze explosive train components. In the course of these investigations, the dynamic responses of several projectiles to transportation and mount handling environments were characterized. While for the particular incidents in question, only the gun launch environments were implicated, it was found that certain transportation environmental shocks were similar, but of much less magnitude and duration than those which produced fuze explosive train action during gun launch. Since transportation safety environments were only incidentally sampled, most of the data presented in this paper are derived from the gun launch phase and are presented as a means of acquainting the explosive safety community with the techniques of measurement, data analysis, and laboratory simulations of environmental shock inputs and components responses. It is hoped that these methods may find application in the entire explosive safety area.

The reported work was performed during the period November 1970 through May 1973. It was a major portion of Naval Ordnance Systems Command sponsored programs designed to determine the causes of and remedial actions for in-service gun ammunition malfunctions. Actions of these investigative programs have been published by Culbertson, Shamblen, and O'Brasky (reference (1)), Shamblen and O'Brasky (reference (2)), Shamblen (reference (3)), and Culbertson (reference (4)).

SYNOPSIS OF MALFUNCTION INVESTIGATIONS

During 1969 and 1970, a series of in-bore ammunition premature incidents were experienced in 5"/38 naval gun firings. Examination of the accumulated in-bore premature history indicated a strong correlation between the observed events and the very early time gun ballistic environment produced by a particular propelling charge assembly denoted as Type A.

During the same 1969-70 time frame, a rash of close-aboard premature (CAP's) functionings were noted in 5"/38 ammunition. Again the correlation between the frequency of these events and the very early time ballistic environment was noted.

In early 1971, a series of close-aboard premature explosions was experienced during 8" naval gun firings. Examination of the 8" firing history revealed that CAP's had occurred only when firing the reduced propelling charge.

In late 1972, a series of in-bore premature explosions took place in the 5"/54 gun system. These explosions were shown to be the result

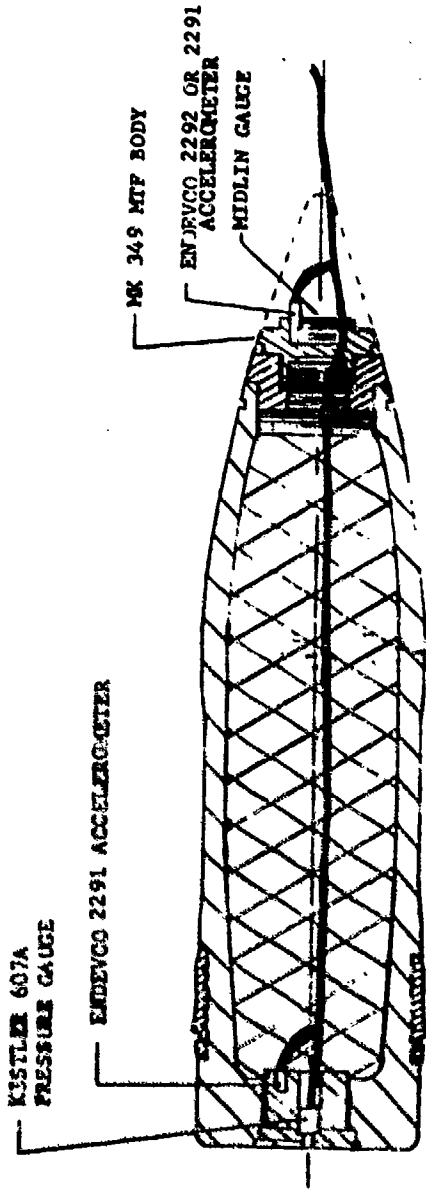
of the interaction between a normal and relatively gentle ballistic environment and a misassembled auxiliary detonating fuze.

In 1972, an in-bore projectile premature destroyed a three-gun 8" turret aboard the USS NEWPORT NEWS. Investigation of this incident revealed that the early time ballistic environment of the propelling charge had interacted with an overly-sensitive detonator in a misassembled auxiliary detonating fuze to produce an in-bore detonation after a very short projectile travel distance (less than 0.1 inch).

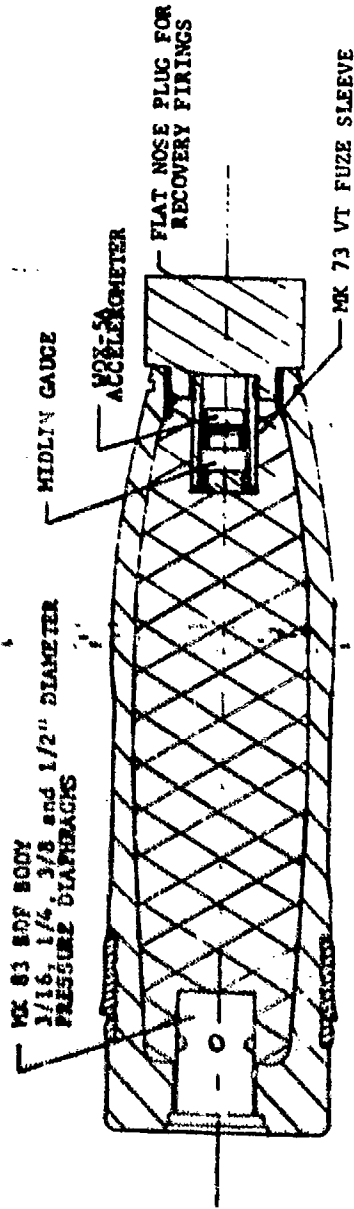
PROCEDURES AND EQUIPMENT

Two principal experimental methods were used to measure the gun ballistic environment and its interaction with ammunition assembly components: first quarter wear life 5"/38 and 8"/55 gun barrels were instrumented as shown by Figure 1; and special test projectile assemblies were instrumented with either peak reading mechanical transducers or continuous recording pressure and acceleration transducers as shown by Figures 2 and 3. The location of these transducers was selected to provide information on the pressure-time history at the base and mouth of the propelling charge and the resulting pressure and shock loading on the projectile structure and components. Instrumentation characteristics were as follows:

- a. The continuous recording piezoelectric pressure transducers were exclusively the KISTLER Model 607A, having a 75 ksi range and a 240 kHz resonant frequency. The continuous recording piezoelectric accelerometers were either ENDEVCO Models 2291 or 2292 having respective



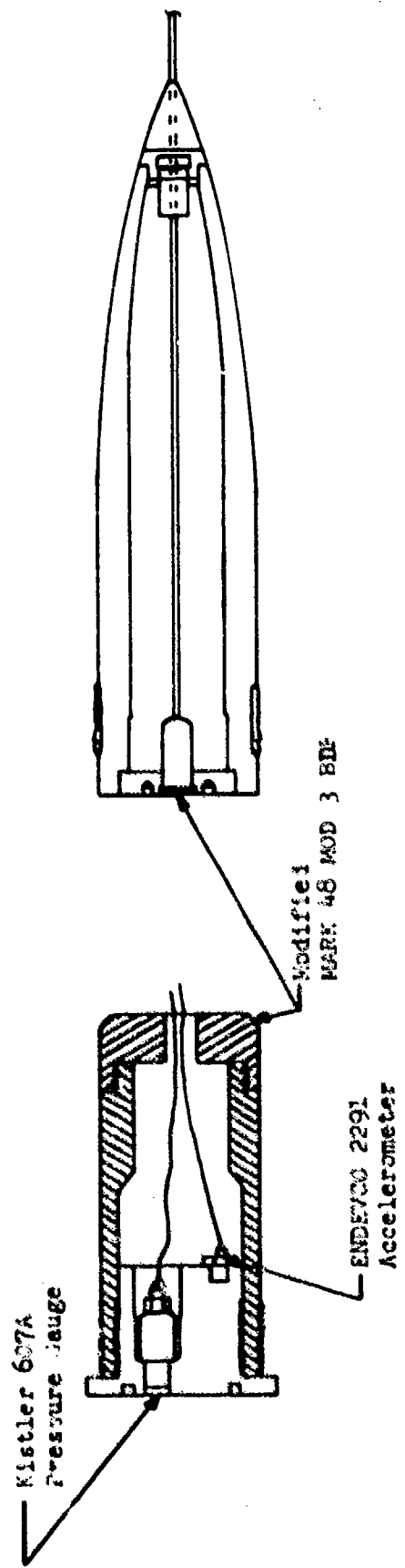
CONTINUOUS RECORDING AND COMBINED MECHANICAL TRANSDUCERS



PEAK READING MECHANICAL TRANSDUCERS

5" PROJECTILE INSTRUMENTATION

FIGURE 2



8" PROJECTILE INSTRUMENTATION

FIGURE 3

range and resonant frequency characteristics of ± 100 kg, 250 kHz and 20 kg, 125 kHz. Slight amplitude errors are to be expected, depending upon transducers (e.g., 11% maximum for the ENDEVCO Model 2291 between 50 and 80 kHz). Low noise coaxial cable was used throughout. Data recording was on Honeywell Test Instruments Model 7620 wide band magnetic tape system, double extended mode, 432 kHz center frequency, D.C. to 80 kHz response at 120 inches per second record speed. End-to-end system response was 80 kHz. For the instrumented projectile experiments, the transducers were "hardwired" through the gun bore to the signal conditioning and recording equipment; this technique provided from 0.5 to 7.0 milliseconds of recording time before adverse cable motion/destruction effects were experienced.

b. Mechanical gages consisted of peak-reading self-recording accelerometers and pressure transducers. The accelerometers were the Mindlin gage copper-ball, used to measure setback shock spectrally at four frequencies, and the NOL WOX-5A, used to measure transverse and spin accelerations. These transducers are described in detail by DeVost (reference (5)). The peak-reading pressure gage consisted of a base detonating fuze body modified to incorporate four peak-pressure-reading diaphragms; the diaphragms were located circumferentially on the fuze body just forward of the threaded portion. These gages were calibrated in an NOL 21" Air Gun Facility, using a setback simulator developed specifically for gun inertial loading studies of projectile fillers.

c. Projectile muzzle velocity data were obtained by use of induction coils or NWL developed doppler radar. The measurement accuracy of these systems is ± 5 ft/sec and ± 2 ft/sec respectively. Primer transit time and gas distribution in the open air burn experiments was obtained from high speed framing camera film (frame rate between 10,000 and 14,000 fps).

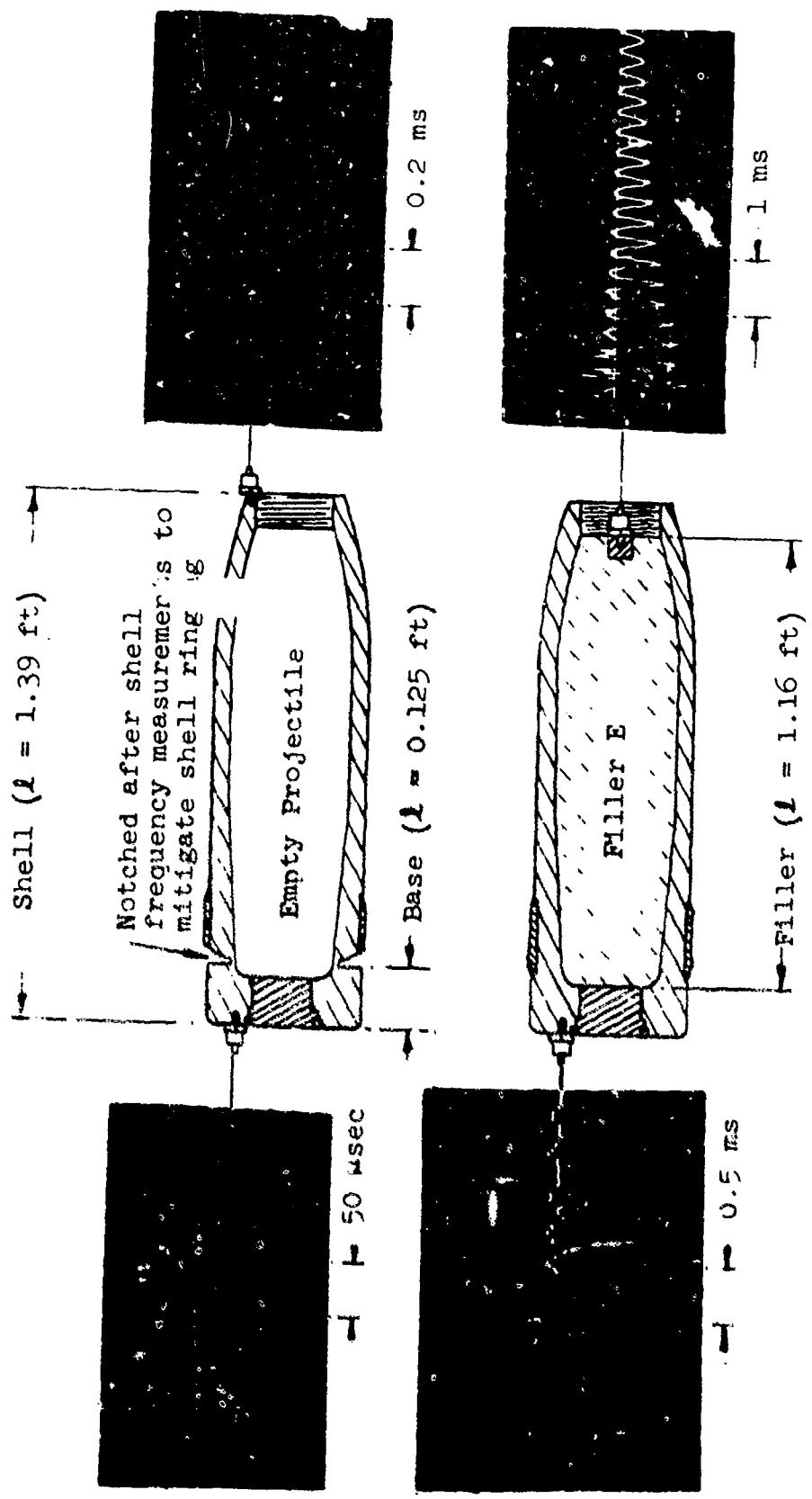
d. Projectiles containing Composition A-3 and Explosive D explosive fillers were fired from 5"/38 and 5"/54 short barreled guns (5"/10 and 5"/16 respectively) to subject the explosive filler to the gun launch forcing function through peak pressure while assuring gentle recovery from sawdust media (recovery velocity 1200 to 1500 ft/sec).

SHOCK SPECTRA ANALYSIS

Shock data analysis consisted of determining the component frequencies of the projectile assemblies used in the investigations and performing computer analysis of the components' response to the pressure and acceleration pulses measured in the ballistic performance studies.

For component frequency analyses, the projectile assemblies were simplified to a three-component structure: base, shell and filler. The fundamental frequencies of individual components were computed using longitudinal sound velocity in materials theory (Aronica, reference (6)), and experimentally measured by monitoring free-body ringing response for the 5" projectiles. A schematic and representative data for the ringing experiments are shown by Figure 4.

For the 5" program, single-degree-of-freedom (sdof) system responses to the experimentally determined gun-projectile pressure and acceleration



COMPONENT FREQUENCY MEASUREMENTS

FIGURE 4

pulses were computed using the NOL Analog Shock-Spectrum Analyzer (Melane, reference (7)). The analog analyzer was used in lieu of digital computer techniques because primary interest was only in the early time, ≤ 1.0 millisecond, portion of the gun ballistic environment; additionally, many of the continuous shock recordings contained large signal errors, at cable destruct times which would have been difficult to correct on the digital system. Response accelerations were obtained for sdof system frequencies of from 430 Hz to 45 kHz; system damping was 2.0% of critical.

For the 8" program, sdof shock spectrum was computed by digital concatenation of the acceleration data taken from the instrumented projectile and converted gun sidewall pressure data by use of subroutine with the MR WISARD computer program (Reed, reference (8)), as shown in Figure 5. Pressure-time recordings were converted directly to acceleration time by changing the pressure calibration of the recorded data to proportional acceleration calibrations by the following:

$$\frac{PA}{W} = \ddot{X}$$

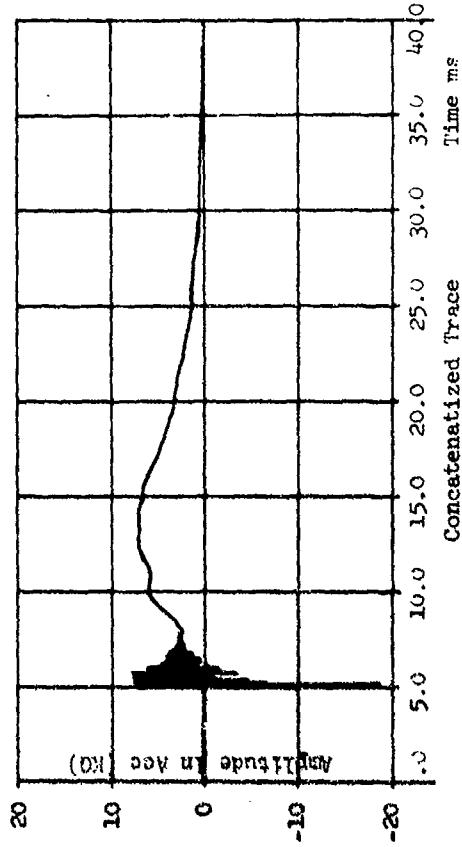
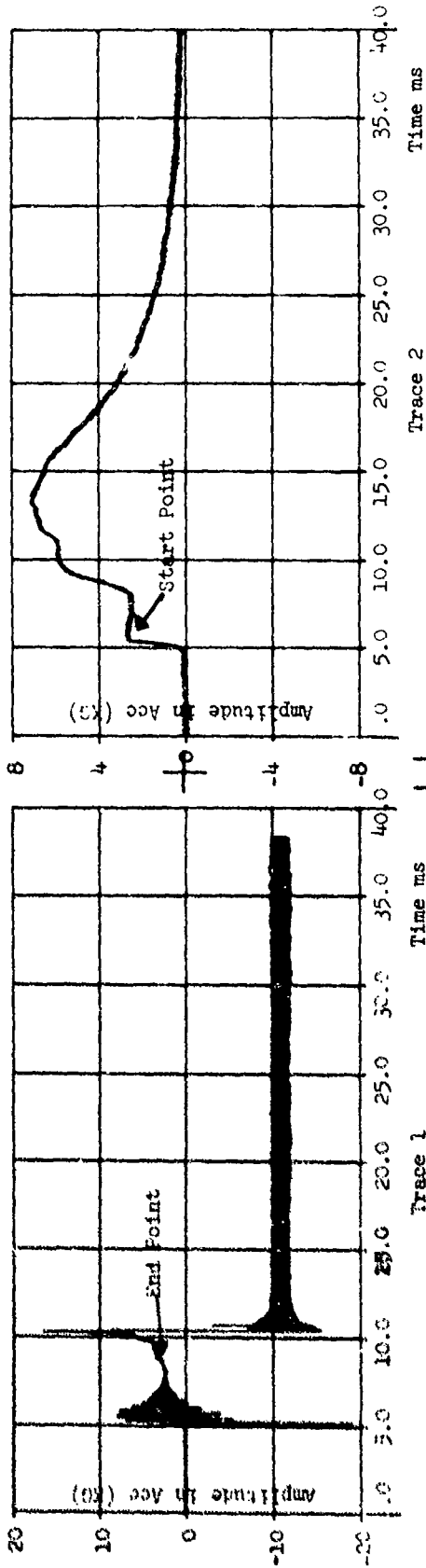
where: P = instantaneous pressure on the projectile base (psi)

A = gun bore area (in²)

W = projectile weight (lb)

\ddot{X} = acceleration (g)

Concatenation of the data records was necessary in order to obtain the complete time history and total spectrum of the projectile shock.



The amplitude of end point on Trace 1 and start point on Trace 2 at the time selected must be equal.

CONCATENATION PROCESS - FULL SERVICE CHARGE

FIGURE 5

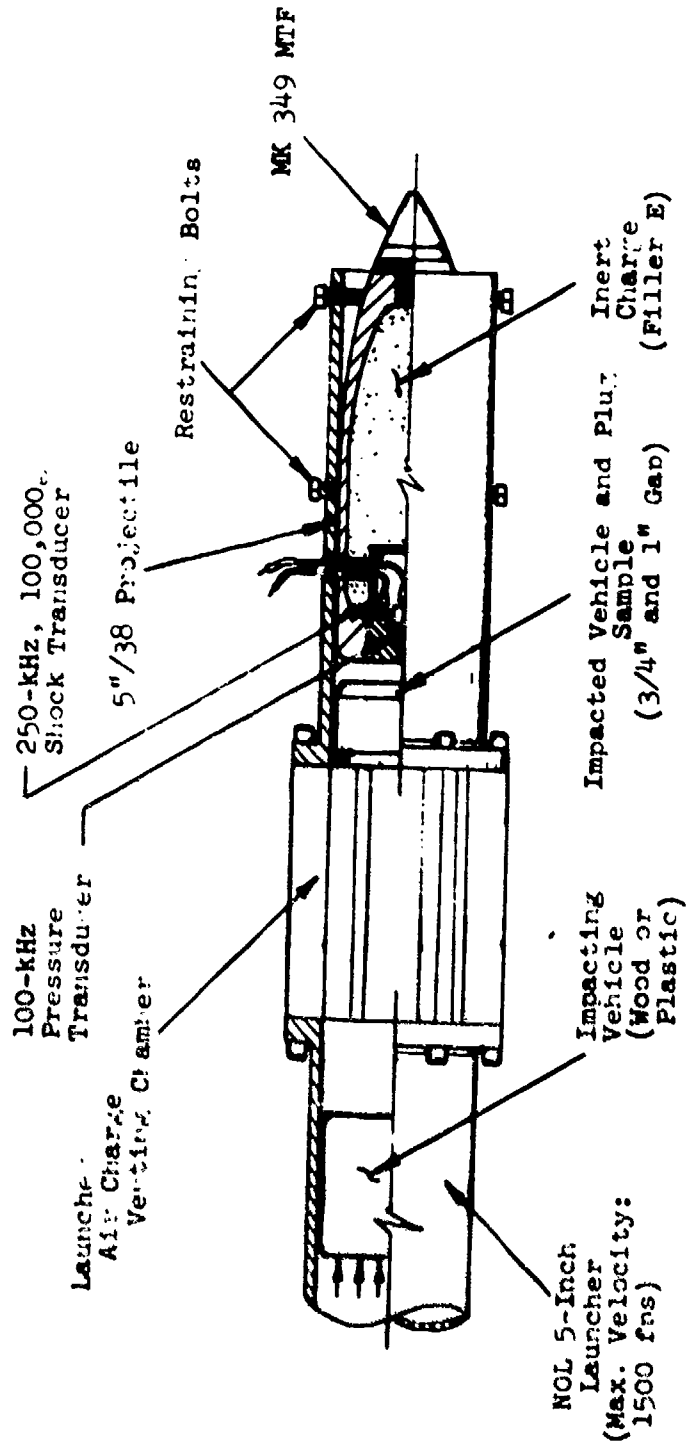
Response accelerations were obtained for sdof system frequencies from 10 Hz to 80 kHz. System damping was 2.0% of critical.

SIMULATION AND CORRELATION STUDIES

Laboratory simulations and analytical modeling were performed during the investigations in order to obtain better understanding of observed experimental results and to minimize costs of full-scale experiments.

For the 5"/38 program, these efforts were primarily concerned with examination of the 5"/38 propelling charge ignition-ammunition interaction phenomena; initial ballistic performance experiments indicated presence of ignition-produced compression waves possibly producing considerable grain and cartridge case closure motion in the Type A propelling charge. Flash X-ray experiments, using an unconfined, fiberglass cartridge case with standard primer, propellant and closure plug components, were performed to obtain a more quantitative understanding of the phenomena (Soper, reference (9)). Concurrently, air gun experiments were performed, as shown schematically by Figure 6, to establish an economical laboratory technique for simulating the observed early-time gun ballistic environment on the base of projectiles. The resulting technique was subsequently used to study the response of specific ammunition components, especially a 5"/38 mechanical time fuze component, to the simulated early time gun environment.

Since it was not possible to duplicate the combined effects of the 8"/55 reduced charge gun firing in the laboratory, the component shocks



AIR GUN SIMULATION FACILITY

FIGURE 6

Reproduced from best available copy.

of in-bore and out-of-bore phenomena, as discussed below were simulated separately and the individual effects on the 8"/55 projectile's base detonating fuze components were studied.

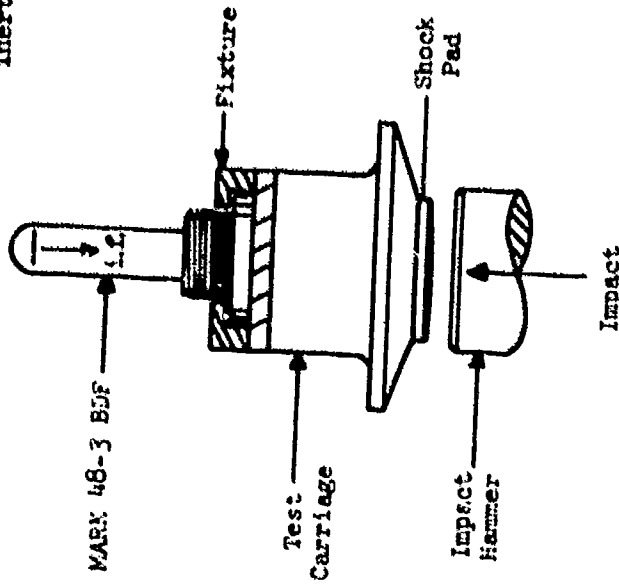
a. Plug Impact Tests - Tests simulating the effects of cartridge case closure plug impacting the base fuze were conducted using the NOL VHg Impact Test Set (DeVost, reference (10)). The test apparatus and impacts are described in Figure 7. Impact levels were similar to those recorded during gun launch of reduced charge propelled instrumented projectiles.

b. Plug Impact and Chugging - An attempt to simulate the combined effects of plug impact and pressure and shock waves in the propelling gases ("chugging") was made by combining two types of shock loads as described below. The effects of plug impact were simulated on the NOL VHg Impact Test Set as described above at the 40 Kg acceleration level. The effects of normal firing and "chugging" were simulated by subjecting the fuzes to either one or three separate shocks of about 7.0 to 7.5 Kg peak acceleration with a duration of about 5 milliseconds (ms). These tests were performed in the NOL 5" Air Gun (Fisher, reference (11)).

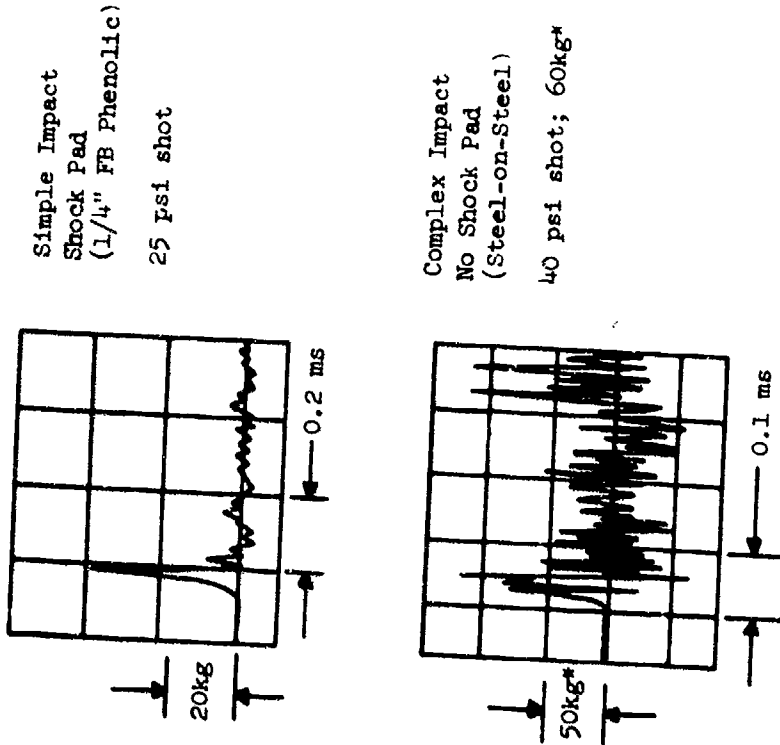
c. Out-of-Bore Drag - Tests were run on fuzes to determine their sensitivity to setforward drag. Based on the assumption that low level projectile oscillation may persist close-aboard after the projectile leaves the gun, out-of-bore drag tests simulating combined projectile drag and oscillation were also run. The tests were performed on drop testers described in Figures 8 and 9. The apparatus were used to

VHig Tester Schematic

(i.f.) Direction of inertial force



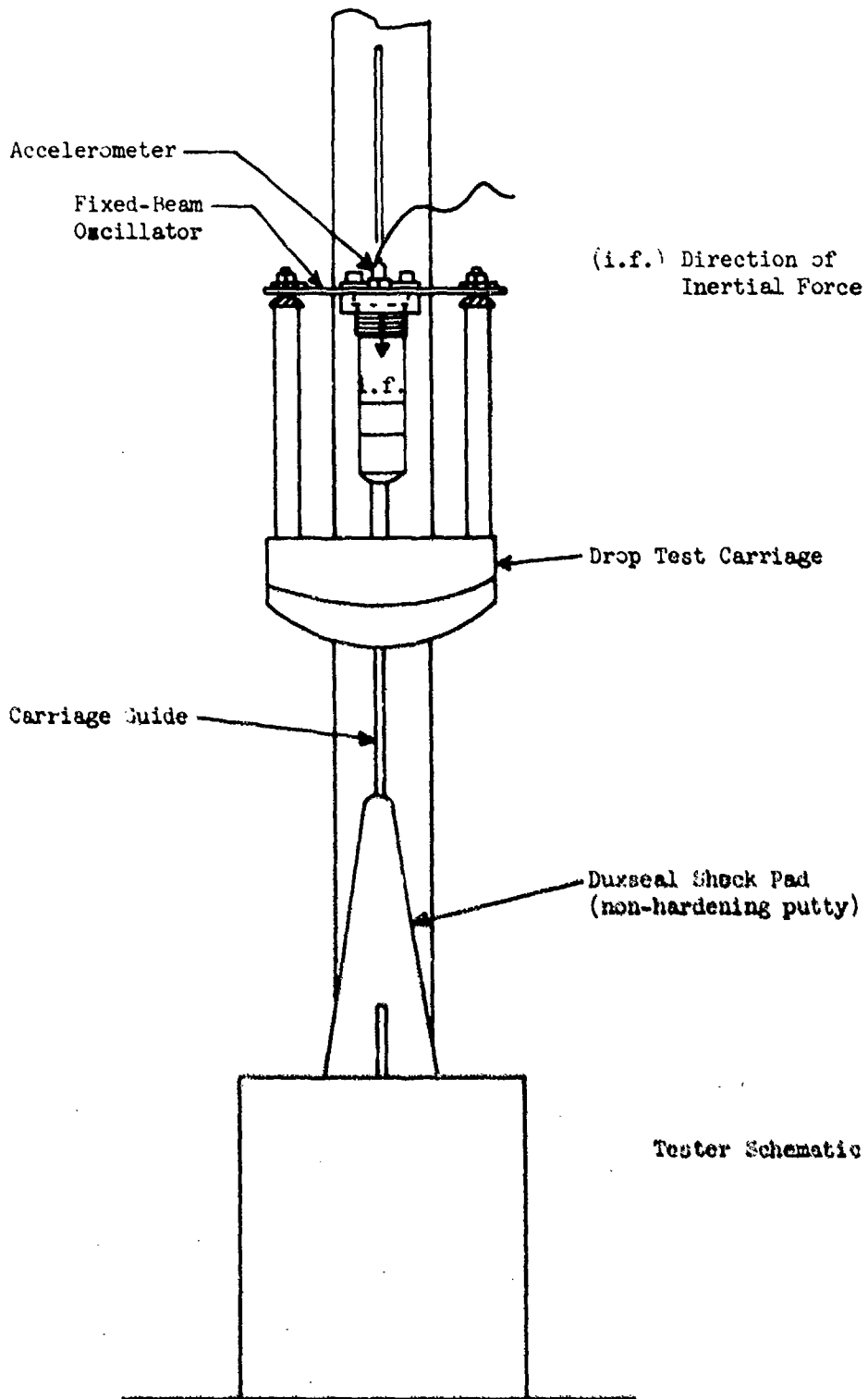
Impact Pulses



*Paired pulse value; 20 psi shot impact was similarly complex and 40 kg (see Table 1)

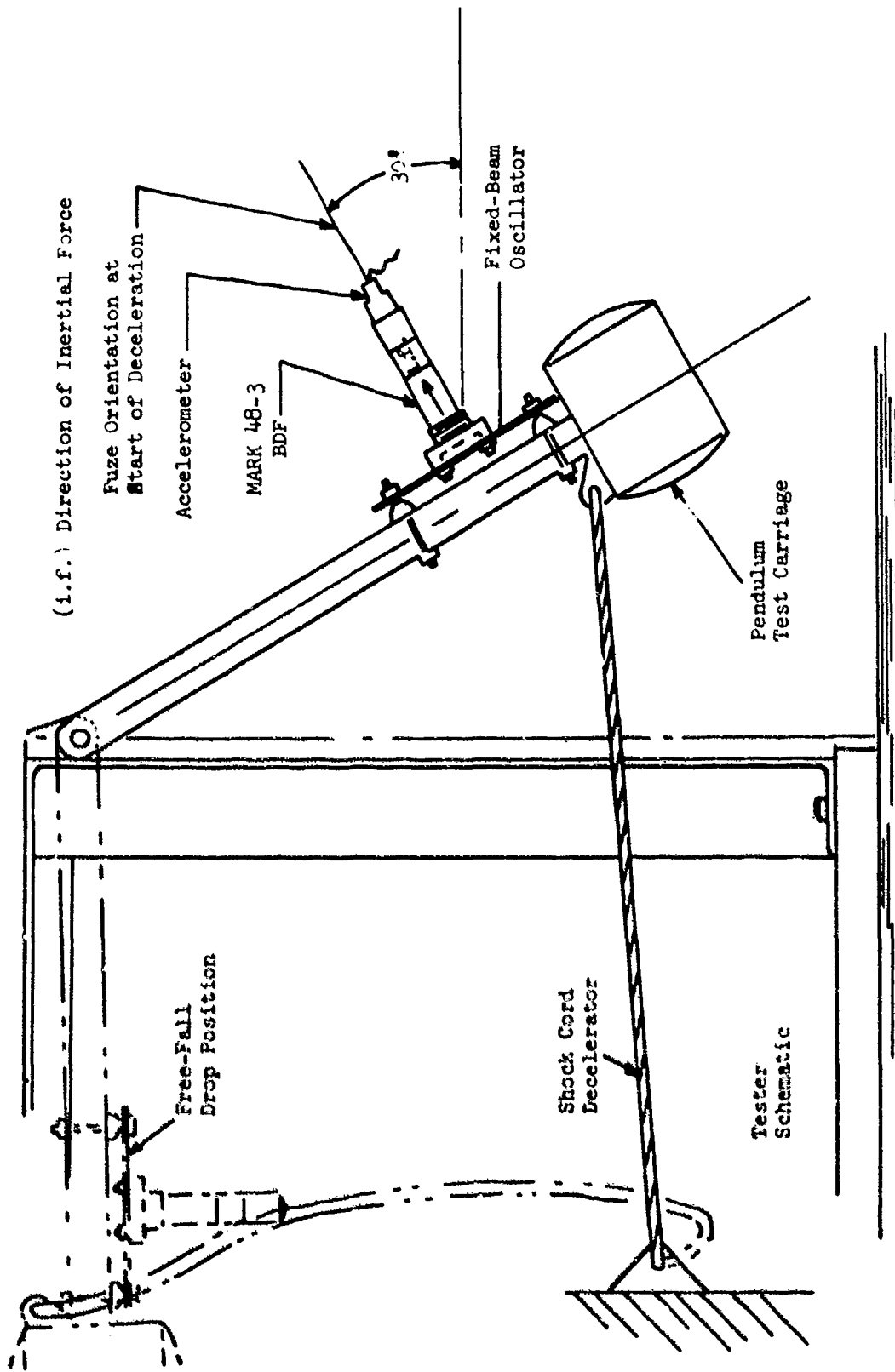
PLUG IMPACT SIMULATION APPARATUS AND OSCILLOGRAMS

FIGURE 7



NOSE-DOWN OUT-OF-BORE SHOCK SIMULATION APPARATUS

FIGURE 8



NOSE-UP OUT-OF-BORE SHOCK SIMULATION APPARATUS

FIGURE 9

produce relatively smooth, long duration pulses to simulate aerodynamic drag, and pulses with superimposed low frequency oscillations to simulate the combined effects of drag and projectile oscillation. In the drag simulation tests, the fuze was mounted rigidly on the carriage; in the combined drag-chugging tests, the fuze was mounted on a fixed beam oscillator as shown in Figures 8 and 9, respectively.

The 5"/54 and 8"/55 investigations of 1972 extended the simulation effort to application to the MARK 54/MARK 55 auxiliary detonating fuze design. The plug impact test, as described above, was applied to fuzes having nominal, partially armed, and completely armed safing and arming devices. The fuzes were also subjected to MIL-STD-313 tests to determine whether misassembled fuzes could be armed in transportation environments.

Over the entire period encompassed by the investigations described in this paper, a simulator, known as a Premature Simulator, was developed. This device, described in reference (12), is a drop tester designed to subject a small amount of explosive, approximately one pound, to the setback pressure and duration achieved in the base region of a projectile during gun launch. Figure 10 is a schematic of this device. The Premature Simulator was used to determine the reaction threshold level for several explosives containing nominal and defective loads.

MAJOR RESULTS AND DISCUSSION - 5" Program

Ballistic Performance Measurements. Data obtained from the high response pressure-time instrumentation in the 5"/38 gun chamber walls

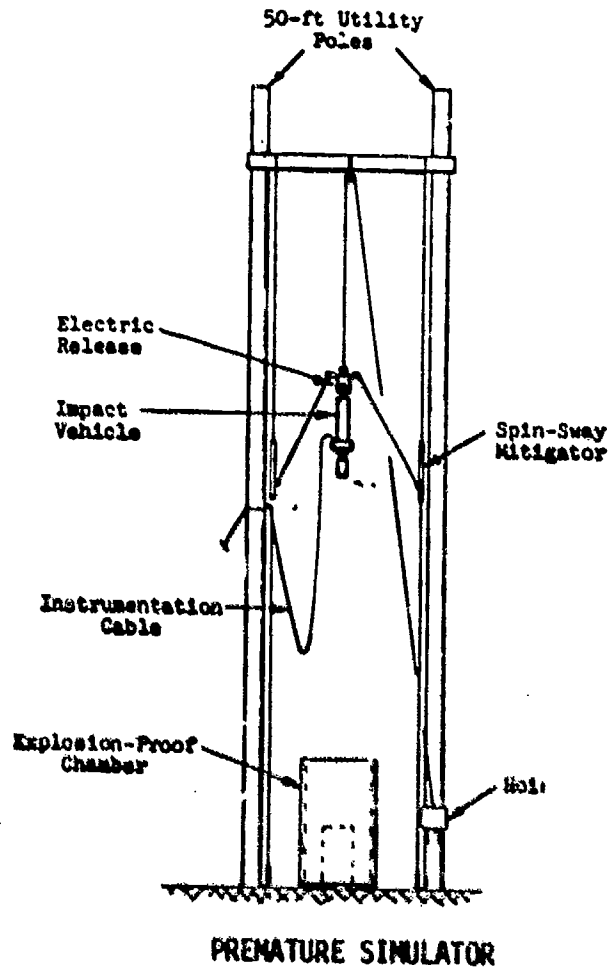
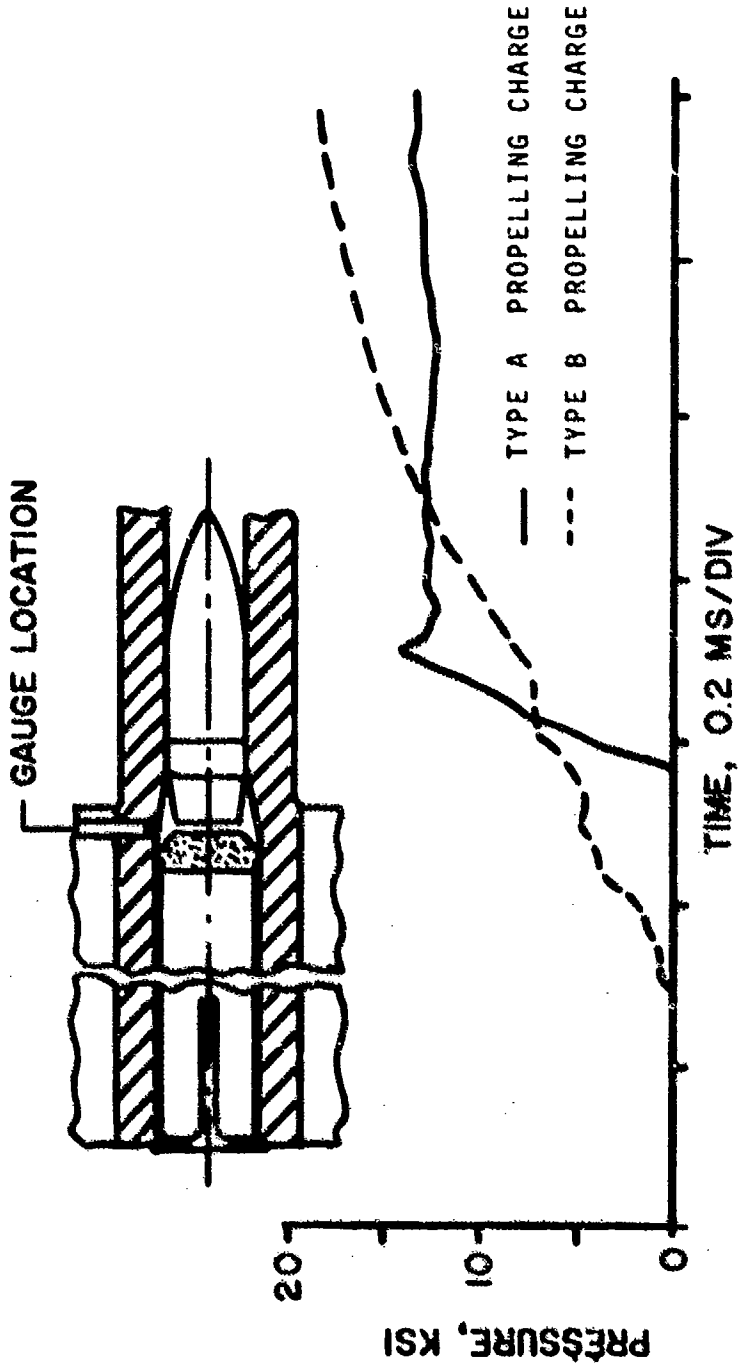


FIGURE 10

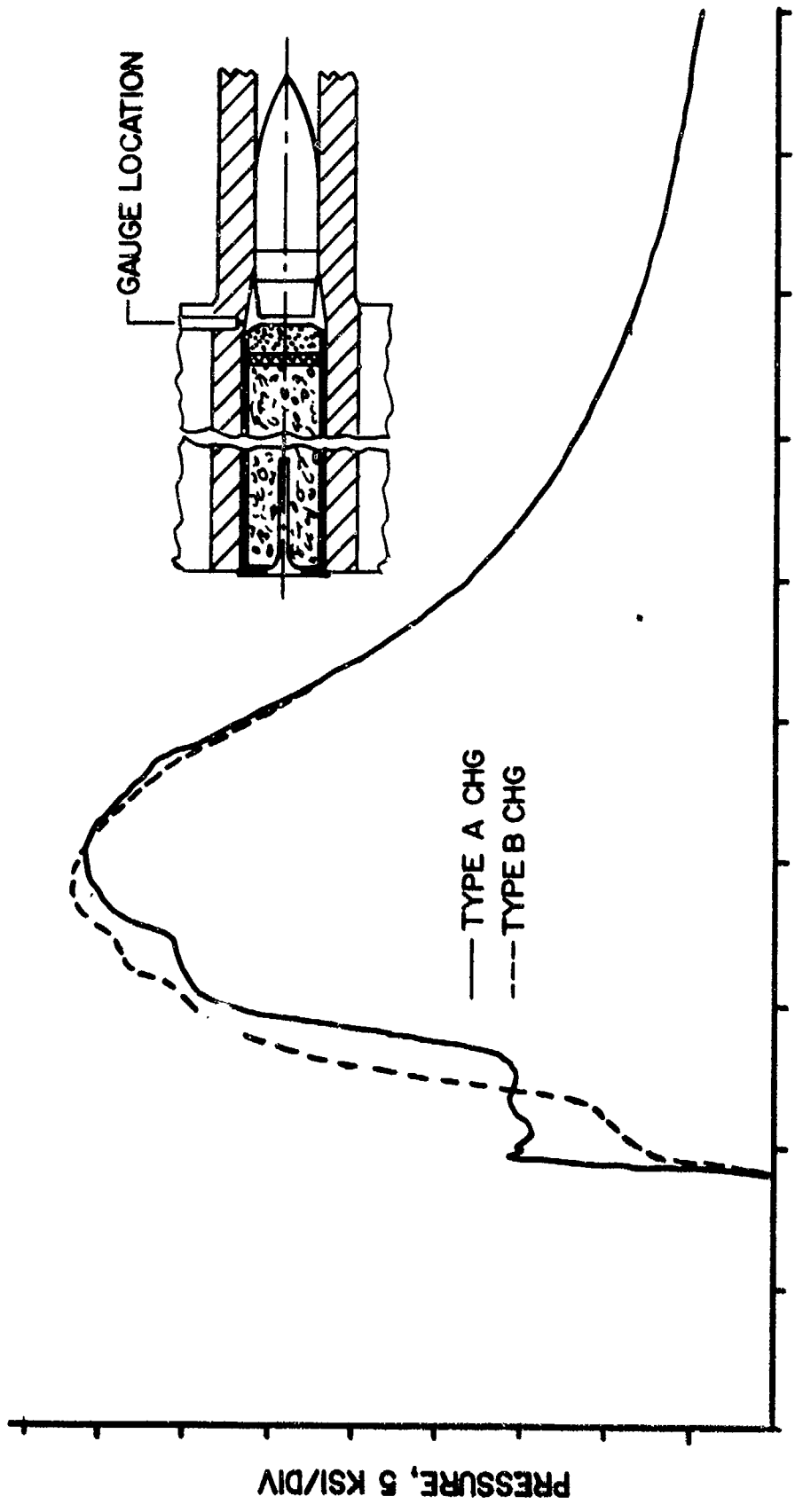
quickly identified a significant difference between Type A and Type B propelling charge ballistic performance; at the cartridge case mouth, the Type A charge consistently produced a characteristic step rise as compared to the more gradual rise characteristic of the Type B charge; see Figure 11 for comparison. The overall pressure-time pulses for both types of charges are compared by Figure 12. In contrast to the classical smooth pressure-time and corresponding acceleration-time profiles usually assumed for gun launched vehicles, analyses of these profiles indicated that strong, combustion-produced, compression wave phenomena were present in both charges but were more severe in the Type A charge. Further analyses, including consideration of pressure measurements made at various distances along the propellant bed, and the detail design characteristics of the charge ignition systems, indicated that the observed wave action was related to initial propellant ignition and subsequent burning-front development.

Data obtained from the instrumented projectile experiments are shown by Table I and Figure 13. While the mechanical gage effort was hampered by projectile recovery problems, useful data were obtained indicating that setback shocks, angular accelerations, and projectile filler base pressures were significantly higher in the rounds fired by the Type A propelling charge than in those fired by the Type B charge. The continuous recording instrumentation provided the essential data needed to define the very early time charge ignition-projectile start period. Recording times ranged from 0.5 to 1.5 milliseconds from initial projectile base pressure rise. These data, as shown by Figure 13,



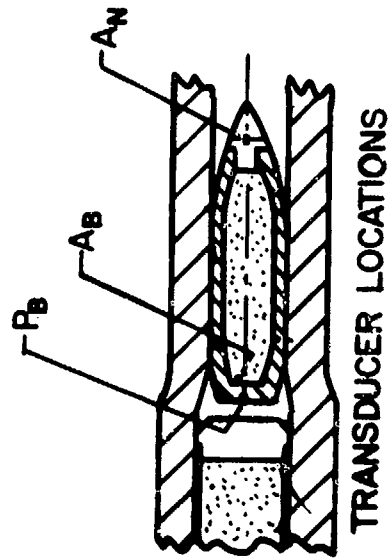
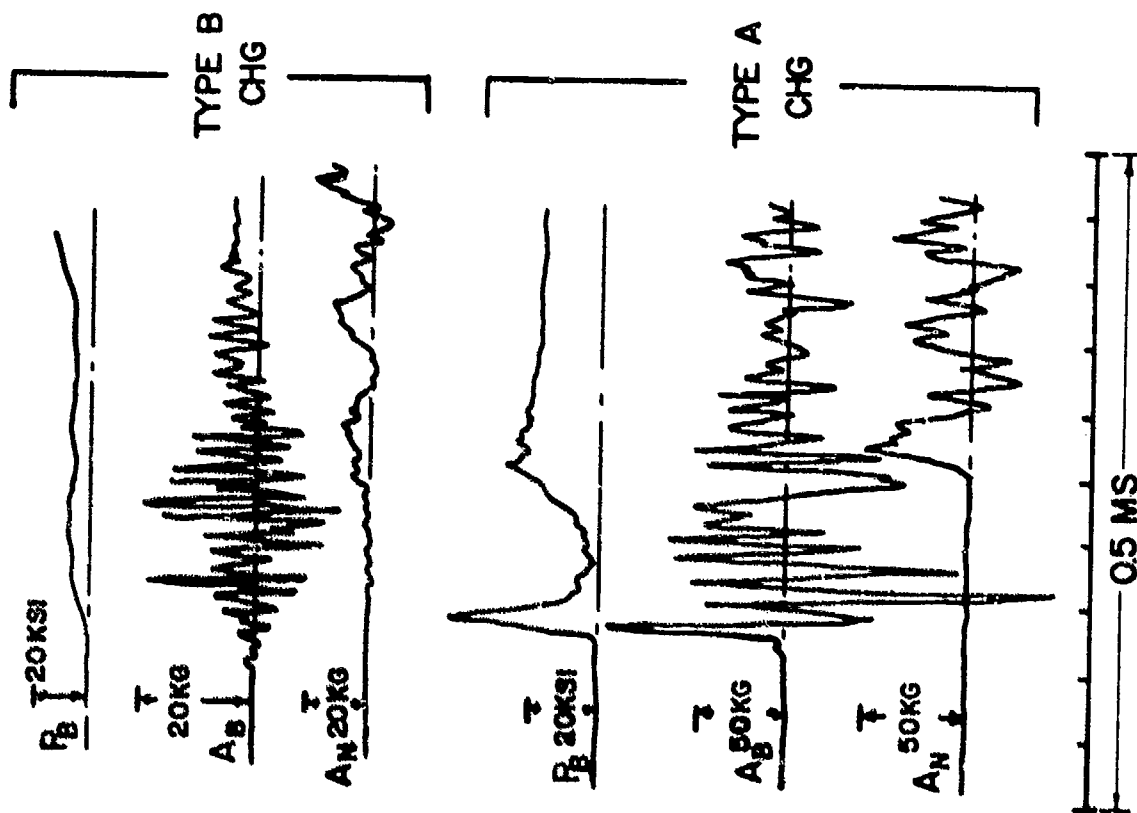
COMPARISON OF INITIAL CASE MOUTH PRESSURE PROFILES
FOR TYPE A AND TYPE B PROPELLING CHARGE

FIGURE 11



COMPARISON OF PRESSURE-TIME PROFILES FOR
 TYPE A AND TYPE B PROPELLING CHARGE

FIGURE 12



TYPICAL DATA RECORDS
FROM
CONTINUOUS RECORDING
INSTRUMENTATION

FIGURE 13

TABLE I
5"/38 MECHANICAL GAUGE DATA

TYPE A PROP. CHARGE (NACO PROPELLANT)					
ROUND NO.	WOX-5A SPIN ACCELERATION		PRESSURE GAUGE		% ABOVE NOMINAL SETBACK PRESSURE*
	BALL DEFORMATION AVG (1/1000)	(RAD/SEC ²)	DIAPHRAGM DEFORMATION 1/1000"	PEAK (PSI)	
1	2.60	585,000	* *	--	--
2	3.75	840,000	61.0	29,500	41.0
3	4.95	1,100,000	70.0	30,400	45.0
TYPE B PROP. CHARGE (PYRO PROPELLANT)					
1	+	--	--	--	--
2	0.0008	180,000	40.0	27,000	13
3	++	--	48.0	28,000	18

*20,900 PSI FOR NACO AND 23,800 PSI FOR PYRO

**FILLER IN THE REGION AROUND THE GAUGE DIAPHRAGMS WERE GOUGED WHEN THE BASE FUZE WAS ASSEMBLED AND WAS NOT IN CONTACT WITH THE DIAPHRAGMS. READINGS WERE VERY LOW.

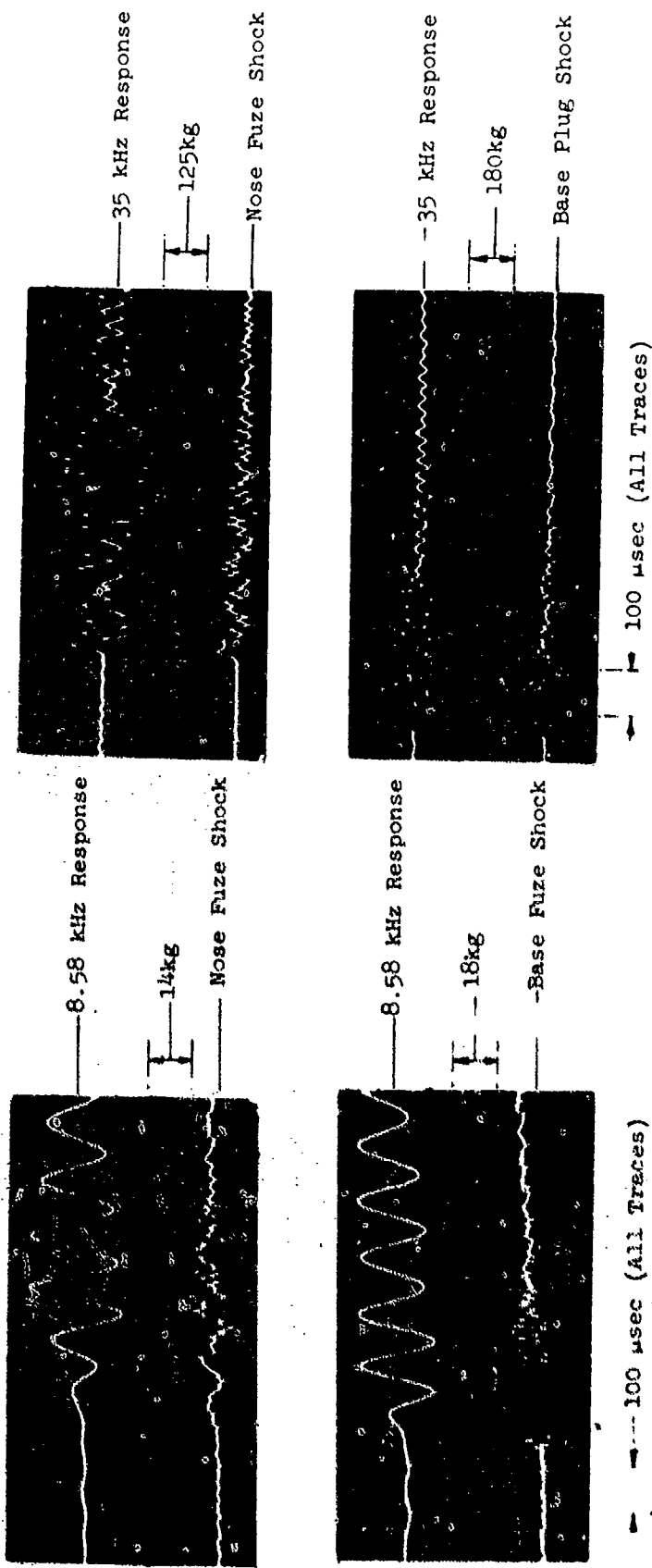
+ROUND BROKE UP; NONE OF THE GAUGES WERE RECOVERED.

++APPARENTLY ROTOR INERTIA FORCE WAS NOT HIGH ENOUGH TO OVERCOME THE SETBACK FRICTIONAL FORCE - THIS HAPPENS FREQUENTLY IN PYRO FIRINGS.

established that the projectiles fired with Type A propelling charges were subjected to significantly more severe early-time shock than were those fired by the Type B charge. Of particular significance was the high amplitude, short-duration pressure pulse observed by the pressure transducer in the projectile base wall; it was reckoned that this pulse was caused by initial impact of the Type A propelling charge closure plug and accelerated propellant grain mass. This was verified and quantified during simulation studies as explained below and, by further analyses and correlations, was found to be the most probable cause of explosive filler initiation in the service premature functionings.

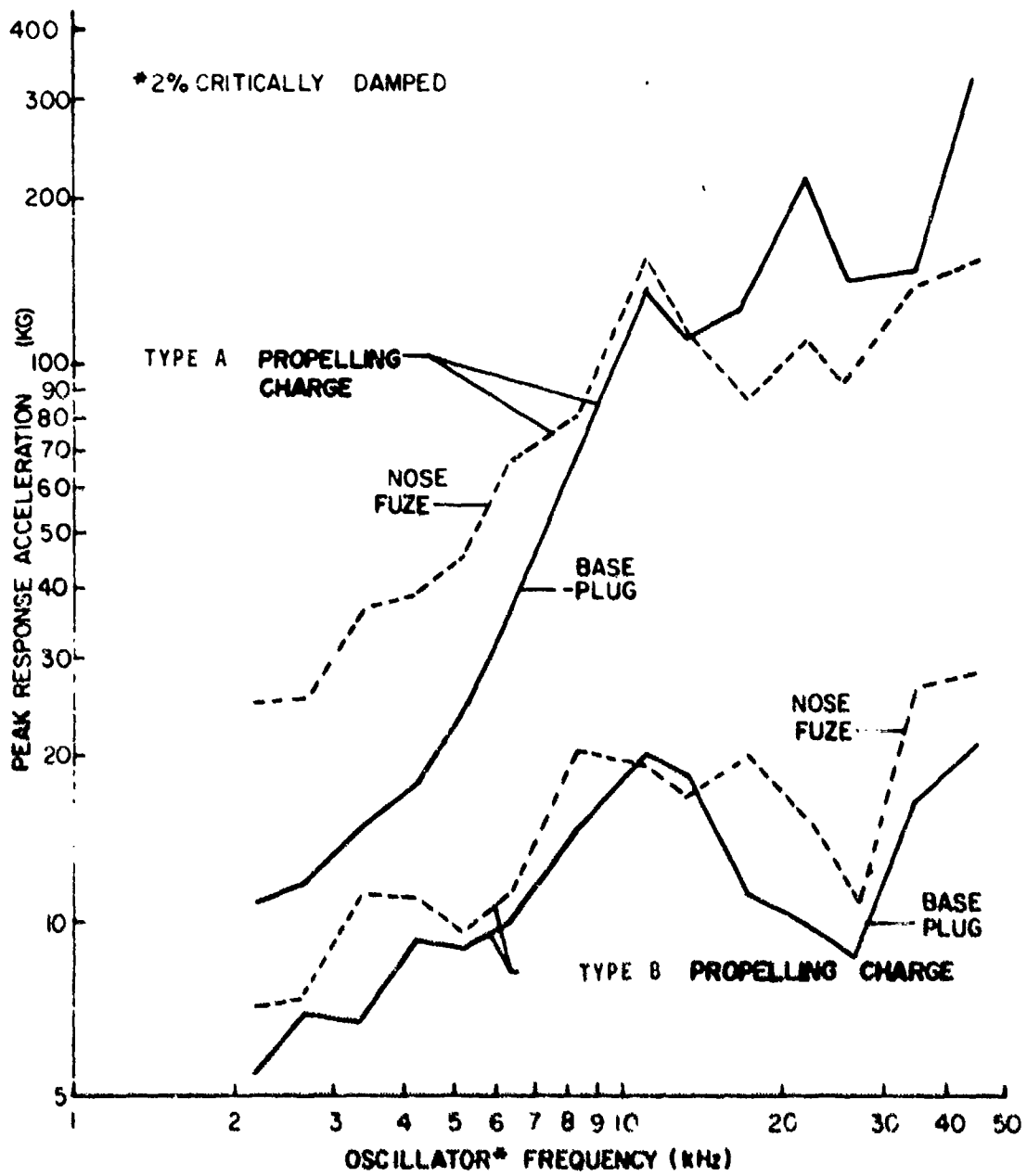
Shock Analysis. Figure 14 shows typical recordings and analog responses of Types A and B propelling charge-produced shocks measured at both projectile base and nose locations. Spectra of the shocks are shown by Figure 15. These data show that the early time shock peaks produced by the Type A propelling charge are more than four times higher than those produced by the Type B charge. As expected, responses approaching the natural frequency of the projectile base (45 kHz) are the highest; responses for the Type A propelling charge are from 1.7 to 21.6 times higher than comparable responses for the Type B propelling charge.

Simulation and Correlation Studies. Typical flash radiographs obtained during the special flash X-ray experiments are shown by Figure 16. These exposures contrast the grain-closure plug performance exhibited by the Type A and Type B propelling charges; for the Type A



RECORDINGS AND ANALOG RESPONSES OF TYPES A AND B PROPELLING CHARGE - PRODUCED SHOCKS IN 5"/38 PROJECTILES

FIGURE 14

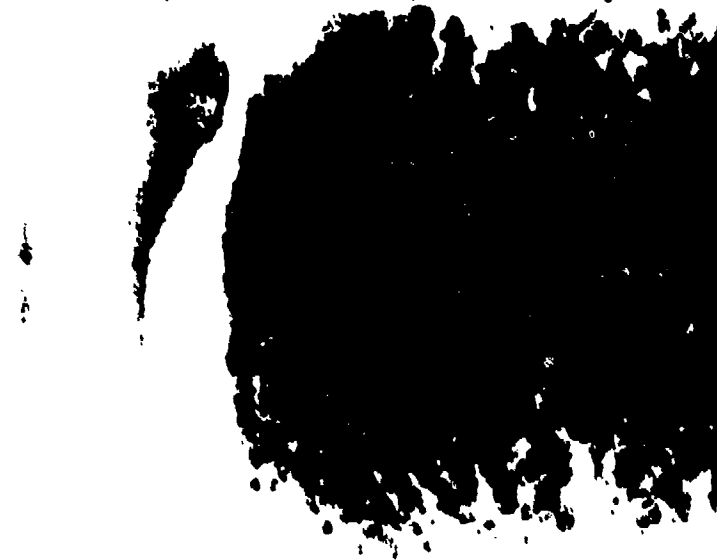


EARLY-TIME SPECTRA OF 5²/38 SETBACK SHOCK

FIGURE 15



TYPE B PROPELLING CHARGE



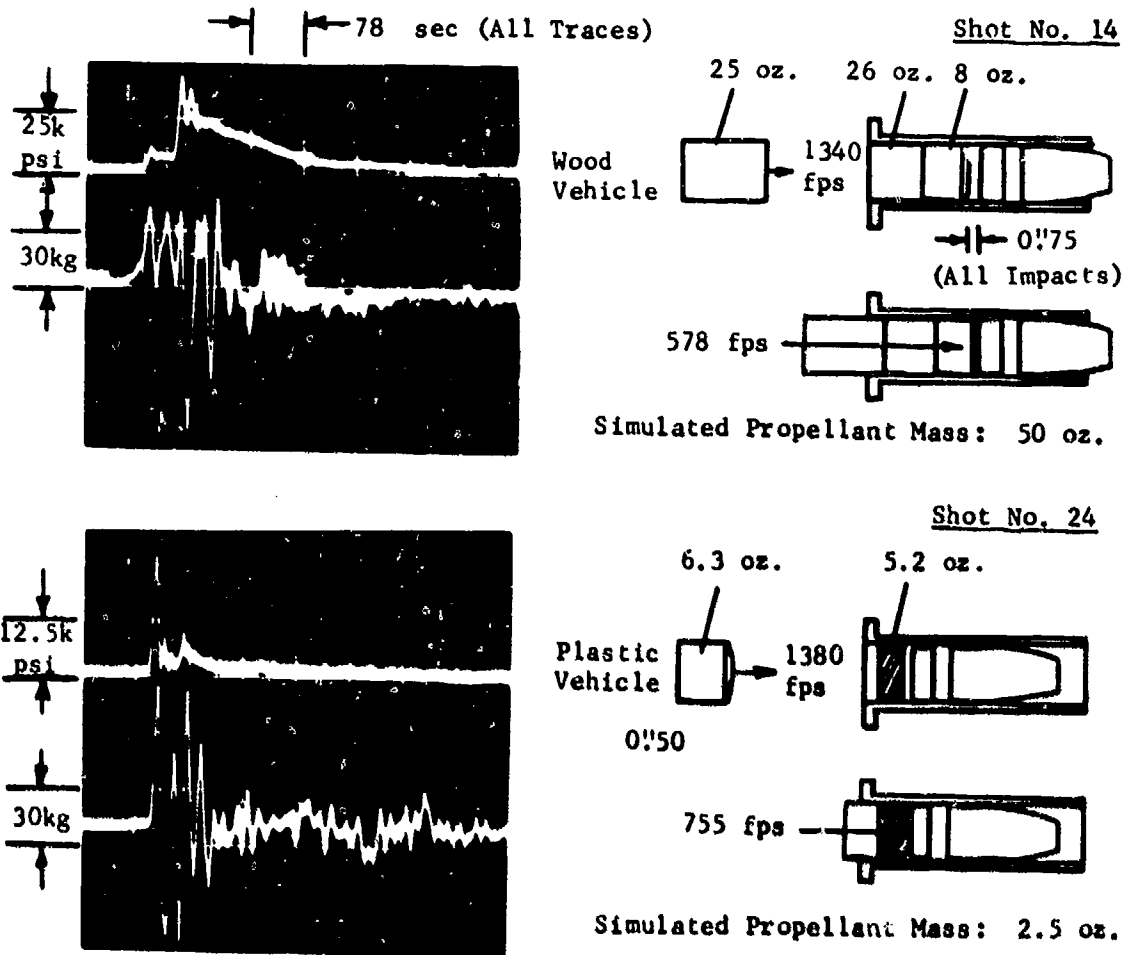
TYPE A PROPELLING CHARGE

FLASH RADIOGRAPHS OF PROPELLING
CHARGE CLOSURE PLUG PERFORMANCE

FIGURE 16

charge, the cork closure plug, originally about three inches thick, has been compressed to approximately 0.5 inch thick, has assumed a convex leading edge shape, and is being forced against the projectile base with an impact velocity of approximately 700 ft/sec; for the Type B propelling charge, the closure plug is disintegrating rather than being forced forward as a homogeneous mass. This action is attributed to differences in propellant grain size and mass and ignition development between the two charges: for the Type A charge, small propellant grains plus relatively small area of initial ignition action result effectively in a rather compact mass of propellant grains and compressed gas being driven forward toward the projectile seat during early ignition; for the Type B charge, larger grain size permits more gas flow forward through the unignited propellant bed, resulting in less propellant motion and sufficient pressure rise against the closure plug to produce the observed plug disintegration.

Typical results of air gun simulations of the closure plug/propellant mass and projectile base impact phenomena are shown by Figure 17; to determine the conditions for equivalency with the measured 5"/38 gun parameters, the simulated propellant mass ranged from two ounces to five pounds while plug impact velocities ranged from 280 to 1420 ft/sec. It is seen that with approximately a 1/2" convex plug leading edge shape, plus approximately 2.5 ounces of simulated propellant mass and an average plug impact velocity of 755 ft/sec, the projectile base pressure and acceleration profiles are essentially identical to those measured in the gun fired instrumented projectile experiments.

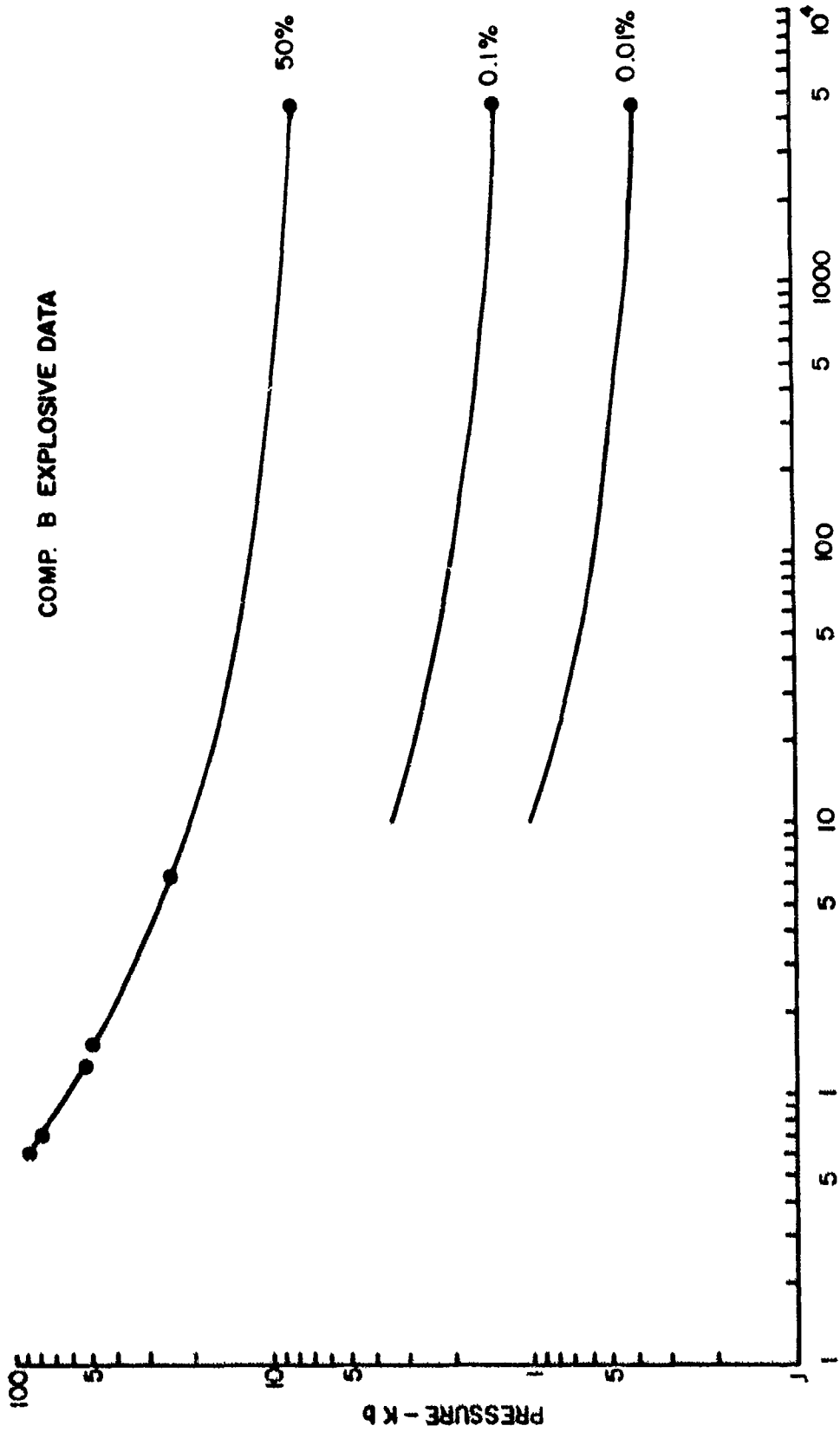


AIR GUN SIMULATION EXPERIMENTS

FIGURE 17

These simulations provided clear evidence that the severe impacts and high impulsive pressures recorded at the base of projectiles using the Type A propelling charge were produced by the grain-closure plug impact phenomena. Further analyses indicated the observed projectile base impact loading was subjecting the explosive filler at the projectile base explosive interface to low level shock pressure pulses of about 0.4 to 1.5 kb with durations of approximately 30 to 50 microseconds. Through examination of available shock initiation data for high explosives, it was possible to construct a family of initiation probability curves for Composition B explosive as a function of pressure level and pulse duration; see Figure 18. Data provided by Schimmel and Weintraub (reference (13)), were particularly useful here since these data allowed unique estimation of the 0.1% and 0.01% initiation probability curves to supplement the normally determined 50% probability curve. Entering these curves with the estimated average impact pulse characteristics, i.e., 1.0 kb and 40 microseconds, a predicted explosive initiation frequency of about one in 10^4 events is obtained. This compares extremely well with the observed service ammunition premature rate of about one in 15×10^3 events; it should be noted here that the Composition A-3 explosive involved in the service prematures is generally acknowledged to be somewhat more sensitive to shock initiation than Composition B explosive for which the initiation probability data were available.

Explosive Load Movement Studies. Thirty-six Composition A-3 loaded 5"/38 projectiles were fired, having explosive fill densities of 1.63, 1.50, 1.45 and 1.30 gm/cc and base gaps of 0.125" and 0.000". Table II



SHOCK INITIATION PROBABILITY CURVES AS FUNCTION OF PULSE CHARACTERISTICS

FIGURE 18

TABLE II

COMPOSITION A-3 EXPLOSIVE LOAD RESPONSE STUDY
LOADING CONDITIONS FOR GUN-FIRED RECOVERY TRIALS

<u>Density of Comp A-3 Loading</u> <u>(gm/cc)</u>	<u>Gap Size</u> <u>(in.)</u>	<u>Sample Size</u>	<u>Remarks</u>
1.63	0.125	6	Note: 1
	0.00	6	Note: 1
1.50	0.125	5	Note: 2, 3
	0.00	1	Note: 3
1.45	0.125	6	Note: 1
	0.00	6	Note: 1
1.30	0.125	6	Note: 2, 3, 4
	0.00	0	
Total		36	

Notes:

- 1 All rounds had Comp A-3 dusted into all base fuze hole plug (BFHP) threads. Graphite marker on increment/interface.
- 2 2 - 3 rounds only had Comp A-3 packed into four BFHP threads nearest explosive cavity.
- 3 Colored (dyed) explosive used to distinguish loading increments.
- 4 Round 6; 1.30 density; Explosive in BFHP threads; 1/8" gap exploded at 52" from breech face.
- 5 All projectiles were 5"/38 MARK 52 MOD 0.

gives the exact conditions. One projectile reacted at 18" of travel. This projectile had a 1.30 gm/cc load with .125" base gap. The 1.60 gm/cc fillers showed no tendency to shift or compact. Figures 19 is a post-firing photograph of typical projectiles. The 1.50 gm/cc fillers compacted slightly, figure 20. The 1.45 gm/cc and 1.30 gm/cc fillers underwent substantial compaction, Figures 21 and 22.

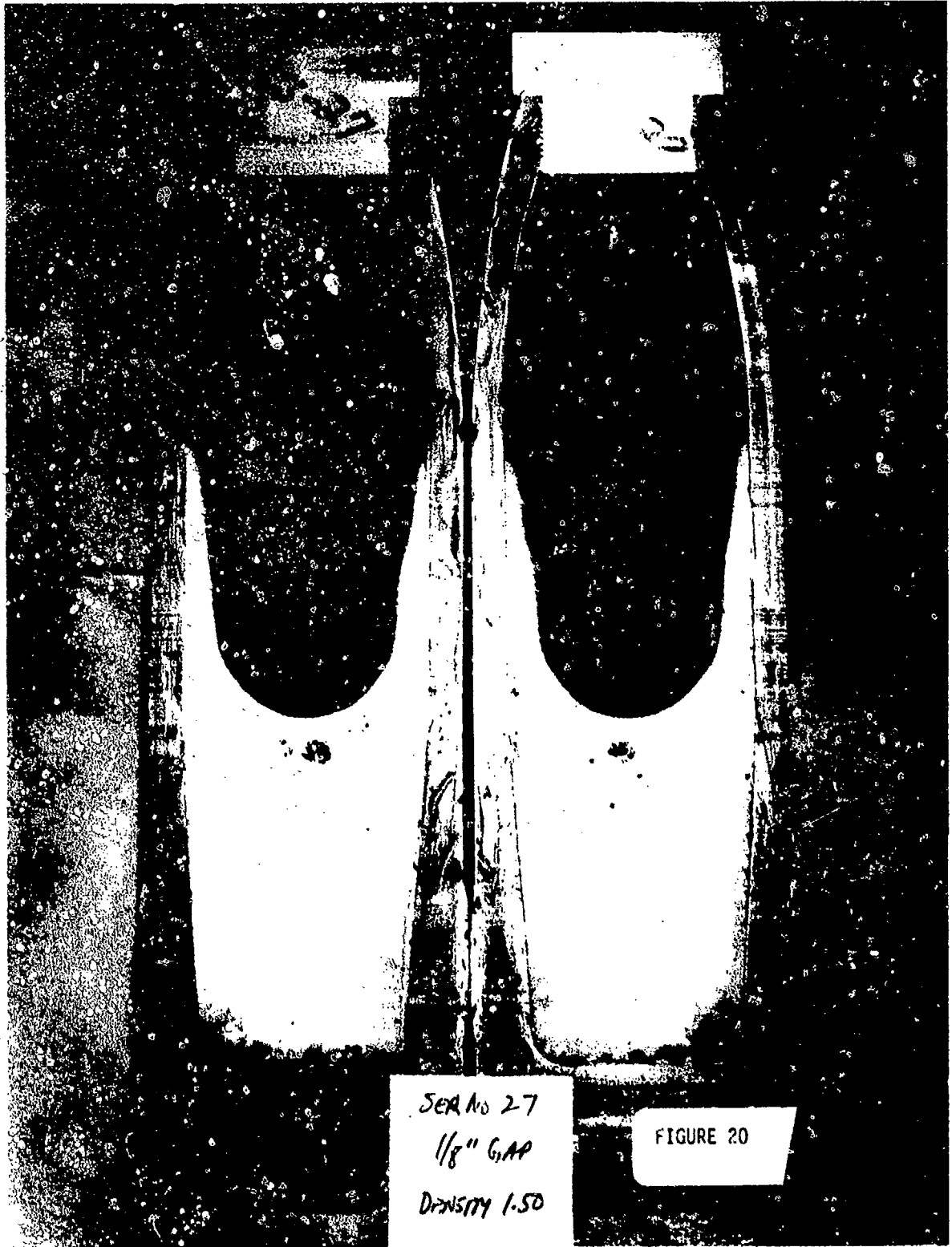
A similar experiment was conducted with 78 5"/54 Explosive D loaded projectiles at density levels of 1.47, 1.51, and 1.55 gm/cc with 0", 1/2" and 2" gaps. Compaction occurred in all cases but no reactions occurred. After firing, the crystalline Explosive D was un-coreable, being reduced to dust.

Premature Simulator Studies. Extensive premature simulator testing has been directed toward assessment of the reaction threshold of Composition A-3 explosive with perfect and defective loads. A summary of these results is presented in Figure 23. The pre-1973 A-3 loads with 1/4" to 1" base gaps were clearly dangerous. This situation confirmed a 1969 series of gun fired experiments. The pre-1973 A-3 loads which did not have gaps had a safety factor of at least two to one. In 1973, a new Comp A-3 bulk density specification was imposed. This specification had the effect of producing a more structurally sound load and reduced the shock sensitivity of the explosive. Following thermal cycling, the new A-3 developed cracks which slightly increased its sensitivity. Even in this case, new Comp A-3 is approximately as sensitive as the best pre-1973 Comp A-3.



Sec No 7
No 640
Jewelry 1.60

FIGURE 19



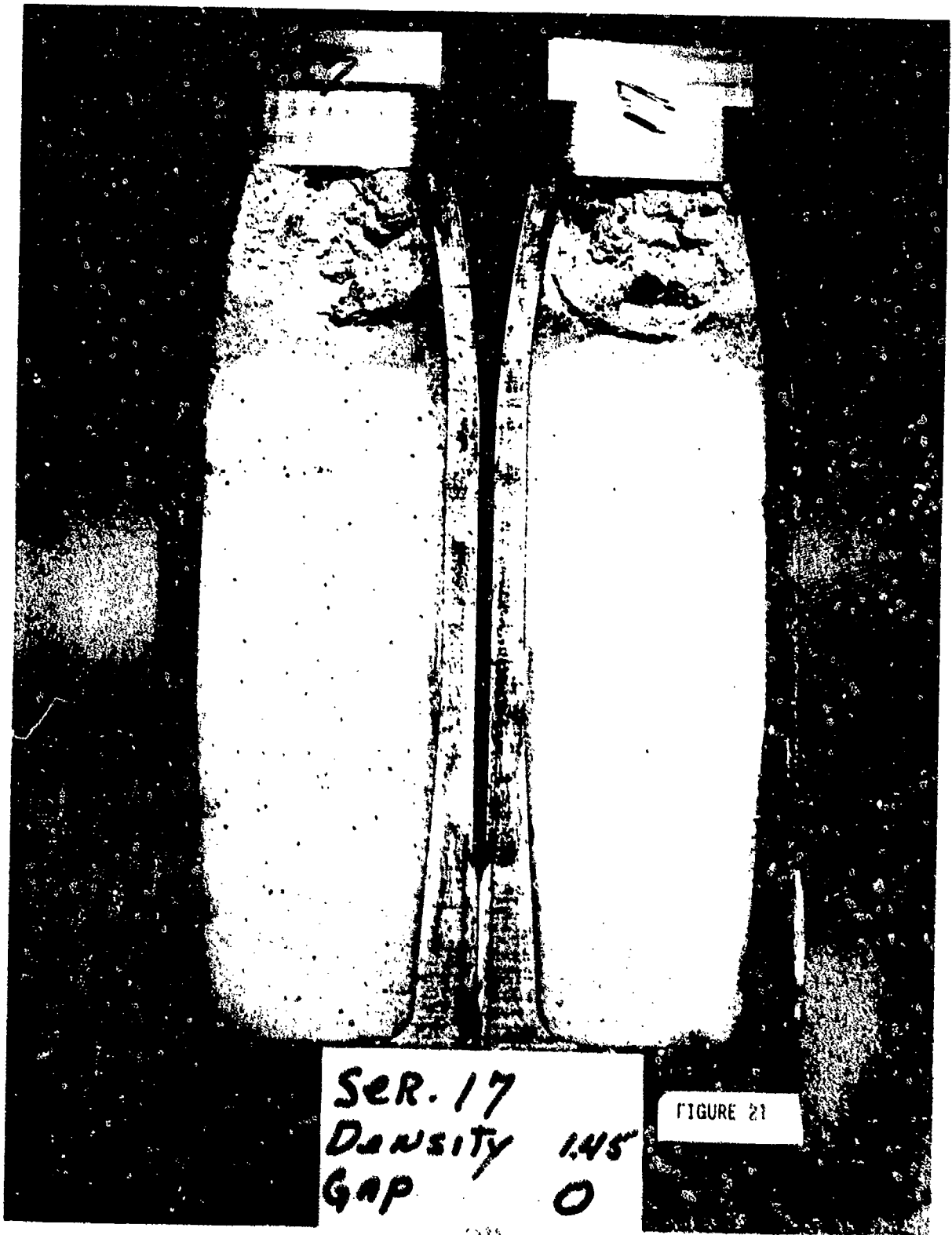
SER No 27

1/8" GAP

DENSITY 1.50

FIGURE 20

1433



SER. 17
DENSITY 1.45
GAP 0

FIGURE 21



SER. No. 41
Density 1.30
1435

FIGURE 2?

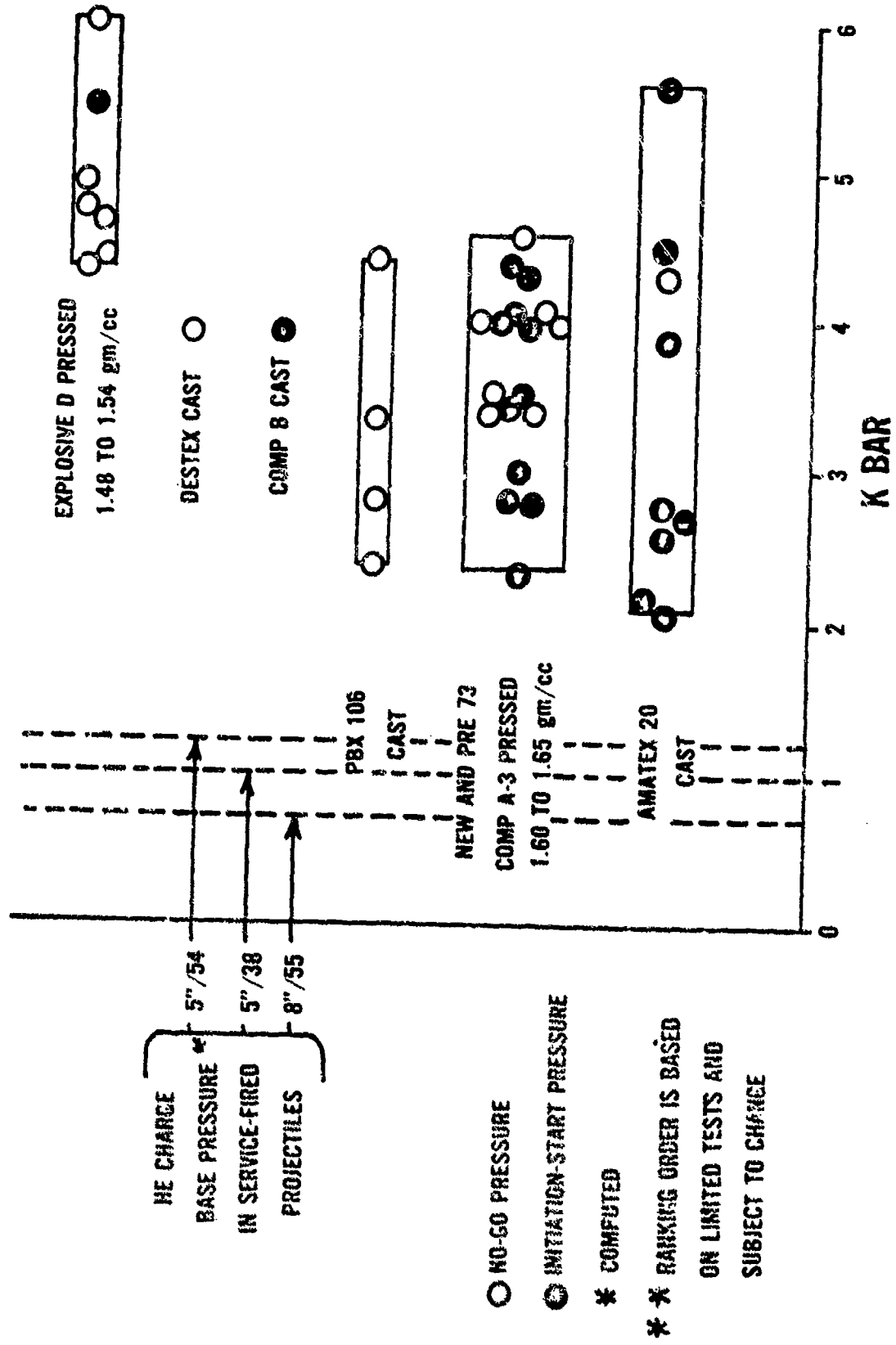


FIGURE 23

A similar experiment was performed with Explosive D with the results indicated in Figure 24. Note that with regard to gun launch safety, Comp A-3 (a sensitive explosive) can have a reaction threshold equivalent to Explosive D, a very insensitive explosive.

Detonator Shock Sensitivity. The MARK 54/MARK 55 auxiliary detonating fuze, Figure 25, uses the MARK 28 detonator which is contained in the fuze rotor. This fuze was implicated in the 8"/55 and 5"/54 malfunctions in 1972. This detonator is quite sensitive. The acceptance test for this detonator is a requirement that 100% of tested detonators will fire if impacted by the firing pin driven by a two-ounce steel ball dropped from a height of 5 inches. The actual test results indicate that the minimum ball drop functioning height was 1.5 inches with 100% functioning at 1.875 inches. The sensitivity of this detonator is reduced by vibration and shock. These inputs cause separations in the train. It was found that plug impact shock can cause this detonator to react whether in the armed or safe rotor position. Since a properly assembled fuze is barrier safe, normally only duds result. In a misassembled fuze, a boosted detonation of the projectile is possible and actually happened in the 8"/55 NEWPORT NEWS incident. Instances have occurred in which the MARK 28 detonator reacted after a 4-foot drop test.

MAJOR RESULTS AND DISCUSSION - 8"/55 Program

Ballistic Performance Measurements. Data obtained from the high-response pressure time instrumentation quickly identified that the 8"

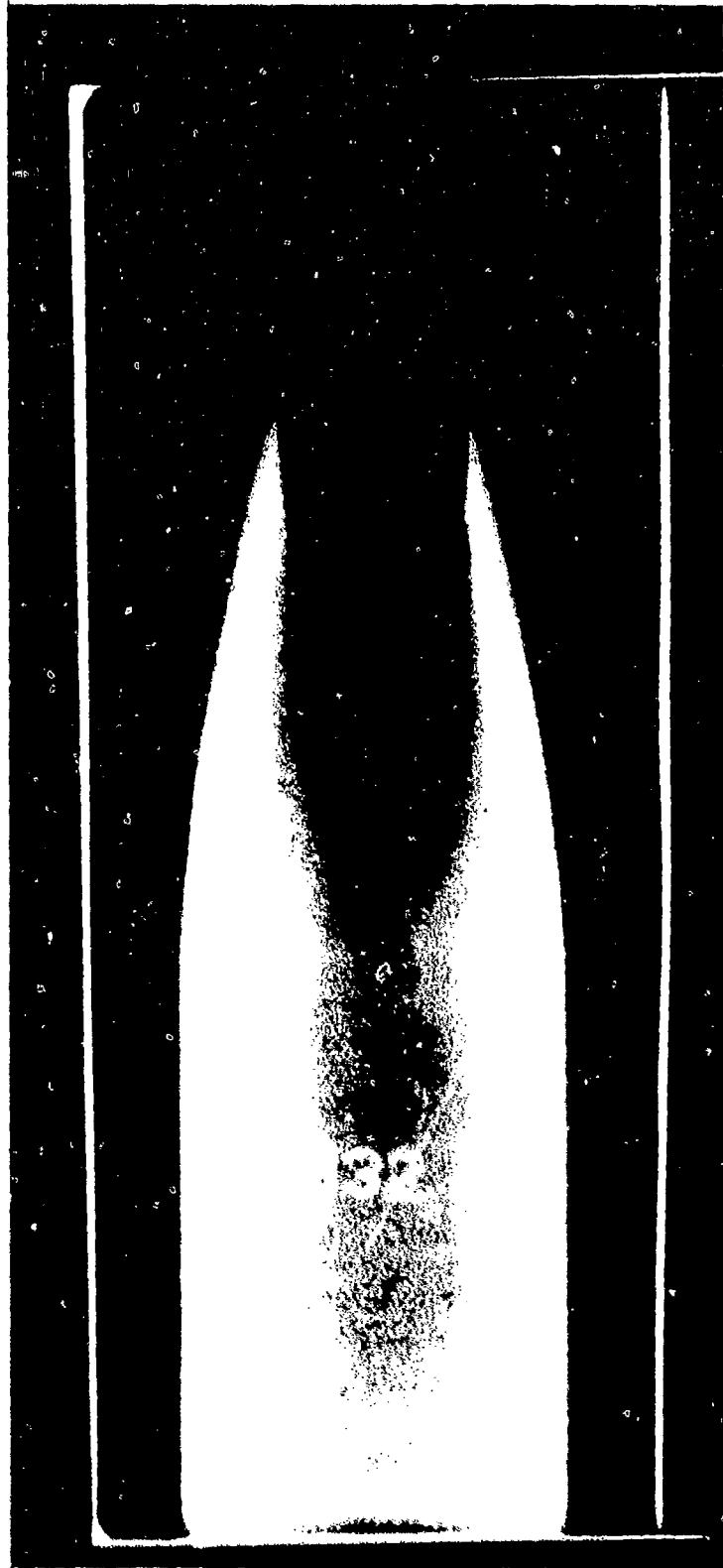
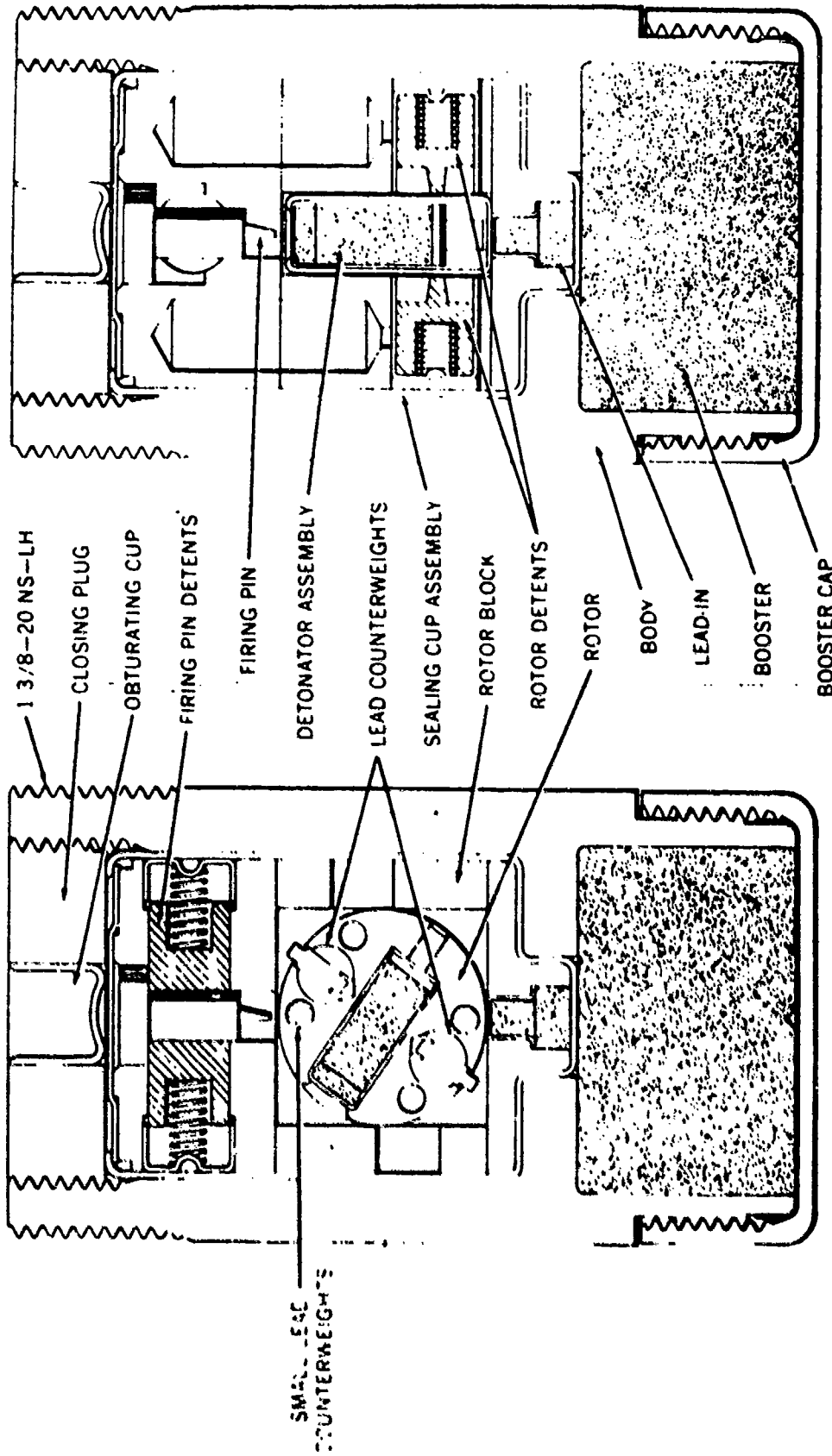


FIGURE 24

Filler movement in nose of Projectile D-2 ($\rho = 1.471$ g/cc, base gap = 0)



ARMED POSITION

ASSEMBLED POSITION

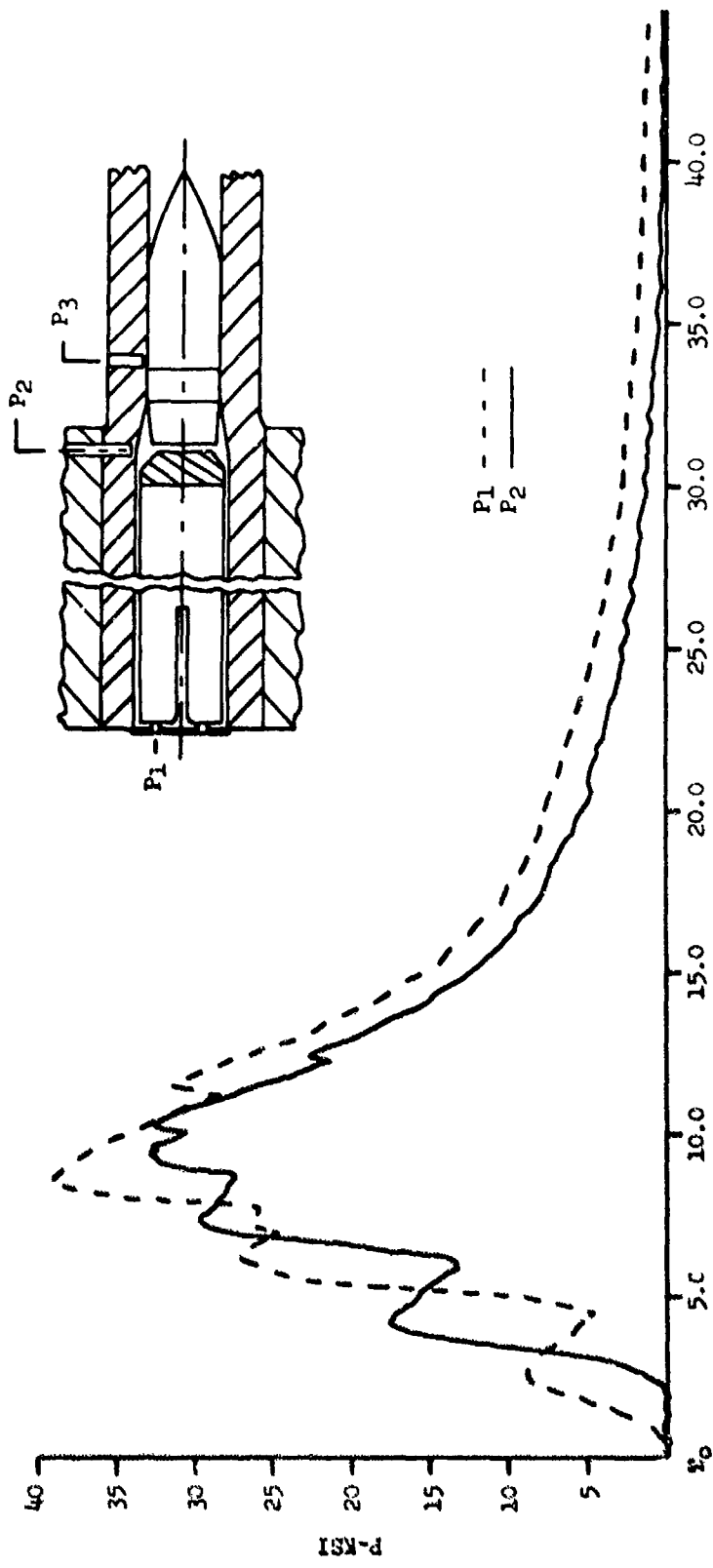
FIGURE 25

reduced charge propelling assemblies exhibited a "chugging" behavior; see Figure 26. The chugging is the result of poor ignition leading to pressure waves traveling through the gas column. In about five out of eight cases these pressure waves became standing shock waves as high as 10,000 psi in magnitude above the fundamental pressure pulse. The "chugging" behavior in conjunction with the base fuze was highly suspect in causing close aboard malfunctions, particularly in view of the fleet premature history.

Further analyses and experimentation with various propellant granulations indicated the observed chugging action was related to initial propellant ignition and subsequent burning. The wave action or chugging was eliminated by replacing the reduced charge propellant with a larger granulation propellant.

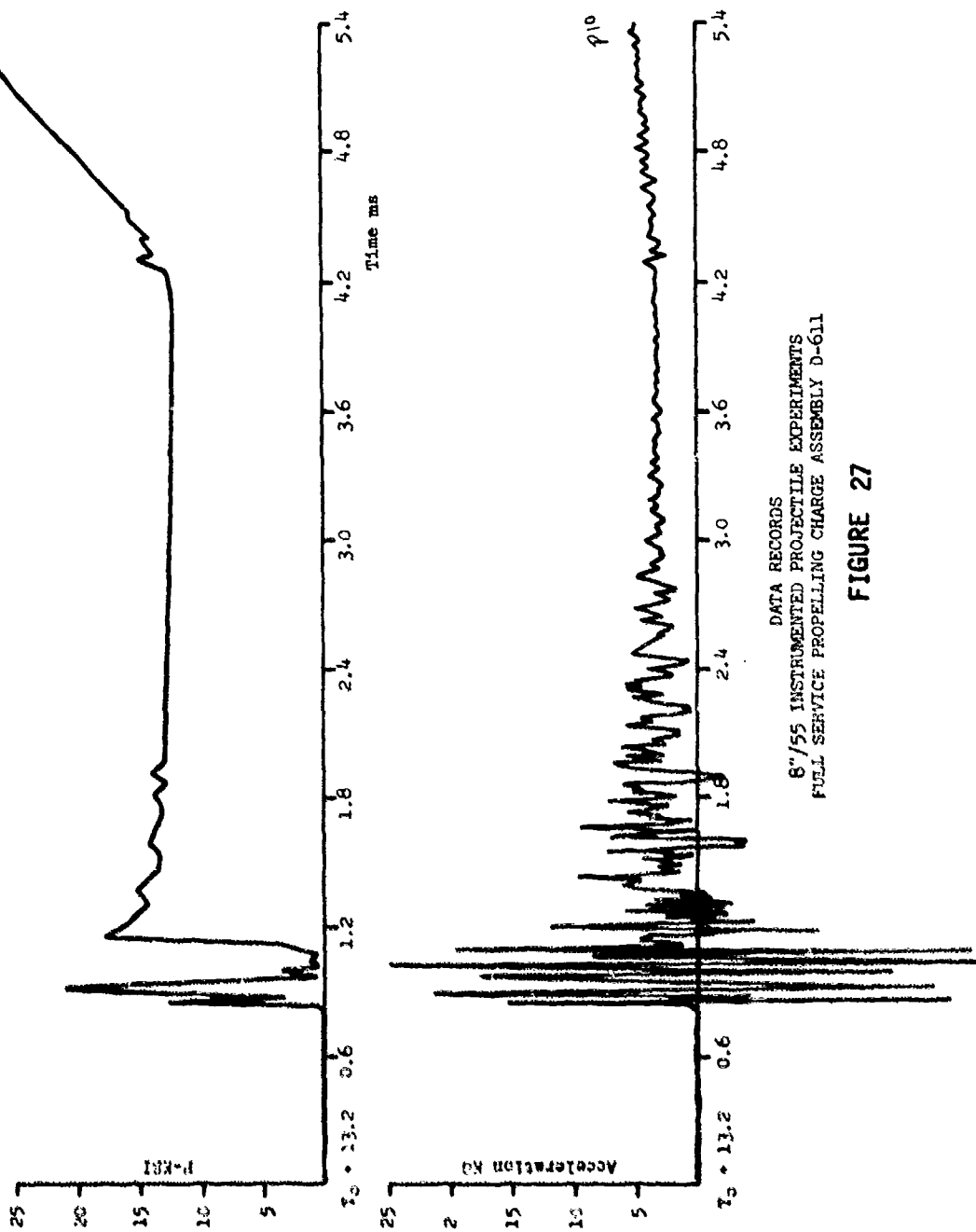
Data obtained from the instrumented projectiles experiments for both the full and reduced charge assemblies (see Figures 27 and 28, respectively, show evidence of cartridge case closure plug impact. However, the measured peak accelerations are about four times greater for the reduced charge propelled round than for the full charge propelled round. The degree of severity of the plug impact depends on the initial burning conditions of the propellant and charge configuration and determines the amplitude of the early time high frequency shocks in the projectile.

Shock Analysis. The computed shock responses, presented in Table III, for the reduced charge are significantly higher than for the full charge at most frequencies, from two to five times as much in the high frequencies



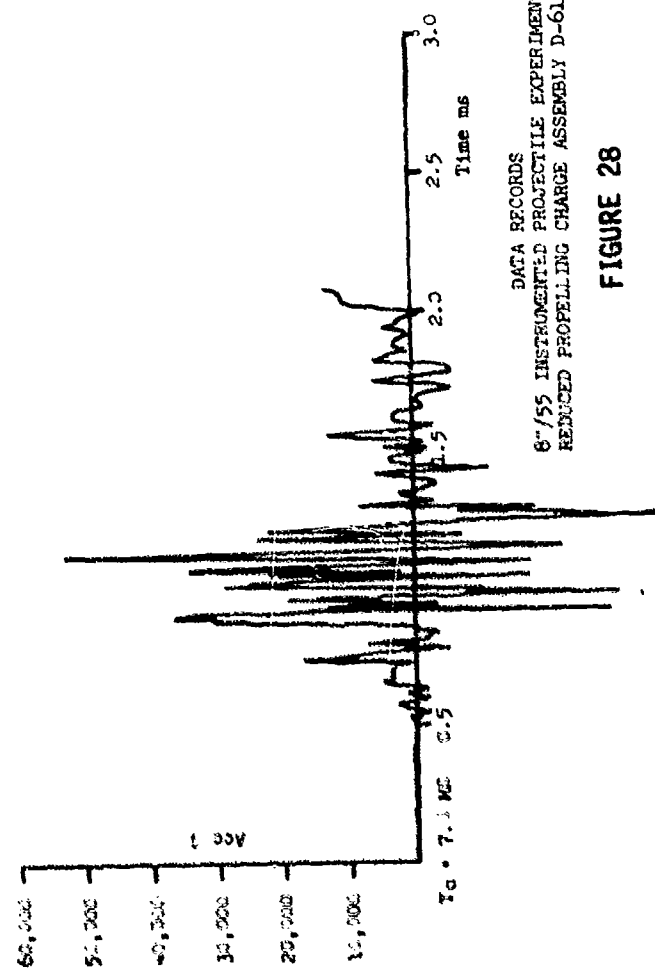
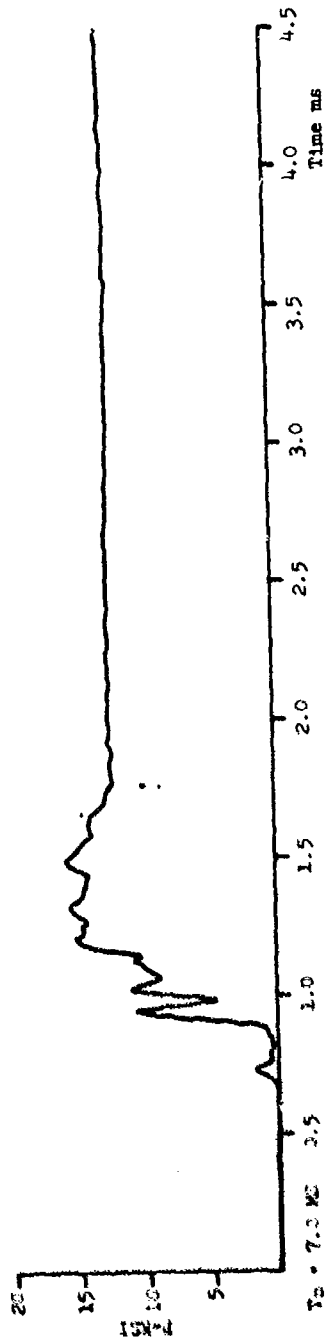
TYPICAL PRESSURE TIME HISTORY D-603/606/612
REDUCED PROPELLING CHARGE ASSEMBLY

FIGURE 26



DATA RECORDS
 8"/55 INSTRUMENTED PROJECTILE EXPERIMENTS
 FULL SERVICE PROPELLING CHARGE ASSEMBLY D-611

FIGURE 27



DATA RECORDS
 87/55 INSTRUMENTED PROJECTILE EXPERIMENTS
 REDUCED PROPELLING CHARGE ASSEMBLY D-612

FIGURE 28

TABLE III

SHOCK RESPONSE SPECTRA - MARK 48 MOD 3 BDF

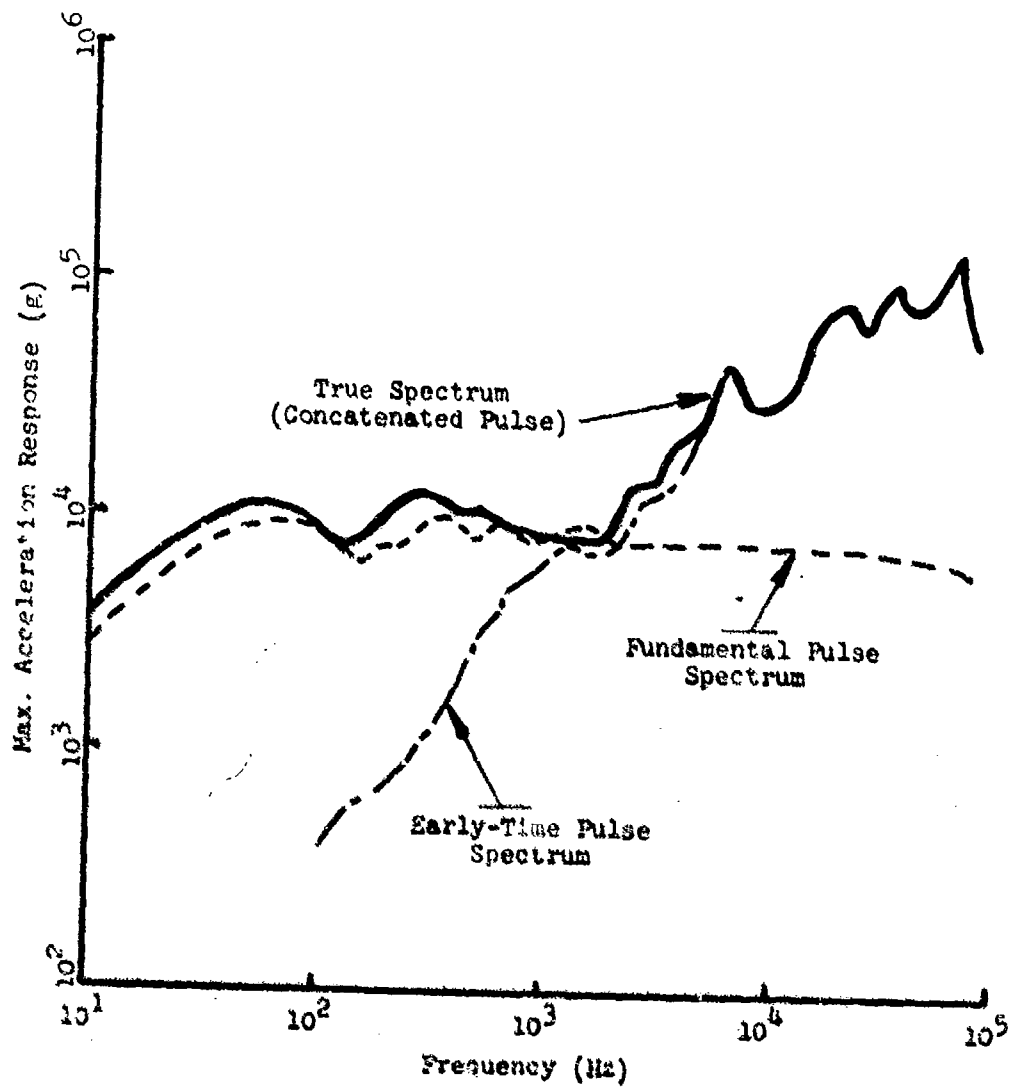
<u>Frequency (Hz)</u>	<u>Service Charge Response Acceleration (g)</u>	<u>Reduced Charge Response Acceleration (g)</u>	<u>Factor*</u>
10	5,131	3,616	0.704
100	9,446	8,083	0.856
1,000	10,300	16,920	1.643
1,995	11,410	13,710	1.201
3,162	14,160	21,500	1.518
5,012	11,070	53,880	4.867
10,000	21,700	83,840	3.865
19,950	52,280	142,800	2.731
31,620	35,510	174,100	4.902
39,810	71,530	157,600	2.203
50,120	62,600	186,500	2.979
63,100	56,400	268,900	4.767
79,430	52,980	160,000	3.020

*Reduced Charge Response/ Service Charge Response

range (3 kHz to 80 kHz). Analyses also indicated that the projectile will be subject to low frequency oscillation in the barrel and may be oscillating several cycles after leaving the barrel. Examination of the physical phenomena involved reveals that the early time high frequency shocks arise from two sources: the impact of the cartridge case closure plug upon the projectile base and subsequent engraving of the rotating band as the projectile enters the rifling. The subsequent low frequency shocks arise from the presence of pressure and standing shock waves in the gas column. Use of the concatenation process to combine both the high and low frequency shock inputs permits computation of the total shock spectrum. A comparison of the total spectrum computed by the concatenation process with early time and fundamental pulse spectra used in earlier analyses of gun setback shock is presented in Figure 29.

Simulation Studies. Results of the plug impact, chugging and out-of-bore drag are presented in Tables IV and V and Figure 30, respectively. These data indicate that either plug impact or chugging, or a combination of both, would sufficiently damage the base fuze anti-creep spring assembly as shown in Figure 31, to permit fuze functioning under low level decelerations of about 3 g's. Such low level decelerations do occur at muzzle exit (out-of-bore drag) and could occur in-bore because of the chugging and resulting projectile oscillations.

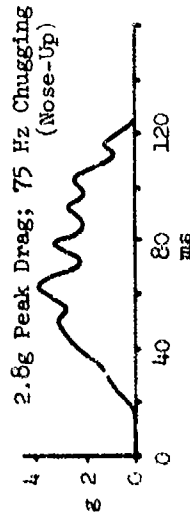
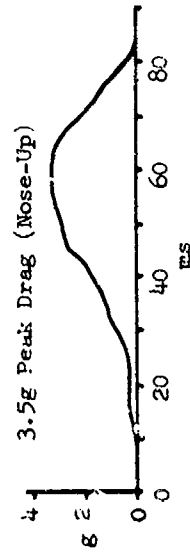
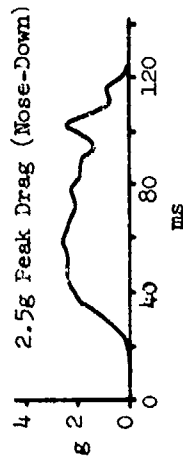
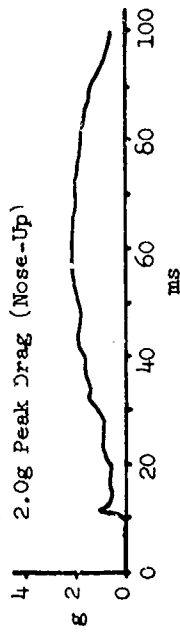
Thus, the ballistic measurements and laboratory tests revealed that the reduced charge assemblies produced a gun environment severe enough to damage base fuze components which degraded the safe-arm integrity of the



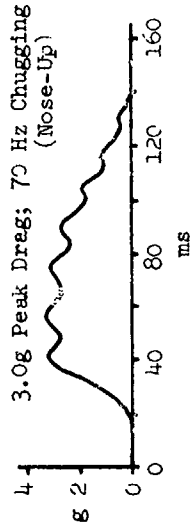
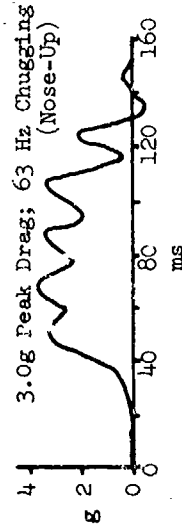
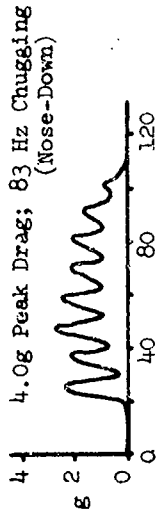
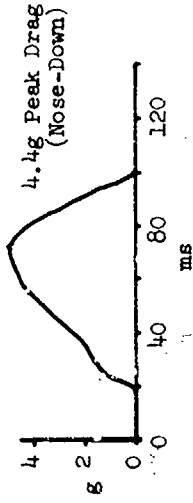
COMPARISON OF PARTIAL SHOCK SPECTRA
WITH TRUE SHOCK SPECTRUM

FIGURE 29

NO PRIMER INDENTATION



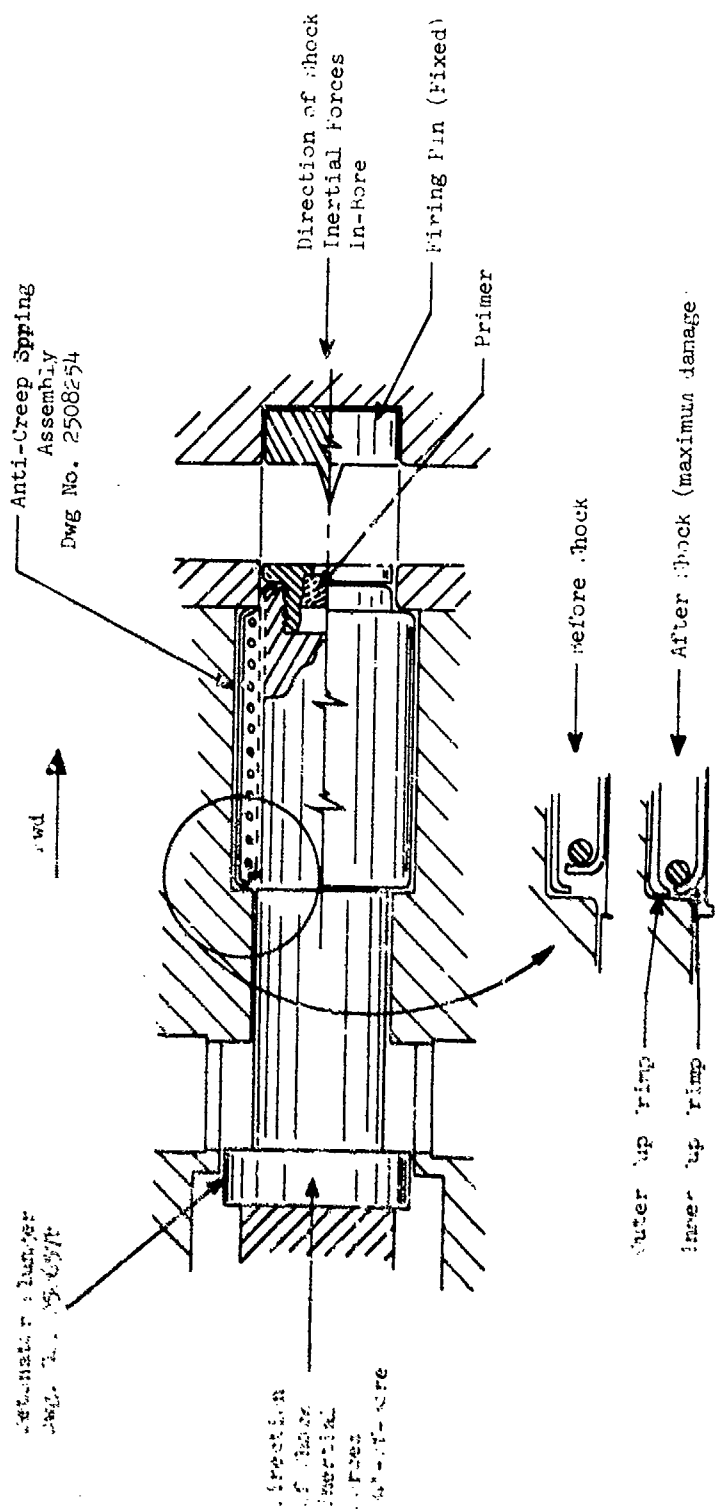
PRIMER INDENTATION



OUT-OF-BORE SHOCK SIMULATION OSCILLOGRAMS

FIGURE 30

view shown in armed mode



ANTI-CREEP SPRING ASSEMBLY (ARMED) - FILING DETAILS

FIGURE 31

TABLE IV
PLUG IMPACT SIMULATION DATA

Fuze No.	Vhg Impact		Anti-Creep Spring Component Elongation ^a (mils)	Estimated Loss in Anti-Creep Spring Force ^a (%)
	Peak (kg)	Type ¹		
1	40 ± 2	Simple	32	19.4
2	40 ± 5	Complex	5	3.06
3	40 ± 5	"	10	6.06
4	40 ± 5	"	22	13.3
5	40 ± 5	"	26	15.8
6	60 ± 10	"	42	39.4

¹See Fig. 7

^aMeasurements made with the plunger and anti-creep spring assembly removed from the fuze. Measurements inside the fuze were not possible.

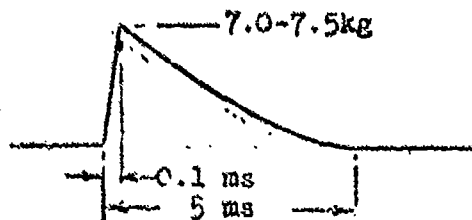
TABLE V

IN-BORE SHOCK SIMULATION DATA

Fuze No.	Plug Impact Shocks (VHg Impact)		Number of Simulated Firing Shocks (Air Gun Shocks ²)	Anti-Creep Spring Component Elongation (mils)	Estimated Loss in Anti-Creep Spring Force (%)
	Peak (kg)	Type ¹			
1	40 ± 3	Simple	3	47	29.7
2	40 ± 5	Complex	3	15	15.2
3	-	-	1	22	12.1
4	40 ± 5	Complex	1	21	3.06
5	40 ± 5	Complex	1	31	12.1
6	-	-	3	28	14.2

¹See Fig. 7

²5-Inch Air Gun smooth shock parameters



fuze to the extent that close-aboard premature projectile explosions were possible.

CONCLUDING REMARKS

In 5"/38 in-bore and 8"/55 close-aboard malfunctions described above, it was shown that the cause of the incidents was the response of the projectile components to the severe shock and dynamic loadings induced by the ballistic environments. To return the subject ammunition to service, two possible courses of action were available. Either the projectile components could be hardened to withstand the existing environment or the detrimental environment would be eliminated. The second course of action was taken as being the most efficacious solution. This solution involved the redesign of the propelling charges to achieve an acceptable ignition and combustion situation.

In the 5"/54 and 8"/55 fuze malfunctions, misassembled fuzes with overly sensitive detonators were implicated. This situation required the X-ray of every round of assembled ammunition at a most inconvenient time--the Easter Offensive in Vietnam. The explosive movement and premature simulator experiments emphasize the importance of the mechanical response of explosives to dynamic loading. The premature simulator has proven an effective tool in evaluating explosive gun-launch sensitivity characteristics.

The detonator sensitivity experiments produced results which reflect upon explosive safety and fuze qualification and acceptance policy. If fuzes are assembled into all-up warheads and these assemblies are subjected to MR-50 type testing, different assemblies may be expected to give different results.

ACKNOWLEDGMENT

By their very nature, ammunition malfunction investigations are interdisciplinary activities involving several stations. Much of the work presented herein would have been far more difficult had it not been for the forthright cooperation provided to the authors by the personnel of the Naval Ordnance Laboratory, White Oak, Silver Spring, Maryland, the Naval Ordnance Station, Indian Head, Maryland, the Naval Weapons Station, Yorktown, Virginia, and the Naval Weapons Station, Concord, California.

REFERENCES

- (1) Culbertson, D. W., Shamblen, M. C., and O'Brasky, J. S., "Investigation of 5" Gun In-Bore Ammunition Malfunctions," Naval Weapons Laboratory Technical Report TR-2624, Dahlgren, Virginia, 1971 (AD 889-970).
- (2) Shamblen, M. C., and O'Brasky, J. S., "Investigation of 8"/55 Close-Aboard Malfunctions," Naval Weapons Laboratory Technical Report TR-2753, Dahlgren, Virginia, 1973.
- (3) Shamblen, M. C., "Investigation of 5"/54 Near Muzzle In-Bore Ammunition Malfunctions," Naval Weapons Laboratory Technical Report TR-2932, 1973.
- (4) Culbertson, D. W., "Investigation of 8"/55 Gun In-Bore Ammunition Malfunction," Naval Weapons Laboratory Technical Report TR-3150, 1974.
- (5) DeVost, V. F., "WOX-5A Accelerometer (Artillery Projectile, Copper-Ball Accelerometer)," Naval Ordnance Laboratory Technical Report 68-85, White Oak, Maryland, 1968.
- (6) Aronica, L., "Sound Velocity and Elastic Moduli Measurements on Several TNT Base Explosive Compositions," NAVORD Report No. 6087, Washington, D. C., 1961.

- (7) Melane, W. W., "Analog Shock Spectrum Analyzer," Naval Ordnance Laboratory Technical Report 67-97, White Oak, Maryland, 1967.
- (8) Reed, R. S., "A digital Computer Program for the Analysis of Wave-Form Data (Multi-Record Wave Investigation for Sine and Random Data - MR WISARD)," Naval Ordnance Laboratory Technical Report 69-38, White Oak, Maryland, 1969.
- (9) Soper, W. G., "Ignition Waves in Gun Chambers," Combustion and Flame 20, 157-162, 1973.
- (10) DeVost, V. F., "VHg Impact Test Set (Design Task Report)", Naval Ordnance Laboratory Technical Report 68-158, White Oak, Maryland, 1968.
- (11) Fisher, J. C., "NOL Shock Testing Facilities," Naval Ordnance Laboratory Report 1056, Third Rev., White Oak, Maryland, 1967.
- (12) NOL Technical Report NOLTR 72-190, 27 July 1972.
- (13) Schimmel, R. T., and Weintraub, G., "Effect of Base Separation and Loading Density on the Setback Sensitivity of Composition A-3," Picatinny Arsenal Technical Report 4147, Dover, New Jersey, 1970.

ABSTRACT

DIPOLE WEST was a series of eleven high explosive experiments conducted by Ballistic Research Laboratories at the Defense Research Establishment, Suffield, in Alberta, Canada, during the summer and fall of 1973. Two of the experiments involved detonation of single, 1080-pound charges; the remaining nine experiments consisted of two 1080-pound charges for each event, detonated simultaneously to within five microseconds. Both pentolite and TNT charges were used.

Purpose of the series was to obtain information on the interaction of shock waves with a real, as contrasted with an ideal, reflecting surface. Results are to be used to modify hydrodynamic airblast codes. An additional purpose was to study fireball interaction and torus formation under double-burst conditions.

Density, particle velocity, stagnation pressure and overpressure were measured at and near the ground surface as well as at and near the ideal reflecting plane (midway between charges). Measurement techniques included pressure transducers, time-of-arrival detectors, high speed photography and late-time aerial photography.

I. OBJECTIVES

The objectives of the DIPOLE WEST experiments were to examine the air blast phenomenology of strong shock on shock, shock on fireball, and fireball flow interactions from the simultaneous detonation of multiple (two) high explosive charges. Because the only method of studying such phenomena in the past has been through theoretical hydrodynamic calculations, major emphasis was given to comparison of the empirical data with calculations. Subsequent upgrading of the computer codes to incorporate realistic boundary conditions is anticipated.

The two parts of the experiment (the horizontal charge separation events and the vertical charge separation events) had somewhat different emphases. The horizontal array was designed to examine:

- 1) The effect of a shock wave on fireball deformation.
- 2) The effect of a shock wave on fireball rise characteristics.

- 3) The effect of neighboring fireball flow fields on fireball rise and expansion.

These effects were to be studied as a function of separation distance and shock strength; the large height of burst (125 feet) was sufficient that effects of shock reflections from the ground could be ignored. In addition, horizontal charge separation events provided a unique opportunity for the detailed study of interactions of three-dimensional shock waves.

The vertical array was designed to examine:

- 1) Shock wave interactions with real and ideal reflecting surfaces.
- 2) The effect of a hard, smooth surface versus that of a rough, soft surface on shock wave interaction.
- 3) Shock fireball interactions and fireball growth and rise.
- 4) The effect of charge orientation by comparison with horizontal arrays having the same separation distance.

Blast parameters of interest for the study were overpressure, overpressure impulse, dynamic pressure, dynamic pressure impulse, propagation velocity, Mach stem formation, and density.

II. OPERATIONAL PLAN

Operations for the DIPOLE WEST experiment began in the late winter and early spring months of 1973. A visual survey of the area was carried out followed by final selection of the site. Contractual arrangements for explosive casting were made with Canadian Arsenals of Montreal. By June, the assessment of the environment was complete, the field survey was finished, and erection of the towers and site construction had begun.

An environmental assessment of the impact of the DIPOLE WEST experiment on the environment was carried out. The conclusions presented were:

- 1) The test will have no significant adverse environmental impact, including very little impact on ecological systems and no impact on endangered species.
- 2) The test preparatory activities will have no more than minor environmental impacts that will be short-lived.

Pertinent details of the assessment, which are published in Reference 1.

A. Project Description

Project DIPOLE WEST consisted of eleven individual tests using spherical, high explosive charges cast of pentolite or TNT in a nominal weight of 1080 pounds. Two charges were simultaneously detonated (to within five microseconds) for nine of the tests; two tests consisted of single charges to provide calibration information and to provide data for comparisons with the multiple bursts. Shots 1 through 6 were fired as parts of the horizontally arrayed series, as presented in Table 1. Charge suspension heights varied from 124 feet to 134 feet, with separation distances of 50 feet, 100 feet, and 165 feet. The prairie soil on the surface was in its natural, hard-packed condition. Shots 7 through 11 were fired as part of the vertically arrayed series, as presented in Table 2. Charge separation distances were 50 feet and 30 feet, with the lower charge at heights of 25 feet and 15 feet for the two separation distances respectively. Ground condition for shots 7 through 9 was that of natural, hard-packed, smooth prairie soil. For shots 10 and 11, a rough, soft, absorbent surface was created by furrowing the soil out to a ground range of 230 feet. Distance between furrows was 14 inches. The average depth of the furrows was also 14 inches.

B. Site Selection

An ideal area to fit all requirements would need to be level from the main camera position across the layout to the backdrop. However, such level areas are not readily available in the south part of the DRES range to which these operations are now restricted. After a preliminary survey, an area was selected 12 miles east of the DRES main laboratory. This area was extensively examined and surveyed to determine the ground conditions in detail and to ensure that lines of sight from the main camera position would provide adequate coverage of all areas of main interest in shock phenomena against the canvas backdrop and smoke puff array. The field layout of the site is shown in Figures 1 and 2.

The gun barrels used in previous blast trials at DRES were installed at the DIPOLE WEST site as instrument mounts for elevated pressure gage measurements. The barrels were lengthened by the addition of 6-inch diameter, 0.432-inch wall thickness "extra heavy" pipe. The welding and machine work for this addition and the drilling required for eleven

pressure gage positions and twelve ABTOAD (Air Blast Time of Arrival Detector) positions on each barrel was done by the DRES experimental model shop.

C. Charge Suspension

The charges were suspended over ground zero by cable between two 200-foot towers. The towers were the commercially available aluminum collapsible, walk-up style. They were placed 400 feet apart with ground zero midway between them. The 5/8-inch wire cable was stretched between the tops of the towers with the ends run through pulleys. Additional pulleys at ground level were anchored in concrete bases. A stationary winch at a position 600 feet south of ground zero provided power for raising the charges.

Figure 3 is a diagram of the horizontal array charge handling system; Figure 4 is a similar diagram for the vertical array system, showing in addition the position of the smoke puff grid. A 3/4-inch manila rope net surrounding each charge was coupled to the desired length of cable and then attached to the 5/8-inch overhead supporting and hoisting cable. In the later vertical array shots, the use of the manila rope net was abandoned because of its bulk. It was replaced by a "seat belt" strap sling arrangement made from nylon webbing 2 inches wide. This system provided a clearer space between the two charges. Raising or lowering the charges was quite easily carried out with the winch system as described above. All charges were armed on the ground and then raised to the height desired. As the charges were raised by the power winch, their positions were monitored from two survey points. When the specified elevations were reached, tethering ropes attached to the charges were secured and a final position survey was taken.

The firing cable dropped straight from the charges to the ground and from there ran directly to the firing box, which was located some 200 feet from ground zero. Control lines from the firing box led directly back to the DRES control bunker.

D. Explosive Casting

The original plan called for spherical TNT charges similar to those used in the 1969 height of burst trials; these charges were produced at Suffield using the DRES plant, molds, equipment, and the same casting techniques that had been used for the previous height of burst trials.

The weight of these TNT spheres was determined by subtracting the amount of TNT remaining after the mold was filled from that originally used. Two separate determinations resulted in an average weight figure of 1080 pounds.

Later, as the program expanded, it was decided that use of pentolite, rather than TNT, would reduce the probability of jetting or similar anomalies in detonation. The firm of Canadian Arsenals Limited, St. Paul L'Ermite, cast the pentolite charges.

III. DATA ACQUISITION SYSTEMS

The systems used to acquire data on DIPOLE WEST were of two general types:

- 1) Systems for recording signals from sensors placed in the blast field.
- 2) Hi-speed cameras for recording smoke puff trajectories and the passage of the shock front over the back drop system.

A. Blast Sensor Instrumentation

Electronic overpressure transducers, electronic stagnation pressure transducers, mechanical self-recording overpressure transducers, and air blast time of arrival detectors (ABTOADS) were placed in the blast field.

1. Overpressure and Stagnation Pressure. The basic units of the pressure data acquisition system for shots 1 through 6 were 14-channel magnetic tape recorders (two Bell & Howell VR-3300's). Eleven channels on each recorder were used for wide-band (dc to 20 kHz) fm recording of data, one channel was used for a multiplexed signal of time reference and time zero, one channel was used for time zero only, and one channel recorded an IRIG B time signal. Reproduction heads and associated electronics were part of the VR-3300 machines. B & F Instruments Model 1-700 signal conditioning equipment was used to supply gage excitation, bridge balancing, and remote shunt calibration. A single step remote shunt calibration was used to detect system gain changes. CEC 1-165 amplifiers were used to amplify the transducer output signal to the level required as input for the fm recording amplifiers. The systems were housed in a

recording van. The DRES control bunker equipment supplied timing signals for the remote operation of the recorders.

The basic units of the pressure data acquisition system for shots 7 through 11 were 32-track magnetic tape recorders (two Sangamo 4784's and two Bell & Howell VR-2800's). Twenty-two channels on each Sangamo were used for recording at a frequency response of dc to 80 kHz, six channels were used for direct recording (400 Hz to 600 kHz) of ABTOAD signals, one channel was used for time zero, one channel for the multiplexed time reference and time zero signals, one channel for IRIG B time, and one channel for a 200 kHz speed reference. Twenty-nine channels on each VR-2800 were used for fm recording (dc to 20 kHz), one channel was used for time zero, one channel for the multiplexed time reference and time zero signals, and one channel for IRIG B. B & F instruments Model 1-700 signal conditioning were used to supply gage excitation, bridge balancing, and remote shunt calibration as for the earlier events. A single step remote calibration was used to detect system gain changes. Newport Laboratories Model 60 dc amplifiers (dc to 100 kHz) were used with the Sangamo 4784 recorders, and CEC 1-165 dc amplifiers (dc to 20 kHz) were used with the VR-2800 systems to amplify the transducer output signals to the required level for the fm recording amplifiers. Manual supervision of the remote operation of the recorders was provided at the DRES control bunker, as it was for the first group of shots.

The Bytrex Model HFG pressure transducer was used in the electronic systems for both overpressure and stagnation pressure measurements. This transducer has a four-arm Wheatstone bridge with two active semiconductor arms and two dummy arms. The semiconductor strain gages are bonded to a force summing column, which is in turn attached to a force collecting diaphragm. The basic configuration is that of a 1 1/8-inch threaded cylinder, three inches long, with a shield over the sensitive area for the diaphragm to protect it from thermal radiation and debris. The transducer is operated with a constant excitation of 20 volts dc and a nominal full scale output of 100 millivolts. The natural frequency of the gage varies from 30 to 80 kHz, depending upon pressure range.

The pressure transducers were mounted on the gun barrels with U-shaped brackets. The bracket arms extended two feet from the barrels so that the measurement points were not perturbed by the barrel. A side-on overpressure gage was mounted on one side with an 18-inch diameter steel

baffle plate. A stagnation pressure gage within a probe was attached to the other side of the U-mount. Surface gages were installed in specially prepared concrete blocks similar to those used in earlier experiments (Reference 2).

The Bytrex gages were statically calibrated in their mounted positions. For calibration, pressure was applied to each gage in six equal steps, ranging from 20% to 120% of a predetermined 100% calibration level. Bottled nitrogen was used as the pressure source. The predicted peak pressure fell between the 80% and 100% level in each case. The linearity was checked and a shunt resistor was added which reproduced the 100% level. This shunt calibration was used as a system gain check a few seconds before actual data acquisition. All gages were recalibrated if it became necessary to move or remount them for any reason. Dynamic testing of the gages was performed in shock tubes at BRL prior to their use in the field.

2. Mechanical Overpressure-Time Gages. Mechanical self-recording overpressure-time gages were used in the low pressure region. These gages, which were developed at BRL, have a flexible diaphragm as the pressure sensing medium. The diaphragm is basically a convoluted flexure disc welded into an interchangeable mount. A recording stylus attached to the diaphragm records its deflection on a moving micro-honed stainless steel regulator spring. A fixed stylus on the diaphragm mount provides a reference position. A third stylus records a time trace (100 Hz) supplied by a generator within the gage. The recording spring also serves as the motor. It is controlled to travel at a rate of 3 inches per second. The gage is activated by means of an externally supplied signal. An arming switch is located on the upper surface of the gage housing. A static calibration is given each sensor before using it in the field.

3. ABTOADs. The ABTOADs were used to determine arrival times of the primary shock waves. Designed and developed by DRES (Reference 3), the detector systems were borrowed from DRES for use on DIPOLE WEST.

ABTOADs were mounted on all four gun barrels. There were twelve ABTOAD units on each gun barrel, four near the ground and eight in an upper region. The lower region ABTOADs were spaced at one-foot intervals from one to four feet above the ground. The upper region ABTOADs were spaced at one-foot intervals from 46 to 53 feet above the ground. The

lower region ABTOADs were used to check arrival times of the Mach stem; those in the upper region provided information in the area of the reflection plane for shots 7, 8, and 11, for which this reflection plane was expected to occur at 50 feet.

B. Photographic Instrumentation

Provisions for shock profile and shock wave radius-time studies by photo-optical means were made by setting up a backdrop line against which the shock wave could be photographed. The backdrop line began at a point on the MCP-GZ (Main Camera Position - Ground Zero) line 400 feet from GZ on the side away from the MCP (Figure 2). It extended along a line making an angle of 80° to the MCP-GZ line to a distance of 325 feet. Ten 30×50 -foot polka dot pattern canvas drops, like those used on previous large scale trials at DRES, were employed through shot 8. During preparations for shot 9, the polka dot backdrops were severely damaged in a freakish wind storm. Replacements were made from stripe pattern drops in the DRES inventory for shots 9 through 11.

For particle trajectory analysis, a smoke puff grid was produced by firing charges in an established pattern (Reference 4). The smoke puffs were placed along a line which passed through ground zero and made an angle of 80° with the MCP-GZ line on the opposite side from the backdrop line. Twenty drops (vertical lines of smoke puffs) were used for shots 7 and 8, sixteen were used for shot 11, and nine for shots 9 and 10. Vertical spacing of the puffs was five feet, starting at three feet above the ground and extending through 58 feet. There were thus a total of twelve smoke puffs per drop. Horizontal spacing varied. For shots 7, 8 and 11 (25 and 75-foot heights of burst) the smoke puff drops began at 25 feet from ground zero with 10-foot spacing. At 45 feet from GZ the spacing changed to 7 feet, and then again to 5 feet at 80 feet from GZ. For shots 9 and 10 (15 and 45-foot heights of burst) the same spacing was used, except that in this case only the first nine drops were placed. White smoke puffs were used for the lower six stations on each drop for contrast with the prairie background, while red smoke puffs were used at the higher positions for contrast with the sky.

IV. DATA REDUCTION

A. Photo-Optical Analysis

The data analysis for the photo-optical results is being carried out by Professor John Dewey at the University of Victoria, British Columbia. Basic film reading equipment is now available there and the necessary computer program analysis systems have been developed.

1. Shock Front Trajectories. A computer program, REDUCE, has been written for the shock wave analysis and tested with data from the 1969 Height-of-Burst series. This program provides geometrical scaling in terms of the surveyed positions of the camera, charges, and photomarkers, and reduces the photogrammetric shock wave data to distance-time values. A further geometrical correction is required because the shock front trajectory viewed from a fixed camera position lies along the semicircular path for which the camera-GZ line is a diameter.

The resulting shock radius-time (R-t) data is then fitted by a least squares program to a curve of the form

$$R = A + Bt + C \ln(1 + t) + D \sqrt{\ln(1 + t)}.$$

The data are weighted inversely with observed radius so as to obtain a fit with constant percentage error throughout the range of the input data. Outputs from this second program, SHOCK, are fitted shock radius values, scaled times and distances, shock velocity, peak particle velocity, peak overpressure (in both atm and psi), and peak density ratio. The program also provides Calcomp graphic display of the output.

The above ad hoc equation has been found valuable for describing a wide variety of monotonically decaying shocks. It satisfies two appropriate boundary conditions; namely, that at $t = 0$ the shock radius may have a positive or negative finite value, and that as $t \rightarrow \infty$ the shock velocity asymptotically approaches the ambient sound velocity. A section of film taken of one of the 1969 tests has been processed with these programs, and results compare favorably with Brode's theoretical calculations for a spherical TNT explosion (Reference 5).

Graphs of overpressure versus distance will be constructed from the DIPOLE WEST photographic data. These will be compared with the pressure transducer measurements as well as with theoretical models.

2. Particle Trajectory Analysis. The program for the evaluation of the particle trajectories was developed by Dewey and is somewhat more involved than that for the shocks, and is still under active development. The principle for the analysis is as follows:

From the film records, the initial coordinates (x_0, y_0) and the coordinates (x, y) at any time t , are measured for each smoke puff. These data are then fitted to functions of the form

$$x = X(x_0, y_0, t) \text{ and } y = Y(x_0, y_0, t).$$

The velocity components at any time or position in the flow field are then obtained from

$$u = \frac{\partial X}{\partial t} \text{ and } v = \frac{\partial Y}{\partial t}.$$

The density field is given by

$$\frac{\rho_0}{\rho} = \left(\frac{x}{x_0} \right) \begin{vmatrix} \frac{\partial X}{\partial x_0} & \frac{\partial Y}{\partial x_0} \\ \frac{\partial X}{\partial y_0} & \frac{\partial Y}{\partial y_0} \end{vmatrix}$$

This analytical technique is now being successfully applied to laboratory data obtained from Mach reflections in shock tube flows.

B. Pressure Transducer and ABTOAD Data

Digitization and plotting of air blast pressures recorded on magnetic tape were carried out by the Albuquerque office of GE-TEMPO, using equipment, personnel, and computer programs available at Air Force Weapons Laboratory (AFWL). The 14-track tapes used for Shots 1 through 6 could be handled directly. The 32-track tapes used for Shots 7 through 11 were first taken to the DNA Playback Center at Nevada Test Site, where they were dubbed to 14-track format before being brought to Albuquerque.

First, the calibration tapes made prior to each shot were digitized and the digits were listed. These tapes contain comparisons between the pressure calibrations and the electronic or shunt calibrations. The digitized calibration levels were averaged and compared by hand. In all cases the shunt calibration was within three percent of the pressure calibration, and in most cases it was within one percent.

The pressure equivalents of the shunt calibrations were punched on cards, along with sampling rates, titles, and other required information. Data from events 1 through 6 were sampled at 100 kilosamples/second. For Shots 7 through 11, data from the Sangamo recorders (designated on the plot titles as systems one and two) were sampled at 400 kilosamples/second and data from the Bell & Howell VR-2800's (systems three and four) were sampled at 200 kilosamples/second. AFWL then prepared a computer tape containing digitized shunt calibration and data files for each channel. Information from the cards appears as a header on each file on this tape.

The direct recorded ABTOAD and time zero signals were handled in the same way. The time zero files were listed so that times from start of digitizing to time zero could be determined accurately.

Next, the digitized data were run through a computer program, ADDGEN3, which equilibrates the pressure from the header information to the shunt calibration level and then applies this to the data file for each channel. Outputs from ADDGEN3 are large working plots and "engineering unit" (EU) computer tapes. The EU tapes were used, finally, as input to another computer program, ROTATE, which prepares the small plots. The EU tapes were also used for calculation of Mach Numbers and dynamic pressures from the overpressure and total pressure records.

V. RESULTS

The eleven tests of the DIPOLE WEST series were successfully carried out between 6 July and 8 November 1973, using the same basic layout for all shots. Presented in Tables 3 and 4 are the firing data and environmental conditions for each of the shots. Fireball anomalies of very minor significance were observed on all the shots. Most of these anomalies occurred in directions which did not affect the instrumentation. An exception to this was Shot 7, in which a jet traveled out directly along the gage line.

A single pentolite charge, fired successfully on July 6, 1973, was the first of the eleven shot series. This calibration shot served to check out the dynamic response of the instrumentation, as well as to provide data from a single charge that could be compared with the double charge data. This single pentolite charge produced a symmetrical fireball and classical, exponentially decaying pressure-time histories. Comparisons

of the pressure-time waveforms recorded at 50 feet north of GZ with those recorded at 50 feet south are shown in Figure 5.

The second shot was the first of four double burst events in the horizontal array part of the series. The two charges for each of these events were approximately the same distance above the surface. For Shots 2 and 3 the TNT charges were approximately two, and one fireball radii apart. The measured air blast parameters along the ground surface are plotted in Figures 6 and 7. A Mach stem was formed on the ideal reflecting plane (the ideal reflecting plane was in the vertical plane midway between the two charges). Depending upon the charge separation distance and the location of the stations in relation to the gage centerline some gage stations were in the Mach region and some were in the regular reflection region. Thus pressures on Shot 2 measured at the ground along the center of the gage line were higher than those measured ten feet to either side. This is shown in Figure 6, where pressures for the stations at 20, 30, and 40 feet are noticeably below those measured at other stations. On Shot 3, the charges were closer together, 1 charge radii, resulting in the Mach stem on the ideal reflecting plane growing faster than on Shot 2. For Shot 4, agreement between the pressure time records obtained at the two points on the ground 82.5 feet north and south of GZ was excellent, as illustrated in Figure 8.

The air blast parameters at ground level for Shot 5 are plotted in Figure 9. With a 100-foot separation between charges, the growth of the Mach stem away from the ideal reflecting plane is relatively slow, and the data indeed show that the Mach stem had not reached a height of ten feet, or maybe more correctly a width of 20 feet, when it arrived at the 20 and 30-foot ground stations. These stations, as previously mentioned, were off-set ten feet from the reflection plane and were in the regular reflection region. The incident and reflected waves at these stations are clearly shown in the records. The blast parameters for Shot 6 are plotted in Figure 10. The only surprise was the maximum overpressure at 90 feet along the surface was 15% lower than expected. This single TNT charge produced a relatively symmetrical fireball and classical, exponentially decaying pressure-time wave forms.

The quality of records from the seventy-eight channels of electronic overpressure and total head pressure instrumentation fielded on Shot 7 was good, even though the anomaly along the gage line produced some unusual features. The influence of the jetting is evident near the ground surface and near the ideal reflecting plane at 50 feet.

Good pressure time information was also obtained from Shots 8 and 9. The air blast parameters are plotted in Figures 11 and 12. As mentioned previously, Shot 9 data was recorded without a zero time reference. Quality of data was otherwise good.

For Shots 10 and 11 over the soft rough surface good pressure time data was recorded as shown in Figures 13 and 14. The arrival time over the roughened surface was longer as shown in Figure 15. The overpressures over the rough real surface was lower than over the ideal reflection surface.

VI. DISCUSSION OF RESULTS

The pressure pulse from the DIPOLE WEST vertically arrayed charges appeared, at the close-in ground surface gage stations, as though it had been produced by a single 1080-pound charge. In Figures 16 and 17, data from the TNT height-of-burst series, conducted in 1969 at DRES, have been scaled to correspond to 1080 and 2160-pound pentolite charge data for comparison with DIPOLE WEST. DIPOLE WEST Shots 8 and 11 pressure records begin to look like those from a 2160-pound charge at 10 psi, while on Shots 9 and 10, the height-of-burst of the lower charge was lower and the separation less so the transfer takes place sooner, at 35 psi.

Shot 6 of the horizontally arrayed series was a single TNT shot at a height-of-burst of 133.7 feet. This event provided, as a secondary benefit, data for the height-of-burst charts developed from the 1969 series.

Diagrams of the progression of the paths of the triple points are presented in Figure 18 for the vertically arrayed Shots 8 and 11. As previously noted, the Mach region from the ideal reflecting plane was almost the same for shots with similar heights of burst. The gage results correlated well with those obtained by photographic means. A slower developing Mach stem was observed at the real surface as a result of the soft, rough ground condition.

Calculated triple point paths are also shown for the 25-foot HOB configuration. These paths are the same because the surfaces were treated identically (in fact, the prediction was constructed from symmetry arguments from a single burst calculation). In order to predict real surface triple point paths, some type of real surface modeling will have to be included in the code. One probable modification is to allow the surface to absorb energy as the shock wave passes over it. How much energy different types of surfaces may be expected to absorb is one of the questions that analysis of the present results is expected to answer.

VII. CONCLUSIONS AND RECOMMENDATIONS

Experimental data was successfully acquired on the rise and expansion of fireballs and on the interactions of shock waves generated by multiple bursts in horizontal and vertical arrays. The path of the triple point and the Mach stem region were identified for two types of real reflecting surfaces and for an ideal reflecting surface at heights of burst of 15 and 25 feet.

Differences in shock wave arrival time and maximum overpressure measured at various points are seen to exist depending on whether the ground surface is hard and smooth or soft and rough. These differences appear to be small, however, and this may indicate that the method used for softening and roughening the surface was not adequate.

Blast parameters such as dynamic pressure, dynamic pressure impulse, particle velocity, and density were undergoing data processing at the time this paper was written and hence were not available for analysis. Limited initial comparisons with theoretical calculations show good correlation, however. Further conclusions must await analysis of the final data.

In light of present knowledge, the following recommendations are made:

- 1) Additional experiments should be conducted with double bursts to allow for further examination of multiburst phenomena. Areas of interest are the examination of scaling relationships and the evaluation of short duration flows over different ground surfaces.
- 2) Multiburst experiments with different sized charges and/or non-simultaneous detonation should be considered.

- 3) Data gaps in the HOB chart above 7.2 feet (scaled to one-pound charges) should be filled by detonating small charges at high levels.

REFERENCES

1. "Environmental Impact Assessment of DIPOLE WEST" General Electric Company, TEMPO, Santa Barbara, California 93102, 30 May, 1973.
2. "Basic Air Blast Studies" Operation Snowball Project Description Vol. 1 by R. E. Reisler, US Army Ballistic Research Laboratories, DASA 1516-1, July 1964.
3. "A Pressure Switch System for Detecting the Arrival of a Shock Front" by F. H. Winfield and others, Suffield Technical Note No. 135, June 1964.
4. "Statically Oriented Smoke - Puff Grids" by B. J. Holsgrove and R. A. Klymchuk, DRES Suffield Technical Paper No. 352 Defence Research Establishment Suffield, Ralston, Alberta, September 1970.
5. "A Calculation of the Blast Wave from a Spherical Charge of TNT" by H. L. Brode, Rand Corporation RM-1965.
6. "The Air Velocity and Density in Blast Waves from TNT Explosives" by J. M. Dewey, Suffield Report No. 207, June 1964.
7. "The Air Velocity in Blast Waves" by J. M. Dewey, Proceeding of the Royal Society, Pages 366-385, 1964.

Table 1. Shot Schedule and Conditions; Horizontally Arrayed Series

Shot No.	Date Fired	Total Charge Weight (lbs)	No. and Material of Charges	Distance Between Charges (ft)	Heights of Burst (ft)		Ground Surface Condition
					1st	2nd	
1	6 July 73	1080	1 Pent	-	124.21	-	Hard, smooth
2	12 July 73	2172	2 TNT	100.61	126.10	125.68	Hard, smooth
3	18 July 73	2172	2 TNT	49.72	128.05	127.92	Hard, smooth
4	24 July 73	2172	2 TNT	165.55	131.99	131.69	Hard, smooth
5	26 July 73	2160	2 Pent	100.15	129.19	128.46	Hard, smooth
6	31 July 73	1086	1 TNT	-	133.71	-	Hard, smooth

Table 2. Shot Schedule and Conditions; Vertically Arrayed Series

Shot No.	Date Fired	Total Charge Weight (lbs)	No. and Material of Charges	Distance Between Charges (ft)	Heights of Burst (ft)		Ground Surface Condition
					1st	2nd	
7	4 Sept 73	2160	2 Pent	46.73	72.19	25.46	Hard, smooth
8	17 Sept 73	2160	2 Pent	49.86	74.31	24.45	Hard, smooth
9	22 Oct 73	2160	2 Pent	30.30	45.45	15.15	Hard, smooth
10	2 Nov 73	2160	2 Pent	30.54	45.46	14.92	Soft, rough
11	8 Nov 73	2160	2 Pent	50.13	74.12	23.99	Soft, rough

Table 3. Firing Data and Environmental Conditions, Shots 1 through 6
Horizontal Array

Shot Number	1	2	3	4	5	6
Firing Date	6 July	12 July	18 July	24 July	26 July	31 July
Firing Time	1430 MDT	0730 MDT	1050 MDT	1704 MDT	1650 MDT	1720 MDT
HOB (Ft.)	124.21	125.68 126.10	127.92 128.05	131.69 131.99	128.46 129.19	133.71
Charge	Pentolite	TNT	TNT	TNT	Pentolite	TNT
Ambient Pressure at GZ (PSI)	13.353	13.553	13.611	13.631	13.572	13.4995
Gnd. Level	13.278	13.504	13.5487	13.571	13.511	13.4381
Charge Height	79.0	60.7	104.2	89.4	104.2	122.0
Temperature °F	70.2	60.0	69.1	78.6	79.7	97.0
Surface	53	42	54	54	38	22
1 Meter						
Relative Humidity %						
Wind Velocity & Direction						
2 Meters	15.2 at 245 T	14.3 at 315 T	3.6 at 060 T	2.0 at 310 T	2.3 at 180 T	4.2 at 290 T
75 Feet					2.0	5.0
Sky Condition	8/10 CB 2/10 AC GZ Obscured By Rain Clouds in Area	4/10 Very Thin CS 25,000 Feet	3/10 CU 3/10 AC 4/10 CS	Clear	7/10 TCU 1/10 AC	4/10 TCU 1/10 CS
300-Ft. Tower Wind Elevation (Ft.)	50	150	300	50	150	300
Direction	253.7	259.1	258.5	321.0	333.6	132.2
Speed (MPH)	27.3	31.7	35.7	17.1	19.8	24.5
				2.0	1.7	3.3
				9.0	9.6	10.9
				2.0	2.1	2.5
				2.0	2.0	2.0
				9.6	10.9	10.9
				274.6	274.9	274.9
				183.0	170.4	191.1
				183.0	170.4	191.1
				274.6	274.9	274.9
				183.0	170.4	191.1
				183.0	170.4	191.1
				274.6	274.9	274.9
				183.0	170.4	191.1
				183.0	170.4	191.1
				274.6	274.9	274.9
				183.0	170.4	191.1
				183.0	170.4	191.1
				274.6	274.9	274.9
				183.0	170.4	191.1
				183.0	170.4	191.1
				274.6	274.9	274.9
				183.0	170.4	191.1
				183.0	170.4	191.1
				274.6	274.9	274.9
				183.0	170.4	191.1
				183.0	170.4	191.1
				274.6	274.9	274.9
				183.0	170.4	191.1
				183.0	170.4	191.1
				274.6	274.9	274.9
				183.0	170.4	191.1
				183.0	170.4	191.1
				274.6	274.9	274.9
				183.0	170.4	191.1
				183.0	170.4	191.1
				274.6	274.9	274.9
				183.0	170.4	191.1
				183.0	170.4	191.1
				274.6	274.9	274.9
				183.0	170.4	191.1
				183.0	170.4	191.1
				274.6	274.9	274.9
				183.0	170.4	191.1
				183.0	170.4	191.1
				274.6	274.9	274.9
				183.0	170.4	191.1
				183.0	170.4	191.1
				274.6	274.9	274.9
				183.0	170.4	191.1
				183.0	170.4	191.1
				274.6	274.9	274.9
				183.0	170.4	191.1
				183.0	170.4	191.1
				274.6	274.9	274.9
				183.0	170.4	191.1
				183.0	170.4	191.1
				274.6	274.9	274.9
				183.0	170.4	191.1
				183.0	170.4	191.1
				274.6	274.9	274.9
				183.0	170.4	191.1
				183.0	170.4	191.1
				274.6	274.9	274.9
				183.0	170.4	191.1
				183.0	170.4	191.1
				274.6	274.9	274.9
				183.0	170.4	191.1
				183.0	170.4	191.1
				274.6	274.9	274.9
				183.0	170.4	191.1
				183.0	170.4	191.1
				274.6	274.9	274.9
				183.0	170.4	191.1
				183.0	170.4	191.1
				274.6	274.9	274.9
				183.0	170.4	191.1
				183.0	170.4	191.1
				274.6	274.9	274.9
				183.0	170.4	191.1
				183.0	170.4	191.1
				274.6	274.9	274.9
				183.0	170.4	191.1
				183.0	170.4	191.1
				274.6	274.9	274.9
				183.0	170.4	191.1
				183.0	170.4	191.1
				274.6	274.9	274.9
				183.0	170.4	191.1
				183.0	170.4	191.1
				274.6	274.9	274.9
				183.0	170.4	191.1
				183.0	170.4	191.1
				274.6	274.9	274.9
				183.0	170.4	191.1
				183.0	170.4	191.1
				274.6	274.9	274.9
				183.0	170.4	191.1
				183.0	170.4	191.1
				274.6	274.9	274.9
				183.0	170.4	191.1
				183.0	170.4	191.1
				274.6	274.9	274.9
				183.0	170.4	191.1
				183.0	170.4	191.1
				274.6	274.9	274.9
				183.0	170.4	191.1
				183.0	170.4	191.1
				274.6	274.9	274.9
				183.0	170.4	191.1
				183.0	170.4	191.1
				274.6	274.9	274.9
				183.0	170.4	191.1
				183.0	170.4	191.1
				274.6	274.9	274.9
				183.0	170.4	191.1
				183.0	170.4	191.1
				274.6	274.9	274.9
				183.0	170.4	191.1
				183.0	170.4	191.1
				274.6	274.9	274.9
				183.0	170.4	191.1
				183.0	170.4	191.1
				274.6	274.9	274.9
				183.0	170.4	191.1
				183.0	170.4	191.1
				274.6	274.9	274.9
				183.0	170.4	191.1
				183.0	170.4	191.1
				274.6	274.9	274.9
				183.0	170.4	191.1
				183.0	170.4	191.1
				274.6	274.9	274.9
				183.0	170.4	191.1
				183.0	170.4	191.1
				274.6	274.9	274.9
				183.0	170.4	191.1
				183.0	170.4	191.1
				274.6	274.9	274.9
				183.0	170.4	191.1
				183.0	170.4	191.1
				274.6	274.9	274.9
				183.0	170.4	191.1
				183.0	170.4	191.1
				274.6	274.9	274.9
				183.0	170.4	191.1
				183.0	170.4	191.1
				274.6	274.9	274.9
				183.0	170.4	191.1
				183.0	170.4	191.1
				274.6	274.9	274.9
				183.0	170.4	191.1
				183.0	170.4	191.1
				274.6	274.9	274.9
				183.0	170.4	191.1
				183.0	170.4	191.1
				274.6	274.9	274.9
				183.0	170.4	191.1
				183.0	170.4	191.1
				274.6	274.9	274.9
				183.0	170.4	191.1
				183.0	170.4	191.1
				274.6	274.9	274.9
				183.0	170.4	191.1
				183.0	170.4	191.1
				274.6	274.9	274.9
				183.0	170.4	191.1
				183.0	170.4	191.1
				274.6	274.9	274.9
				183.0	170.4	191.1
				183.0	170.4	191.1
				274.6	274.9	274.9
				183.0	170.4	191.1
				183.0	170.4	191.1
				274.6	274.9	274.9
				183.0	170.4	191.1
				183.0	170.4	191.1
				274.6	274.9	274.9
				183.0	170.4	191.1
				183.0	170.4	191.1
				274.6	274.9	274.9
				183.0		

Table 4. Firing Data and Environmental Conditions Shots 7 through 11
Vertical Array

Shot Number	7	8	9	10	11
Firing Date	4 Sept.	17 Sept.	22 Oct.	2 Nov.	8 Nov.
Firing Time	1650 MDT	1730 MDT	1156 MDST	1400 MDST	1535 MDST
HOB (Ft.)	72.185 25.455	74.307 24.447	45.45 15.15	45.46 14.92	74.12 23.99
Ambient Pressure GZ (PSI)					
Gnd. Level	13.59	13.521	13.491	13.689	13.683
Charge Height	13.58 13.56				
Temperature °F					
Surface	97	82.5	59.8		
1 Meter	72.1	67.5	57.5	21.3	-2.4
Relative Humidity %	37	31	55	81	60
Wind Velocity & Direction					
2 Meters	7.9 at 330	2.5 at 150	3.8 at 245	7.2 at 030	Calm
75 Feet	10.0	6.5	4.5 at 245	7.5 at 030	Calm
Sky Condition	Clear	Bright 4/10 CI	Sun Moderate 6/10 CI	Sun Slightly Visible 7/10 CI	Sun Fairly Bright 4/10 AC 3/10 CI
Surface Condition	Hard. Smooth	Hard. Smooth	Hard. Smooth	Soft, Rough	Soft, Rough

Cloud Abbreviations: CI - cirrus
AC - alto-cumulus

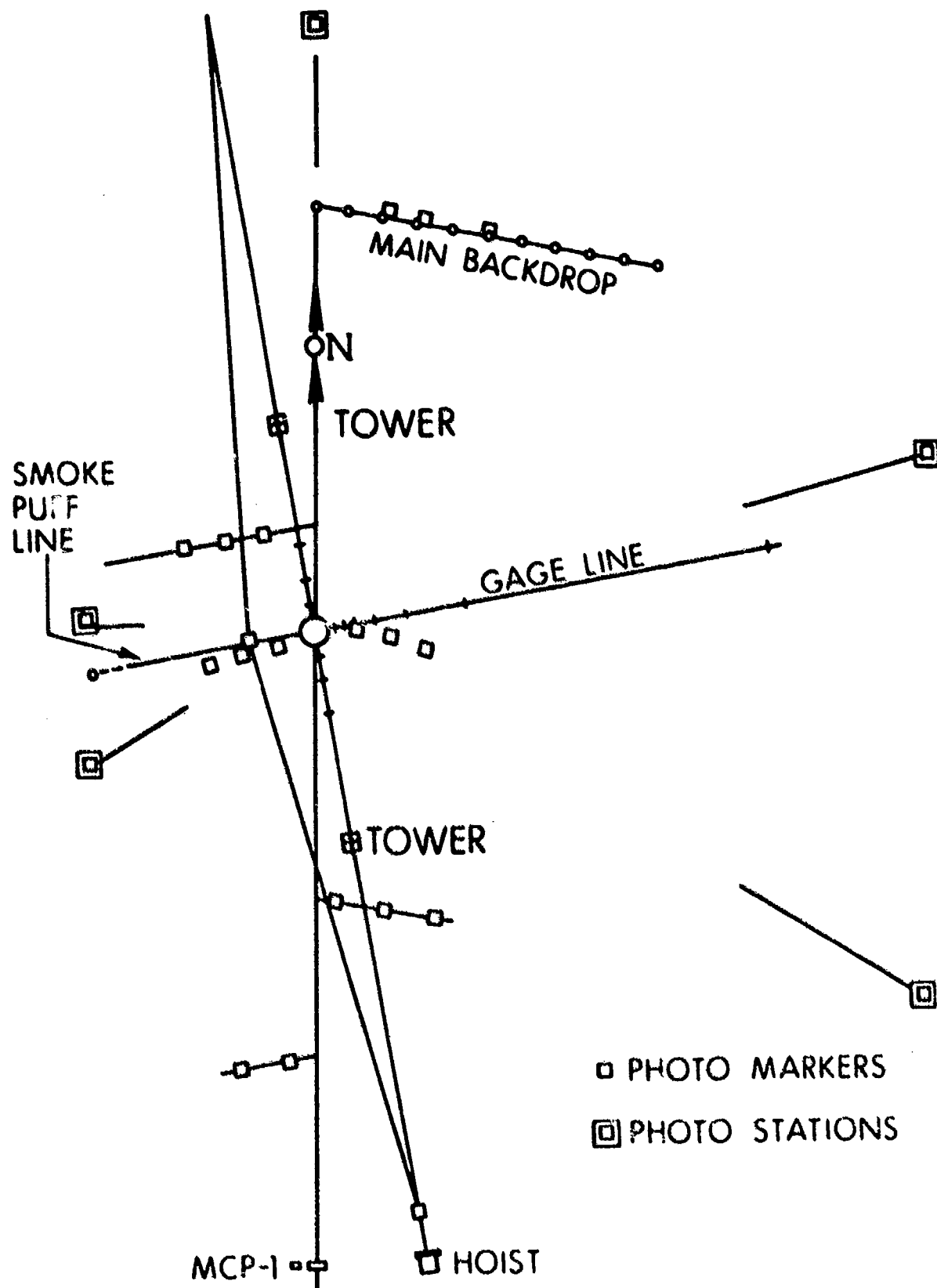


Figure 1. Field Layout of DIPOLE WEST Site

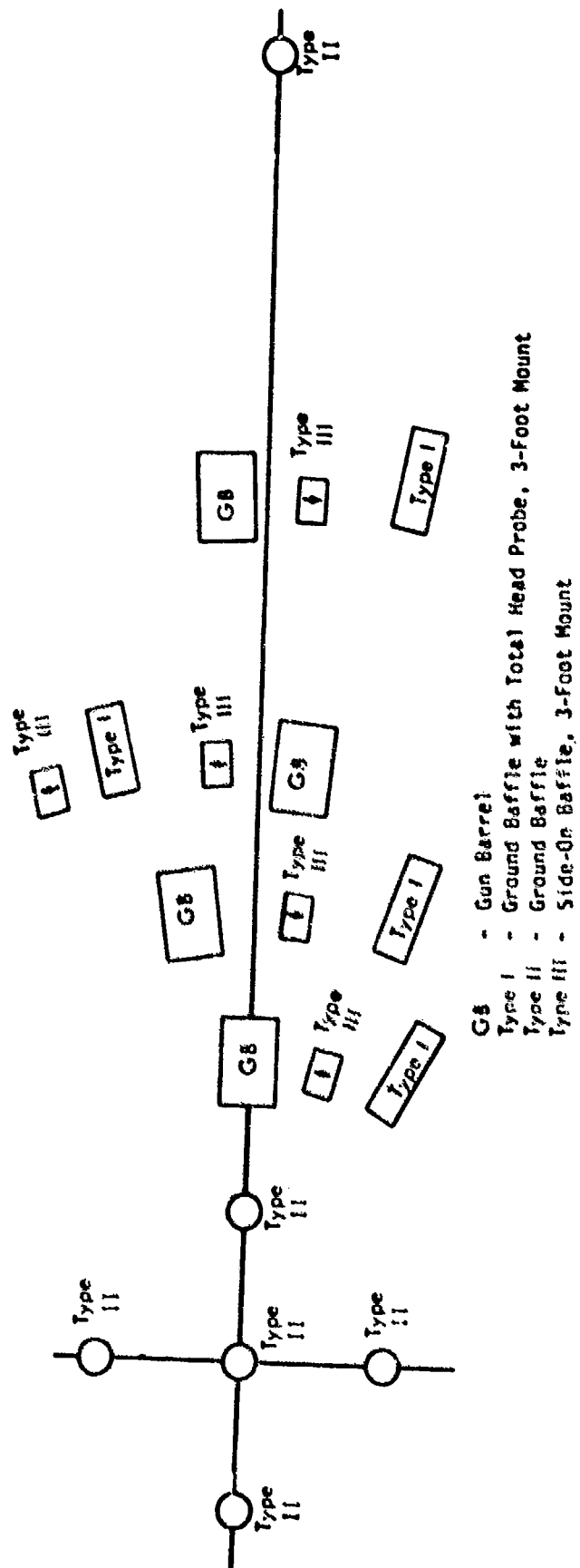


FIGURE 2. Detail of Field Layout, Ground Zero Area

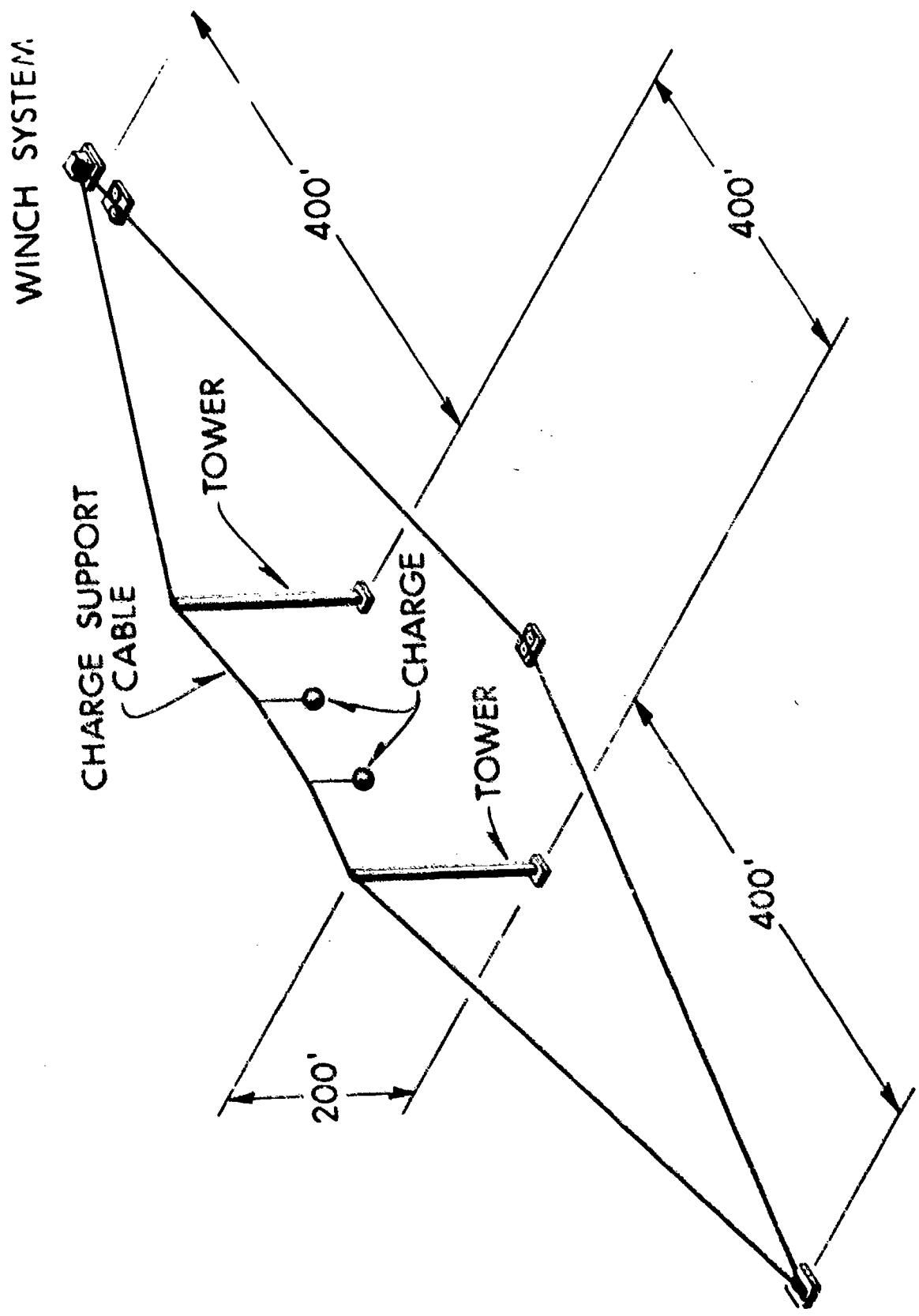


Figure 3. Diagram of the Horizontal Array Charge Handling System

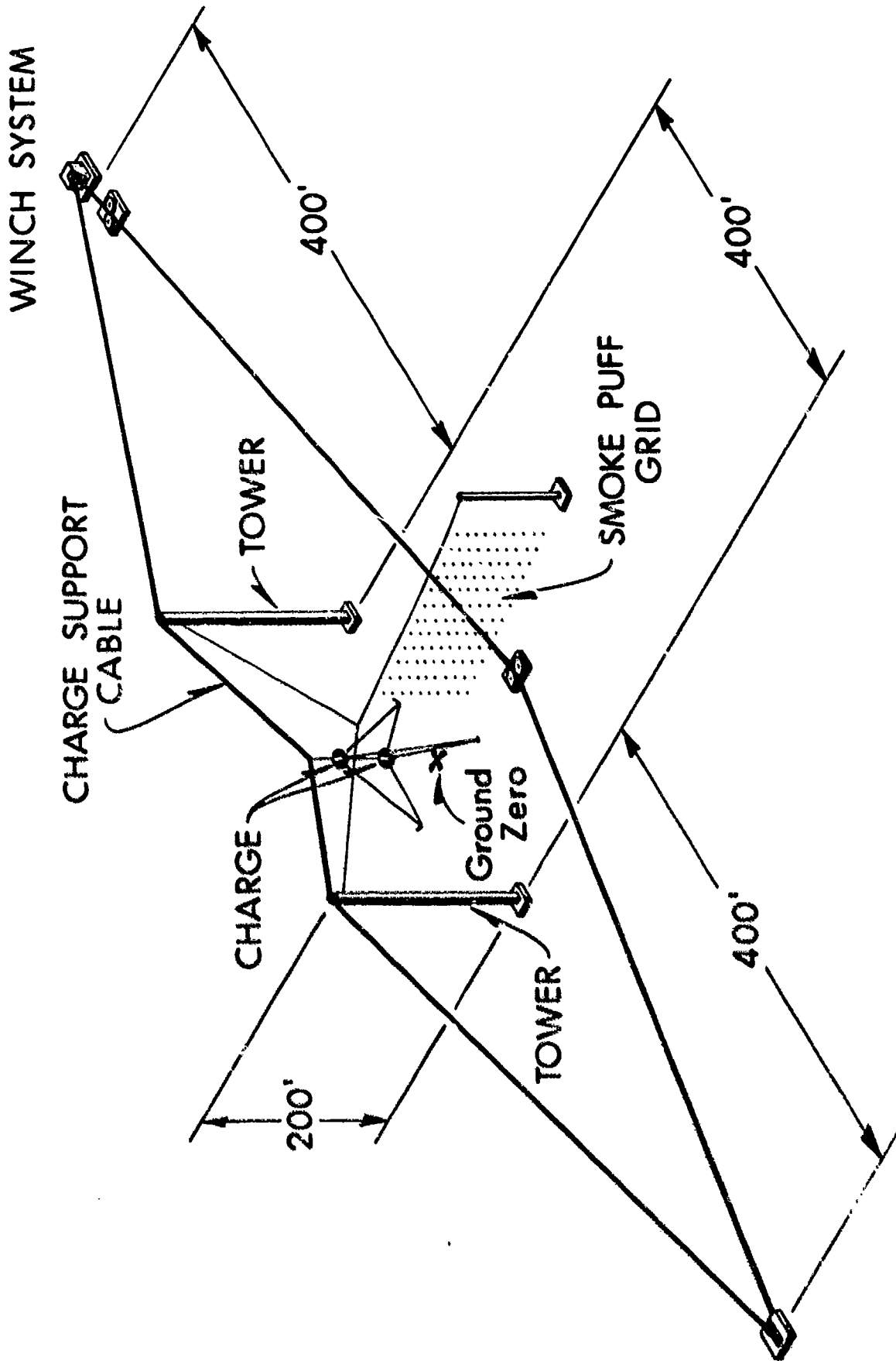


Figure 4. Diagram of the Vertical Array Charge Handling System

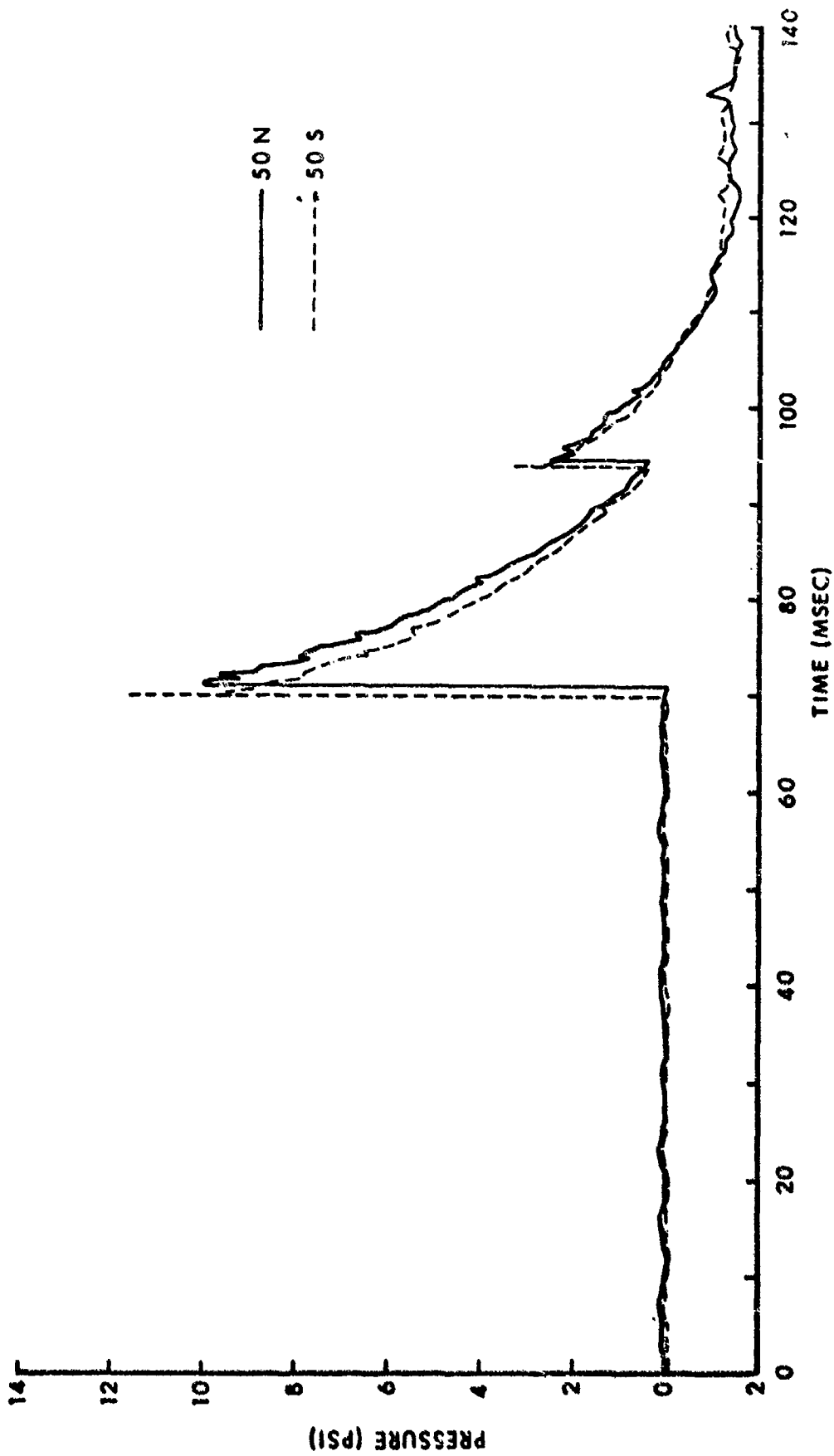


Figure 5. Comparison of Pressure Records 50 Feet from Instrument Ground Zero; Shot 1

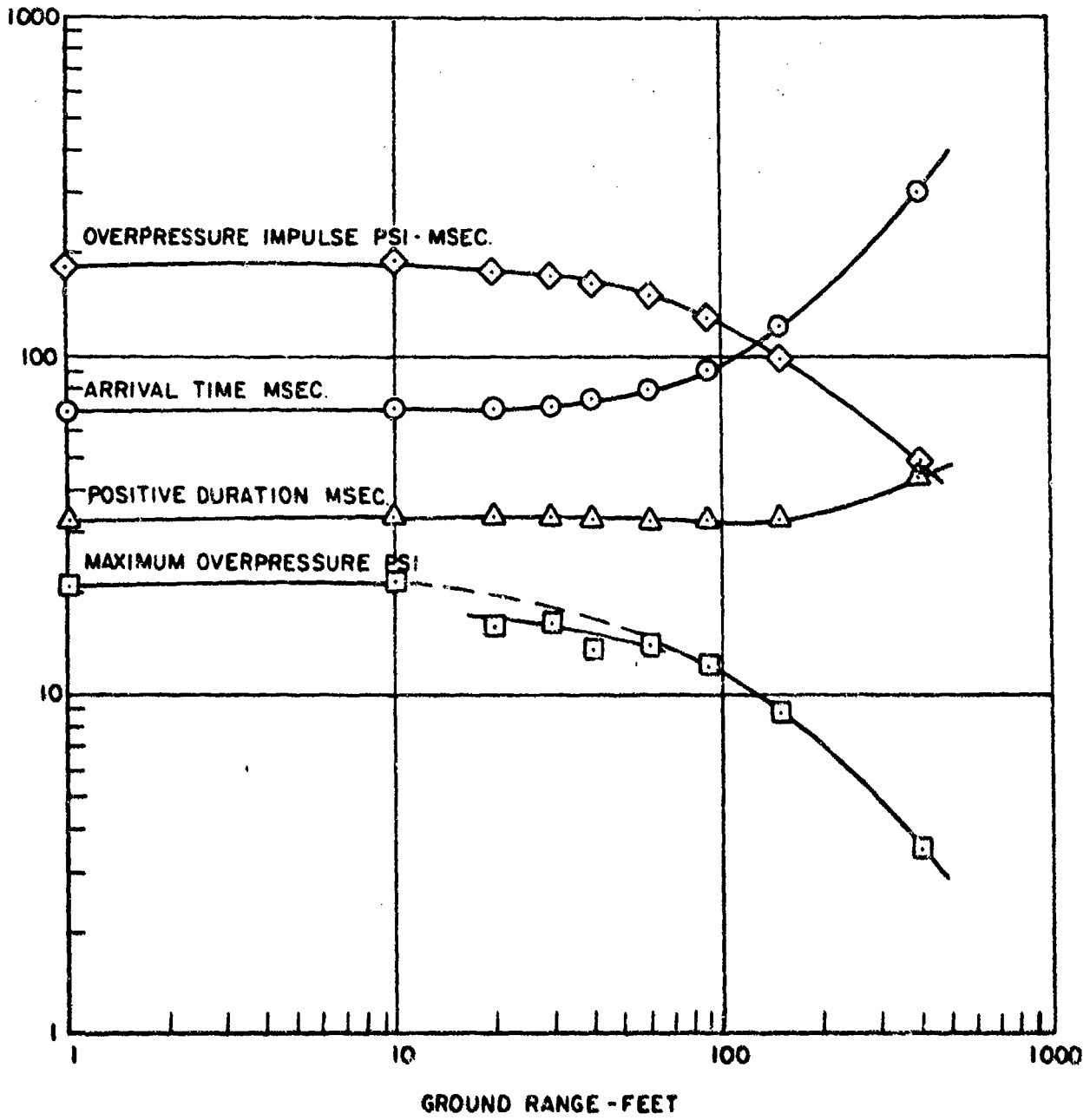


Figure 6. Air Blast Parameters at Ground Level Versus Ground Range; Shot 2

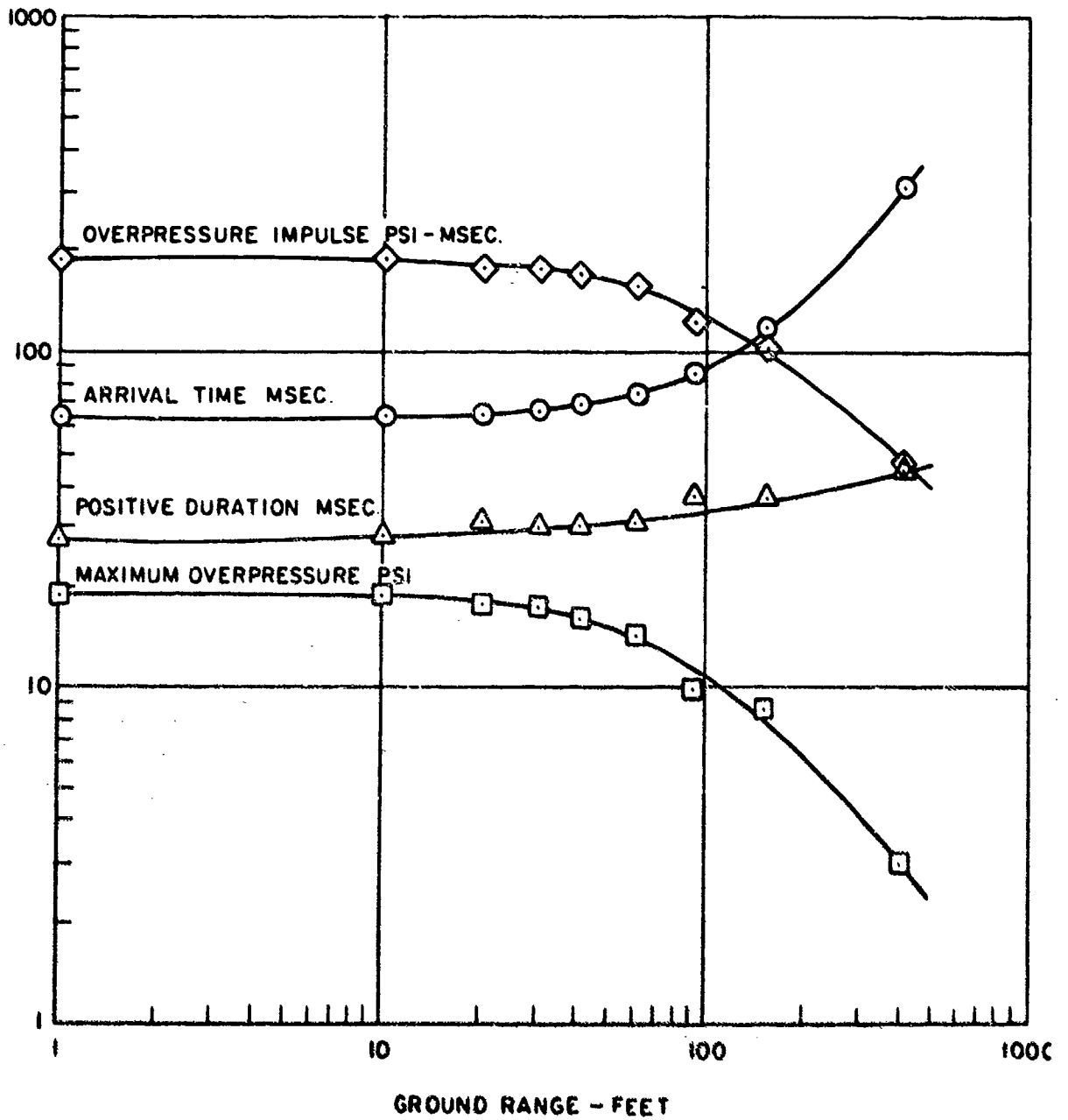


Figure 7. Air Blast Parameters at Ground Level Versus Ground Range; Shot 3

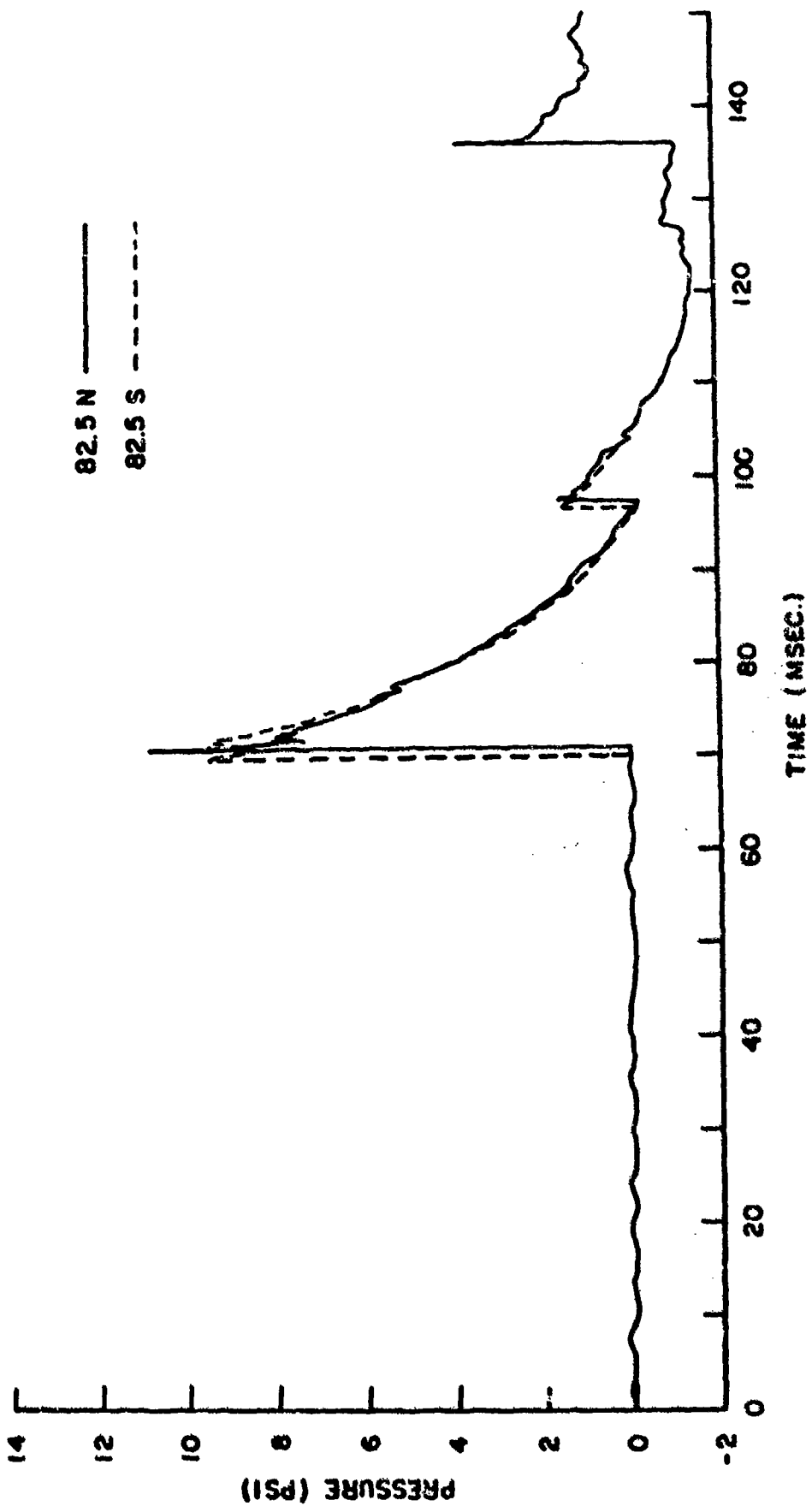


Figure 8. Comparison of Pressure Records 82.5 Feet from Instrument Ground Zero; Shot 4

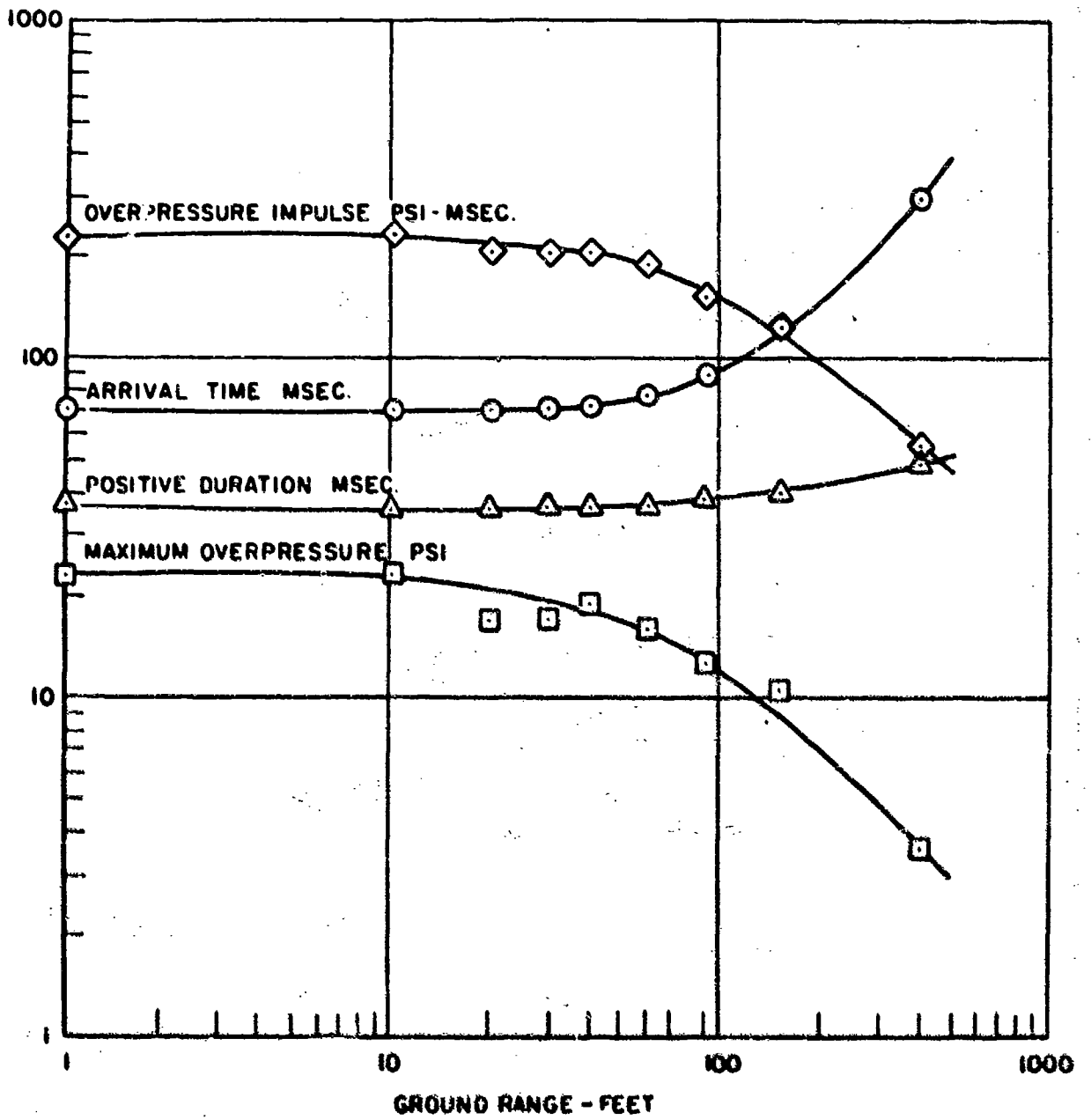


Figure 9. Air Blast Parameters at Ground Level Versus Ground Range; Shot 5

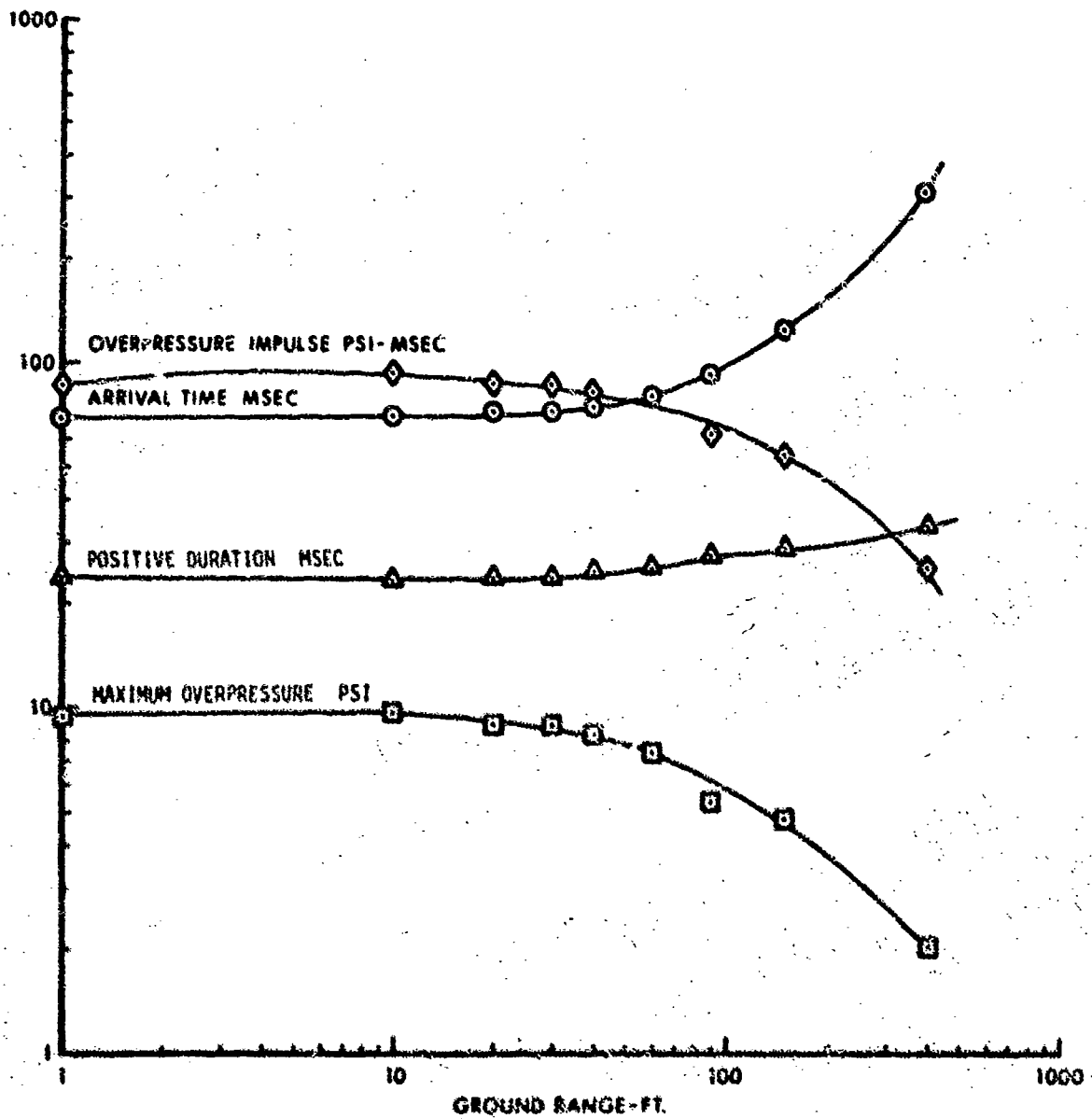


Figure 10. Air Blast Parameters at Ground Level Versus Ground Range; Shot 6

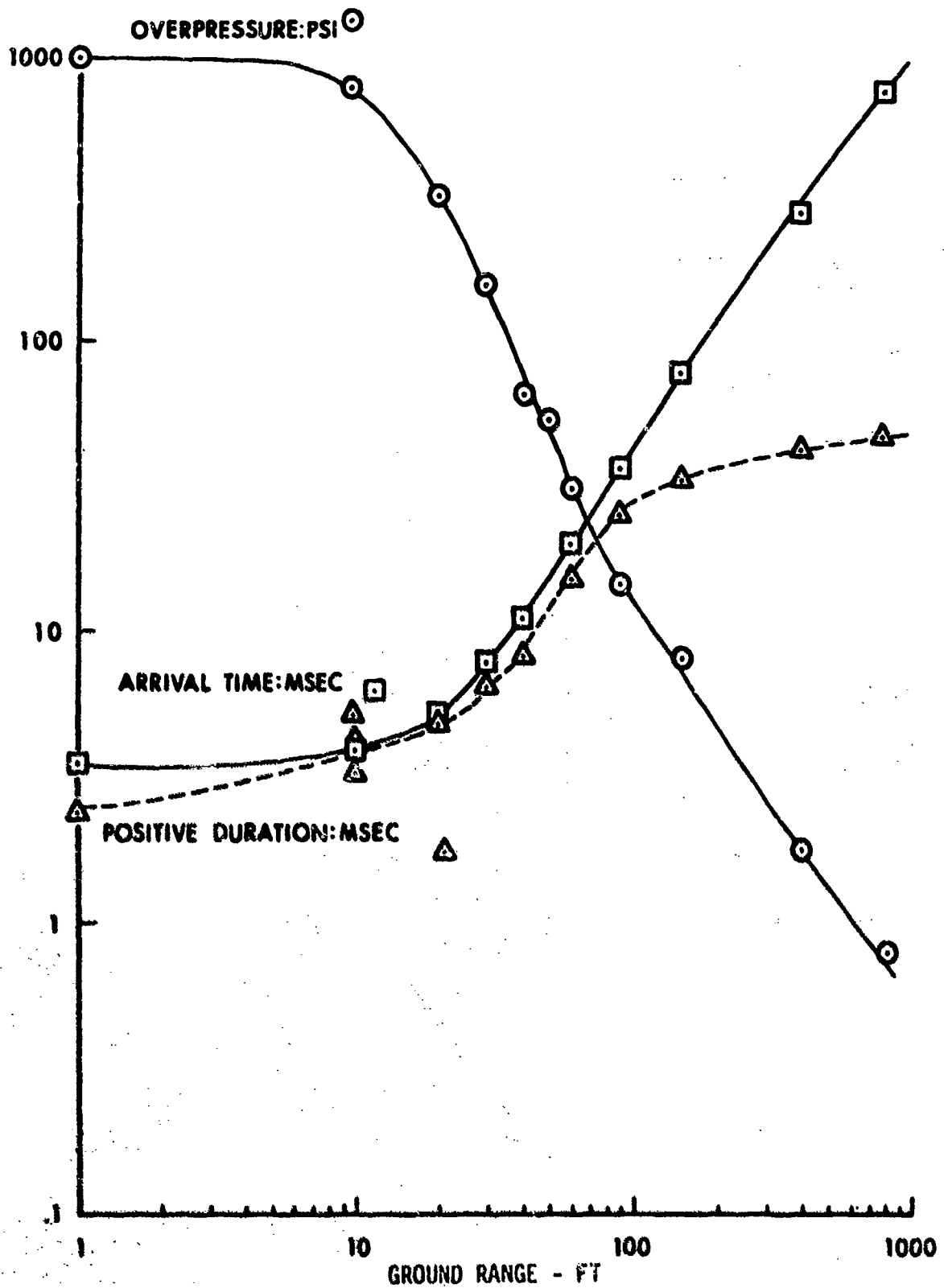
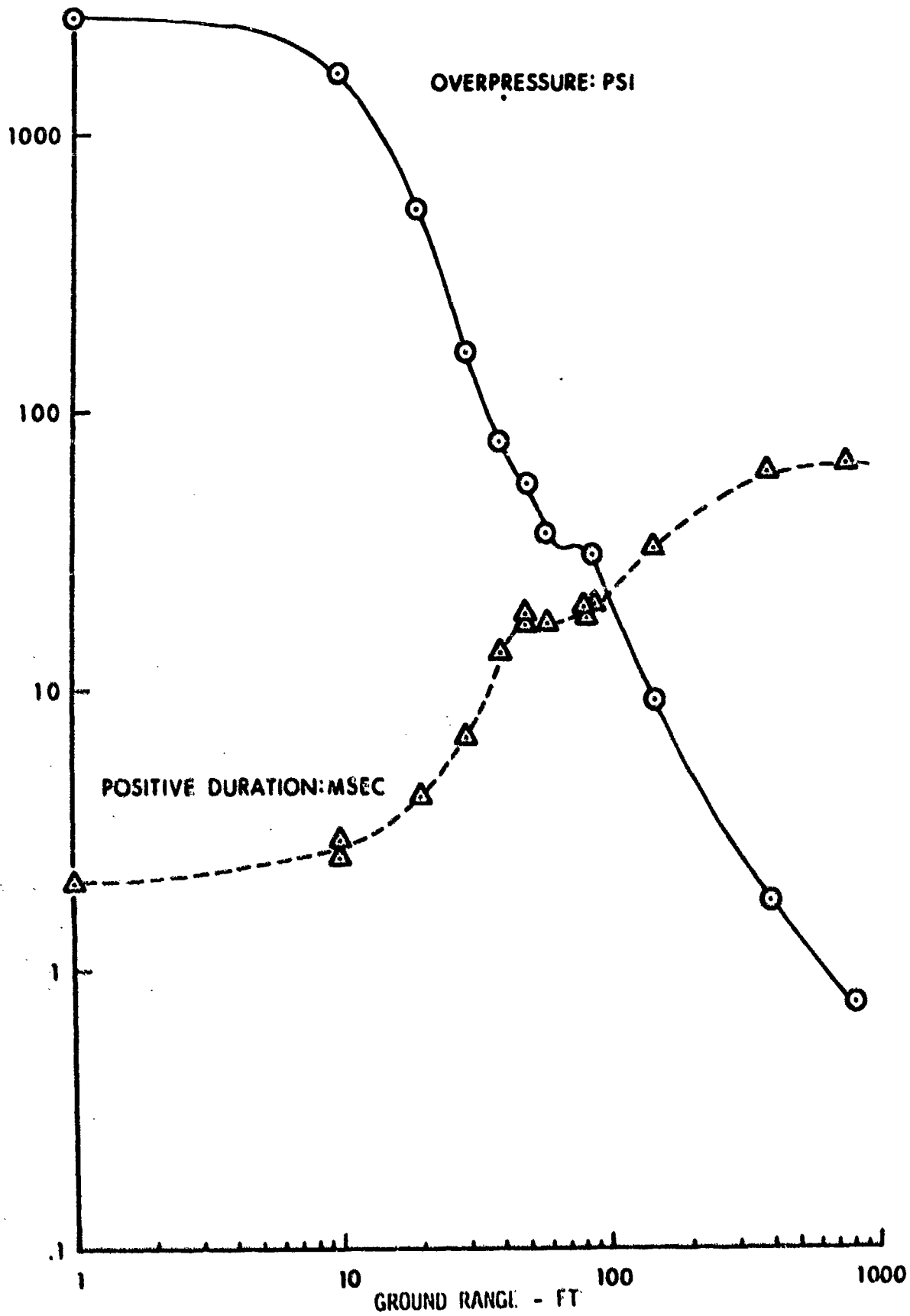


Figure 11. Air Blast Parameters at Ground Level Versus Ground Range; Shot 8

Figure 12. Air Blast Parameters at Ground Level Versus Ground Range: Shot 9



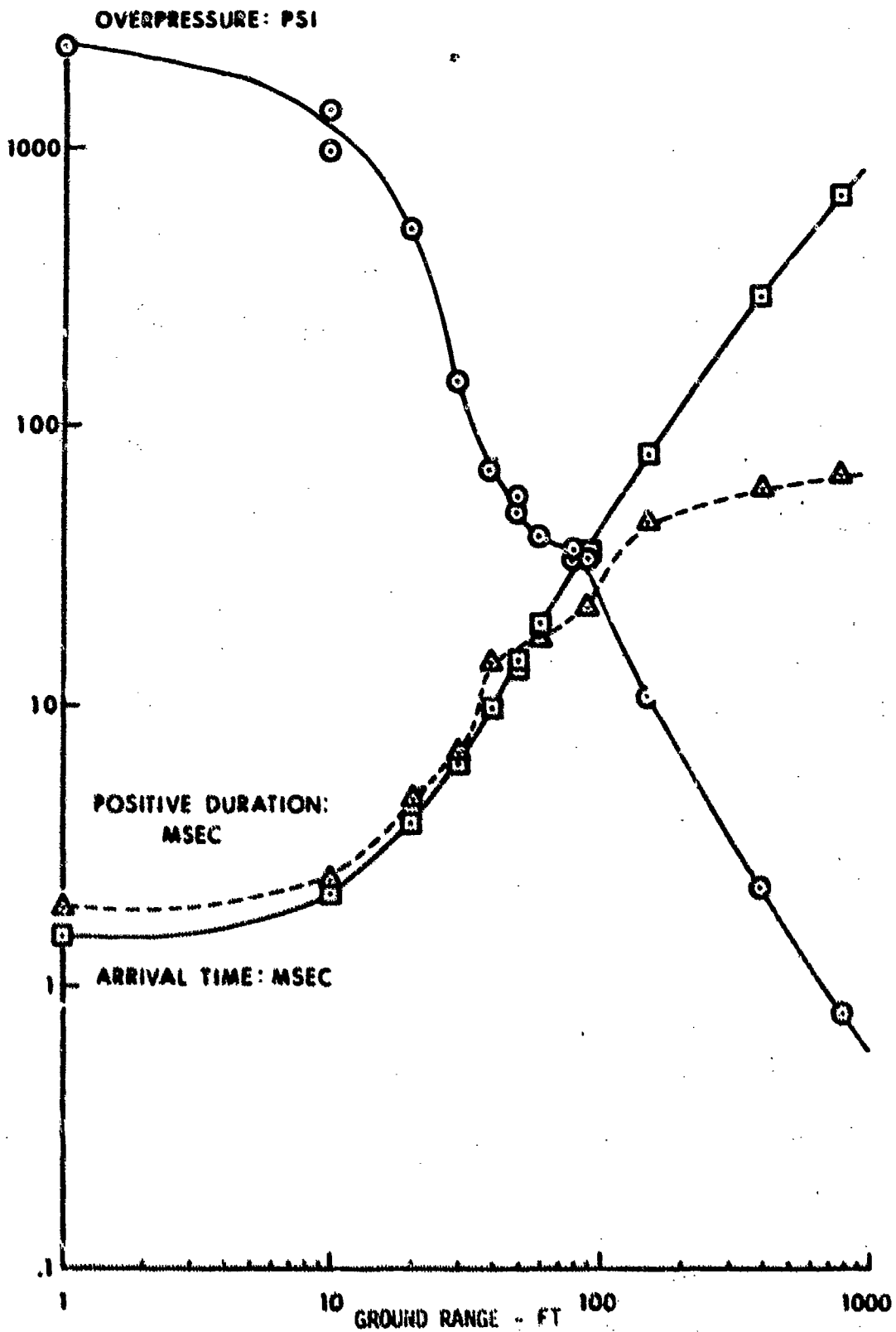


Figure 13. Air Blast Parameters at Ground Level Versus Ground Range; Shot 10

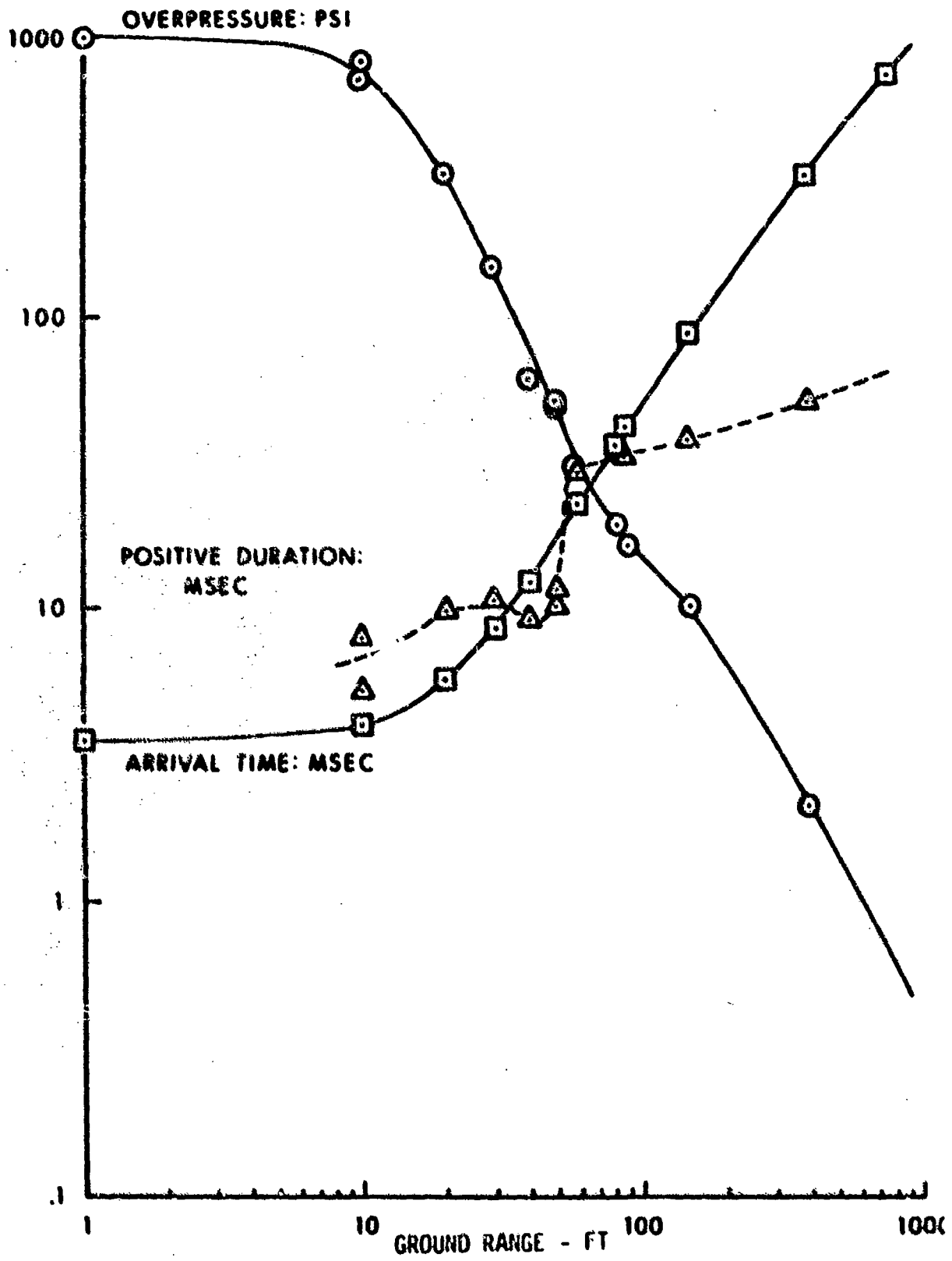


Figure 14. Air Blast Parameters at Ground Level Versus Ground Range; Shot 11

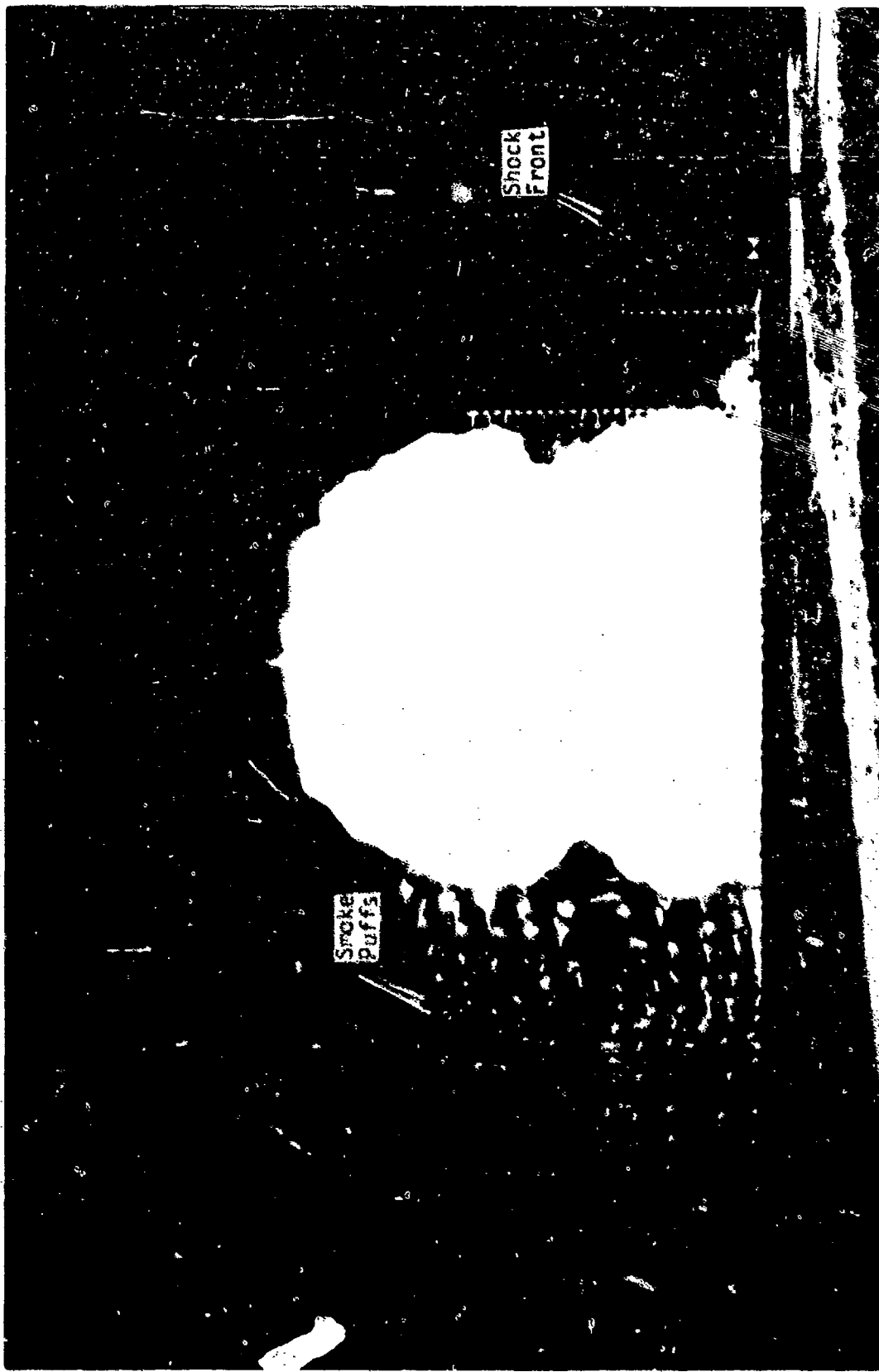


Figure 15. Shot 10 Combined Fireballs at 0.05 Seconds After Detonation

Figure 16. Comparison of Overpressure Data from Shots 8 and 11, with Data from HOB 1969 Series

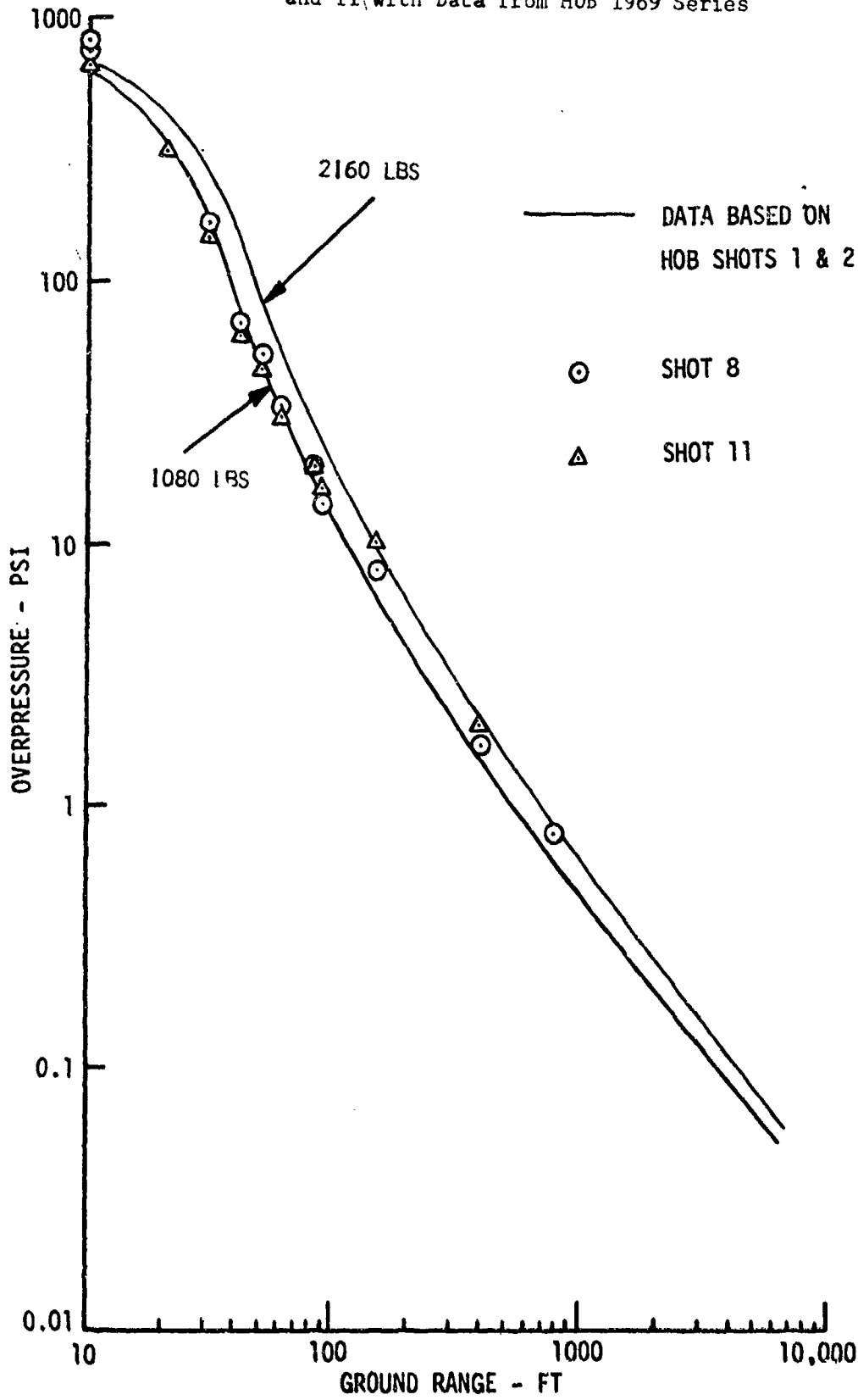
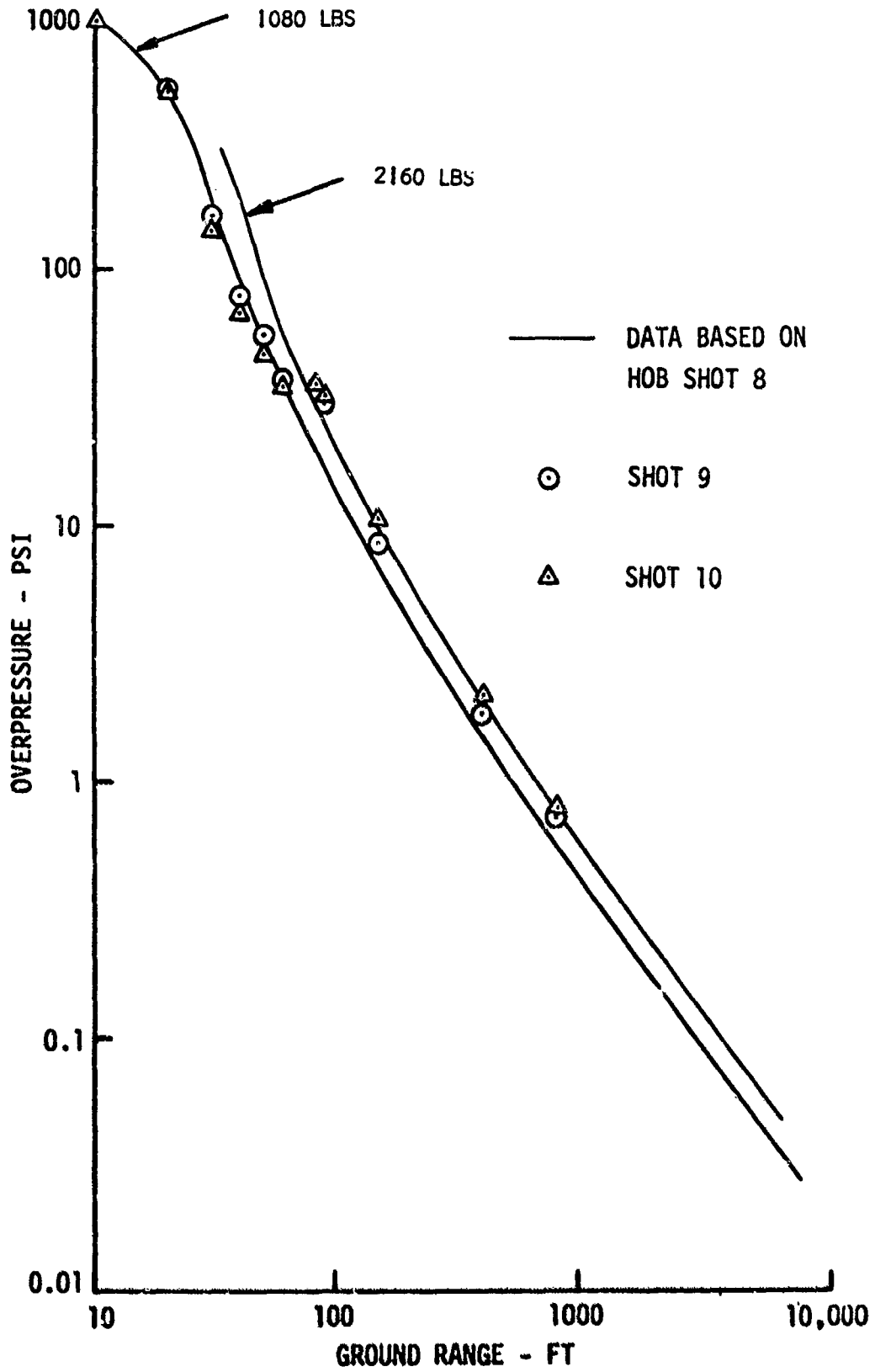


Figure 17. Comparison of Overpressure Data from Shots 9 and 10 with Data from HOB 1969 Series



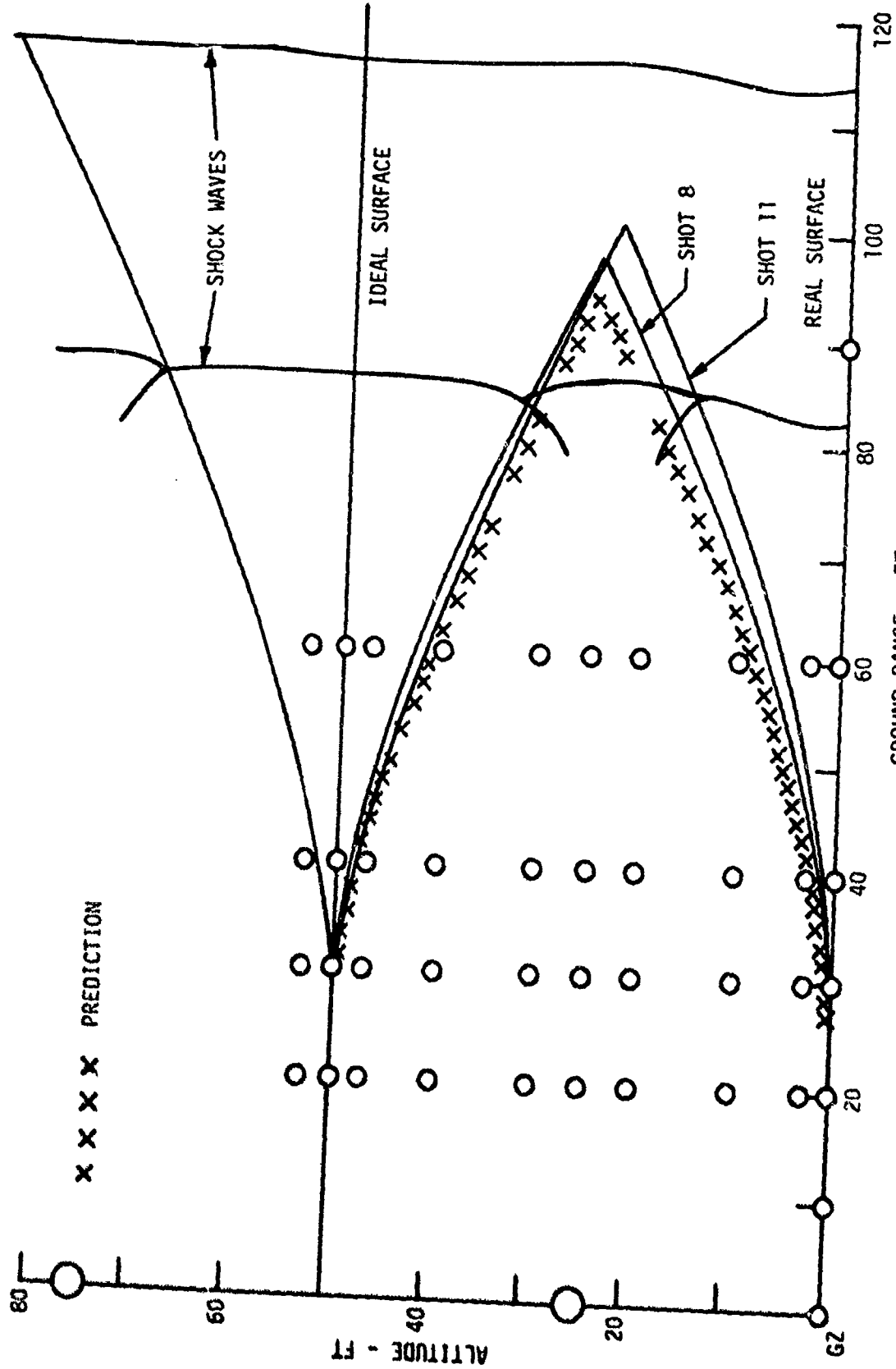


Figure 18. Reconstructed Triple Point Path and Shock Wave Diagram for 25-Foot HOB Events

MEASUREMENT OF PRESSURES AND IMPULSES OF GASEOUS EXPLOSIONS AT HIGH INITIAL PRESSURES

by

A. B. Wenzel

Southwest Research Institute
San Antonio, Texas

ABSTRACT

This paper presents the results of laboratory scale experiments based on a model analysis using Hopkinson's and/or Sachs' scaling laws of gaseous explosions in an oil or gas well bore as a function of initial pressures.

The pressure-time history of various mixtures of oxygen-methane and air-methane at high initial pressures was recorded. The properties of the gaseous explosion were measured using piezoelectric and piezoresistive transducers. All conclusions made were derived from the output measurements of transducers. The results of this program show that the detonation pressure-time history can be controlled by varying the gas ratio mixtures and the initial confined pressures. Also, at stoichiometric mixtures the peak reflected pressure was found to be 75 times greater than the initial pressure. Gaseous detonations have the advantageous characteristic that they yield low peak pressures and high impulses relative to other types of explosives, making them attractive for mining, quarrying, and/or oil and gas recovery techniques.

INTRODUCTION

Gaseous explosions have been experienced ever since man began handling quantities of volatile solvents and combustible gases. Numerous accidents involving gaseous explosives have been recorded in the literature and summarized in Reference 1. All of the accidental explosions reported in Reference 1 involved the explosion of unconfined vapor clouds produced by the dispersion of flammable liquid or vapor spills.

Gaseous explosions have been studied experimentally and analytically by many investigators. The literature is full of references concerning the work done in this area. However, all of the work cited in the literature refers itself to either of the two kinds of gas explosions, which are:

deflagration and detonation. Furthermore, all these investigators studied these explosions at atmospheric or subatmospheric pressure conditions.

Deflagration denotes the simple burning of a gas mixture, with the flames being propagated almost entirely by thermal conduction in the gas. They propagate at up to sonic speed in the gas mixture, and the flame temperatures can be calculated by elementary thermodynamics. Pressure rises can also be calculated from the increase in the number of moles of gas and the temperature rise. Flame speed is slow enough that the pressure rise can be largely dissipated by an outward gas flow which is simply a wind.

Detonation in gases is similar to deflagration in that it comprises a flame running through the gaseous mixture with the evolution of heat and a resultant pressure rise. They differ in that detonation propagates at supersonic rather than subsonic speeds and generates a shock wave. Blast pressures can be up to a thousand times as high as burning pressures, but are usually on the order of five to ten times as high.

More energy is required to initiate a detonation than to ignite a deflagration. However, a deflagration can shock up to a detonation. The amount of energy needed to initiate a full-blown detonation is variable with gas composition.

Detonation velocities also depend upon gas composition, and for the case of hydrogen, methane, ethane and propane-oxygen mixtures, the burning velocity is considerably lower for either lean or rich fuel mixtures than at stoichiometric mixtures.^{2*}

A common characteristic of gaseous explosions is the fact that the peak pressures generated are considerably lower than a solid or liquid explosive, but the time duration phase of the pressure-time history (i. e., the impulse) is much longer than that of solid or liquid explosives. This characteristic is what makes gaseous explosions so destructive when loading a structure. The loading of structures by gas explosion is still of the impulsive type, in spite of longer durations than for condensed explosives. That is, the duration of loading is in many cases of the order of, or smaller than, the characteristic response time of the structure corresponding to its natural frequencies.

As pointed out earlier, to the author's knowledge, the study of gaseous explosives at high initial pressures has not been previously investigated.

The motivation for undertaking such a study came as a result of some relatively recent work conducted by Blackstone and Wenzel,³ where oxygen-methane mixtures were studied at cryogenic temperatures. These studies

*Superscript numbers denote references listed at the end of this paper.

revealed that this explosive mixture was more energetic than Pentaerythritol-Tetranitrate (PETN) and appeared to have about the same degree of handling hazard as PETN and was three times as safe as nitromethane and five times as safe as n-propyl nitrate. 3-4

These results suggested the possible use of this type of explosive for mining, oil and gas stimulation, and oil shale retorting applications.

Since the majority of the above mentioned applications would require the use of this type of explosive mixture at initial pressures of several orders of magnitude greater than atmospheric pressures, a program to investigate gaseous explosions at high initial pressures was undertaken. This paper presents the results of laboratory scale experiments based on a model analysis of a gaseous explosion in an oil or gas well bore.

The pressure-time history of various mixtures of oxygen-methane and air-methane at high initial pressures was recorded. The properties of the gaseous explosion was measured using piezoelectric and piezoresistive transducers. All conclusions made were derived from the output measurements of the transducers.

DESIGN OF THE EXPERIMENT

To measure the properties of the gaseous explosion as a function of initial pressures, an experimental apparatus was designed such that the explosive gas mixture could be thoroughly ignited at specific initial pressures and at known gas ratios, with an instrumented firing chamber which could readily be modified to vary gases, ratio of gas compositions, pressures, and firing chamber configurations. The rationale for the design of the apparatus was based on a model analysis of an oil or gas well bore where the detonation takes place at or near the bottom of the hole. Hole diameter, hole length, initial pressure, initial temperature, fuel-oxygen ratio, total explosion energy, explosion pressure, explosion temperature, and time were the parameters considered to derive the scale factors. A detailed discussion of the derivation of the model law based on Hopkinson's and/or Sachs' scaling laws is given in Reference 5. This model law not only guided the design of the test apparatus, but also helped interpret the results from the scaled experiments. The overall test apparatus designed and built for these tests is depicted schematically in Figure 1.

A brief discussion of the charging system, the test chamber, the firing system and the instrumentation are discussed in the following paragraphs.

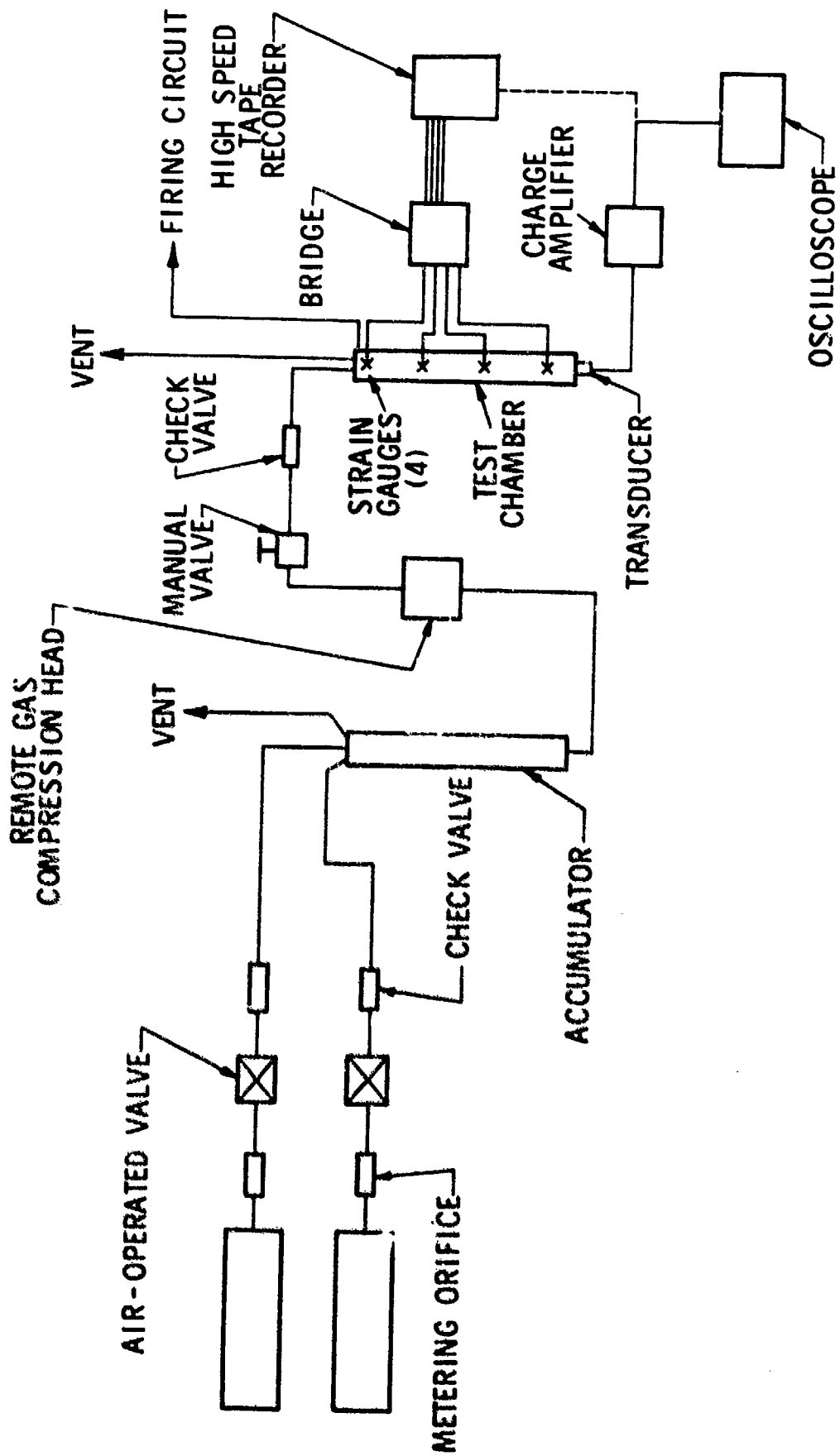
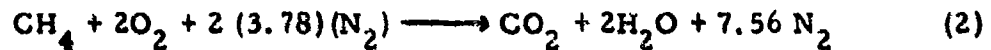


Figure 1. Schematic Of Experimental Apparatus

Gas Charging System

Oxygen, methane, and air used for these tests were obtained commercially in 330-ft³ bottles. Each gas was fed individually at a regulated pressure through a metering orifice and high-pressure tubing to an air-operated solenoid valve. The pneumatically operated valves were electrically controlled by switches located in the control center. From the air-operated solenoid valve, the gas flowed through a 20,000-psi check valve to either the accumulator or directly to the test chamber, depending on the initial test pressure desired. To control the quantity of gases supplied to the test chamber and obtain proper mixing, it was decided to feed the gases into a mixing chamber, through orifices for which the flow was at sonic velocity.

Different orifice sizes were selected to control the gas mixture and to measure their effect on the pressure time history of the explosion. The chemical reaction of the gases considered (methane-oxygen and methane-air) was assumed to be as follows:



The metering orifices function on the principle of critical mass flow. This approach was chosen because it appears practical and feasible for controlling downhole mixtures in an operational system.

The mass flow rate equation for sonic flow is given by

$$W = CAP \sqrt{\left(\frac{gY}{RT}\right) \left(\frac{2}{Y+1}\right) \left(\frac{Y+1}{Y-1}\right)} \quad (3)$$

where

W = mass flow rate

C = orifice discharge coefficient

A = throat area of orifice area

P = upstream absolute gas pressure

g = gravitational constant

Y = ratio of specific heats of working gases

R = gas constant (universal gas constant/molecular weight)

T = upstream absolute temperature

The derivation of this relation assumes isentropic discharge, negligible upstream velocity relative to the discharge velocity, and uniform discharge velocity distribution, including negligible boundary layer formation.

For all the test conditions, the source pressure was always twice or greater than the final mixed pressure in order to use the sonic flow equations. Relating to Eq. (1), the ratio of the molecular weights of oxygen (O_2) to methane (CH_4) is

$$\frac{O_2}{CH_4} = 4 \quad (4)$$

Assuming that the initial pressure, temperature and the orifice coefficients are the same for O_2 and CH_4 , then applying Eqs. (3) and (4) enables one to calculate the orifice size for stoichiometric mixtures.

Other percentages of stoichiometric mixtures for oxygen or air can be computed from the following equations:

$$\% O_2 = (0.367) \left(\frac{D_{O_2}}{D_{CH_4}} \right)^2 \times 100 \quad (5)$$

$$\% Air = (0.0814) \left(\frac{D_{Air}}{D_{CH_4}} \right)^2 \times 100 \quad (6)$$

where D_{O_2} , D_{Air} and D_{CH_4} are orifice diameters.

The initial pressures in this program were varied from atmospheric up to 1500 psi. To achieve the higher initial pressures, an accumulator and a high pressure pump were used. The accumulator consisted simply of a 1-1/2-in. I.D., 3-in. O.D., 40-3/4-in.-long steel tube. The gaseous mixture was held in this tube at 500 to 1000 psi and then pumped to the desired level. The high-pressure pump was a 3000-psi gas compression head driven hydraulically by a remotely located air pump. For these tests, a 60,000-psi check valve and a manually operated needle valve were installed in the flow line between the gas compression head and the test chamber. This was thought necessary to ensure that the gas compression head was not damaged by the high pressures generated when the explosive mixtures were detonated. Figure 2 shows the experimental setup with the accumulator, high-pressure pump and check valve.

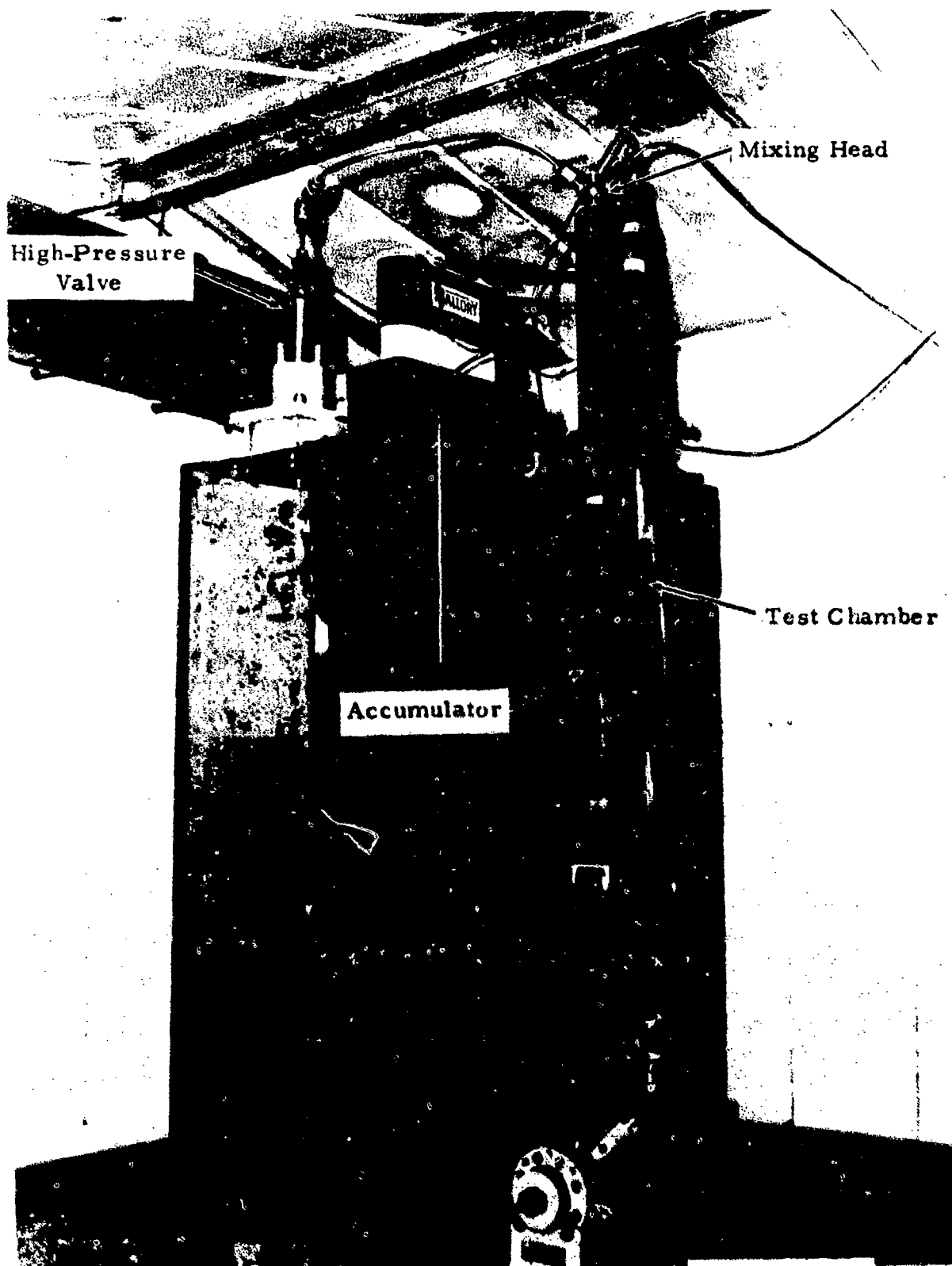


FIGURE 2. "LARGE TUBE" EXPERIMENTAL SETUP USING ACCUMULATOR, HIGH-PRESSURE PUMP AND CHECK VALVES

Test Chamber

To check the scaling laws, the test chambers used in this program were designed in accordance with the model law given in Reference 5 to simulate an 8-in. O.D. by 50-ft-deep hole located in the pay zone (i. e., the pay zone may well be located several thousand feet below the surface, which would affect the initial pressure in the pay zone). There were essentially two basic test chambers used throughout this program: one referred to as the large chamber consisting of 1/2-in. I.D. by 60 in. long, with a wall thickness of 1/2 in., and the other test chamber referred to as the "small tube" consisting of 1/4-in. I.D. test chamber by 30 in. long. These chambers were designed to withstand pressures in excess of 100,000 psi. Figure 3 shows the experimental setup utilizing the "large test chamber" without the accumulator chamber. Note that this test setup was instrumented with strain gauges mounted at four equally spaced points along the exterior wall for sensing pressures and detonation wave arrival times. A quartz piezoelectric pressure transducer was mounted at the bottom of the chamber to record reflected pressure-time histories. Filling and venting were done via the mixing head mounted in the top of the test chamber, and the firing squib system was mounted through the chamber wall near the top.

Firing System

Different spark systems were attempted to initiate the gas at high initial pressures. These systems varied from ordinary high voltage spark-gap wires to automotive-spark plugs. Although initiations were obtained with these devices, the data were not repeatable. Therefore, an electrical pyrotechnic squib mounted across the spark plug gap was used as a firing device. The squibs were ignited by a current supply from a 6-volt battery, controlled from a firing switch located in the control center.

Instrumentation

The primary dynamic measurement made in this program was the reflected pressure at the opposite end of the tube from where detonation of the gas mixtures was initiated. The instrumentation system used for this purpose, shown in Figure 4, consisted of a 0 to 100,000-psi range piezoelectric transducer connected to a charge amplifier, with the output of the amplifier connected to a cathode ray oscilloscope for photographic recording of the pressure-time data trace. The oscilloscope was triggered from the firing switch, initiating the ignition system used on each test. Two examples of pressure data recorded on film using an oscilloscope are presented in Figure 5. Note the familiar fast rise time and exponential decay pressure-time record experienced in detonation measurements. Subsequent pulses represent reflected waves which have traveled back and forth through the test chamber. In some cases, where the particular test conditions caused a delayed detonation, a magnetic tape recorder was used in parallel

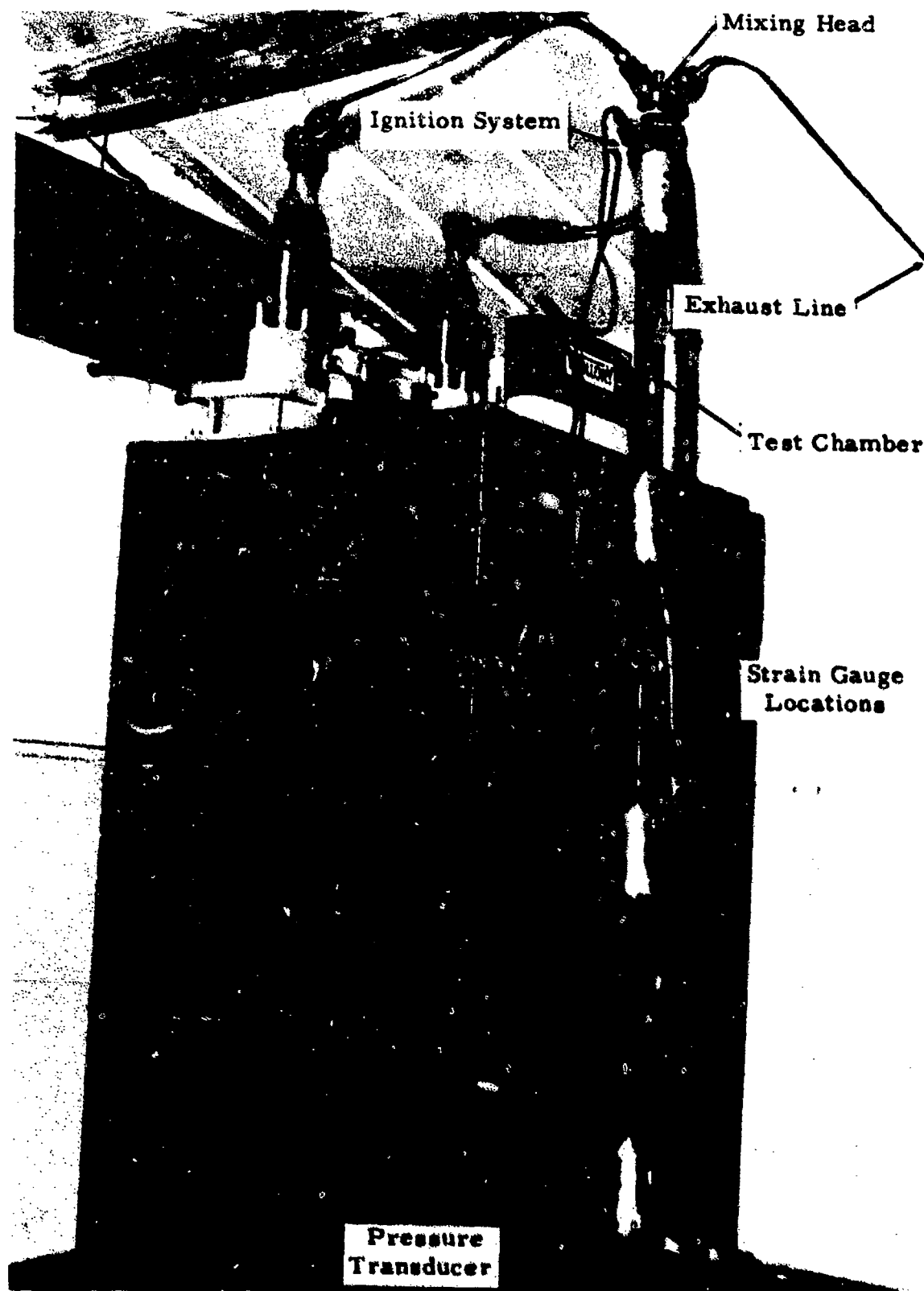
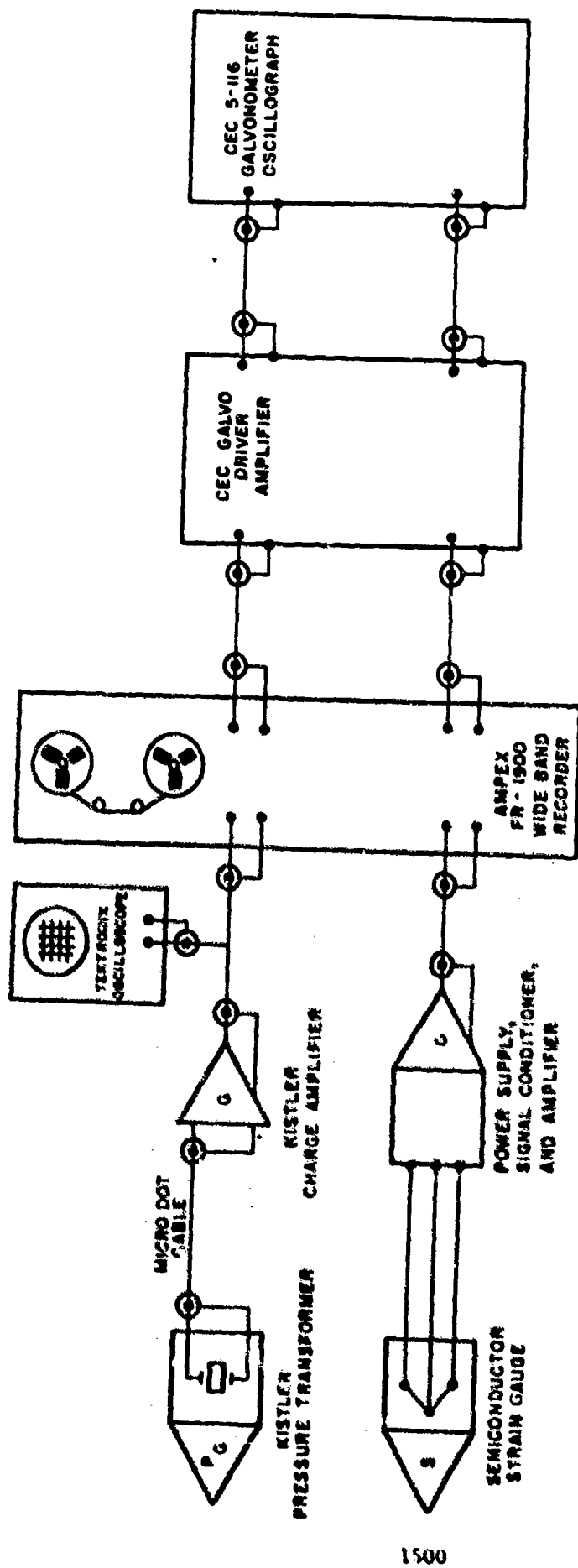
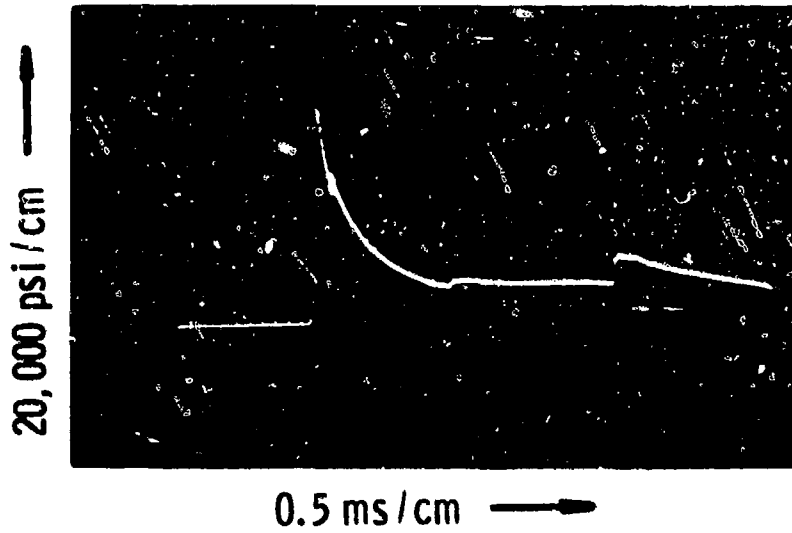


FIGURE 3. "LARGE TUBE" EXPERIMENTAL SETUP

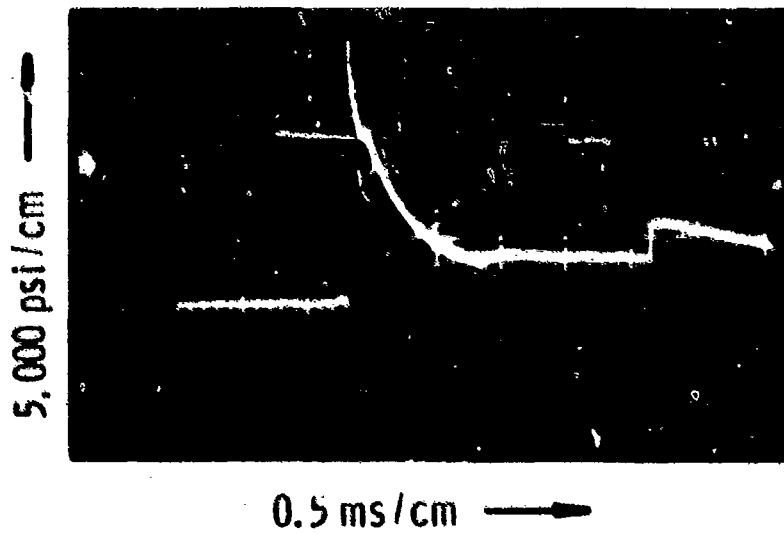


1500

Figure 4. Schematic Pressure And Time Of Arrival Instrumentation System



(a) Pressure-Time Polaroid Photograph, Test No. 8



(b) Pressure-Time Polaroid Photograph, Test No. 12

FIGURE 5. EXAMPLES OF PRESSURE DATA OBTAINED ON OSCILLOSCOPE

to record the pressure data. Figure 6 illustrates pressure measurements made using the magnetic tape recorder.

As mentioned earlier, the pressure chamber was strain-gauged on the outer surface at four stations along the length of the tube. These measurements provided time of arrival data from which the velocity of the pressure pulse generated was obtained. Because of the wide range of pressures expected at the start of the program, including pressures lower than 10,000 psi, and the thickness of the tube, external strain levels estimated from thick-walled cylinder equations were of the order of 50 μ in. per inch. To obtain a good voltage signal above the magnitude of the "noise" that is inherent in this type of dynamic testing, semiconductor strain gauges were used to measure the time of arrival. Theoretically, the magnitude of the side-on pressure generated inside the tube can be derived from the strains measured. However, because of the content of noise on the recorded strain data, interpretation of the magnitudes proved futile.

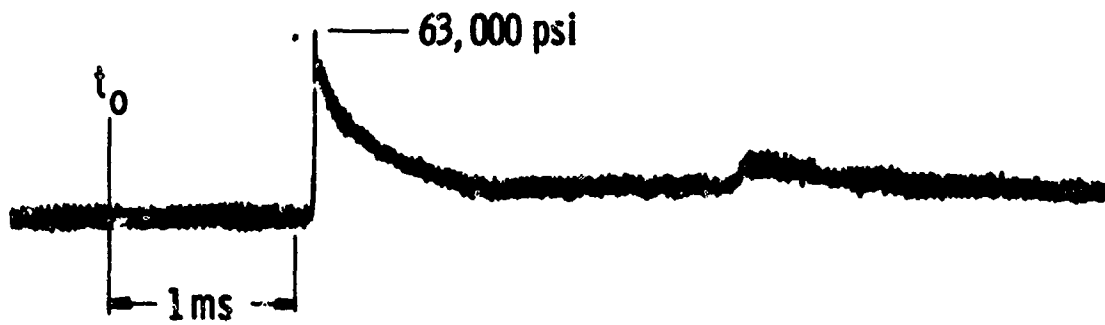
TEST PROGRAM AND RESULTS

There were 80 shots fired during this program. Several gas mixtures were used with the larger of the two test chambers, and only one gas mixture was tested in the smaller test chamber to determine the effect of scaling.

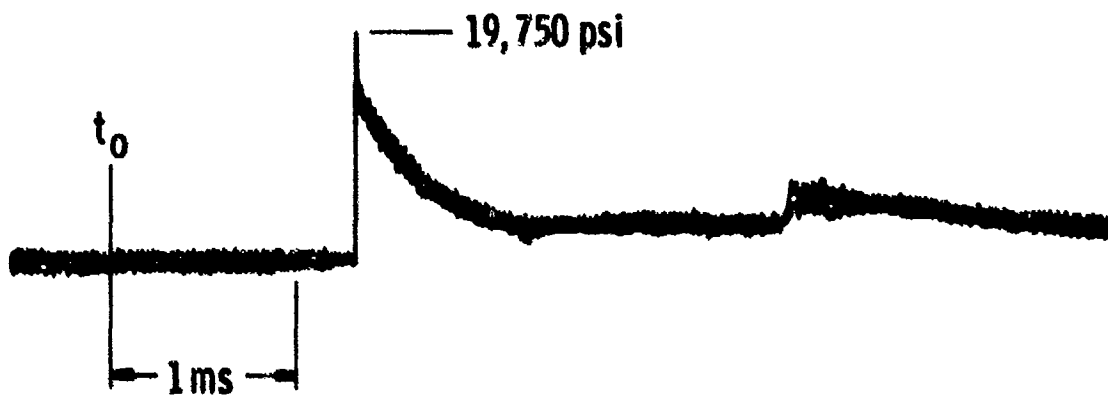
The program was essentially subdivided by the percent of stoichiometric mixture of oxygen to methane and percent of stoichiometric ratios of air to methane. This division is summarized in Table I.

TABLE I. SUMMARY OF TEST PROGRAM

<u>% O₂ to CH₄</u>	<u>Size of Test Chamber</u>
112	large
112	small
229	large
72	large
57	large
23	large
<u>% Air to CH₄</u>	
73	large
93	large



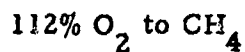
(a) Pressure-Time Oscillograph Trace, Test No. 8



(b) Pressure-Time Oscillograph Trace, Test No. 12

Figure 6. Example of Pressure Measurements Made Using Magnetic Tape Recorder

A discussion of the results obtained for each different setup is given below.



Initial tube pressures ranged from 0 to 800 psi, and peak reflected pressures ranged from 575 to 63,000 psi. These results are plotted in Figure 7. For this case, the normally reflected pressure (P_r) appears to be a linear function of the initial test chamber pressure (p_0). The slope of the line (P_r/p_0) is 75. For the shot that yielded 63,000 psi, the center of the spark plug was blown out.

During these tests an attempt was made to alternately and separately introduce the gases into the pressure tube. Detonation was not achieved in either case.

From the pressure-time histories, the approximate specific impulse was obtained by integrating the area under the trace obtained. Impulses for this series of tests ranged from 0.2 to 31.5 psi-sec. Figure 8 is a plot of the specific impulse versus initial test chamber pressure. The values seemed to group into a linear relationship.

Detonation velocities were obtained by measuring the time of arrival of the wave sensed by the externally mounted strain gauges at four stations located 17 in. apart.

Normalizing all of the strain gauge data to the first station located near the ignition source, in order to obtain a common initial time base, a plot of time of arrival versus distance was obtained and is shown in Figure 9. The time-of-arrival data points shown in Figure 9 were obtained at the wide range of initial pressures. Although there is some scatter in the points due to initial pressure dependency, it appears that velocity is not a strong function of initial pressure. The author selected to show a linear relationship in order to extract an average detonation velocity across the initial pressure range. A value of 7,550 ft/sec was obtained from the slope of the linear function selected. This value compared well with the 7400 ft/sec detonation velocity reported in References 6 and 7. From these measurements, it was concluded that a sustained detonation of the gas mixture did occur in the test chamber.

A series of tests using this stoichiometric mixture was conducted to check the effects of scaling by using a smaller diameter and shorter test chamber. Initial pressures tested ranged from 250 to 600 psi. The reflected pressures ranged from 29,000 to 79,000 psi. These results are plotted in Figure 10 and compared with the straight line obtained from similar tests using the larger tube. Note that the pressures for the smaller tube are

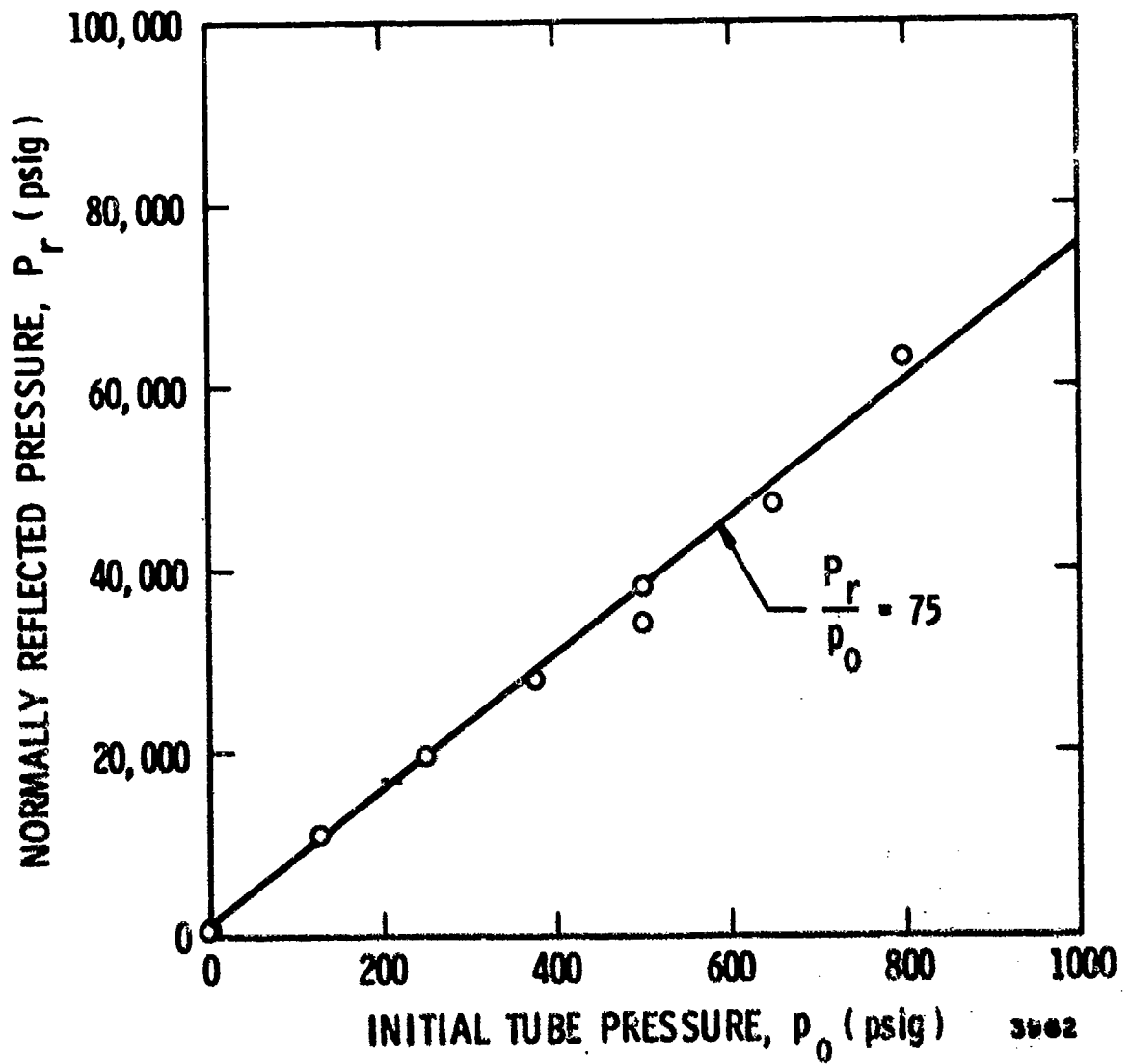


FIGURE 7. REFLECTED PRESSURES FOR LARGE CHAMBER WITH 112.5% O_2 TO CH_4

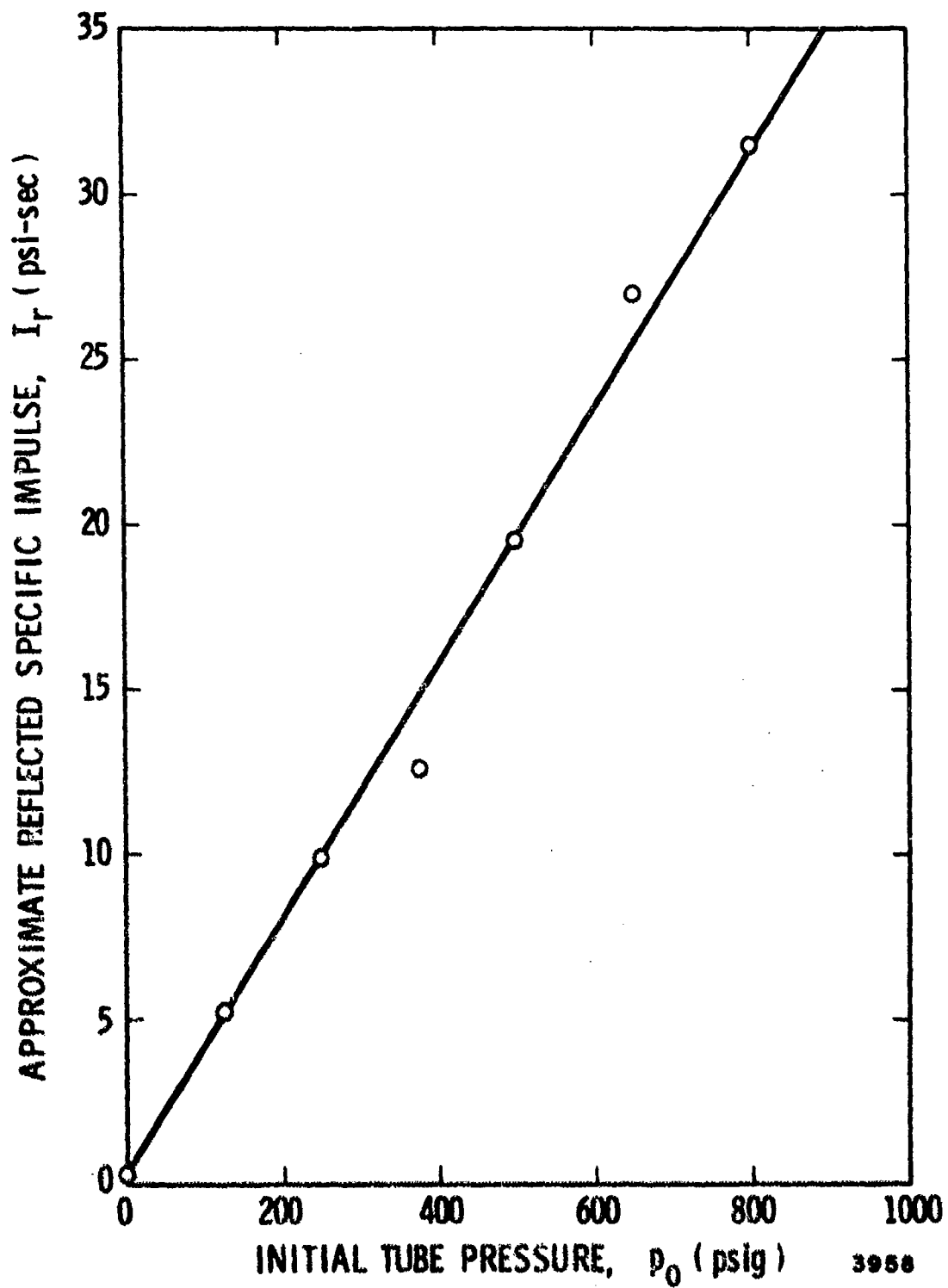


FIGURE 8. REFLECTED IMPULSE FOR LARGE CHAMBER
WITH 112.5% O_2 TO CH_4

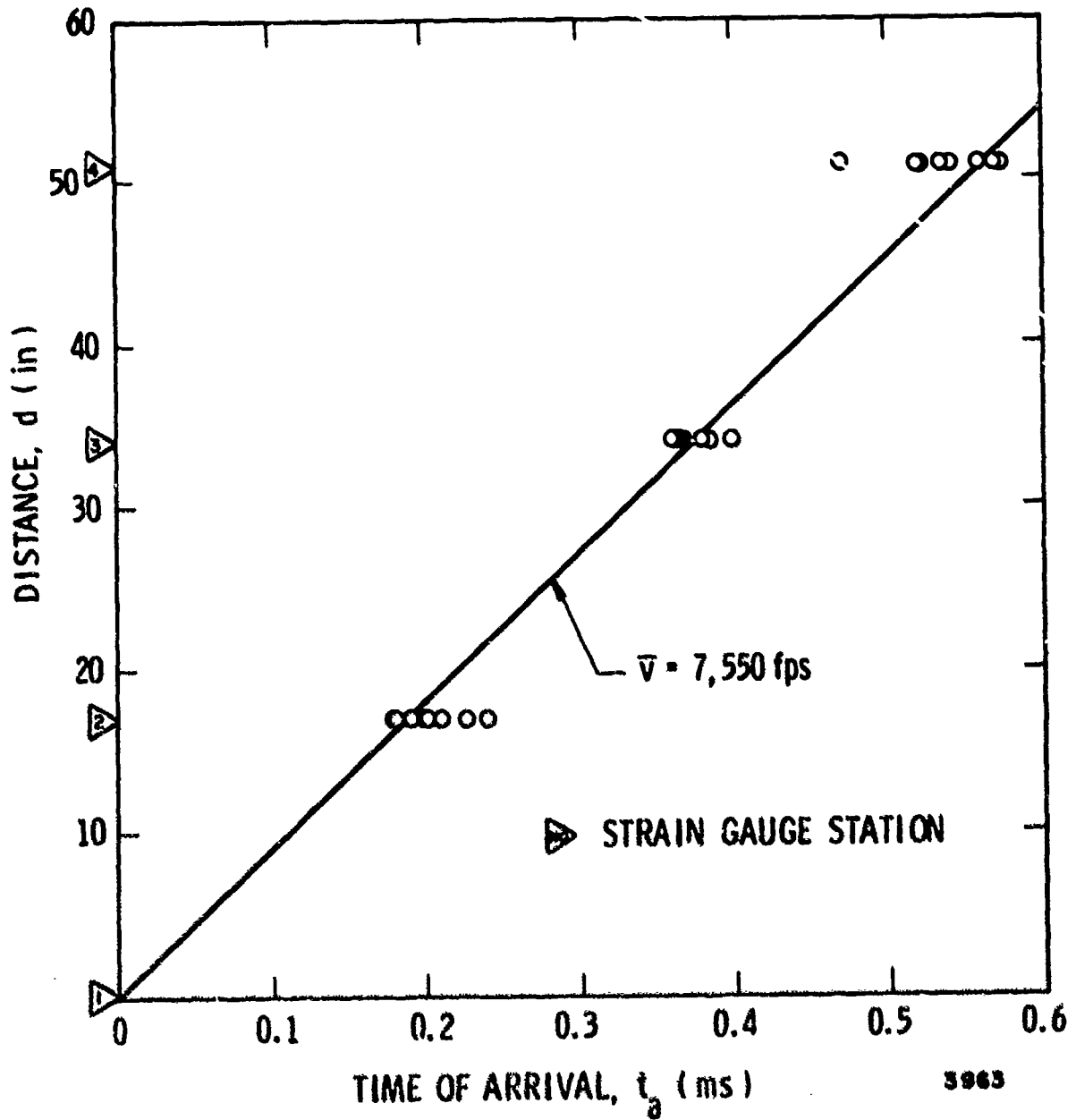


FIGURE 9. TIMES OF ARRIVAL FOR LARGE CHAMBER WITH 112.5% O₂ TO CH₄

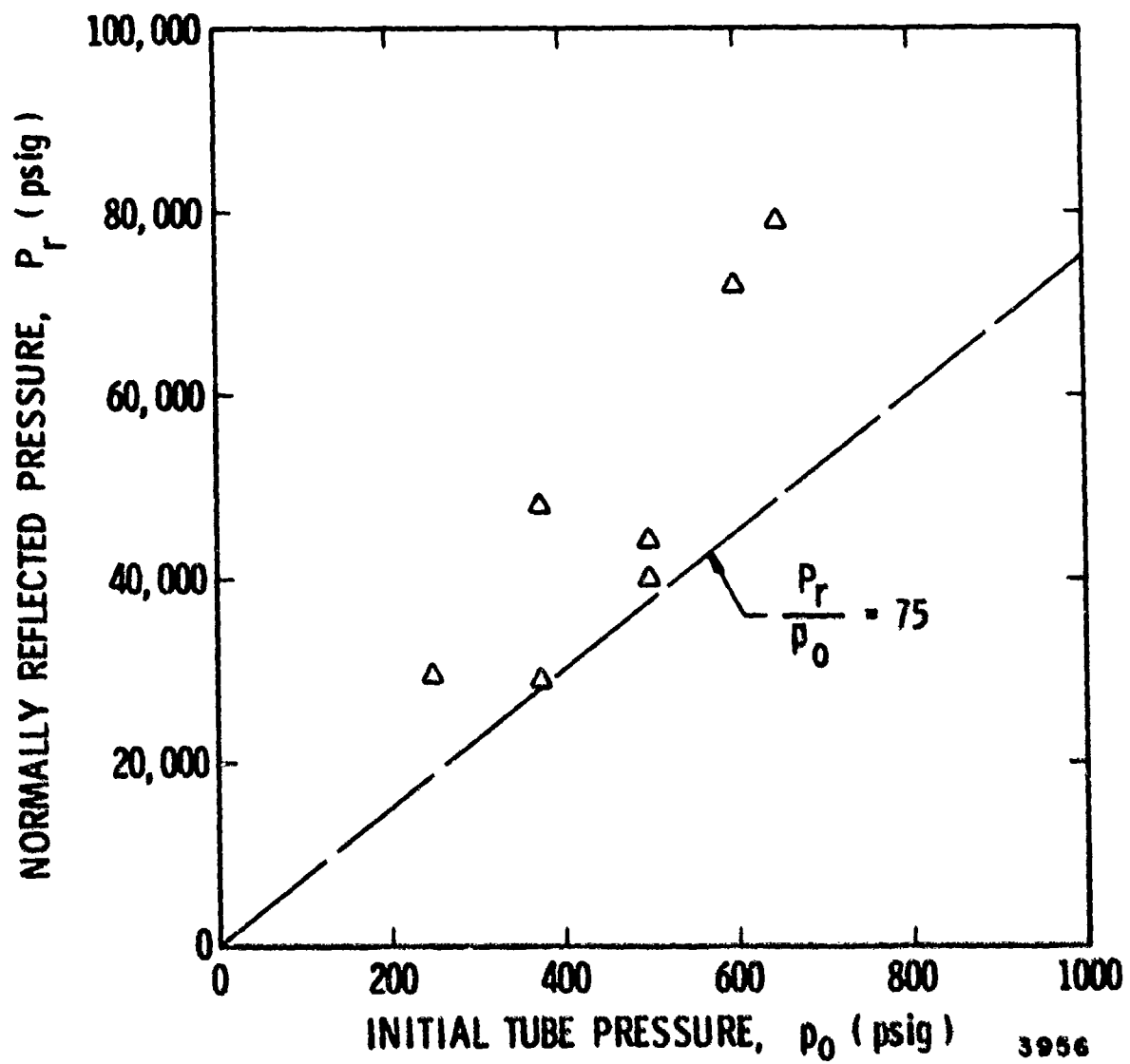


FIGURE 10. REFLECTED PRESSURES FOR SMALL CHAMBER WITH 112.5% O₂ TO CH₄

greater than those obtained from the larger tube. These differences may be a result of the experimental setup. Because of the dimension of the small tube, it was impossible to introduce the initiating squib system through the side without pre-initiating the squib, damaging it, and/or allowing leakage in the system. Therefore, a larger diameter initiating chamber was welded directly to the smaller tube to house the ignition system. Later it was found that this abrupt change in diameter could have caused an increase in pressure caused by the multiple reflection generated in the system and also the change in flow characteristics induced from the change in diameters. Hence, the multiplier factor was approximately 25% higher than in the larger diameter tube.

Considering these factors, this difference does not invalidate the scaling, and perhaps scaling should be further investigated using a larger diameter tube than those used in this program so that replica models can be constructed. On the shot yielding 79,000 psi, the pressures were great enough to blow out the tubing immediately above the test chamber. The impulses obtained from this series of tests ranged from 3.0 to 13.4 psi-sec and are plotted in Figure 11. According to the model law, impulses scale directly with the scale factor λ . For this particular test, the smaller tube was one-half the dimension of the larger tube, and, therefore, to compare directly, one must multiply the impulse obtained with the smaller tube by a factor of 2. The data obtained compare well when multiplied by a factor of 2.5, but data scatter is great enough that the scaling law is not necessarily invalidated. The time of arrival when applying the scale factor of 2.5 compared well with the times obtained with the larger tube.

229% O₂ to CH₄

These tests were conducted to measure the effects of an oxygen-rich mixture consisting of 229.0% of O₂ to CH₄. The initial pressure tested was 500 psi, and the reflected peak pressure measured was 65,000 psi. On this shot, the transducer diaphragm was damaged beyond repair. Even though a peak pressure was obtained, the trace record was not good enough to measure an impulse, primarily because of the very short duration of the pulse. Because the transducer was damaged, there is a question on the validity of the peak pressure measured. The time of arrival was 0.7 millisecond. This shot was repeated, introducing a new Kistler 607-C4 transducer. The record obtained was difficult to interpret, and, therefore, no data were obtained.

73% O₂ to CH₄

These tests were conducted to measure the effects of an oxygen lean mixture consisting of 73% of O₂ to CH₄.

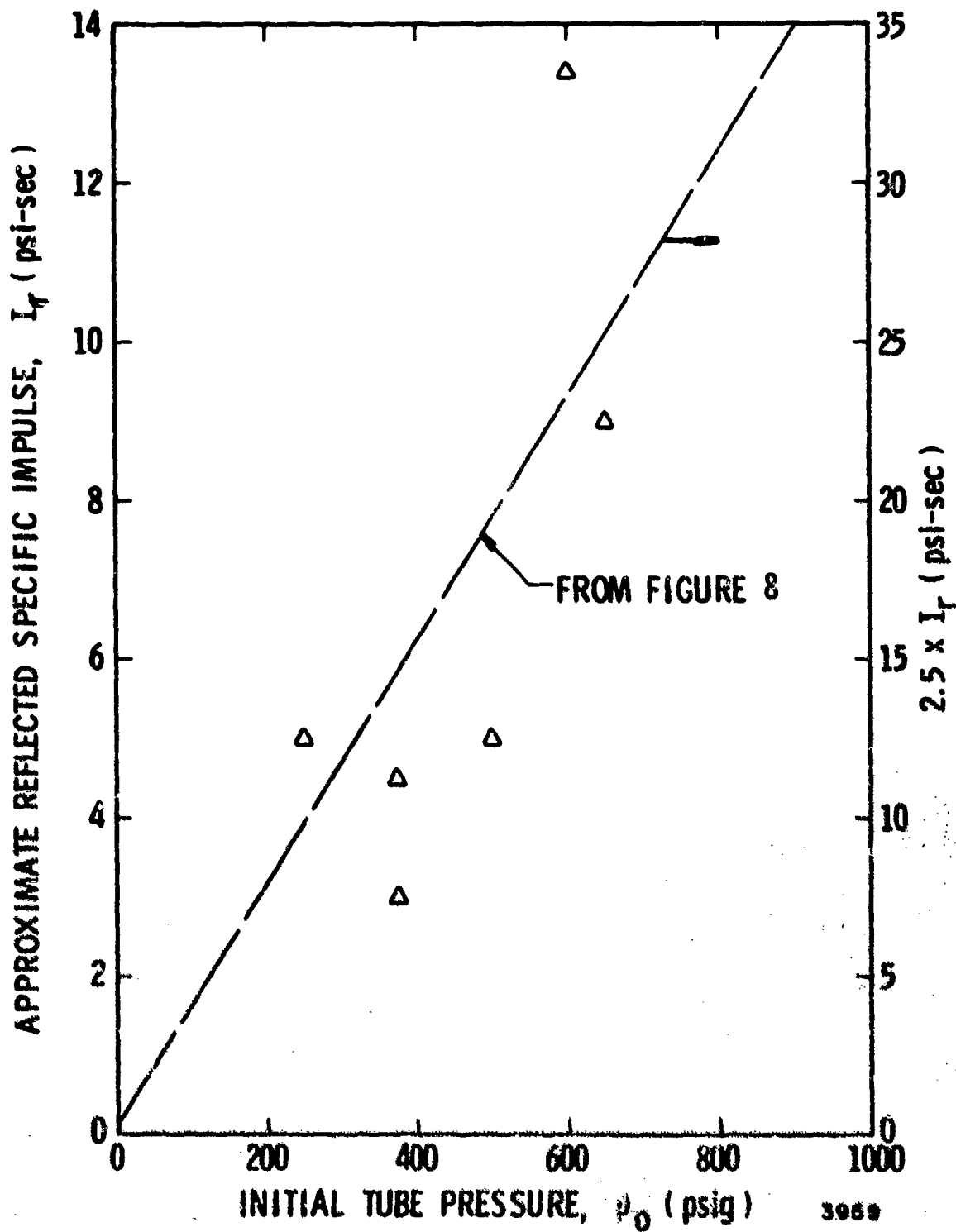


FIGURE 11. REFLECTED IMPULSE FOR SMALL CHAMBER WITH 112.5% O₂ TO CH₄

Initial pressures ranged from 125 to 650 psi, and the peak reflected pressures ranged from 2500 to 66,000 psi. These pressure data are plotted in Figure 12 and compared with the line given in Figure 7. A line drawn through the data points produced a ratio of $(P_r/p_o) \approx 36$. This is roughly half of the multiplier factor obtained at 112%. Impulses ranged from 2.6 to 7.2 psi-sec, which were considerably lower than those obtained at 112%. These results indicate that for oxygen lean mixtures the peak pressure and impulses are reduced. However, the impulses are still relatively high.

The average velocity obtained from the strain gauge time of arrival was 9280 ft/sec. Note that this is a higher value than the one obtained at 112%. However, since all of these data were normalized to the first strain gauge location, not knowing the scatter at this location, the absolute differences in the velocities could be considerably lower. As pointed out in Reference 7, wide variance in both detonation velocities and pressures can be obtained by simply changing gas mixture ratios. This was apparently observed in these experiments.

57% O₂ to CH₄

Initial pressures tested were at 500 psi and 1500 psi, respectively. The reflected peak pressures obtained ranged from 20,000 to 30,000 psi, for a constant setting of 500 psi. At the initial pressure of 1500 psi, no reflected pressures or impulses were recorded because of an error in oscilloscope settings. However, considerable damage was experienced on this test. The ignition squib-spark plug system was completely blown out of the test chamber, allowing the gases to vent to the test building. Considerable damage was done to the building. The pressure transducer was also damaged beyond repair. Although no data were measured, our previous experience in this program indicated that any time a pressure line ruptured and the center of the spark plug was blown out, the pressures exceeded 60,000 psi. Furthermore, blow-out of the pressure lines occurred at 79,000 psi. From these observations, one can summarize that, in order to completely blow out the transducer from its high-pressure fitting, the pressures must have exceeded 60,000 psi, and perhaps could have been greater than 80,000 psi.

23% O₂ to CH₄

All the tests at this mixture were conducted at an initial pressure of 500 psi. A modification to the ignition system was made for some of the tests conducted with this mixture.

Tests initiated with the squib-spark plug system described earlier yielded reflected peak pressures which scattered from 8800 to 39,000 psi. The impulses scattered between 3.1 and 8.7 psi-sec. When two squibs were introduced, the reflected peak pressures varied between 53,000 and 62,000 psi

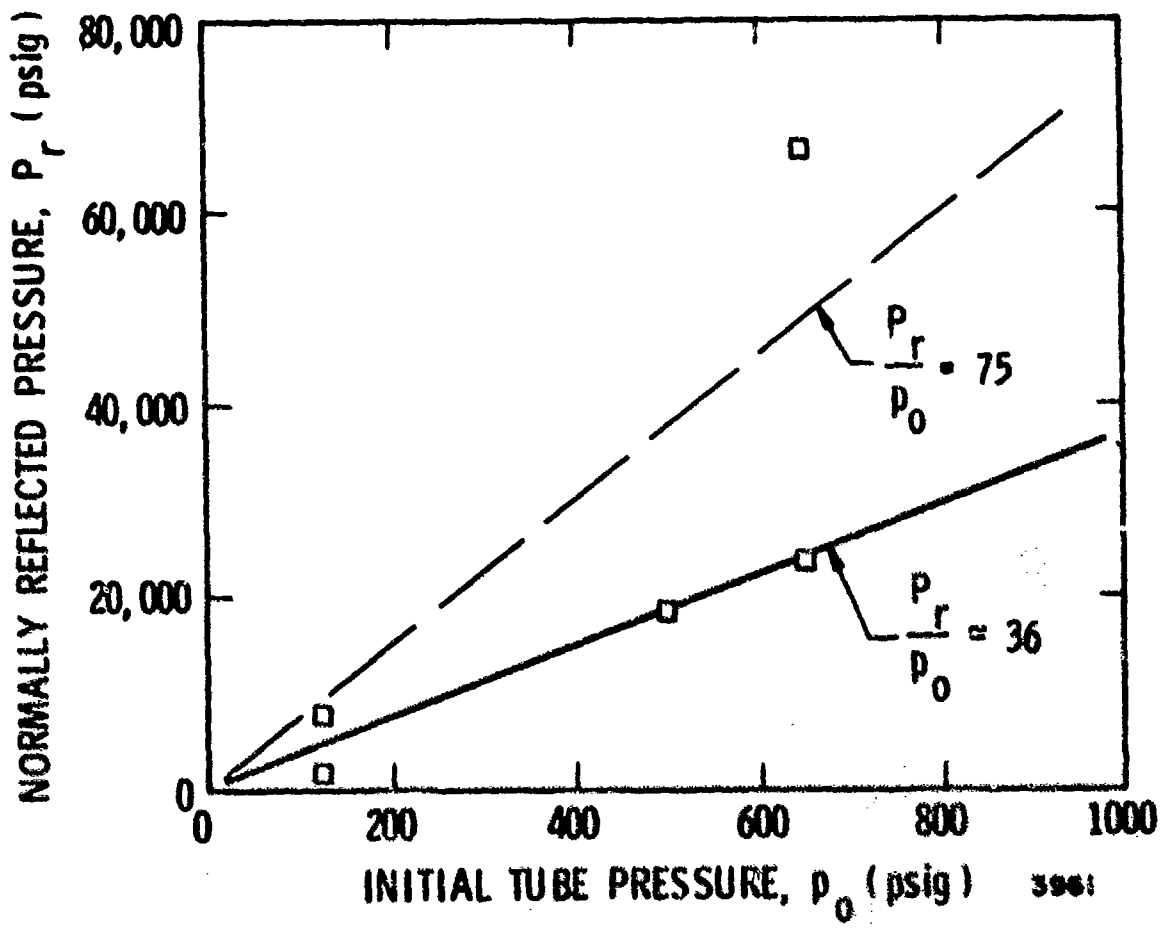


FIGURE 12. REFLECTED PRESSURES FOR LARGE CHAMBER WITH 72% O₂ TO CH₄

for a constant 500-psi initial pressure. The impulses ranged between 10.0 and 10.3 psi-sec.

From these tests it appears that the method of ignition is very important in the efficiency of the detonation produced. Nevertheless, the pressures produced at high initial pressures are considerably greater than those produced at 100% stoichiometric ratios at atmospheric pressures.

Air-Methane Mixtures (73% and 93% Air to CH₄)

The purpose of these tests was to measure the effects of two ratios of air-methane mixtures. Three tests were conducted using mixtures containing 73% air to CH₄. The first shot was initiated with a one-squib system at 500-psi initial pressure. The time required to ignite the squib was 30 seconds. No data output was recorded from the transducer. Direct observation revealed that the test chamber was warm, and a small amount of carbon was found in the exhaust line, suggesting that a low-grade reaction might have occurred. The second shot was a repeat of the first except that two squibs were used in the ignition system. The results were the same as the first test.

The third test was conducted utilizing two squibs for ignition at 1000-psi initial pressure. The results were the same as before, experiencing a definite thermal gradient from top to bottom of the test chamber. The lower portion of the test chamber was warmer than the upper.

One test was conducted with a mixture of 93% air to CH₄. The initial pressure for this test was 1000 psi, and two squibs were used for ignition. The pressure record from this test showed a very slow buildup of pressure to 2500 psi maximum and was sustained at this level for a period of approximately 0.5 second. This result implies that the mixture burned and did not detonate. At this point, it was decided that either a better ignition system was needed to drive this mixture to detonation; or one must utilize a stoichiometric O₂-CH₄ mixture with various percentages of air or nitrogen. The results of this program indicate that this new mixture may reduce the peak reflected pressures generated from a stoichiometric mixture reaction and perhaps increase the impulse.

CONCLUSIONS

The principal conclusions and observations reached as a result of the test conducted in this program are:

- (1) For nearly stoichiometric gas mixture ratios of 112.5% O₂ to CH₄, the normally reflected pressure (P_r) appears to be a linear function of the initial test chamber pressure (p_0)

for the initial pressures tested. The multiplier obtained from the slope of the line (P_r/p_0) is 75. The impulses generated from this mixture ranged from 0.2 to 31.5 psi-sec and indicated a linear relationship between specific impulse and initial test chamber pressure.

- (2) To achieve detonation with the ignition system used, the working gases must be introduced at the same time and mixed as they are being pumped into the chamber.
- (3) The pressure data obtained in the smaller diameter tube were greater by approximately 25% than those obtained in a larger diameter tube, for tests using the same (112.5% O_2 to CH_4) gas mixture ratio. This difference was attributed to the smaller tube not being a replica model of the large tube, and, therefore, it was felt that this difference did not invalidate scaling. The same percentage difference was observed in the impulse data, and the same conclusion drawn from the pressure data applies to the impulse data.
- (4) Gas mixtures of 229% O_2 to CH_4 yielded inconclusive results due to damage of the transducers. On one shot the reflected peak pressure measured at 500 psi and initial pressure was 65,000 psi. This pressure was considerably higher than the pressures measured at near stoichiometric mixtures for the same initial pressures.
- (5) At an oxygen-to-methane mixture of 73%, a linear function was again established between initial and reflected pressures. A ratio of $P_r/p_0 \approx 36$ was obtained for this mixture, which is roughly half of the multiplier factor obtained at near stoichiometric ratios. The impulses obtained for this ratio ranged between 2.6 and 7.2 psi-sec, which are much lower than the values obtained near stoichiometric ratios. The average detonation velocity obtained for this ratio was 9280 ft/sec.
- (6) Gas mixtures of 57.3% O_2 to CH_4 yielded similar results in pressure and impulse to those obtained at 72% O_2 to CH_4 , with larger scatter in the pressure data than in the impulse data for a constant initial pressure of 500 psi. At 1500 psi initial pressure, considerable damage to the experimental setup and transducer was experienced. From experimental observations it was concluded that the pressures must have exceeded 60,000 psi, and perhaps could have been greater than 80,000 psi for the damage experienced.
- (7) Gas mixtures of 23% O_2 to CH_4 yielded large scatter in pressure and impulse data for the same initial pressures when

initiated with a single squib system. For the same initial pressures using a double squib ignition system, the pressures and impulses were considerably larger than the single ignition system, suggesting that the method of ignition is very important in the efficiency of the detonation produced.

- (8) Air-methane mixtures tested up to 1000-psi initial pressures did not produce high order detonation with the ignition systems used. However, large impulses were experienced.
- (9) From the results obtained in this test program, it has been shown that the detonation pressure-time history can be controlled by varying the gas ratio mixtures and the initial confined pressures. Gaseous detonations have the advantageous characteristic that they yield low peak pressures and high impulses relative to other types of explosives, making them attractive for mining, quarrying, and/or oil and gas recovery techniques.

REFERENCES

1. Strehlow, R. A., "Unconfined Vapor-Cloud Explosions--An Overview," International Symposium on Combustion at Pennsylvania State University, 1972.
2. Zabetakes, M. G., "Flammability Characteristics of Combustible Gases and Vapors," Bureau of Mines Bulletin 627, U. S. Department of Interior, 1965.
3. Blackstone, W. R., and Wenzel, A. B., "Explosive Sensitivity and Reaction Intensity of Cryogenic Explosives," Final Report, Project G2-3060, Southwest Research Institute, 1971.
4. Every, R. L., and Thieme, J. O., "Liquid Oxygen and Liquid Methane Mixtures as Rocket Monopropellants," Journal of Spacecraft and Rockets, Vol. 2, No. 5, pp. 787-789, October 1965.
5. Wenzel, A. B., "Feasibility Studies of Gaseous Explosive Mixtures as a Secondary Gas-Oil Recovery Technique," Final Report, Project 02-3567, Southwest Research Institute, 1973.
6. Klima, R. J., and Fugelso, L. E., "1500-psi Dynamic Load Simulator," Proceedings of the 2nd Conference on Military Applications of Blast Simulation, 1971.
7. Fedderson, D. W., "Explosive Gas Forming," Proceedings of the 1st International Conference of the Center for High Energy Forming, Estes Park, Colorado, June 19-23, 1967.

PRESSURE RELIEF AND DECAY IN INTERNAL EXPLOSIONS

by

R.G.S. Sewell & G.F. Kinney
Naval Weapons Center
China Lake, CA

Damage from hydrostatic pressure rise in an internal explosion can in principle be reduced by venting to prevent the rise. Venting phenomena are treated in some detail in a recent report (reference 1). Here basic relations of thermodynamics and compressible fluid flow provide an expression for rate of pressure change due to venting, dP/dt , as

$$dP/dt = - \frac{C_D A P}{V} \sqrt{\frac{RT}{M}} \left[k \left(\frac{2k}{k+1} \right)^{1/2} \left(\frac{2}{k+1} \right)^{1/k} - 1 \right] \quad (1)$$

where C_D is the discharge coefficient for flow through vent area A , V the volume of confined gas and R the molar gas constant. Here gas pressure P , its temperature T formula mass M , and specific heat ratio k are instantaneous bulk values that may vary during the venting process. The relation presumes adiabatic conditions.

For internal explosion of a fuel-air mixture with appreciable hydrostatic pressure rise and associated gas leakage through vents, average values for these variables above can be assigned. A representative average temperature is 2700 K, a representative formula mass for the gases is 28.9, and a representative specific heat ratio for them is 1.25. Also a discharge coefficient of unity may be assigned for transient flow conditions. Then

$$dP/dt = -725 (A/V)P \quad (2)$$

for SI metric units of the meter and the second. It is convenient to write this relation in the form $dP/dt = k_2 P$, where k_2 , the rate constant for pressure decay becomes

$$k_2 = -725 (A/V) \quad (3)$$

Let us consider next, rise rates for the pressure in an internal explosion. Such an explosion ordinarily results from chemical reactions, rates of which depend on many items such as effective concentrations. For gases, the effective concentration is proportional to the pressure. The basic relation for rate of the chemical reaction of concern here, becomes in greatly simplified form

$$dP/dt = k_1 P \quad (4)$$

where rate constant k_1 is to be evaluated empirically for the particular explosion of concern.

Comparing rate equations (2) and (4) it can be seen that if the pressure decay rate of equation (2) is greater than pressure rise rate of equation (4), no hydrostatic pressure rise occurs. On the other hand if pressure rise rate is greater than pressure decay rate, the pressure increases and rate of chemical reaction in the explosion increases exponentially until a maximum pressure is reached. A critical situation exists where the two rates of pressure change are equal and opposite. This can be represented symbolically in the form

$$k_1 + k_2 = \text{zero} \quad (5)$$

Rate constant k_2 of above expressions (5) and (3) involves a vent area. If requirements of equation (5) are met, this area becomes a critical vent area for that explosion. Vents larger than this prevent runaway hydrostatic pressure rise and so may greatly alleviate damage effects. Vents smaller than critical, however, cannot prevent a runaway pressure rise that may be quite damaging.

The concept of a critical venting area for an internal explosion is here applied to two explosion situations. The first is a fuel-air explosion in a confined volume such as a ship compartment, a grain elevator, or a motor boat hull. The other concerns a store of propellant, either rocket propellant or cannon propellant.

For an internal explosion in a confined volume of fuel-air mixture, the chemical reaction is that of combustion. The rate of this reaction, and also the associated rate of pressure rise, is proportional to the pressure itself as noted above. The rate is also proportional to the area of reaction front of the combustion fireball. Now it has been observed (reference 2) that for both thermal and mechanical reasons the surface area of this fireball quickly approaches the surface area S of the confining volume. Also, the pressure rise caused by a given amount of reaction is inversely proportional to total volume V of the fuel-air mixture. Pressure rise rate equation (4) can thus be written in the form

$$dP/dt = B(S/V)P$$

where B is a constant of proportionality whose value is to be determined. Written in alternative form, $d \ln P = B(S/V)dt$, and integrating from initial pressure P_0 at time t_0 to pressure P at time t

$$\ln(P/P_0) = B(S/V)t \quad (6)$$

Measurements on many internal explosions are described in reference 2, and its extensive data permit ready evaluation of proportionality constant B of equation (6). Convenient for this purpose are pressure-time traces; these typically show an exponential type of pressure buildup during its early phases. For evaluation of constant B a point near maximum buildup is selected. For a typical completely confined explosion, one with no vent, and where initial turbulence is induced mechanically

$$B = \frac{\ln(P/P_0)}{t(S/V)} = 5.0 \text{ m/s} \quad (7)$$

for SI metric units of the meter and the second. The corresponding pressure rise rate constant of relation (4) becomes

$$k_1 = 5.0 (S/V)$$

for internal surface area S in square meters and confining volume V in cubic meters, and rate constant k_1 in units of per second. This numerical value 5.0 pertains to an explosion with an initially turbulent fuel-air mixture. For initial quiescent conditions the pressure rises somewhat more slowly giving a corresponding numerical value 0.85 for the above rate relation.

For the critical venting area in a confined fuel-air explosion, this relation is combined with equation (5), as

$$5.0 (S/V) - 725 (A/V) = \text{zero}$$

and the critical area A^* found as

$$A^* = 0.007 S \tag{8}$$

where S is the internal surface of the confining volume. This important relation indicates that a venting area greater than seven-tenths of one percent of the internal surface area of a confining volume will prevent runaway hydrostatic pressure rise in an internal explosion. This is a relatively small vent. Also, it is important to note that the volume of the system to be vented has no direct effect on critical venting area requirement.

For an internal explosion with initially quiescent conditions the critical vent area can be found to be even smaller, only 0.12 percent of confining surface area, or a remarkably small amount. Where venting is for safety reasons the larger vent, where turbulence is presumed, would undoubtedly be preferred.

Venting equations (1), (2), and (3) on which the above observations are based actually apply only for hydrostatic overpressures above some minimum amount, typically about 0.8 bars (reference 1). Thus the actual maximum pressure rise for an internal explosion in a critically vented volume is about

0.8 bars; vents larger than the critical vent limit pressure rises, to even smaller overpressures.

Next let us consider venting a possible explosion of a store of propellant in a container. Here the rate of pressure relief is as described in above equations (1), (2), and (3). However, rates of pressure rise follow relations quite different from the rise rate equations above. For a propellant, gases of the explosion are generated by a surface burn effect at a rate proportional to the pressure and to the burn surface area S_B . Expressed symbolically

$$\text{rate of burn } \propto S_B P \quad (9)$$

where a constant of proportionality is to be evaluated experimentally. For a conventional rocket propellant the linear rate of burn is about one centimeter per second at 135 bars, and from this the proportionality constant is 7.4×10^{-5} meters per second-bar.

To translate such a burn rate into a pressure rise rate, the mass rate is found by multiplying by the material density of propellant ρ . For this a typical value is 1.65 g/ml, or 1650 kg/m³ in SI units, as pertains to cellulose nitrate. Mass rate is then converted to mole rate for gas formation, dn/dt , by dividing by formula mass M for gases formed. A typical formula mass is 28.9 g/mol, or 0.0298 kg/mol in SI units. Pressure rise rate is then obtained through the ideal gas law as

$$\frac{dP}{dt} = \frac{RT_B}{V} \frac{dn}{dt} = \frac{RT_B \rho S_B}{VM} P = k_1 P \quad (10)$$

where R is the molar gas constant, 8.314×10^{-5} bar-m³/mol - K, and T_B the burn temperature, the temperature at which the gases are formed. This typically is about 2500°K in a closed container.

Introducing numerical values into equation (10) and solving for the pressure rise rate constant k_1 as used in equation (4),

$$k_1 = 0.88 (S_B/V) \quad (11)$$

for the propellant store with total burn surface S_B burning in confined volume V . (This is a greatly simplified adaptation of an important equation in interior ballistics.)

This rate constant is introduced into equation (5) to give

$$0.88 (S_B/V) = 725 (A/V)$$

and the critical vent area A for this store of explosives found as

$$A^* = 0.0012 S_B \quad (12)$$

where S_B is the total area of the burn surface. Thus the critical vent area for a propellant store depends on burn surface and not on volume of its storage container. This conclusion is quite analogous to one deduced above for the critical vent area for a fuel-air explosion in a confined space.

Burn surface for a propellant depends on both grain size and configuration. Let us select for study a typical cannon propellant with cylindrical grains 10 mm long, 3 mm in diameter, and a single longitudinal perforation with diameter of one millimeter. Then by geometry the surface area per grain is 1.382 cm^2 , and volume of propellant material per grain is 0.0628 cm^3 . For a bulk loading density of 0.5 grams per cubic centimeter, each grain represents $0.0628 \times 0.5 = 0.0314$ grams of propellant load. The surface to mass ratio for this load becomes $1.382/0.0314 = 44 \text{ cm}^2/\text{g}$, or $4.4 \text{ m}^2/\text{kg}$ in SI metric units. Substituting into equation (12) the critical vent for a store of this propellant with mass m_p becomes

$$A^* = 0.0053 m_p \quad (13)$$

A container with one kilogram of this propellant thus requires a vent with 53 square centimeters area in order to prevent an initially quiescent burn, as from accidental ignition, from becoming a runaway explosion. In practice, a reasonable margin for safety is prudent and an appreciably larger vent would be provided.

An interesting deduction to be made from equation (13) concerns behavior of this propellant powder in a typical cannon, for example a 90 mm gun. Here the open gun barrel could be a vent; its vent area is 0.00636 square meters. The corresponding mass of this propellant for critical venting becomes $0.00636/.00533$ or 1.2 kilograms, closely. If an open gun (one without projectile or wadding) were loaded with more powder than this and it then uniformly ignited, the powder would explode, for its gases could not be vented. On the other hand less than 1.2 kilograms of this powder in the open gun would not explode; it could only burn but probably with ejection of burning grains.

Next, let us apply the above relations to another limiting situation, that of a completely unconfined store of propellant. This unconfined store represents the ultimate in venting area. For a hemispherical store this surface area is also the venting area, or $\pi l^2/2$, where l is the length along the diameter of the store. Mass of propellant in this store is given as the product of volume and loading density. For a loading density of 0.5 g/cm^3 , propellant mass is $500 \pi l^3/12$. Equation (13) with these values indicates that

$$A^* = \pi l^2/2 = 0.0053 \times 500 \times \pi l^3/12$$

Solving for diameter of this critical store where its surface is also a critical venting area, this becomes 2.3 meters. Corresponding mass contained in this store is a limit or critical mass; here this is computed as 1500 kilograms, or 1.5 metric tons. For a propellant with this grain size and configuration, then a store of 1.5 tons represents a critical mass. A hemispherical store larger than this if uniformly ignited always explodes; a smaller store would show only deflagration with reduced damage potential.

As another application of the above relations let us consider influence of grain size of a propellant such as a ball powder with its spherical grains. The rate constant for the pressure rise relation for burning of this powder can be estimated closely by equation (10); however, for convenience let us accept burn characteristics similar to those described above. Then the rate constant of equation (11) is $k_1 = 0.88 S_B/V$, where S_B is the burn surface area (m^2) for a powder stored in a container with volume V (m^3).

Now the surface for a single grain of this powder with diameter d is πd^2 . Its volume is $\pi d^3/6$, and for a loading density of 0.6 g/cm^3 this volume corresponds to an average mass of $600 \pi d^3/6$ (SI units). The burn surface to mass ratio becomes $10^{-2}/d$, or $S_B = 10^{-2} m_p/d$, where m_p is mass of the powder. Introducing into equation (12), the critical vent area is obtained as

$$A^* = 1.2 \times 10^{-5} m_p/d \quad (14)$$

for SI units of kilograms for mass of propellant, meters for grain diameter, and square meters for vent area.

Applying this relation to a powder with grains one millimeter in diameter, the minimum vent area to prevent explosion of one kilogram of this powder is found to be 0.012 m^2 , or 120 square centimeters. For ordinary one kilogram containers, this is a somewhat unattainable value. Powders with smaller grains require even larger vent areas which are even more difficult to provide. It may be concluded that one kilogram stores of such powders if accidentally ignited would always produce explosions that could not be vented.

SUMMARY

Critical venting area for an internal explosion is that minimum area needed to prevent runaway hydrostatic pressure rise. An equation that mathematically defines this critical venting area is developed from basic considerations of thermodynamics, compressible fluid flow, and chemical kinetics.

Critical vent area for explosion of a turbulent fuel-air mixture in a confined space is computed from the above relation to be some seven-tenths of one percent of the internal surface of the confining volume, and is independent of the confining volume itself. An initially quiescent fuel-air mixture burns at a somewhat slower rate and so shows an even smaller critical vent area that also is independent of volume.

Critical vent area for a store of propellants is found to depend only on burn surface of propellant; that is, on the amount, on grain size and configuration--but not on volume of the storage container. Critical vent areas for stores of a typical cannon propellant and for a ball powder are computed; these are different but each is proportional to mass of the stored propellant.

A limit situation with a propellant is a completely unconfined store; here surface area of the store is the vent area, and this also is the maximum available vent area for that store. Mass of propellant in an unconfined store such that its surface area is also the critical vent area is a critical mass for that propellant. Stores with a larger mass than this would, if uniformly ignited, always explode while smaller stores would only burn relatively quietly. An equation which predicts this critical mass is derived and a sample calculation included.

REFERENCES

1. *Venting of Explosions*, G. F. Kinney and R. G. S. Sewell, Naval Weapons Center. TM-2448 (July 1974).
2. *Explosion Development in Closed Vessels*, John Nagy et al, Bureau of Mines RI 7507 (1971).

BLAST ENVIRONMENT FROM FULLY AND
PARTIALLY VENTED EXPLOSIONS IN CUBICLES

Messrs W. A. Keenan & J. E. Tancreto
Civil Engineering Laboratory
NCBC Port Hueneme, CA

INTRODUCTION

The U. S. Army Armament Command (ARMCOM) is modernizing ammunition facilities, including equipment and protective structures, used in the manufacture, processing and storage of conventional munitions. Structures which serve to prevent explosion propagation, damage to material, or injury to personnel are being designed to comply with the Army TM5-1300 (Navy NAVFAC P-397) Manual, "Structures to Resist the Effects of Accidental Explosions." [1]. The manual contains methods and criteria to establish the output from an explosion in its environment and its effect on that environment in terms of blast, fragments and structural response.

In the plant modernization program it was found that the TM5-1300 manual lacks complete information in chapter 4 on the blast environment from partially confined explosions, i.e., explosions in an air space confined by one or more walls, such as cubicles which serve to direct and control the output from an accidental explosion. Consequently, Picatinny Arsenal (Manufacturing Technology Directorate) sponsored experiments at CEL (Civil Engineering Laboratory) to develop methods and criteria for predicting the blast environment in and around cubicles. Ammann and Whitney, Consulting Structural Engineers, New York, under contract to Picatinny Arsenal, provided technical guidance throughout the study.

The CEL experiments involved exploding a range of charge weights inside several small-scale cubicles representing various sizes, shapes, vent areas and charge densities. A four-wall cubicle was tested with a restricted roof opening of various sizes to provide data on partially vented cubicles.* Two three-wall cubicles, each with and without a roof, were tested to collect data on fully vented cubicles.* The charge weight (W) varied from 0.50 to 3.00 pounds of Composition B explosive, charge density (W/V) from 0.009 to 0.375 lb/ft³, and the degree of venting (A/V) from 0.010 to 1.00 ft²/ft³. The blast pressure history was measured inside the cubicle and outside at scaled distances (R/W^{1/3}) from 1.42 to 63.0 ft/lb^{1/3}. The blast environment was related to scaled parameters, involving A, V, W and R, in the form of design charts and equations to aid the designer in predicting the positive and negative

*Distinction between full and partial venting depends on the duration of gas pressures generated inside the cubicle compared to the average duration of shock pressures acting on the cubicle walls. If the gas duration exceeds the shock duration, the partially confined explosion is classified as a partially vented explosion.

pressures, duration and impulse outside fully and partially vented cubicles and the peak gas pressure, impulse, and duration inside partially vented cubicles. A detailed description of the experiments and analysis of the results are contained in Reference 2.

This paper presents and discusses some significant findings from the CEL study, including a series of design charts for predicting the blast environment in and around fully and partially vented cubicles, sample problem solutions which illustrate applications of the design charts, and the influence of cubicle and charge parameters on safe-separation distance requirements for those cases where blast environment, not fragments, dictate safety requirements.

CONFINED EXPLOSIONS

Explosions generate pressures from shock waves produced by the detonation. If the explosion is confined inside an enclosed or partially vented cubicle, gaseous by-products of the explosion generate gas pressures, in addition to the shock pressures. The initial shock wave strikes the walls of the cubicle and is reflected. The reflected waves produce extremely high blast pressures on the walls. The blast pressures rapidly decay as the energy in the shock wave rapidly dissipates.

In the same time period, the gas pressures rise inside the cubicle to some peak value and then gradually decay as gas temperatures drop and gas pressures are vented from the cubicle. The peak gas pressure is characteristically low compared to the peak blast pressure. However, when the vent area is small, the duration of the gas pressure can be many times greater than the duration of the blast pressure. If the vent area is increased, the duration of the gas pressure will decrease. At some critical vent area, the duration of the gas pressure will equal the duration of the blast pressure. This critical vent area can define the division between fully and partially vented explosions.

In terms of structural response, the gas pressure pulse can be far more damaging than the shock pulse, depending on the duration of the gas pulse, t_g , relative to the duration of the shock pulse, t_0 . If $t_g/t_0 < 1$, the explosion is classified as a fully vented explosion and the gas pulse, if any, can be neglected in the design of the cubicle. Figure 1b is typical of the pressure pulse inside a fully vented cubicle. For $t_g/t_0 > 1$, the explosion is classified as a partially vented explosion and both the gas and shock pulses must be considered in the design of the cubicle. Figure 1a is typical of the pressure pulse inside a partially vented cubicle. The importance of the gas impulse increases with t_g/t_0 until at some large value of t_g/t_0 , the shock pulse can be neglected since its energy is insignificant compared to that in the gas pulse. Therefore, in presenting methods and criteria for blast environment in and around cubicles, it is useful for design purposes to delineate between fully and partially vented explosions.

PARTIALLY VENTED EXPLOSIONS

Definition

The scaled duration of positive pressure measured inside the cubicles is plotted in Figure 2 as a function of the scaled vent area, $A/W^{2/3}$. The unshaded data points denote cases where $t_g > t_0$. The shaded points denote cases where it appeared that $t_g < t_0$.

The family of lines shown in Figure 2 connect data points representing the same value of W/V . The solid lines are straight, parallel and connect all data points corresponding to $t_g > t_0$. The dashed lines connect the data point believed to correspond to $t_g < t_0$. The dashed lines are also straight and parallel but their slopes are greater.

Between the ends of the solid and dashed lines is a zone which defines the transition from $t_g > t_0$ (partially vented cubicle) to $t_g < t_0$ (fully vented cubicle). There is insufficient experimental data to exactly define the transition zone but the zone can be bounded. It was discovered that a line which falls just "below" all unshaded data points is described by

$$A/V^{2/3} = 0.21 \quad (1)$$

Equation 1 is considered a reasonable upper bound to the transition zone corresponding to $t_g = t_0$. Similarly, a line which falls just "above" all shaded data points is described by

$$A/V^{2/3} = 0.60 \quad (2)$$

Equation 2 is considered a reasonable lower bound to the transition zone corresponding to $t_g = t_0$. In other words, the parameter $A/V^{2/3}$, with a value some where between $0.21 < A/V^{2/3} < 0.60$, defines the division between a fully and partially vented explosion, at least for the range of test parameters. Note that $A/V^{2/3}$ is independent of charge weight and a dimensionless parameter and, therefore, independent of the physical size of the cubicle and charge.

To be conservative, it is recommended for design purposes that a cubicle be considered partially vented if $A/V^{2/3} < 0.60$. This criterion implies, as illustrated in Figure 2, that the practical sizes of three-wall cubicles with and without a roof and four-wall cubicles without a roof are fully vented cubicles ($A/V^{2/3} > 0.60$).

Blast Environment Inside Cubicle

Peak Gas Pressure. The peak gas pressure, p_g , measured inside the test cubicles is plotted as a function of W/V in Figure 3. The figure includes experimental data reported in Reference 3 for Composition B charges ($0.0016 < W/V < 0.0259$ lb/ft³) inside a relatively large four-wall cubicle with a circular vent hole in its roof. The curved line in Figure 3 is the predicted peak gas pressures using an NOL computer program [4].

The measured peak gas pressures and NOL predicted values are in excellent agreement for a degree of venting, $A/V < 0.010 \text{ ft}^2/\text{ft}^3$. (Similar agreement was found by Proctor and Filler in comparing NOL predictions with peak gas pressures measured by H.R.W. Weibull for a wide range of charge to volume ratios, $0.00125 < W/V < 0.287 \text{ lb}/\text{ft}^3$, but for relatively small vent areas, $7.6 \times 10^{-6} < A/V < 60 \times 10^{-4} \text{ ft}^2/\text{ft}^3$) [4]. For larger degrees of venting ($A/V > 0.010$), the data points in Figure 3 fall well below the NOL curve and for a fixed degree of large venting, the difference increases with W/V . For example, for points with $A/V = 0.043$ and 0.031 , the measured gas pressures are lower by 27% at $W/V = 0.0069$, 31% at $W/V = 0.069$, 39% at $W/V = 0.145$ and 52% at $W/V = 0.287$. Some of the differences may stem from possible errors in interpreting the measured pressure histories but this source of error could account for no more than perhaps 20% of the difference.

It is concluded from Figure 3 that p_g depends on W/V and, to a lesser degree on A/V . For $A/V < 0.010$, venting has no appreciable influence on p_g but for $A/V > 0.010$ the decrease in p_g can be significant, especially for large values of W/V . Experiments are needed to find the relationship between p_g and W/V for large values of A/V . Until this relationship is found, it is recommended that the NOL curve for gas pressure be used for predicting design loads for $A/V < 0.010 \text{ ft}^2/\text{ft}^3$ and a value 25% less for $A/V > 0.010 \text{ ft}^2/\text{ft}^3$.

Impulse of Gas and Shock Pressures. The scaled peak impulse of the gas pressure measured inside the cubicles is plotted in Figure 4 as a function of the scaled vent area, $A/W^{2/3}$. The unshaded data points denote cases where the total impulse of the gas pressure, i_g , far exceeded the total impulse of the shock pressure, i_s .

The family of solid lines in Figure 4 connect data points having the same value of W/V . The best fit lines are straight and parallel, at least within the range of experimental data. These lines are described by

$$i_g/W^{1/3} = 569 (A/W^{2/3})^{-0.78} (W/V)^{-0.38} \quad \text{for } A/V^{2/3} < 0.21 \quad (3)$$

Equation 3 has some error because it is derived from impulse data which include the combined impulse from gas and shock pressures. However, any error in Equation 3 from this source is considered insignificant since all data points originate from pressure-time histories which clearly show the shock impulse was insignificant compared to the gas impulse.

There is no experimental data to define the exact shape of the lines in Figure 4 for $0.21 < A/V^{2/3} < 0.60$. To provide compatibility with the impulse curves in the TMS-1300 Design Manual for a fully vented cube, the shape of the dashed lines in Figure 4 were drawn so that at $A/V^{2/3} = 0.60$, the effective duration of the shock pressure, t'_s , given by Equation 4-1 of the TMS-1300 Design Manual [1] is equal to the effective duration of the gas pressure, $t'_g = 2 i_g/p_g$. By this scheme, the impulse

curves in Figure 4 provide a smooth transition from a partially vented cube to a fully vented cube and are compatible with the pressure loading obtained from the TM5-1300 Design Manual for a fully vented cube.

The instrumentation in the CEL experiments did not allow measurements of the shock pressure impulse. For example, in the partially vented cubicles the shock impulse could not be isolated from the much larger gas impulse. In the fully vented cubicles, where the gas impulse was insignificant, the shock pressures were too severe for the pressure transducers. However, Figures 4-17 through 4-62 of the TM5-1300 Design Manual already contain curves for predicting the average shock impulse on the wall of a cubicle.

It is recommended for design purposes that Figure 4 be used to predict the gas impulse for $A/V^{2/3} < 0.60$ and Figures 4-17 through 4-62 of the TM5-1300 Design Manual be used to predict the shock impulse for any value of $A/V^{2/3}$. A procedure for predicting i_g for $A/V^{2/3} > 0.60$ is not necessary since one will find in using the above recommendations that for $A/V^{2/3} > 0.60$, $i_g < i_s$, $t_g' < t_o'$ and $p_g < p_r$, i.e. for $A/V^{2/3} > 0.60$, the shock pressure pulse completely masks the gas pressure pulse, and, therefore, dictates the pressure-time design loading for the cubicle.

Duration of Gas and Shock Pressures. The family of straight lines shown in Figure 2 can be expressed in the form

$$t_g/W^{1/3} = 2.26 [AW^{1/3}/V]^{-0.86} \quad \text{for } A/V^{2/3} < 0.21 \quad (4)$$

$$t_o/W^{1/3} = 0.654 [AW^{1/3}/V]^{-1.14} \quad \text{for } A/V^{2/3} > 0.60 \quad (5)$$

The term $AW^{1/3}/V$ in Equations 4 and 5 is defined as the scaled degree of venting.

Equations 4 and 5 are compared with experimental data in Figure 5. As expected, the unshaded data points ($t_g > t_o$) fall along the solid line (Equation 4) and the shaded data points ($t_g < t_o$) fall along the dashed line (Equation 5). The transition zone, defined in Figure 2 by $0.21 < A/V^{2/3} < 0.60$, falls between these lines and is represented in Figure 5 by a series of reverse curves which are tangent to the solid and dashed lines. Note in Figure 5 that the relative position of the transition lines depends on W/V . For $0.21 < A/V^{2/3} < 0.60$, one must enter Figure 5 with known values of both $AW^{1/3}/V$ and W/V to determine the duration of the positive pressure. It is important to note that the duration obtained from Figure 5 is the duration of the exponentially decaying pressure pulse.

For convenience in design, the exponential pressure pulse is replaced by an equivalent triangular-shaped, pressure-time pulse having the same total impulse. It is recommended that the effective gas duration, t_g' , of the equivalent triangular gas pulse be calculated as

$$t'_g = 2 i_g / p_g \quad (6)$$

where i_g = Total gas impulse obtained from Figure 4

p_g = Peak gas pressure obtained from Figure 3

Further, it is recommended that the effective shock duration, t'_o , of the equivalent triangular shock pulse be calculated from Equation 4-1 of TMS-1300 Design Manual [1].

Blast Environment Outside Cubicle

Personnel or fragile buildings may be located in the near vicinity of a cubicle containing explosives. An accidental explosion may produce a blast environment outside the cubicle which constitutes a high hazard to personnel or an unacceptable level of damage to the buildings. In this case, it may be necessary to confine and partially vent the explosion inside a cubicle to reduce the blast environment at some distance from the charge to a safe level. To accomplish this, the designer must know the influence of the size and vent area of the cubicle and the weight and location of the charge on the exterior blast environment at any range from a cubicle.

Peak Positive Pressure. Pressure data from the CEL tests of partially vented cubicles can be described, as shown in Reference 2, by Equation 7.

$$p_{so} = 464 \left(\frac{AW^{1/3}}{V} \right)^{0.37} \left(\frac{R}{W^{1/3}} \right)^{-1.58} \quad \text{for } A/V^{2/3} < 1.0 \quad (7)$$

Equation 7 describes the leakage pressures from partially vented cubicles ($A/V^{2/3} < 0.60$). However, since data from an open-top cube ($A/V^{2/3} = 1.0$) also fits Equation 7, $A/V^{2/3} < 1.0$ is given as the limit. Note that leakage pressures depend on the scaled degree of venting, $AW^{1/3}/V$, and the scaled distance from the charge, $R/W^{1/3}$.

Equation 7 indicates that p_{so} is more sensitive to R than A/V . For example, to decrease p_{so} by say 50%, either R must be increased 55% or A/V decreased 84.6%. The important point is that the designer can still "buy considerable distance" by reducing A/V . Where real estate is a premium, controlling p_{so} by adjusting A/V may be the only solution.

Equation 7 was used to construct the design chart shown in Figure 6. The chart is useful in selecting the degree of venting needed to limit the leakage pressure to a safe level at any distance from a partially vented explosion. It is recommended that Figure 6 be used for design purposes provided $A/V^{2/3} < 1.0$.

Peak Positive Impulse. Frequently, blast pressures outside a cubicle are very short in duration compared to the fundamental period of vibration of structures located in the near vicinity of the cubicle. In this case, the blast loading is applied very quickly as an impulse which simply imparts an initial velocity to the structure. Resulting peak deflections and the extent of structural damage depend on the peak positive impulse, i_s .

In Reference 2, the impulse data from the CEL cubicles was used to construct the design chart for impulse shown in Figure 7. The chart is useful for selecting the vent area needed to limit the peak positive impulse at any range outside a partially vented explosion. The chart should yield reasonable values of $i_s/W^{1/3}$ within the range of the test data, i.e., $0.072 < W/V < 0.289$ and $0.008 < AW^{1/3}/V < 0.721$. For large values of $AW^{1/3}/V$, Figure 7 indicates that $i_s/W^{1/3}$ is almost independent of $AW^{1/3}/V$ and approaches the value from an unconfined surface burst. As $AW^{1/3}/V$ decreases in value, $i_s/W^{1/3}$ becomes more sensitive to $AW^{1/3}/V$ until for values of $AW^{1/3}/V \approx 0.02$, a given change in $AW^{1/3}/V$ produces almost an identical percentage change in $i_s/W^{1/3}$.

It is recommended that Figure 7 be used for design purposes to predict the peak positive impulse outside partially vented cubicles.

Duration of Positive Pressure. Most theoretical procedures for predicting the dynamic response of structures are based on a triangular pressure-time pulse. Consequently, for design purposes, the actual pressure pulse with an exponential decay is approximated by an equivalent triangular pressure-time pulse [1]. The duration of the actual pulse is replaced by an fictitious duration, t'_0 , such that the peak pressure, p_{s0} , and total impulse, i_s , of the actual and equivalent pulses are identical.

$$t'_0/W^{1/3} = 2 (i_s/W^{1/3})/p_{s0} \quad (8)$$

Values of $t'_0/W^{1/3}$ from Equation 8 and measured values of $t_0/W^{1/3}$ are plotted versus $R/W^{1/3}$, for several values of $AW^{1/3}/V$, in Reference 2. A smooth curve through the data points is an s-shaped curve, characteristic of the relationship for an unconfined surface burst. Measured values of $t_0/W^{1/3}$ are in fair agreement with Equation 8, except for $R/W^{1/3} < 5$ and very small degrees of scaled venting. In other words, the exponential decay in actual pressure is much greater for very small degrees of venting and scaled distances.

Equation 8 is recommended for design purposes, except for very small scaled degrees of venting ($AW^{1/3}/V < 0.01$) and scaled distances ($R/W^{1/3} < 5$).

Design Problem

The following problems and their solution serve to illustrate the use of the various charts for constructing the pressure-time loadings (shown in Figure 1) in and around a partially vented cubicle. The first problem illustrates the case where the gas pressures dominate the loading function. The second problem illustrates the case for a fully vented cubicle where shock pressures dominate the loading.

Problem 1. A four-wall cube with a hole in its roof contains 17 pounds of Composition B explosive located at the geometric center of the cubicle. The length of each wall is 10 feet. The vent hole in the roof is 3.0 feet in diameter. (a) Is the cubicle partially vented? (b) Calculate the pressure-time loading (Figure 1) acting on a wall, and (c) Calculate the pressure-time loading outside the cubicle at a point 24 feet from the charge.

Solution. (a) Given $W = 17$ lb, $A = \pi D^2/4 = \pi(3.0)^2/4 = 7.1$ ft² and $V = 10 \times 10 \times 10 = 1,000$ ft³. Therefore, $A/V^{2/3} = 7.1/(1,000)^{2/3} = 0.07$. Since $A/V^{2/3} < 0.60$, the cubicle is partially vented and gas pressures must be considered in the loading.

(b) $W/V = 17/1,000 = 0.017$ and $AW^{1/3}/V = 0.018$. From Figure 3, $p_g = 135$ psi. From Figure 5, $t_g/W^{1/3} = 70$ or $t_g = 70(17)^{1/3} = 180$ msec. From Figure 4, $i_g/W^{1/3} = 2,540$ or $i_g = 2,540(17)^{1/3} = 6,530$ psi-msec. For design purposes, the effective duration of the equivalent triangular load pulse from Equation 6 is $t'_g = 2i_g/p_g = 2(6,530)/135 = 97$ msec. From chapter 4 of Reference 1, $i_s/W^{1/3} = 200$ or $i_s = 200(17)^{1/3} = 514$ psi-msec. From Equation 4-1 of Reference 1, $t'_o/W^{1/3} = 1.3$ or $t'_o = 1.3(17)^{1/3} = 3.3$ msec. For design purposes, the fictitious peak shock pressure is $p_r = 2i_s/t'_o = 2(514)/3.3 = 311$ psi. The calculated pressures, impulses and time durations apply to the load diagram shown in Figure 1a.

(c) Given $R = 244$ ft and $AW^{1/3}/V = 0.018$. Therefore, $R/W^{1/3} = 244/(17)^{1/3} = 9.4$ ft/lb^{1/3}. From Figure 6, $p_{s0} = 3.0$ psi. From Figure 7, $i_s/W^{1/3} = 2.4$ or $i_s = 2.4(17)^{1/3} = 6.16$ psi-msec. From Equation 8, the effective duration of the equivalent triangular pulse is $t'_o = 2i_s/p_{s0} = 2(6.16)/3.0 = 4.1$ msec. The calculated pressures, impulses and time duration apply to the load diagram shown in Figure 1b.

Problem 2. The vent hole in the roof of the cubicle described in Problem 1 is increased to 8.75 feet in diameter. (a) Is the cubicle fully vented? (b) Calculate the pressure-time loading acting on a wall.

Solution. (a) Given $D = 8.75$ ft. Therefore, $A = \pi D^2/4 = \pi(8.75)^2/4 = 60$ ft². $V = 1,000$ ft³. Therefore, $A/V^{2/3} = 60/(1,000)^{2/3} = 0.60$. Since $A/V^{2/3} > 0.60$, the cubicle is fully vented and no gas pressure must be considered in the design loading, as confirmed by the following calculations.

(b) $W/V = 0.017$ and $AW^{1/3}/V = 60(17)^{1/3}/1,000 = 0.157$. From Figure 3, $p_g = 135$ psi. From Figure 5, $t_g/W^{1/3} = 5.6$ or $t_g = 5.6(17)^{1/3} = 14.4$ msec. From Figure 4, $i_g/W^{1/3} = 87$ or $i_g = 87(17)^{1/3} = 223$ psi-msec. For design purposes, from Equation 6, the effective gas duration is $t'_g = 2i_g/p_g = 2(223)/135 = 3.3$ msec. From Equation 4-1 of Reference 1, $t'_o/W^{1/3} = 1.3$ or $t'_o = 1.3(17)^{1/3} = 3.3$ msec. For design purposes, the fictitious peak shock pressure is $P_r = 2i_g/t'_o = 2(223)/3.3 = 311$ psi. Note that $t_g > t'_o$ but $t'_g < t'_o$ and therefore the cubicle is fully vented as indicated by the calculations in (a). The calculated pressures, impulses and time durations apply to the load diagram shown in Figure 1b.

FULLY VENTED EXPLOSIONS

According to the CEL criterion, an explosion is fully vented if $A/v^{2/3} > 0.60$. Within the practical range of aspect ratios, three-wall cubicles with or without a roof satisfy this criterion. But the TM5-1300 Design Manual already contains charts for predicting the pressure loading inside three-wall cubicles [1]. Therefore, the following discussion of fully vented explosions is limited to procedures for predicting the blast environment outside three-wall cubicles.

Blast Environment Outside Three-Wall Cubicles

Consider a charge detonated at the geometric center of a three-wall cubicle without a roof. The expanding shock wave and resulting reflected waves eventually produce an erratic train of shock waves escaping to the outside of the cubicle by passing unobstructed through the open front wall and roof and by spilling over the top of the side and backwalls.

At points outside the open front wall, the train of waves quickly merge to reinforce the shock front and the peak pressure and impulse, at essentially any range, exceed those from an unconfined surface burst. A typical relationship for peak pressures outside the open front wall is shown in Figure 8.

At points behind the side and backwalls, the wave train, by spilling over the back and sidewalls, forms a highly turbulent vortex at the free edges of the walls. At first, the vortex is small but rapidly grows in size with time. Evidence that a vortex indeed forms behind a barrier wall and grows to considerable size is shown in a study by Teel [5]. The vortex apparently distorts the shock front because the peak pressure and impulse at points close-in to the cubicle are much less than those from an unconfined surface burst. A typical relationship found for peak pressures behind a sidewall is shown in Figure 9. Note that at a critical distance from the wall, depending on the charge weight and cubicle geometry, the peak pressure (and impulse) is maximum and beyond this critical distance the peak pressure (and impulse) decreases with increasing scaled distance. The pressure corresponding to the peak in the pressure curve (Figure 9) is referred to as $p_{g0}(\max)$ and the portion of the curve to the right of the peak is referred to as the envelope curve.

Peak Positive Pressure. Envelope curves for the measured peak positive pressure, p_{s0} , behind the front, back and sidewalls of the three-wall cubicles, with and without a roof, are shown in Figures 10 and 11, respectively. At all scaled distances, p_{s0} is greatest behind the front wall, less behind the sidewalls and least behind the backwall. The curves apply to both cube and rectangular shaped cubicles.

The maximum peak pressure, $p_{s0}(\max)$, was found to depend on both the cubicle geometry and W/V , as shown in Figure 12. The peak positive pressure, p_{s0} , from Figures 10 and 11 must never exceed $p_{s0}(\max)$ from the appropriate curve in Figure 12. Consequently, Figures 10 and 11 must be used in conjunction with Figure 12, especially for small values of $R/W^{1/3}$ and W/V where one will find that $p_{s0}(\max)$ from Figure 12 is less than p_{s0} from Figures 10 and 11.

It is recommended for design purposes that Figures 10, 11, and 12 be used to predict the peak pressure at any range outside three-wall cubicles with or without a roof.

Peak Positive Impulse. The scaled positive impulse, $i_g/W^{1/3}$, behind the walls of a three-wall cubicle diminishes with increasing $R/W^{1/3}$ in a manner similar to that shown in Figures 8 and 9 for peak pressure. The impulse data shows a clear influence of cubicle geometry and W/V on $i_g/W^{1/3}$. For peak pressures, W/V effected p_{s0} only at close-in ranges but for peak impulse, W/V was found to influence $i_g/W^{1/3}$ at all ranges. For both cube and rectangular shaped three-wall cubicles, $i_g/W^{1/3}$ decreases with increasing W/V and $R/W^{1/3}$.

Design curves and equations to predict $i_g/W^{1/3}$ are presented in Reference 2. Typical relationships derived from the data include the following.

Behind the open front wall of a cube shaped cubicle,

$$i_g/W^{1/3} = 110 (W/V)^{-0.16} (R/W^{1/3})^{-1.05} \quad (9)$$

for $R/W^{1/3} \geq 7$ and $W/V < 2.1$.

Behind the open front wall of a rectangular shaped cubicle,

$$i_g/W^{1/3} = 96.6 (W/V)^{-0.15} (R/W^{1/3})^{-1.04} \quad (10)$$

for $R/W^{1/3} \geq 10$ and $W/V \approx 1.0$.

Behind the sidewalls of both the cube and rectangular shaped cubicles,

$$i_g/W^{1/3} = 71 (W/V)^{-0.09} (R/W^{1/3})^{-0.95} \quad (11)$$

for $R/W^{1/3} \geq 20$ and $W/V < 1.0$.

Behind the backwall of the cube and rectangular shaped test cubicles there was no clear trend in the impulse data or clear influence of W/V or cubicle geometry.

The lines described by Equations 9, 10, and 11 are nearly parallel to the curve for an unconfined surface burst. Therefore, a critical value of W/V exists, according to the equations, such that $i_g/W^{1/3}$ outside the cubicle is identical to that from an unconfined surface burst. For any W/V greater than this critical value, the line relating $i_g/W^{1/3}$ and $R/W^{1/3}$ should fall, it seems, on the unconfined surface burst curve. For this reason, an upper limit for W/V is given for Equations 9, 10 and 11.

At small scaled distances, the $i_g/W^{1/3}$ curves bend over and peak out in a manner similar to the p_{SO} curves. For points close-in behind the open front wall, the curves bend over and tend to merge with the unconfined surface burst curve. This trend is attributed to the shock waves reflecting off the side and backwalls which have not yet reached and reinforced the primary shock front. Behind the side and backwalls, impulse curves bend over and peak but there appears to be no consistent relationship between the peak and W/V or the cubicle geometry.

It is recommended for design purposes that Equations 9, 10, 11 and similar equations and charts for impulse presented in Reference 2 be used to predict the peak positive impulse outside a three-wall cubicle.

Duration of Pressure. No detailed analysis of $t_o/W^{1/3}$ was made (although the data is tabulated in Reference 2) but a correlation of the data indicates that (1) $t_o/W^{1/3}$ increases with decreasing W/V , (2) the influence of W/V on $t_o/W^{1/3}$ diminishes with increasing $R/W^{1/3}$, and (3) at large $R/W^{1/3}$, the effect of W/V is negligible and $t_o/W^{1/3}$ approaches that from an unconfined surface burst.

It is recommended for purposes of design that the effective duration, t'_o , be calculated from Equation 8.

Design Problem

The following problems and their solution serve to illustrate the use of the various charts for constructing the pressure-time loading, shown in Figure 1b, outside a fully vented cubicle.

Problem 1. Design a three-wall cube without a roof to contain 125 pounds of Composition B explosive. The pressures any where behind the back and side walls must not exceed 10 psi. (a) What wall dimensions are required? (b) What will the peak pressure be behind the side, back and front walls at a range of 200 feet?

Solution. (a) Given $W = 125$ lb and $p_{SO}(\max) = 10$ psi. From line A in Figure 12 the required $W/V = 0.017$ or $V = 125/0.017 = 7,350$ ft³. For a cube, $L = V^{1/3} = (7,350)^{1/3} = 19.4$ ft. Therefore, the length and height of the side and back walls must be 19.4 ft.

(b) Given $R = 200$ ft, $W = 125$ lb, and $V = 7,350$ ft³. Therefore, $R/W^{1/3} = 200/(125)^{1/3} = 40$ and $W/V = 0.017$. From Figure 10, $p_{HO} = 1.0$ psi behind backwall, 1.5 psi behind sidewall and 1.8 psi behind open front wall.

Problem 2. A rectangular-shaped, three-wall cubicle contains 3,375 pounds of Composition B explosive. The ground surface is flush with the floor ($h = H$) and the walls are 10 feet high. The lengths of the side and back walls are 20 and 40 feet, respectively. Calculate the design loading (p_{so} , i_s , and t'_o) for a point 300 feet from the charge behind the sidewall.

Solution. Given $W = 3,375$ lb, $V = 10 \times 20 \times 40 = 8,000$ ft³, and $R = 300$ ft. Therefore, $R/W^{1/3} = 300/(3,375)^{1/3} = 20$ and $W/V = 3,375/8,000 = 0.42$. From Figure 10, $p_{so} = 5$ psi. From Equation 11, $i_s/W^{1/3} = 71(0.42)^{-0.09}(20)^{-0.95} = 4.46$ or $i_s = 4.46(3,375)^{1/3} = 66.9$ psi-msec. For design purposes, the effective duration of the pressure from Equation 8 is $t'_o = 2(66.9)/5 = 26.8$ msec.

PROPOSED DESIGN CRITERIA

Design criteria for predicting the loading in and around fully and partially vented cubicles are summarized in Tables 1 and 2. The design criteria for the loading inside fully vented cubicles are compatible with procedures recommended in the TMS-1300 Design Manual [1]. Design criteria for the loading outside cubicles are limited to $h = 0$ for four-wall cubicles and $h = H$ for three-wall cubicles. (A semi-empirical procedure is described in Reference 2 for estimating the blast environment for other values of h .)

REFERENCES

1. NAVFAC P-397 Manual; Structures to Resist the Effects of Accidental Explosions. Department of the Army, Navy and Air Force; Washington, D.C., Jun 1969 (also Army TMS-1300 and AFM-88-22).
2. Civil Engineering Laboratory. Technical Report R- : Blast Environment From Fully and Partially Vented Explosions in Cubicles, by W. A. Keenan and J. E. Tancreto, Port Hueneme, CA (to be published).
3. Naval Civil Engineering Laboratory. Technical Report R-780: Determination of Blast Leakage Pressures and Fragment Velocity for Fully Vented and Partially Vented Protective Cubicles, by John M. Ferritto, Port Hueneme, CA, Dec 1972.
4. J. F. Proctor and W. S. Filler, "A Computerized Technique for Blast Loads From Confined Explosions," Minutes of the 14th Annual Explosives Safety Seminar, p. 99, Nov 1972.
5. Ballistics Research Laboratory. BRL Memorandum Report No. 1536: A Study of Flow Patterns in Aircraft Revetments, by George Teel and George Coulter, Aberdeen, MD, Feb 1964.
6. Picatinny Arsenal. Technical Report 4168: Full and Model Scale Tests of Bay Structures, by S. Levy, et al, Dover, New Jersey, Feb 1971.

LIST OF SYMBOLS

A	Total vent area of the cubicle (ft ²)
D	Diameter of charge or opening in roof (ft)
h	Vertical distance from top of cubicle roof, wall or pipe stack vent down to the ground surface or horizontal plane of interest (ft)
H	Interior height of cubicle wall from floor to roof (ft)
i _s	Unit positive impulse of shock pressure (psi-msec)
i _g	Unit positive impulse of gas pressure (psi-msec)
L	Length (ft)
P _g	Peak positive gas pressure (psi)
P _r	Peak reflected shock pressure (psi)
P _{s0}	Peak positive incident pressure (psi)
P _{s0(max)}	Maximum peak positive pressure (psi)
R	Horizontal range from charge to point of interest (ft)
R'	Skew range from charge to point of interest (ft)
t _g	Duration of exponential decay in gas pressure (msec)
t' _g	Effective duration of gas pressure (msec)
t ₀	Duration of exponential decay in shock pressure (msec)
t' ₀	Effective duration of shock pressure (msec)
t _w	Thickness of cubicle wall (ft)
V	Internal volume of cubicle (ft ³)
W	Total weight of explosive (lb)

Table 1. Proposed Design Criteria for Loading Inside Fully and Partially Vented Cubicles

Cubicle	Parameter					
	i_s	t'_o	P_r	i_g	P_g	t'_g
Fully Vented $A/\sqrt{2/3} > 0.60$	Figures 4-17 through 4-62 of TMS-1300 Design Manual [1]	Equation 4-1 of TMS-1300 Design Manual [1]	$2i_g/t'_o$	a	a	a
Partially Vented $A/\sqrt{2/3} \leq 0.60$			$2i_g/t'_o$	Figure 4	Figure 3	$2i_g/p_g$

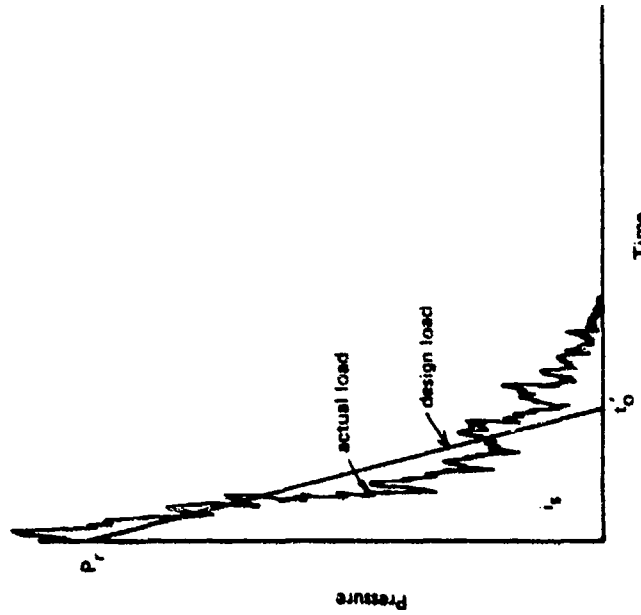
^a Gas pressure not a factor in loading since $t'_g/t'_o \leq 1.0$.

Table 2. Proposed Design Criteria for Loading Outside Fully and Partially Vented Cubicles

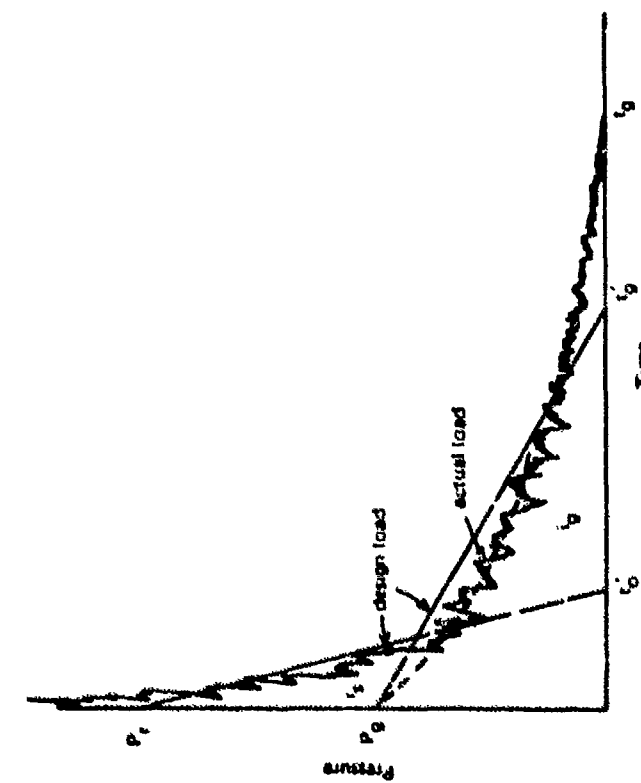
Cubicle	Parameter			
	Direction	P_{sc}	i_s	t'_o
Four-wall cubicles with $A/\sqrt{2/3} \leq 1.0$	Any	Figure 6 ^a	Figure 7 ^a	$2i_g/p_{so}$
Three-wall cubicles with $A/\sqrt{2/3} > 0.60$	Behind open front wall Behind side wall Behind back wall	Figures 10, 11 and 12	Equations 7, 8, 10 and 11 ^b Figures B11, 12, 17 and 18 ^b Equations 9 and 12 ^b Figures B13, 14, 19, 20 ^b Figures B15, 16, 21, 22 ^b	$2i_g/p_{so}$

^a For $h = 0$; for $h > 0$ use semi-empirical procedure described in text.

^b Figure numbers refer to Figures in Reference 2; For $h = H$; for $h < H$ use semi-empirical procedure described in text.



(a) Loading inside partially vented cubicle,
 $A/V^{2/3} < 0.60$.



(b) Loading inside full vented cubicle
 $(A/V^{2/3} > 0.60)$ and outside both
 fully and partially vented cubicles.

Figure 1. Blast loading from fully and partially vented cubicles.

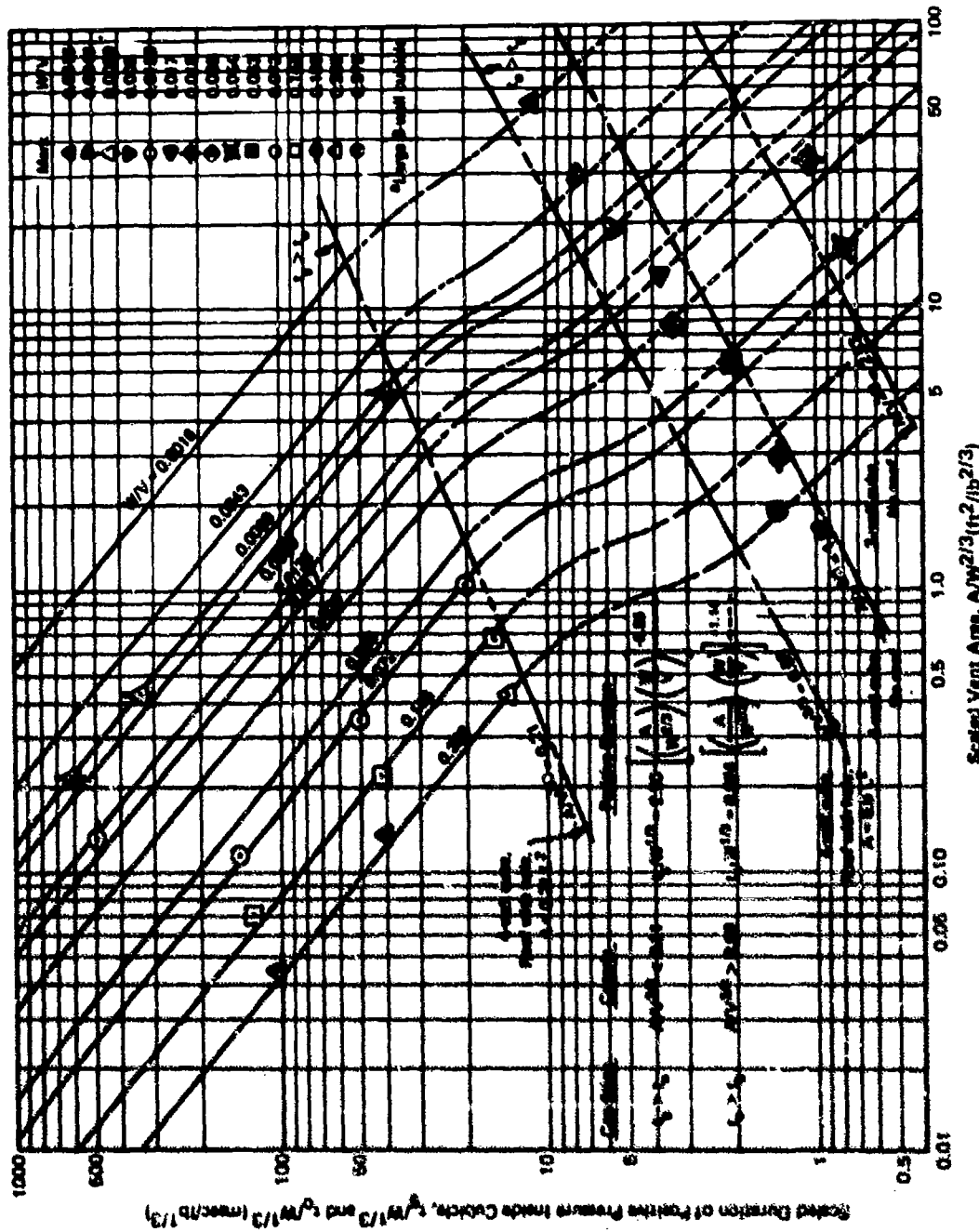


Figure 2. Scaled duration of positive pressure inside four-wall cubicle versus scaled vent area and cubicle volume.

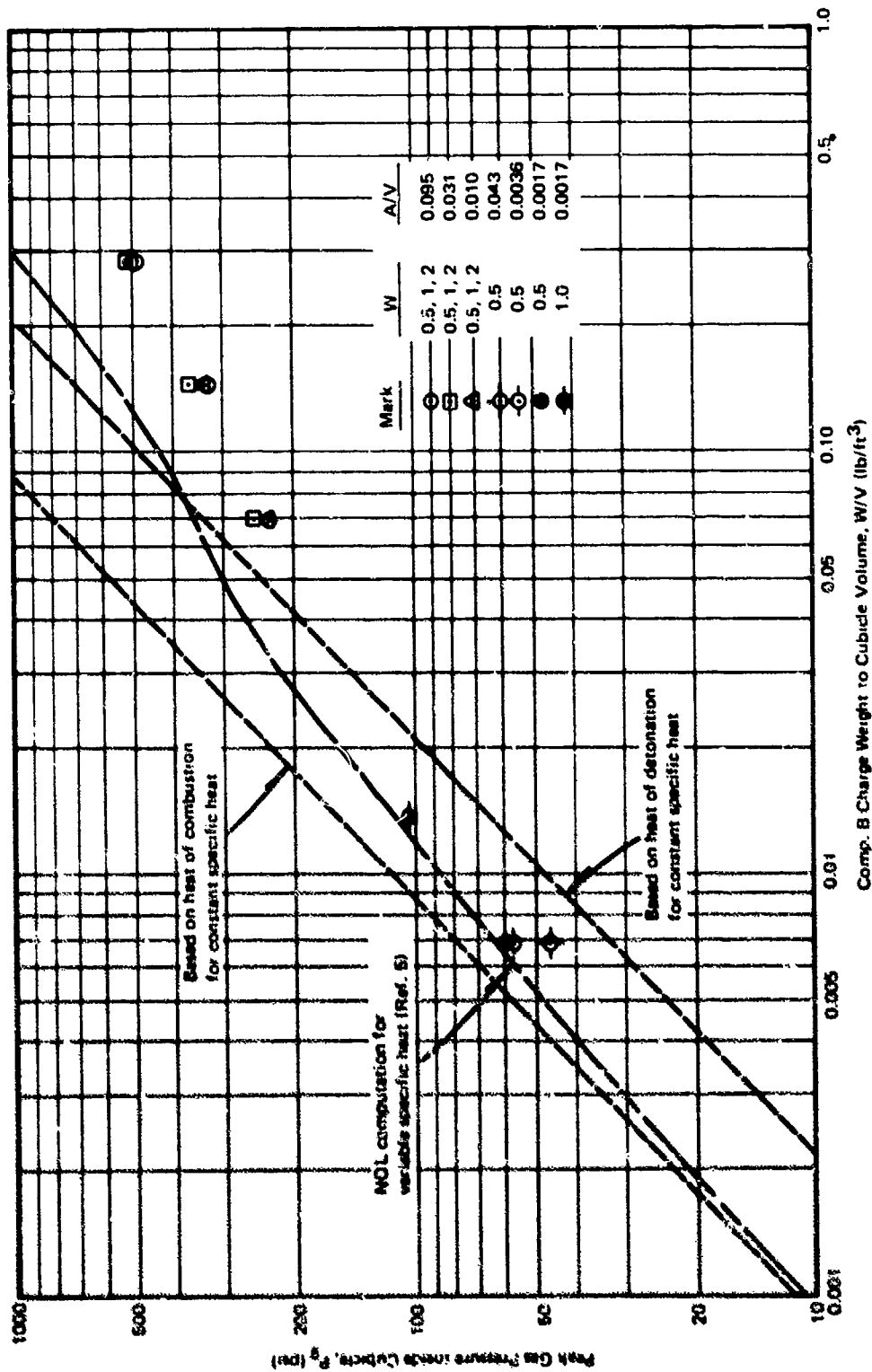


Figure 3. Peak gas pressure from partially vented explosion of Composition B in four-wall cubicle.

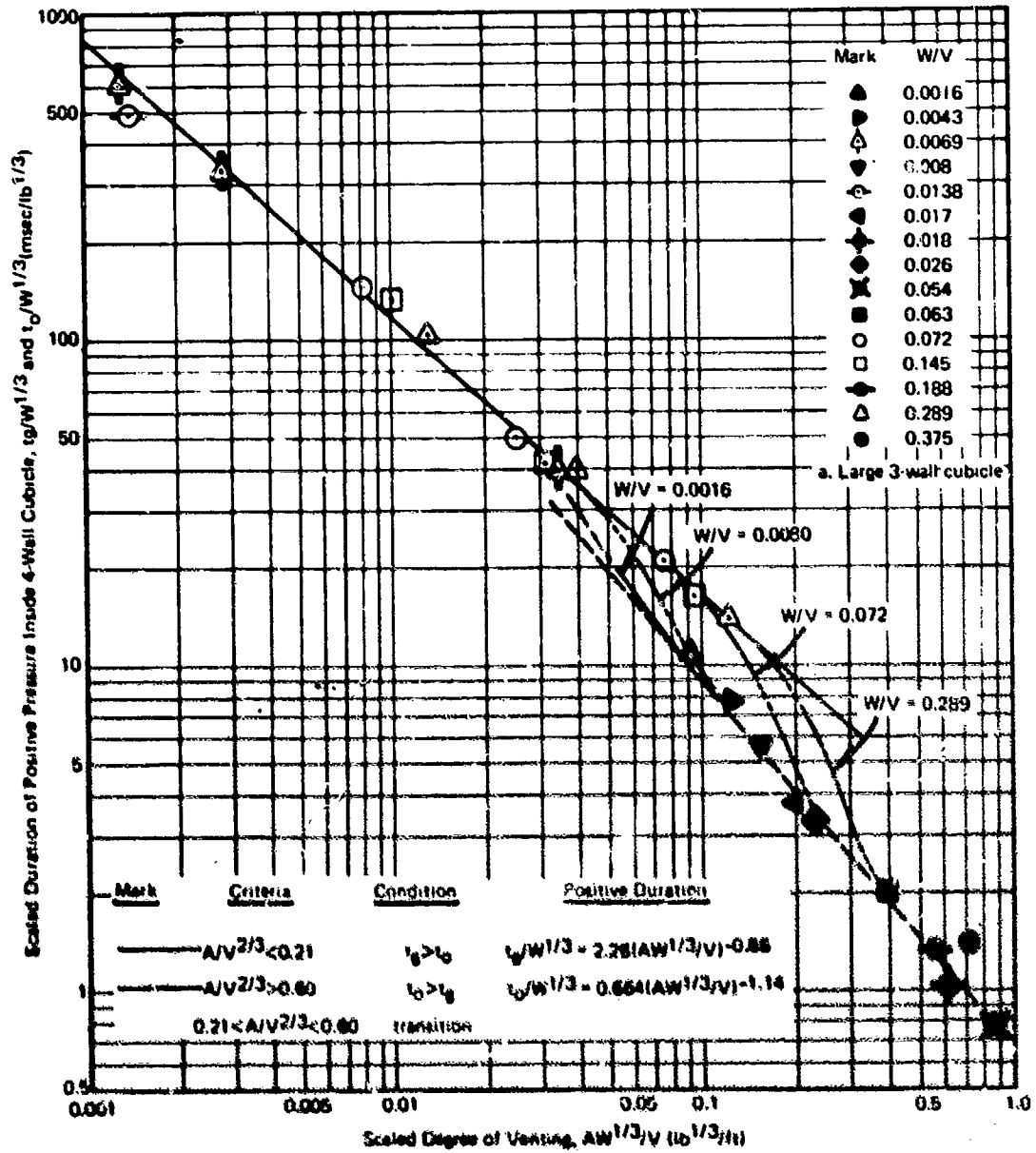


Figure 5. Design chart for scaled duration of positive pressure inside a cubicle versus scaled degree of venting.

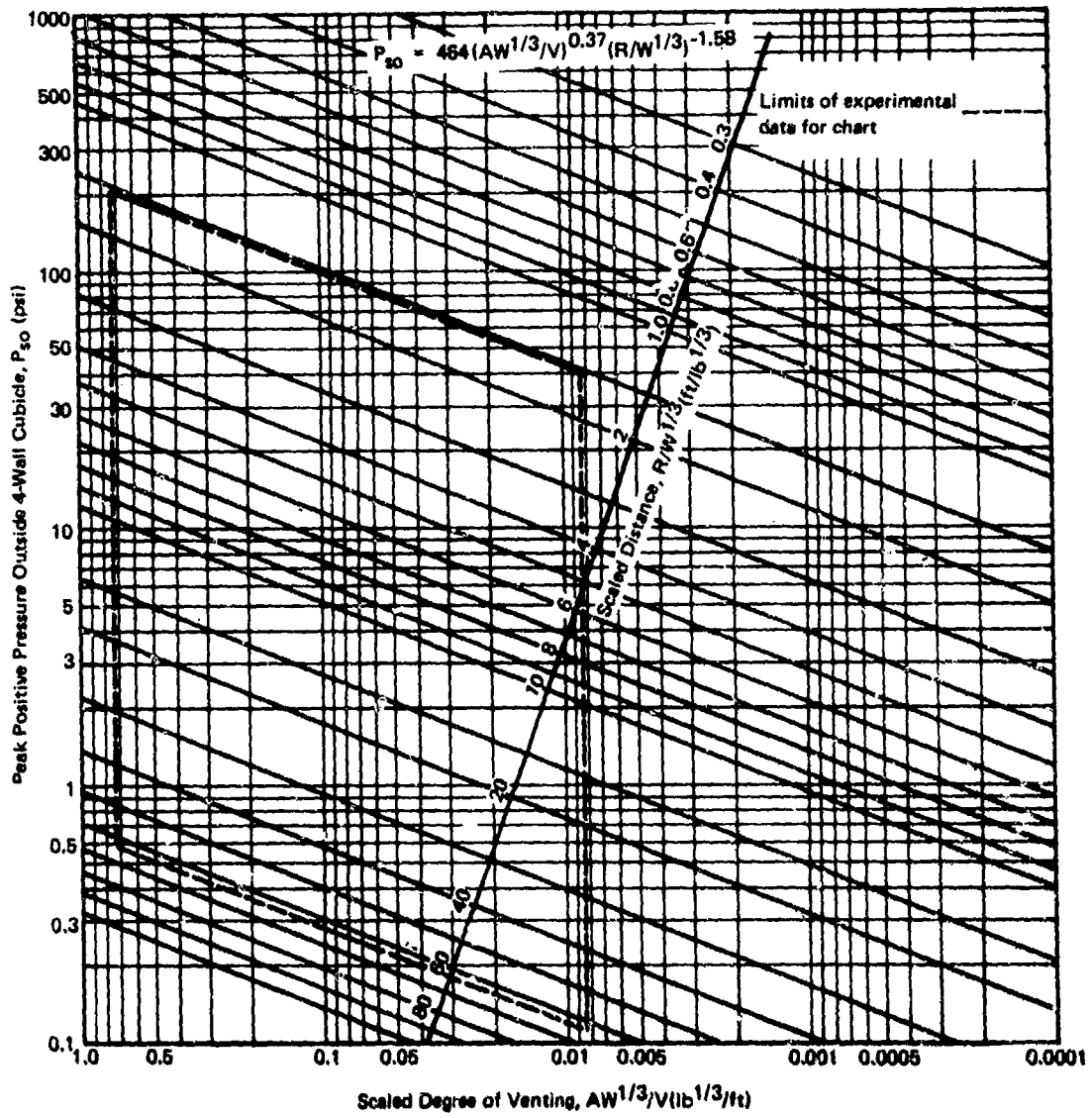


Figure 6. Design chart for vent area required to limit pressures at any range outside a four-wall cubicle.

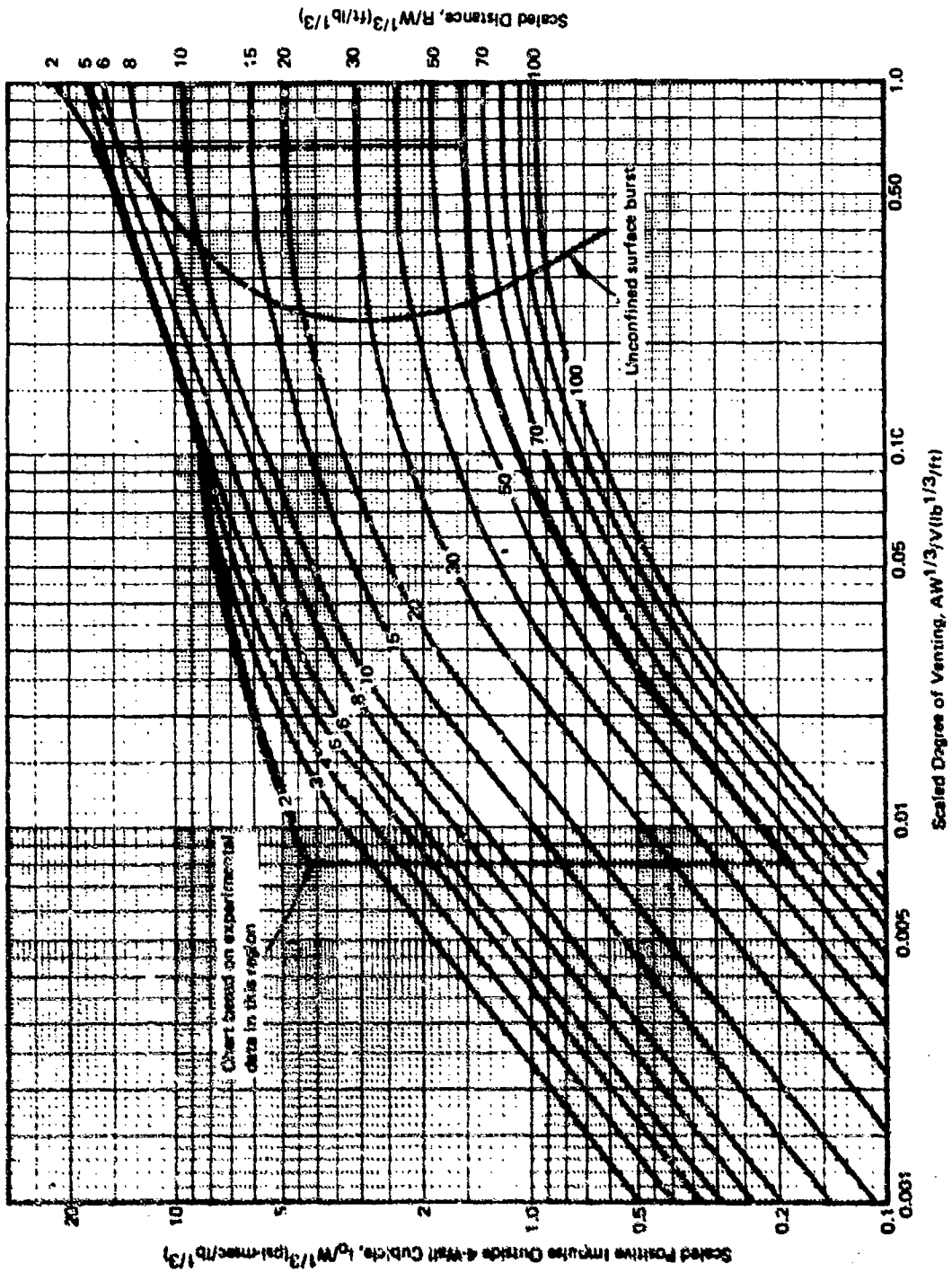


Figure 7. Design chart for vent area required to limit positive impulse at any range outside a four-wall cubicle.

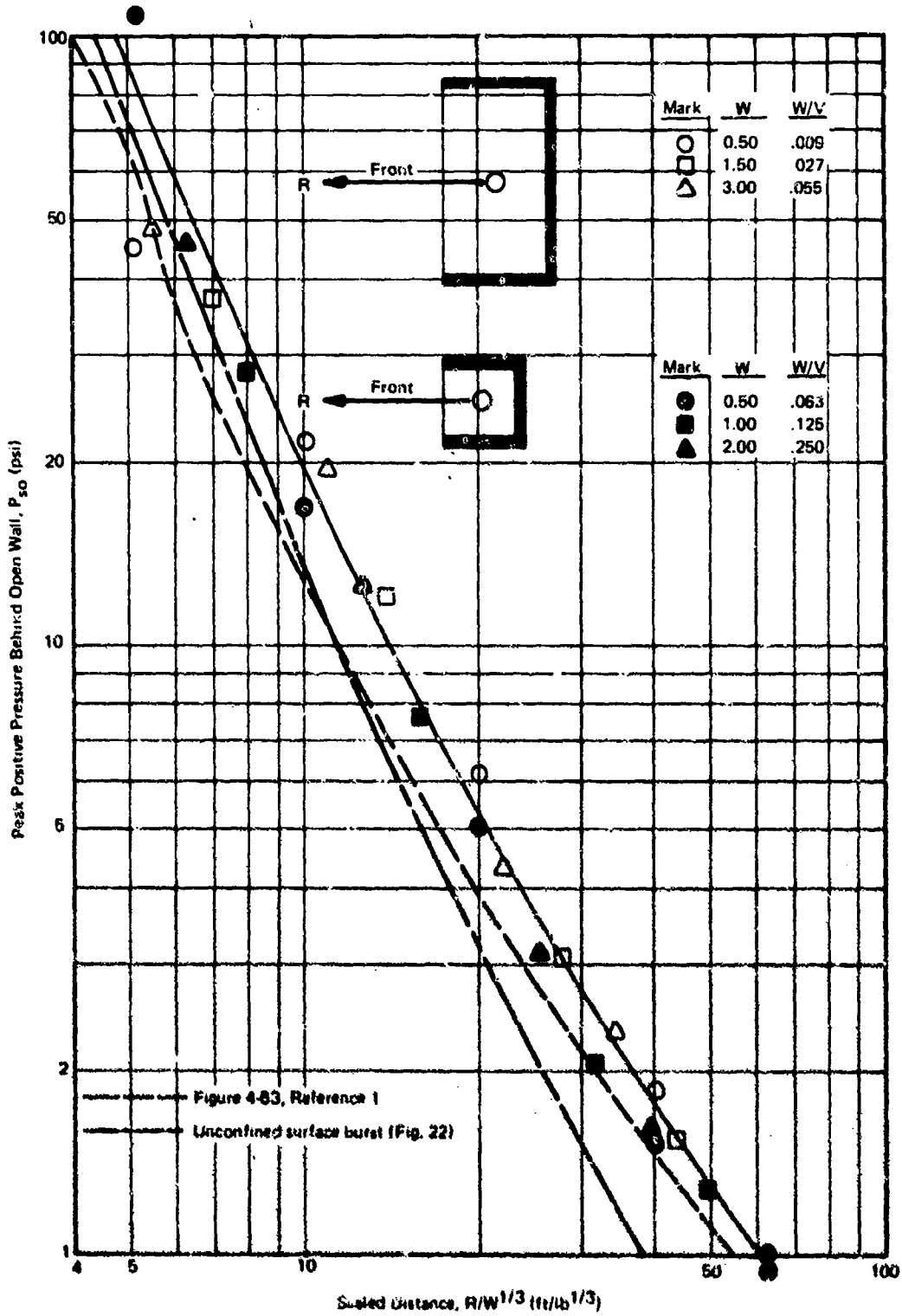


Figure 8. Peak positive pressure behind open wall of three-wall cubicles without a roof.

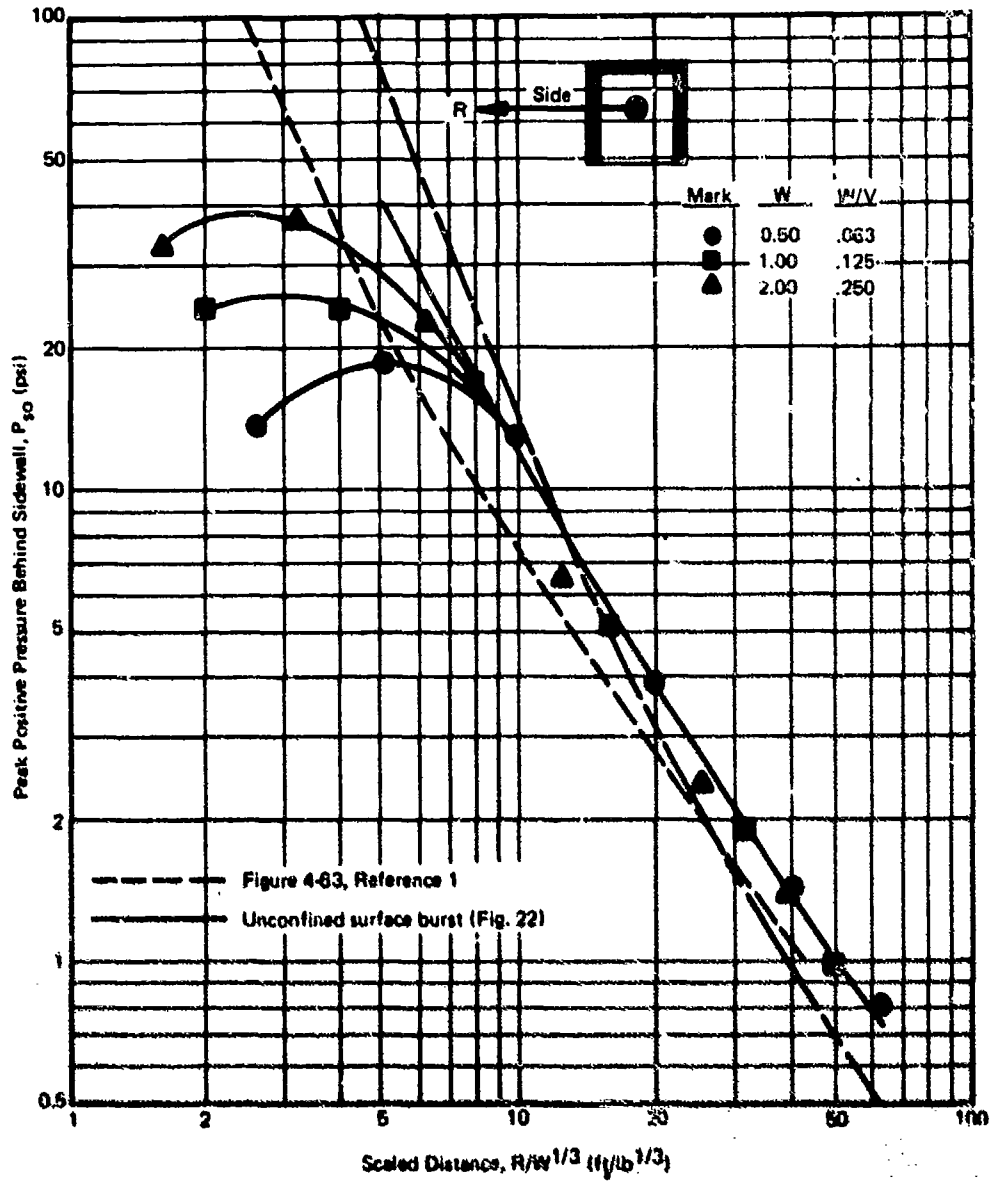


Figure 9. Peak positive pressure behind sidewall of small three-wall cubicle without roof.

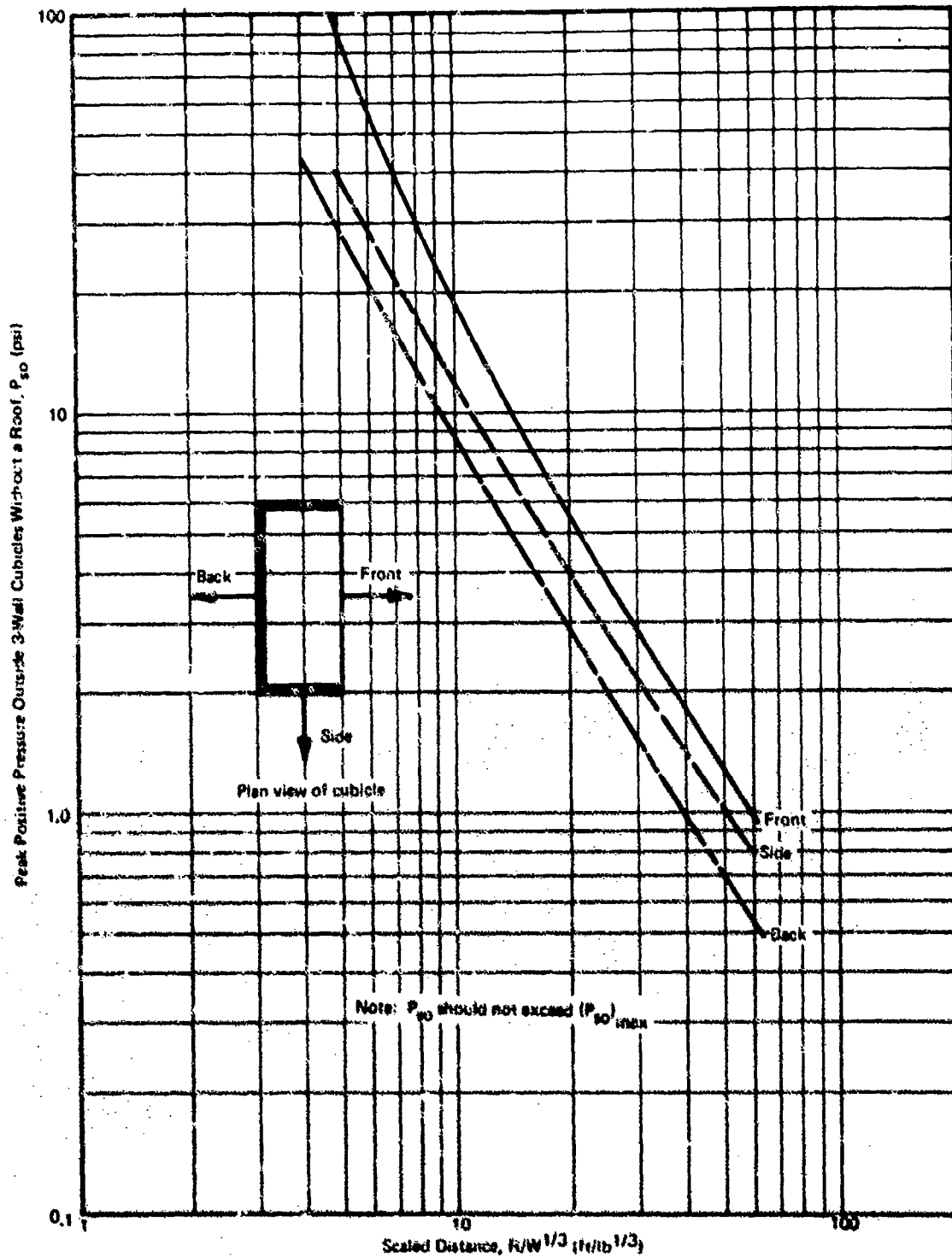


Figure 10. Envelope curves for peak positive pressure outside three-wall cubicles without a roof.

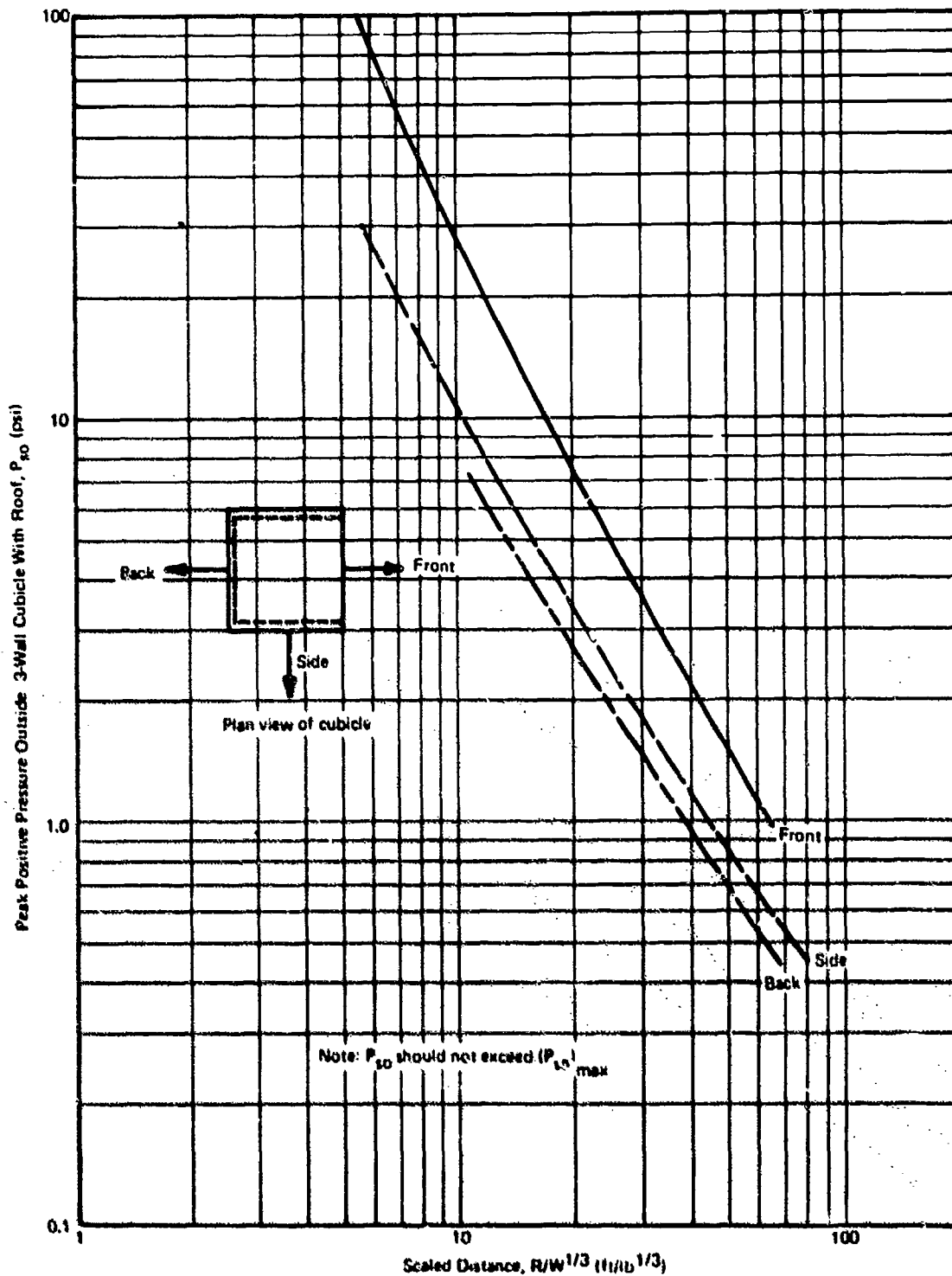


Figure 11. Envelope curves for peak positive pressure outside three-wall cubicles with a roof.

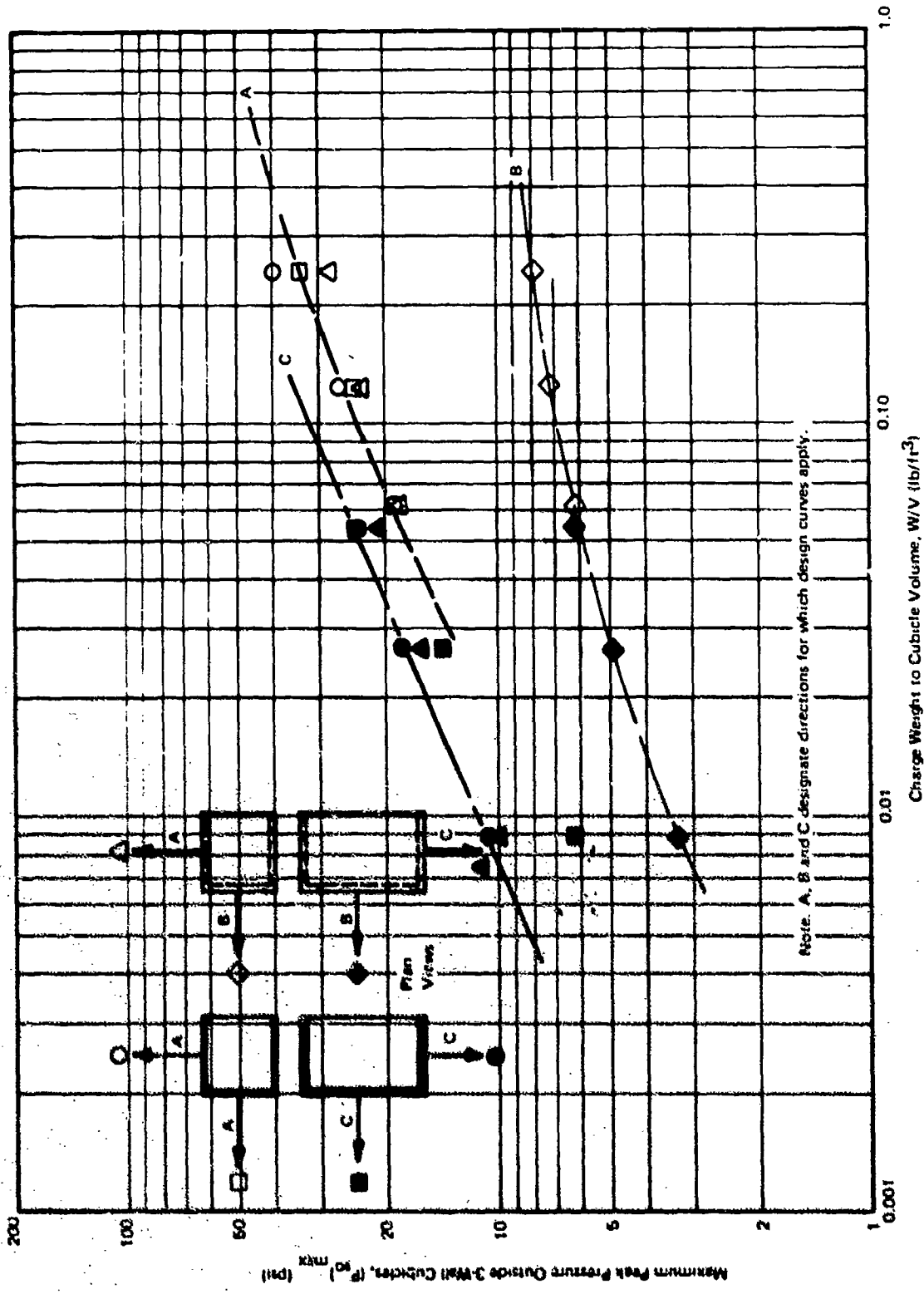


Figure 12. Envelope curves for maximum peak pressure outside three-wall cubicles.

PERSONAL ASPECTS OF PUBLIC AFFAIRS

Mr. J. J. Foley
HQ, US Army Materiel Command
Alexandria, VA

When the Army started to plan Operation CHASE (cut holes & sink 'em) in 1968, - some reaction was expected. The sheep kill in Utah had raised quite a fuss and the admission that nerve gas was stored on Okinawa got a lot of attention in 1969. - But no one was prepared for the depth and breadth of the public's reaction to CHASE.

After all, ocean dumps had been made many times before and aroused little or no comment. In fact, - since 1964, - ocean dumping had been the Army's preferred method of disposal.

However, the Army's 1968 plan to transport chemical agents and munitions from several inland depositories by train to a seaport for transfer to a hull which they would be towed out aways and sunk by the Navy, - stirred up a storm that wouldn't die. It's intensity caught everyone by surprise.

After two years had passed and all interested parties had cleared the plan, the Army moved two trainloads of obsolete chemical munitions through hostile territory. Despite the worst fears of its severest critics, all went well.

Interesting and successful as Operation CHASE was, I did not choose it as the anchor for my remarks today for those reasons. I chose it because, in my mind at least, it represented a watershed in the way government relates to people. The lessons learned during 1968, 69 and 70,

when public outrage was at its highest, are universally applicable not only in handling subsequent government actions but those undertaken by private industry as well.

People from General Motors, for instance, who under-rated the impact of Ralph Nader, are aware of them, so are the people who fronted for Onassis in New Hampshire when he decided to build an oil refinery there; so are people in the Atomic Energy Commission who planned a string of low-cost, privately operated nuclear power generating stations.

Something basic changed in American life during the 1960's and early 1970's and we who work in the public affairs trade, and those who hire and pay us, should examine this change carefully. Many observers will agree that aroused public opinion stopped a war, ended the careers of two presidents, turned the automobile business upside down, and continues to challenge the status quo with impressive success.

Putting away this broader consideration for the moment, I'd like to discuss Operation CHASE in its role as a watershed public affairs case -- the first of its kind.

It was the first Army action to fall under provisions of the 1969 National Environmental Protection Act (NEPA) which directed that each Federal agency contemplating an action affecting the quality of the human environment should prepare and coordinate with all interested parties a paper describing the proposed action and summarizing its environmental impact and adverse environmental effects. The "interested parties" included all Federal, State and local agencies having jurisdiction or special expertise...including public bodies.

In the uptight atmosphere of 1969, you can just image the comments on the Operation CHASE impact statement. Of course, these comments were in the public domain and this brought public affairs officers into a jungle of new technical, legal, administrative and pathological terms with which they were unacquainted. They began to learn.

In addition, Operation CHASE was one of the first major Army actions taken under the Freedom of Information Act, signed by President on the fourth of July 1966 to be effective a year later. More prosaically, the President signed a piece of legislation amending Section 3 of the Administrative Procedures Act which denied to individual agencies the right to handle their own files in any way they deem proper.

The Attorney General attempted to ease the implementation of this new openness by issuing a memorandum dated June 1967 setting forth some guidelines. The key ones read as follows:

...that disclosure be the general rule, not the exception;

...that all individuals have equal rights of access;

...that the burden be on the government to justify the withholding of a document, not the person who requests it;

...that individuals improperly denied access to documents have a right to seek injunctive relief in the courts; and

...that there be a change in government policy and attitude.

"At the same time"...the Attorney General continued..."this law gives assurance to the individual citizen that his private rights will not be violated. The individual deals with the government in a number of protected relationships which could be destroyed if the right to know were not modulated by principles of confidentiality and privacy. Such materials as tax reports, medical and personnel files, and trade secrets must remain outside the zone of accessibility."

Although the press was slow to use FOI, as it came to be known, other parties were not. By 1969, the Consumers Union had taken the Veterans' Administration to court over the release of brand names of products tested prior to procurement. Since then, other Federal agencies have been taken to court. They include the Securities Exchange Commission, the Renegotiation Board, the General Services Administration, the Federal Trade Commission, HUD, the National Labor Relations Board, the Department of Justice, the Environmental Protection Agency, the Department of Transportation, the Federal Communications Commission, and the Selective Service System. You name one, its been sued, and the judgment probably has gone against the government.

Defense and Army regulations implementing the FOI reflected these guidelines. If a record was unclassified, out it went, and not through the public affairs office, either. Gone were the days when a publication could be reviewed by layers of headquarters staffs before a decision would be reached for or against release.

Public affairs officers now must respond to press queries arising from documents they have never seen or heard of before...and lack the scientific background to evaluate. Requests for all kinds of chemical/biological records came in beginning in 1967 and 1968. Some papers dated back to World War I, some concerned World War II, Korea and Vietnam. More and more of this type of information was released into the public domain by operational staff members rather than public information officers. In many cases, the raw materials contained in these released records served to feed protest movements and make disposal programs similar to CHASE that much more difficult to execute.

In addition to the complicating effects of NEPA and FOI, other events occurring around the same time also contributed to a hostile public environment. Of these, Vietnam and all its sorrows, - played by print and television to a fare-the-well, - sensitized all who read and viewed and in the end overwhelmed all. A look through the New York Times Index for those years of CHASE, - 1968-9 and 70, - is substantiating. It is recommended to all who would learn from the past.

Rarely does one look up from day to day activities in order to ascertain the sweep of events over time and thereby place man and his duty in perspective. A scanning review of these indexes can be helpful in such an effort as the following selected excerpts indicate:

In 1968 when CHASE was in its initial planning phase, the troop strength in Vietnam hit its top, 540,500. President Johnson withdrew from consideration for nomination after Gene McCarthy took forty percent of the vote in the New Hampshire primaries. Approximately forty-five hundred sheep were killed by lethal gas during testing in Utah. Robert Kennedy joined McCarthy in a race for the nomination and was assassinated in Los Angeles. Martin Luther King was assassinated in Memphis. Ralph Abernathy led his people into Resurrection City along the Mall in Washington, DC. The Democratic National Convention turned into a shambles in Chicago and Columbia University exploded.

During 1968...the new President started to withdraw troops from Vietnam. 250 to 300,000 people demonstrated in Washington against the war. An incident involving twenty-three persons on Okinawa revealed presence of nerve gas overseas. The President issued his proclamation against aggressive chemical warfare. On the whole, it wasn't too bad a year. Things seemed to be settling down.

But the first six months of 1970 turned grim. People in Seattle demonstrated convincingly against receipt of nerve gas shipments from overseas. LTG Peers released his report on Songmy. US officials admitted that the Vietnam defoliation program might not be as harmless as previously announced. Millions of Americans celebrated "earth day" in April. In May, the President sent troops into Cambodia and hell broke loose. The tragedy at Kent State followed. College campuses all over the country reacted strongly. 75 to 100,000 demonstrated in Washington. The Senate voted 81 to 10 to repeal the Tonkin Gulf Resolution. In August, the FCC held that the President had used television to such an extent in defending his war policies that networks now must make prime time available to his critics. And on and on and on.

Well, this is enough to sketch out the state of the public mind when the Army decided to make another routine ocean dump of some old leakers.

But the Army and all the rest of government learned that the public no longer considered routine ocean dumping routine any more. Nor was it going to accept as inevitable personal risk, unsafe cars, dangerous working conditions, radioactive nuclear generating plants. Nor would it accept as inevitable environmental deterioration of seacoasts, timberlands, rivers, coal fields.

Government public affairs officers had to re-learn something all had known and perhaps had forgotten: their power to manipulate public opinion is highly overrated. An aroused public brushes aside anyone or anything starting in its path, right, wrong or maybe.

The volatility of the Vietnam war years has passed and most of the physical demonstrations have ended but the one lesson has once again been established beyond a question of a doubt: the people have the ultimate power to effect change. The Freedom of Information Act and the National Environmental Protection Act are only the forerunners of a body legislation that seeks to equalize the legal position of the consumer with that of the supplier, casting the government in the role of an honest broker between the two.

So, in supporting his management, the modern public affairs officer now must bring information about the public in before he creates information to go out.

The film that follows illustrates this public affairs approach. The responsible Army public affairs officers triumphed over innumerable difficulties in planning, coordinating and executing Operation CHASE. They did an excellent job of briefing all who had the need to know, all who demanded to know, all who just wanted to know, before any movement took place.

And then, when everyone was onboard, the Army demonstrated its operational skills by executing an extremely difficult logistics movement with a professionalism that drew the admiring comments from its severest critics.

Now...the film. (Available on request to DAIO.)

LIST OF ATTENDEES

AARON, COL Jerome, USA	USAMC, Alexandria, VA
ADAMIETZ, F. P.	Sierra Army Depot, Herlong, CA
ALISON, John	Northrop Corp., Arlington, VA
ALLAN, D. S.	A. D. Little, Cambridge, MA
ALLISON, LTC J. C., USAF	HQ USAF/IGI, Wash, DC
ALSOP, B. E.	Embassy of Australia, Wash, DC
AMLIE, Dr. June T.	USN Ship R&D Ctr, Bethesda, MD
ANDERSON, CAPT B. A., USMC	Camp Pendleton, CA
ANDERSON, R. W.	Agbabian Assoc., El Segundo, CA
ANDREWS, S. B.	NWL Dahlgren, VA
ANSALVISH, F. B.	Aberdeen Proving Ground, MD
ARONSON, C. J.	NOL Silver Spring, MD
ARORA, K. K.	Gen American Transp Corp, Niles, IL
ATKISSON, J. B.	Jet Propulsion Lab, Pasadena, CA
BACHTELL, N. D.	DDESB, Wash, DC
BACKOFEN, J. E.	Battelle Labs, Columbus, OH
BAILEY, M. R.	USAMC Fld Safety Agency, Charlestown, IN
BAKER, C. F.	Lawrence Livermore Lab, CA
BAKER, G. A.	NAD Hawthorne, NV
BAKER, Dr. W. E.	SW Res Inst, San Antonio, TX
BALDWIN, W. J.	DSA, Alexandria, VA
BALLANCE, N. B.	NOS Indian Head, MD
BARAN, Chester	1605 AB Wg, Azores
BEARDEN, LTC J. L., USAF	AFISC/SES, Norton AFB, CA
BEGLEY, L. D.	Camp Walker, Taegu, Korea
BENT, R. L.	Sperry Rand Corp, Louisiana AAP, LA
BIASUTTI, G. S.	Biazzi Soc. AN. Vevey, Switzerland
BIBLE, W. B.	Martin Marietta Alum Sales, Milan, TN
BISHOP, R. H.	2750 AB Wg/SE, W-P AFB, OH
BLANKENSHIP, J. H.	USAMC Surety Fld Ofc, Dover, NJ
BODDORFF, Deane	Hercules Inc, Wilmington, DE
BOGGS, W. H.	NASA, Kennedy SC, FL
BOX, J. R.	Robins AFB, GA
BRADWORD, W. J.	Olin Corp., Stamford, CT
BRASWELL, A. T.	Red River Army Depot, Texarkana, TX
BRAUN, E. F.	DCASR, Detroit, MI
BREEN, C. F.	NASA, Hampton, VA
BRETTEL, E. G.	Day & Zimmermann, Kansas AAP, KS
BROCK, N. H.	Air Prod & Chmls Inc, Allentown, PA
BRODELL, R. L.	NOL Silver Spring, MD
BROUDY, P. M.	Frankford Arsenal, Philadelphia, PA
BROWER, G. H.	POMF Atlantic, Charleston, SC
BROWN, C. J.	BRL, Aberdeen PG, MD
BROWN, W. D.	Iowa AAP, Burlington, IA

BRYAN, K. M.
 BUCHANAN, H. G.
 BUCKNER, A. K.
 BURCH, Austin
 BURKE, E. F.
 BURNER, MAJ R.
 BURNS, W. J.
 BYRD, J. L.

CADY, C. M.
 CALLAHAN, H. L.
 CAMERA, E.
 CAMPBELL, C. D.
 CAMPBELL, C. J.
 CANTRELL, MAJ Frederick
 CAREW, D. L.
 CARPER, W. E.
 CASIMO, S. P.
 CASTLEBERRY, LTC A. R., USAF
 CAVIN, D. L.
 CHANG, Wei-Jhing
 CLONINGER, J. R.
 COFFEY, C. E.
 COFFIN, J. P.
 COLLINS, W. B.
 COMBS, CDR M. F., USN
 CONLEY, J. H.
 COOPER, J. D.
 COOPER, R. E.
 CORBIN, C. C.
 CORNEY, CAPT J. K., USAF
 COST, T. B.
 COUCH, Gerald
 COULSON, J. R.
 COURTRIGHT, W. C.
 CRAIG, E. L.
 CROSLY, W. A.
 CRUPI, J. S.
 CRUZ, I. T.
 CUMNOCK, F. L.
 CUTSHALL, J. S.

DALL, COL Burt, USA
 DAVIS, J. O.
 DEANS, H. L.
 DeGIOVANNI, Joseph
 DeIREGNO, Lawrence
 DEMBERG, Edmund
 DEMBO, M. M.

Tooele Army Depot, UT
 BRL, Aberdeen PG, MD
 Kansas AAP, Parsons, KS
 AEC, Los Alamos, NM
 Olin Corp., St. Marks, FL
 DCASR, N.Y., NY
 Dept of Transportation, Wash, DC
 AMC Ammunition Center, Savanna, IL

Badger AAP, Baraboo, WI
 Black & Veatch, Kansas City, MO
 Biazzi Soc. AN., Vevey, Switzerland
 USA Foreign Science & Tech Ctr, VA
 USARMCOM, Rock Island Arsenal, IL
 HQ Dir Ord Svcs, Vauxhall Barracks, UK
 ADC, Ent AFB, CO
 NAVSEASYSKOM Safety Sch, NAD Crane, IN
 Aberdeen Proving Ground, MD
 SAC, Offutt AFB, NE
 NAD Hawthorne, NV
 Bureau of Explosives, Edison, NJ
 Olin Corp., St. Marks, FL
 DuPont Co., Martinsburg, WV
 Thiokol Corp., Bristol, PA
 ADTC, Eglin AFB, FL
 NOMTF, White Sands Msl Range, NM
 Aberdeen Proving Ground, MD
 NWS Charleston, SC
 BuAlcohol, Tob, Firearms, Treasury Dept, Wash, DC
 NAD Crane, IN
 AFAL, Eglin AFB, FL
 USATECOM, White Sands Msl Range, NM
 United Technology Ctr, Sunnyvale, CA
 DuPont Co., Wilmington, DE
 Los Alamos Scientific Lab, NM
 NWS Concord, CA
 Detector Electronics Corp., Minn., MN
 OASN(I&L), Wash, DC
 NWS Yorktown, VA
 Pine Bluff Arsenal, AR
 Sacramento Air Log Ctr, McClellan AFB, CA

Edgewood Arsenal, Aberdeen PG, MD
 Sandia Labs, Albuquerque, NM
 DDESB, Wash, DC
 Hercules Inc., Cumberland, MD
 DCASR, Dallas, Texas
 Picatinny Arsenal, Dover, NJ
 USA Engineer Div, Huntsville, AL

DEXTER, R. F.
DIAS, W. C.
DOBBIE, J. M.
DOBBS, N. G.
DONNADIEU, Roger
DOWDY, R. W.
DOWLING, T. P.
DOYLE, J. R.
DRAKE, R. W.
DUNN, J. A.
DUNN, J. H.
DUNN, M. L.

ECCLESTON, H. F.
EDDY, W. J.
EDGERTON, J. H.
EDWARDS, C. R.
EHRINGER, A. G.
EILO, C. W.
ELKINS, L. O.
ELSASSER, F. M.
ERICKSON, C. L.
ESPARZA, E. D.
EVERETT, L. A.
EWING, H. M.

FARMER, M. D.
FARR, A. H.
FEIL, LTC J. A., USAF
FENGER, F. H.
FIDELL, F. J.
FIEDOREK, Joseph
FINKEL, M. G.
FISCHER, COL G. F., USAF
FLACK, D. E. J.
FLETCHER, E. R.
FLYNN, W. F.
FOLEY, J. J.
FORBUS, K. V.
FORSTEN, Irving
FORSYTHE, F. J.
FGSMIRE, D. F.
FOWLER, R. G.
FOWLER, W. T.
FRIEDMAN, N. J.

GAITHER, Donald
GIRBLE, J. W.
GILCHRIST, A. B.

BuAlcohol, Tob, Firearms, Treasury Dept, Wash, DC
Vandenberg AFB, CA
A. D. Little, Cambridge, MA
Ammann & Whitney, N.Y., NY
Societe Nat des Poudres et Expl, Paris, France
Agabian Assoc, El Segundo, CA
Trojan-U.S. Powder, Allentown, PA
Sandia Labs, Kirtland AFB, NM
Los Alamos Scientific Lab, NM
Picatinny Arsenal, Dover, NJ
Baldwin Electronics Inc, Camden, AR
DDESB, Wash, DC

NOL Silver Spring, MD
NAVFACENCOM, Alexandria, VA
MIMC Tr Eng Agency, Newport News, VA
Radford AAP, Radford, VA
AMC Ammunition Center, Savanna, IL
Hercules Inc., Wilmington, DE
Eglin AFB, FL
60 MAW, Travis AFB, CA
USAMC Ammunition Center, Savanna, IL
SW Res Inst, San Antonio, TX
DCASR, Philadelphia, PA
Sacramento Army Depot, Sacramento, CA

Lexington-Blue Grass AD, KY
ADTC, Eglin AFB, FL
DCASR, Boston, MA
Tudor Engr Co., San Francisco, CA
Frankford Arsenal, Philadelphia, PA
Dept of Interior, MESA, Pittsburgh, PA
USAM Sys Analysis Acty, Aberdeen PG, MD
HQ USAF/LGTN, Wash, DC
Royal Ord Factory, Renfrewshire, Scotland
Lovell Foundation, Albuquerque, NM
Redstone Arsenal, AL
USAMC, Alexandria, VA
Anniston Army Depot, AL
Picatinny Arsenal, Dover, NJ
Joliet AAP, Joliet, IL
Tyndall AFB, FL
ICI United States, Charlestown, IN
Radford AAP, Radford, VA
Picatinny Arsenal, Dover, NJ

NAD Crane, IN
NAVAIRSYSCOM, Wash, DC
Letterkenny Army Depot, Chambersburg, PA

GILL, J. O.
GILMORE, A. E.
GLADDEN, W. L.
GOGLIUCCI, Anthony
GOLDBERG, Dr. Harold
GOLDSTEIN, Raymond
GOOCH, T. R.
GORA, T. F.
GOTT, R. W.
GUARIENTI, R. P.

HAHN, J. C.
HALCOMB, R. N.
HALL, Clyde
HALL, P. H.
HALTER, D. I.
HALTOM, P. T.
HAMILTON, A. E.
HAMILTON, Norl
HAMMONDS, R. G.
HANNA, R. J.
HANNAH, M. M.
HARPER, J. D.
HARRIS, R. M.
HART, C. E.
HARTON, E. E., Jr.
HAWES, J. M.
HEESEMAN, Al
HELLE, C. J.
HELMS, E. D.
HENDERSON, W. P.
HERMAN, R. C.
HERNANDEZ-FRAGOSO, COL I., USA
HIGGINS, J. M.
HILL, J. H.
HILL, W. V.
HILLARD, L. F.
HILLMAN, R. S.
HOLLANDER, W. V.
HOLLOWAY, B. G.
HORNE, K. E.
HUFFINGTON, N. J., Jr.
HUFFMAN, COL J. P., USAF
HUOT, LTC F. A., Canadian Fcs

IERARDI, M. P.
INGRAM, J. K.
INGRAM, P. L.
ISAACS, N. D.
ISENBERG, P. E.

NAPEC, NAD Crane, IN
NAPEC, NAD Crane, IN
United Technology Ctr, Sunnyvale, CA
Picatinny Arsenal, Dover, NJ
NAVSEASYSKOM, Wash, DC
Picatinny Arsenal, Dover, NJ
Thiokol Corp., Huntsville, AL
Picatinny Arsenal, Dover, NJ
Hercules Inc., Magna, UT
Lawrence Livermore Lab, Livermore, CA

Martin Marietta Corp., Orlando, FL
Martin Marietta Corp., Cocoa B., FL
Austin Powder Co., McArthur, OH
437th MAWG, Charleston AFB, SC
Red River Army Depot, Texarkana, TX
USA Log Mgt Ctr, Red River AD, TX
NAPEC, NAD Crane, IN
ICI United States Inc, Chattanooga, TN
Yuma Proving Ground, AZ
Boeing Co., Seattle, WA
63d MAW, Norton AFB, CA
Los Alamos Scientific Lab, NM
Red River AD, Texarkana, TX
NWL Dahlgren, VA
Dept of Transportation, Wash, DC
USAMC, Alexandria, VA
Wyle Laboratories, Norco, CA
Ranington Arms Inc., Sao Paulo, Brazil
Holston Defense Corp., Kingsport, TN
Edgewood Arsenal, Aberdeen PG, MD
DDESB, Wash, DC
USAMC, Alexandria, VA
Mason & Hanger-Silas Mason, Grand Is, NE
Calesco Ind. Inc., E. Camden, AR
Black & Veatch, Kansas City, MO
USARPAC, San Francisco, CA
Martin Marietta Aerospace, Denver, CO
Olin Corp., New Haven, CT
Volunteer AAP, Chattanooga, TN
Jet Research Ctr, Arlington, TX
BRL, Aberdeen PG, MD
IGD (AFISC/SEV), Norton AFB, CA
National Defence HQ, Ottawa, Canada

NOL Silver Spring, MD
USAEWES, Vicksburg, MS
Anniston Army Depot, AL
MRC Corp., Baltimore, MD
Olin Corp., St. Marks, FL

JAMISON, J. E.	Mason & Hanger-Silas Mason Co, Burl, IA
JENKINS, D. M.	NWL Dahlgren, VA
JOHNSON, L. J., Jr.	NASA, Langley Res Ctr, Hampton, VA
JOHNSON, R. E.	Olin Corp, Badger AAP, Baraboo, WI
JOHNSON, R. E.	StratWpnsFacyPac, Silverdale, WA
JONES, C. P.	NAVSEASYSCOM, Wash, DC
JONES, F. M.	Aerojet Solid Prop Co, Sacramento, CA
KAHLER, R. J.	Mason & Hauger-Silas Mason Co, Amarillo, TX
KATIC, J. R.	Olin Corp, Badger AAP, Baraboo, WI
KAWKA, John	AFISC, Norton AFB, CA
KEEFER, J. H.	BRL, Aberdeen Proving Ground, MD
KEETCH, A. K.	Dugway Proving Ground, UT
KELLEY, COL P. G., USA	DDESB, Wash, DC
KELLEY, S. C.	USAEWES, Lawrence Liv Lab, Livermore, CA
KERNS, A. J.	Picatinny Arsenal, Dover, NJ
KIM, Ki-Bong	Jet Propulsion Lab, Pasadena, CA
KINDIG, LCDR J. N., USN	NMC Point Mugu, CA
KINEKE, J. H.	BRL, Aberdeen PG, MD
KING, P. V.	Edgewood Arsenal, Aberdeen PG, MD
KINGERY, C. N.	BRL, Aberdeen PG, MD
KIRTLEY, Don	Hercules Inc., Wilmington, DE
KLEIN, CAPT P. F., USN	Chairman, DDESB, Wash, DC
KNASEL, B. L.	DDESB, Wash, DC
KNUTSON, CAPT D. W., USN	Cfc Ch of Naval Operations, Wash, DC
KOINAKIS, W. J.	BRL, Aberdeen PG, MD
KOMOS, J. N.	DSA, Alexandria, VA
KORSLUND, A. R.	Boeing Aerospace Co., Hill AFB, UT
KRESS, J. A.	NAPEC, NAD Crane, IN
KRISTOFF, F. T.	Hercules Inc., Radford AAP, VA
LAGAMMA, V. E.	DCASR, N. Y., NY
LAIDLAW, B. G.	Dept of Natl Defence, Ralston, Alberta, Canada
LANCASTER, J. M.	USARMCOM, Rock Island Arsenal, IL
LANDRUM, CDR R. G., USN	NWS Concord, CA
LARIMER, F. M.	Fed Cartridge Corp, Twin Cities AAP, MN
LARSEN, T. E.	Detector Elec Corp., Minn., MN
LASSEIGNE, A. H.	General Electric Co, Bay St. Louis, MS
LATHAM, J. F.	NAD Earle, Colts Neck, NJ
LAYBOURNE, J. D.	Umatilla Depot Activity, Hermiston, OR
LEACH, T. M.	NAVSEASYSCOM Safety Sch, NAD Crane, IN
LEANDER, R. C.	Thiokol Corp, Marshall, TX
LEARY, W. F.	HQ USAREUR & 7th Army, Germany
LEONARD, Larry	NAD Crane, IN
LERWILL, R. J.	USA Test & Eval Com, Aberdeen PG, MD
LEVEY, D. V.	Gearhart-Owen Ind., Ft. Worth, TX
LEWIS, Hamilton	DuPont Co, Wilmington, DE
LEWIS, H. L.	NOSSOPAC, San Diego, CA
LEWIS, W. R.	Red River Army Depot, Texarkana, TX

LINDLER, H. E.
LOGAN, J. E.
LONADIER, F. D.
LOPEZ, H. R.
LYMAN, Ms Ona R.
LYNCH, C. G.
LYNCH, Dr. R. H.

McBRIDE, William
McCARTIN, LT J.J., USCG
McCAY, W. C.
McCLOSKEY, G. W.
McDONALD, J. P.
McDOWELL, R. C.
McGAUGHY, R. V.
McINTYRE, F. L.
McKOWN, G. L.
McLAIN, W. H.
MALCOLM, CDR N. T., Canadian Fcs
MANSFIELD, M. B.
MAPLES, J. D.
MARSICOVETE, J. R.
MARSISCHKY, G. W.
MATHIS, J. M.
MEAD, J. M.
METCALF, H. L.
MIGUEL, J.
MILLER, R. J.
MILTON, LTC J. P., USAF
MINIX, CAPT J. H., USA
MITCHELL, W. D.
MITTERNIGHT, C. P.
MONDANO, R. L.
MORAN, E. P.
MULLINS, R. K.
MURPHY, J. L.
MYERS, R. L.
MYERS, R. L.

NAPADENSKY, Mrs Hyla S.
NASH, J. T.
NELSON, G. A.
NEWCOMB, F. N.
NEWTON, C. B.
NICKERSON, H. D.

OAKES, R. M.
O'DRISCOLL, J. J.
OLIVER, R. E.

USAMC Fld Safety Agency, Charlestown, IN
Western Electric Co, Greensboro, NC
Monsanto Res Corp, Miamisburg, OH
NOS Indian Head, MD
BRL, Aberdeen PG, MD
NAD Crane, IN
Ministry of Defence, British Embassy, Wash, DC

NWS Yorktown, VA
USCG, Jacksonville, FL
Longhorn AAP, Marshall, TX
Indiana AAP, Charlestown, IN
NAD Crane, IN
USAMC, Alexandria, VA
Picatinny Arsenal, Dover, NJ
General Electric Co, Bay St Louis, MS
Edgewood Arsenal Res Lab, Bay St Louis, MS
SW Res Inst, San Antonio, TX
National Defence HQ, Ottawa, Canada
UTC Eastern Test Range, Cape Canaveral, FL
Redstone Arsenal, AL
Picatinny Arsenal, Dover, NJ
NAVSEASYS COM Sch Dept, NAD Crane, IN
Martin Marietta Corp, Vandenberg AFB, CA
Uniroyal Inc, Joliet, IL
Ofc ASD(I&L), Wash, DC
NUSC Newport, RI
Uniroyal Inc., Joliet, IL
1st St Air Div, SAC, Vandenberg AFB, CA
USA Inst for Mil Asst, Ft Bragg, NC
USAMICOM, Redstone Arsenal, AL
NAD Crane, IN
CMI Operations/3M Co, Chelmsford, MA
ARMCOM, Rock Island, IL
Lawrence Livermore Lab, Livermore, CA
Thiokol Corp, Huntsville, AL
USAMC Fld Safety Agency, Charlestown, IN
Olin Corp, St. Marks, FL

IIT Res Inst, Chicago, IL
USA CofEngrs, Huntsville, AL
NUC San Diego, CA
USA Human Engr Lab, Aberdeen PG, MD
AFCMD, Kirtland AFB, NM
NAVFACENGCOCOM, Alexandria, VA

Sierra Army Depot, Herlong, CA
Southern Railway System, Atlanta, GA
NavShipR&D Ctr, Portsmouth, VA

O'KONSKI, A. R.
OLSEN, F. N.
OPEL, M. C.
ORNELLAS, G. S.
OZENGHAR, H. H.

PAKULAK, J. M.
PELLEREAU, MAJ GEN P. J. M.
PENA, A. O.
PEPE, Ron
PERKINS, R. G.
PERRY, MAJ R., USA
PETERSEN, A. H.
POLLEY, C. J.
POLLOCK, B. D.
PORZEL, F. B.
POWELL, J. L.
PRATT, Victor
PRICE, P. D.
PRIOR, L. C.
PRITCHARD, G. C.

RACHEL, C. K.
RACHMELER, BR GEN Louis
RANDALL, H. J.
RANKIN, J. E.
RAUSIN, COL G. D., USAF
RAY, D. E.
REDDEN, J. E.
REDDY, P. D.
REDMAN, C. W.
REED, J. W.
REEVES, H. J.
REGAN, L. F.
REICH, Claude
REILLY, F. E.
REISBICK, CAPT J.N.P., USAF
REMPFER, E. J.
REZETKA, W. L.
RHODES, D. B.
RICCARDI, S. A.
RICHMOND, D. R.
RIIKONEN, ENS D. A., USCG
RINDNER, R. M.
RITTMAN, H. T.
RIZZO, F. J.
ROBERTS, J. H.
ROBERTSON, T. R.
RODIO, P. A.

Ofc Proj Mgr Prod Base Mod & Exp, PicArs, NJ
Boeing Aerospace Co, Seattle, WA
ICI United States Inc, Charlestown, IN
14th Naval Dist Staff, HI
DSA, Los Angeles, CA

NWC China Lake, CA
Ordnance Board, MOD, United Kingdom
NOMTF, White Sands Msl Range, NM
IIT Research Inst, Chicago, IL
DDESB, Wash, DC
Mil Ocean Terminal, Sunny Pt, NC
Detector Electronics Corp, Minn., MN
AMMRC, Watertown, MA
Picatinny Arsenal, Dover, NJ
NOL Silver Spring, MD
Olin Corp, Marion, IL
Dugway Proving Ground, UT
Picatinny Arsenal, Dover, NJ
Jet Propulsion Lab, Pasadena, CA
NWC China Lake, CA

Hughes Aircraft Co, Tucson, AZ
Ofc ASA(I&L), Wash, DC
DCASR, Burlingame, CA
USAMC, Alexandria, VA
DDESB, Wash, DC
USARMCOM, Rock Island, IL
Olin Corp, Marion, IL
Agbahian Assoc, El Segundo, CA
Alaskan Air Command
Sandia Labs, Albuquerque, NM
BRL, Aberdeen PG, MD
AMC, Alexandria, VA
MESA, Dept of Interior, Denver, CO
Picatinny Arsenal, Dover, NJ
TAC HQ, Langley AFB, VA
Frankford Arsenal, Phila., PA
Pac Msl Range, Point Mugu, CA
Lone Star AAP, Texarkana, TX
Olin Corp, St. Marks, FL
Lovell Foundation, Albuquerque, NM
HQ USCG, Wash, DC
Picatinny Arsenal, Dover, NJ
DuPont Co, Wilmington, DE
USA Natick Labs, Natick, MA
AMC Ammunition Center, Savanna, IL
Dept of Energy, Mines & Resources, Canada
USAMC, Alexandria, VA

ROSSI, J. M.
ROTHERY, C. M.
ROURE, Ingenieur General J. J.
ROYLANCE, H. M.
RUTLEDGE, R. G.

SAFFIAN, L. W.
SAINDON, B. W.
SANCHEZ, F. B.
SAVAIKO, B. M.
SAVOY, G. A.
SAWYER, R. B.
SCHAICH, CAPT E., German AF
SCHIFFMAN, T. H.
SCHILDER, C. B.
SCHULTZ, L. F.
SCHWAMB, D. F.
SCHWARTZ, R. M.
SCOTT, Dr. R. A., Jr.
SEAVERS, R. H.
SEELY, L. A.
SEWELL, R. G. S.
SHALABI, G. K.
SHAMBLIN, M. C.
SHAW, R. F., Jr.
SHAW, W. A.
SHEFFIELD, O. E.
SHULTZ, J. E.
SIMPSON, J. L.
SIMS, W. H.
SIPIA, J. A.
SIRIANNE, R. A.
SIRLS, J. M.
SKAAR, K. S.
SKINNER, C. S.
SLIWA, A. F.
SLYKER, R. W.
SMITH, R. L.
SNEED, J. A.
SOULE, K. O.
SPANNBAUER, D. G.
SPENCER, J. R.
STANDLEY, R. S.
STAPOR, B. C.
STARK, C. G.
STEPHANS, LTC R. A., USA
STEVENS, C. J.
STONESIFER, R. C.
STOFFERS, F. W.

Picatinny Arsenal, Dover, NJ
DCASR, St. Louis, MO
Bur of Explosives, Paris, France
NAVSEASYSKOM, Wash, DC
Martin Marietta Corp., Denver, CO

Picatinny Arsenal, Dover, NJ
Rocky Mountain Arsenal, Denver, CO
NWL Dahlgren, VA
USA Electronics Com, Ft Monmouth, NJ
Hercules Inc., Magna, UT
DDESB, Wash, DC
Ministry of Defence, Fed Repub of Germany
Gen American Res Div, Niles, IL
HQ DA (DAIG-SD), Wash, DC
Lockheed Msls & Space Co, Sunnyvale, CA
Letterkenny Army Depot, Chambersburg, PA
Day & Zimmermann, Philadelphia, PA
DDESB, Wash, DC
Redstone Arsenal, Huntsville, AL
ARO Inc, Arnold AFS, TN
NWC China Lake, CA
Olin Corp, Badger AAP, Baraboo, WI
NWL Dahlgren, VA
Honeywell Inc, New Brighton, MN
Civil Engr Lab, Port Hueneme, CA
Picatinny Arsenal, Dover, NJ
BUMED, Dept of the Navy, Wash, DC
Martin Marietta Aerospace, Denver, CO
NOOSO Atlantic, Portsmouth, VA
Frankford Arsenal, Philadelphia, PA
Tr & Doctrine Com, Ft Monroe, VA
Martin Marietta Alum Sales Inc, Milan, TN
NWC China Lake, CA
Booz-Allen & Hamilton Inc, Cleveland, OH
NAVSEASYSKOM, Wash, DC
NWC Point Mugu, CA
Hercules Inc, Sunflower AAP, KS
Defense Nuclear Agency Fld Com, NM
Rockwell Int Corp, Canoga Park, CA
DCASR, Atlanta, GA
Lake City AAP, Independence, MO
Armco Steel Corp, Middletown, OH
Tracor Jitco Inc, Rockville, MD
Hq Command, USAF, Bolling AFB, Wash, DC
Volunteer AAP, Chattanooga, TN
NAVFACENGCOR, Alexandria, VA
DCASD, Ft Benjamin Harrison, IN
Jet Propulsion Lab, Pasadena, CA

STUCKEY, G. K.
SULLIVAN, E. P.
SULLIVAN, L. W.
SWATOSH, J. J.
SWINK, S. O.

TALLEY, R. R.
TANCRETO, J. E.
TAYLOR, J. O.
TAYLOR, W. J.
TEICHMANN, E. C.
TETER, J. S.
THOMAS, W. C.
TINKER, W. L.
TOLLINGER, LCDR J. N., USN
TURNER, Dean
TURNER, H. R.
TUTTLE, MAJ W. D., USAF

VALENZUELA, C. Y.
VANDERBILT, S. J.
VAN ERP, Dirk
VINSON, J. L.
VOEGLEIN, J. F.

WALKER, W. L.
WALL, M. F.
WALTZ, G. S.
WASCHLER, A. L.
WATSON, R. R.
WATSON, R. W.
WEALS, F. H.
WEBSTER, MAJ L. C., USA
WEISS, R. R.
WEISSMAN, S. L.
WELLER, J. F.
WENZEL, A. B.
WESTINE, P. S.
WHITNEY, H. W.
WILCOX, W. R.
WILLEY, R. L.
WILLIS, F. M.
WILSCH, L. R.
WILSON, P. D.
WINNEY, LTC W. E., USA
WISE, J. S.
WOSLAND, N. C.
WRAY, G. H.
WYATT, DR. R. M. H.

USARMCOM, Rock Island, KIL
Atlantic Research Corp, Gainesville, VA
NASA, Langley Res Center, Hampton, VA
IIT Research Institute, Chicago, IL
Jet Propulsion Lab, Pasadena, CA

NAVFACENGCOM, San Bruno, CA
Civil Engineering Lab, Port Hueneme, CA
NAVFACENGCOM, San Bruno, CA
Atlas Powder Co., Wilmington, DE
60th Ordnance Group, Germany
Tudor Engineering Co., San Francisco, CA
NUC San Diego, CA
NS San Diego, CA
NAD Earle, Colts Neck, NJ
ODCSLOG, DA, Wash, DC
Etowah Mfg Co., Inc., Gadsden, AL
HQ AFISC, Norton AFB, CA

Yuma Proving Ground, AZ
31st AD Arty Brig, Homestead AFB, FL
Keller & Gannon Cons Engrs, San Fran, CA
Remington Arms Co, Independence, MO
Edgewood Arsenal, Aberdeen PG, MD

NAD Crane, IN
Thiokol Corp., Marshall, TX
Pueblo Army Depot, CO
Aberdeen Proving Ground, MD
Ministry of Defence, London, UK
Bureau of Mines, Dept of Interior, Pittsb, PA
NWC China Lake, CA
USAEWES, Lawrence Livermore Lab, CA
USAMC, Redstone Arsenal, AL
Ammann & Whitney, New York, NY
NAPEC, NAD Crane, IN
SW Res Institute, San Antonio, TX
SW Res Institute, San Antonio, TX
AMMRC, Watertown, MA
General Electric Co, Bay St Louis, MS
NOL Silver Spring, MD
DuPont Co, Martinsburg, WV
Lowry AFB, CO
Pacific Missile Range, Pt Mugu, CA
USARMCOM, Rock Island, IL
NSR&DC Portsmouth, VA
USAM Sys Analysis Agency, Aberdeen PG, MD
Day & Zimmermann Inc, Texarkana, TX
Explosives R&D Estab, United Kingdom

YANTOSIK, G. D.
YOUNG, G. A.

ZAKER, Dr. T. A.
ZAUGG, M. M.

USAMC Surety Fld Ofc, Dover, NJ
NOL Silver Spring, MD

DDESB, Wash, DC
Tooele Army Depot, UT